@00576P08694044

Star 13

# PRATT & WHITNEY AIRCRAFT

ats -26908

File with N76-22355

East Hartford, Connecticut 06108

In reply please refer to
KDS:REF:jan - MERL, J-Mezz

24 May 1976

To: National Aeronautics and Space Administration
Lewis Research Center
21000 Brookpark Road
Cleveland, Ohio 44135

Attention: Mr. F. H. Harf, MS 49-3

Subject: Final Technical Report on Alloy and Structural Optimization of a Directionally Solidified Lamellar Eutectic Alloy - NASA CR-135000 (PWA-5300)

Reference: Contract No. NAS 3-17811

Attachment: One (1) camera ready copy of subject report

Enclosed herewith is one (1) camera ready copy of the subject report. This report is submitted to fulfill the requirements of the Reports of Work Section, paragraph C5, of the referenced contract.

Distribution of this report is being made in accordance with the distribution list furnished by the National Aeronautics and Space Administration Contracting Officer. The distribution list is included at the end of the report.

UNITED TECHNOLOGIES CORPORATION
Pratt & Whitney Aircraft Division

Keith D. Sheffler

K. D. Sheffler
Program Manager

cc: Naval Plant Representative Office (ltr. only)
Pratt & Whitney Aircraft
East Hartford, Connecticut 06108

| 1. Report No. | 2. Government Accession No. | 3. Recipient's Catalog No. |
|---|---|---|
| NASA CR-135000 | | |

| 4. Title and Subtitle | 5. Report Date |
|---|---|
| ALLOY AND STRUCTURAL OPTIMIZATION OF A DIRECTIONALLY SOLIDIFIED LAMELLAR EUTECTIC ALLOY | May 1976 |
| | 6. Performing Organization Code |

| 7. Author(s) | 8. Performing Organization Report No. |
|---|---|
| K. D. Sheffler, R. H. Barkalow, J. J. Jackson, and A. Yuen | PWA-5300 |
| | 10. Work Unit No. |
| 9. Performing Organization Name and Address<br>Pratt & Whitney Aircraft Division,<br>United Technologies Corporation<br>East Hartford, Connecticut | 11. Contract or Grant No.<br>NAS3-17811 |
| | 13. Type of Report and Period Covered<br>Contractor Report |
| 12. Sponsoring Agency Name and Address<br>National Aeronautics and Space Administration<br>Washington, D. C. 20546 | 14. Sponsoring Agency Code |

15. Supplementary Notes

Project Manager Fredric H. Harf, Materials and Structures Division, NASA-Lewis Research Center, Cleveland, Ohio

16. Abstract

Mechanical property characterization of a directionally solidified Ni-20%Cb-2.5%Al-6%Cr cellular eutectic turbine blade alloy shows excellent long time creep stability and indicates intermediate temperature transverse tensile ductility and shear strength to be somewhat low for turbine blade applications. Alloy and structural optimization significantly improves these off-axis properties with no loss of longitudinal creep strength or stability. The optimized alloy-structure combination is a carbon modified Ni-20.1% Cb-2.5%Al-6.0%Cr-0.06%C composition processed under conditions producing plane front solidification and a fully lamellar microstructure. With current processing technology, this alloy exhibits a creep-rupture advantage of 39°C (70°F) over the best available nickel base superalloy, directionally solidified MAR M200+ Hf. Optimized transverse tensile and rupture ductilities of 1 to 2 percent are similar to those of hafnium free directionally solidified MAR M200, which has been used for solid blade applications in a high performance military engine. While improved by about 20 percent, shear strength of the optimized alloy remains well below typical superalloy values.

| 17. Key Words (Suggested by Author(s)) | | 18. Distribution Statement |
|---|---|---|
| Eutectic | Nickel Alloys | Unclassified - Unlimited |
| Directional Solidification | Anisotropy | |
| Mechanical Properties | Turbine Alloys | |

| 19. Security Classif. (of this report) | 20. Security Classif. (of this page) | 21. No. of Pages | 22. Price* |
|---|---|---|---|
| Unclassified | Unclassified | 328 | $6.00 |

* For sale by the National Technical Information Service, Springfield, Virginia 22151

## FOREWORD

This report describes work performed by the Pratt & Whitney Aircraft Division of the United Technologies Corporation for the Lewis Research Center of the National Aeronautics and Space Administration under Contract NAS3-17811. The program was administered for Pratt & Whitney Aircraft by Dr. K. D. Sheffler, Program Manager, with assistance provided by Dr. R. H. Barkalow, Mr. J. J. Jackson, and Mr. A. Yuen. Dr. G. R. Leverant and Dr. M. L. Gell acted as consultants to the program. Special recognition is due Mrs. D. A. Boychuck for her efforts in the areas of metallographic preparation, microstructural interpretation, and the keeping of extensive and accurate records for this program. Preparation and screening of materials for the Phase II solidification studies were performed at the United Technologies Research Center (UTRC) under the supervision of Dr. E. R. Thompson and Dr. F. D. Lemkey. Instrumented impact testing for Phase IV was conducted at UTRC under the supervision of Dr. C. O. Houlse. The NASA Project Manager was Mr. F. H. Harf, with Dr. H. R. Gray acting as a consultant. Results of parallel company-sponsored research programs are included in this report where appropriate.

## TABLE OF CONTENTS


| Section | | Page |
|---|---|---|
| I. | SUMMARY | 1 |
| | A. Baseline Alloy Characterization | 1 |
| | B. Microstructure and Chromium Variation Studies | 1 |
| | C. Alloy Modification | 2 |
| | D. Substantiation of Optimized Alloys | 2 |
| | E. Comparison With Superalloys | 3 |
| II. | INTRODUCTION | 4 |
| III. | EXPERIMENTAL DETAILS | 7 |
| | A. Preparation of Test Material | 7 |
| | B. Test Procedures | 7 |
| IV. | PHASE I – BASELINE ALLOY CHARACTERIZATION | 10 |
| | A. Test Program | 10 |
| | B. Long Time Stability | 10 |
| | 1. Discussion of Results | 10 |
| | 2. Metallographic Evaluation of Tested Creep Specimens | 11 |
| | C. Shear Strength Evaluation | 14 |
| | 1. Ultimate Shear Strength Results | 14 |
| | 2. Shear Creep Test Results | 14 |
| | D. Transverse Strength Evaluation | 15 |
| | 1. Tensile Test Results | 15 |
| | 2. Transverse Creep Results | 16 |
| | E. Evaluation of Notch Sensitivity | 16 |
| | 1. Combination Smooth-Notch Tension Test Results | 16 |
| | 2. Combination Smooth-Notch Stress Test Results | 17 |
| | F. Phase I Summary | 17 |
| V. | PHASE II – MICROSTRUCTURE AND CHROMIUM VARIATION STUDIES | 19 |
| | A. Phase II, Part A - Solidification Studies | 19 |
| | 1. Gradient Measurements | 19 |
| | 2. Critical G/R Determinations | 20 |
| | 3. Microstructural Characterizations | 21 |
| | a. Interlamellar Spacing | 21 |
| | b. Volume Fraction $Ni_3Cb$ Phase | 22 |
| | c. Eutectic Grain Size | 23 |

## TABLE OF CONTENTS (Cont'd)


| Section | | Page |
|---|---|---|
| | B. PHASE II, Part B - Mechanical Behavior | 23 |
| | 1. Creep Strength | 23 |
| | a. Test Program | 24 |
| | b. Processing Details | 24 |
| | c. Lamellarity, Lamellar Spacing and Chromium Effects | 25 |
| | d. Lamellar Spacing Effects in the Chromium Free Alloy | 26 |
| | 2. Transverse Tensile Ductility | 28 |
| | 3. Transverse Creep | 30 |
| | 4. Longitudinal Tensile Strength | 31 |
| | 5. Effects of Chromium on Thermal Fatigue | 31 |
| | C. Phase II Summary | 32 |
| VI. | PHASE III – ALLOY MODIFICATION | 34 |
| | A. Alloy Screening | 34 |
| | 1. Boron | 35 |
| | 2. Zirconium and Hafnium | 36 |
| | B. Alloy Optimization | 37 |
| | 1. Carbon Level Optimization | 37 |
| | 2. Metallurgical Evaluation of Carbon Modified Castings | 37 |
| | C. Processability - Property Balance Optimization | 40 |
| | 1. Solidification Rate Effects | 41 |
| | 2. Tantalum Modification | 42 |
| | D. Evaluation of Thermal Treatments | 43 |
| | E. Critical G/R Determination | 44 |
| | F. Phase III - Summary | 45 |
| VII. | PHASE IV – SUBSTANTIATION OF OPTIMIZED ALLOYS | 46 |
| | A. Test Program | 46 |
| | B. Off-Axis Properties | 46 |
| | 1. Transverse Tensile and Creep Results | 47 |
| | 2. Shear Properties | 48 |
| | 3. Transverse Low Cycle Fatigue | 49 |
| | C. Impact Results | 49 |
| | D. Longitudinal Creep Evaluation | 50 |
| | E. Microstructural Stability | 51 |
| | 1. Eutectic Microstructures | 51 |
| | 2. Coating Stability | 51 |
| | F. Phase IV Summary | 52 |
| VIII. | CONCLUSIONS | 53 |
| IX. | REFERENCES | 54 |

## TABLE OF CONTENTS (Cont'd)


| Section | | Page |
|---|---|---|
| APPENDICES | | 251 |
| Appendix A | Castings Evaluated | 252 |
| Appendix B | Methods Used for Analysis of Tension Test Results | 262 |
| Appendix C | Quantitative Metallographic Measurements | 265 |
| Appendix D | Microstructures Found in Typical Modified Slab Castings Evaluated in Phase III | 278 |
| Appendix E | Minor Element Chemical Analysis | 294 |
| Appendix F | Phase II and Phase III 760°C (1400°F) Transverse Tension Tests | 303 |
| Appendix G | Phase III Longitudinal Creep Tests | 311 |
| DISTRIBUTION LIST | | 315 |

## I. SUMMARY

Directionally solidified eutectics are a unique new class of alloys which have the potential to meet the increased strength and temperature demands that will be placed on advanced gas turbine materials. The objective of this contract was to characterize the mechanical behavior of a cellular $\gamma'(Ni_3Al)$ precipitation strengthened $\gamma - \delta$ $(Ni\text{-}Ni_3Cb)$ eutectic turbine blade alloy (designated $\gamma/\gamma' - \delta$), which was developed recently under NASA sponsorship at the United Technologies Research Center, and to investigate approaches for improving the balance of properties parallel and perpendicular to the direction of primary reinforcement. The experimental program conducted to achieve this objective included four phases, which are described in the following paragraphs.

### A. BASELINE ALLOY CHARACTERIZATION

Phase I was devoted to characterization of the cellular Ni-20%Cb-2.5%Al-6% Cr* baseline alloy. Results showed excellent long time (> 1000 hours) creep stability of the eutectic microstructure, and indicated that intermediate temperature (704-760°C/1300-1400°F) transverse ductility and shear strength were the key properties requiring improvement for turbine applications. Transverse tensile and creep ductilities on the order of 0.2 to 0.5 percent were measured in this temperature range, as compared to values between 3 and 20 percent at higher temperatures. The 704°C (1300°F) shear strength of the eutectic was 300 MPa (44 ksi), less than half that of B-1900 (≈ 700 MPa/100 ksi), a conventional nickel-base superalloy. Metallographic evaluation confirmed that off-axis failure of the cellular structure occurs preferentially on cellular grain boundaries.

### B. MICROSTRUCTURE AND CHROMIUM VARIATION STUDIES

The influence of chromium level on process-structure and structure-property relationships was investigated in Phase II. Results of solidification studies showed that chromium increases the critical G/R for plane front solidification from ≈ 5C° hr/cm² in the absence of Cr to 55C° hr/cm² at the 1 percent level. Further increases to 120 and 150C° hr/cm² were measured at chromium levels of 3 and 6 percent. Chromium also decreases the solidification rate - lamellar spacing constant ($\lambda^2 R$), which causes lamellar spacing to decrease with increasing chromium level at a constant solidification rate. Creep test results showed that refinement of lamellar spacing increases creep strength in both fully lamellar (plane front solidified) and cellular microstructures, with fully lamellar specimens, solidified at the highest rate producing plane front solidification, having the highest creep strengths. At high solidification rates (above 6 cm per hour in the chromium free alloy), a transition from intra- to intergranular deformation causes the creep strength of the fully lamellar structure to decline. Chromium increases the creep strength of fully lamellar structures having equivalent lamellar spacings, with the largest increase occurring in the range of 0 to 1 percent Cr. Microstructure has a significant influence on intermediate temperature transverse ductility. At 760°C (1400°F), respective average transverse tensile ductilities of 0.28 and 0.33 percent were measured in fully lamellar specimens containing 1 and 6 percent chromium, as compared to average values of 0.06 and 0.18 percent in corresponding cellular structures. Intermediate temperature transverse rupture ductility is also increased from about 0.5 percent in the

*Unless otherwise stated, all compositions are reported in weight percent.

cellular structure to 1.6 percent in the lamellar structure. High temperature (1038°C/ 1900°F) transverse ductilities of the lamellar structure remain above 3 percent.

## C. ALLOY MODIFICATION

The influence of small additions of quinary elements such as carbon, zirconium, hafnium, or boron on intermediate temperature transverse tensile ductility was investigated in Phase III. Various approaches to development of an optimum balance of longitudinal and transverse properties were also investigated in this phase. Results of initial screening trials showed that carbon was the only element having a beneficial influence, with an average 760°C (1400°F) transverse tensile ductility of 0.49 percent being measured in carbon modified alloys containing both 1 and 6 percent chromium. Zirconium and hafnium had no influence on transverse ductility, while boron had an embrittling effect. Optimum carbon charge levels of 0.08 and 0.06 percent, respectively, were identified in the 1 and 6 percent Cr compositions. Solidification studies showed that carbon has a slight, beneficial influence on processability (critical G/R). Heat treatment studies indicated that a 24-hour age at 899°C (1650°F) increased the 760°C (1400°F) average transverse tensile ductility of the lamellar base composition 6% Cr alloy to 0.47 percent, and had no influence on the carbon modified composition. Creep test results indicated that carbon has no influence on longitudinal creep strength. These results also showed that the creep strength of the 1 percent Cr alloy is increased by refinement of lamellar spacing and by the addition of tantalum, but the improvements are not sufficient to match the best creep properties of the 6 percent Cr alloy. Based on these results, the base composition and 0.06 percent carbon modified 6 percent Cr alloys processed under conditions producing plane front solidification (fully lamellar microstructure) were identified as the two alloy-structure combinations having the best property balance. These two candidate alloy-structure combinations were subjected to further evaluation in Phase IV to select the optimum combination having the best potential for successful turbine applications.

## D. SUBSTANTIATION OF OPTIMIZED ALLOYS

Properties evaluated on the two candidate alloy-structure combinations in Phase IV included shear and transverse creep and tensile, longitudinal creep, impact, transverse low cycle fatigue, and microstructural stability. Test results indicated significant increases of the key off-axis properties identified as requiring improvement in Phase I, with no loss of longitudinal strength or microstructural stability. The application of a NiCoCrAlY overlay coating was found to increase the 760°C (1400°) average transverse tensile ductility of the carbon modified alloy from 0.49 to 0.85 percent. A smaller increase from 0.49 to 0.55 percent, was found in the fully lamellar base composition. Respective 760°C (1400°F) transverse rupture ductilities of 1.7 and 2 percent were measured in the base composition and carbon modified alloys. Intermediate temperature shear strength of the carbon modified alloy was increased to 390 MPa (56 ksi), as compared to values of 340 and 300 MPa (49 and 44 ksi) measured on the lamellar and cellular base compositions. Impact resistance of the carbon modified alloy was comparable to values measured on the baseline alloy after a 1500-hour age at 849°C (1560°F). Limited transverse low cycle fatigue results indicate that carbon improves the 760°C (1400°F) transverse low cycle fatigue life, with no influence being found at 982°C (1800°F).

## E. COMPARISON WITH SUPERALLOYS

Based on these results, a Ni-20.1%Cb-2.5%Al-6%Cr-0.06%C modified composition directionally solidified under conditions producing a fully lamellar microstructure is recommended as the optimum alloy-structure combination for turbine application of $\gamma/\gamma'$-$\delta$. With current processing technology, this alloy exhibits a 40 percent improvement of longitudinal stress capability at 1000°C (1832°F), which translates to a 39°C (70°F) temperature advantage over the best available nickel base superalloy (DS MAR-M200 + Hf). The intermediate temperature transverse ductility of the optimized eutectic alloy is comparable to that of directionally solidified MAR M-200 without hafnium, which has been used for solid blade applications in a high performance military engine. It appears that the design limiting property of the eutectic may be intermediate temperature shear strength. While significant improvements are obtained by the addition of carbon, the 390 MPa (56 ksi) strength measured on the optimized alloy remains well below typical superalloy levels of 700 MPa (100 ksi).

## II. INTRODUCTION

The increasing performance demands on modern gas turbine engines necessitate the use of turbine materials with improved elevated temperature and strength capability. The turbine blade environment is a particularly critical one because rotating components are subjected to severe combinations of stress and temperature. Directionally solidified eutectics are a unique new class of materials which have the potential to meet the performance demands of advanced turbine designs. Directionally solidified nickel-base eutectic superalloys containing $Ni_3Cb$ ($\delta$ phase) reinforcing platelets in a $\gamma'$ strengthened nickel-base matrix have a potential temperature advantage of 56 to 83°C (100 to 150°F) over the best conventional nickel-base superalloy when tested in the direction of reinforcement[1]. However, to realize the potential strength/temperature advantage of this class of alloys, it is desirable that the transverse and shear properties be improved to support the loads imposed in the root attachment area, as well as the transverse airfoil thermal fatigue strains which may exist in advanced hollow turbine blades.

The objectives of this program were to characterize the mechanical behavior of a $\delta$ reinforced directionally solidified eutectic alloy (Ni-20% Cb-2.5% Al-6% Cr) which was recently developed under NASA sponsorship at the United Technologies Research Center[2], and to investigate approaches for improvement of the shear and transverse properties of the material while maintaining processability and longitudinal creep strength. The program for accomplishment of these objectives included four major phases. The first phase was devoted to characterization of the long time creep stability, elevated temperature shear, transverse strength, and notch sensitivity of the baseline Ni-20% Cb-2.5% Al-6% Cr alloy. Results of these tests provided baseline property values which were used to assess improvements achieved in the remaining three phases, which were devoted to microstructural evaluation and testing of structural and compositional modifications of the baseline alloy. The purpose of the second phase was to determine the influence of chromium variations in the range of zero to six weight percent on processability, strength, and thermal fatigue resistance, while Phase III involved evaluation of the influence of minor elements such as hafnium, zirconium, carbon, and boron on processability and off-axis properties. The objective of the fourth phase was to substantiate the mechanical properties of two optimized alloy-structure combinations selected from results of the second and third phases. A more detailed discussion of these objectives and the background leading to their identification as areas requiring investigation on this contract, is included in the following paragraphs.

As shown by Lemkey[2] the addition of aluminum to the binary Ni-$Ni_3Cb$ ($\gamma$ - $\delta$) directionally solidified (DS) eutectic originally described by Quinn, et. al.[3], Figure 1, produces a monovariant alloy* which can be directionally solidified under suitable growth conditions to produce an aligned composite structure consisting of alternating lamellae of $\gamma$ nickel and $\delta$ $Ni_3Cb$ (Figure 2a). On cooling below the solidus temperature, $\gamma'$ ($Ni_3Al$) phase precipitates from the (Ni-Al-Cb) $\gamma$ solid solution producing a typical superalloy-type $\gamma/\gamma'$ microstructure reinforced by the $\delta$ lamellae (Figure 2b). The combination of $\gamma'$ precipitation hardening and $\delta$ reinforcement provides for high longitudinal strength and creep resistance over the entire temperature range experienced by turbine airfoil materials.

*Approximate composition Ni-21.6%Cb-2.5%Al

Processing conditions exert a primary influence on the microstructure of the $\gamma/\gamma' - \delta$ eutectic. Important parameters include precise alloy composition, rate of advance of the solid-liquid interface (R), and temperature gradient in the liquid at the interface (G, illustrated in Figure 3). Solidification rate controls the spacing between successive lamellae ($\lambda$, Figure 2b) through the relationship $\lambda^2 R$ = constant. As shown in Figure 4, Lemkey[2] has characterized the rate-spacing relationship in the monovariant Ni-Cb-Al eutectic. The degree of alignment achieved in the eutectic microstructure is controlled by the ratio of thermal gradient to solidification rate, G/R. At G/R conditions above a critical value, G/R*, fully coupled plane front growth occurs and a microstructure such as that shown in Figure 5a is achieved. This structure consists entirely of aligned lamellae of the matrix and reinforcing phases, and contains a clearly defined columnar grain structure which is approximately equiaxed in the transverse plane. At G/R conditions below the critical value, plane front growth is not achieved, and microstructures such as that shown in Figure 5b are produced. Two significant differences from the plane front structure are evident in this photomicrograph. First, the eutectic grains are no longer equiaxed in the transverse plane, but are elongated parallel to the lamellae. Second, the structure includes small intergranular triangular "cells" of non-lamellar material. Lemkey and Thompson have shown that the critical G/R above which plane front microstructures such as that shown in Figure 5a are produced in the monovariant $\gamma/\gamma' - \delta$ eutectic is relatively low, on the order of 3-5C° hr/cm$^2$[4]. One of the major objectives of this program was to assess the influence of lamellar versus cellular structures on the mechanical properties of the directionally solidified eutectic.

Because composition ranges must be specified for commercial production of $\gamma/\gamma' - \delta$ turbine hardware, it is necessary to consider the influence of compositional variations on microstructure. Off-eutectic solidification results in structures such as that shown in Figure 6a for Cb lean and in Figure 6b for Cb rich compositions. Off-composition effects may be found in both lamellar (plane front) and cellular microstructures. For example, the structure shown in Figure 6a may be characterized as cellular and $\gamma$ dendritic, resulting from directional solidification of a hypoeutectic (Cb lean) composition at G/R conditions below the critical value for plane front solidification. The structure shown in Figure 6b is lamellar but contains $\delta$ dendrites, indicating a plane-front solidified hypereutectic (Cb rich) composition. Previous work[5] has shown that the presence of primary $\gamma$ phase seriously degrades the creep strength of $\gamma/\gamma' - \delta$. It was desired in the present study to more thoroughly characterize the influence of off-eutectic as well as the previously noted lamellar-cellular structure variation on the mechanical behavior of $\gamma/\gamma' - \delta$.

In an effort to improve high temperature oxidation resistance, Lemkey investigated the addition of chromium to $\gamma/\gamma' - \delta$[2]. While quantitative measurements were not made, it was observed that this quaternary addition caused a substantial increase in the critical G/R of the eutectic, so that the optimized alloy which emerged from Lemkey's study (approximate composition Ni-20%Cb-2.5%Al-6%Cr)* exhibited a cellular microstructure when directionally solidified in the best available gradient at a specified rate of 3 cm/hr (Figure 7). In addition to possessing better oxidation resistance, the 6 percent chromium containing $\gamma/\gamma' - \delta$ alloy ap-

*The exact level of Cb required for fully coupled eutectic growth depends slightly on process conditions and specific levels of other additions such as chromium. Specific compositions evaluated will be noted where appropriate.

peared to have significantly better creep properties than the non-chromium containing monovariant eutectic composition when processed under similar conditions. Major objectives of the current program were to further investigate the mechanical properties of the cellular 6 percent chromium alloy developed on the previous contract, and to study in more detail the influence of chromium level on both processability and properties. The first of these two objectives was approached in Phase I, while chromium variation studies were performed in the second phase together with the structure-property studies mentioned earlier.

The third phase of this program was an investigation of approaches for improvement of the "off-axis" mechanical properties of $\gamma/\gamma'$-$\delta$. As with most materials having a directional microstructure, the mechanical properties of $\gamma/\gamma'$-$\delta$ are anisotropic. Of particular concern were the strength in shear parallel to the direction of lamellar alignment (freezing direction), which relates to the capability of the eutectic to sustain the relatively large shear loads imposed in the root attachment area of advanced turbine blades, and the ductility of the material loaded in tension at right angles (transverse) to the freezing direction.

Preliminary studies demonstrated that both shear and transverse failures of the cellular microstructure occurred by a grain boundary fracture mechanism[5], Figure 8, suggesting that approaches which are used to improve the grain boundary strength of conventional nickel base superalloys might be effective for improvement of off-axis properties in the eutectic alloy. Studies of the influence of both microstructural and compositional modifications with minor elements such as C, Hf, B, and Zr, which are known to be effective grain boundary strengtheners in conventional nickel base superalloys, therefore were undertaken in the third phase of this program. At the conclusion of Phase III, two candidate optimized alloys were selected for a more extensive evaluation of mechanical properties in Phase IV.

## III. EXPERIMENTAL DETAILS

This section will describe general experimental procedures used for processing and evaluating the test material. Certain specialized techniques, such as the quantitative metallographic analyses performed in Phase II, will be described in subsequent sections together with the experimental programs for each of the four phases.

### A. PREPARATION OF TEST MATERIAL

Two primary methods were used for directional solidification of test materials. The first of these methods employed a water-quench Bridgman apparatus having a thermal gradient (G) on the order 300 to 500°C/cm (1400 to 2300°F/inch), Figure 9. This apparatus produced material in the form of nominal 0.9 to 1.3 cm (0.375 to 0.5 inch) diameter by 20 cm (8 inch) long bars. Starting materials of > 99.9 percent purity were pre-alloyed and conventionally chill cast in the form of bars having the appropriate diameter to fit the inside diameter of a 99.8 percent pure recrystallized alumina crucible. Directional solidification was accomplished in a dynamic argon atmosphere by lowering the crucible out of the induction heated hot zone and past the water spray ring at the desired rate. Because of geometry limitations, only longitudinal tests (applied stress parallel to the freezing direction) were performed on specimens produced in this apparatus.

Material for off-axis tests (applied stress not parallel to the freezing direction) was produced in a modified Bridgman apparatus (Figure 10) having a separate recrystallized alumina melting crucible which permitted casting of complex shapes in a conventional alumina shell mold. Most of these castings were produced in the form of nominal 0.3 to 2.5 cm (0.125 to 1 inch) thick by 5 to 10 cm (2 to 4 inch) wide by 20 cm (8 inch) long slabs with the solidification direction parallel to the long dimension. Elemental charges of > 99.9 percent purity were melted under vacuum and poured into a mold of the desired geometry which was then withdrawn under argon from an induction heated chamber at the desired rate. Temperature of the liquid metal was maintained at about 1600°C (2900°F), which provided a gradient on the order of 75 to 125°C/cm with the most generally used 0.64 cm (0.25 inch) slab thickness. Longitudinal as well as off-axis tests were performed on material cast in this furnace, as described in subsequent sections. A list of all castings evaluated during the program is included in Appendix A.

To simulate the surface condition expected in engine application of $\gamma/\gamma' - \delta$, some of the specimens evaluated during the program were tested with a protective coating applied according to a standard Pratt & Whitney Aircraft specification, PWA 270. This nominal Ni-23%Co-17%Cr-12.5%Al-0.3%Y coating was applied to the specimen surface by an electron beam vapor deposition technique. Following application, the coated surface was glass bead peened and subjected to a 4 hour thermal treatment at 1079°C (1975°F).

### B. TEST PROCEDURES

Where applicable, mechanical tests were conducted according to appropriate ASTM procedures and specifications. All elevated temperature tests were performed in air using resistance heated furnaces controlled to within ±1.7°C (3°F), except for the Phase IV transverse low cycle fatigue tests, where temperature was controlled to ±2.8°C (5°F) by induction heating.

The various specimen geometries used for evaluation of mechanical properties are shown in Figures 11 through 18. Tensile and creep properties were generally measured using the specimen shown in Figure 11, which incorporates a pair of dimples on each shoulder for attachment of a high temperature extensometer. Displacements between these dimples were measured with a LVDT (linear variable differential transformer) having a guaranteed resolution of ±2.5μm (100μ inch),which provided an overall accuracy of ±0.01 percent strain with the 2.5 cm (1 inch) reduced section. Measurement of fracture strain using this method is discussed in Appendix B. Unless otherwise noted, elevated temperature tension tests were conducted with a crosshead extension rate of 125 μm (0.005 inch) per minute. For creep testing of thin [0.32 cm, (0.125 inch)] slab castings evaluated in Phase III, a sheet type specimen (Figure 12) was used. No extensometry was employed with this specimen.

Notch sensitivity was evaluated using a specimen having a machined notch ($K_t$ = 3.2) together with a smooth section with a reduced diameter equal to that of the net section at the notch root (Figure 13). Smooth section failure of this specimen was interpreted as an absence of notch sensitivity. Failure at the notch with reduced properties as compared to typical smooth section values indicated that the material was notch sensitive, while notch failure with properties typical of smooth section test results indicated that the material was essentially notch neutral.

Shear tests were conducted using the specimen and test method developed by Iosipescu[7] which is illustrated in Figure 14. This test method was selected in preference to the more commonly used double-offset notched tension or bolt-head shear test methods because it provides a highly uniform distribution of pure shear stress which is insensitive to machining tolerances. For sustained load (creep) tests, extensometer arms were attached to the test fixture so that shear offset could be measured as a function of time at load. While shear strain values could not be calculated from these offset measurements because of the infinitesimally small "gage section" of the notched specimen, the strain-time records provided at least a qualitative indication of creep curve shape with sustained shear loading.

Thermal fatigue properties were evaluated by fluidized bed testing of the wedge-type specimen shown in Figure 15. The geometry of the casting produced in the modified Bridgman furnace to obtain this specimen is shown in Figure 16. This specimen was alternately immersed in hot (1038°C/1900°F) and cold (room temperature) fluidized beds at intervals of one minute. Testing was interrupted periodically for zyglo inspection, with the number of cycles to crack sizes of 0.4, 0.8, and 1.6 mm (0.016, 0.031 and 0.063 inch) being recorded.

Impact tests were conducted on the specimen shown in Figure 17. Specimen orientation was defined in terms of the orientation of the principle tensile stress developed at the root of the notch. Thus a longitudinal test was defined as being impacted perpendicular to the freezing direction, while a transverse test was impacted parallel to the freezing direction. The test machine was instrumented to record force versus tup penetration as well as total energy required to fracture the specimen.

Low cycle fatigue properties were measured using the tubular specimen shown in Figure 18. Strain controlled isothermal low cycle fatigue tests were conducted at a frequency of 0.08 Hz

(5 cycles/minute) on specimens having the previously discussed PWA 270 overlay coating on the outside diameter and a low aluminum ($\approx$ 12 percent) diffusion aluminide coating on the inside diameter. Axial strain was controlled using an LVDT extensometer which was located on the specimen ends and was calibrated by optical measurement of fiduciary marks on the specimen surface. Loads were recorded from a load cell included in the load train.

## IV. PHASE I – BASELINE ALLOY CHARACTERIZATION

The objective of this phase of the program was to characterize selected mechanical properties of the cellular Ni-20%Cb-2.5%Al-6%Cr baseline alloy developed by Lemkey[2]. Specific properties studied included long time creep stability, elevated temperature shear strength, transverse strength, and notch sensitivity. Details of the test program are discussed below.

### A. TEST PROGRAM

Tests conducted on this phase of the program are summarized in Table I. Long time stability was evaluated by comparison of long time (>1000 hours) creep test results with previously available data generated from shorter time (<300 hours) tests. Twelve creep tests were conducted using the specimen shown in Figure 11, six to rupture and six to one percent creep strain, with four of the six one percent creep specimens being retested to rupture at higher stresses. Tests were conducted at 871 and 1038°C (1600 and 1900°F) with stresses being chosen to provide lives in excess of 1000 hours using a Larson-Miller curve representing results of previously conducted short time tests.

Shear strength was evaluated in short time and sustained load (tensile and creep) tests using the method illustrated in Figure 14 with the shear stress acting parallel to the growth direction of the aligned structure. Ultimate shear strength was measured at 704, 871, and 1038°C (1300, 1600, and 1900°F). Shear creep tests were conducted at 704 and 871°C (1300 and 1600°F). To provide comparative data for evaluation of the relative performance of the eutectic alloy in shear, duplicate tests were also conducted on a conventionally cast nickel base superalloy (B-1900).

To evaluate the performance of the aligned microstructure in off-axis loading, tensile and creep tests were conducted on the specimen shown in Figure 11 at 704 and 1038°C (1300 and 1900°F) with the tensile axis oriented at 90 degrees to the growth direction.

Notch sensitivity was evaluated in tension and creep at 760 and 1038°C (1400 and 1900°F) using the combination smooth/notch specimen shown in Figure 13 with the tensile axis oriented parallel to the growth direction.

Material for the creep stability and notch sensitivity tests was produced in bar form at a rate of 3 cm (1.2 inches) per hour using the water quench Bridgman apparatus shown in Figure 9. Shear and transverse specimens were obtained from slab castings produced at 1.3 cm (0.5 inches) per hour in the modified Bridgman furnace (Figure 10). Representative microstructures found in each of these types of castings are shown in Figure 19.

### B. LONG TIME STABILITY

#### 1. Discussion of Test Results

Creep data obtained from long time creep tests are plotted in Figure 20. One percent creep and rupture life results are summarized in Table II together with specific test conditions for

each specimen. These results indicate excellent long time creep stability, as shown by comparison with previously generated short time test data (Figures 21 and 22).

Results of rupture tests performed on specimens with one percent prior creep are presented in Table III. Rupture life fractions shown in this table represent the ratio of accumulated test time to predicted rupture life (calculated from the Larson-Miller curve, Figure 22) at each of the stress and temperature combinations applied to the specimen. Summation of these life fractions provides an average of about ¾ at 1038°C (1900°F), and approximately unity at 871°C (1600°F). Examination of prior creep curves for the four upload tests (Figure 20) shows that both of the 1038°C (1900°F) specimens were undergoing tertiary creep when uploaded, whereas both 871°C (1600°F) specimens were in steady state creep at the time of upload. These observations indicate that uploading of this material in third-stage creep at 1038°C (1900°F) causes accelerated failure, and that the linear damage rule does not apply under these conditions, whereas uploading in second-stage at 871°C (1600°F) provides results which are consistent with the concept of linear damage.

As discussed in a subsequent section of this report, metallographic examination revealed an incipient neck in the 1038°C (1900°F) 94 MPa (13.6 ksi) nominal stress test which was removed from test at one percent extension (specimen A74-573-02). The presence of this neck is consistent with the above observation that all three specimens tested at these conditions were in third-stage creep at one percent prior strain. Because of this observation, the first of the two 1038°C (1900°F) upload specimens which reached one percent strain (specimen A74-685-02) was unloaded and cooled to room temperature for remeasurement of specimen diameter prior to uploading. While a slight neck may have been present in this specimen, no measurable localized reduction of diameter could be found, and the specimen was therefore reheated and loaded to the higher stress level using the original cross sectional area reduced by one percent for stress calculation. This procedure is conservative in that it results in the application of a higher load than would be calculated on the basis of a locally reduced (necked) cross sectional area. Based on the failure to detect a neck in specimen A74-685-02, the one percent diameter reduction was also used for calculation of the higher stress level for specimen A74-685-01, as well as for the two specimens uploaded at 871°C (1600°F), which were in steady state creep at the time of uploading, as noted previously. To maintain a consistent procedure, the latter three specimens were unloaded prior to application of the higher load.

Because some concern was felt regarding the possible influence of stress relief during unloading on properties measured at higher stress levels after reloading, creep rates observed prior to and after uploading were compared. Inspection of the creep curves for the four uploaded tests (Figure 23) shows very small amounts (<0.03 percent) of "primary" creep strain after reloading at the higher stress levels, indicating that recovery during unloading did not significantly influence subsequent creep behavior at either test temperature.

## 2. Metallographic Evaluation of Tested Creep Specimens

Metallographic examination of specimens tested in the long time creep stability program indicates that the aligned microstructure produced by directional solidification of the 6% Cr

$\gamma/\gamma'$ - $\delta$ eutectic alloy is completely stable with respect to spheroidization or coarsening of the $\delta$ phase reinforcing platelets. Certain microstructural changes were observed as a result of the creep exposure but none of these changes degrade long time creep properties, as indicated by the test results (Figures 21 and 22). The changes observed include ripening of the $\gamma'$ phase, precipitation of $\delta$ phase platelets in a Widmanstatten morphology in the $\gamma/\gamma'$ phase, and precipitation of a second phase which has been tentatively identified as $\gamma/\gamma'$ [8, 9] in the $\delta$ platelets. As shown in Figures 24 and 25, $\gamma'$ ripening in the matrix was found only in specimens tested at 1038°C (1900°F), while Widmanstatten $\delta$ precipitation was most prominent at 871°C (1600°F). Neither of the changes which occur in the matrix phase ($\gamma'$ ripening and Widmanstatten $\delta$ precipitation) appear to be stress dependent, being found about equally in stressed and unstressed areas. Precipitation of the Widmanstatten $\delta$ phase appears to occur preferentially in cellular regions, but is also found in eutectic $\gamma/\gamma'$ lamellae. Precipitation of $\gamma/\gamma'$ in the $\delta$ phase appears to be strain dependent, being found only in secondary necks and in areas immediately adjacent to the fracture, suggesting a strain induced precipitation phenomenon. This observation is consistent with results presented by Breinan[9], who found a similar precipitate which was concentrated near the fracture in $\delta$ reinforced creep specimens of various compositions, and which appeared to nucleate on slip planes in untwinned regions of the $\delta$ phase. The precipitation found by Gray occurred in cyclic oxidation specimens where strain levels were undefined[8]. As mentioned above, comparison of the short and long time rupture results in Figure 22 demonstrate clearly that the occurrence of this precipitation within the $\delta$ phase does not influence the long time creep stability of $\gamma/\gamma'$ - $\delta$. This conclusion is supported by Gray's post-exposure creep results which were equivalent to results obtained on as-cast specimens at 1038°C (1900°F)[8].

Examination of longitudinal flats polished on the tested creep specimens shows a tendency for necking and failure in areas of the microstructure which are slightly more cellular than normal (Figures 26 through 28). This tendency for preferential deformation in cellular bands is more easily observed in unbroken specimens because gross localized plastic deformation tends to obscure microstructural detail near a fracture. Cellular microstructures observed in the necked areas of specimens removed from test at one percent extension are shown in Figures 26 and 27. The neck found in specimen A74-573-02 tested at 1038°C (1900°F) is extremely shallow, as indicated by the fact that it can be resolved only in the section which is polished just through the coating (Figure 26a) and not on the mid-radius section on which microstructural observations were made (Figure 26b). Multiple necks found in specimen A74-216-02 tested at 871°C (1600°F) were better developed and can be easily resolved on the $\approx$ ¼ radius section shown in Figure 27. The cellular microstructure observed in a secondary neck found in rupture specimen A74-698-02 tested at 871°C (1600°F) is shown in Figure 28.

The occurrence of cellular bands in the directionally solidified eutectic creep specimens is typical for material grown in the water-quench Bridgman apparatus which was used to produce the specimens tested in this program, and is presumed to result from transient thermal and/or mechanical perturbations of the steady state solidification conditions. The occurrence of necking and failure in these bands is typical of previously observed behavior of the directionally solidified 6% Cr $\gamma/\gamma'$-$\delta$ eutectic alloy[5] and indicates that improved processing methods which promote lamellarity may provide a creep strength advantage for the $\gamma/\gamma'$ - $\delta$ alloy which is even greater than that which is presently available with current processing technology.

Typical fracture profiles for the four sets of rupture conditions investigated in the long time stability program are shown in Figure 29. As mentioned above, the excessively cellular microstructure generally found in the area of failure tends to be obscured by localized plastic deformation at the fracture, particularly at 1038°C (1900°F) where localized deformation is most pronounced. Failure at the higher test temperature occurs by a combined tensile-shear mode, with substantial amounts of interlamellar shear parallel to the tensile axis (Figures 29c and 29d). Fracture at 871°C (1600°F) tends to involve less shear and interlamellar crack propagation, with relatively flat facets being observed across individual grains (Figures 29a and 29b).

The photomicrographs presented in Figure 29 also show the occurrence of void formation in some of the tested specimens. Voids found in specimens A74-698-02 and A74-685-02 tested respectively at 871 and 1038°C (1600 and 1900°F) are shown at higher magnification in Figure 30. The mechanism of void formation appears to involve rupture of $\delta$ lamellae followed by propagation of the $\delta$ phase crack into adjacent $\gamma$ lamellae. The occurrence and intensity of void formation did not correlate with applied test conditions, and, in fact, was not consistent among specimens tested at identical conditions. The explanation for this effect is not obvious.

During the course of post-test examination, it was noted that some of the long time creep specimens appeared to have suffered moderate to severe surface degradation, as shown in Figure 31. Metallographic evaluation indicated that no coating was present in these areas (Figure 32). A review of processing records revealed that the coating, and in some cases substrate stock, were removed during the glass bead peening operation which was performed prior to diffusion heat treatment of the coating. Coating removal was not noted prior to test initiation because the surface appearance of the bare substrate is virtually identical to the appearance of the PWA 270 coating after diffusion treatment. The creep performance noted in Figures 21 and 22 must be considered exceptional in view of the fact that a good number of the long time specimens represented were essentially uncoated.

Examination of long time creep specimens which were coated over the entire gage section shows good coating performance (Figure 33). The structure of the diffusion zone formed during exposure is somewhat different at the two test temperatures investigated. A relatively equiaxed grain structure is observed at 871°C (1600°F) (Figure 33b), while the diffusion zone formed at 1038°C (1900°F) has a more acicular structure (Figure 33a). The identity of the phase(s) contained in these diffusion zone structures is not presently known.

As shown in Figure 32a and 32c, an unidentified precipitate having a nonmetallic appearance was observed in uncoated areas of specimen A74-685-02. A similar precipitate was seen in uncoated areas of A74-685-01 but was not found in any of the other long time creep specimens. Similar precipitates have been noted after static high temperature exposure of carbon-containing $\gamma/\gamma'$-$\delta$ oxidation coupons[10], indicating that the precipitate is a carbide and that the casting from which the two precipitate-containing specimens was taken (casting A74-685) contained unintentional carbon additions. The previously discussed creep results obtained from these two specimens indicate that the presence of carbon does not significantly influence the high temperature load bearing capability of the 6%Cr $\gamma/\gamma'$-$\delta$ alloy.

## C. SHEAR STRENGTH EVALUATION

### 1. Ultimate Shear Strength Results

Results of shear strength tests on directionally solidified 6%Cr $\gamma/\gamma'$-$\delta$ and conventionally cast B-1900 alloy are compared in Table IV and Figure 34. These results indicate that the shear strength of the eutectic in the direction of structural alignment varies from 43 percent of the shear strength of B-1900 at 704°C (1300°F) to 55 percent at 1038°C (1900°F). This result was not unexpected in view of the highly directional nature of the directionally solidified eutectic structure. These results also show that the ultimate strength in pure shear is well in excess of the resolved shear stress for failure in conventional tension with the tensile axis oriented at 45 degrees to the growth direction, indicating that the tensile stress which acts normal to the shear direction in uniaxial tensile loading significantly influences fracture behavior.

One of the slabs cast for evaluation of shear properties contained a band of fully lamellar microstructure, which is compared with the more typical cellular microstructure in Figure 35. To compare the shear strength properties of the two microstructures, one of the eutectic shear specimens tested at each temperature was taken from the lamellar band, and the other was taken from the more typical cellular area. With the possible exception of the 1038°C (1900°F) data, the results presented in Table IV indicate no significant influence of structure on shear strength or ductility.

Metallographic examination of tested specimens indicates that deformation and fracture of both microstructures is predominantly intergranular at all three temperatures (Figures 36 through 39). This observation suggests that the strength difference noted at 1038°C (1900°F) probably results from random variability rather than from a systematic dependence of shear strength on structure.

### 2. Shear Creep Test Results

Results of shear creep tests conducted on B-1900 and directionally solidified 6%Cr $\gamma/\gamma'$-$\delta$ alloys at 704 and 871°C (1300 and 1600°F) are presented in Table V. "Creep" shear offset versus time curves obtained from each test are shown in Figures 40 through 43. The test results are summarized on a Larson-Miller plot in Figure 44, where the Iosipescu creep shear data are compared with the resolved shear stress for failure in conventional creep testing of

B-1900 alloy and of 6%Cr $\gamma/\gamma'$-$\delta$ alloy with the tensile axis oriented at 45 degrees to the growth direction. As with the ultimate shear strength results, this comparison shows that the rupture life in pure shear is well in excess of the life in conventional rupture with an equivalent resolved shear stress, indicating that the tensile stress which exists normal to the shear direction in the conventional test significantly influences the shear fracture of both test materials. Comparison of these results on the basis of applied shear stress for rupture in 100 hours at various temperatures (Figure 45) indicates the same trend.

Metallographic examination of broken creep shear test specimens indicates a failure mode comparable to that observed in the ultimate shear strength specimens; i.e., failure almost exclusively occurs at grain boundary and/or cell wall areas of the microstructure. A typical example of this failure mode observed at 871°C (1600°F) is shown in Figure 46.

## D. TRANSVERSE STRENGTH EVALUATION

### 1. Tensile Test Results

Results of transverse tension tests show the marked anisotropy of the highly directional eutectic structure (Figure 47). At high temperatures (1038°C/1900°F), transverse ductility is adequate (Table VI). At intermediate temperatures, the transverse ductility is very low; fracture strains measured as described in Appendix B are less than 0.25 percent at 704°C (1300°F) (Figure 48). Improvement of this property was one of the prime objectives of the alloy modification studies conducted in the third phase of this contract, as discussed in Section VI.

Examination of the transverse specimens tested at 704°C (1300°F) indicates that failure occurred near the center of the gage section with little evidence of prior plastic deformation, while the specimens tested at 1038°C (1900°F) exhibit evidence of significant plastic deformation with fracture occurring near the end of the gage section in both cases (Figure 49).

Metallographic examination of the 704°C (1300°F) failure indicates significant intergranular fracture (Figure 50) with little evidence of plastic deformation in the microstructure. There is occasional evidence of limited transgranular fracture in cases where an intergranular fracture path was not favorably oriented for propagation of the advancing crack. Of the numerous secondary cracks visible in Figure 50, all but one are intergranular, with a marked tendency for the intergranular separation to occur at loeations where grains composed of lamellae oriented approximately perpendicular to the tensile axis intersect grains composed of lamellae oriented approximately parallel to the tensile axis. One such crack shows evidence of crack arrest when propagation proceeds from an intergranular nucleation site into an adjacent grain which is oriented to favor interlamellar propagation. No evidence of secondary cracking is found in areas removed from the fracture surface of the 704°C (1300°F) specimens.

Fracture at 1038°C (1900°F) appears to occur by a combination of intergranular cavitation and shear along those grain boundaries which are oriented at 45 degrees to the tensile axis, with significant amounts of plastic deformation apparent (Figure 51). Evidence of intergranular cavitation is found throughout the gage section of both 1038°C (1900°F) specimens (Figure 52).

### 2. Transverse Creep Results

Results of transverse creep tests conducted at 704 and 1038°C (1300 and 1900°F) are presented in Figures 53 and 54 and in Table VII. These results are compared with longitudinal properties in Figure 55. While this comparison involves material produced at different rates of growth, the highly anisotropic nature of the directionally solidified eutectic is evident. Comparison of transverse creep elongations (Table VII and Figures 53 and 54) with elongations measured in tensile failure (Table VI) indicates that transverse rupture ductility is significantly greater than transverse tensile fracture strain.

Metallographic examination of broken transverse creep specimens shows failure mechanisms very similar to those observed in transverse tensile fractures. At 1038°C (1900°F), failure occurs primarily by a shear deformation mode, while at 704°C (1300°F) the fracture is relatively flat and perpendicular to the tensile axis (Figure 56). Specimens tested at 1038°C (1900°F) show substantial reduction of area and significant plastic deformation throughout the gage section. Reduction of area and plastic deformation in areas of the gage section remote from the fracture are minimal at 704°C (1300°F). Failure at 1038°C (1900°F) occurs by a process of intergranular shear (Figure 57a), while fracture at the lower test temperature occurs primarily by tensile separation across grain boundary and/or cell wall areas (Figure 57b).

## E. EVALUATION OF NOTCH SENSITIVITY

### 1. Combination Smooth-Notch Tension Test Results

Results of combination smooth-notch tensile tests (Table VIII) indicate that the baseline eutectic alloy is notch insensitive at 1038°C (1900°F) and is notch neutral at 760°C (1400°F) Yield and ultimate strength values in these tests, including the low temperature notch failure results, are consistent with previous smooth specimen data (Figure 47), as are ductility values for the smooth section failures.

Examination of the 760°C (1400°F) fractures (Figure 58) shows the smooth section failure to be relatively flat and faceted while the notched fracture surface is distinctly fissured by grain boundary and cell wall separation. This longitudinal secondary cracking associated with the notched failure is attributed to the triaxial state of stress in the vicinity of the notch root. Examination of the longitudinal microstructure in the notched zone of both 760°C (1400°F) specimens (Figure 59) confirms the presence of the longitudinal secondary cracks in the notch failure, and indicates similar longitudinal secondary cracking near the notch root in the specimen which failed in the smooth section. Figure 60 shows the longitudinal cracks to be intergranular in both specimens, with some tendency for cracking at the interface between the $\delta$ dendrites and the eutectic and for cracking of the $\delta$ dendrites themselves.

Examination of the microstructure in the vicinity of the 760°C (1400°F) smooth section fracture surface (Figure 61) shows fracture of the individual grains to be relatively smooth, with distinct differences between the angle of fracture across adjacent grains.

The fracture appearance at 1038°C (1900°F) (Figure 62) is distinctly different from that observed for the smooth section fracture at 760°C (1400°F), with the fracture profile across individual grains being highly irregular. A significant amount of intergranular separation is also observed, as well as some tendency for void nucleation in areas adjacent to the fracture surface. Examination of the structure in the notch zone of the two specimens broken at 1038°C (1900°F) indicates minimal microstructural damage in the vicinity of the notch root (Figure 63).

### 2. Combination Smooth-Notch Stress Rupture Test Results

Results of duplicate stress-rupture tests conducted on combination smooth-notch specimens at 760°C (1400°F) and 758 Mpa (110 ksi) (Table IX) indicate that the 6%Cr $\gamma/\gamma'$-$\delta$ eutectic alloy is notch sensitive under the test conditions employed. With a few exceptions, stress-rupture tests on smooth specimens at these conditions would be expected to run over 100 hours to rupture (Figure 22) as compared to the approximately 25 hour life observed for the notched failures. This result was not unexpected in view of the fact that other high strength materials are known to be notch sensitive under selected conditions of temperature, strain rate, and stress state [11].

Longitudinal and transverse sections through the fracture zone of these samples are shown in Figure 64. In both specimens, the longitudinal profile shows a typically transgranular fracture mode, while the transverse section indicates a tendency for grain boundary separation under the multiaxial stress state in the vicinity of the notch.

Results of the 1038°C (1900°F) tests (Table IX) indicate the material to be notch neutral in creep at this temperature, with one specimen breaking in the gage section and the other breaking at the notch but at a life essentially equivalent to average smooth section properties. The smooth section fracture is typical of 1038°C (1900°F) creep failures (Figure 65a), involving ductile tearing with significant plastic deformation and some void formation near the fracture surface. Void formation is also observed near the notch fracture (Figure 65b), but with less evidence of localized plastic deformation. As shown in Figure 66a, the triaxial stress state at the notch root caused secondary cracking at grain boundary and/or cell wall areas parallel to the stress axis. Carbide contamination is also observed in this specimen (Figure 66b), but no direct evidence can be found to indicate that the presence of carbides contributed to notch rather than smooth section failure.

## F. PHASE I SUMMARY

Excellent creep stability is demonstrated by results of long time ($>$ 1,000 hours) creep tests, which agree with predictions made from a Larson-Miller curve based on shorter ($<$ 300 hours) tests. Microstructural evaluation shows no degradation of the eutectic microstructure in specimens tested as long as 2100 hours at 1038°C (1900°F). As with certain other nickel-base superalloys, the eutectic is notch sensitive in creep at 760°C (1400°F). Notch sensitive behavior is not found in tension at this temperature, or in either tension or creep at 1038°C (1900°F).

Results of transverse and shear tests on the cellular baseline alloy indicate two properties of particular concern for turbine blade applications. The first is intermediate temperature (704 to 760°C/1300-1400°F) transverse ductility. Respective 704°C (1300°F) average transverse tensile and rupture ductilities of 0.2 and 0.5% were measured on coated cellular specimens. The second concern is shear strength, which is about half that of B-1900, a conventionally-cast nickel-base superalloy. Failure evaluation confirmed that off-axis fracture of the cellular structure occurs primarily at cellular grain boundaries.

## V – PHASE II – MICROSTRUCTURE AND CHROMIUM VARIATION STUDIES

This phase was undertaken to improve the understanding of both process-structure and structure-property relationships in directionally solidified $\gamma/\gamma'$-$\delta$ alloys containing various levels of chromium. Process-structure relationships were characterized in the first part of this phase by measuring the influence of thermal gradient, solidification rate, and chromium content on interlamellar spacing, volume fraction of fully lamellar microstructure and volume fraction of the $Ni_3Cb$ reinforcing phase. Results of these experiments were used to define process conditions for the second part, where the influence of chromium level and microstructure on both longitudinal and off-axis mechanical behavior was investigated.

### A. PHASE II, PART A – SOLIDIFICATION STUDIES

As discussed in Section II, Lemkey characterized the solidification rate lamellar spacing relationship and determined the critical G/R (G/R*) for plane front solidification of the chromium free $\gamma/\gamma'$-$\delta$ eutectic [2,4]. The purpose of this study was to determine the influence of chromium on these processing characteristics and on the volume fraction of the $Ni_3Cb$ reinforcing phase. The experimental plan involved directional solidification of $\gamma/\gamma'$-$\delta$ eutectic alloys containing four chromium levels (0, 1, 3, and 6 weight percent) at a variety of growth rates in two Bridgman furnaces with significantly different gradients. The first of these furnaces was the high gradient water-quench apparatus described in Section III (Figure 9). This furnace was used to investigate solidification behavior at high values of G/R. For studies at low G/R levels, a resistance heated low gradient furnace (Figure 67) was used to avoid the need to solidify at very high rates, where steady state heat transfer conditions are not assured, to achieve low G/R growth conditions.

#### 1. Gradient Measurements

To determine values of critical G/R, it first was necessary to measure the thermal gradient for each furnace. For purposes of economy in experimental effort, it was desired to solidify at multiple rates in each of the G/R determination runs. Therefore, it was necessary to document gradient as a function of both growth rate and vertical position in the ingot in each furnace. The basic experimental configuration for gradient determination was identical for both furnaces, and consisted of a thermocouple located within a 2mm ID X 4mm OD X 76 cm long (0.08 X 0.160 X 30 inch) protection tube placed in the center of a 1.3 cm (0.5 inch) crucible containing a 6%Cr $\gamma/\gamma'$-$\delta$ melt (Figure 68). The tube was sealed at the top with a flexible cement to provide an inert atmosphere for protection of the thermocouple wire. The use of a flexible seal allowed the thermocouple to be repositioned upward at any desired interval during the solidification experiment to measure the gradient at various locations and/or growth rates in the same melt.

Preliminary experiments were performed with Pt-6% Rh/Pt-30% Rh thermocouples; however, because of the high melt temperatures used to maximize gradient, difficulty was encountered with incipient melting of the thermocouple wires. Subsequent experiments were therefore

performed with W/W -26% Re thermocouples, which proved highly satisfactory. The only difficulty encountered with the temperature measurements involved electronic interference from the RF coil on the high gradient apparatus. To avoid this problem, a procedure was adopted involving momentary RF power interruptions, which allowed the true thermocouple output to be measured at periodic intervals on a rapid response recording instrument.

Results of the gradient determinations are presented in Figures 69 and 70 in the form of temperature versus distance plots. Measurements of thermal gradient (defined as the slope of the temperature versus distance curve in the liquid at the 6%Cr $\gamma/\gamma'$-$\delta$ solidus temperature) were made from expanded plots of the data presented for each determination. Results of these measurements are noted on each curve in Figures 69 and 70 and are summarized in Table X. Some variability is noted in these measurements, particularly in the high gradient furnace. Because of this variability, it was difficult to evaluate possible systematic variations of G with either rate or location. To separate the two effects, the influence of solidification rate on gradient was evaluated by plotting the ratio of the gradient measured at higher rates to the gradient measured at the same location in the ingot at the lowest rate studied in each furnace. Values of this ratio are plotted as a function of solidification rate in Figure 71. These results indicate no significant influence of solidification rate on thermal gradient within the range of rates investigated in each furnace.

Based on the conclusion that rate did not influence gradient, all of the determinations made at a given location in each furnace were averaged for evaluation of possible location effects. These averages, noted in Table X, indicate that there may be a small, systematic influence of location on gradient; however, because of the variability observed at each location, it was felt that a reliable characterization of this trend could not be made from the available data. Therefore, it was elected to specify a single value of gradient for each furnace, to be used for calculation of G/R values at all ingot locations. As noted in Table X, these values are 68 and 360°C/cm for the low and high gradient furnaces, respectively.

### 2. Critical G/R Determinations

Compositions and processing conditions investigated for determination of G/R* as a function of chromium content are summarized in Figure 72. Most of these castings were solidified at multiple rates to allow investigation of more than one G/R value in each bar. Longitudinal flats ground on each of these bars were examined to select areas of microstructure which were typical of each solidification condition. Each bar was then sectioned at these locations (noted in Figure 72) for evaluation of transverse microstructure. Photomicrographs obtained at these locations are presented in Figures 73 through 76.

Critical G/R for the 1, 3 and 6 percent chromium alloys was determined from quantitative point count measurements of volume fraction of lamellar structure (see Appendix C) produced by each of the processing combinations investigated (Table XI). Results of these measurements were plotted as a function of G/R to determine G/R* for each chromium level, as shown in Figure 77.

To correlate these results with Lemkey's determination, ingots of the chromium free alloy were included in the current study. Examination of the chromium free microstructures pre-

sented in Figure 73 indicates that none of the chromium free alloys produced was of exactly the eutectic composition. Recognizing the hypoeutectic nature of some of the structures shown in Figure 73, it is apparent that G/R* was not exceeded, and therefore was not defined in any of the runs made in this series of experiments. Since the data obtained in this study are not in conflict with the previously reported chromium free $\gamma/\gamma'$-$\delta$ G/R* value of $< 5C^{\circ}$ hr/cm$^2$[4], this value has been used for correlation with G/R* values obtained from the 1, 3 and 6 percent Cr alloys (Figure 78).

To rationalize the influence of chromium on critical G/R, published values of liquidus and solidus temperatures in the Ni-Cb-Al-Cr system[12] are correlated with G/R* in Figure 79. This correlation is consistent with the criterion for plane front solidification suggested by Cline and Walter[13]:

$$G/R \geqslant \frac{\Delta T}{D}$$

where $\Delta$ T is the liquidus-solidus temperature range and D is the diffusion coefficient in the liquid phase. Calculation of the slope of the relatiohship shown in Figure 79 indicates a diffusion coefficient on the order of $2 \times 10^{-5}$ cm$^2$/sec, which is of the correct order for diffusion in the liquid.

### 3. Microstructural Characterizations

Ingots produced for the G/R* determinations were studied together with material obtained from other sources[5] to evaluate the influence of chromium level and processing conditions on various microstructural characteristics of the DS $\gamma/\gamma'$-$\delta$ alloy. These studies included measurements of the volume fraction lamellar structure ($V_\ell$), interlamellar spacing ($\lambda$), and volume fraction of the $Ni_3Cb$ reinforcing phase ($V_\delta$). Volume fraction measurements were made by the method of point counting, while interlamellar spacings were measured directly on photomicrographs of known magnification. Procedures and detailed results are included in Appendix C. Significant findings are discussed below.

#### a. Interlamellar Spacing

Results of interlamellar spacing measurements (Table XII) show a systematic influence of chromium level on lamellar spacing. At a solidification rate of 3 cm/hr, for example, the data indicate that $\lambda$ varies from 5.2$\mu$m in the chromium free alloy to 3.3$\mu$m in the 6 percent Cr alloy.

As noted earlier, Lemkey's study of the chromium free alloy indicated that the dependence of lamellar spacing on solidification rate obeys a relationship of the form $\lambda^2 R = C$[2]. To determine the applicability of this relationship to the chromium-containing alloys, the lamellar spacing measurements noted in Table XII were plotted against $R^{-1/2}$ for each chromium level investigated (Figure 80). Results of regression analysis on these data (Table XIII) show that the 95 percent confidence intervals on the regression intercept overlap the origin for the 0, 1 and 3 percent chromium data, which means that there is no reason to reject the hypothesis that the above relationship holds for these alloys, independent of processing and structure.

Confidence intervals on the 6 percent Cr regression intercept indicate that the 6Cr results do not obey the $\lambda^2 R = C$ relationship at either the 95 or the 99 percent confidence level. However, if these data are separated into high and low gradient groups, the regression results show no reason to reject the accepted relationship for each data group. It is not possible to determine from the available data whether there is a real influence of gradient on lamellar spacing at the 6 percent chromium level, or whether the normally observed $\lambda^2 R = C$ relationship is, in fact, not obeyed by the 6 percent chromium alloy.

To summarize the results of the lamellar spacing measurements, a combined plot was prepared which includes data at all four chromium levels (Figure 81). Because the hypothesis that a $\lambda^2 R = C$ relationship exists between $\lambda$ and R could not be rejected on a statistical basis for the 0, 1 and 3 percent Cr alloys, a constrained regression line was forced through the origin to represent the results for each of these three alloys in Figure 81. Because the grossly cellular microstructure observed in the low gradient 6% Cr alloys is not directly relevant to the microstructure anticipated in application of this material, only the high gradient 6% Cr results were included in Figure 81, with a constrained regression line being used to represent the assumed functional relationship.

To rationalize the observed variation of lamellar spacing with chromium content, an effort was made to correlate the lamellar spacing constant C (square of the slope of the $\lambda$ versus $R^{-1/2}$ curve, Table XII) with alloy composition. Presuming that the variation of C results from diffusion rate variations in the liquid, factors which might affect diffusion rate were examined. Assuming further that the relatively small compositional variations studied were unlikely to substantially influence the diffusion coefficient, it was postulated that differences in the rate of diffusion between alloys must result from differences in the composition gradients between the bulk liquid and the $\gamma$ and $\delta$ phases. As shown in Table XIV, the average atomic percentage of nickel present in the liquid is relatively close to the percentage present in the $Ni_3Cb$ phase for all four alloys studied, while the percentage of columbium present in the liquid is just slightly over half of the amount present in $Ni_3Cb$. This observation leads to the hypothesis that columbium diffusion is probably a rate controlling factor in determination of lamellar spacing. A plot of the lamellar spacing constant as a function of the difference between the atomic percentage of columbium in the liquid and in the $Ni_3Cb$ phase ($\Delta Cb$) (Figure 82) shows a linear dependence of C on $\Delta Cb$, which supports the hypothesis that diffusion of Cb through the liquid is the rate determining step in the mass transport kinetics which control lamellar spacing, and suggests that the variation of lamellar spacing with chromium level results from the influence of chromium on the eutectic composition, and not from a direct influence of chromium on the solidification process.

### b. Volume Fraction $Ni_3Cb$ Phase

Measurements of the volume fraction of lamellar $Ni_3Cb$ present in plane front microstructures are summarized in Table XV. Results for the 0, 1 and 6 percent chromium alloys were obtained on fully lamellar, dendrite free microstructures produced at or near G/R* in the present study. Because the 3 percent Cr bars produced in the present study were $\delta$ dendritic, fully lamellar dendrite free material produced in a previous study[5] was used for the 3 percent Cr $V_\delta$ measurements. The $V_\delta$ value reported for 2 percent chromium

was obtained on previously grown fully lamellar, δ dendritic (2.2 volume percent) material, and therefore must be interpreted with some caution.

A plot of $V_\delta$ versus chromium content (Figure 83) indicates a systematic and apparently linear increase in volume fraction of $Ni_3Cb$ from about 34 percent in the chromium free alloy to about 40 percent in the 6 percent chromium alloy. These results correlate well with the volume fraction $Ni_3Cb$ value of 42.5 percent reported by Lemkey for a 9 percent chromium, 1 percent Al alloy[14] and are presumed to be responsible, at least in part, for the reported improvement of creep strength in the 6 percent Cr alloy as compared to the chromium free alloy tested with comparable lamellar spacing[12].

### c. Eutectic Grain Size

Another microstructural property which appears to vary with composition and processing condition is the size and shape of the eutectic "grains". From the photomicrographs presented in Figure 73 through 76, it would appear that bars processed in the high gradient furnace have a substantially finer grain size than material produced at the lower gradient. Grain shape appears to vary with G/R in the same way as the percentage of lamellar structure. In fully lamellar structures, the grains are approximately equiaxed, whereas in the partially cellular structures the "grains" (lamellar areas) are much longer parallel to the lamellae than across the lamellae. The influence of these variations in grain size and shape on mechanical behavior is discussed in a following section.

## B. PHASE II, PART B – MECHANICAL BEHAVIOR

The objective of this part of Phase II was to investigate the influence of microstructure and chromium level on mechanical behavior. Based on results obtained in Phase I, emphasis was placed on evaluation of longitudinal creep strength and intermediate temperature (704 to 760° C/1300 to 1400°F) transverse tensile ductility, with longitudinal tensile strength, transverse creep, and fluidized bed thermal fatigue behavior also being characterized.

### 1. Creep Strength

Metallographic examination of longitudinal creep specimens tested in Phase I indicated that creep deformation occurs preferentially in areas of increased cellularity (cellular bands), suggesting that creep strength may be related to lamellarity of the microstructure. One purpose of this study was to systematically investigate the relationship between creep strength and lamellarity. It was reported by Lemkey that creep strength is increased by refinement of lamellar spacing[2]; a systematic investigation of this effect was also desired. Lemkey also reported that chromium improved creep strength; however, his comparison was not made on materials of identical microstructure. A third objective of the present study was to determine the influence of chromium on the creep strength of materials having identical microstructures.

a. Test Program

Based on results of the previously discussed solidification studies, three closely related test programs were designed to meet the three objectives noted above. The first of these (Table XVI) was designed to investigate the influence of interlamellar spacing and degree of lamellarity on creep strength. Two chromium levels (1 and 6 percent) were included to investigate possible interactions between chromium level and microstructural effects. Because of critical G/R limitations, lamellar spacing effects could be studied only in cellular microstructures in this set of tests. A second set of tests (Table XVII) was therefore designed to evaluate lamellar spacing effects in the fully lamellar chromium free alloy, which has a low critical G/R and can be solidified plane front over a wide range of rates. Based on results of the first set of tests, which indicated that the fully lamellar microstructure provided the best creep properties at both chromium levels studied, a third set of tests was conducted to measure creep strength on a fully lamellar 3 percent chromium alloy solidified at a rate which produced a lamellar spacing equivalent to that of the fully lamellar specimens evaluated in the first set of tests. Results of these tests, together with results from the chromium free specimens produced at 6 cm/hr, provided the desired information concerning the effect of chromium on the creep strength of materials with equivalent microstructures (i.e., fully lamellar structure with equivalent lamellar spacing).

**b. Processing Details**

Most of the material for the three sets of longitudinal creep tests was produced in the form of bars in the high-gradient Bridgman furnace (Figure 9). To develop the lower gradients required to produce the 4 $\mu$m spacing cellular structures investigated in the first set of tests (Table XVI), various geometries were directionally solidified in the modified Bridgman furnace (Figure 10). The 120°C/cm gradient was achieved with a cluster mold containing four 1.3 cm (0.5 inch) diameter bars. The 160°C/cm gradient was obtained with a single 1 cm (0.38 inch) diameter bar mold processed on the centerline of the modified Bridgman furnace.

Initial efforts to produce the fully lamellar 6 percent chromium test material required for the first set of tests were not successful because of the occurrence of cellular bands in otherwise lamellar castings. Because cellular bands have been shown to have an unfavorable influence on creep behavior, the presence of these bands was considered unacceptable. Their occurrence was eliminated through the use of modified processing methods which are discussed below.

The occurrence of cellular bands in an otherwise fully lamellar microstructure produced under nominal G/R conditions above the critical value was attributed to transient thermal and/or mechanical perturbations of the steady state growth conditions which appear to be an intrinsic feature of the water-quench Bridgman process. These perturbations are assumed to cause a transient reduction in the instantaneous value of G/R at the solid-liquid interface. The approach used to eliminate cellular bands involved modifications which increased the steady state gradient in the Bridgman furnace so that the temporarily reduced G/R experienced during normal perturbations remained above G/R*. Two changes were made to accomplish this objective. First, to increase the perimeter-to-area ratio of the casting cross-section, which

is known to promote higher gradients[15], the casting diameter was reduced from the normally used 1.3 cm (0.5 inch) to 1 cm (0.38 inch). Second, the superheat in the liquid portion of the ingot was increased about 50°C (90°F). While the first process change had no disadvantages for this program, where the maximum diameter of the desired test specimen was 0.64 cm (0.25 inch), increasing the superheat had the disadvantage of increasing the tendency for mold-metal reactions, which tend to contaminate the test material with nonmetallic inclusions, particularly near the top of the ingot where the longest exposure occurs. This problem was particularly severe with the 6 percent Cr alloy grown at 2 cm/hr because of the long exposure time associated with the low growth rate. For this reason, test material could be obtained only from the lower half of the fully lamellar 2 cm/hr 6 percent Cr castings.

### c. Lamellarity, Lamellar Spacing and Chromium Effects

Results of creep tests conducted in this evaluation are presented in Tables XVIII and XIX. The effects of chromium level, lamellarity, and lamellar spacing in cellular structures on creep strength are summarized together with typical microstructures in Figure 84. In addition to differences in lamellar spacing and amount of cellular structure, these photomicrographs also show significant differences in grain size among the various compositions and solidification conditions investigated. Since all grain boundaries are essentially parallel to the stress axis in the aligned eutectic structure, these test results have been interpreted assuming that grain size has no influence on creep strength. The validity of this assumption will be examined more carefully in a later section.

Several important conclusions may be drawn from evaluation of the results summarized in Figure 84. First, the fully lamellar microstructure provides creep strengths which are superior to the creep strengths of cellular microstructures with comparable lamellar spacing at all chromium levels where this effect was investigated. Second, refinement of the lamellar spacing improves the creep strengths of cellular structures, but not sufficiently to match the strengths of fully lamellar material. This second conclusion is important because it indicates that the strengthening produced by lamellar spacing refinement does not fully counterbalance the weakening caused by increased cellularity at high solidification rates, so that the maximum creep strength potential of the $\gamma/\gamma'$-$\delta$ eutectic cannot be realized at solidification rates above the critical value for plane front solidification.

A third important conclusion obtained from examination of these results concerns the influence of chromium on creep strength. Comparison of 1038°C (1900°F) rupture life results from fully lamellar 0, 1, 3, and 6 percent Cr specimens produced with equivalent lamellar spacing shows a continuous but nonuniform increase of life with chromium content (Figure 85). To rationalize this observation, the established Larson-Miller curve for the 6 percent Cr alloy (Figure 22) was used to convert these results to stress for 100 hour rupture life, which is plotted versus atomic percent chromium in Figure 86. This plot shows a more uniform increase of creep strength (as opposed to rupture life) with chromium addition, but continues to indicate a disproportionate strength increase on going from the chromium free to the 1 percent chromium alloy.

The absence of a saturation effect in these data may indicate that more than solid solution hardening is involved with the creep strength increase provided by the addition of chromium to $\gamma/\gamma' - \delta$. Measurement of $\gamma'$ size as a function of Cr, Table XX, indicated that there was no significant refinement in $\gamma'$ size with increasing chromium content to account for the strength increase. Pederson[16] has suggested that composite creep strength should show an essentially linear increase with increasing volume fraction of the reinforcing phase in the range of 0.2 to 0.8, indicating that the effect of chromium on the creep strength of $\gamma/\gamma'-\delta$ may also be related to the previously discussed influence of chromium on the volume fraction of the $Ni_3Cb$ phase, which increased from 0.34 in the chromium free alloy to 0.40 in the 6 percent Cr alloy. It would thus appear that both solid solution strengthening and volume fraction effects are involved with chromium induced creep strengthening of $\gamma/\gamma'-\delta$, but sufficient data are not available from this study to separate these effects.

Fracture appearance of the specimens discussed above is shown in Figures 87 through 89. The most obvious difference in fracture appearance among these specimens is associated with testing conditions. Specimens tested at 760°C/758 MPa (1400°F/110 ksi) (Figures 87 and 88, d through f, and 89b) have relatively flat, faceted fractures with short, longitudinal steps between grains. The higher temperature fractures, on the other hand, exhibit a more irregular fracture appearance, with evidence of significant plastic deformation near the fracture surface in most cases. Some evidence of shear deformation is observed in the low temperature fractures; this phenomenon is particularly evident in the 3 percent Cr alloy, Figure 89b. There does not appear to be any major influence of composition or microstructure on fracture appearance at 760° (1400°F). Specimens tested at 1038°C (1900°F) show significant variations of fracture appearance, but these variations do not appear to correlate uniquely with either composition or microstructure.

### d. Lamellar Spacing Effects in the Chromium Free Alloy

The influence of solidification rate on the transverse microstructure of the chromium free specimens evaluated in this study is shown in Figure 90. Lamellar spacings measured at each solidification rate are in good agreement with results from the solidification studies conducted in Part A (Figure 91). Examination of the photomicrographs presented in Figure 90 also shows a significant decrease of transverse grain size with increasing solidification rate, similar to that observed by Shaw[17] in the lamellar Cd-Zn eutectic (Figure 92). The significance of this observation is discussed in later paragraphs.

Creep results are listed in Table XIX together with measurements of lamellar spacing and transverse grain diameter made in the gauge section of each specimen. A plot of rupture life versus solidification rate (Figure 93) shows an increase of life with freezing velocity in the range of 1 to 6 cm (0.4 to 2.4 inches)/hr. When plotting in terms of stress for a minimum creep rate of $10^{-4}$ $hr^{-1}$ **, the data in this range of solidification rates appear to correlate with $\lambda^{-1/2}$ on a Hall-Petch type plot (Figure 94).

Above 6 cm (2.4 inches)/hr, rupture life decreases continuously up to the highest rate investigated. This result was not expected and is not easily rationalized. Examination of the previously discussed transverse microstructures (Figure 90) indicates that the 17 and 38 cm

**Calculated from the measured minimum creep rates using a stress exponent of 5.4, measured at 1038°C (1900°F) in Phase I.

(6.7 and 15 inches) per hr microstructures are very slightly cellular, which can reduce creep properties; however, examination of Figure 90f shows that plane front solidification was achieved at 100 cm (40 inches)/hr, indicating that the slight cellularity present of 17 and 38 cm (6.7 and 15 inches)/hr is not a major factor in the observed strength decline at high solidification rates.

Metallographic examination of typical fracture profiles found in specimens tested at each of the six solidification rates (Figure 95) shows a change in fracture mode which may account at least in part for the unexpected variation of rupture life with solidification rate. At the lower rates, the primary failure mode appears to involve transgranular shear deformation, with little evidence of cavitation or grain boundary sliding. At the higher solidification rates, increasing evidence of intergranular shear parallel to the loading axis is seen. Closer examination of the specimen solidified at 100 cm (40 inches)/hr shows extensive deformation at grain boundaries (Figure 96). The data plotted in Figure 97 show a trend toward a continuous decline of rupture ductility with increasing solidification rate which is consistent with the apparent transition from a primarily transgranular to a predominantly intergranular deformation mode.

To further rationalize the behavior observed at high solidification rates, an effort was made to correlate the measured creep properties with grain size. Shown in Figure 98 is a plot of minimum creep rate versus transverse grain diameter for specimens solidified at rates between 6 and 100 cm (2.4 and 40 inches)/hour. While this correlation is satisfactory in the sense that creep rate increases with decreasing grain diameter, as expected where grain boundary sliding is the predominant deformation mechanism, the slope of the curve is very large compared to results normally obtained on polycrystalline materials. Electron micrographs presented in Figure 99 show no basic change in the structural nature of the grain boundaries at high solidification rates which might account for this anomalously high sensitivity of creep rate to grain diameter.

Another microstructural characteristic which has been correlated with creep properties is grain aspect ratio (GAR, ratio of grain length to transverse grain diameter). The influence of GAR on creep behavior is not entirely clear. Wilcox presents results which suggest that GAR is more important than grain size in determining the creep properties of wrought, oxide dispersion strengthened materials having an elongated grain structure[18]. However, results reported by Filippi indicate an opposite effect; i.e., that creep strength correlates with grain size but not with GAR[19]. To investigate possible GAR effects in the directionally solidified eutectic, attempts were made to measure grain length at various solidification rates. As shown in Figure 100, there is an apparent variation of grain length with solidification rate; however, because of the very large apparent grain aspect ratio found in the eutectic (estimated) to be on the order of 50 or greater) accurate measurements of grain length could not be made. (Wilcox reports being unable to measure grain length at aspect ratios above 12[18]). Thus, while it would appear on a qualitative basis that there is a significant reduction of grain aspect ratio with increasing solidification rate, which is consistent with the observed creep strength reduction according to the argument of Wilcox[18], a quantitative correlation between creep strength and grain aspect ratio could not be established because of the extremely large grain aspect ratios found in the eutectic.

Another factor which was investigated as possibly contributing to accelerated creep failure of high solidification rate structures was the previously discussed precipitation of $\gamma/\gamma'$ within the $\delta$ phase. It was thought that bridging of the thin $\delta$ lamellae produced at the higher solidification rates might proceed more rapidly than bridging of the thicker lamellae found at the lower rate. Results of electron microscopy studies indicated that, as in the cellular long time stability specimens, precipitation in the $\delta$ phase occurred only in highly strained areas (i.e., in secondary necks and adjacent to the fracture). The amount of acicular precipitate depended on the thickness of the $\delta$ lamallae. In the low growth rate material, 1-6 cm/hr, the $\delta$ lamellae were wide enough to permit multiple precipitation across each $\delta$ lamellae (Figure 101a). At high growth rates, 17-100 cm/hr, the thin lamellae permitted only one or two $\gamma/\gamma'$ particles to precipitate across each $\delta$ platelet (Figure 101b). The relationship of precipitate volume to $\delta$ thickness suggests that bridging of the $\delta$ lamellae probably proceeds at about equal rates in both high and low growth rate materials, and therefore is not a likely explanation for the decline in creep strength at high growth rates. In addition, the fact that precipitation occurred only near the fracture or in necked regions may indicate that the local state of stress has a strong influence on the initiation of the precipitation process. In areas where the stress remained uniaxial or in essentially unstressed locations such as the grip section, no $\gamma'$ precipitation was observed.

Based on the above evidence, it is concluded that the occurrence of a maximum creep life at intermediate solidification rates is caused by a change in the deformation and fracture mode from predominantly intragranular at low solidification rates (large lamellar spacings) to predominantly intergranular at high solidification rates (small lamellar spacings). Based on the absence of any apparent change in the structural nature of the grain boundary, it is proposed that this transition results from strengthening of the grain interior by refinement of lamellar spacing at high solidification rates. Results indicate that at low solidification rates the deformation is predominantly intragranular and that significant intragranular strengthening is achieved by refinement of lamellar spacing. As the solidification rate increases, the strength of the grain becomes equal to the strength of the boundary so that both intra- and intergranular deformation occurs. At high solidification rates, the strength of the refined grain is greater than the strength of the unchanged boundary, and deformation becomes predominantly intergranular. It is assumed that if grain size did not change, the creep strength would remain approximately constant or increase slightly at higher solidification rates. However, since both grain size and possibly grain aspect ratio decrease at high growth rates, the creep strength decreases with increasing rate in the range where grain boundary sliding is the predominant deformation mode.

### 2. Transverse Tensile Ductility

Test results obtained in Phase I confirmed previous observations indicating that intermediate temperature transverse tensile ductility is a key mechanical property requiring improvement for successful turbine applications of $\gamma/\gamma'$-$\delta$. A series of tests therefore was conducted in this phase of the program to determine the influence of both chromium level and microstructure on this critical property. Test materials were cast in slab form in the modified Bridgman furnace. Transverse fracture strains were measured at 760°C (1400°F) as described in Appendix B on lamellar and cellular specimens with chromium levels of 1 and 6 percent. Test

results are presented in Table XXI. These results are analyzed on a Weibull plot in Figure 102. This plot clearly shows significant differences between the various alloy-structure combinations evaluated. The most important differences are between the lamellar and cellular microstructures. The transverse ductility of the lamellar microstructure is more than four times that of the cellular structure in the 1 percent chromium composition and nearly double in the 6 percent chromium containing alloy. Chromium is seen to have a large influence on the transverse ductility of the cellular microstructure. A smaller but apparently real influence is also observed in the lamellar structure.

Metallographic examination of tested specimens shows a significant difference in fracture mode for the lamellar and cellular microstructures which is thought to be responsible for the improved transverse ductility. As noted previously in Section IV, transverse failure of the cellular structure occurs almost exclusively by a grain boundary fracture mode. As shown in Figure 103, failure of the lamellar structure occurs by a mixed mode, with three distinct types of fracture path being found. As illustrated in Figure 103a, these include intergranular fracture (areas A), interlamellar fracture [i.e., intragranular cracking parallel to the lamellae (area B)], and translamellar fracture, involving intragranular crack propagation across the lamellae (area C). This transition to a mixed fracture mode indicates that while grain boundary cracking continues to contribute, it is no longer the single cause of failure in the lamellar structure.

The failure of interfacial delamination to become the dominant fracture mode in lamellar structures is taken to be an encouraging sign. It means that the intrinsic strength of the interface, which has been found to be a weak point in other lamellar eutectic systems [20] is high and that further improvements of ductility might be expected if grain boundary failure could be completely eliminated as a contributing failure mode in transverse loading.

The translamellar cracking seen in Figure 103a often appears to be associated with lamellar "growth faults" (labeled "D"). Such faults were long thought to be an intrinsic characteristic of lamellar eutectics, and have been the object of considerable research [21-24]. Malmejac has recently demonstrated that lamellar faulting can be dramatically reduced by processing under extremely stable laboratory conditions [25]; however, it seems unlikely that $\gamma/\gamma'$-$\delta$ can be grown free of such faults in a production environment.

Another observation made during the course of these tests concerns the influence of off-composition microstructures on transverse ductility. While a comprehensive evaluation of this effect was not made, a small number of slightly columbium rich (hypereutectic) 1 percent chromium specimens were tested. Results of a single test on a fully lamellar, $\delta$ dendritic 1 percent chromium specimen (E329B) indicated ductility comparable to the baseline (Table XXI), despite the presence of a $\delta$ dendrite on the fracture surface (Figure 104a). Results from specimens E318F and E318G were confused by the partially cellular microstructure which resulted in low ductility failure in grain boundary cell wall regions (Figure 104b). However, it is significant to note that failure in the $\delta$ dendritic cellular structure continues to occur in the intergranular mode, indicating that the dendrite-eutectic grain interface possesses better cohesive strength than the grain boundary/cell wall areas, and thus does not represent a preferred fracture path in the cellular microstructure.

In summary, it has been demonstrated that the fully lamellar microstructure possesses significantly better intrinsic transverse ductility than the cellular microstructure at chromium levels of 1 and 6 percent. This improvement appears to be associated with a change of fracture mode from almost exclusively intergranular failure in the cellular structure to mixed intergranular, interlamellar and translamellar cracking in the lamellar structure. Preliminary results indicate that a small volume fraction of dendritic $\delta$ phase does not seriously degrade transverse ductility. It was also found that increasing chromium level from 1 to 6 percent provides a slight improvement of transverse ductility in both microstructures investigated.

### 3. Transverse Creep

The objective of these tests was to investigate the influence of chromium level on the transverse creep properties of $\gamma/\gamma'$-$\delta$. Based on results discussed in the preceding sections, process conditions were selected to produce fully lamellar microstructures with equivalent lamellar spacings in specimens containing 1, 3, and 6 percent chromium. Test material was produced in the slab form in the modified Bridgman furnace. Creep tests were performed on specimens of the design shown in Figure 11 machined with the tensile axis oriented at 90 degrees to the growth direction.

Test results are presented in Table XXII together with previously discussed results obtained on cellular material tested in Phase I, and results obtained on other programs[5]. Comparison of these results on a Larson-Miller plot (Figure 105) leads to two significant conclusions. The first concerns the influence of chromium on transverse creep strength. In the intermediate temperature range 704 to 760°C (1300 to 1400°F), it would appear that chromium does not have a significant influence on transverse creep strength; results obtained on alloys containing 1, 3, and 6 percent Cr all tend to lie within the same scatter band in this temperature range. At higher temperatures (1038°C/1900°F), it would appear that the 6 percent Cr alloy may have some advantage over the two lower chromium levels investigated. The second conclusion concerns the influence of microstructure on transverse creep strength. The Phase I results obtained on 6 percent Cr specimens having a cellular microstructure tend to lie at or near the bottom of the scatter band defined by the intermediate temperature results, and are slightly lower than results obtained on the lamellar 6 percent Cr alloy at the higher test temperature. It would thus appear that the lamellar microstructure may have a small advantage over the cellular structure with respect to transverse creep strength.

Metallographic examination of the typical fully lamellar transverse creep specimens shown in Figure 106 indicates a distinct difference in the deformation found at high and intermediate temperatures, which is similar to the difference found in cellular specimens tested in Phase I. Specimens tested in the 704-760°C (1300-1400°F) temperature range show little evidence of plastic deformation, while specimens tested at 1038°C (1900°F) exhibit numerous shear offsets which often indicate an intergranular shear deformation mode. Fracture profiles included in Figure 107 confirm the major contribution of grain boundary shear to the high temperature deformation process, and show no significant influence of chromium level on the failure mode in either test temperature range. Photomicrographs included in Figures 107d, e, and f show both transgranular and intergranular fracture components at the intermediate test temperatures. As shown by comparison of Figures 108a and b, this failure

mode is different from that found in the previously tested cellular material, where transverse creep failures were almost exclusively intergranular.

### 4. Longitudinal Tensile Strength

The primary objective of this series of tests was to evaluate the influence of an overlay coating on the longitudinal tensile ductility of the fully lamellar 1 percent Cr and 6 percent Cr alloys in the temperature range of 316 to 649°C (600 to 1200°F). Previous work on Contract NAS 3-16792 indicated that the application of overlay coatings, including PWA 270, could in some cases severely degrade tensile ductility in this temperature range [25]. Material for these tests was produced in the water-quench Bridgman furnace at respective growth rates of 2 and 4 cm/hr for the 6 percent and 1 percent chromium alloys, which provided fully lamellar microstructures of equivalent lamellar spacing in both compositions. To evaluate coating effects, one half of the specimens (Figure 11) were coated with $\approx 60\mu m$ (0.0025 inches) of the previously described PWA 270 overlay coating. Duplicate tests were conducted on coated and uncoated specimens of each composition at 316, 482, and 649°C (600, 900 and 1200°F).

While the results of these tests (Table XXIII) show some influence of coating on tensile ductility, elongations measured in the coated condition range from 3.4 to 14.8 percent indicating that coating-related ductility reductions are not a problem with the 60 $\mu$m (0.0025 inches) coating thickness investigated. As shown in Figure 109, there is no significant difference between the fracture profiles found in coated and uncoated specimens.

### 5. Effect of Chromium on Thermal Fatigue

The influence of chromium on the thermal fatigue behavior of $\gamma/\gamma'$-$\delta$ was evaluated by fluidized bed testing of wedge type specimens (Figure 15) with chromium levels of 0, 1, 3 and 6 percent. Solidification rates were adjusted to provide equivalent lamellar spacings ($\sim 5\mu m$) for all four compositions, as indicated in Table XXIV. Because chromium has a strong influence on the critical G/R for plane front growth, equivalent microstructures could not be obtained at all of the chromium levels tested, as shown in Figure 110. Essentially plane front microstructures were achieved with the 0 and 1 percent Cr alloys (Figure 110a and b), while the 3 percent and 6 percent Cr alloys were very slightly to moderately cellular (Figure 110c and d). The 1 percent chromium alloy contains a relatively small volume fraction of primary $\delta$ phase.

Based on results obtained in a recent NASA-sponsored coating program[25], the thermal fatigue specimens were coated with $\approx 6\mu m$ (0.0025 inches) NiCrAlY plus $\approx 6\mu m$ (0.00025 inches) platinum rather than the NiCoCrAlY coating (PWA 270) used elsewhere in this program. Coated specimens were tested by alternate immersion in hot (1038°C/1900°F) and cold (room temperature) fluidized beds at intervals of one minute. Testing was interrupted periodically for Zyglo inspection, with the number of cycles to crack sizes of 0.4, 0.8 and 1.6 mm (1/64, 1/32, and 1/16 inch) being recorded. Three series of four tests each were conducted, with one specimen of each chromium level being included in each series. The four specimens included in each series were mounted together in a wire basket, so that each specimen in the series was exposed to identical cycling conditions.

Interpretation of results from the first series of tests (Table XXV) was confused by the occurrence of both longitudinal and transverse cracking at all four chromium levels (Figure 111). Examination of the tested specimens indicated that longitudinal crack initiation occurred in the area of spot welds made to temporarily attach holding fixtures for overlay coating (Figure 111a). Metallographic examination of untested specimens revealed pre-existing longitudinal cracks in the area of these welds. The ends of the remaining specimens were therefore ground to remove the pre-existing cracks, and the remaining two series of tests were successfully completed without longitudinal cracking.

Results of the second and third series of tests (Table XXV) were averaged to evaluate the influence of chromium on thermal fatigue life (Table XXVI). Within the range of experimental scatter, these averages show no systematic influence of chromium on the thermal fatigue behavior of $\gamma/\gamma'$-$\delta$. Analysis of the fluidized bed strain-temperature cycle indicates a strain range $\geqslant 0.5$ percent. This high strain range accounts for the relatively low lives experienced by all alloys. The lives are consistent with those obtained with out-of-phase thermomechanical fatigue cycling at comparable strain ranges in other programs [26, 27].

## C. PHASE II SUMMARY

Chromium increases the critical ratio of thermal gradient-to-solidification rate (critical G/R) for plane front solidification from $\approx 5C^\circ$ hr/cm$^2$ in the absence of Cr to $55C^\circ$ hr/cm$^2$ at the 1 percent Cr level. Further increases to 3 and 6 percent Cr cause smaller increases of critical G/R, with respective values of 120 and $150C^\circ$ hr/cm$^2$ being measured at these levels. The increase of critical G/R correlates with the increase of melting range caused by the addition of chromium. Increasing chromium systematically reduces the solidification rate-lamellar spacing constant ($\lambda^2$ R). At a rate of 3 cm (1.25 inches)/hr, lamellar spacing decreases from $\approx 5.2\mu$m in the chromium free composition to $\approx 3.3\mu$m at 6 percent Cr. Chromium increases the volume fraction of the $Ni_3$ Cb reinforcing phase from $\approx 34$ percent at zero percent chromium to $\approx$ at 40 percent at 6 percent chromium.

Results of creep tests on alloys containing 1 and 6 percent chromium indicate that lamellar (plane front solidified) microstructures have better creep strength than cellular microstructures. Increasing solidification rate up to 6 cm (2.4 inches)/hr increases the creep strength of the lamellar microstructure in a chromium-free $\gamma/\gamma'$ - $\delta$ alloy. Further increases of solidification rate reduce creep strength. At low rates, the strength increase correlates with $\lambda^{-1/2}$ on a Hall-Petch type plot. The strength decline at higher rates is attributed to a change of deformation mode from primarily intragranular of low rates (large $\lambda$) to primarily intergranular at high rates (small $\lambda$). Refinement of lamellar spacing by increased solidification rate raises the creep strength of the cellular microstructure in the 1 and 6 percent Cr alloys (which cannot be plane front solidified at high rates because of their higher critical G/R's), but the strength increase is not sufficient to match the creep strengths of corresponding lamellar materials. The creep strength of lamellar alloys of equivalent lamellar spacing increases monotonically with chromium level in the range of 0 to 6 percent, with the largest increases occurring in the range of 0 to 1 percent Cr.

Both microstructure and chromium level influence intermediate temperature transverse tensile ductility, with microstructure having the largest effect. At 1 percent Cr, average transverse tensile ductilities of the lamellar and cellular structures are 0.28 and 0.06 percent. Average transverse tensile ductilities of the lamellar and cellular 6 percent Cr alloy are 0.33 and 0.18 percent. Microstructure also affects transverse rupture ductility, which is higher than transverse tensile ductility. Average ductilities of 1.6 and 0.5 percent were measured on lamellar and cellular specimens of the 6 percent Cr alloy. The lamellar structure also shows a small transverse creep strength advantage at both intermediate and high temperatures.

Fluidized bed thermal fatigue tests on specimens coated with $\approx$ 60$\mu$m (.0025 in) of NiCoCrAlY plus $\approx$ 6$\mu$m (.0025 in) platinum indicate that chromium has no influence on thermal fatigue life in the range of 0 to 6 percent. Low temperature (316 to 650°C/600 to 1200°F) longitudinal tensile ductility of NiCoCrAlY overlay coated ($\approx$ 60$\mu$m/ (.0025 in thick) 1 and 6 percent chromium alloys is in the range of 3.4 to 14.8 percent, which is more than adequate for turbine blade applications.

# VI. PHASE III – ALLOY MODIFICATION

The objectives of this Phase were to investigate alloy modifications to improve the shear and transverse properties of $\gamma/\gamma'$- $\delta$, and to identify two candidate alloy – structure combinations having an optimum balance of longitudinal and transverse properties and processability. Based on previous studies [5], and on Phase I and II results which indicate that off-axis failures of $\gamma/\gamma'$- $\delta$ always include a significant component of grain-boundary fracture, the approach investigated for off-axis property improvement involved the addition of minor elements such as C, Hf, Zr, and B, which are known to strengthen grain boundaries in conventional and directionally solidified nickel-base superalloys. A list of modifications evaluated is provided in Table XXVII. The first part of the following discussion summarizes the results of initial screening studies, which indicated carbon to be the most promising addition for improvement of off-axis properties. Optimization of the off-axis carbon benefits is described in Section VI.B, while development of an optimum balance between longitudinal and transverse properties and processability is discussed in Section VI.C. Sections VI.D and VI.E describe results of thermal treatment studies and critical G/R determinations on the optimized alloys. Specific processing details and compositions of the castings evaluated are listed in Appendix A. Detailed test results are included in Appendices D through G.

## A. ALLOY SCREENING

The objective of this part of Phase III was to determine the influence of C, B, Zr, and Hf additions (alone and in various combinations) on the off-axis mechanical behavior and processability of $\gamma/\gamma'$-$\delta$. Off-axis property effects were evaluated by measurements of intermediate temperature [760°C (1400°F)] transverse fracture strain (see Appendix B). Processability effects were qualitatively evaluated by observing the influence of each addition on microstructure. Test material was produced in the modified Bridgman furnace (Figure 10) in the form of 0.6 x 7.5 cm (0.25 x 3 inch) slab castings having a 1.3 cm (0.5 inch) bar cast integrally along one or both edges, as illustrated in Figure 112. These bars were used primarily for initial metallographic screening prior to sectioning for detailed chemical, metallographic and mechanical property evaluation.

Minor element effects were investigated in both lamellar and cellular microstructures and in base compositions containing chromium levels of 1 and 6 percent. Specific additions screened are included in Table XXVII. Because of the relatively high critical G/R of the 6 percent Cr base alloy, and the deleterious influence which all of the modifications except carbon were found to have on processability, most of the modified 6 percent Cr castings investigated had a cellular microstructure, with minor element effects in the lamellar microstructure being studied primarily in the 1 percent Cr base composition.

The influence of minor element modification on transverse tensile ductility is summarized in Figure 113. These results indicate that, of the four additions evaluated, carbon is the only element which provides any significant benefit to transverse ductility. Zirconium and hafnium have relatively little effect, while boron is definitely deleterious. No synergistic interactions were found between any of the combinations of minor element additions investigated. While the beneficial effect of carbon is found in combination with both zirconium or hafnium,

neither of these species enhance the effect. Similarly, the deleterious effect of boron is found in combination with zirconium. In castings containing both boron and carbon, the deleterious influence of boron predominates. As shown by comparison of the four charts included in Figure 113, similar effects were found in all four base alloy-structure combinations studied. While some small beneficial effects were found in the cellular microstructure, none of the modifications studied increased the transverse ductility of cellular test materials sufficiently to match the properties of the corresponding baseline lamellar microstructures, providing additional support for previous conclusions concerning the desirability of the lamellar structure for optimum properties.

A review of the microstructures found in various areas of representative castings evaluated in this program (presented in Appendix D) shows the deleterious influence which all of the modifications except carbon have on processability. This reduced processability is responsible for the fact that only carbon modifications were investigated in the lamellar 6 percent Cr alloy, since lamellar microstructures could not be produced in this composition with boron, zirconium, or hafnium additions. More specific comments concerning the effects of boron, zirconium, and hafnium on structure and properties are included in the following paragraphs. A detailed descussion of results obtained with carbon is presented in the next section.

### 1. Boron

Chemical analysis results summarized in Figure 114a indicate that boron segregates upward during directional solidification of the boron modified 1 percent Cr composition. Because the first 4 to 5 cm of metal in contact with the chill plate solidifies very rapidly (see Figure 10), minimal boron segregation is noted at low g (fraction solidified) values, with the average of the analyses obtained in the chill zone being about equal to the charge level. Severe upward segregation is noted above the chill zone, with the average analyses being about 10 to 15 percent of charge levels in the lower third of the directionally solidified zone. The addition of carbon or zirconium together with boron does not appear to significantly alter the boron segregation behavior. Results obtained with the boron modified 6 percent Cr composition are different. At charge levels of 0.02 and 0.05 percent, no segregation is found, with most of the analyses being equal to the amount charged. At a charge level of 0.01 percent, significant losses are seen, which may be the result of difficulty in accurately weighing the extremely small charge needed for this low level. Presuming that this is the cause of the low analyses obtained in the 0.01 percent Zr, 6 percent Cr casting, it would appear that chromium must significantly alter the solubility of boron in $\gamma/\gamma'$-$\delta$, which would account for the difference in segregation behavior between the 1 and 6 percent Cr compositions.

Photomicrographs included in Appendix D indicate that boron slightly alters the eutectic composition, so that both 1 and 6 percent Cr castings produced with the base alloy columbium levels are slightly $\delta$ dendritic. These photomicrographs also show the deleterious effect of boron on processability. While quantitative measurements of lamellarity were not made in most cases, the difference in cellularity between the typical baseline 6 percent Cr slab microstructure (Figure 19) and the structures shown in Appendix D for a boron-modified, 6 percent Cr slab produced under nominally identical processing conditions is immediately obvious. In the 1 percent Cr alloy, where segregation occurs, lamellar microstructures are found in low

boron areas, with the structure degenerating as boron levels increase at high g values.

In addition to degrading processability, boron appears to promote the formation of a new phase in the cellular microstructure, labeled "A" in several of the photomicrographs included in Appendix D. As shown in Figure 115, a similar phase was found in several of the zirconium and hafnium modified castings. While also found in a Hf + C modified casting, the presence of this phase was not detected in any of the carbon modified castings evaluated, and therefore is attributed to the presence of hafnium in the Hf + C composition. Results of electron probe microanalysis performed on the 1 percent Hf casting E312 (Figure 116) show that Hf is concentrated in this phase, which is also rich in Al relative to the other phases present. Inspection of the atom percentages tabulated in Table XXVIII suggests that the phase is $\gamma'$ of the form $(Ni, Cr)_x(Cb, Al, Cr)_y$ with x slightly above the stoichiometric value of 0.75. The measured microhardness of this phase ($\approx$ 430 to 480 DPH) is consistent with this interpretation, as is its appearance with those modifications (Hf, Zr, and B) which are known to promote formation of $\gamma'$ in solidification of conventional nickel-base superalloys. The relatively large size, blocky morphology, and location suggest that this phase forms during solidification rather than as a solid state precipitate.

Typical fracture profiles found in various boron and boron + zirconium modified transverse tension test specimens are shown in Figure 117. As with the base alloy tests discussed in Section V.B.2, transverse failure of the cellular microstructures appears to occur almost exclusively by a grain boundary fracture mode, while failure of the lamellar structure occurs by the previously discussed mixed fracture mode. The presence of significant amounts of secondary grain boundary cracking in the lamellar boron modified specimen (Figure 117a) suggests that fracture initiation may continue to be a grain boundary related phenomenon in this composition, which may account for the boron related ductility loss. This hypothesis is consistent with the observation that boron tends to segregate strongly to grain boundaries in conventional nickel-base superalloys.

### 2. Zirconium and Hafnium

Behavior of these two reactive metal species in $\gamma/\gamma' - \delta$ is very similar in many respects. Like boron, both zirconium and hafnium alter the eutectic composition to lower columbium levels, degrade processability (as shown by photomicrographs included in Appendix D), and promote the formation of free $\gamma'$ (Figure 115). However, unlike boron, neither of the reactive metal additions behaves in a predictable way insofar as correlation between charge and analyzed levels is concerned. As shown in Figures 118 and 119, analyzed values generally are significantly below charge levels and vary greatly from casting to casting. While a general trend toward upward segregation of zirconium and downward segregation of hafnium is noted in these data, unique correlation with fraction solidified values (such as that shown for boron in Figure 114) are not possible because of variations in the analyzed levels. This variability is attributed to reactivity with crucible and mold materials, which is known to be a problem with the addition of zirconium and hafnium to conventional nickel-base superalloys.

As noted previously, neither zirconium nor hafnium appear to have a major effect on off-axis ductility (Figure 113). As shown in Figure 120, fracture profiles found in broken transverse

tensile specimens are similar to those found in the base composition alloys (Figure 103), except for the Hf + C modified specimen E329H, which was hypoeutectic ($\gamma$ dendritic). In this case, separation at dendrite-eutectic boundaries is evident, suggesting that the $\gamma$ dendritic microstructure may be more detrimental to transverse ductility than the $\delta$ dendritic microstructure, which was discussed in section V.B.2. Based on this evidence, and on results generated in Phases I and II and in other studies[5] which indicates that the hypoeutectic ($\gamma$ dendritic) microstructures are detrimental to longitudinal creep strength, while slightly hypereutectic ($\delta$ dendritic) structures show no apparent creep debit with respect to baseline properties, it is clear that hypoeutectic compositions are to be avoided in $\gamma/\gamma' - \delta$, while slightly hypereutectic microstructures appear to be acceptable.

## B. ALLOY OPTIMIZATION

Results discussed above indicate that of the four minor element modifications evaluated, carbon shows the most promise for improvement of off-axis mechanical properties in $\gamma/\gamma' - \delta$. This section will describe the influence of carbon level on the transverse ductility, casting behavior, and microstructure of alloys containing 1 and 6 percent chromium.

### 1. Carbon Level Optimization

The influence of carbon level on the transverse ductility of fully lamellar 1 and 6 percent Cr castings is summarized in Tables XXIX and XXX. The results in Table XXIX indicate that analyzed carbon levels of 0.05 percent or above are needed to obtain a beneficial effect in the 1 percent Cr composition. Results for the 6 percent Cr alloy (Table XXX) indicate enhanced ductilities with analyzed levels in the range of 0.02 to 0.03 percent and above.

A Weibull analysis of results from the lamellar carbon modified alloys is compared with the previously discussed base composition results in Figure 121. This analysis demonstrates the statistical significance of the transverse ductility enhancement provided by carbon, and indicates no detectable difference between the 1 and 6 percent Cr carbon modified compositions. The Weibull plot of the carbon modified results also shows a distinct concave-down curvature, which indicates that the lower bound of the probability distribution is non-zero[28]. Further analysis of the carbon modified results indicates that this lower bound is on the order of 0.19 percent. Subtraction of this value from the measured data results in a linear Weibull plot, as shown in Figure 122.

### 2. Metallurgical Evaluation of Carbon Modified Castings

To learn more about the behavior of carbon in $\gamma/\gamma' - \delta$, and to investigate possible reasons for the beneficial influence on transverse ductility, a comprehensive evaluation of the carbon modified castings listed in Table XXVII was undertaken. Results of chemical analysis, light and electron microscopy, x-ray diffraction, and electron probe studies are discussed in the following paragraphs.

Results of chemical analysis for carbon (Figure 123) show significant variability at low g values, where large dendritic MC carbides are found to form at charge levels greater than 0.08 percent (See Figure 127a). Factors promoting the formation of these carbides are discussed

in more detail in a subsequent paragraph. Most of the analyses obtained in the vicinity of the chill zone tend to be slightly below charge level, indicating that formation of the large carbides depletes the adjacent matrix areas of carbon. In cases where a large carbide is included in the analyzed sample, analyses above 0.7 percent have been obtained. More consistent analyses are obtained at higher g values and for charge levels below 0.08 percent, where the large carbides do not form. At lower charge levels, retention appears to be somewhat better in the 6 percent Cr composition. Early castings made with elemental carbon additions exhibited significant variations of analyzed carbon level, which were traced to problems with incomplete solutioning of the elemental charge. In the case of casting E389, for example, analyses of $\approx$ 0.05 percent C were obtained with a charge level of 0.15 percent, and a large piece of undisolved carbon was found in the bottom of the melt crucible after the pour. Later castings, including the lower carbon level 6 percent Cr slabs, were made with a nickel-carbon master alloy, which probably accounts for the improved retention.

As noted previously, the addition of carbon does not appear to degrade the processability of $\gamma/\gamma'$- $\delta$. A slight alteration of the eutectic composition is noted in the 6 percent Cr alloy, with the best microstructure being obtained with 20.1 percent columbium. As shown by a review of the processing details and microstructural comments included in Appendix A, lamellar microstructures were obtained in carbon modified compositions with the same process conditions which produced plane front solidification in the analogous base compositions. These qualitative observations are confirmed by quantitative measurements described in a later section, which indicate that carbon actually reduces the critical G/R of the 6 percent Cr composition by a slight amount.

The influence of carbon on the lamellar eutectic microstructure is shown in Figure 124. These photomicrographs show subtle alterations in the nature of the lamellar structure, which are more pronounced at the lower chromium level. These alterations include modification of the appearance of the lamellar faulting noted earlier in Figure 103a, alteration of the grain boundary geometry to a slightly more irregular configuration, and a reduction of interlamellar spacing (See Figure 125). While it is possible that these microstructural alterations may be associated with the transverse ductility enhancement provided by carbon, the fact that comparable ductilities are measured in carbon modified alloys with chromium levels of both 1 and 6 percent indicates that the more pronounced alterations seen in the 1 percent Cr alloy are probably not a major factor in the ductility enhancement.

Fracture profiles examined in carbon modified specimens (Figure 126) are not significantly different from those found in base composition specimens (Figure 103). Transverse fracture in the cellular carbon modified 6 percent Cr material occurs almost exclusively in grain boundary and cell wall areas, while failure of lamellar carbon-modified specimens occurs by the previously discussed mixed fracture mode at both levels of chromium studied.

Another factor which was investigated in an effort to rationalize the carbon-related ductility enhancement was the morphology and distribution of carbides found in the carbon modified castings. Photomicrographs presented in Figure 127 show the formation of two basically different types of carbide. At charge levels of 0.08 percent and above, the previously noted large dendritic carbides (Figure 127a) are found. While these large carbides generally are confined

to a relatively narrow band just above the chill zone, isolated dendritic carbides have been found at much higher locations (See Appendix D). High charge levels (0.2 percent) and high solidification rates [130 cm (12 inches)/hr] promote the formation of dendritic carbides at relatively high g values. The presence of these massive dendritic carbides has an undesirable influence on transverse ductility, as shown by tests E319E, E420T1, and E421T1 (listed in Appendix F). An example of a dendritic carbide found on the fracture surface of a low-ductility transverse test specimen is shown in Figure 128. Carbon charge levels above 0.08 percent also promote the formation of smaller dendritic surface carbides which would be considered undesirable because they might interfere with coating acceptance and also might tend to have a deleterious influence on fatigue behavior.

The second type of carbide, found in all carbon modified castings (except E314, which analyzed below 60 ppm carbon), is illustrated in Figures 127b and c. In the cellular microstructure, these relatively fine carbides tend to be distributed preferentially in cellular areas (Figure 127b). No preferential grain boundary distribution is found in the lamellar structure, as shown in Figure 127c. It appears that there may be some tendency for the fine carbides to form preferentially at lamellar faults and to occupy a specific habit plane in the $\gamma/\gamma'$ phase, although this type of distribution is not universally found. Scanning electron micrographs included in Figure 129 show the preferential distribution of fine carbides to the $\gamma/\gamma'$, but also indicate occasional formation in the $\delta$ phase. The rounded shape and occasional presence in the $\delta$ phase suggest that these carbides form during solidification rather than by precipitation in the solid state. The inability to find a preferential grain boundary distribution of carbides indicates a relatively low probability that the presence of the fine carbide phase is responsible for the carbon-related ductility enhancement.

To determine the composition of the fine interlamellar carbides formed in the lamellar microstructure, extraction residues were examined in the electron probe microanalyzer and the transmission electron microscope. Electron diffraction patterns obtained on extracted carbides indicate that they are of the MC type. X-ray diffraction patterns obtained from chemically extracted residues confirm this identification and show no other carbide types present. Microprobe analysis shows the carbides to be Cb rich, with no other elements being detected.

Other factors evaluated in an effort to find a significant difference between the base composition and carbon modified alloys which might account for the carbon-related ductility enhancement included measurements of the $\gamma'$ size and volume fraction of the $Ni_3Cb$ reinforcing phase, and experiments to detect the possible presence of carbon in solution in the $\delta$ phase. As shown in Figure 130, the addition of carbon apparently increases the volume fraction of $\delta$ in the 6 percent Cr composition, but appears to have no influence on $\gamma'$ size. Measurements of $\gamma'$ size in a carbon modified 6 percent Cr water-quench Bridgman bar solidified at 2 cm (0.8 inch)/hr indicates an average size of 0.49$\mu$m, which is very close to the value of 0.51$\mu$m measured in an identically processed base composition bar (Table XX). The increase in the amount of reinforcing phase is not thought to be related to the ductility enhancement.

Because alloying can influence twinning behavior, which is the major deformation mode in the $Ni_3Cb$ phase, attempts were made to chemically analyze for the presence of carbon in $\delta$ by selective dissolution of the $\gamma/\gamma'$ matrix. These efforts were not successful because of the

presence of undissolved carbides in the residue. However, x-ray diffraction results obtained from the mixed residue (Table XXXI) show no shift of lattice parameter which might indicate the presence of carbon in solution in the $Ni_3Cb$ phase.

To summarize the results of the alloy optimization study, it would appear that in the 1 percent Cr base composition an analyzed carbon level of 0.05 percent or above is needed to achieve the beneficial effect of carbon on transverse ductility. Reference to Figure 123 indicates that a charge level on the order of 0.08 percent is required to reproducibly achieve this minimum analyzed level. Because this charge level can cause the formation of undesirable dendritic carbides near the chill zone, careful casting design will be required to avoid the occurrence of dendritic carbides in carbon modified 1 percent Cr turbine blade castings. In the 6 percent Cr composition, more latitude is available in terms of an optimum carbon charge level. The ductility benefit is found with charge levels in the range of 0.04 to 0.06 percent, where the dendritic carbide formation does not occur. This relatively large range of nondendrite forming carbon levels which produce a ductility enhancement in the 6 percent Cr composition is desirable from a foundry practice viewpoint, because it provides some latitude for establishment of a chemistry specification.

The mechanism responsible for the ductility enhancement provided by carbon was not determined, despite an extensive evaluation of microstructural, x-ray, and electron probe results. The mixture of intergranular, interlamellar, and translamellar fracture modes found in the lamellar structure does not appear to change substantially as a result of modification with carbon. No preferential distribution of carbides to the grain boundaries is found, nor is any evidence of carbon in solution in the $Ni_3Cb$ phase, which might alter deformation modes. Based on the absence of any clearly defined microstructural evidence, such as grain boundary carbide precipitation, which would explain the increased transverse ductility provided by carbon, consideration was given to other possibilities. The primary possibility under consideration is the cleansing of the melt by removal of additional oxygen and nitrogen. (The importance of eliminating these gaseous species has been recognized for some time in superalloy melt practice by melting under vacuum). Oxygen would be removed in the eutectic by direct reaction with carbon, and nitrogen by diffusion into the carbon monoxide bubbles rising through the melt. Reduction in the level of these impurities would tend to reduce the number of impurity atoms at the solid-liquid interface during unidirectional solidification which should reduce the critical G/R for plane front growth. In fact, G/R for carbon-modified 6 percent Cr material was determined to be 140 $C^\circ$ hr/$cm^2$ compared to 150 $C^\circ$ hr/$cm^2$ for the carbon free alloy as discussed in a subsequent section. Recommended future work in this area would include a more detailed evaluation of the concentration of impurity species at grain boundaries.

## C. PROCESSABILITY-PROPERTY BALANCE OPTIMIZATION

The objective of the effort described in this section was to investigate approaches for achievement of an optimum balance between longitudinal creep strength, transverse ductility, and processability. Based on previously discussed results which have shown that plane front solidification is desirable for optimization of both longitudinal and transverse properties, these efforts were concentrated on production and evaluation of lamellar test materials. While the Phase II results also show that the creep properties of the 6 percent Cr composition are better than the properties of the 1 percent Cr composition, the much lower critical G/R of

the 1 percent Cr composition (55 versus 150 C° hr/cm$^2$) makes it extremely attractive from a processability viewpoint. Efforts were therefore undertaken to determine if longitudinal creep strength improvements could be achieved in the lamellar 1 percent Cr alloy without reducing the previously optimized transverse ductility. Parallel studies were also conducted in the 6 percent Cr composition.

Two approaches for achievement of creep strength improvements were investigated. The first was reduction of lamellar spacing by processing at increased solidification rates, which was shown in Phase II to improve the creep strength of the lamellar microstructure in the range of solidification rates where grain boundary sliding is not the predominant deformation mechanism (up to 6 cm/hr in the chromium free composition). The second approach was modification with tantalum, which was shown by Lemkey to have a potentially beneficial effect on the creep strength of $\gamma/\gamma' - \delta$[29].

## 1. Solidification Rate Effects

A primary objective of this effort was to investigate solidification rate effects with process conditions which simulate as closely as possible the procedures used to fabricate $\gamma/\gamma'$-$\delta$ turbine blades, which can be produced with a fully lamellar microstructure at solidification rates as high as 1.3 cm (0.5 inch)/hr in the 6 percent Cr base composition [30, 31]. Thus, while plane front solidification could have been achieved at higher solidification rates in the higher-gradient water-quench Bridgman furnace, the studies described in this section were performed with slab material processed in the lower gradient modified Bridgman furnace because it more closely simulates the current blade casting process. Because the critical G/R of the 1 percent Cr alloy is relatively low, it was possible to produce lamellar microstructures in 0.6 cm (0.25 inch) thick 1 percent Cr modified Bridgman slab castings at relatively high rates [up to 2.5 cm (1.0 inch)/hr. To investigate slab properties in 6 percent Cr castings made at rates above 0.6 cm (0.25 inch)/hr, it was necessary to use the thinner 0.3 cm (0.125 inch) casting illustrated in Figure 131. The reduced perimeter/area ratio of this casting promotes a higher thermal gradient, which allows plane front solidification conditions to be achieved at higher solidification rates. The sheet-type specimen illustrated in Figure 12 was used to evaluate the rupture properties of the thin slab castings.

Results of creep tests conducted on this part of the program are included in Appendix G. These results are summarized in Figure 132 together with the previously discussed Phase II results. These data indicate that, with the exception of one result, the rate-spacing relationship found in the 1 and 6 percent Cr base compositions is comparable to that measured for the chromium free alloy in Phase II.

Results obtained on the carbon modified 1 percent Cr alloy did not behave exactly as expected. Within the range of 1.3 to 2.5 cm (0.5 to 1.0 inch)/hr, no increase of creep strength was found (Table XXXII). Measurement of lamellar spacings in these castings indicates that spacing did not change with rate as much as expected, so that when plotted in Figure 132 the carbon modified results are clustered in a relatively small grouping.

Based on the results discussed above, it would appear that increasing solidification rate within the range where plane front solidification can be achieved should produce improved creep strengths with simulated blade process conditions. However, it does not appear likely that the rate increases alone will improve the creep strength of 1 percent Cr $\gamma/\gamma'$-$\delta$ alloys sufficiently to match the best properties available from the 6 percent Cr alloy.

## 2. Tantalum Modification

The second approach which was investigated for development of an optimum balance of properties in $\gamma/\gamma'$- $\delta$ was modification with tantalum. This modification was evaluated in both base composition and carbon modified 1 and 6% Cr alloys, as summarized in Table XXXIII. Typical photomicrographs from the tantalum modified castings (Figure 133) indicate that the addition of three percent tantalum significantly increases the critical G/R of both the 1 and 6 percent Cr compositions. Plane front solidification could not be achieved in the tantalum modified 1 percent Cr alloy at rates above 0.6 cm (0.25 inch)/hr, indicating that the critical G/R of this modification is comparable to that of the 6 percent Cr base composition (150C°hr/cm$^2$). A lamellar microstructure could not be obtained in the tantalum modified 6 percent Cr alloy at any solidification rate investigated, indicating that tantalum also increases critical G/R at the higher chromium level.

Creep test results from this study are listed in Appendix G. The influence of carbon and tantalum on rupture life is summarized in Table XXXIII. Several conclusions may be drawn from examination of these results. First, modification with carbon does not significantly influence the creep strength of either base composition. Second, tantalum by itself has a small beneficial effect on the creep strength of the 1 percent Cr composition. However, the benefit is not sufficient to match the properties of either the base composition or carbon modified 6 percent Cr alloys, which have processabilities comparable to the tantalum modified 1 percent Cr alloy. Third, the creep strength of the cellular tantalum modified 6 percent Cr alloys does not equal that of the lamellar base composition and carbon modified 6 percent Cr alloys. These results indicate that the best balance between processability and longitudinal creep strength is obtained with the base composition and carbon modified 6 percent chromium alloys.

Results of 760°C (1400°F) transverse tension tests conducted on the tantalum modified castings (Appendix F) are summarized in Table XXXIV. These results indicate that tantalum degrades transverse ductility in every alloy-structure combination evaluated.

In summary, it would appear that the addition of tantalum is not a viable approach to development of an optimum balance of properties and processability in the $\gamma/\gamma'$-$\delta$ directionally solidified eutectic alloys investigated in this program, and that the two alloy-structure combinations having the best balance between longitudinal creep strength, transverse ductility, and processability are the base composition and carbon modified 6 percent Cr alloys, processed at the maximum rate producing a fully lamellar microstructure.

## D. EVALUATION OF THERMAL TREATMENTS

The objective of this part of Phase III was to determine the influence of thermal treatments on the transverse ductility of the fully lamellar base composition and carbon modified alloys identified in the previous section as having an optimum balance of properties and processability.

Results of preliminary experiments performed to determine the $\gamma'$ solvus temperature of the base composition 6 percent Cr alloy are provided in Figure 134. These photomicrographs indicate that the solvus temperature is in the range between 1160 and 1171°C (2120 and 2140°F). Based on this result, several thermal treatments were selected for evaluation of transverse ductility. These treatments are listed in Table XXXV together with coded designations which will be used for subsequent reference to each treatment. The 2200(4) and 2110 (4) exposures were selected to provide complete and partial solutioning of the $\gamma'$ phase. The partially solutioned microstructure was investigated on the basis of results of Dreshfield[32] which suggest that this thermal treatment, in conjunction with an aging cycle, may prove beneficial to transverse ductility. The 1975 (4) treatment was selected to simulate a typical coating thermal cycle. Aging treatments in the range of 871 to 899°C (1600-1650°F) were investigated both alone and in conjunction with each of the three higher temperature treatments discussed above.

Typical microstructures found in baseline and carbon modified coupons exposed to each of the seven thermal treatments listed in Table XXXVI are shown in Figures 135 through 137 together with photomicrographs of virgin (as-cast) material. Insofar as basic microstructure is concerned, there appears to be essentially no difference in the response of the baseline and carbon modified alloys to thermal treatment. As anticipated from results of the $\gamma'$ solvus determination, the 2200(4) treatment provides complete solutioning of the $\gamma'$ phase, while the 2110(4) and 1975(4) treatments leave progressively larger amounts of undissolved coarse $\gamma'$. It would appear that some reprecipitation of $\gamma'$ may occur on cool-down from the full solutioning treatment, although this $\gamma'$ is too fine to be clearly resolved at the magnification examined. Aging of the as-cast and solution treated material (both fully and partially solutioned) causes essentially no change to the $\gamma'$ morphology which can be detected in the light microscope. The primary observable influence of the aging treatment appears to be precipitation of Widmanstatten $\delta$ in the matrix. This precipitation was observed in the Phase I long time creep specimens tested in the same temperature range (Figure 24 a and b) and was shown to have little influence on mechanical properties (Figure 22). As shown in Figure 137, none of the thermal treatments applied appear to alter significantly the distribution or morphology of the carbide phase in the carbon modified composition, indicating the carbide solutioning temperature to be above 1204°C (2200°F). This observation is consistent with the previously stated hypothesis that the carbides form during solidification rather than by precipitation from the solid state.

Results of 760°C (1400°F) transverse tension tests on virgin and thermally exposed specimens (Appendix F) are summarized in Table XXXVI. These results indicate that aging, either alone or in conjunction with the partial solution or simulated coating treatments, provides a substantial improvement in the transverse ductility of the baseline alloy. This effect is not

seen in the presence of carbon. Solution treatment is obviously deleterious to the transverse ductility of either composition; aging provides a partial recovery of this solution treatment related ductility loss in the carbon modified composition, but not in the baseline alloy. The partial solutioning treatment is deleterious in the carbon modified but not the baseline composition. As with the full solution treatment, aging of the partially solution treated carbon modified alloy provides a partial recovery of the ductility loss. The simulated coating treatment does not appear to have any significant influence on the transverse ductility of either composition.

In summary, it would appear that a full solutioning treatment is to be avoided in both compositions, and that aging appears to be desirable for transverse ductility enhancement of the fully lamellar base composition 6 percent Cr alloy. Based on results of early studies conducted in this laboratory [5], and on more recent results obtained by Dreshfield[32] which show that thermal treatments involving a solutioning cycle do not improve the high temperature creep strength of the 6% Cr $\gamma/\gamma' - \delta$ alloy, the solution treatment related transverse ductility loss is not considered a problem, since there is no reason to apply this treatment to the alloy. The absence of a deleterious influence from the simulated coating treatment is a good result, since results obtained on other programs indicate that a coating will be required for turbine application of $\gamma/\gamma' - \delta$[25].

## E. CRITICAL G/R DETERMINATION

The objective of this part of Phase III was to determine the critical G/R for the base composition and carbon modified 6 percent Cr alloys. While a critical G/R determination was performed previously on the base composition 6 percent Cr alloy in Phase II, it was considered desirable to repeat this determination together with the determination on the carbon modified composition to provide as nearly as possible identical experimental conditions for a critical comparison of processability between the two alloys.

Procedures used for determination of critical G/R in this Phase were essentially identical to those described in Section V. A. except that a different water-quench Bridgman furnace was employed. Because gradient can vary slightly from rig to rig, new gradient determinations were performed for the current study. Plots of temperature versus traverse distance obtained from gradient runs made immediately prior to and immediately after the critical G/R castings produced in this phase (Figure 138) indicate an average gradient on the order of 280°C/cm for the furnace used. Photomicrographs of base composition and carbon modified 6 percent Cr castings directionally solidified at various rates in this furnace are shown in Figure 139. Measurements of volume fractions of lamellar microstructure made on these photomicrographs are plotted versus G/R in Figure 140. Results from the base alloy (closed circles) are consistent with results obtained previously in Phase II (open circles), which indicate a critical G/R of 150C° hr/cm$^2$ for this composition. Results obtained on the carbon modified composition (□ symbol) indicate that carbon reduces the critical G/R slightly, to a value of about 140C° hr/cm$^2$.

## F. PHASE III SUMMARY

Modification with carbon increases the average 760°C (1400°F) transverse tensile ductility of the fully lamellar 1 and 6 percent Cr alloys to 0.49 percent. Smaller benefits occur in cellular microstructures, with the transverse ductility of cellular carbon modified specimens being less than corresponding lamellar base composition properties. A 24 hour aging treatment at 899°C (1650°F) increases the average transverse ductility of the lamellar 6 percent Cr base composition to 0.47 percent, and has no influence on the carbon modified 6 percent Cr alloy. The addition of zirconium or hafnium has no effect on transverse ductility, while boron has an embrittling effect.

The optimum carbon charge level for transverse ductility enhancement is 0.06 percent in the 6 percent Cr alloy and 0.08 percent in the 1 percent Cr alloy. The higher carbon addition in the 1 percent Cr alloy causes formation of undesirable large MC carbide dendrites at low g (fraction solidified) values. These carbides do not form at the lower optimum charge levels in the 6 percent Cr alloy. Results of solidification studies show that carbon slightly decreases the critical G/R of the 6 percent Cr alloy to about 140C° $hr/cm^2$.

Modification with carbon does not degrade longitudinal creep strength. Reduction of lamellar spacing by raising solidification rate increases the longitudinal creep strength of the fully lamellar 1 and 6 percent Cr alloys. However, the creep strength of the lamellar 1 percent Cr alloy is not increased sufficiently to match the best properties of the 6 percent Cr alloy.

The addition of 3 percent tantalum causes large increases in the critical G/R of both the 1 and 6 percent Cr alloys. While this modification increases the creep strength of the lamellar 1 percent Cr alloy, the improvement is not sufficient to equal the properties of the 6 percent Cr alloy. Lamellar microstructures could not be achieved in the tantulum modified 6 percent Cr alloy because of the substantially increased critical G/R. The creep properties of cellular tantalum containing 6 percent Cr specimens are below those of the lamellar base composition.

## VII. PHASE IV – SUBSTANTIATION OF OPTIMIZED ALLOYS

Phase III results discussed in the preceding section indicate that the two alloys having the best balance between longitudinal and transverse properties and processability are the base and carbon modified 6 percent Cr compositions, processed at the maximum rate producing plane front solidification. The objective of this phase was to substantiate the mechanical properties and long time thermal stability of these two alloy-structure combinations, leading to selection of an optimized alloy for further evaluations involving stress analysis, thermomechanical fatigue, and root subcomponent testing of an advanced hollow, high work eutectic turbine blade[33].

### A. TEST PROGRAM

Specific properties evaluated in Phase IV include shear and transverse creep and tensile, longitudinal and transverse impact, transverse low cycle fatigue (LCF), longitudinal creep, and long time microstructural stability. Mechanical tests were conducted using specimens and procedures described in Section III. All properties were evaluated on slab castings produced at 0.6 cm (0.25 inch)/hr, with longitudinal creep properties also being evaluated on water-quench Bridgman bars solidified at 2 cm (0.8 inch)/hr. Carbon modified castings were produced with a charge carbon level of 0.06 percent, which is at the high end of the range that provides enhanced transverse ductility but does not promote carbide dendrite formation. All specimens, except the shear and impact bars, were overlay coated with $\approx$ 60 $\mu$m (0.0025 in) of the previously discussed PWA 270 NiCoCrAlY coating. In addition, the inside diameter of the tubular transverse LCF specimens was coated with $\approx$ 25 $\mu$m (0.001 in) of a low aluminum grade aluminide coating. Coated specimens received a 1975(4)* thermal treatment as an integral part of the coating diffusion anneal process. This thermal treatment was also applied to all uncoated specimens. Based on results of Phase III, base composition specimens were evaluated in the aged 1650 (24)* condition. Results of selected tests on unaged lamellar base composition specimens indicated that within the range of experimental scatter the aging treatment had no significant influence on any properties other than transverse ductility. Results from aged and unaged specimens were therefore averaged for subsequent comparison of lamellar base composition properties with other alloy-structure combinations.

### B. OFF-AXIS PROPERTIES

Off-axis test results for the two candidate optimized alloys (Tables XXXVII through XLIII) are compared with available cellular baseline properties in Figure 141. This comparison shows significant improvements of most properties for which comparative baseline data are available. In most cases, the off-axis property improvements are greater in the carbon modified composition in the intermediate temperature range. A more detailed discussion of specific test results is included in the following sections.

*See Table XXXV for explanation of thermal treatment codes.

## 1. Transverse Tensile and Creep Results

Results of transverse tensile and creep tests on the two candidate optimized alloys (Tables XXXVII and XXXVIII) are summarized together with average properties of directionally solidified MAR M-200 (with and without hafnium) in Figure 142 and Tables XXXIX and XL. These results confirm the large improvements of intermediate temperature transverse tensile and rupture ductility found in Phases II and III, and show adequate high temperature transverse ductility for all alloy-structure combinations evaluated. Two results are of particular note. First, comparison of the Phase III and Phase IV intermediate temperature tensile results on the carbon modified composition indicates that overlay coating significantly improves the transverse tensile ductility of this composition (0.85 percent coated versus 0.49 percent uncoated). A smaller improvement (0.54 percent coated versus 0.47 percent uncoated) is noted for the lamellar base composition. Comparison of previously discussed Phases I and II results indicates virtually no coating related transverse tensile ductility improvement for the cellular base composition (0.21 percent coated versus 0.18 percent uncoated). The second notable result concerns the intermediate temperature transverse rupture ductility of the optimized eutectic alloys, which is significantly greater than the transverse tensile ductility in the same temperature range. The highest transverse rupture ductilities, on the order of 2 percent, are measured on the lamellar carbon modified alloy, which also has the highest transverse tensile ductility, slightly under 1 percent. A similar difference was found for the lamellar and cellular base composition alloys, where intermediate temperature rupture ductilities of 1.7 percent (lamellar) and 0.54 percent (cellular) were measured, as compared to respective transverse tensile ductilities of 0.47 and 0.21 percent.

Transverse strength improvements found in the candidate optimized alloys are marginal. The test results indicate modest improvements of tensile and creep strength at intermediate temperatures, with no improvement evident at high temperatures.

Fracture profiles included in Figures 143 and 144 are similar to those discussed in Sections V and VI. Intermediate temperature transverse tensile fractures occur by the previously described mixed intergranular, interlamellar and translamellar mode. Intermediate temperature creep fractures appear to involve a similar type of failure together with a major component of grain boundary shear. High temperature transverse failures occur predominantly by grain boundary shear in both tensile and creep deformation.

An unusual phenomenon found in the coated carbon modified specimen having the highest 760°C (1400°F) tensile fracture strain (E511 H, 1.38 percent) was the occurrence of secondary cracking at locations remote from the primary fracture. Shown in Figure 145 is a subsurface secondary crack found in this specimen. The fact that this crack is located exclusively in the grain boundary indicates that transverse crack initiation may continue to be grain boundary related in the optimized microstructure.

Comparison of the eutectic and MAR M-200 data included in Figure 142 and Tables XXXIX and XL indicates that the high temperature transverse properties of these two types of directionally solidified materials are not greatly different. High temperature tensile and rupture ductilities are comparable as are high temperature transverse tensile strengths. While the high

temperature transverse creep strength of the eutectic is somewhat lower, the major difference is found in the intermediate temperature range where the rupture strength of the eutectic is less than half that of the directionally solidified superalloys. The significance of these reduced properties is currently being evaluated [33].

A similar situation exists with regard to interpretation of the transverse ductility results. Comparison of the optimized eutectic and directionally solidified superalloy rupture ductilities listed in Table XL indicates that, presuming transverse creep stresses do not exceed the strength capabilities as discussed above, intermediate temperature transverse rupture ductility of the eutectic should be adequate. The adequacy of the optimized transverse tensile ductility is more difficult to assess. The comparison in Table XL indicates that the average 760°C (1400°F) transverse tensile ductility of the optimized eutectic is higher than that of directionally solidified MAR M-200 without hafnium, which has seen service in a high performance military engine. However, the comparison must be interpreted with some caution because of the previously discussed variability of the eutectic fracture strain measurements. Weibull analysis of the Phase IV carbon modified test results, shown in Figures 146 and 147, indicates that the coating increases the characteristic fracture strain from 0.52 to 0.94 percent. The limited results plotted in Figure 147 confirm that the transverse ductility of hafnium free directionally solidified MAR M-200 is in the same range as the optimized eutectic results.

In summary, the transverse test results obtained on the optimized alloys show substantial improvements in the transverse ductility of $\gamma/\gamma' - \delta$ as a result of microstructural and compositional modification, and from the addition of an overlay coating, with the best properties being measured on the coated, fully lamellar carbon modified composition, which appears to possess transverse ductility characteristics similar to those of non-hafnium modified directionally solidified MAR M-200. However, sufficient information is not yet available to determine if the optimized transverse properties are adequate for turbine blade applications of $\gamma/\gamma' - \delta$. Both analytical and subcomponent evaluations are presently being conducted to provide additional information concerning this question.

### 2. Shear Properties

Shear test results on the candidate optimized alloys (Tables XLI and XLII) are compared with Phase I baseline and superalloy results in Figures 148 and 149. These results show significant improvements of shear strength, particularly in the carbon modified composition. Examination of the broken test specimens indicates mixed mode failure, with a large component of grain boundary shear, at both test temperatures and for both optimized alloy – structure combinations (Figures 150 and 151). Comparison of the optimized eutectic results with the B-1900 data generated in Phase I indicates that, while significant improvements have been achieved, the optimized eutectic properties are still below typical superalloy shear strengths.

### 3. Transverse Low Cycle Fatigue

Results of transverse low cycle fatigue tests conducted on the two candidate optimized alloys are presented in Table XLIII and are summarized together with prior results on the cellular baseline alloy[27] in Figure 152. These results indicate the carbon modified alloy to be better than the lamellar base composition at 760°C (1400°F), with no apparent difference at 982°C (1800°F). The coincidence of the 760°C (1400°F) carbon modified and 427°C (800°F) cellular baseline results indicates that the carbon modified properties are superior to the baseline properties, since increasing temperature is known to have a deleterious influence on fatigue strength. As seen by comparison of the test results with predictions based on the method of universal slopes, the slope of the eutectic log $\epsilon$ - log N relationship is significantly smaller than predicted at low and intermediate temperatures. Location of the crack initiation site was difficult to determine on the failed test specimens, particularly at 760°C (1400°F). At 932°C (1800°F), detectable initiation sites were located on the inside diameter of the tubular specimen. No indications of secondary cracking were found at either test temperature.

## C. IMPACT RESULTS

Subsize, instrumented Charpy impact tests were performed on the two candidate optimized alloys in the longitudinal and transverse orientations (defined in Section III) at room temperature and 760°C (1400°F). Results of these tests (Table XLIV) indicate that carbon reduces impact resistance in both orientations and at both temperatures investigated. The reduction appears larger at room temperature than at 760°C (1400°F). While preferential crack initiation and/or propagation at carbides may be involved with the carbon-related impact strength reduction, the small size of the carbides makes it difficult to document such an effect at optical magnifications (Figures 153 and 154).

The photomicrograph, Figure 154d, and comments included in Table XLIV indicate that some of the transverse specimens were cellular or $\delta$ dendritic. A review of the results indicates that, unlike transverse tensile and creep properties, impact resistance does not appear to be highly sensitive to microstructure. Support for this hypothesis is found by comparison of the longitudinal room temperature lamellar base composition average of 2.33J (1.72 ft. lb.) with Lemkey's reported value of 2.29J (1.69 ft. lb.) for the cellular baseline alloy[2]. It is interesting to note that aging of the cellular baseline alloy for 1500 hours at 849°C (1560°F) reduces the toughness to 1.61J (1.19 ft. lb.)[2], which is in the range of the carbon modified alloy.

## D. LONGITUDINAL CREEP EVALUATION

Results of slab and Bridgman bar creep tests on the candidate optimized alloys (Table XLV) are compared with a computer generated least-squares curve representing previous 3 cm (1.2 inch)/hr cellular Bridgman bar results in Figure 155. This comparison indicates that the average optimized Bridgman bar results are comparable to prior Bridgman bar properties, while the 0.6 cm (0.25 inch)/hr optimized slab results are slightly lower but still substantially above the properties of the best available nickel base superalloy, directionally solidified MAR M-200 + Hf. Based on the previously discussed relationship between solidification rate, lamellar spacing, and creep strength (Figure 132), the property debit found at 0.6 cm (0.25 inch)/hr was not unexpected, and is not considered to be representative of properties to be expected in hollow eutectic airfoils, which can be produced fully lamellar at 1.3 cm (0.5 inch)/hr with current process technology [30, 31]. Efforts are being made on a concurrent Air Force sponsored program to develop test methods for measurement of machined-from-blade (MFB) creep properties on hollow eutectic airfoils produced at 1.3 cm (0.5 inch)/hr to confirm this hypothesis[30]. The equivalence of the 2 cm (0.75 inch)/hr optimized Bridgman bar results with prior 3 cm per hour cellular Bridgman bar properties was not expected. Based on Phase II microstructural optimization studies, the properties of the 2 cm (0.75 inch)/hr lamellar Bridgman bars were expected to be significantly better than prior cellular 3 cm (1.2 inch) per hour properties. Examination of the tabular data (Table XLV) indicates that the Bridgman bar results were not only lower than expected, but also exhibited significant variability, particularly at the lower test temperature (760°C/1400°F). Both the variability and the lower than expected average properties could be attributed to the presence of cellular bands and nonmetallic inclusions in the Bridgman bars tested in this Phase. Process difficulties which led to these microstructural defects are discussed below.

As described in Section V. B.1.b., the production of fully lamellar, band free Bridgman bars at 2 cm (0.75 inch)/hr requires a careful balance between excessive superheat, which promotes mold-metal reactions leading to nonmetallic inclusions (See Ref. 29, P. 53), and inadequate superheat, which reduces gradient and causes the formation of cellular bands. Phase II results indicated that a superheat temperature of about 1750°C (3180°F), produced lamellar microstructures with minimal oxide contamination in the bottom half (shorter exposure time) of 2 cm (0.75 inch)/hr Bridgman bars. As shown in Figure 156a, efforts to produce test material for Phase IV with identical process conditions resulted in moderate to heavy oxide contamination along the entire length of the 2 cm (0.75 inch)/hr bars tested in this phase. Attempts to process with reduced superheat resulted in cellular banding, as shown in Figure 156b. The increased reactivity encountered in processing of the Phase IV Bridgman bars was attributed to a change in crucible vendor. This was demonstrated by processing of a Phase IV test bar (A76-010) in a single remaining crucible from the old lot. The bottom half of this bar had an oxide-free, lamellar microstructure comparable to that found in the Phase II test bars.

As noted earlier, the lower than expected properties measured on the Phase IV Bridgman bars can be attributed to the cellular bands and nonmetallic inclusions discussed above. As indicated by the comments in Table XLV and the microstructural evidence shown in Figures 157 and 158, premature creep failures can be directly correlated with these microstructural defects. As shown by the results of test A76-010-01, properties comparable to those discussed in Phase II were obtained in the defect-free bar produced in a crucible from the old lot.

## E. MICROSTRUCTURAL STABILITY

### 1. Eutectic Microstructure

The thermal stability of the optimized alloy microstructures was evaluated by metallographic examination of static (unstressed) coupons exposed 1000 hours in air at 871 and 1038°C (1600 and 1900°F), and of a 1038°C (1900°F) coated carbon modified creep specimen which was tested to rupture in 743 hours at 110 MPa (16 ksi). Results of these examinations, included in Figures 159 and 160, indicate excellent thermal stability of the optimized lamellar eutectic structure, comparable to that found in the cellular baseline structure studied in Phase I. As in the baseline alloy, $\gamma'$ ripening was seen in both static and stressed exposures at 1038°C (1900°F), while Widmanstatten $\delta$ precipitation was observed at 871°C (1600°F). Comparison of the base composition and carbon modified exposure coupons indicates that the 871°C (1600°F) Widmanstatten $\delta$ precipitation is less copious in the carbon containing alloy. This effect is attributed to depletion of columbium from solid solution in the $\gamma/\gamma'$ matrix by formation of the columbium rich MC carbides in the carbon modified composition. Some $\gamma'$ ripening is also evident in the carbon modified material exposed at 871°C (1600°F). This is attributed to the smaller amount of Widmanstatten $\delta$, which apparently serves as a physical barrier to $\gamma'$ agglomeration at 871°C (1600°F) in the base composition. As shown in Figure 161, no change in the carbide distribution occurs as a result of air exposure.

### 2. Coating Stability

While none of the coated specimens were examined prior to testing, coating microstructures found in the 760°C (1400°F) transverse tension test specimens (Figures 162 a and b) were considered representative of the as-deposited condition. Coating acceptance appears to be comparable on both the base composition and carbon modified substrates, with the development of a thin but well defined diffusion zone in both compositions. As seen in Figure 162b, the diffusion zone in the carbon modified alloy contains a relatively uniform dispersion of fine carbides, with a narrow carbide-depleted zone in the adjacent substrate. High temperature creep exposure increases the thickness of the diffusion zone, with a concomitant increase in the density of diffusion zone carbide precipitation and depth of carbide depletion in the substrate of the carbon modified composition. For the 743 hour creep exposure shown in Figure 161d, the depletion has penetrated slightly past the mid-radius position of the 0.3 cm

(0.125 inch) diameter test bar (about 1 mm/.040 in). The migration of carbon and the continued presence of carbides in the center of the specimen indicates that substantial carbon must remain in solution in the carbide depleted zone. Examination of 760°C (1400°F) creep specimen indicates no depletion of carbides beyond that found in as-coated specimen (Figure 163). Presuming that the scavenging mechanism proposed in Section VI is correct, the coating related carbon migration found at high temperatures should not influence properties.

## F. PHASE IV SUMMARY

Based on the results of Phases II and III, the fully lamellar base composition and 0.06 percent carbon modified 6 percent chromium alloys were selected for further evaluation of mechanical properties. Results of this evaluation show that overlay coating of the carbon modified 6 percent chromium alloy increases the average 760°C (1400°F) transverse tensile ductility from 0.49 to 0.85 percent. A smaller improvement, from 0.47 to 0.54 percent, occurs in the coated lamellar base composition 6 percent chromium alloy. The average 760°C (1400°F) transverse rupture ductility of the coated carbon modified alloy is 2 percent.

Modification with carbon raises intermediate temperature shear strength by 20 percent and increases shear rupture life by a factor of three over the baseline alloy. Carbon reduces impact resistance of the virgin baseline alloy to a value comparable to that obtained after aging of the baseline alloy for 1500 hours at 849°C (1560°F). Limited results indicate that carbon improves transverse low cycle fatigue life at 760° (1400°F) with no apparent effect at 982°C (1800°F). Creep results indicate that carbon does not degrade creep strength and show that long time creep stability of the carbon modified alloy is excellent.

Based on these results, the Ni-20.1%Cb-2.5%Al-6.0%Cr-0.06%C modified composition directionally solidified under conditions producing plane front solidification is recommended as the optimum alloy-structure combination for turbine applications of $\gamma/\gamma'$-$\delta$.

## VIII. CONCLUSIONS

The objective of this program was to characterize the mechnical behavior of a Ni-20.0%Cb-2.5%Al-6%Cr cellular eutectic alloy and to investigate approaches for improving the balance between longitudinal and transverse properties. Results of the baseline alloy characterization show excellent long time creep stability and indicate intermediate temperature transverse tensile ductility (on the order of 0.2 percent) and shear strength (≈ 300 MPa, 44 ksi) to be the off-axis properties of greatest concern for turbine blade applications. Both of these properties were significantly improved by alloy and structural optimization with no loss of longitudinal creep strength or stability. The alloy-structure combination identified as having the best balance of properties is a carbon modified Ni-20.1%Cb-2.5%Al-6%Cr-0.06%C composition processed under conditions producing plane front solidification. With current processing technology, this alloy exhibits a temperature advantage of 39°C (70°F) [which translates to a 40 percent improvement of longitudinal stress capability at 1000°C (1832°F)] over the best available nickel-base superalloy, directionally solidified MAR M-200 + Hf. While the improved transverse tensile and rupture ductilities of the optimized eutectic alloy remain limited (on the order of 1 to 2 percent), they are similar to those of hafnium free directionally solidified MAR M-200 which has seen service as solid blades in a high performance military engine. It appears that the design limiting property of the eutectic may be intermediate temperature shear strength. While a 20 percent improvement was achieved, the optimized eutectic shear strength of 390 MPa (56 ksi) continues to be well below typical superalloy levels of ≈ 700 MPa (100 ksi). Analytical and subcomponent test programs are being conducted to evaluate the capability of the optimized eutectic alloy to sustain advanced design hollow blade root attachment and airfoil fatigue loads[33].

## IX. REFERENCES


1. Gell, M. and Donachie, M. J., "Directionally Solidified Eutectics for Use in Advanced Gas Turbine Engines," Proceedings of the Sixth SAMPE National Technical Conference, Dayton, Ohio, October 8-10, 1974.

2. Lemkey, F. D., "Eutectic Superalloys Strengthened by δ $Ni_3Cb$ Lamellae and γ′ $Ni_3Al$ Precipitates," NASA CR-2278, November 1973.

3. Quinn, R. T., Kraft, R. W. and Hertzberg, R. W., "Structure and Elevated Temperature Mechanical Behavior of a Unidirectionally Solidified Ni-$Ni_3Nb$ Eutectic Alloy," Trans. ASM, Vol. 62 (1969), p. 38.

4. Lemkey, F. D. and Thompson, E. R., United Aircraft Research Laboratories, "Eutectic Superalloys Strengthened by Aligned δ, $Ni_3Cb$ Lamellae, γ′, $Ni_3Al$ Precipitates and Reduced Interlamellar Spacing," published in The Microstructure and Design of Alloys, Proceedings of the Third International Conference on the Strength of Metals and Alloys, Vol. 1, Institute of Metals, 1973.

5. Barkalow, R. H., Jackson, J. J., Gell, M. L., and Leverant, G. R., "Mechanical Behavior of the Directionally Solidified γ/γ′-δ Eutectic Alloy," Proceedings of the Conference on In-Situ Composites – II, Bolton Landing, New York, September 5-7, 1975. In Press.

6. Duerden, I. J. and Hume-Rothery, W., "The Equilibrium Diagram of the System Niobium-Nickel," J. Less Common Metals, Vol. 11 (1966), p. 381.

7. Iosipescu, N., "New Accurate Method for Single Shear Testing of Metals," Jour. Materials, Vol. 2, No. 3, 1967, p 537.

8. Gray, H. R. and Sanders, A., "Effect of Thermal Cycling in a Mach 0.3 Burner Rig on Properties and Structure of Directionally Solidified γ/γ′- δ Eutectic," Proceedings of the Conference on In-Situ Composites - II, Bolton Landing, New York, Sept. 5-7, 1975. In Press. See also same title, NASA TM X3271, October 1975.

9. Breinan, E. M., McCarthy, G. P., and Thompson, E. R., "The Effect of Microstructure on the Creep Behavior of Eutectic Alloys," Proceedings of the Conference on In-Situ Composites - II, Bolton Landing, New York, Sept. 5-7, 1975. In Press. See also Breinan, E. M., "Eutectic Composites," Final Technical Report, ONR Contract N00014-71-C-0393, Report No. R75-911184-16, December 1975.

10. Strangman, T. E. and Benden, R. S., "Refinement of Promising Casting Compositions for Directionally Cast Eutectics," Seventh Quarterly Technical Progress Narrative, Contract NAS3-18920, 15 April 1976.

11. Wilson, D. J., "Sensitivity of Creep-Rupture Properties of Waspaloy Sheet to Sharp-Edged Notches in the Temperature Range 1000 to 1400°F," Jour. of Basic Engineering Trans. ASME, Vol. 94, March 1972, p. 13.

## REFERENCES (Cont'd)


12. Thompson, E. R. and Kraft, E. H., "The Response of Complex Eutectic Alloys to Directional Solidification," Final Report, Contract DAHC04-72-C-0041, Army Research Office, Durham, May 1975.

13. Cline, H. E., and Walter, J. L., "The Effect of Alloy Additions on the Rod-Plate Transition of the Eutectic NiAl-Cr," Met. Trans., Vol. 1 (1970), p. 2907.

14. Lemkey, F. D. and Thompson, E. R., "Eutectic Superalloys Strengthened by $\delta_3 Ni_3 Cb$ Lamellae and $\gamma'$, $Ni_3 Al$ Precipitates," Proceedings of the Conference on In-Situ Composites, Lakeville, Conn., NMAB 308-II, Vol. 2, p. 105. Published by the National Academy of Sciences, January 1973.

15. Curran, P. M., and Erickson, J. S., "Directional Solidification of $Ni_3 Cb$ Reinforced Eutectic Turbine Blades," Final Report, Contract N00019-73-C-0252, May 1974.

16. Pederson, O. B., "Creep Strength of Discontinuous Fiber Composites," Jl. Mat. Sci., Vol. 9 (1974), p. 948.

17. Shaw, B. J., "Room Temperature Mechanical Properties of Cadmium-Zinc Lamellar Eutectic Alloys," Acta Met., Vol. 15 (1967), p. 1169.

18. Wilcox, B. A., and Clauer, A. H., "The Role of Grain Size and Shape on Strengthening of Dispersion-Hardened Nickel Alloys," Acta Met., Vol. 20, (1972), p. 743.

19. Filippi, A. M., "The Effect of Forging History on the Strengthened Microstructure of TDNiCr (Ni-20Cr-2$ThO_2$)," Met. Trans., Vol. 6A (1975), p. 2171.

20. Sheffler, K.D., Hertzberg, R. W., and Kraft, R. W., "Elevated Temperature Mechanical Properties and Fracture Behavior of a Ni-$Ni_3$ Ti Eutectic Alloy," Trans. ASM, Vol. 62, 1969, p. 105.

21. Kraft, R. W. and Albright, D. L., "Microstructure of Unidirectionally Solidified Al-$CuAl_2$ Eutectic," Trans. AIME, Vol. 221, 1961, p. 95.

22. Kraft, R. W. and Albright, D. L., "Crystallographic Substructure of Lamellar Al-$CuAl_2$ Eutectic," Trans. AIME, Vol. 224, 1962, p. 1176.

23. Kraft, R. W., Lemkey, F. D., and George, F. D., "Quantitative Metallographic Analysis of Linear Features in Anisotropic Structures. Substructure of Lamellar Eutectic Alloy". Trans. AIME, Vol. 224, 1962, p. 1037.

24. Hopkins, R. H., "A Rapid Technique for Observation of Three Dimensional Microstructures; Application to Analysis of Faulted Structure in a Eutectic Alloy" Masters Thesis, Lehigh University, January 1965.

## REFERENCES (Cont'd)


25. Malmejac, Y., "Controlled Growth of Al-$Al_2Cu$ Eutectic Crystals and Improvement of Their Morphological Stability," Proceedings of the Conference on In-Situ Composites, Bolton Landing, New York, Sept. 2-5, 1975, In Press.

26. Felten, E. J., Strangman, T. E., and Ulion, N. E., "Coatings for Directional Eutectics," Final NASA CR-134735, October 1974.

27. Hayes, C. W. and Jackson, J. J., "Applied High Temperature Technology Program," Final Technical Report AFAPL-TR-75-44, (Volume I), AFAPL Contract F33657-71-C-0789, October 1975.

28. Weibull, W., Fatigue Testing and Analysis of Results, Pergamon Press, New York, 1961, p.224.

29. Lemkey, F. D., and McCarthy, G., "Quaternary and Quinary Modifications of Eutectic Superalloys Strengthened by $\delta$, $Ni_3Cb$ Lamellae and $\gamma'$, $Ni_3Al$ Precipitates," NASA-CR-134678, February 1975.

30. Schulmeister, L. F., Cybulsky, M., and Erickson, J. S., "Reduced Cost Processing for Eutectic Airfoils," Contract F33615-74-C-5018.

31. Salkeld, R. W., Erickson, J. S., and Taylor, K. E., "Directional Solidification of $Ni_3Cb$ Reinforced Eutectic Turbine Blades," Contract No. N62269-75-C-0121.

32. Tewari, S. N. and Dreshfield, R. L., "Heat Treating of a Lamellar Eutectic Alloy ($\gamma/\gamma'$-$\delta$)," NASA TMX-71833.

33. Sheffler, K. D. and Jackson, J.J., "Stress Analysis, Thermomechanical Fatigue Evaluation, and Root Subcomponent Testing of Hollow Blades of Gamma/Gamma Prime - Delta Eutectic Alloy," Contracts NAS3-19714 and NAS3-19732, NASA CR-135005, to be published.

## TABLE I

## SUMMARY OF TESTS CONDUCTED TO CHARACTERIZE THE MECHANICAL BEHAVIOR OF CELLULAR 6CR $\gamma/\gamma' - \delta$ DIRECTIONALLY SOLIDIFIED EUTECTIC ALLOY

| Type of Test | Material | Coating[1] | Test Temperature °C | Test Temperature °F | Specimen[2] Number | Casting Type |
|---|---|---|---|---|---|---|
| Long Time Creep | 6Cr $\gamma/\gamma' - \delta$ | PWA 270 | 871 | 1600 | A74-216-02 | Bar |
| Long Time Creep | 6Cr $\gamma/\gamma' - \delta$ | PWA 270 | 871 | 1600 | A74-676-01 | Bar |
| Long Time Creep | 6Cr $\gamma/\gamma' - \delta$ | PWA 270 | 871 | 1600 | A74-676-02 | Bar |
| Long Time Rupture | 6Cr $\gamma/\gamma' - \delta$ | PWA 270 | 871 | 1600 | A74-698-02 | Bar |
| Long Time Rupture | 6Cr $\gamma/\gamma' - \delta$ | PWA 270 | 871 | 1600 | A74-698-01 | Bar |
| Long Time Rupture | 6Cr $\gamma/\gamma' - \delta$ | PWA 270 | 871 | 1600 | A74-580-02 | Bar |
| Long Time Creep | 6Cr $\gamma/\gamma' - \delta$ | PWA 270 | 1038 | 1900 | A74-573-02 | Bar |
| Long Time Creep | 6Cr $\gamma/\gamma' - \delta$ | PWA 270 | 1038 | 1900 | A74-685-02 | Bar |
| Long Time Creep | 6Cr $\gamma/\gamma' - \delta$ | PWA 270 | 1038 | 1900 | A74-685-01 | Bar |
| Long Time Rupture | 6Cr $\gamma/\gamma' - \delta$ | PWA 270 | 1038 | 1900 | A74-561-01 | Bar |
| Long Time Rupture | 6Cr $\gamma/\gamma' - \delta$ | PWA 270 | 1038 | 1900 | A74-652-01 | Bar |
| Long Time Rupture | 6Cr $\gamma/\gamma' - \delta$ | PWA 270 | 1038 | 1900 | A74-650-01 | Bar |
| Shear Strength | 6Cr $\gamma/\gamma' - \delta$ | None | 704 | 1300 | E-203-3 | Slab |
| Shear Strength | 6Cr $\gamma/\gamma' - \delta$ | None | 704 | 1300 | E-214-21 | Slab |
| Shear Strength | 6Cr $\gamma/\gamma' - \delta$ | None | 871 | 1600 | E-214-37 | Slab |
| Shear Strength | 6Cr $\gamma/\gamma' - \delta$ | None | 871 | 1600 | E-214-22 | Slab |
| Shear Strength | 6Cr $\gamma/\gamma' - \delta$ | None | 1038 | 1900 | E-203-2 | Slab |
| Shear Strength | 6Cr $\gamma/\gamma' - \delta$ | None | 1038 | 1900 | E-214-25 | Slab |
| Shear Strength | B-1900 | None | 704 | 1300 | E-571-15 | Slab[3] |
| Shear Strength | B-1900 | None | 704 | 1300 | E-571-110 | Slab[3] |
| Shear Strength | B-1900 | None | 871 | 1600 | E-571-13 | Slab[3] |
| Shear Strength | B-1900 | None | 871 | 1600 | E-571-18 | Slab[3] |
| Shear Strength | B-1900 | None | 1038 | 1900 | E-571-16 | Slab[3] |
| Shear Strength | B-1900 | None | 1038 | 1900 | E-571-19 | Slab[3] |
| Shear Creep | 6Cr $\gamma/\gamma' - \delta$ | None | 704 | 1300 | E-203-7 | Slab |
| Shear Creep | 6Cr $\gamma/\gamma' - \delta$ | None | 704 | 1300 | E-203-8 | Slab |
| Shear Creep | 6Cr $\gamma/\gamma' - \delta$ | None | 871 | 1600 | E-214-3-10 | Slab |
| Shear Creep | 6Cr $\gamma/\gamma' - \delta$ | None | 871 | 1600 | E-203-5 | Slab |
| Shear Creep | B-1900 | None | 704 | 1300 | E-571-1-7 | Slab[3] |
| Shear Creep | B-1900 | None | 704 | 1300 | E-571-1-12 | Slab[3] |
| Shear Creep | B-1900 | None | 871 | 1600 | E-571-1-11 | Slab[3] |
| Shear Creep | B-1900 | None | 871 | 1600 | E-571-1-4 | Slab[3] |

## TABLE I (Cont'd)

| Type of Test | Material | Coating[1] | Test Temperature °C | Test Temperature °F | Specimen[2] Number | Casting Type |
|---|---|---|---|---|---|---|
| Transverse Tension | 6Cr $\gamma/\gamma'$ - $\delta$ | PWA 270 | 704 | 1300 | E-134-1 | Slab |
| Transverse Tension | 6Cr $\gamma/\gamma'$ - $\delta$ | PWA 270 | 704 | 1300 | E-134-2 | Slab |
| Transverse Tension | 6Cr $\gamma/\gamma'$ - $\delta$ | PWA 270 | 1038 | 1900 | E-134-3 | Slab |
| Transverse Tension | 6Cr $\gamma/\gamma'$ - $\delta$ | PWA 270 | 1038 | 1900 | E-134-4 | Slab |
| Transverse Creep | 6Cr $\gamma/\gamma'$ - $\delta$ | PWA 270 | 704 | 1300 | E-259-3B | Slab |
| Transverse Creep | 6Cr $\gamma/\gamma'$ - $\delta$ | PWA 270 | 704 | 1300 | E-259-5B | Slab |
| Transverse Creep | 6Cr $\gamma/\gamma'$ - $\delta$ | PWA 270 | 1038 | 1900 | E-259-4B | Slab |
| Transverse Creep | 6Cr $\gamma/\gamma'$ - $\delta$ | PWA 270 | 1038 | 1900 | E-259-1A | Slab |
| Smooth-Notch Tension | 6Cr $\gamma/\gamma'$ - $\delta$ | None | 760 | 1400 | A74-055-01 | Bar |
| Smooth-Notch Tension | 6Cr $\gamma/\gamma'$ - $\delta$ | None | 760 | 1400 | A74-055-02 | Bar |
| Smooth-Notch Tension | 6Cr $\gamma/\gamma'$ - $\delta$ | None | 1038 | 1900 | A74-275-01 | Bar |
| Smooth-Notch Tension | 6Cr $\gamma/\gamma'$ - $\delta$ | None | 1038 | 1900 | A74-275-02 | Bar |
| Smooth-Notch Stress Rupture | 6Cr $\gamma/\gamma'$ - $\delta$ | None | 760 | 1400 | A74-268-01 | Bar |
| Smooth-Notch Stress Rupture | 6Cr $\gamma/\gamma'$ - $\delta$ | None | 760 | 1400 | A74-268-02 | Bar |
| Smooth-Notch Stress Rupture | 6Cr $\gamma/\gamma'$ - $\delta$ | None | 1038 | 1900 | A74-384-01 | Bar |
| Smooth-Notch Stress Rupture | 6Cr $\gamma/\gamma'$ - $\delta$ | None | 1038 | 1900 | A74-894-02 | Bar |

Notes: 1. PWA 270-electron beam vapor deposited NiCoCrAlY.

2. For Phase I castings, the first letter of the specimen identification indicates the furnace in which the Phase I castings were made, with E indicating the modified Bridgman and A the water quench Bridgman. For water quench Bridgman castings, the last number indicates the location in the casting from which the specimen was obtained, with "-01" indicating the bottom and "-02" the top of the bar. The same general scheme applies less exactly to the modified Bridgman castings, with higher suffix numbers generally indicating higher locations in the slab.

3. Conventionally cast (not directionally solidified).

TABLE II

RESULTS OF LONG TIME CREEP TESTS ON COATED CELLULAR 6 CR $\gamma/\gamma'$ - $\delta$ DS EUTECTIC ALLOY GROWN IN THE FORM OF 1.3 CM (0.5 IN.) DIAMETER BRIDGMAN BAR AT A RATE OF 3 CM/HR

| Specimen Number | Test Temperature °C | Test Temperature °F | Stress MPa | Stress ksi | 1% Creep Life, Hours | Rupture Life, Hours | Prior Creep % | % Elongation | % RA | Minimum Creep Rate, Hours$^{-1}$ |
|---|---|---|---|---|---|---|---|---|---|---|
| A74-216-02 | 871 | 1600 | 331 | 48.0 | 2280 | * | -- | -- | -- | $2.5 \times 10^{-6}$ |
| A74-676-01 | 871 | 1600 | 317 | 46.0 | 2975 | ** | -- | -- | -- | $2.3 \times 10^{-6}$ |
| A74-676-02 | 871 | 1600 | 317 | 46.0 | 2769 | ** | -- | -- | -- | $2.9 \times 10^{-6}$ |
| A74-698-02 | 871 | 1600 | 356 | 51.6 | 1073 | 1913 | 2.3 | 2.6 | 3.5 | $6.2 \times 10^{-6}$ |
| A74-698-01 | 871 | 1600 | 354 | 51.4 | 1717 | 2764 | 3.8 | 4.7 | 3.5 | $3.9 \times 10^{-6}$ |
| A74-580-02 | 871 | 1600 | 356 | 51.6 | 1874 | 3578 | 5.2 | 6.4 | 7.4 | $3.9 \times 10^{-6}$ |
| A74-573-02 | 1038 | 1900 | 94 | 13.6 | 1232 | * | -- | -- | -- | $4.5 \times 10^{-6}$ |
| A74-685-02 | 1038 | 1900 | 92 | 13.3 | 1478 | *** | -- | -- | -- | $2.4 \times 10^{-6}$ |
| A74-685-01 | 1038 | 1900 | 92 | 13.3 | 1843 | *** | -- | -- | -- | $2.5 \times 10^{-6}$ |
| A74-561-01 | 1038 | 1900 | 108 | 15.7 | 664 | 846 | 1.8 | N.M. | 8.8 | $1.2 \times 10^{-5}$ |
| A74-652-01 | 1038 | 1900 | 114 | 16.5 | 1070 | 1234 | 1.8 | 2.8 | 4.0 | $5.7 \times 10^{-6}$ |
| A74-650-01 | 1038 | 1900 | 107 | 15.6 | +++ | 2071 | +++ | 3.5 | 3.3 | +++ |

* Terminated at 1%.

** Terminated at 1% and re-tested to rupture at 871°C/446 MPa (1600°F/60 ksi nominal) – See Table III

*** Terminated at 1% and re-tested to rupture at 1037°C/152 MPa (1900°F/20 ksi nominal) – See Table III

+++ Extensometer failed.

NOTES: N. M. indicates not measured because of experimental difficulties.
Stresses based on original (uncoated) specimen diameter, adjusted for coating loss where observed (see text)
Coating: $\approx 64\mu m$ (0.0025 in.) NiCoCrAlY overlay coating
"Prior Creep" is the last extension reading obtained prior to (usually within 2 hours of) failure.

## TABLE III

## RESULTS OF STRESS RUPTURE TESTS ON COATED CELLULAR 6 Cr $\gamma/\gamma' - \delta$ DS EUTECTIC SPECIMENS WITH ≈ 1% PRIOR CREEP
(See Table II)

| Specimen Number | Temperature °C | Temperature °F | Prior Stress MPa | Prior Stress ksi | Prior Test Time at Upload, Hr | Prior Extension at Upload, Percent | Upload Stress MPa | Upload Stress ksi | Rupture Life Hrs. | Percent* Elongation | Percent* RA | Creep Rate at Upload, $Hr^{-1}$ Before | Creep Rate at Upload, $Hr^{-1}$ After | Calculated Stress Exponent | Rupture Life Fraction** Low Stress | Rupture Life Fraction** High Stress | Rupture Life Fraction** Total |
|---|---|---|---|---|---|---|---|---|---|---|---|---|---|---|---|---|---|
| A74-676-01 | 871 | 1600 | 317 | 46.0 | 2976.5 | 1.000 | 417 | 60.5 | 742.1 | 3.1 | 10.3 | $2.x310^{-6}$ | $1.3x10^{-5}$ | 6.3 | 0.49 | 0.58 | 1.07 |
| A74-676-02 | 871 | 1600 | 317 | 46.0 | 2784.1 | 1.004 | 417 | 60.5 | 601.2 | 2.7 | 8.8 | $2.9x10^{-6}$ | $1.3x10^{-5}$ | 5.5 | 0.46 | 0.47 | 0.93 |
| A74-685-02 | 1038 | 1900 | 92 | 13.3 | 1488.7 | 1.016 | 141 | 20.4 | 42.4 | 2.9 | 8.4 | $1.4x10^{-5}$ | $1.5x10^{-4}$ | 5.7 | 0.61 | 0.12 | 0.73 |
| A74-685-01 | 1038 | 1900 | 92 | 13.3 | 1855.3 | 1.028 | 141 | 20.4 | 17.1 | 3.1 | 4.3 | $2.1x10^{-5}$ | $1.8x10^{-4}$ | 5.1 | 0.76 | 0.05 | 0.81 |

* Total, Including Prior Deformation

** Ratio of Test Time Accumulated at Each Stress and Temperature to Rupture Life Predicted From Larson-Miller Curve

Material Cast in the Form of 1.3 cm (0.5 in.) Diameter Bridgman Bars Solidified at a Rate of 3 cm/hr.
Stresses Based on Original (Uncoated) Specimen Diameter, Adjusted for 1% Reduction of Cross Sectional Area Resulting From 1% Prior Creep
Coating: ≈64μm (0.0025 in.) PWA 270

## TABLE IV

## RESULTS OF IOSIPESCU-TYPE ULTIMATE SHEAR STRENGTH TESTS CONDUCTED ON CELLULAR 6 Cr $\gamma/\gamma' - \delta$ DIRECTIONALLY SOLIDIFIED EUTECTIC AND CONVENTIONALLY CAST B-1900 ALLOYS

| Specimen Number | Test Material | Test Temperature °C | Test Temperature °F | Ultimate Shear Strength MPa | Ultimate Shear Strength ksi | Shear Offset at Fracture mm | Shear Offset at Fracture in x $10^3$ | Eutectic Structure |
|---|---|---|---|---|---|---|---|---|
| E-203-3 | 6Cr $\gamma/\gamma'-\delta$ | 704 | 1300 | 302 | 43.8 | .081 | 3.2 | ≈ 75% lamellar |
| E-214-21 | 6Cr $\gamma/\gamma'-\delta$ | 704 | 1300 | 305 | 44.3 | .071 | 2.8 | fully lamellar |
| E-214-37 | 6Cr $\gamma/\gamma'-\delta$ | 871 | 1600 | 239 | 34.7 | .079 | 3.1 | ≈ 75% lamellar |
| E-214-22 | 6Cr $\gamma/\gamma'-\delta$ | 871 | 1600 | 239 | 34.7 | .064 | 2.5 | fully lamellar |
| E-203-2 | 6Cr $\gamma/\gamma'-\delta$ | 1038 | 1900 | 142 | 20.6 | .071 | 2.8 | ≈ 75% lamellar |
| E-214-25 | 6Cr $\gamma/\gamma'-\delta$ | 1038 | 1900 | 113 | 16.4 | .084 | 3.3 | fully lamellar |
| E-571-15 | B-1900 | 704 | 1300 | 720 | 104.5 | .259 | 10.2 | -- |
| E-571-110 | B-1900 | 704 | 1300 | 704 | 102.2 | .371 | 14.6 | -- |
| E-571-13 | B-1900 | 871 | 1600 | 501 | 72.7 | .216 | 8.5 | -- |
| E-571-18 | B-1900 | 871 | 1600 | 480 | 69.7 | .196 | 7.7 | -- |
| E-571-16 | B-1900 | 1038 | 1900 | 227 | 33.0 | .211 | 8.3 | -- |
| E-571-19 | B-1900 | 1038 | 1900 | 234 | 33.9 | .185 | 7.3 | -- |

Note: Eutectic alloy cast in slab form with a growth rate of 1.3 cm (0.5 in.)/hour

## TABLE V

## RESULTS OF IOSIPESCU-TYPE CREEP SHEAR TESTS CONDUCTED ON CELLULAR 6Cr $\gamma/\gamma'$ - $\delta$ DIRECTIONALLY SOLIDIFIED EUTECTIC AND CONVENTIONALLY CAST B-1900 ALLOYS

| Specimen Number | Test Material | Test Temperature °C | Test Temperature °F | Applied Shear Stress MPa | Applied Shear Stress ksi | Shear Rupture Life, Hours |
|---|---|---|---|---|---|---|
| E-203-7 | 6Cr $\gamma/\gamma'$-$\delta$ | 704 | 1300 | 172 | 25 | >3600* |
| E-203-8 | 6Cr $\gamma/\gamma'$-$\delta$ | 704 | 1300 | 172 | 25 | 1635.8 |
| E-214-310 | 6Cr $\gamma/\gamma'$-$\delta$ | 871 | 1600 | 69 | 10 | 192.3 |
| E-203-5 | 6Cr $\gamma/\gamma'$-$\delta$ | 871 | 1600 | 83 | 12 | 24.0 |
| 571-1-7 | B-1900 | 704 | 1300 | 482 | 70 | 283.4 |
| 571-1-12 | B-1900 | 704 | 1300 | 482 | 70 | 325.0 |
| 571-1-4 | B-1900 | 871 | 1600 | 220 | 32 | 107.0 |
| 571-1-11 | B-1900 | 871 | 1600 | 220 | 32 | 107.3 |

*Test discontinued

Note: Eutectic test material grown in slab form at a solidification rate of 1.3 cm (0.5 in.) per hour

## TABLE VI

## RESULTS OF TENSION TESTS ON COATED CELLULAR 6Cr $\gamma/\gamma'$ - $\delta$ DIRECTIONALLY SOLIDIFIED EUTECTIC SPECIMENS TESTED WITH THE TENSILE AXIS ORIENTED 90° TO THE GROWTH DIRECTION

| Specimen Number | Test Temperature °C | Test Temperature °F | 0.2% Yield Stress** MPa | 0.2% Yield Stress** ksi | Ultimate Strength** MPa | Ultimate Strength** ksi | Fracture Strain, % | Total Elongation % | Percent RA |
|---|---|---|---|---|---|---|---|---|---|
| E-134-1 | 704 | 1300 | N.M. | N.M. | 693 | 100.6 | 0.15 | 0.7 | Nil |
| E-134-2 | 704 | 1300 | 736 | 106.8 | 736 | 106.8 | 0.27 | 0.6 | Nil |
| E-134-3 | 1038 | 1900 | 203 | 29.5 | 265 | 38.4 | N.M. | 2.9 | 6.0 |
| E-134-4 | 1038 | 1900 | 217 | 31.5 | 261 | 37.9 | N.M. | 5.3 | Nil |

* Approximately 60$\mu$m (2.5 mils) NiCoCrAlY overlay coating
**Based on substrate (uncoated) cross sectional area.
Material grown in slab form at a rate of 1.3 cm (0.5 in.)/hour

N.M. indicates not measured

## TABLE VII

## RESULTS OF CREEP TEST CONDUCTED ON COATED CELLULAR 6Cr $\gamma/\gamma'$ - $\delta$ DIRECTIONALLY SOLIDIFIED EUTECTIC ALLOY WITH THE STRESS AXIS ORIENTED AT 90° TO THE GROWTH DIRECTION

| Specimen Number | Temperature °C | Temperature °F | Stress** MPa | Stress** ksi | 1% Creep Life, Hours | Rupture Life, Hours | Minimum Creep Rate, Hour$^{-1}$ | Percent Elongation | Percent RA |
|---|---|---|---|---|---|---|---|---|---|
| E-259-3B | 704 | 1300 | 241 | 34.9 | – | >3500*** | 6.4x10-7 | >.47 | – |
| E-259-5B | 704 | 1300 | 241 | 34.9 | – | 1681.2 | 8.1x10-7 | 0.54 | 1.70 |
| E-259-4B | 1038 | 1900 | 38.1 | 5.5 | 40 | 244.2 | 2.3x10-4 | 10.2 | 18.1 |
| E-259-1A | 1038 | 1900 | 38.1 | 5.5 | 74 | 255.6 | 1.1x10-4 | 5.1 | 9.7 |

Material grown in slab form at a rate of 1.3 cm (0.5 in.) per hour

* Approximately 60 $\mu$m (2.5 mils) NiCoCrAlY overlay coating
** Stress calculated using original (uncoated) specimen diameter
*** Test discontinued

## TABLE VIII

## COMBINATION SMOOTH-NOTCH TENSION TEST RESULTS FOR CELLULAR 6Cr $\gamma/\gamma'$ - $\delta$ DIRECTIONALLY SOLIDIFIED EUTECTIC ALLOY

| Specimen Number | Test Temperature °F | Test Temperature °C | 0.2% Y.S. ksi | 0.2% Y.S. MPa | UTS ksi | UTS MPa | Percent Elongation | Failure Location |
|---|---|---|---|---|---|---|---|---|
| A74-055-01 | 1400 | 760 | 143 | 984 | 149 | 1030 | 16.8 | Smooth |
| A74-055-02 | 1400 | 760 | 140 | 966 | 145 | 998 | – | Notch |
| A74-275-01 | 1900 | 1038 | 88.5 | 610 | 88.5 | 610 | 16.0 | Smooth |
| A74-275-02 | 1900 | 1038 | 95.1 | 656 | 96.7 | 667 | 7.3 | Smooth |

Material grown in the form of 1.3 cm (0.5 in) diameter Bridgman bars solidified at 3 cm/hr.

## TABLE IX

## RESULTS OF SMOOTH-NOTCHED STRESS-RUPTURE TESTS ON CELLULAR 6Cr $\gamma/\gamma'$ - $\delta$ DIRECTIONALLY SOLIDIFIED EUTECTIC ALLOY

| Specimen Number | Temperature °C | Temperature °F | Stress MPa | Stress ksi | Rupture Life, Hours | Percent Elongation | Failure Location |
|---|---|---|---|---|---|---|---|
| A74-268-01 | 760 | 1400 | 758 | 110 | 26.6 | – | Notch |
| A74-268-02 | 760 | 1400 | 758 | 110 | 24.4 | – | Notch |
| A74-384-01 | 1038 | 1900 | 152 | 22 | 504.2 | 7.8 | Smooth Section |
| A74-894-02 | 1038 | 1900 | 152 | 22 | 240 | – | Notch |

Material grown in the form of 1.3 cm (0.5 in) diameter Bridgman bars solidified at 3 cm/hr.

TABLE X

RESULTS OF GRADIENT DETERMINATIONS IN HIGH AND LOW GRADIENT DIRECTIONAL SOLIDIFICATION APPARATUS (GRADIENT VALUES GIVEN IN C°/cm)

High Gradient Apparatus

| Run Number | Solidification Rate cm/hr | Thermocouple Location, cm* 2.5 | 7.6 | 12.7 |
|---|---|---|---|---|
| A74-722 | 3 | 350 | -- | -- |
| A74-730 | 3 | -- | 325 | 415 |
| A74-735 | 3 | 375 | 280 | 390 |
| A74-733 | 5 | 310 | -- | -- |
| A74-733 | 10 | -- | 410 | -- |
| A74-733 | 20 | -- | -- | 390 |
| Average | | 340 | 345 | 390 |

Average of 9 determinations: 360°C/cm

Low Gradient Apparatus

| Run Number | Solidification Rate cm/hr | Thermocouple Location, cm* 2.5 | 7.6 | 12.7 |
|---|---|---|---|---|
| A74-732 | 2 | 62 | 70 | 72 |
| A74-747 | 3 | 65 | -- | -- |
| A74-747 | 6 | -- | 67 | -- |
| A74-747 | 9 | -- | -- | 70 |
| Average | | 64 | 69 | 71 |

Average of 6 determinations: 68°C/cm

*Refers to distance of thermocouple above bottom of crucible.

TABLE XI

SUMMARY OF MEASUREMENTS OF VOLUME FRACTION LAMELLAR STRUCTURE IN DIRECTIONALLY SOLIDIFIED $\gamma/\gamma' - \delta$ EUTECTIC ALLOYS

| Run No. | Wt. Pct. Chromium | Solidification Rate (R) cm/hr | Gradient (G) °C/cm | G/R | Volume Fraction Lamellar Structure | Standard Deviation | 95 Percent Confidence Interval | (G/R)/ (G/R)* |
|---|---|---|---|---|---|---|---|---|
| A74-748 | 1 | 5.0 | 360 | 72 | 1.000 | – | – | 1.31 |
| | 1 | 10.0 | 360 | 36 | 0.760 | 0.041 | 0.029 | 0.65 |
| A74-767 | 1 | 1.25 | 68 | 54 | 1.000 | – | – | 0.98 |
| | 1 | 1.50 | 68 | 45 | 0.885 | 0.040 | 0.029 | 0.82 |
| A74-745 | 3 | 3.0 | 360 | 120 | 1.000 | – | – | 1.00 |
| | 3 | 5.0 | 360 | 72 | 0.777 | 0.032 | 0.023 | 0.60 |
| A74-739 | 3 | 7.0 | 360 | 51 | 0.699 | 0.035 | 0.025 | 0.43 |
| A74-752 | 3 | 2.0 | 68 | 34 | 0.615 | 0.031 | 0.022 | 0.28 |
| | 3 | 3.0 | 68 | 23 | 0.580 | 0.029 | 0.021 | 0.19 |
| A74-761 | 6 | 2.5 | 360 | 144 | 0.980 | 0.020 | 0.014 | 0.96 |
| | 6 | 3.0 | 360 | 120 | 0.873 | 0.036 | 0.026 | 0.80 |
| | 6 | 3.5 | 360 | 103 | 0.772 | 0.038 | 0.027 | 0.69 |
| | 6 | 4.0 | 360 | 90 | 0.742 | 0.048 | 0.034 | 0.60 |
| A74-757 | 6 | 1.0 | 68 | 68 | 0.608 | 0.069 | 0.049 | 0.45 |
| | 6 | 1.5 | 68 | 45 | 0.568 | 0.064 | 0.046 | 0.30 |
| | 6 | 2.0 | 68 | 34 | 0.535 | 0.046 | 0.033 | 0.23 |

TABLE XII

SUMMARY OF INTERLAMELLAR SPACING MEASUREMENTS ON DIRECTIONALLY-SOLIDIFIED $\gamma/\gamma'$-$\delta$ EUTECTIC ALLOYS GROWN IN THE FORM OF 1.3 CM (0.5 INCH) DIAMETER BRIDGMAN BARS. MEASURED AT 200X UNLESS OTHERWISE SPECIFIED

| Run No. | Wt. % Cr | Solidification Rate (R) cm/hr | $R^{-1/2}$ $(cm/sec)^{-1/2}$ | Thermal Gradient °C/cm | Vol. Pct. Lamellar Structure | Interlamellar $\mu$m | No. of Measurements | Standard Deviation | 95% Confidence Interval |
|---|---|---|---|---|---|---|---|---|---|
| A72-623 | 0 | 10.0 | 19.0 | N.M.+ | – | 2.7*, ** | 10 | 0.5 | ± 0.3 |
| A71-651 | 0 | 2.0 | 42.2 | N.M.+ | – | 6.8 | 7 | 1.1 | ± 1.1 |
| A74-756 | 0 | 10.0 | 19.0 | 360 | – | 2.7 | 10 | 0.2 | ± 0.1 |
| | 0 | 20.0 | 13.4 | 360 | – | 2.0* | 10 | 0.5 | ± 0.4 |
| A74-774 | 0 | 20.0 | 13.4 | 360 | – | 1.9* | 10 | 0.3 | ± 0.2 |
| | 0 | 40.0 | 9.5 | 360 | – | 1.4* | 10 | 0.2 | ± 0.1 |
| A74-762 | 0 | 3.0 | 34.6 | 68 | – | 5.2 | 11 | 1.1 | ± 0.8 |
| | 0 | 5.0 | 26.8 | 68 | – | 4.4 | 10 | 1.1 | ± 0.8 |
| | 0 | 7.0 | 22.7 | 68 | – | 4.1 | 11 | 0.7 | ± 0.4 |
| A74-775 | 0 | 5.0 | 26.8 | 68 | – | 4.2 | 10 | 0.6 | ± 0.5 |
| | 0 | 7.0 | 22.7 | 68 | – | 3.7 | 11 | 0.3 | ± 0.2 |
| | 0 | 9.0 | 20.0 | 68 | – | 3.4 | 10 | 0.5 | ± 0.4 |
| A73-079 | 1 | 2.5 | 37.9 | N.M.+ | N.M. | 4.7 | 8 | 0.5 | ± 0.4 |
| A74-748 | 1 | 5.0 | 26.8 | 360 | 1.000 | 3.2 | 10 | 0.2 | ± 0.2 |
| | 1 | 10.0 | 19.0 | 360 | 0.760 | 2.7 | 10 | 0.3 | ± 0.2 |
| A74-767 | 1 | 0.71 | 71.2 | 68 | 1.000 | 9.4 | 15 | 0.8 | ± 0.5 |
| | 1 | 1.0 | 60.0 | 68 | 1.000 | 8.5 | 11 | 1.2 | ± 0.8 |
| | 1 | 1.25 | 53.7 | 68 | 1.000 | 7.6 | 10 | 0.9 | ± 0.7 |
| | 1 | 1.5 | 49.0 | 68 | 0.885 | 6.5 | 20 | 1.3 | ± 0.6 |
| A73-080 | 3 | 2.5 | 37.9 | N.M.+ | 1.000 | 4.1 | 6 | 0.3 | ± 0.3 |
| A74-739 | 3 | 7.0 | 22.7 | 360 | 0.699 | 2.3* | 13 | 0.5 | ± 0.3 |
| A74-745 | 3 | 3.0 | 34.6 | 360 | 1.000 | 3.6 | 20 | 0.4 | ± 0.2 |
| | 3 | 5.0 | 26.3 | 360 | 0.777 | 3.2 | 20 | 0.4 | ± 0.2 |
| A74-752 | 3 | 2.0 | 42.4 | 68 | 0.615 | 5.1 | 20 | 1.0 | ± 0.5 |
| | 3 | 3.0 | 34.6 | 68 | 0.581 | 4.0 | 20 | 0.5 | ± 0.2 |

TABLE XII (Cont'd)

| Run No. | Wt. % Cr | Solidification Rate (R) cm/hr | $R^{-1/2}$ $(cm/sec)^{-1/2}$ | Thermal Gradient °C/cm | Vol. Pct. Lamellar Structure | Interlamellar $\mu$m | No. of Measurements | Standard Deviation | 95% Confidence Interval |
|---|---|---|---|---|---|---|---|---|---|
| A74-363 | 6 | 2.0 | 42.4 | N. M.+ | 1.000 | 4.2 | 11 | 0.5 | ± 0.3 |
| A74-761 | 6 | 2.5 | 37.9 | 360 | 0.980 | 3.5 | 12 | 0.4 | ± 0.3 |
| | 6 | 3.0 | 34.6 | 360 | 0.873 | 3.3 | 15 | 0.4 | ± 0.3 |
| | 6 | 3.5 | 32.1 | 360 | 0.772 | 3.0 | 10 | 0.3 | ± 0.2 |
| | 6 | 4.0 | 30.0 | 360 | 0.742 | 2.7 | 11 | 0.2 | ± 0.1 |
| A74-757 | 6 | 1.0 | 60.0 | 68 | 0.608 | 7.2 | 30 | 1.9 | ± 0.7 |
| | 6 | 1.5 | 49.0 | 68 | 0.568 | 5.6 | 10 | 1.5 | ± 1.0 |
| | 6 | 2.0 | 42.4 | 68 | 0.535 | 4.8 | 20 | 1.5 | ± 1.1 |

\+ N.M. - Not Measured - Thought to be on the order of 300°C/cm.

* Measured at 1000X.

** Compares with value of 2.6 (+0.4, −0.7) reported by F. D. Lemkey[2].

TABLE XIII

RESULTS OF LINEAR REGRESSION ANALYSIS ON DS $\gamma/\gamma' - \delta$ LAMELLAR SPACING VS RATE$^{-1/2}$ DATA

| Wt. Pct. Chromium | Free Regression Coefficients | | Constrained Regression Coefficient | Lamellar Spacing Constant (C) X $10^{10}$ |
|---|---|---|---|---|
| | $b_1$ (slope) | $b_0$ (intercept) | ($b_1$) | $cm^3/sec$ X $10^{10}$ |
| 0 | 0.15459 ± 0.01659 | −0.13044 ± 0.37643 | 0.14951 ± 0.00764 | 2.235 ± 0.229 |
| 1 | 0.13995 ± 0.02036 | −0.26394 ± 0.98777 | 0.13486 ± 0.00688 | 1.819 ± 0.186 |
| 3 | 0.12581 ± 0.04569 | −0.45597 ± 1.54528 | 0.11258 ± 0.00863 | 1.267 ± 0.194 |
| 6 | 0.15318 ± 0.02099 | −2.00064 ± 0.88300** | | |
| 6 high* | 0.11497 ± 0.02900 | −0.72986 ± 1.03443 | 0.09466 ± 0.00505 | 0.896 ± 0.096 |
| 6 low* | 0.13729 ± 0.08136 | −1.06196 ± 4.16328 | | |

* 6 high – 6Cr high gradient results only
6 low – 6Cr low gradient results only
** 99% confidence interval = ± 1.33767

Free Regression Equation: $\lambda = b_0 + b_1 R^{-1/2}$

Constrained Regression Equation: $\lambda = b_1 R^{-1/2}$ ($\lambda^2 R = C = b_1^2$)

Indicated Ranges are 95% Confidence Intervals Obtained from Regression Analysis

TABLE XIV

COMPOSITION OF $\gamma/\gamma' - \delta$ EUTECTIC ALLOYS IN ATOMIC PERCENT

| Alloy | Composition, Atomic Percent | | | | |
|---|---|---|---|---|---|
| | Ni | Cb | Al | Cr | ΔCb* |
| Cr Free | 79.85 | 14.42 | 5.73 | – | 10.58 |
| 1 w/o Cr | 79.05 | 14.06 | 5.71 | 1.18 | 10.94 |
| 3 w/o Cr | 77.26 | 13.52 | 5.68 | 3.54 | 11.48 |
| 6 w/o Cr | 74.21 | 13.11 | 5.65 | 7.03 | 11.89 |

*Difference between atomic percent Cb in the liquid and in the $Ni_3Cb$ phase.

TABLE XV

SUMMARY OF VOLUME FRACTION $Ni_3Cb$ MEASUREMENTS
ON FULLY LAMELLAR STRUCTURES
(DENDRITE FREE EXCEPT AS NOTED)

| Run No. | Wt. % Cr | Solidification Rate, R cm/hr | Thermal Gradient, G °C/cm | G/R | Volume Fraction Lamellar $Ni_3Cb$ | Standard Deviation | 95% Confidence Interval | Number of Determinations |
|---|---|---|---|---|---|---|---|---|
| A74-775 | 0 | 5.0 | 68 | 14 | 0.326 | – | | 1 |
| | 0 | 7.0 | 68 | 10 | 0.358 | – | | 1 |
| | 0 | 9.0 | 68 | 8 | 0.327 | 2.6 | | 3 |
| A74-756 | 0 | 20.0 | 360 | 18 | 0.344 | 1.9 | | 5 |
| A74-774 | 0 | 40.0 | 360 | 9 | 0.343 | 1.2 | | 5 |
| (Average) | | | | | 0.340 | 1.8 | ± 0.010 | 15 |
| A74-767 | 1 | 0.7 | 68 | 96 | 0.373 | – | | 1 |
| | 1 | 1.0 | 68 | 68 | 0.363 | – | | 1 |
| | 1 | 1.25 | 68 | 54 | 0.366 | 1.2 | | 5 |
| A74-748 | 1 | 5.0 | 360 | 72 | 0.350 | 1.1 | | 5 |
| (Average) | | | | | 0.360 | 1.3 | ± 0.008 | 12 |
| A73-082 | 2 | 2.5 | * | * | 0.361** | 2.6 | ± 0.014 | 15 |
| A73-080 | 3 | 2.5 | * | * | 0.369 | 2.0 | ± 0.010 | 17 |
| A74-761 | 6 | 2.5 | 360 | 144 | 0.403 | 3.1 | ± 0.015 | 18 |

* Gradient on the order of 300C°/cm; exact value not known.

** $Ni_3Cb$ dendritic structure; 2.2 Vol. % $Ni_3Cb$ dendrites not included in indicated value.

TABLE XVI

TEST MATRIX FOR EVALUATION OF THE EFFECT OF MICROSTRUCTURE ON CREEP STRENGTH

| | Fully Lamellar | | ≈ 75% Lamellar | |
|---|---|---|---|---|
| Alloy | $\lambda \approx 2\mu m$ | $\lambda \approx 4\mu m$ | $\lambda \approx 2\mu m$ | $\lambda \approx 4\mu m$ |
| 1% Cr | | $G/R > 55C^\circ$ hr/cm$^2$<br>$G \geqslant 220C^\circ$/cm<br>R = 4 cm/hr<br>$\lambda = 4.1\mu m$ | $G/R = 30C^\circ$ hr/cm$^2$<br>$G \cong 390C^\circ$/cm<br>R = 13 cm/hr<br>$\lambda = 2.2\mu m$ | $G/R = 30C^\circ$ hr/cm$^2$<br>$G = 160C^\circ$/cm<br>R = 4 cm/hr<br>$\lambda = 4.1\mu m$ |
| 6% Cr | | $G/R > 150C^\circ$ hr/cm$^2$<br>$G \geqslant 300C^\circ$/cm<br>R = 2 cm/hr<br>$\lambda = 4.1\mu m$ | $G/R = 80C^\circ$ hr/cm$^2$<br>$G \cong 400C^\circ$/cm<br>R = 5 cm/hr<br>$\lambda = 2.2\mu m$ | $G/R = 80C^\circ$ hr/cm$^2$<br>$G \cong 160C^\circ$/cm<br>R = 2 cm/hr<br>$\lambda = 4.1\mu m$ |

TABLE XVII

COMPOSITIONS AND PROCESS CONDITIONS USED TO EVALUATE THE INFLUENCE OF LAMELLAR SPACING ON CREEP STRENGTH OF THE CHROMIUM-FREE $\gamma'/\gamma' - \delta$ DIRECTIONALLY SOLIDIFIED EUTECTIC ALLOY

| Solidification Rate, cm/hr | Columbium Level, Percent |
|---|---|
| 1 | 20.6 |
| 2 | 20.8 |
| 6 | 21.2 |
| 17 | 21.6 |
| 38 | 21.9 |
| 100 | 22.3 |

# TABLE XVIII

## CREEP TEST RESULTS ON PARTS A AND B OF TASK III MECHANICAL PROPERTY EVALUATION

| Specimen Number | Chromium Level, Percent | Growth Rate cm/hr | Test Temperature °C | Test Temperature °F | Applied Stress MPa | Applied Stress ksi | Life, Hours 1% Creep | Life, Hours Rupture | Minimum Creep Rate $Hour^{-1}$ | Prior* Creep Percent | Percent Elongation | Percent R.A. | Measured Lamellar Spacing μm | Measured Volume Fraction Cellular Structure |
|---|---|---|---|---|---|---|---|---|---|---|---|---|---|---|
| A74-1064-02 | 1 | 4 | 760 | 1400° | 758 | 110 | 129 | 202 | $3.4x10^{-5}$ | 4.1 | 5.6 | 16 | 3.7 | 0 |
| A74-1036-01 | 1 | 4 | 760 | 1400 | 758 | 110 | 148 | 227 | $2.8x10^{-5}$ | 5.7 | 6.7 | 9 | 3.9 | 0 |
| A74-1055-01 | 1 | 4 | 1038 | 1900 | 152 | 22 | 191 | 222 | $1.0x10^{-5}$ | 3.0 | 4.5 | 12 | 4.1 | 0 |
| A74-1055-02 | 1 | 4 | 1038 | 1900 | 152 | 22 | 101 | 114 | $5.1x10^{-5}$ | 1.7 | 3.2 | 38 | 3.6 | 0 |
| A75-026-01 | 6 | 2 | 760 | 1400 | 758 | 110 | 515 | 800 | $9.2x10^{-6}$ | 2.7 | 3.4 | 4 | 4.6 | 0.17** |
| A75-451-01 | 6 | 2 | 760 | 1400 | 758 | 110 | 668 | 1015 | $8.7x10^{-6}$ | 2.2 | 3.6 | 7 | 3.9 | 0 |
| A74-1020-01 | 6 | 2 | 1038 | 1900 | 152 | 22 | 510 | 556 | $1.1x10^{-5}$ | 1.7 | 4.0 | 16 | 4.0 | 0 |
| A75-421-01 | 6 | 2 | 1038 | 1900 | 152 | 22 | 138 | 252 | $5.4x10^{-5}$ | 4.5 | 6.9 | 15 | 4.0 | 0 |
| A74-1132-02 | 1 | 13 | 760 | 1400 | 758 | 110 | 60 | 105 | $9.9x10^{-5}$ | 4.3 | 4.8 | 20 | 2.7 | 0.13 |
| A74-1139-01 | 1 | 13 | 760 | 1400 | 758 | 110 | 42 | 87 | $1.4x10^{-4}$ | 4.3 | 7.2 | 4 | 2.4 | 0.14 |
| A74-1129-01 | 1 | 13 | 1038 | 1900 | 152 | 22 | 46 | 87 | $1.5x10^{-4}$ | 6.2 | 16.0 | 18 | 2.5 | 0.14 |
| A74-1129-02 | 1 | 13 | 1038 | 1900 | 152 | 22 | 64 | 114 | $1.1x10^{-4}$ | 6.2 | 11.5 | 15 | 2.6 | 0.13 |
| A75-017-01 | 6 | 5 | 760 | 1400 | 758 | 110 | 640 | 1211 | $7.8x10^{-6}$ | 3.2 | 3.8 | 5 | 2.8 | 0.27 |
| A75-011-01 | 6 | 5 | 760 | 1400 | 758 | 110 | - | 272 | $8.7x10^{-6}$ | 0.5 | 0.9 | 6 | 2.4 | 0.24 |
| A75-003-02 | 6 | 5 | 1038 | 1900 | 152 | 22 | 103 | 188 | $7.5x10^{-5}$ | 6.6 | 9.1 | 16 | 2.5 | 0.29 |
| A75-011-02 | 6 | 5 | 1038 | 1900 | 152 | 22 | 108 | 177 | $8.6x10^{-5}$ | 5.4 | 7.9 | 16 | 2.4 | 0.25 |
| E369A-02 | 1 | 4 | 760 | 1400 | 758 | 110 | 16 | 28 | $3.8x10^{-4}$ | 1.6 | 1.8 | 3 | 4.3 | 0.12 |
| E369B-01 | 1 | 4 | 760 | 1400 | 758 | 110 | 23 | 60 | $2.6x10^{-4}$ | 3.0 | 4.5 | 6 | 4.4 | 0.15 |
| E369B-02 | 1 | 4 | 1038 | 1900 | 152 | 22 | 8 | 24 | $1.5x10^{-3}$ | 7.0 | 11.5 | 7 | 4.5 | 0.13 |
| E369C-01 | 1 | 4 | 1038 | 1900 | 152 | 22 | 12 | 31 | $1.5x10^{-3}$ | 8.2 | 15.4 | 59 | 4.1 | 0.16 |
| E357-02 | 6 | 2 | 760 | 1400 | 758 | 110 | - | 254 | $1.2x10^{-5}$ | 0.6 | 1.3 | Nil | 4.3 | 0.32 |
| E370-02 | 6 | 2 | 760 | 1400 | 758 | 110 | 372 | 393 | $1.2x10^{-5}$ | 1.1 | 2.2 | 3 | 4.9 | 0.35 |
| E361-01 | 6 | 2 | 1038 | 1900 | 152 | 22 | 93 | 142 | $2.2x10^{-5}$ | 8.9 | 14.5 | 11 | 4.2 | 0.25 |
| E361-02 | 6 | 2 | 1038 | 1900 | 152 | 22 | 59 | 129 | $1.5x10^{-4}$ | 8.5 | 13.8 | 15 | 4.3 | 0.29 |
| A75-204-01 | 3 | 3 | 760 | 1400 | 758 | 110 | 294 | 406 | $1.8x10^{-5}$ | 2.2 | 3.5 | 11 | 3.7 | 0 |
| A75-301-01 | 3 | 3 | 760 | 1400 | 758 | 110 | 298 | 444 | $1.4x10^{-5}$ | 3.3 | 4.4 | 10 | 4.0 | 0 |
| A75-254-01 | 3 | 3 | 1038 | 1900 | 152 | 22 | 152 | 175 | $3.5x10^{-5}$ | 1.8 | 3.8 | 8 | 3.8 | 0 |
| A75-259-01 | 3 | 3 | 1038 | 1900 | 152 | 22 | 196 | 227 | $1.3x10^{-5}$ | 2.0 | 5.1 | 13 | 3.9 | 0 |

* Extension measured immediately prior to (within two hours of) failure

** Measured in a cellular band at the fracture surface, balance of specimen lamellar

TABLE XIX

RESULTS OF CREEP TESTS CONDUCTED ON CHROMIUM-FREE $\gamma/\gamma'$-$\delta$ EUTECTIC ALLOY AT 1038°C/152 MPa (1900°F/22 KSI)

| Specimen No. | Growth Rate cm/hr. | Lamellar* Spacing μm | Transverse* Grain Size μm | Life, Hours 1% | Life, Hours Rupture | Minimum Creep Rate $hr^{-1}$ | Prior** Creep Percent | Percent Elongation | Percent RA | Stress for*** Minimum Creep Rate of $10^{-4}$ $hr.^{-1}$ MPa | Stress for*** Minimum Creep Rate of $10^{-4}$ $hr.^{-1}$ ksi |
|---|---|---|---|---|---|---|---|---|---|---|---|
| A75-313-01 | 1 | 8.4 | 183 | 6 | 10.2 | $1.5\times10^{-3}$ | 2.6 | 6.5 | 0.9 | 91.6 | 13.3 |
| A75-313-02 | 1 | 8.4 | 168 | 4 | 10.4 | $2.6\times10^{-3}$ | 9.4 | 13.7 | 48.8 | 82.7 | 12.0 |
| A75-184-01 | 2 | 6.2 | 97.5 | 9 | 19.6 | $7.1\times10^{-4}$ | 4.7 | 10.4 | 28.4 | 105.4 | 15.3 |
| A75-184-02 | 2 | 4.8 | 78.6 | 18 | 29.9 | $3.8\times10^{-4}$ | 5.5 | 9.9 | 37.3 | 117.8 | 17.1 |
| A75-229-01 | 6 | 3.8 | 41.8 | 40 | 60.1 | $1.3\times10^{-4}$ | 3.9 | 8.4 | 10.3 | 114.7 | 21.0 |
| A75-229-02 | 6 | 3.2 | 47.9 | 50 | 75.1 | $6.8\times10^{-5}$ | 4.3 | 7.0 | 5.6 | 162.6 | 23.6 |
| A75-298-01 | 17 | 2.1 | 36.0 | 26 | 53.5 | $2.5\times10^{-4}$ | 6.0 | 11.6 | 16.4 | 127.5 | 18.5 |
| A75-298-02 | 17 | 2.1 | 37.2 | 27 | 57.4 | $2.5\times10^{-4}$ | 9.1 | 11.9 | 17.3 | 127.5 | 18.5 |
| A75-235-01 | 38 | 1.6 | 32.6 | 15 | 39.1 | $7.0\times10^{-4}$ | 5.2 | 8.8 | 7.2 | 106.1 | 15.4 |
| A75-235-02 | 38 | 1.5 | 32.9 | 13 | 37.7 | $7.8\times10^{-4}$ | 6.3 | 10.6 | 8.7 | 104.0 | 15.1 |
| A75-224-01 | 100 | 0.86 | 27.0 | 5.1 | 21.1 | $1.9\times10^{-3}$ | 4.8 | 11.1 | 9.3 | 87.5 | 12.7 |
| A75-224-02 | 100 | – | – | 1.0 | 10.2+ | $5.1\times10^{-3}$ | 6.1 | 12.5 | 1.7 | 73.7 | 10.7 |

\+ Off-axis fracture (tensile axis not aligned with growth direction).

* Measured in gage section of test specimen.

** Extension measured immediately prior to (within two hours of) failure.

*** Calculated assuming a stress exponent of 5.4.

TABLE XX

MEASUREMENT OF $\gamma'$ SIZE AS A FUNCTION OF CHROMIUM CONTENT

| Chromium Content Wt % | Solidification Rate cm/hr | $\gamma'$ Size $\mu$m |
|---|---|---|
| 0 | 6 | 0.75 |
| 1 | 4 | 0.77 |
| 3 | 3 | 0.75 |
| 6 | 2 | 0.51 |

TABLE XXI

INFLUENCE OF MICROSTRUCTURE AND CHROMIUM LEVEL ON THE 760°C (1400°F) TRANSVERSE TENSILE PROPERTIES OF THE $\gamma/\gamma'$-$\delta$ DIRECTIONALLY SOLIDIFIED EUTECTIC ALLOY

| Specimen Number | Percent Chromium | Solidification Rate | | Microstructure | 0.2% offset Yield | | Ultimate Strength | | Failure Strain |
|---|---|---|---|---|---|---|---|---|---|
| | | cm/hr | in/hr | | MPa | ksi | MPa | ksi | Percent |
| E371 B1 | 1 | 1.3 | 1/2 | Cellular | – | – | 536 | 77.8 | 0.05 |
| E371 B2 | 1 | 1.3 | 1/2 | Cellular | – | – | 426 | 61.9 | 0.01 |
| E371 B3 | 1 | 1.3 | 1/2 | Cellular | – | – | 605 | 87.8 | 0.09 |
| E371 B4 | 1 | 1.3 | 1/2 | Cellular | – | – | 491 | 71.3 | 0.05 |
| E371 B5 | 1 | 1.3 | 1/2 | Cellular | – | – | 556 | 80.7 | 0.07 |
| E318 F | 1 | 1.3 | 1/2 | Cellular, $\delta$ Dendritic | – | – | 517 | 75.0 | 0.05 |
| E318 G | 1 | 1.3 | 1/2 | Cellular, $\delta$ Dendritic | – | – | 574 | 88.3 | 0.08 |
| | | | Average | | – | – | 529 | 76.8 | 0.06 |
| | | | Standard Deviation | | – | – | 59 | 8.5 | 0.03 |
| E318 B | 1 | 30 | 12 | Cellular, fine grain | – | – | 498 | 72.3 | 0.01 |
| E318 C | 1 | 30 | 12 | Cellular, fine grain | – | – | 491 | 71.3 | 0.02 |
| E318 D | 1 | 30 | 12 | Cellular, fine grain | – | – | 451 | 65.4 | 0.03 |
| | | | Average | | – | – | 480 | 69.7 | 0.02 |
| | | | Standard Deviation | | – | – | 26 | 3.7 | 0.01 |
| E436 T1 | 1 | 1.3 | 1/2 | lamellar | 607 | 88.1 | 621 | 90.1 | 0.42 |
| E436 T2 | 1 | 1.3 | 1/2 | lamellar | 595 | 86.4 | 610 | 88.5 | 0.40 |
| E436 T3 | 1 | 1.3 | 1/2 | lamellar | 609 | 88.4 | 615 | 89.3 | 0.35 |
| E436 T4 | 1 | 1.3 | 1/2 | lamellar | 569 | 82.6 | 584 | 84.7 | 0.38 |
| E318-1 | 1 | 1.3 | 1/2 | lamellar | 628 | 91.1 | 629 | 91.3 | 0.20 |
| E318-2 | 1 | 1.3 | 1/2 | lamellar | 636 | 92.3 | 640 | 92.9 | 0.26 |
| E318-3 | 1 | 1.3 | 1/2 | lamellar | 616 | 89.4 | 640 | 92.9 | 0.36 |
| E318-4 | 1 | 1.3 | 1/2 | lamellar | 678 | 98.4 | 688 | 99.8 | 0.26 |

TABLE XXI (Cont'd)

| Specimen Number | Percent Chromium | Solidification Rate cm/hr | Solidification Rate in/hr | Microstructure | 0.2% offset Yield MPa | 0.2% offset Yield ksi | Ultimate Strength MPa | Ultimate Strength ksi | Failure Strain Percent |
|---|---|---|---|---|---|---|---|---|---|
| E318-5 | 1 | 1.3 | 1/2 | lamellar | 672 | 97.5 | 679 | 98.5 | 0.24 |
| E318-6 | 1 | 1.3 | 1/2 | lamellar | 566 | 82.1 | 595 | 86.4 | 0.28 |
| E314 H | 1 | 1.3 | 1/2 | lamellar | 598 | 86.8 | 616 | 89.4 | 0.34 |
| E314 J1 | 1 | 1.3 | 1/2 | lamellar | 609 | 88.4 | 632 | 91.7 | 0.26 |
| E435 T1 | 1 | 1.3 | 1/2 | lamellar | 610 | 88.5 | 610 | 88.5 | 0.20 |
| E435 T2 | 1 | 1.3 | 1/2 | lamellar | – | – | 591 | 85.7 | 0.15 |
| E435 T3 | 1 | 1.3 | 1/2 | lamellar | 561 | 81.4 | 585 | 84.9 | 0.32 |
| E435 T4 | 1 | 1.3 | 1/2 | lamellar | 636 | 92.3 | 636 | 92.3 | 0.24 |
| E435 T5 | 1 | 1.3 | 1/2 | lamellar | 617 | 89.5 | 625 | 90.7 | 0.24 |
| E329 B | 1 | 1.3 | 1/2 | lamellar, δ dendritic | 595 | 86.3 | 595 | 86.3 | 0.20 |
| | | | Average | | 612 | 88.8 | 622 | 90.2 | 0.28 |
| | | | Standard Deviation | | 32 | 4.7 | 29 | 4.2 | 0.08 |
| E355 E | 1 | 0.6 | 1/4 | lamellar | – | – | 616 | 89.4 | 0.18 |
| E355 G | 1 | 0.6 | 1/4 | lamellar | 640 | 92.9 | 640 | 92.9 | 0.21 |
| | | | Average | | 640 | 92.9 | 628 | 91.2 | 0.20 |
| | | | Standard Deviation | | – | – | 17 | 2.5 | 0.02 |
| E363 T6 | 6 | 1.3 | 1/2 | Cellular | 610 | 88.5 | 652 | 94.7 | 0.27 |
| E525 C | 6 | 1.3 | 1/2 | Cellular | – | – | 600 | 87.1 | 0.17 |
| E525 E | 6 | 1.3 | 1/2 | Cellular | – | – | 639 | 92.7 | 0.12 |
| E525 F | 6 | 1.3 | 1/2 | Cellular | – | – | 641 | 93.0 | 0.19 |
| E625 G | 6 | 1.3 | 1/2 | Cellular | – | – | 645 | 93.6 | 0.19 |
| E525 H | 6 | 1.3 | 1/2 | Cellular | 628 | 91.2 | 637 | 92.4 | 0.23 |
| E525 K | 6 | 1.3 | 1/2 | Cellular | – | – | 656 | 95.2 | 0.14 |
| E525 L | 6 | 1.3 | 1/2 | Cellular | – | – | 626 | 90.9 | 0.12 |
| | | | Average | | | | 637 | 92.5 | 0.18 |
| | | | Standard Deviation | | | | 18 | 2.5 | 0.05 |

TABLE XXI (Cont'd)

| Specimen Number | Percent Chromium | Solidification Rate cm/hr | Solidification Rate in/hr | Microstructure | 0.2% offset Yield MPa | 0.2% offset Yield ksi | Ultimate Strength MPa | Ultimate Strength ksi | Failure Strain Percent |
|---|---|---|---|---|---|---|---|---|---|
| E497 T2 | 6 | 0.6 | 1/4 | Lamellar | 651 | 94.5 | 681 | 98.8 | 0.35 |
| E497 T3 | 6 | 0.6 | 1/4 | Lamellar | 670 | 97.2 | 670 | 97.2 | 0.20 |
| E434 T1 | 6 | 0.6 | 1/4 | Lamellar | 627 | 91.0 | 652 | 94.7 | 0.35 |
| E434 T2 | 6 | 0.6 | 1/4 | Lamellar | 627 | 91.0 | 652 | 94.7 | 0.32 |
| E363 T1 | 6 | 0.6 | 1/4 | Lamellar | 629 | 91.2 | 652 | 94.6 | 0.39 |
| E363 T2 | 6 | 0.6 | 1/4 | Lamellar | 656 | 95.2 | 684 | 99.2 | 0.42 |
| E433 T1 | 6 | 0.6 | 1/4 | Lamellar | 629 | 91.2 | 643 | 93.2 | 0.27 |
| E433 T2 | 6 | 0.6 | 1/4 | Lamellar | 596 | 86.4 | 621 | 90.0 | 0.40 |
| E433 T3 | 6 | 0.6 | 1/4 | Lamellar | 635 | 92.1 | 653 | 94.7 | 0.30 |
| E433 T4 | 6 | 0.6 | 1/4 | Lamellar | 617 | 89.5 | 654 | 94.9 | 0.40 |
| E433 T5 | 6 | 0.6 | 1/4 | Lamellar | 631 | 91.5 | 665 | 96.5 | 0.38 |
| E447 B | 6 | 0.6 | 1/4 | Lamellar | 566 | 82.1 | 624 | 90.5 | 0.44 |
| E447 K | 6 | 0.6 | 1/4 | Lamellar | 654 | 94.9 | 755 | 109.6 | 0.55 |
| E448 B | 6 | 0.6 | 1/4 | Lamellar | 647 | 93.9 | 658 | 95.5 | 0.26 |
| E448 H | 6 | 0.6 | 1/4 | Lamellar | 728 | 105.7 | 754 | 109.4 | 0.35 |
| E452 B | 6 | 0.6 | 1/4 | Lamellar | 448 | 65.0 | 465 | 67.5 | 0.25 |
| E452 E | 6 | 0.6 | 1/4 | Lamellar | – | – | 607 | 88.1 | 0.14 |
| E452 G | 6 | 0.6 | 1/4 | Lamellar | – | – | 618 | 89.7 | 0.19 |
| | | | Average | | 625 | 90.8 | 650 | 94.4 | 0.33 |
| | | | Standard Deviation | | 59 | 8.5 | 61 | 8.9 | 0.10 |
| E341 A | 6 | 1.3 | 1/2 | Cellular, δ Dendritic | – | – | 522 | 75.8 | 0.03 |
| E341 B | 6 | 1.3 | 1/2 | Cellular, δ Dendritic | – | – | 527 | 76.6 | 0.02 |
| E341 C | 6 | 1.3 | 1/2 | Cellular, δ Dendritic | – | – | 545 | 79.1 | 0.06 |
| E372 B | 6 | 1.3 | 1/2 | Cellular, δ Dendritic | – | – | 385 | 55.9 | 0.02 |
| E402 K | 6 | 25 | 10 | Cellular, fine grain | – | – | 396 | 57.5 | 0.01 |
| E402 L | 6 | 25 | 10 | Cellular, fine grain | – | – | 476 | 69.1 | 0.02 |
| E497 T1 | 6 | 0.6 | 1/4 | Cellular | – | – | 557 | 80.9 | 0.08 |

## TABLE XXII

## RESULTS OF TRANSVERSE CREEP TESTS CONDUCTED ON DIRECTIONALLY SOLIDIFIED $\gamma/\gamma'$ -$\delta$ ALLOY

| Casting Number | Charge Composition Percent Cb | Cr | C | Rate Solidification cm/hr | in/hr | Specimen Identification | Microstructure | Stress MPa | KSI | Temperature °C | °F | Rupture Life Hours | Prior Creep Percent | Total Elongation Percent | Parameter $To_R(20+\log t)$ |
|---|---|---|---|---|---|---|---|---|---|---|---|---|---|---|---|
| E288 | 21.2 | 1 | -- | 1.3 | 1/2 | 8 | lamellar | 413 | 60 | 760 | 1400 | 0.1 | 0.2 | 1.1 | 35.3 |
| | | | | | | 10 | lamellar | 345 | 50 | 760 | 1400 | 1.9 | 0.8 | 0.3 | 37.7 |
| | | | | | | 9 | lamellar | 310 | 45 | 760 | 1400 | 12.3 | 0.8 | 1.6 | 39 |
| | | | | | | 11 | lamellar | 276 | 40 | 760 | 1400 | 36.5 | 1.6 | 2.1 | 40 |
| E406 | 21.0 | 1 | -- | 1.3 | 1/2 | G | lamellar | 310 | 45 | 700 | 1300 | 458 | 2.5 | N.M. | 39.9 |
| | | | | | | F | lamellar | 310 | 45 | 700 | 1300 | Broken in Set-up | | | |
| | | | | | | H | lamellar | 41.3 | 6 | 1038 | 1900 | 55.2 | 26.6 | 27.1 | 51.3 |
| | | | | | | E | lamellar | 41.3 | 6 | 1038 | 1900 | Broken in Set-up | | | |
| E384 | 20.5 | 3 | -- | 1.0 | 3/8 | B | lamellar | 345 | 50 | 700 | 1300 | 151.8 | | N.M. | 39.0 |
| | | | | | | C | lamellar | 310 | 45 | 700 | 1300 | 318.4 | 2.6 | 5.6 | 39.6 |
| | | | | | | D | lamellar | 41.3 | 6 | 1038 | 1900 | 44.1 | | 22.5 | 51.1 |
| | | | | | | E | lamellar | 41.3 | 6 | 1038 | 1900 | 44.7 | | 12.8 | 51.1 |
| E259 | 20.0 | 6 | -- | 1.3 | 1/2 | 3B | cellular | 241 | 34.9 | 700 | 1300 | >3500 | >0.47 | | >41.1 |
| | | | | | | 5B | cellular | 241 | 34.9 | 700 | 1300 | 1681 | 0.54 | | 40.9 |
| | | | | | | 4B | cellular | 38.1 | 5.5 | 1038 | 1900 | 244 | 10.2 | | 52.8 |
| | | | | | | 1A | cellular | 38.1 | 5.5 | 1038 | 1900 | 256 | 5.1 | | 52.9 |
| E363 | 20.0 | 6 | -- | 1.3 | 1/2 | T5 | cellular | 310 | 45 | 760 | 1400 | 5.1 | 0.63 | 0.8 | 38.0 |
| E363 | 20.0 | 6 | -- | 0.6 | 1/4 | T3 | lamellar | 310 | 45 | 760 | 1400 | 51.0 | .68 | 1.0 | 40.4 |
| E407 | 20.0 | 6 | -- | 0.6 | 1/4 | F | lamellar | 345 | 50 | 700 | 1300 | 18.8 | | 1.7 | 37.4 |
| | | | | | | D | lamellar | 310 | 45 | 700 | 1300 | 267.0 | 1.2 | 2.1 | 39.5 |
| | | | | | | C | lamellar | 41.3 | 6 | 1038 | 1900 | Broken in Set-up | | | |
| | | | | | | E | lamellar | 41.3 | 6 | 1038 | 1900 | 279.3 | | 24.0 | 53.0 |
| E434 | 20.0 | 6 | -- | 0.6 | 1/4 | T3 | lamellar | 310 | 45 | 760 | 1400 | 4.4 | | 1.5 | 38.4 |

TABLE XXIII

RESULTS OF LONGITUDINAL TENSION TESTS CONDUCTED ON THE PHASE II MECHANICAL PROPERTY EVALUATION

| Specimen Number | Chromium Content Percent | Surface Condition | Test Temperature °C | Test Temperature °F | 0.2% Offset Yield Strength MPa | 0.2% Offset Yield Strength ksi | Ultimate Tensile Strength MPa | Ultimate Tensile Strength ksi | Percent Elongation | Percent R.A. |
|---|---|---|---|---|---|---|---|---|---|---|
| A75-354-01 | 1 | Bare | 316 | 600 | 985 | 142.9 | 1115 | 161.8 | 24.5 | 20.4 |
| A75-359-02 | 1 | Bare | 316 | 600 | 1017 | 147.6 | 1088 | 157.9 | 9.4 | 20.6 |
| A75-363-01 | 1 | Bare | 482 | 900 | 995 | 142.7 | 1289 | 187.1 | 48.7 | 34.6 |
| A75-370-01 | 1 | Bare | 482 | 900 | 995 | 144.4 | 1312 | 190.4 | 48.4 | 32.5 |
| A75-363-02 | 1 | Bare | 650 | 1200 | 891 | 129.3 | 1084 | 157.4 | 15.3 | 40.0 |
| A75-370-02 | 1 | Bare | 650 | 1200 | 959 | 139.2 | 1094 | 158.8 | 24.4 | 37.6 |
| A75-351-01 | 1 | Coated | 316 | 600 | -- | -- | 994 | 144.2 | 0.2* | -- |
| A75-351-02 | 1 | Coated | 316 | 600 | 1071 | 155.4 | 1183 | 171.7 | 6.4 | 10.5 |
| A75-375-01 | 1 | Coated | 482 | 900 | 1062 | 154.1 | 1219 | 176.9 | 7.1 | 7.9 |
| A75-377-01 | 1 | Coated | 482 | 900 | 1052 | 152.7 | 1232 | 178.8 | 14.8 | 19.4 |
| A75-379-01 | 1 | Coated | 650 | 1200 | 1023 | 148.5 | 1171 | 169.9 | 10.6 | 16.5 |
| A75-379-02 | 1 | Coated | 650 | 1200 | 985 | 142.9 | 1149 | 166.8 | 11.5 | 19.1 |
| A75-505-01 | 6 | Bare | 316 | 600 | 978 | 141.9 | 1094 | 158.8 | 3.9 | 9.7 |
| A75-516-01 | 6 | Bare | 316 | 600 | 1013 | 147.0 | 1110 | 161.1 | 4.5 | 9.1 |
| A75-412-01 | 6 | Bare | 482 | 900 | 980 | 142.2 | 1142 | 165.7 | 24.0 | 22.8 |
| A75-449-01 | 6 | Bare | 482 | 900 | 954 | 138.5 | 1095 | 158.9 | 12.5 | 13.9 |
| A75-467-01 | 6 | Bare | 650 | 1200 | 782 | 113.5 | 1129 | 163.8 | 18.5 | 32.2 |
| A75-481-01 | 6 | Bare | 650 | 1200 | 927 | 134.6 | 1122 | 162.8 | 18.6 | 30.8 |

TABLE XXIII

| Specimen Number | Chromium Content Percent | Surface Condition | Test Temperature °C | Test Temperature °F | 0.2% Offset Yield Strength MPa | 0.2% Offset Yield Strength ksi | Ultimate Tensile Strength MPa | Ultimate Tensile Strength ksi | Percent Elongation | Percent R.A. |
|---|---|---|---|---|---|---|---|---|---|---|
| A75-501-01 | 6 | Coated | 316 | 600 | 991 | 143.9 | 1109 | 160.9 | 3.4 | 10.4 |
| A75-470-01 | 6 | Coated | 316 | 600 | 1031 | 149.6 | 1145 | 166.2 | 4.6 | 7.1 |
| A75-443-01 | 6 | Coated | 482 | 900 | 939 | 136.3 | 1109 | 160.9 | 6.9 | 15.8 |
| A75-511-01 | 6 | Coated | 482 | 900 | 1060 | 153.8 | 1268 | 184.0 | 6.6 | 2.6 |
| A75-446-01 | 6 | Coated | 650 | 1200 | 928 | 134.7 | 1139 | 165.3 | 12.2 | 18.6 |
| A75-460-01 | 6 | Coated | 650 | 1200 | 923 | 133.9 | 1104 | 160.2 | 4.7 | 9.3 |

*Failed at microstructural defect.

TABLE XXIV

COMPOSITIONS AND SOLIDIFICATION RATES FOR DIRECTIONALLY SOLIDIFIED $\gamma/\gamma'$-$\delta$ THERMAL FATIGUE WEDGE BLANKS

| Composition, Percent | | | | Solidification Rate | |
|---|---|---|---|---|---|
| Ni | Cb | Al | Cr | cm/hr | in/hr |
| Bal. | 21.3 | 2.5 | 0 | 3.2 | 1.25 |
| Bal. | 21.2 | 2.5 | 1 | 2.5 | 1.00 |
| Bal. | 20.5 | 2.5 | 3 | 1.9 | 0.75 |
| Bal. | 20.0 | 2.5 | 6 | 1.3 | 0.50 |

TABLE XXV

RESULTS OF FLUIDIZED BED THERMAL FATIGUE TESTS ON $\gamma/\gamma'$-$\delta$ ALLOY

| Specimen Number | Chromium Level (Percent) | Pinpoint Indication | Cycles to Indicated Crack Length | | | Total Cycles Applied |
|---|---|---|---|---|---|---|
| | | | 0.4 mm (1/64 in.) | 0.8 mm (1/32 in.) | 1.6 mm (1/16 in.) | |
| Series I** | | | | | | |
| E354 A1 | 0 | >80 | 140 | 800 | – | 1146 |
| E346 A1 | 1 | 180 | 260 | 593* | 926 | 1146 |
| E351 A1 | 3 | 260 | 475* | 691 | – | 1146 |
| E340 A1 | 6 | >100 | 140 | 791 | – | 1146 |
| Series II | | | | | | |
| E354 A2 | 0 | 288 | 363* | 438 | – | 588 |
| E346 B1 | 1 | 288 | 363* | 438 | 588 | 588 |
| E351 B1 | 3 | 288 | 363* | 438 | 588 | 588 |
| E340 A2 | 6 | 288 | 338* | 388* | 438 | 588 |
| Series III | | | | | | |
| E354 B2 | 0 | 50 | 150 | 250 | 550 | 1000 |
| E346 B2 | 1 | >250 | 350 | 550 | 1000 | 1000 |
| E351 B2 | 3 | 50 | 150 | 250 | 550 | 1000 |
| E340 B1 | 6 | 250 | 350 | 450 | 550 | 1000 |

* Interpolated

** Not valid data because of simultaneous occurrence of longitudinal cracking (see text).

TABLE XXVI

AVERAGE OF SECOND AND THIRD SERIES OF THERMAL FATIGUE TESTS

| Chromium Level Percent | Cycles to Indicated Crack Size | | | |
|---|---|---|---|---|
| | Pinpoint | 0.4 mm (1/64 in.) | 0.8 mm (1/32 in.) | 1.6 mm (1/16 in.) |
| 0 | 169 | 256 | 344 | 569 |
| 1 | 294 | 356 | 494 | 794 |
| 3 | 169 | 256 | 344 | 569 |
| 6 | 269 | 344 | 419 | 494 |

TABLE XXVII

SLAB CASTINGS EVALUATED IN PHASE III
(SEE APPENDIX A FOR COMPLETE COMPOSITIONS AND PROCESSING DETAILS)

| Alloy Modification | Chromium Level of Base Composition | | | |
|---|---|---|---|---|
| | 1 Percent | | 6 Percent | |
| None | F1665 | | D2-40 | |
| | E355 | | E447 | |
| | | | E448 | |
| | | | E452 | |
| | | | E493 | |
| | | | E517 | |
| | | | E523 | |
| Carbon | E313 | 0.10% C | E319 | 0.10% C |
| | E314 | 0.02% C | E320 | 0.02% C |
| | E385 | 0.10% C | E372 | 0.10% C |
| | E389 | 0.15% C | E388 | 0.10% C |
| | E394 | 0.08% C | E416 | 0.10% C |
| | E418 | 0.10% C | E453 | 0.06% C |
| | E420 | 0.20% C | E459 | 0.08% C |
| | E421 | 0.10% C | E468 | 0.04% C |
| | E422 | 0.05% C | E469 | 0.08% C |
| | E423 | 0.08% C | E471 | 0.10% C |
| | E424 | 0.10% C | E472 | 0.12% C |
| | E425 | 0.10% C | E473 | 0.10% C |
| | E426 | 0.15% C | | |
| | E432 | 0.10% C | | |
| Boron | E323 | 0.04% B | E333 | 0.05% B |
| | E324 | 0.01% B | E334 | 0.01% B |
| | E382 | 0.06% B | | |
| | E398 | 0.02% B | | |
| Zirconium | E315 | 0.10% Zr | E268 | 0.10% Zr |
| | E383 | 0.2% Zr | E332 | 0.10% Zr |
| | E427 | 0.2% Zr | E365 | 0.20% Zr |
| | E437 | 0.2%Zr | | |
| Hafnium | E312 | 1.0% Hf | E322 | 1.0% Hf |
| | E353 | 1.0% Hf | | |
| | E359 | 1.0% Hf | | |
| Tantalum | E414 | 3.0% Ta | E419 | 3.0% Ta |
| | E417 | 3.0% Ta | | |
| | E450 | 3.0% Ta | | |

TABLE XXVII (continued)

| Alloy Modification | Chromium Level of Base Composition | | | |
|---|---|---|---|---|
| | 1 Percent | | 6 Percent | |
| Carbon + Boron | E397 | 0.08% C + 0.06% B | E368 | 0.05% C + 0.02% B |
| Carbon + Zirconium | E395 | 0.08% C + 0.2% Zr | E366 | 0.02% C + 0.2% Zr |
| | E428 | 0.08% C + 0.2% Zr | | |
| Carbon + Hafnium | E328 | 0.05% C + 0.6% Hf | E339 | 0.05% C + 0.6% Hf |
| | E391 | 0.08% C + 1.0% Hf | E367 | 0.10% C + 0.6% Hf |
| | E392 | 0.15% C + 1.0% Hf | | |
| Carbon + Tantalum | E431 | 0.10% C + 3.0% Ta | E430 | 0.10% C + 3.0% Ta |
| Boron + Zirconium | E325 | 0.02% B + 0.06% Zr | E338 | 0.02% B + 0.06% Zr |
| | E396 | 0.06% B + 0.2% Zr | | |

TABLE XXVIII

RESULTS OF ELECTRON PROBE MICROANALYSIS OF UNIDENTIFIED PHASE IN CASTING E-312 (Ni-21.2%Cb-2.5%Al-1%Hf)

| | Composition | | | | | |
|---|---|---|---|---|---|---|
| | Atomic Percent | | | Weight Percent | | |
| Element | δ Phase | Unidentified Phase | γ/γ′ Matrix | δ Phase | Unidentified Phase | γ/γ′ Matrix |
| Ni | 77.1 | 78.5 | 83.5 | 70 | 80 | 83 |
| Cb | 20.9 | 8.1 | 7.6 | 30 | 13 | 12 |
| Al | 1.2 | 10.7 | 6.6 | 0.5 | 5 | 3 |
| Cr | 0.6 | 1.1 | 2.3 | 0.5 | 1 | 2 |
| Hf | 0.2 | 1.6 | 0 | 0.5 | 5 | 0.1 |

TABLE XXIX

INFLUENCE OF CARBON LEVEL ON THE 760°C (1400°F) TRANSVERSE FRACTURE STRAIN OF THE 1% Cr $\gamma/\gamma'$-$\delta$ DIRECTIONALLY SOLIDIFIED EUTECTIC ALLOY (FOR COMPLETE TEST RESULTS SEE APPENDIX G)

| Specimen Number | Analyzed Carbon (Percent) | Fracture Strain (Percent) | Average |
|---|---|---|---|
| E418T1 | 0.08 | 0.40 | 0.36 |
| E418T2 | 0.08 | 0.26 | |
| E418T3 | 0.08 | 0.40 | |
| E432T2 | 0.08 | 0.38 | |
| E313H | 0.07[1] | 0.76 | 0.42 |
| E313J | 0.07[1] | 0.48 | |
| E385B | 0.07[1] | 0.30 | |
| E385C | 0.07[1] | 0.31 | |
| E385D | 0.07[1] | 0.23 | |
| E385E | 0.07[1] | 0.38 | |
| E423T1 | 0.07 | 0.25 | |
| E423T2 | 0.07 | 0.56 | |
| E418T4 | 0.07 | 0.39 | |
| E418T5 | 0.07 | 0.53 | |
| E418T6 | 0.06 | 0.45 | 0.45 |
| E394F | 0.05[1] | 0.53 | 0.59 |
| E394G | 0.05[1] | 0.54 | |
| E389F | 0.05[1] | 0.75 | |
| E389G | 0.05[1] | 0.54 | |
| E422T1 | 0.03 | 0.30 | 0.28 |
| E422T2 | 0.03 | 0.34 | |
| E426T2 | 0.03 | 0.21 | |
| E426T1 | 0.02 | 0.22 | 0.22 |
| Average Base Composition (Phase II Results) | | | 0.22 |

[1] Estimated from Slab Analysis

TABLE XXX

INFLUENCE OF CARBON LEVEL ON THE 760°C (1400°F) TRANSVERSE FRACTURE STRAIN OF THE 6% Cr $\gamma/\gamma'$-$\delta$ DIRECTIONALLY SOLIDIFIED EUTECTIC ALLOY (FOR COMPLETE TEST RESULTS SEE APPENDIX G)

| Specimen Number | Analyzed Carbon (Percent) | Fracture Strain (Percent) | Average |
|---|---|---|---|
| E416C | 0.10 | 0.60 | |
| E416B | 0.10 | 0.46 | 0.51 |
| E459F | 0.10 | 0.46 | |
| E473F | 0.09 | 0.34 | 0.34 |
| E472F | 0.08 | 0.60 | |
| E472G | 0.08 | 0.29 | |
| E472H | 0.08 | 0.26 | |
| E459H | 0.08 | 0.35 | 0.53 |
| E416E | 0.08 | 0.69 | |
| E471H | 0.08 | 0.82 | |
| E471J | 0.08 | 0.69 | |
| E459K | 0.07 | 0.46 | |
| E469K2 | 0.07 | 0.32 | |
| E469K5 | 0.07 | 0.35 | |
| E469K6 | 0.07 | 0.45 | |
| E416G | 0.07[1] | 0.30 | 0.45 |
| E473K | 0.07 | 0.90 | |
| E472J | 0.07 | 0.34 | |
| E453F | 0.06 | 0.45 | |
| E388C | 0.06[1] | 1.02 | 0.52 |
| E388E | 0.06[1] | 0.20 | |
| E416J | 0.06 | 0.40 | |
| E453G | 0.05 | 0.59 | 0.45 |
| E453H | 0.05 | 0.30 | |
| E468H | 0.03 | 0.53 | 0.60 |
| E468J | 0.03 | 0.66 | |
| E468G | 0.02 | 0.44 | 0.44 |
| Base Composition Average (Phase II Results) | | | 0.33 |

1)Estimated from Slab Analysis

TABLE XXXI

RESULTS OF $Ni_3Cb$ X-RAY LATTICE PARAMETER MEASUREMENTS IN 6% Cr BASE COMPOSITION AND CARBON MODIFIED DIRECTIONALLY SOLIDIFIED EUTECTIC ALLOYS

| Lattice Vector | Lattice Parameter, m X $10^{10}$ | |
|---|---|---|
| | Base Composition[1] | Carbon Modified[2] |
| a | 5.1055 | 5.1077 |
| b | 4.2384 | 4.2337 |
| c | 4.5416 | 4.5440 |
| Unit Cell Volume ($m^3$ x $10^{30}$) | 98.276 | 98.262 |

0.02% difference

[1]Average of 2 measurements
[2]Average of 3 measurements

TABLE XXXII

INFLUENCE OF SOLIDIFICATION RATE ON THE 1038°C/152 MPa (1900°F/22KSI) RUPTURE LIFE OF FULLY LAMELLAR 1% Cr $\gamma/\gamma'$-$\delta$ ALLOY

| Solidification Rate | | Rupture Life, Hours | |
|---|---|---|---|
| cm/hr. | in./hr. | Base Composition | Carbon Modified |
| 0.6 | 1/4 | 30 | --- |
| 1.3 | 1/2 | 30 | 31 |
| 1.9 | 3/4 | ---- | 27 |
| 2.5 | 1.0 | ---- | 27 |

TABLE XXXIII

INFLUENCE OF TANTALUM ON THE RUPTURE LIFE (IN HOURS) OF $\gamma/\gamma$- $\delta$ DIRECTIONALLY SOLIDIFIED EUTECTIC ALLOY

| Chromium Level Percent | Creep[1] Test Conditions | Cellular Microstructure | | | | Lamellar Microstructure | | | |
|---|---|---|---|---|---|---|---|---|---|
| | | Base Composition | Ta Modified | C Modified | Ta + C Modified | Base Composition | Ta Modified | C Modified | Ta + C Modified |
| | A | 0.4 | 0.5 | --- | 0.1 | 36 | --- | 30[2] | --- |
| 6 | B | 57 | 21 | --- | 27 | 53 | --- | 40 | --- |
| | C | 96 | 88 | --- | 57 | 110[2] | --- | 105 | --- |
| | A | --- | 0.6 | --- | --- | 20[2] | 18 | 19 | 0.8 |
| 1 | B | --- | 16 | --- | --- | 10 | 11 | 9 | 10 |
| | C | --- | 35 | --- | --- | 30 | 43 | 28 | 26 |

[1]Test Conditions:
- A 760°C/758 MPa (1400°F/110 KSI)
- B 982°C/276 MPa (1800°F/40 KSI)
- C 1038°C/152 MPa (1900°F/22 KSI)

[2]Estimated from Larson-Miller Plot

TABLE XXXIV

INFLUENCE OF TANTALUM ON THE 760°C (1400°F) TRANSVERSE FRACTURE STRAIN (IN PERCENT) OF THE $\gamma/\gamma' \cdot \delta$ DIRECTIONALLY SOLIDIFIED EUTECTIC ALLOY

| | Cellular Microstructure | | | | Lamellar Microstructure | | | |
|---|---|---|---|---|---|---|---|---|
| Level Percent | Base Composition | Ta Modified | C Modified | Ta + C Modified | Base Composition | Ta Modified | C Modified | Ta + C Modified |
| 6 | 0.18 | 0.07 | 0.25 | 0.07 | 0.33 | --- | 0.49 | --- |
| 1 | 0.06 | 0.01 | --- | --- | 0.28 | 0.13 | 0.44 | 0.18 |

TABLE XXXV

THERMAL TREATMENTS INVESTIGATED IN TASK IV

| Thermal Treatment Code | Exposure Time Hours | Treatment Temperature °C | Treatment Temperature °F |
|---|---|---|---|
| 2200(4) | 4 | 1204 | 2200 |
| 2110(4) | 4 | 1154 | 2110 |
| 1975(4) | 4 | 1079 | 1975 |
| 1650(24) | 24 | 899 | 1650 |
| 1600(24) | 24 | 871 | 1600 |

TABLE XXXVI

SUMMARY OF HEAT TREATMENT RESULTS

| Thermal[1] Treatment Code | Fracture Strain, Percent Baseline | Fracture Strain, Percent Carbon Modified |
|---|---|---|
| As Cast[2] | 0.33 | 0.49 |
| 2200(4) | 0.26 | 0.23 |
| 2110(4) | 0.31 | 0.29 |
| 1975(4) | 0.32 | 0.47 |
| 1650(24) | 0.54 | 0.44 |
| 2200(4)+1600(24) | 0.20 | 0.33 |
| 2110(4)+1650(24) | 0.58 | 0.42 |
| 1975(4)+1650(24) | 0.47 | 0.45 |

[1]For explanation of thermal treatment code see Table XXXV

[2]Average results from Phase II

TABLE XXXVII

RESULTS OF TRANSVERSE TENSION TESTS ON FULLY LAMELLAR 6% Cr $\gamma/\gamma'$-$\delta$ DIRECTIONALLY SOLIDIFIED EUTECTIC ALLOY WITH AND WITHOUT CARBON. ALL SPECIMENS COATED WITH ≈60 μm (2.5 mils) PWA 270 NiCoCrAlY OVERLAY COATING. MATERIAL CAST IN SLAB FORM DIRECTIONALLY SOLIDIFIED AT A RATE OF 0.6 cm (0.25 inch) PER HOUR.

| Specimen Identification | Material [1] | Thermal Treatment Code [2] | Test Temperature °C | Test Temperature °F | Ultimate Strength MPa | Ultimate Strength KSI | 0.2% Yield Strength MPa | 0.2% Yield Strength KSI | Fracture Strain Percent |
|---|---|---|---|---|---|---|---|---|---|
| E466J | B | 1975(4) + 1650 (24) | 760 | 1400 | 715 | 103.8 | 689 | 100.0 | 0.53 |
| E480B | B | 1975(4) + 1650 (24) | 760 | 1400 | 635 | 92.1 | 602 | 87.4 | 0.55 |
| E535G | C | 1975(4) | 760 | 1400 | 753 | 109.3 | 734 | 106.5 | 0.35 |
| E511F | C | 1975(4) | 760 | 1400 | 752 | 109.1 | 716 | 103.9 | 0.55 |
| E511L | C | 1975(4) | 760 | 1400 | 722 | 104.8 | 678 | 98.4 | 0.58 |
| E501G | C | 1975(4) | 760 | 1400 | 686 | 99.6 | 640 | 92.9 | 0.58 |
| E511J | C | 1975(4) | 760 | 1400 | 797 | 115.7 | 749 | 108.7 | 0.75 |
| E501F | C | 1975(4) | 760 | 1400 | 749 | 108.7 | 695 | 100.9 | 0.87 |
| E535E | C | 1975(4) | 760 | 1400 | 787 | 114.2 | 724 | 105.1 | 1.20 |
| E511G | C | 1975(4) | 760 | 1400 | 783 | 113.7 | 719 | 104.3 | 1.35 |
| E511H | C | 1975(4) | 760 | 1400 | 762 | 110.6 | 739 | 107.3 | 1.38 |
| E480D | B | 1975(4) + 1650 (24) | 1038 | 1900 | 246 | 35.7 | 198 | 28.7 | 4.0 |
| E480C | B | 1975(4) + 1650 (24) | 1038 | 1900 | 240 | 34.8 | 198 | 28.7 | 4.2 |
| E501H | C | 1975(4) | 1038 | 1900 | 246 | 35.7 | 212 | 30.7 | 1.8 |
| E503B | C | 1975(4) | 1038 | 1900 | 275 | 39.9 | 220 | 31.9 | 4.2 |

1 B indicates Base Composition
C indicates 0.06% carbon modified

2 See Table XXXV for explanation of thermal treatment codes

TABLE XXXVIII

RESULTS OF TRANSVERSE CREEP TESTS ON FULLY LAMELLAR 6% Cr $\gamma/\gamma'$-$\delta$ DIRECTIONALLY SOLIDIFIED EUTECTIC ALLOY WITH AND WITHOUT CARBON. ALL SPECIMENS COATED WITH ≈60 μm (2.5 mils) PWA 270 NiCoCrAlY OVERLAY COATING. MATERIAL CAST IN SLAB FORM, DIRECTIONALLY SOLIDIFIED AT A RATE OF 0.6 cm (0.25 inch) PER HOUR.

| Specimen Identification | Material[1] | Thermal Treatment Code[2] | Stress | | Temperature | | Rupture Life | Elongation | Larson Miller Parameter |
|---|---|---|---|---|---|---|---|---|---|
| | | | MPa | KSI | °C | °F | Hours | Percent | (c = 20) |
| E480E | B | 1975(4) + 1650(24) | 276 | 40 | 760 | 1400 | 64.7 | 1.8 | 40.6 |
| E480F | B | 1975(4) + 1650(24) | 276 | 40 | 760 | 1400 | 65.9 | 1.4 | 40.6 |
| E534B | B | 1975(4) | 276 | 40 | 760 | 1400 | 15.3 | 1.3 | 39.4 |
| E534C | B | 1975(4) | 276 | 40 | 760 | 1400 | 45.7 | 2.1 | 40.3 |
| E513C | C | 1975(4) | 276 | 40 | 760 | 1400 | 118.5 | 1.7 | 41.1 |
| E513D | C | 1975(4) | 276 | 40 | 760 | 1400 | 143.1 | 2.3 | 41.2 |
| E466H | B | 1975(4) + 1650(24) | 41 | 6 | 1038 | 1900 | 228.4 | 20.3 | 52.8 |
| E466I | B | 1975 (4) + 1650(24) | 41 | 6 | 1038 | 1900 | 575.7 | 20.5 | 53.7 |
| E503C | C | 1975(4) | 41 | 6 | 1038 | 1900 | 173.8 | 18.0 | 52.5 |
| E513B | C | 1975(4) | 41 | 6 | 1038 | 1900 | 165.4 | 11.4 | 52.4 |

1 B indicates base composition
C indicates 0.06% carbon modified

2 See Table XXXV for explanation of thermal treatment codes

TABLE XXXIX

SUMMARY OF TRANSVERSE TENSILE STRENGTHS

| Alloy-Structure Combination | 760°C (1400°F) 0.2% Yield Strength MPa | KSI | Ultimate Strength MPa | KSI | 1038°C (1900°F) 0.2 Yield Strength MPa | KSI | Ulimate Strength MPa | KSI |
|---|---|---|---|---|---|---|---|---|
| Base composition 6 Cr $\gamma/\gamma'$-$\delta$ cellular | – | – | 714(1) | 103.7(1) | 210 | 30.5 | 263 | 38.1 |
| Base composition 6 Cr $\gamma/\gamma'$-$\delta$ lamellar | 646 | 93.7 | 675 | 98.0 | 198 | 28.7 | 243 | 35.3 |
| Carbon modified 6 Cr $\gamma/\gamma'$-$\delta$ lamellar | 710 | 103.1 | 754 | 109.5 | 216 | 31.3 | 260 | 37.8 |
| DS MAR-M200 | 689 | 100 | 805 | 117 | 220 | 32 | 269 | 39 |
| DS MAR-M200+Hf | 689 | 100 | 805 | 117 | 220 | 32 | 269 | 39 |

(1) 700°C (1300°F) Test Temperature

TABLE XL

SUMMARY OF TRANSVERSE TENSILE AND RUPTURE DUCTILITIES

| Alloy Structure Combination | Average Transverse Fracture Strain Percent | | Average Transverse Rupture Elongation Percent | |
|---|---|---|---|---|
| | 700-760°C (1300-1400°F) | 982-1038°C (1800-1900°F) | 700-760°C (1300-1400°F) | 982-1038°C (1800-1900°F) |
| Base composition 6 Cr $\gamma/\gamma'$-$\delta$ cellular | 0.21 | 4.1 | 0.5 | 7.7 |
| Base composition 6 Cr $\gamma/\gamma'$-$\delta$ lamellar | 0.54 | 4.1 | 1.7 | 20.4 |
| Carbon modified 6 Cr $\gamma/\gamma'$ - $\delta$ lamellar | 0.85 | 3.0 | 2.0 | 14.7 |
| DS MAR-M200 | 0.68(1) | 1.1(1) | ~1.5 | ~3 |
| DS MAR-M200 + Hf | 2.6(1) | 3.9(1) | ~3 | ~10 |

(1) Uncoated to simulate engine service condition in root attachment.

TABLE XLI

RESULTS OF ULTIMATE SHEAR STRENGTH TESTS ON FULLY LAMELLAR 6% Cr $\gamma/\gamma'$-$\delta$ DIRECTIONALLY SOLIDIFIED EUTECTIC ALLOY WITH AND WITHOUT CARBON. MATERIAL CAST IN SLAB FORM, DIRECTIONALLY SOLIDIFIED AT A RATE OF 0.6 cm (0.25 inch) PER HOUR.

| Specimen Identification | Material[1] | Thermal Treatment Code[2] | Test Temperature °C | Test Temperature °F | Ultimate Shear Strength MPa | Ultimate Shear Strength ksi |
|---|---|---|---|---|---|---|
| E482F | B | 1975(4) + 1650(24) | 760 | 1400 | 333 | 48.3 |
| E489E | B | 1975(4) + 1650(24) | 760 | 1400 | 339 | 49.2 |
| E508E | C | 1975(4) | 760 | 1400 | 389 | 56.5 |
| E513F1 | C | 1975(4) | 760 | 1400 | 380 | 55.1 |
| E489C | B | 1975(4) + 1650(24) | 870 | 1600 | 260 | 37.7 |
| E489F | B | 1975(4) + 1650(24) | 870 | 1600 | 271 | 39.4 |
| E508H | C | 1975(4) | 870 | 1600 | 304 | 44.1 |
| E503D | C | 1975(4) | 870 | 1600 | 307 | 44.5 |

1 B indicates base composition
C indicates 0.06% carbon modified

2 See Table XXXV for explanation of thermal treatment code

TABLE XLII

RESULTS OF CREEP SHEAR TESTS ON FULLY LAMELLAR 6% Cr $\gamma/\gamma'$-$\delta$ DIRECTIONALLY SOLIDIFIED EUTECTIC ALLOY WITH AND WITHOUT CARBON. MATERIAL CAST IN SLAB FORM, DIRECTIONALLY SOLIDIFIED AT A RATE OF 0.6 cm (0.25 inch) PER HOUR.

| Specimen Identification | Material[1] | Thermal Treatment Code[2] | Shear Stress MPa | Shear Stress KSI | Temperature °C | Temperature °F | Shear Rupture Life Hours | Larson Miller Parameter (c = 20) |
|---|---|---|---|---|---|---|---|---|
| E489D | B | 1975(4) + 1650(24) | 179 | 26 | 760 | 1400 | 33.2 | 40.0 |
| E496G | B | 1975(4) + 1650(24) | 179 | 26 | 760 | 1400 | 76.8 | 40.7 |
| E496E | B | 1975(4) | 179 | 26 | 760 | 1400 | 74.3 | 40.7 |
| E496F | B | 1975(4) | 179 | 26 | 760 | 1400 | 64.1 | 40.6 |
| E508C | C | 1975(4) | 179 | 26 | 760 | 1400 | 83.4 | 40.8 |
| E503E | C | 1975(4) | 179 | 26 | 760 | 1400 | 121.8 | 41.1 |
| E508G | C | 1975(4) | 179 | 26 | 760 | 1400 | 360.1 | 42.0 |
| E482D | B | 1975(4) + 1650(24) | 83 | 12 | 870 | 1600 | 88.8 | 45.2 |
| E482E | B | 1975(4) + 1650(24) | 83 | 12 | 870 | 1600 | 45.9 | 44.6 |
| E496H | B | 1975(4) | 83 | 12 | 870 | 1600 | 119.8 | 45.5 |
| E508D | C | 1975(4) | 83 | 12 | 870 | 1600 | 216.3 | 46.0 |
| E508F | C | 1975(4) | 83 | 12 | 870 | 1600 | 379.9 | 46.5 |

1 B indicates base composition
C indicates carbon modified

2 See Table XXXV for explanation of thermal treatment code

TABLE XLIII

RESULTS OF TRANSVERSE LOW CYCLE FATIGUE TESTS ON FULLY LAMELLAR 6% Cr $\gamma/\gamma'$-$\delta$ DIRECTIONALLY SOLIDIFIED EUTECTIC ALLOY WITH AND WITHOUT CARBON. TUBULAR SPECIMENS COATED WITH $\approx$ 60 $\mu$m (2.5 mils) PWA 270 NiCoCrAlY OVERLAY COATING ON THE OUTSIDE DIAMETER AND $\approx$ 25 $\mu$m (1 mil) LOW ALUMINUM ALUMINIDE ON THE INSIDE DIAMETER. MATERIAL CAST IN SLAB FORM DIRECTIONALLY SOLIDIFIED AT A RATE OF 0.6 cm (0.25 inch) PER HOUR.

| Specimen Identification | Material[1] | Thermal Treatment Code[2] | Temperature °C | Temperature °F | Strain Range Percent | Cycles to[3] Failure | Comments |
|---|---|---|---|---|---|---|---|
| E510B | B | 1975(4) + 1650(24) | 760 | 1400 | 0.52 | 35 | |
| E510D | B | 1975(4) + 1650(24) | 760 | 1400 | 0.51 | 246 | |
| E524B1 | C | 1975(4) | 760 | 1400 | 0.52 | >3500 | Runout – Uploaded as E524B2 |
| E524B2 | C | 1975(4) | 760 | 1400 | 0.59 | 364 | 3500 prior cycles at 0.52% |
| E524D | C | 1975(4) | 760 | 1400 | 0.64 | 203 | |
| E510E1 | B | 1975(4) + 1650(24) | 982 | 1800 | 0.31 | >2914 | Runout – Uploaded as E510E2 |
| E510E2 | B | 1975(4) + 1650(24) | 982 | 1800 | 0.42 | 903 | 2914 prior cycles at 0.31% |
| E510G | B | 1975(4) + 1650(24) | 982 | 1800 | 0.37 | 605 | |
| E524C | C | 1975(4) | 982 | 1800 | 0.38 | 761 | |
| E524E | C | 1975(4) | 982 | 1800 | 0.44 | 484 | |

1 B indicates base composition
C indicates carbon modified

2 See Table XXXV for explanation of thermal treatment code

3 Failure defined as separation of specimen into two pieces

TABLE XLIV

RESULTS OF IMPACT TESTS ON FULLY LAMELLAR 6% Cr $\gamma/\gamma'$-$\delta$ DIRECTIONALLY SOLIDIFIED EUTECTIC ALLOY WITH AND WITHOUT CARBON. MATERIAL CAST IN SLAB FORM, DIRECTIONALLY SOLIDIFIED AT A RATE OF 0.6 cm (0.25 inch) PER HOUR.

| Specimen Identification | Material[1] | Thermal Treatment Code[2] | Orientation[3] | Temperature °C | Temperature °F | Maximum Stress MPa | Maximum Stress KSI | Energy at Max. Stress[4] Joules | Energy at Max. Stress[4] ft-lb | Total Energy Joules | Total Energy ft-lb. | Comments |
|---|---|---|---|---|---|---|---|---|---|---|---|---|
| E492B | B | 1975(4) + 1650(24) | Longitudinal | 20 | 68 | 790 | 114.5 | 1.38 | 1.02 | 2.58 | 1.90 | |
| E492C | B | 1975(4) + 1650(24) | Longitudinal | 20 | 68 | 751 | 109.0 | 1.74 | 1.28 | 2.09 | 1.54 | |
| E513H | C | 1975(4) | Longitudinal | 20 | 68 | 764 | 110.8 | 1.35 | 1.00 | 1.63 | 1.20 | |
| E513I | C | 1975(4) | Longitudinal | 20 | 68 | 611 | 88.6 | 0.71 | 0.52 | 1.41 | 1.04 | |
| E500C | B | 1975(4) + 1650(24) | Transverse | 20 | 68 | 407 | 59.0 | 0.50 | 0.37 | 0.66 | 0.49 | |
| E500D | B | 1975(4) + 1650(24) | Transverse | 20 | 68 | 390 | 56.5 | 0.47 | 0.34 | 0.56 | 0.41 | |
| E503F | C | 1975(4) | Transverse | 20 | 68 | 328 | 47.6 | 0.22 | 0.16 | 0.43 | 0.32 | |
| E503G | C | 1975(4) | Transverse | 20 | 68 | 284 | 41.2 | – | – | 0.38 | 0.28 | |
| E492D | B | 1975(4) + 1650(24) | Longitudinal | 760 | 1400 | 826 | 119.7 | 2.65 | 1.95 | 3.76 | 2.77 | |
| E492E[5] | B | 1975(4) + 1650(24) | Longitudinal | 760 | 1400 | 939 | 136.2 | – | – | – | – | |
| E513J | C | 1975(4) | Longitudinal | 760 | 1400 | 932 | 135.1 | 1.90 | 1.40 | 3.25 | 2.40 | |
| E513K | C | 1975(4) | Longitudinal | 760 | 1400 | 839 | 121.7 | 1.58 | 1.17 | 2.59 | 1.91 | |
| E500E | B | 1975(4) + 1650(24) | Transverse | 760 | 1400 | 435 | 63.2 | 0.51 | 0.37 | 0.71 | 0.52 | |
| E500F | B | 1975(4) + 1650(24) | Transverse | 760 | 1400 | 416 | 60.3 | 0.51 | 0.38 | 0.64 | 0.47 | Cellular, $\delta$ dendritic |
| E503H | C | 1975(4) | Transverse | 760 | 1400 | 468 | 67.9 | 0.30 | 0.22 | 0.60 | 0.44 | $\delta$ dendritic |
| E503I | C | 1975(4) | Transverse | 760 | 1400 | 414 | 60.0 | – | – | 0.49 | 0.36 | Cellular, $\delta$ dendritic |

1 B indicates base composition
C indicates carbon modified

2 See Table XXXV for explanation of thermal treatment code

3 See Section 4 for definition of orientation

4 Energy absorbed prior to reaching maximum stress

5 Specimen did not break

TABLE XLV

RESULTS OF LONGITUDINAL CREEP TESTS ON 6% Cr $\gamma/\gamma'$-$\delta$ DIRECTIONALLY SOLIDIFIED EUTECTIC ALLOY WITH AND WITHOUT CARBON. ALL SPECIMENS COATED WITH $\approx$ 60 $\mu$m (2.5 mils) PWA 270 NiCoCrAlY OVERLAY COATING.

| Specimen Identification | Material[1] | Type of Casting[2] | Thermal Treatment Code[3] | Stress MPa | Stress KSI | Temperature °C | Temperature °F | Rupture Life Hours | Elongation[4] Percent | Larson Miller Parameter (c = 20) | Comments |
|---|---|---|---|---|---|---|---|---|---|---|---|
| A75-804-01 | B | Bar | 1975(4) + 1650(24) | 758 | 110 | 760 | 1400 | 48.7 | 1.0 | 40.3 | Failed at oxide inclusion |
| A75-824-01 | B | Bar | 1975(4) + 1650(24) | 758 | 110 | 760 | 1400 | 22.4 | 1.0 | 39.7 | Failed at oxide inclusion |
| A75-806-01 | B | Bar | 1975(4) | 758 | 110 | 760 | 1400 | 82.8 | 11.1 | 40.8 | Failed at cellular band |
| A76-010-01 | B | Bar | 1975(4) | 758 | 110 | 760 | 1400 | >670 | | | |
| E465F | B | Slab | 1975(4) + 1650(24) | 758 | 110 | 760 | 1400 | 55.6 | 1.3 | 40.4 | |
| E465G | B | Slab | 1975(4) + 1650(24) | 758 | 110 | 760 | 1400 | 46.5 | 1.2 | 40.3 | |
| E496J | B | Slab | 1975(4) | 758 | 110 | 760 | 1400 | 92.7 | 1.0 | 40.9 | |
| E496K | B | Slab | 1975(4) | 758 | 110 | 760 | 1400 | 171.9 | 1.2 | 41.4 | |
| A75-882-01 | C | Bar | 1975(4) | 758 | 110 | 760 | 1400 | 254.3 | 1.1 | 41.7 | Failed at oxide inclusion |
| A75-884-01 | C | Bar | 1975(4) | 758 | 110 | 760 | 1400 | 62.2 | 0.7 | 40.5 | Failed at oxide inclusion |
| A75-887-01 | C | Bar | 1975(4) | 758 | 110 | 760 | 1400 | 59.5 | 0.9 | 40.5 | Failed at oxide inclusion |
| A75-908-01 | C | Bar | 1975(4) | 758 | 110 | 760 | 1400 | 225.1 | 0.9 | 41.6 | Failed at oxide inclusion |
| E508I | C | Slab | 1975(4) | 758 | 110 | 760 | 1400 | 49.2 | 0.9 | 40.3 | |
| E508J | C | Slab | 1975(4) | 758 | 110 | 760 | 1400 | 22.0 | 0.7 | 39.7 | |
| E503L | C | Slab | 1975(4) | 689 | 100 | 760 | 1400 | 179.5 | 0.9 | 41.4 | |
| E513N1 | C | Slab | 1975(4) | 689 | 100 | 760 | 1400 | >1600 | – | | |
| A75-815-01 | B | Bar | 1975(4) + 1650(24) | 152 | 22 | 1038 | 1900 | 179.9 | 4.1 | 52.5 | |
| A75-857-01 | B | Bar | 1975(4) + 1650(24) | 152 | 22 | 1038 | 1900 | 173.5 | 4.3 | 52.5 | |
| A75-382-01 | B | Bar | 1975(4) | 152 | 22 | 1038 | 1900 | 149.6 | N.M. | 52.3 | Failed at cellular band |
| A75-810-01 | B | Bar | 1975(4) | 152 | 22 | 1038 | 1900 | 156.3 | 6.3 | 52.4 | Failed at cellular band |

# TABLE XLV (Cont'd)

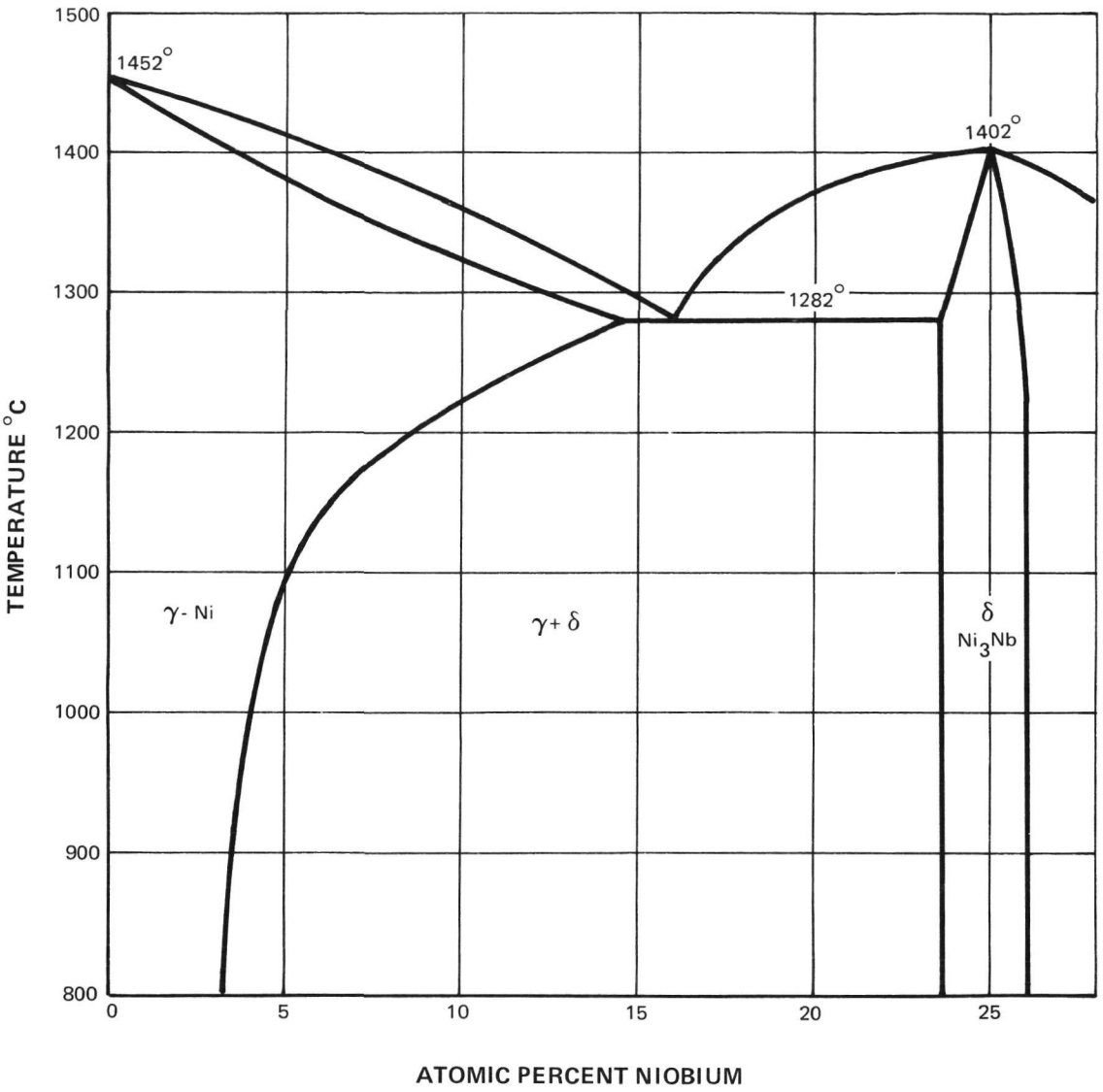
| Specimen Identification | Material[1] | Type of Casting[2] | Thermal Treatment Code[3] | Stress MPa | Stress KSI | Temperature °C | Temperature °F | Rupture Life Hours | Elongation[4] Percent | Larson Miller Parameter (c = 20) | Comments |
|---|---|---|---|---|---|---|---|---|---|---|---|
| E465H | B | Slab | 1975(4) + 1650(24) | 152 | 22 | 1038 | 1900 | 136.0 | 8.4 | 52.2 | |
| E465I | B | Slab | 1975(4) + 1650(24) | 152 | 22 | 1038 | 1900 | 169.3 | 7.0 | 52.5 | |
| E496L | B | Slab | 1975(4) | 152 | 22 | 1038 | 1900 | 230.2 | 7.8 | 52.8 | |
| A75-890-01 | C | Bar | 1975(4) | 152 | 22 | 1038 | 1900 | 32.0 | 1.9 | 50.8 | Failed at oxide inclusion |
| A75-891-01 | C | Bar | 1975(4) | 152 | 22 | 1038 | 1900 | 354.3 | N.M. | 53.0 | |
| A75-904-01 | C | Bar | 1975(4) | 152 | 22 | 1038 | 1900 | 248.0 | 4.8 | 52.9 | |
| A75-905-01 | C | Bar | 1975(4) | 152 | 22 | 1038 | 1900 | 189.0 | 2.7 | 52.6 | |
| E508K | C | Slab | 1975(4) | 152 | 22 | 1038 | 1900 | 156.9 | 6.5 | 52.4 | |
| E503J | C | Slab | 1975(4) | 152 | 22 | 1038 | 1900 | 124.3 | 7.1 | 52.1 | |
| E503K | C | Slab | 1975(4) | 110 | 16 | 1038 | 1900 | 445.3 | 9.5 | 53.5 | |
| E513M1 | C | Slab | 1975(4) | 110 | 16 | 1038 | 1900 | 742.6 | 7.5 | 54.0 | |

1 B indicates base composition C indicates 0.06% carbon modified

2 Bar indicates Bridgman bar solidified at 2 cm (0.8 inch) per hour. Slab indicates modified Bridgman slab casting solidified at 0.6 cm (0.25 inch) per hour.

3 See Table XXXV for explanation of thermal treatment code

4 N.M. indicates not measured




R14-29

Figure 1 Nickel Rich Portion of the Ni-Nb Equilibrium Phase Diagram After Durden and Hume-Rothery[6]

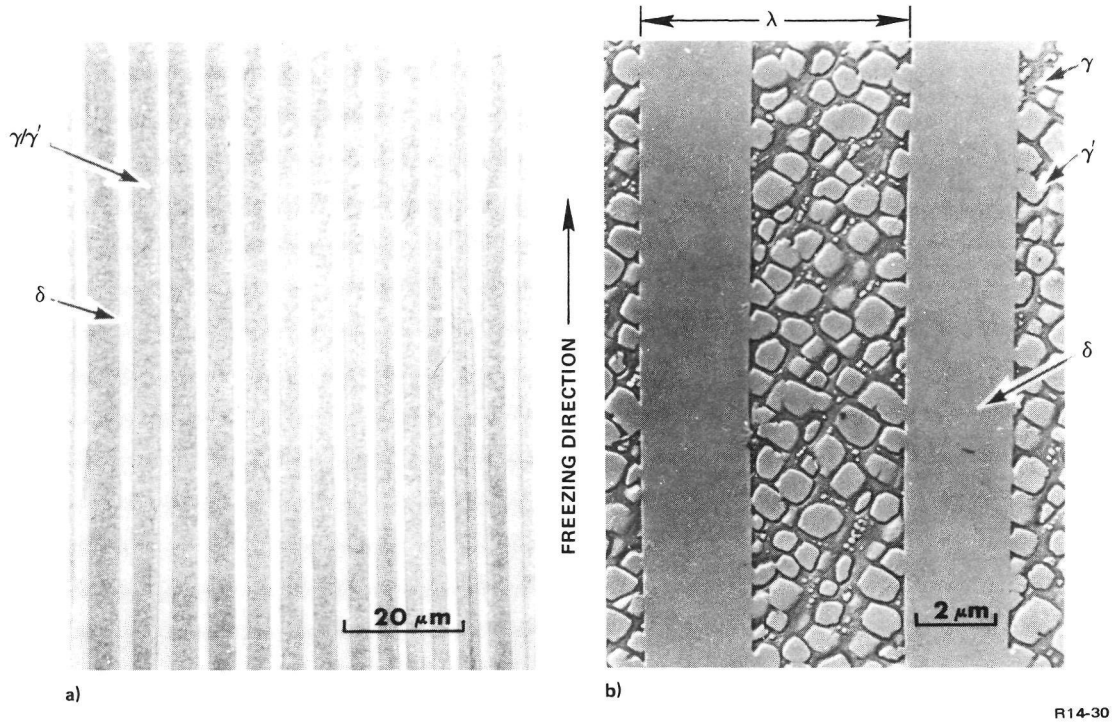



Figure 2 Microstructure of Directionally Solidified $\gamma/\gamma'$-$\delta$ Eutectic Alloy (J7986-39)

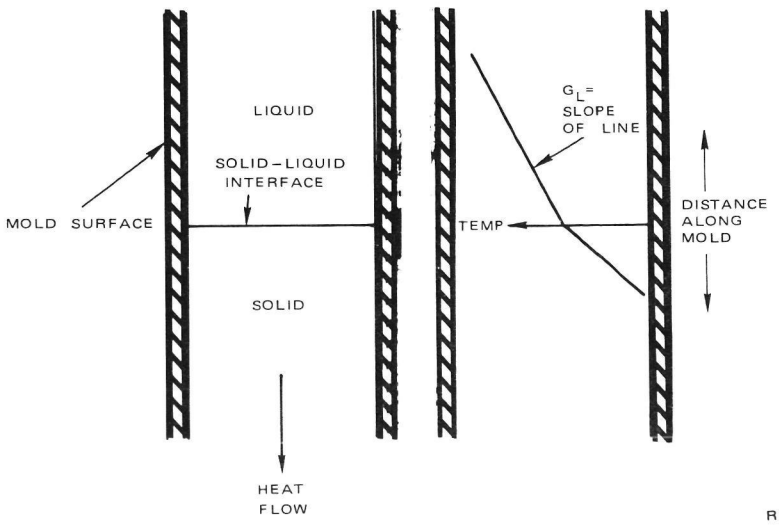



Figure 3 Schematic Drawing Illustrating the Temperature Gradient in Liquid G

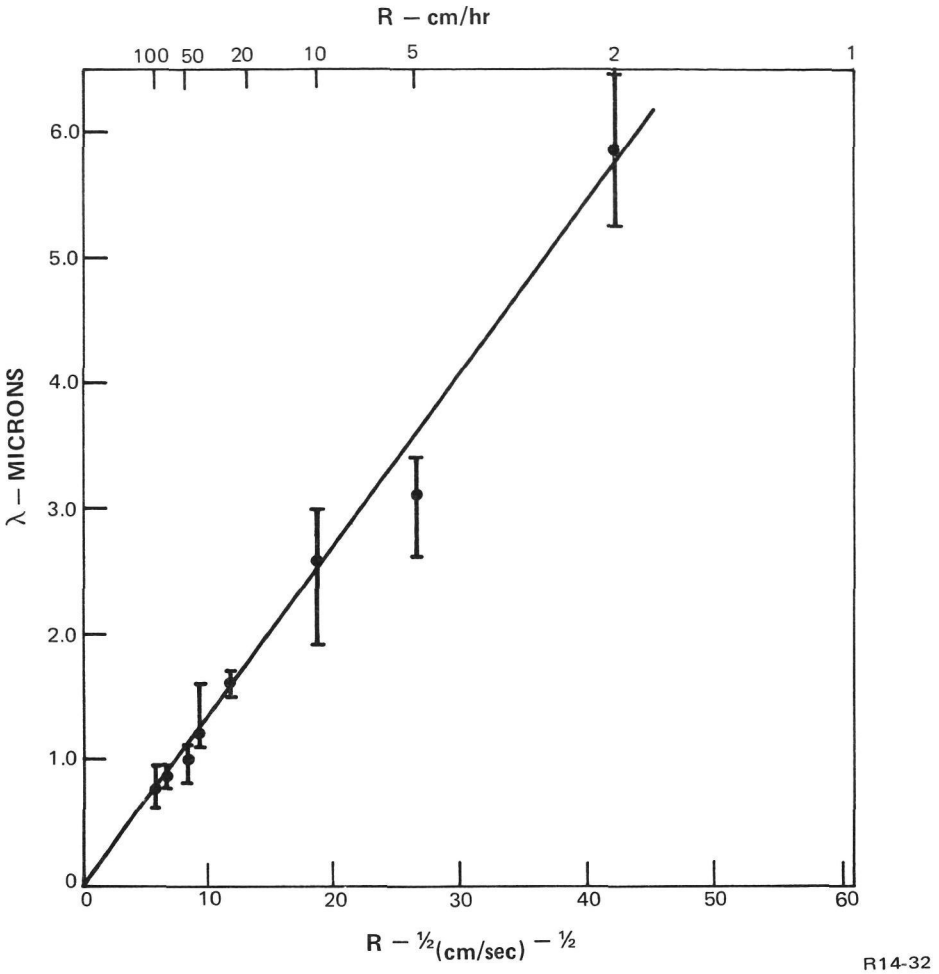



Figure 4 Interlamellar Spacing of $\gamma/\gamma'$ - $\delta$ (Ni-21.0-22.2 w/o Cb 2.5 w/o Al) as a Function of Freezing Rate After Lemkey[2]

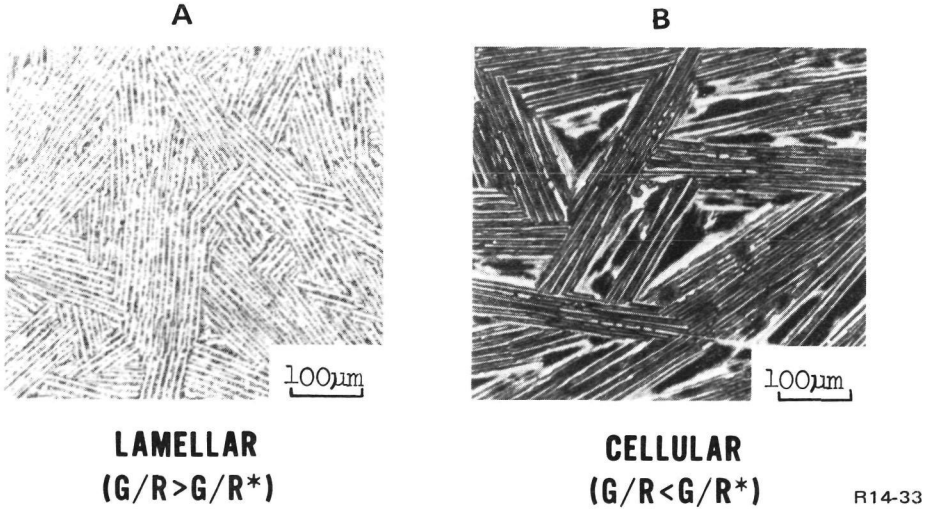
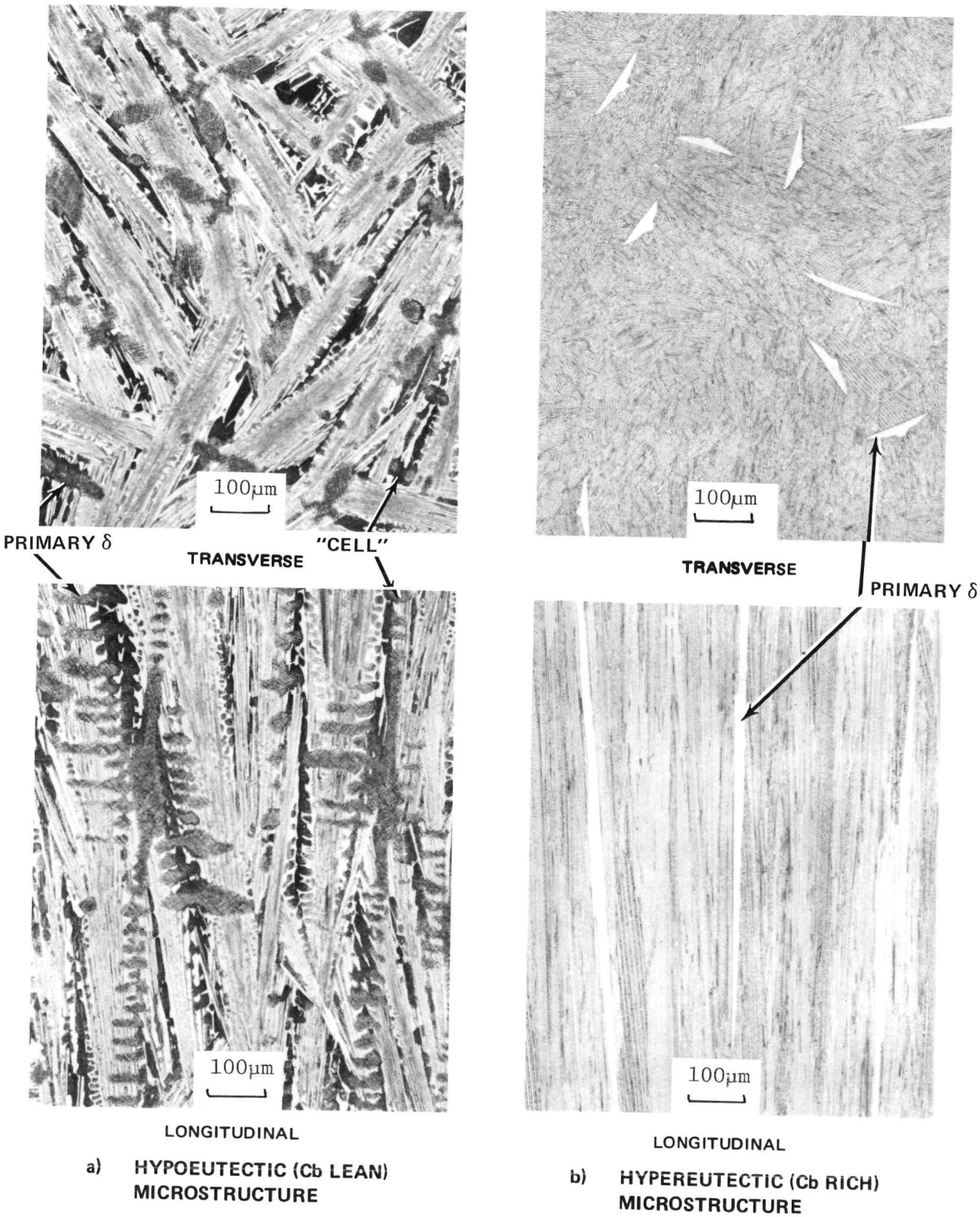
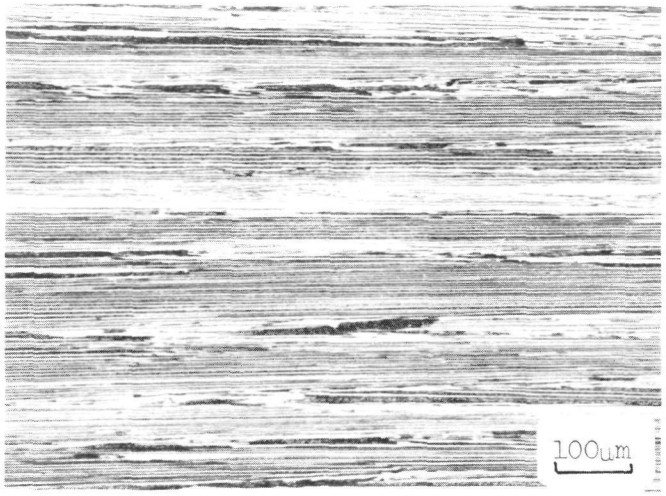



Figure 5 Transverse Microstructures Observed In $\gamma/\gamma'$-$\delta$ Directionally Solidified Eutectic Alloys As Affected By Gradient/Rate Ratio

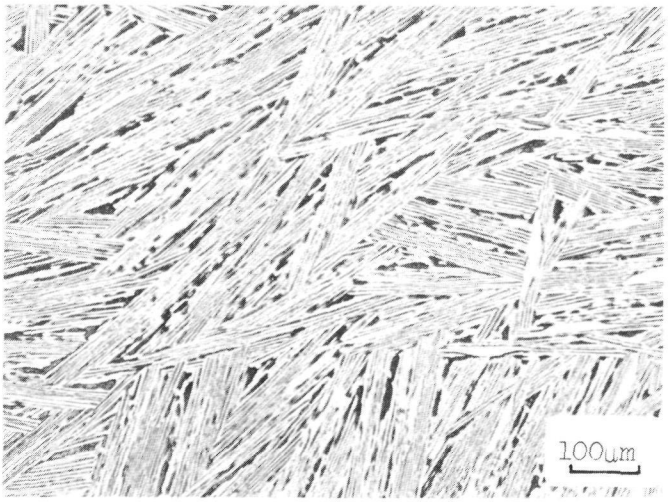



R14-34

Figure 6 Longitudinal and Transverse Microstructures of Hypo and Hypereutectic Directionally Solidified $\gamma/\gamma'$ - $\delta$ Alloys



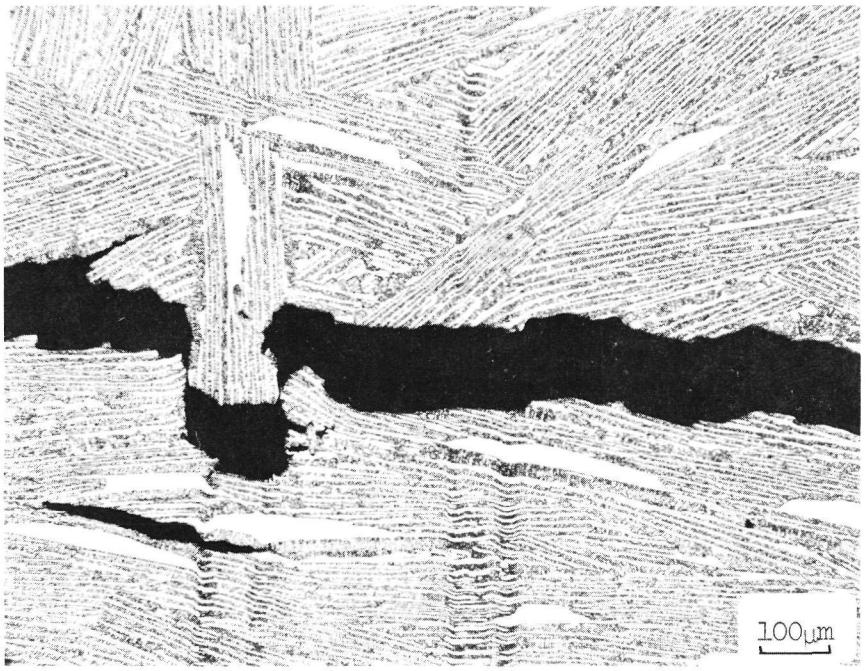

**LONGITUDINAL**




**TRANSVERSE**

R14-35

Figure 7 Typical Microstructure of 6 Percent Cr $\gamma/\gamma'$ - $\delta$ Alloy Directionally Solidified at 3 cm/hr in a High Gradient ($G \approx 360°C/cm$) Bridgman Apparatus




E323-C4 (B454)

R14-36

Figure 8 Grain Boundary Failure Found in Cellular $\gamma/\gamma' - \delta$ Specimen Loaded in Tension Transverse to the Growth Direction

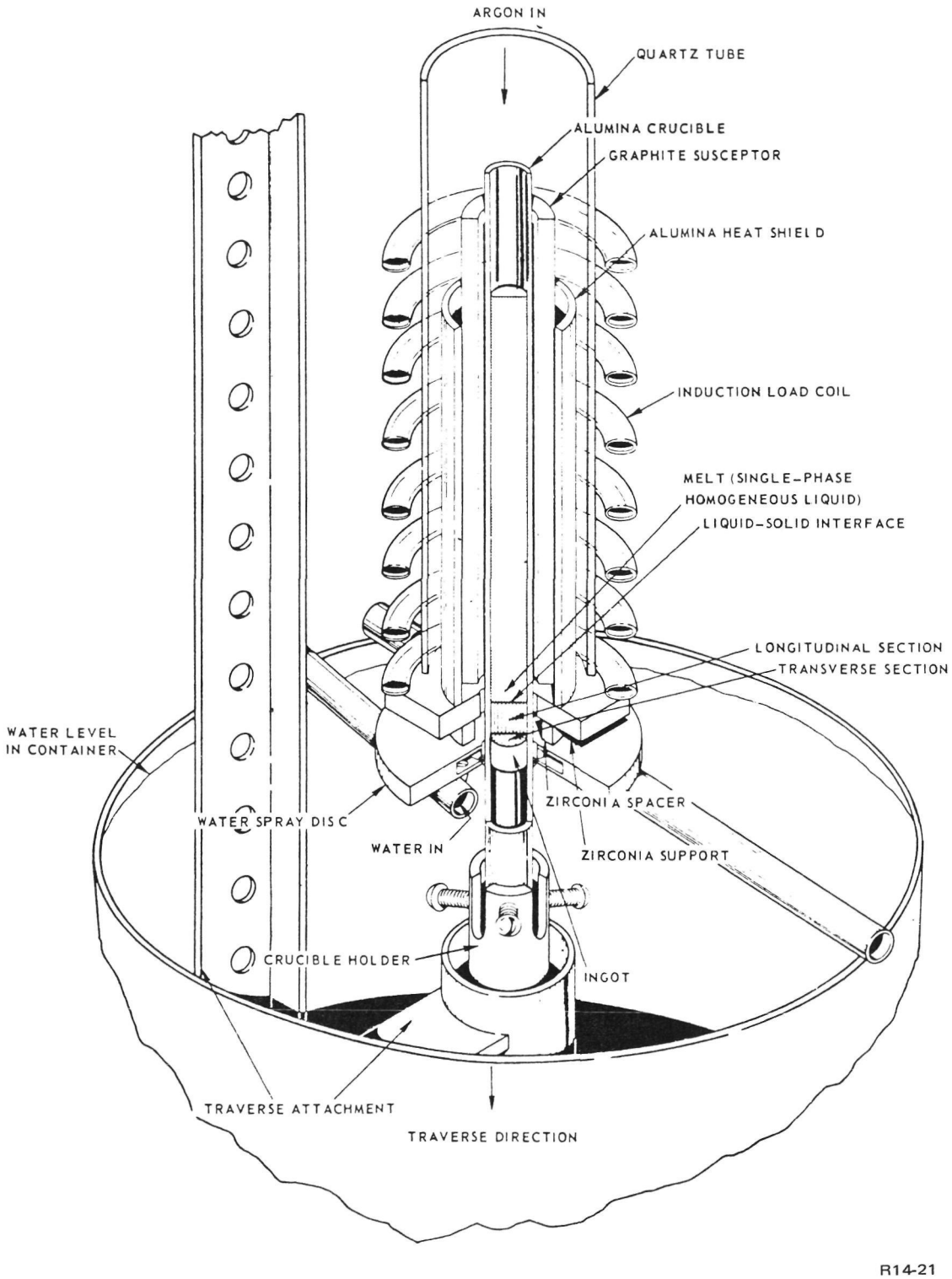



Figure 9 Schematic Diagram of Water-Quench Laboratory Bridgman Apparatus

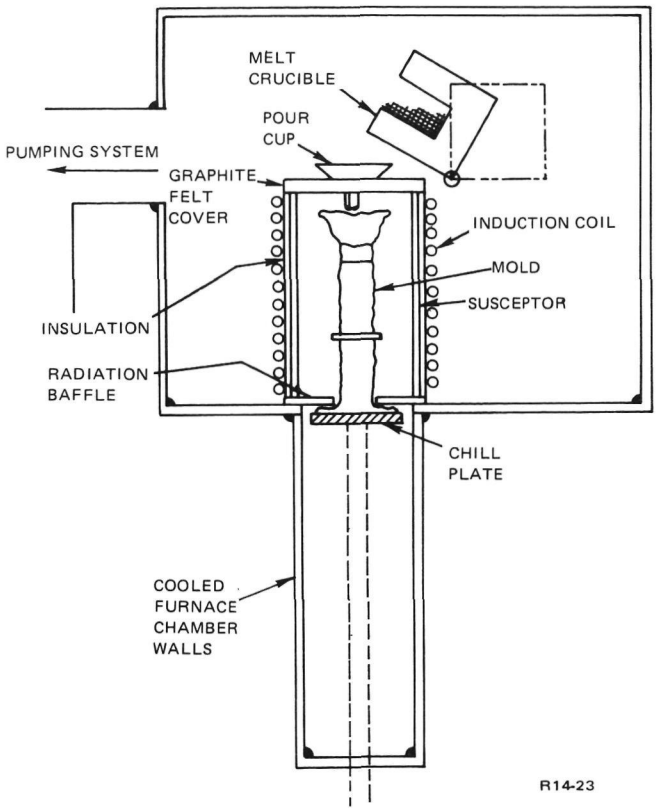



Figure 10 Schematic Diagram of Modified Bridgman Furnace

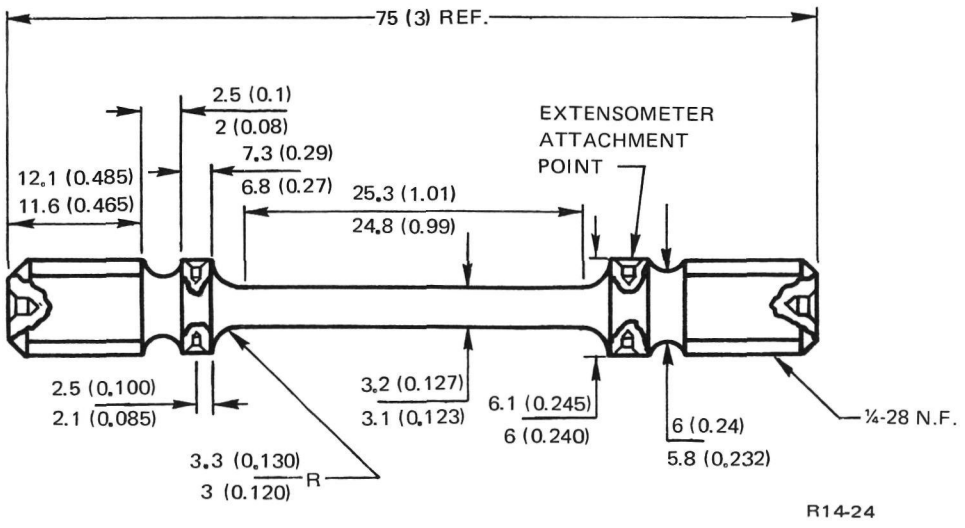



Figure 11 Tensile and Creep Test Specimen. Dimensions are mm (inches) Except Threads

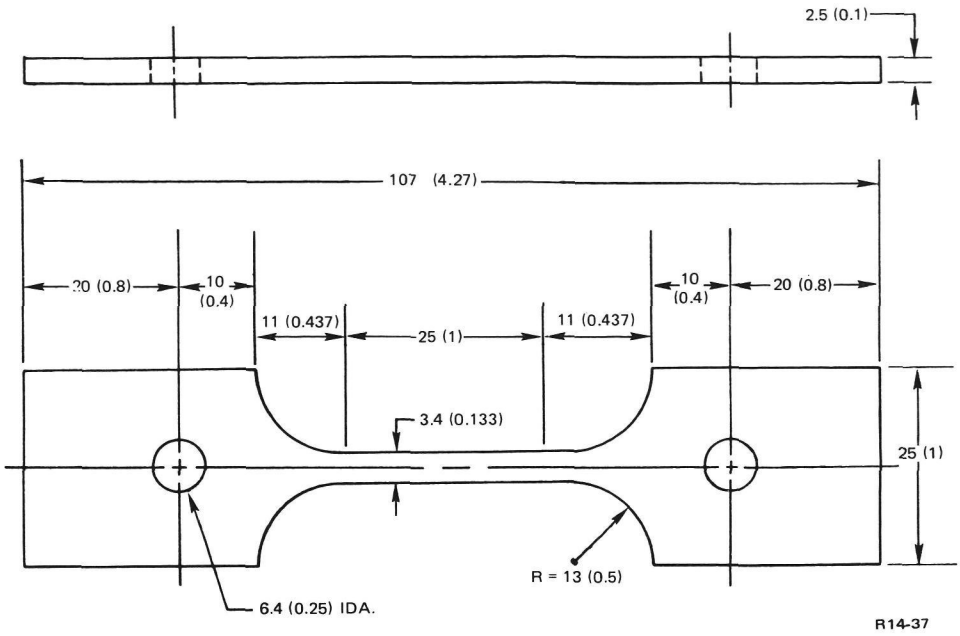



Figure 12 Sketch of the Thin Slab Stress Rupture Specimen. Dimensions are mm (inches)

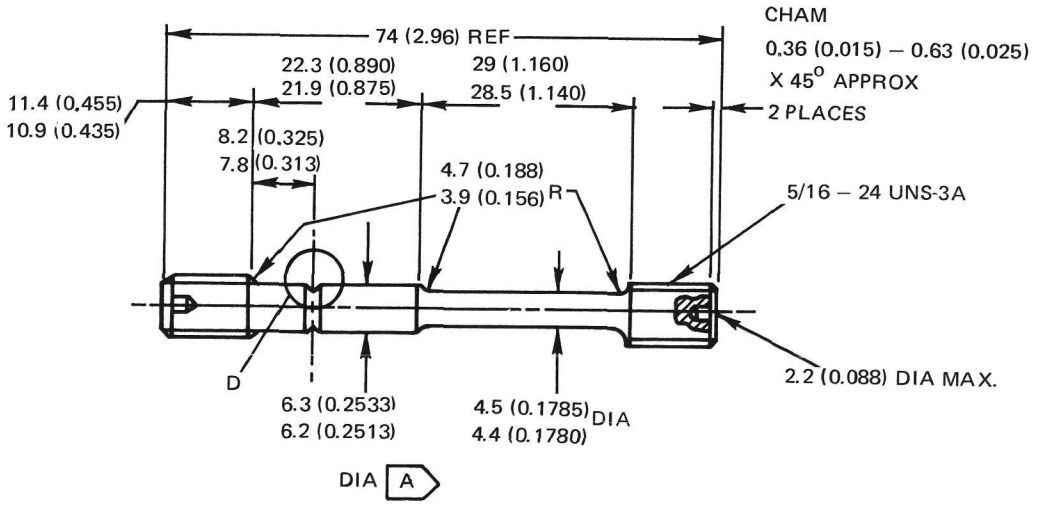
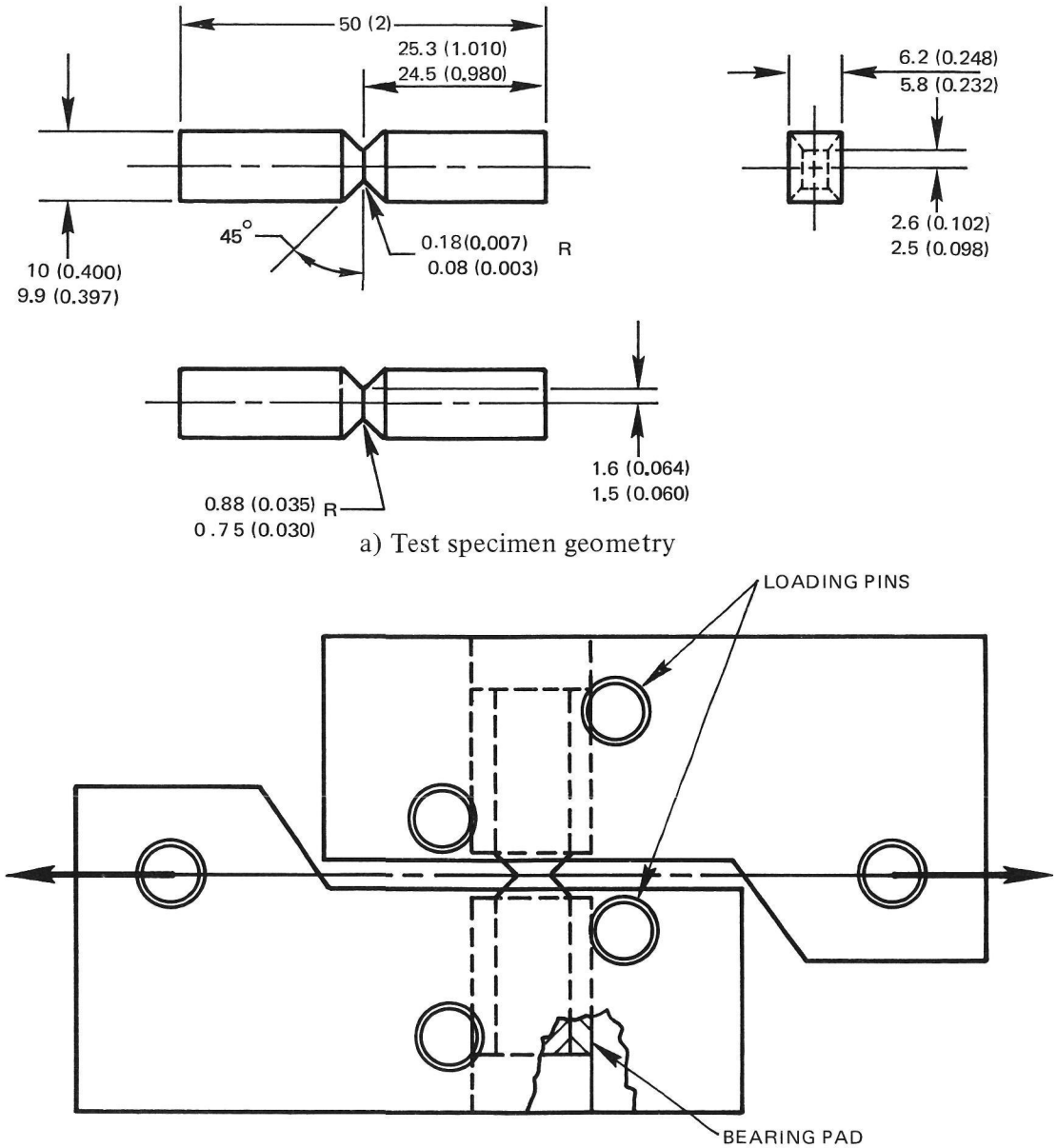



Figure 13 Combination Notch/Smooth Sample. Dimensions are mm (inches) Except Threads




R14-26

Figure 14 Test Method Used for Evaluation of Elevated Temperature Shear Properties. Dimensions are mm (inches)

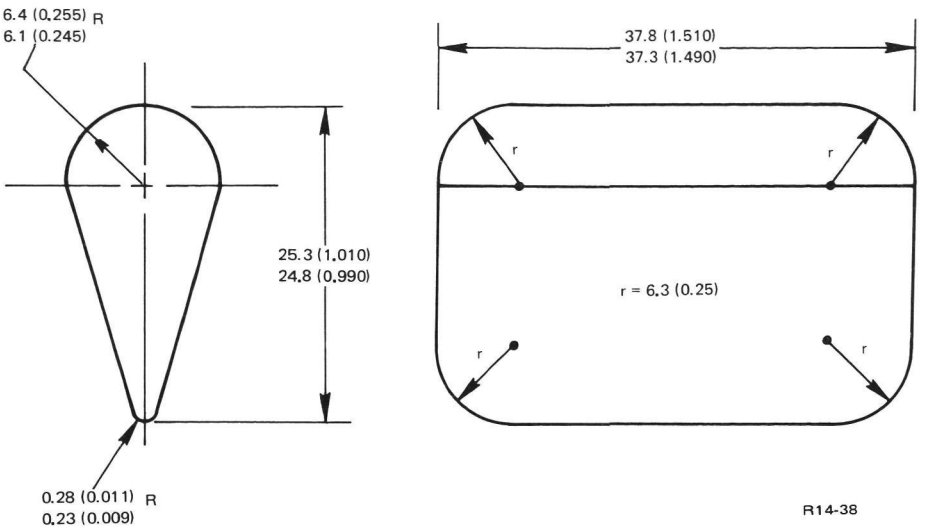



Figure 15 Fluidized Bed Thermal Fatigue Test Specimen. Dimensions are mm (inches)

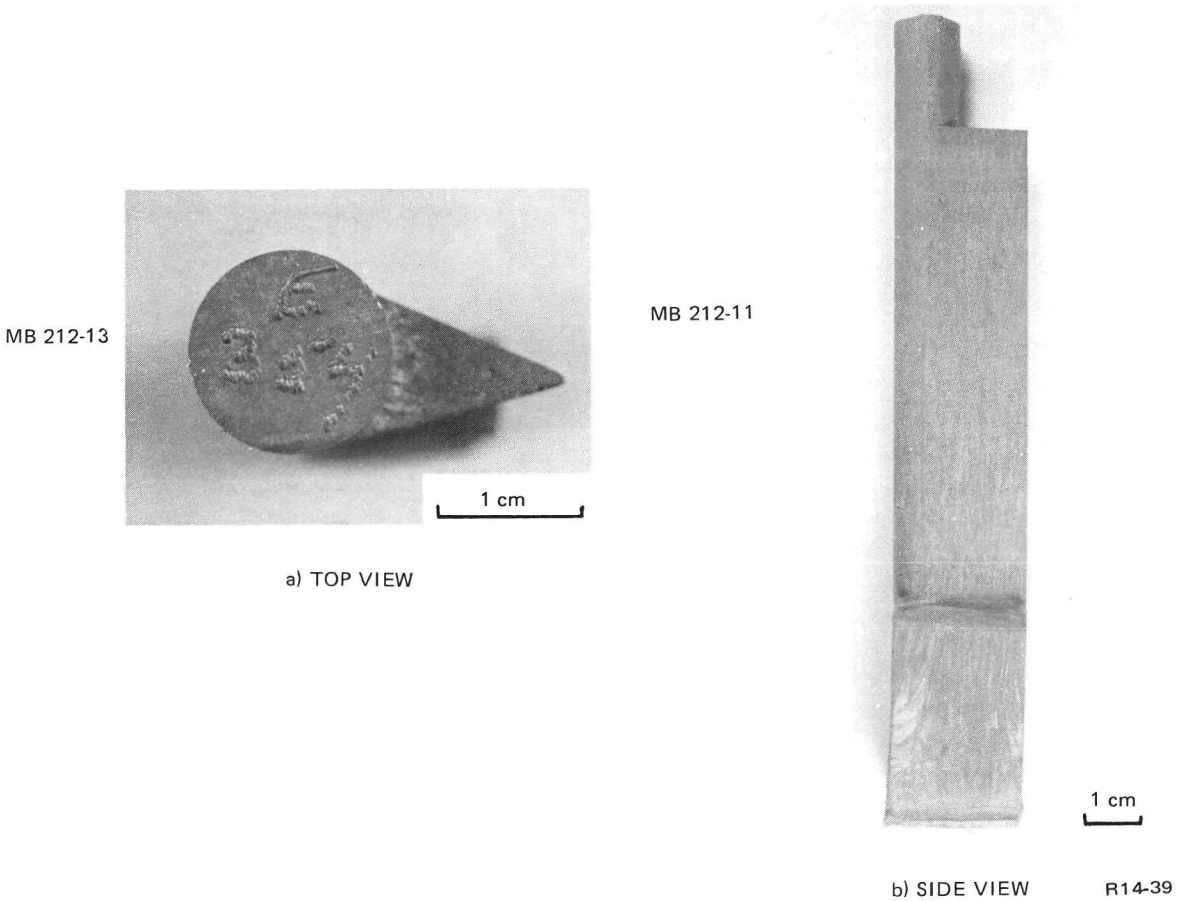



Figure 16 Casting Design Used for Thermal Fatigue Wedges

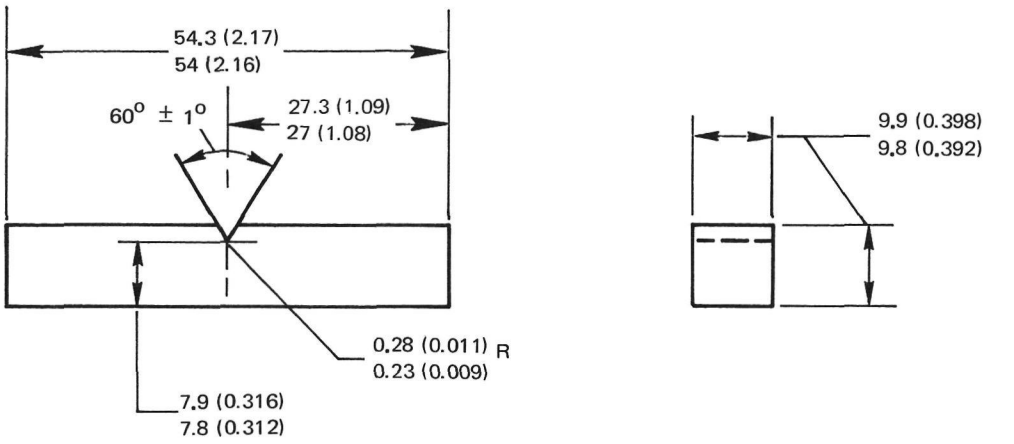



Figure 17 Notched Charpy Impact Specimen. Dimensions are mm (inches)

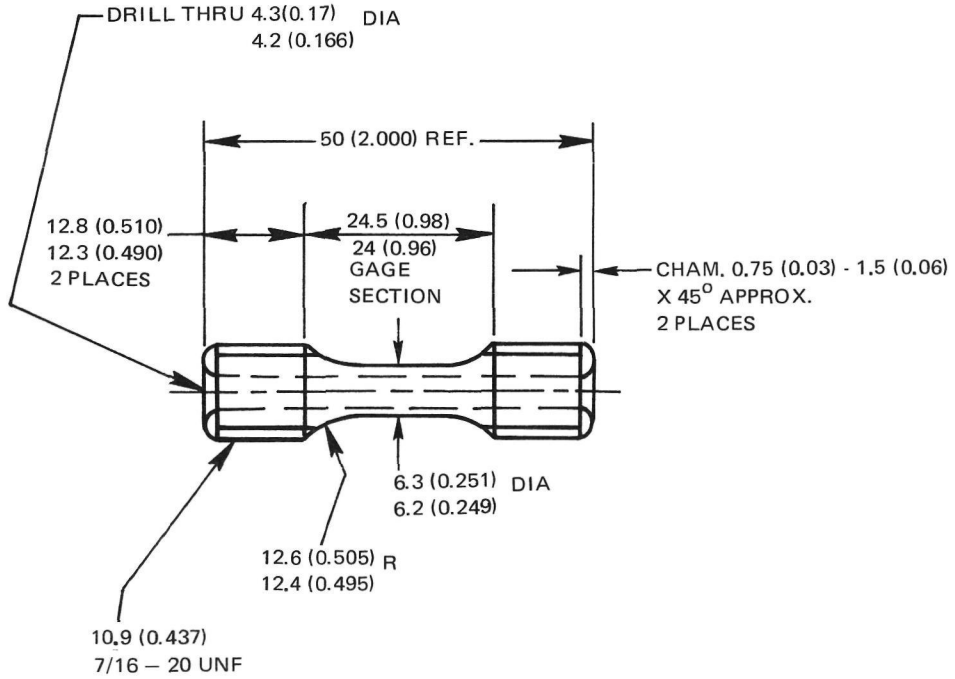
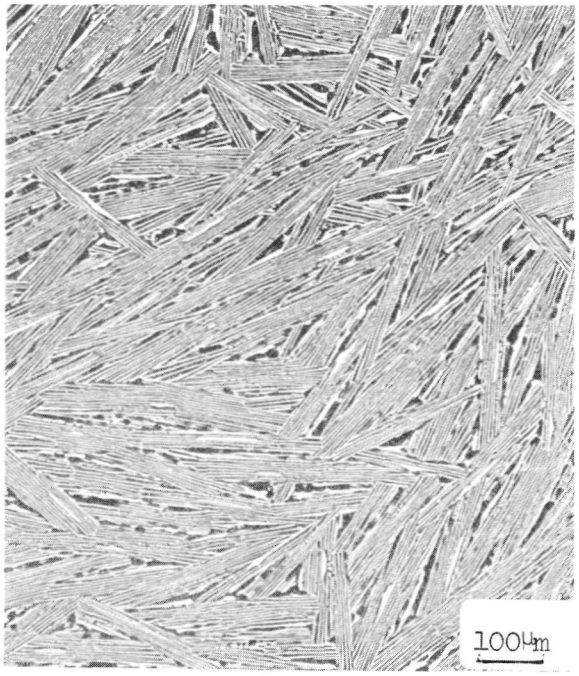
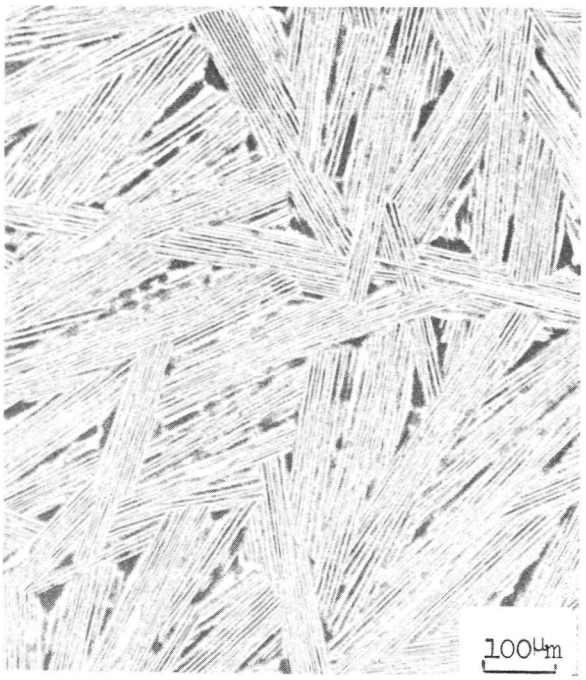



Figure 18 Specimen (MERL-2A) for Determining Transverse LCF of Coated Directionally Solidified Eutectic Material. Dimensions are mm (inches) Except Threads



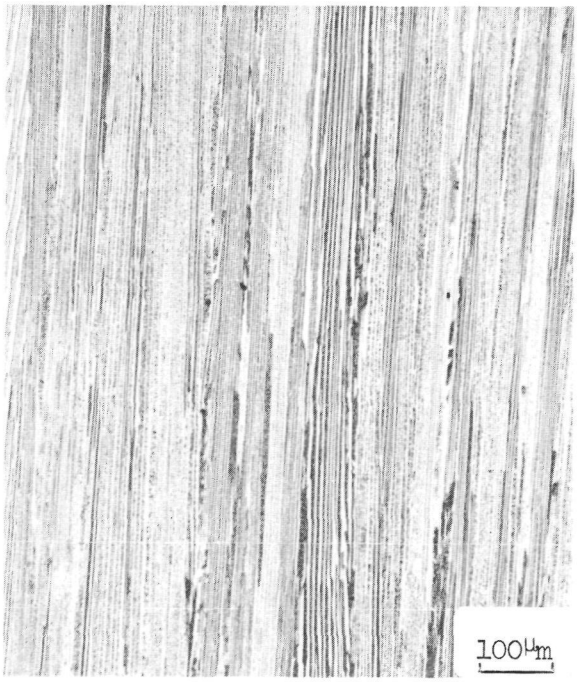

MB 707-3 (B480)

**TRANSVERSE**




MB 707-1 (MIDDTN B 430)

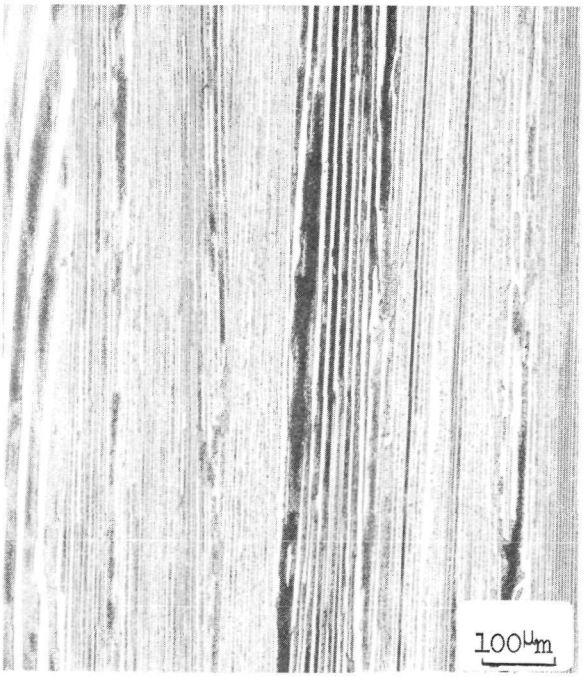
**TRANSVERSE**




MB 707-4 (J479)

**LONGITUDINAL**

a) Water-quench Bridgman bar structure. Solidification rate 3 cm/hr.




MB 707-2 (MIDDTN. B430)

**LONGITUDINAL**

b) Modified Bridgman slab structure. Solidification rate 1.3 cm/hr.

R14-22

Figure 19 Typical Microstructure of Cellular 6 Cr $\gamma/\gamma'$ - $\delta$ Eutectic Alloy Directionally Solidified Under the Indicated Conditions

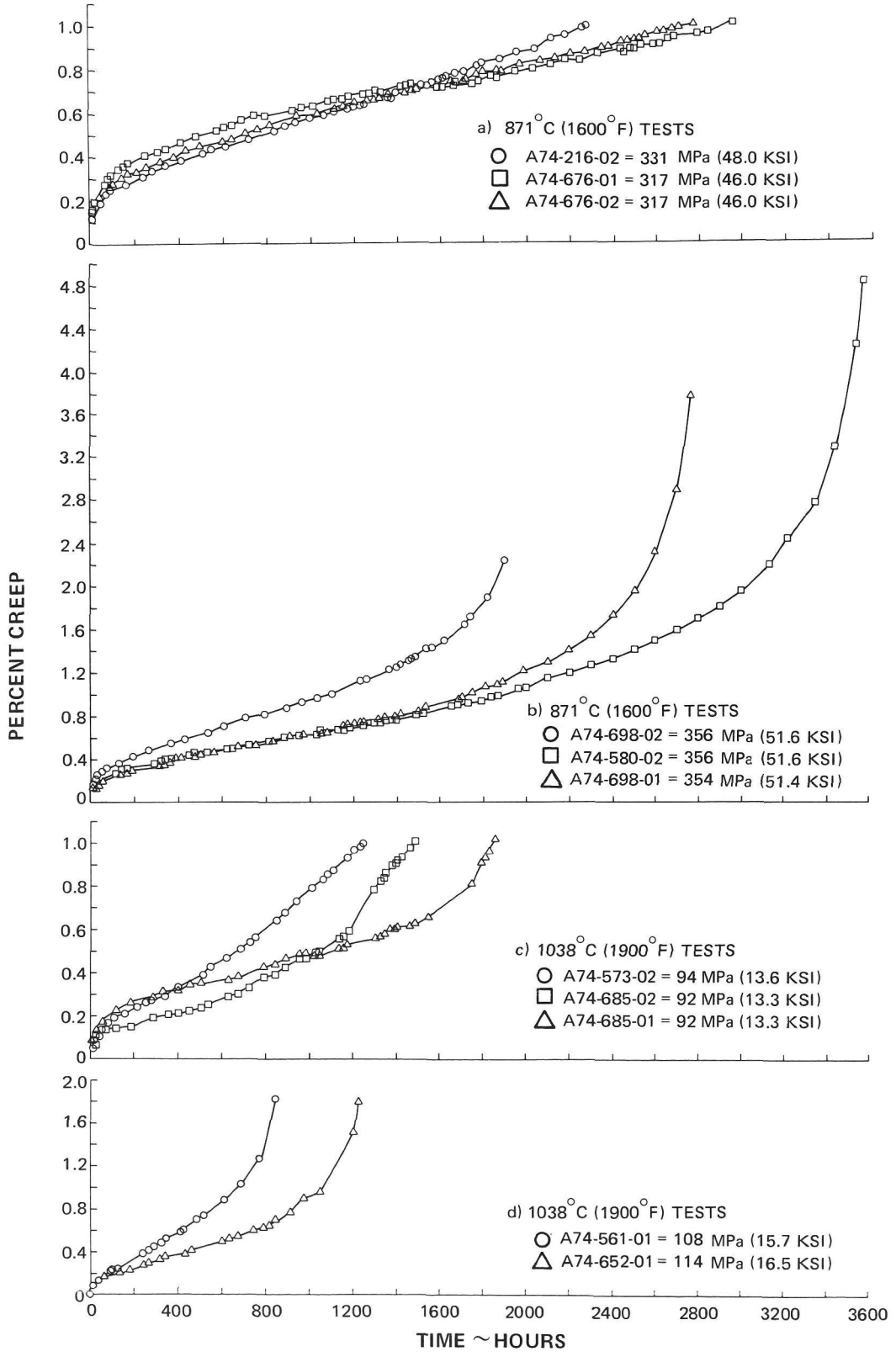
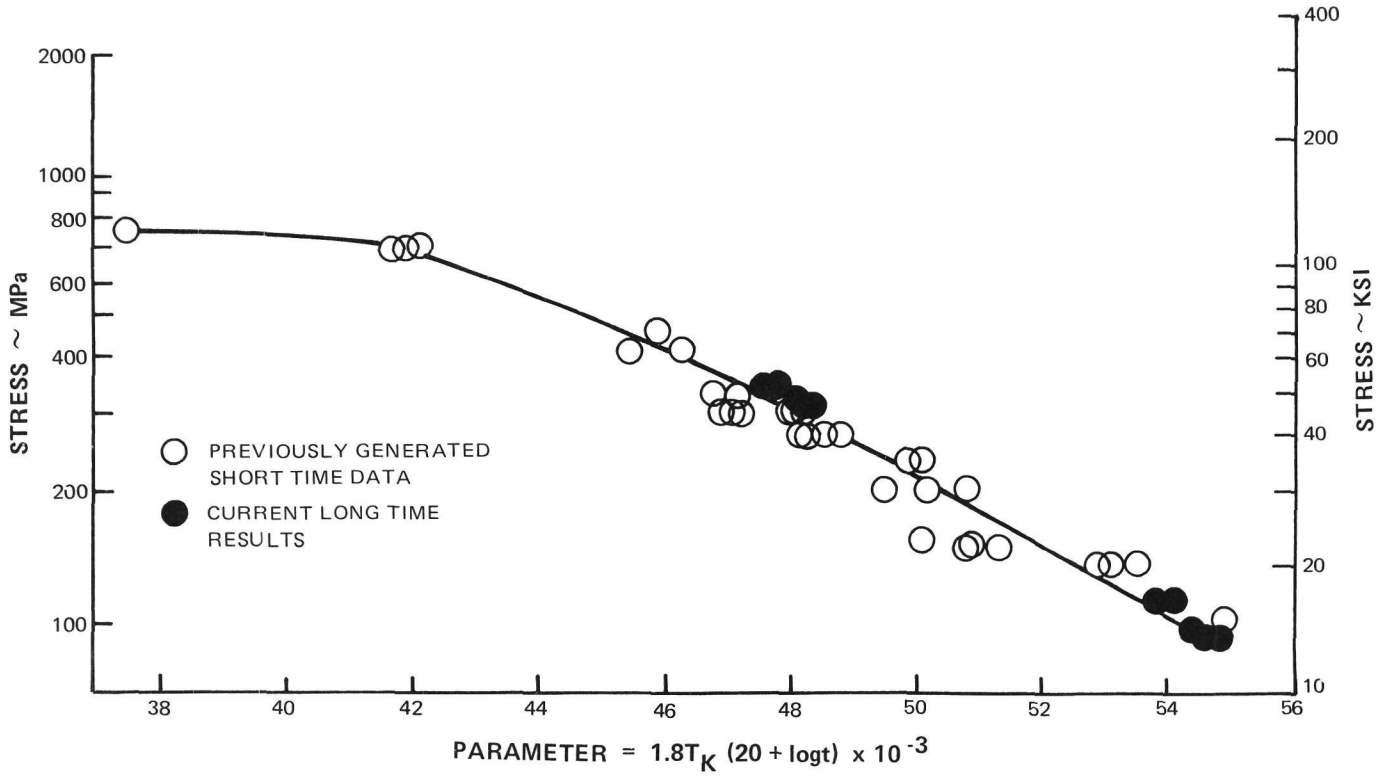



Figure 20 Long Time Creep Results for Cellular 6 Cr $\gamma/\gamma'$-$\delta$ Directionally Solidified Eutectic Alloy Grown in the Form of 1.3 cm (0.5 inch) Diameter Bridgman Bars Solidified at a Rate of 3 cm/hour




R14-28

Figure 21 Comparison of Long Time One Percent Creep Life Results Generated on the Current Program With Previous Short Time Data for Cellular 6 Cr $\gamma/\gamma' - \delta$ Directionally Solidified Eutectic Alloy. Material Grown in the Form of 1.3 cm (0.5 inch) Diameter Bridgman Bars Solidified at a Rate of 3 cm/hour

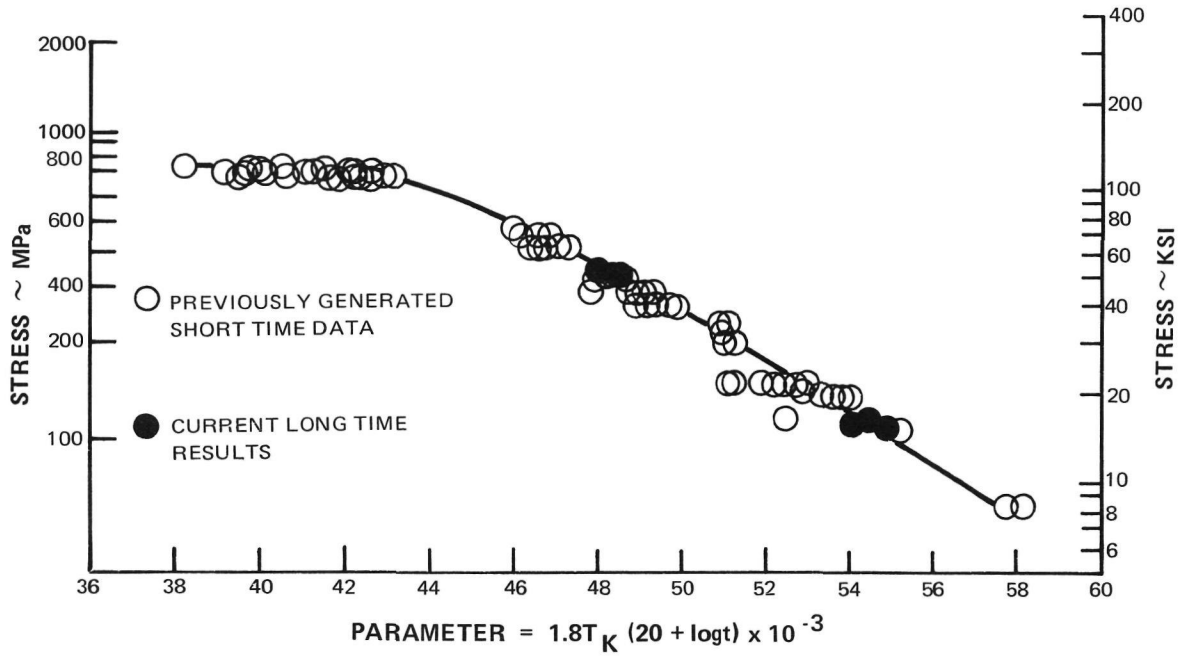
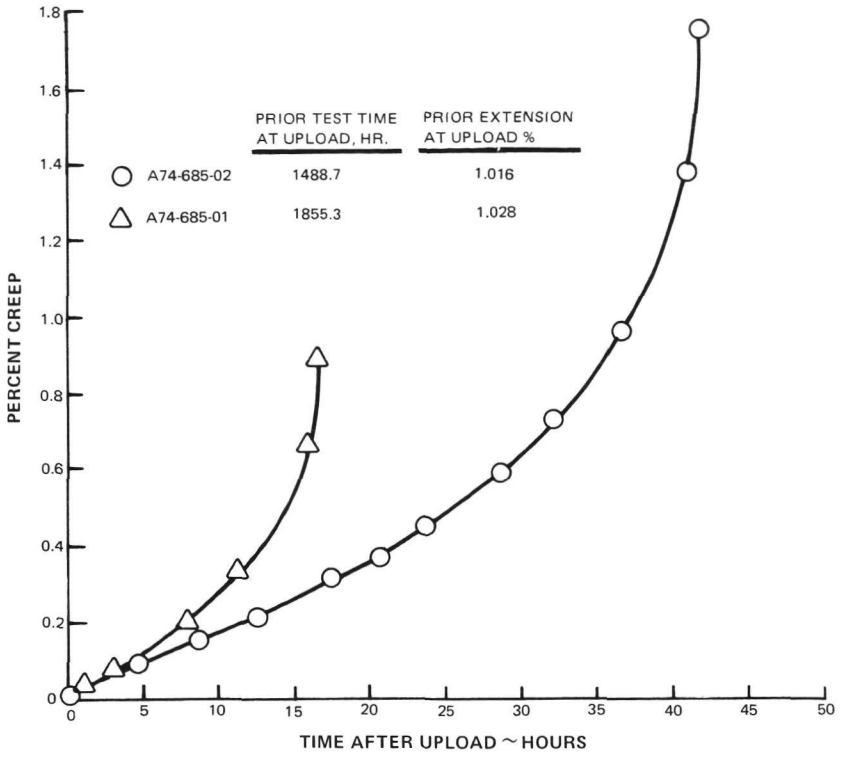
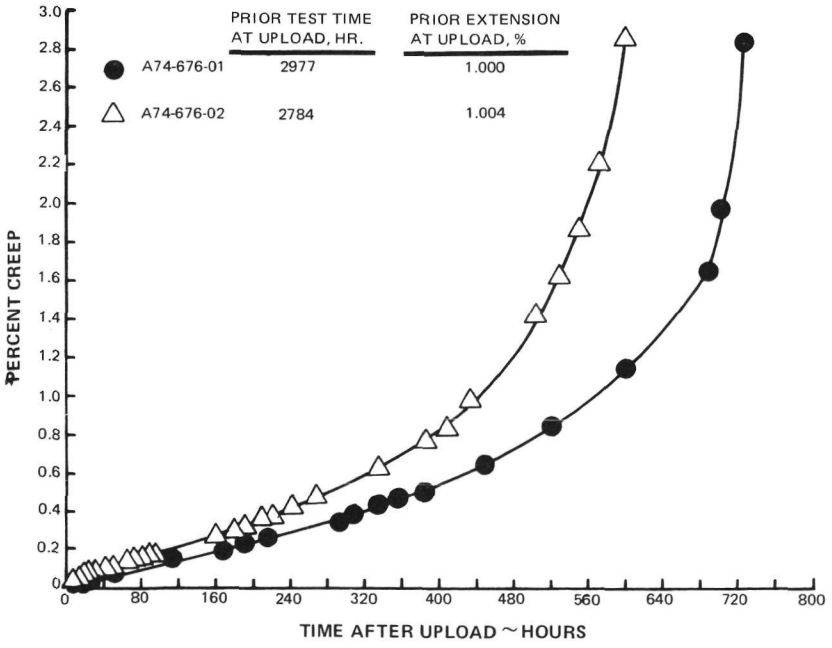



Figure 22 Comparison of Long Time Rupture Life Generated on the Current Program With Previous Short Time Data for Cellular 6 Cr $\gamma/\gamma'$ - $\delta$ Directionally Solidified Eutectic Alloy. Material Grown in the Form of 1.3 cm (0.5 inch) Diameter Bars Solidified at a Rate of 3 cm/hour



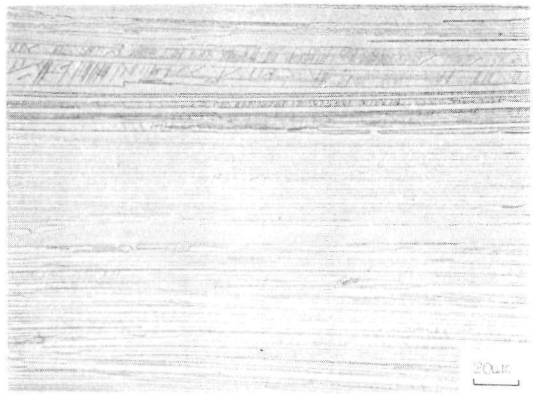

a) Specimens Uploaded to 141 MPa (20.4 ksi) at 1038°C (1900°F) After Testing to ≈ One Percent Strain at 92 MPa (13.3 ksi) at the Same Temperature




b) Specimens Uploaded to 417 MPa (60.5 ksi) Nominal Stress at 871°C (1600°F) After Testing to One Percent Extension at 317 MPa (46 ksi) at the Same Temperature

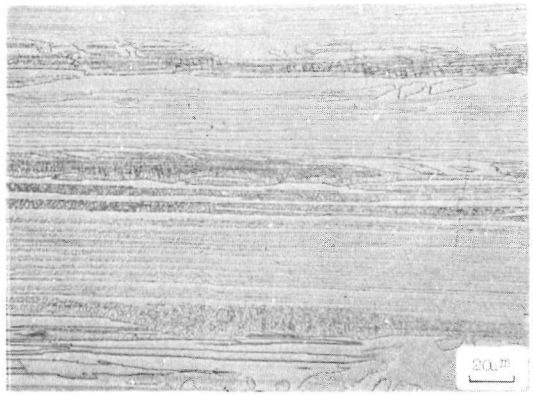
R14-43

Figure 23 Creep Results for Cellular 6 Cr $\gamma/\gamma'$ - $\delta$ Directionally Solidified Eutectic Alloy Creep Specimens After Uploading



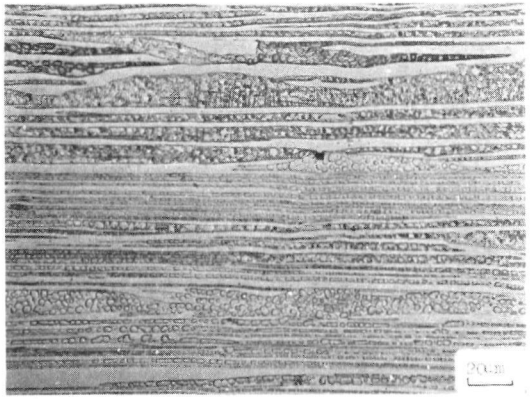
MB 75-18 (B478)

a) Specimen A74-216-02 exposed ≈ 2300 hours at 871°C (1600°F), unstressed area of specimen shoulder.



MB 75-17 (B478)

b) Specimen A74-216-02 exposed ≈ 2300 hours at 871°C (1600°F) and 331 MPa (48 ksi).



MB 75-6 (B481)

c) Specimen A74-685-02 exposed ≈ 1500 hours at 1038°C (1900°F), unstressed area of specimen shoulder.

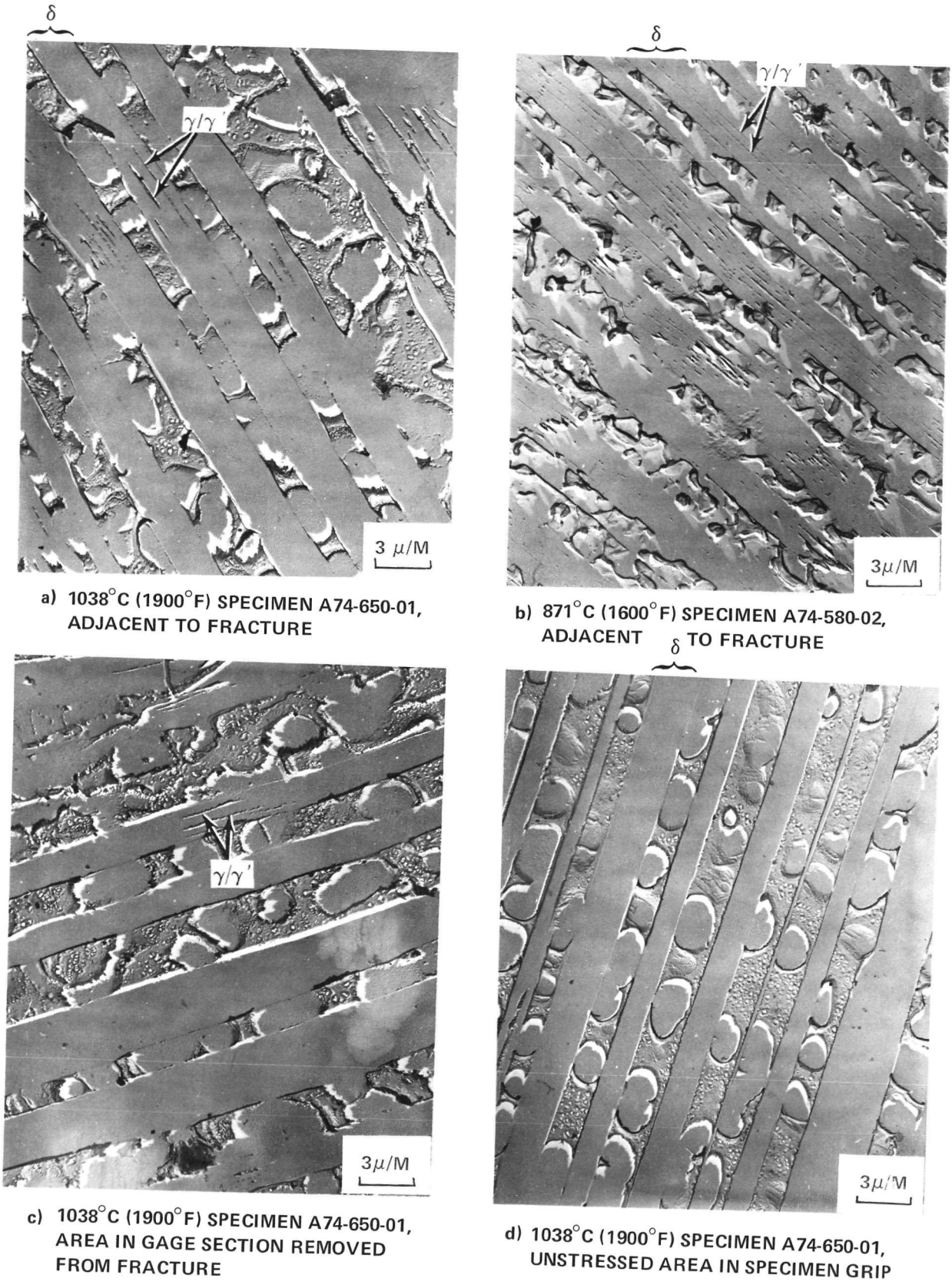


MB 75-7 (B481)

d) Specimen A74-685-02 exposed ≈ 1500 hours at 1038°C (1900°F) with sequentially applied stresses of 92 and 141 MPa (13.3 and 20.4 ksi).

Figure 24 Influence of Long Time Thermal Creep Exposure on the Microstructure of Cellular 6 Cr $\gamma/\gamma'$ - $\delta$ Directionally Solidified Eutectic Alloy

R14-44




a) 1038°C (1900°F) SPECIMEN A74-650-01, ADJACENT TO FRACTURE

b) 871°C (1600°F) SPECIMEN A74-580-02, ADJACENT TO FRACTURE

c) 1038°C (1900°F) SPECIMEN A74-650-01, AREA IN GAGE SECTION REMOVED FROM FRACTURE

d) 1038°C (1900°F) SPECIMEN A74-650-01, UNSTRESSED AREA IN SPECIMEN GRIP

Figure 25 Illustrating Precipitation of a Second Phase Presumed to be $\gamma/\gamma'$ in $\delta$ Lamellae Adjacent to 1038°C (1900°F) Long Time Creep Fracture

R14-45

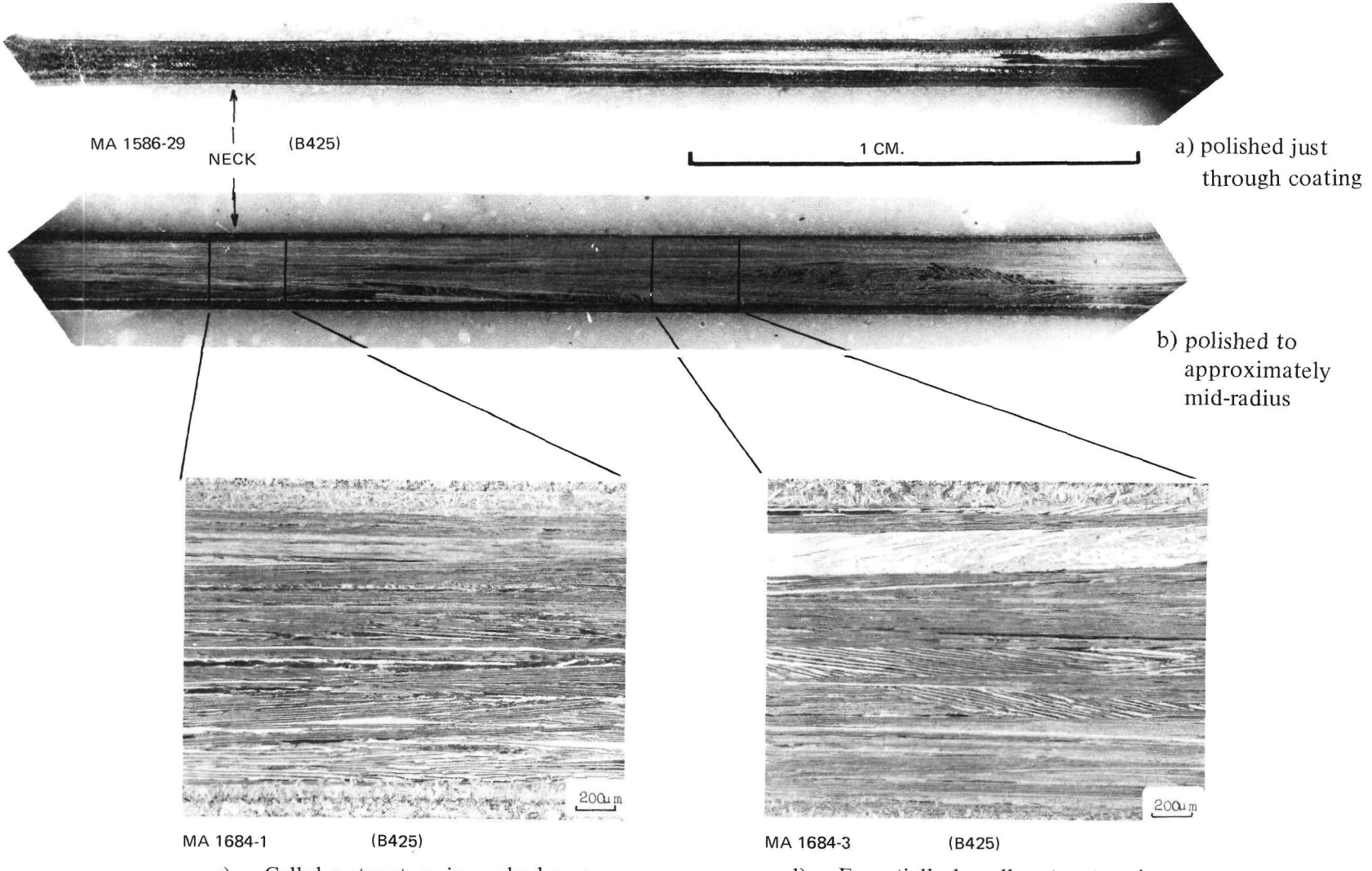



Figure 26 Comparison of Excessively Cellular and Essentially Lamellar Microstructures Found in Necked and Unnecked Areas of Specimen A74-573-02 Tested to One Percent Extension in 1232 Hours at 1038°C/94 MPa (1900°F/13.6 ksi)

R14-46

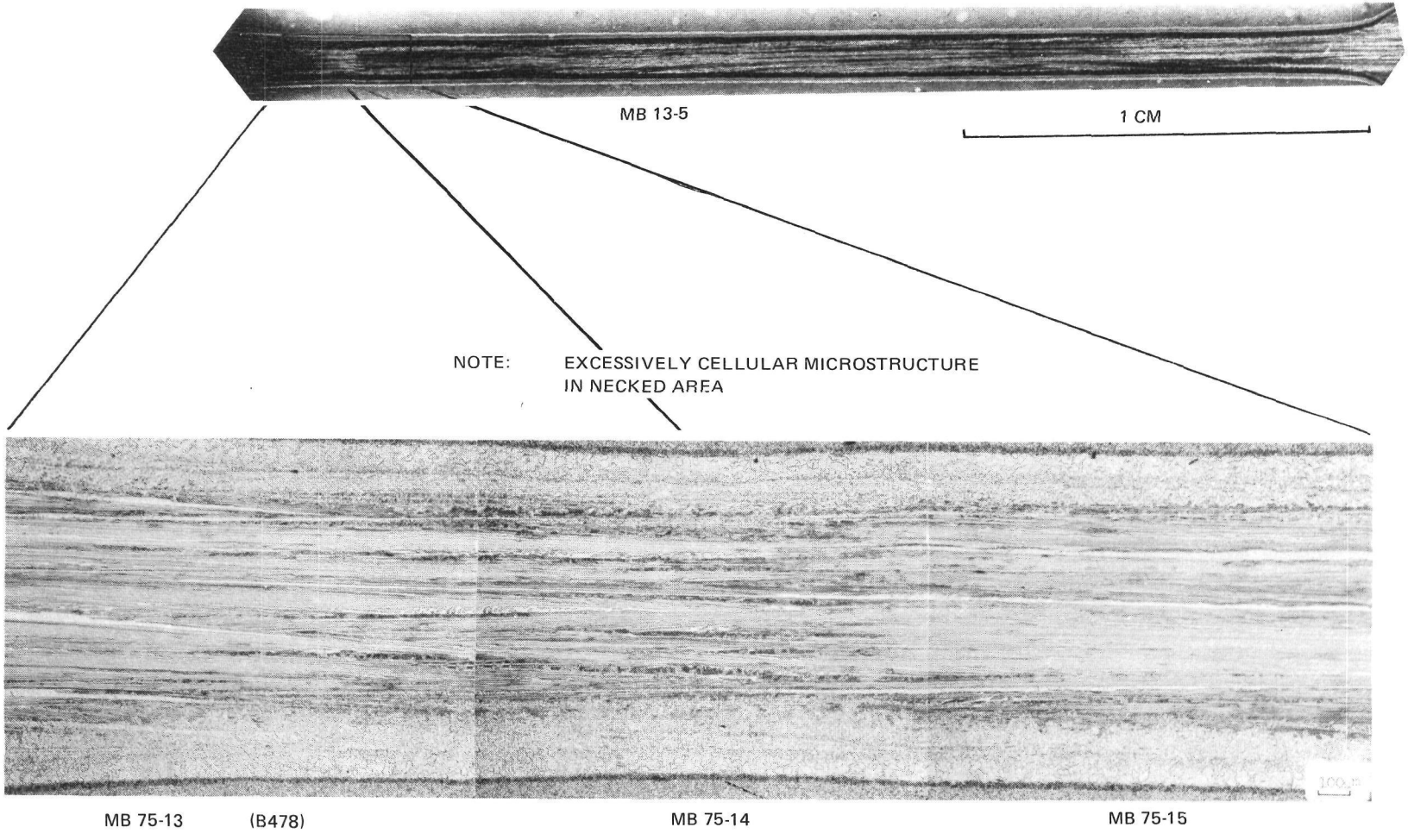



Figure 27 Cellular Microstructure Observed in Necked Area of Specimen A74-216-02 Tested to One Percent Extension at 871°C/331 MPa (1600°F/48 ksi)

R14-47

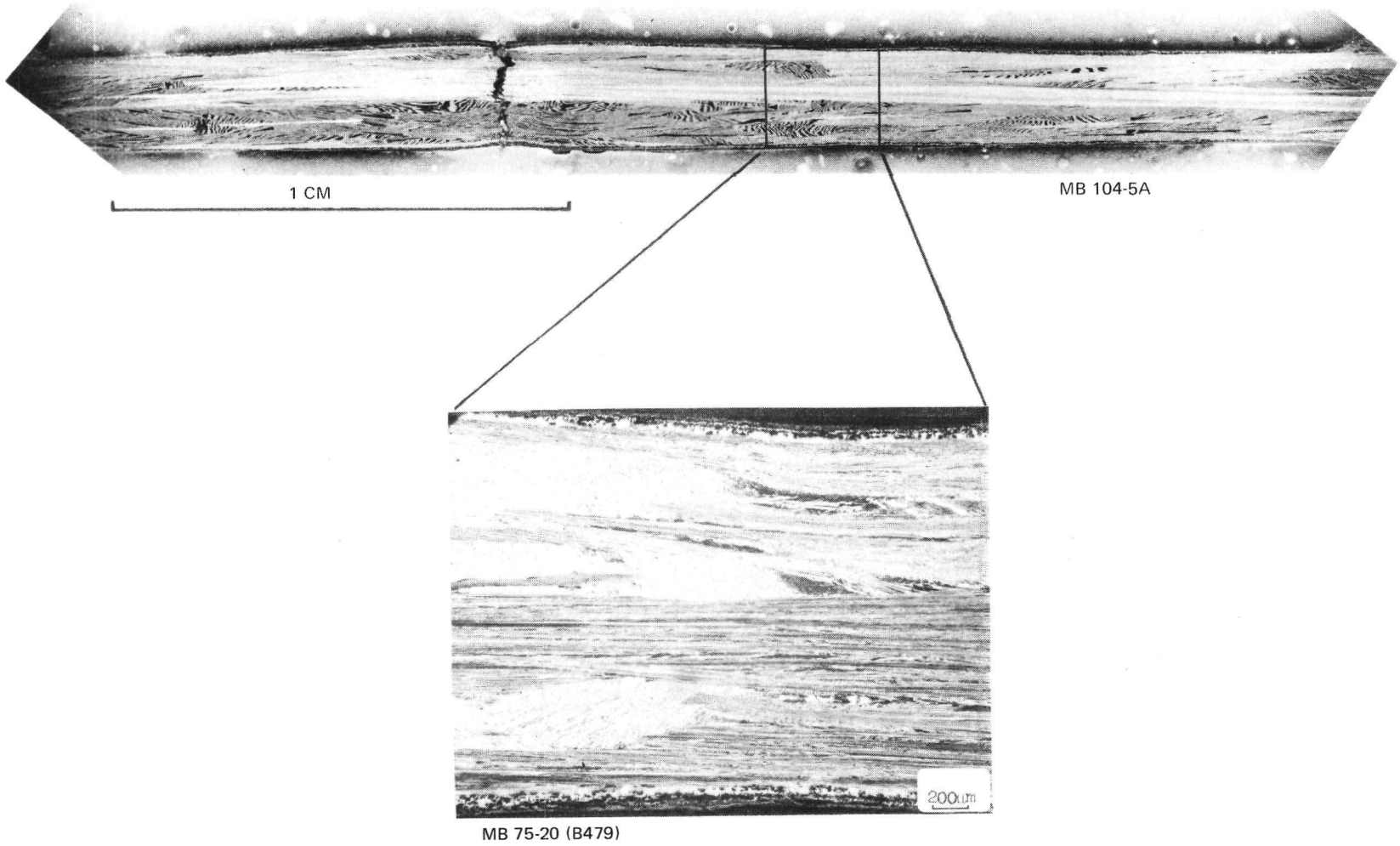
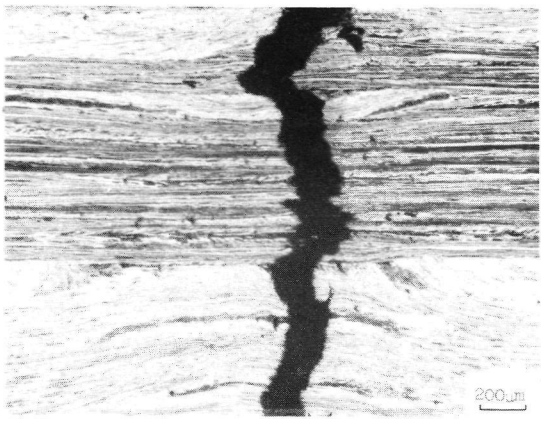


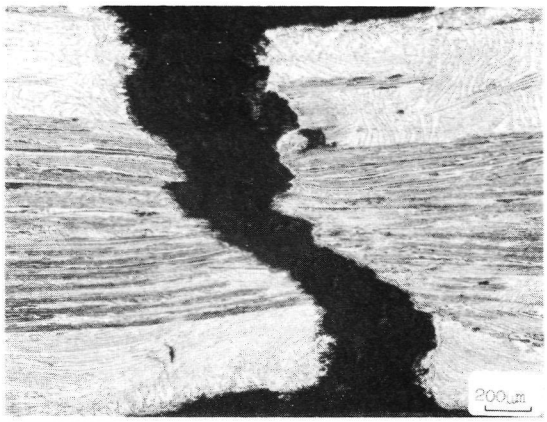

Figure 28 Cellular Microstructure Observed in Secondary Neck Found in Specimen A74-698-02 Ruptured in 1073 Hours at 871°C/356 MPa (1600°F/51.6 ksi)

R14-48



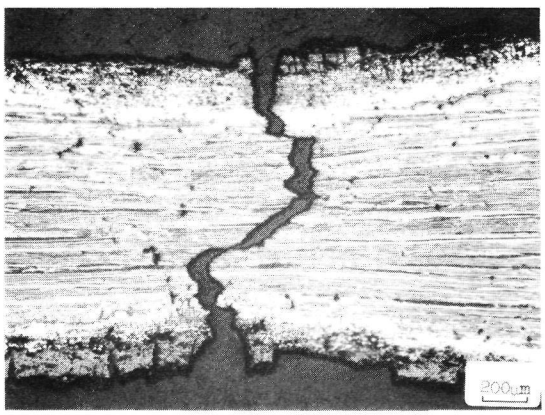

MB 75-19 (B479)

a) Specimen A74-698-02 ruptured in 1073 hours at 871°C/356 MPa (1600°F/51.6 ksi).



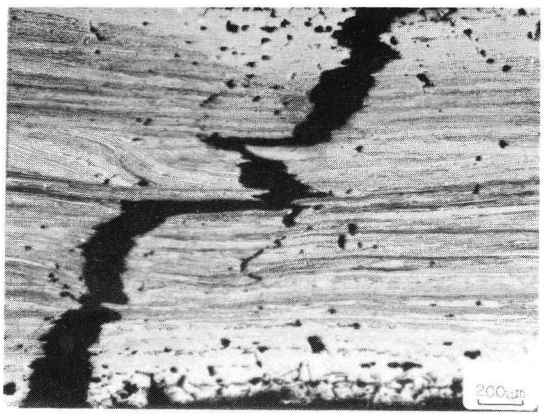

MB 75-10 (B480)

c) Specimen A74-561-01 ruptured in 846 hours at 1038°C/108 MPa (1900°F/15.7 ksi).




(B527)

b) Specimen A74-676-02 creep tested 2784 hours to 1% extension at 871°C/317 MPa (1600°F/46 ksi) and retested 601 hours to rupture at 871°C/417 MPa (1600°F/60.5 ksi).




MB 75-1 (B481)

d) Specimen A74-685-02 creep tested 1489 hours to 1% extension at 1038°C/92 MPa (1900°F/13.3 ksi) and retested 42 hours to rupture at 1038°C/141 MPa (1900°F/20.4 ksi).

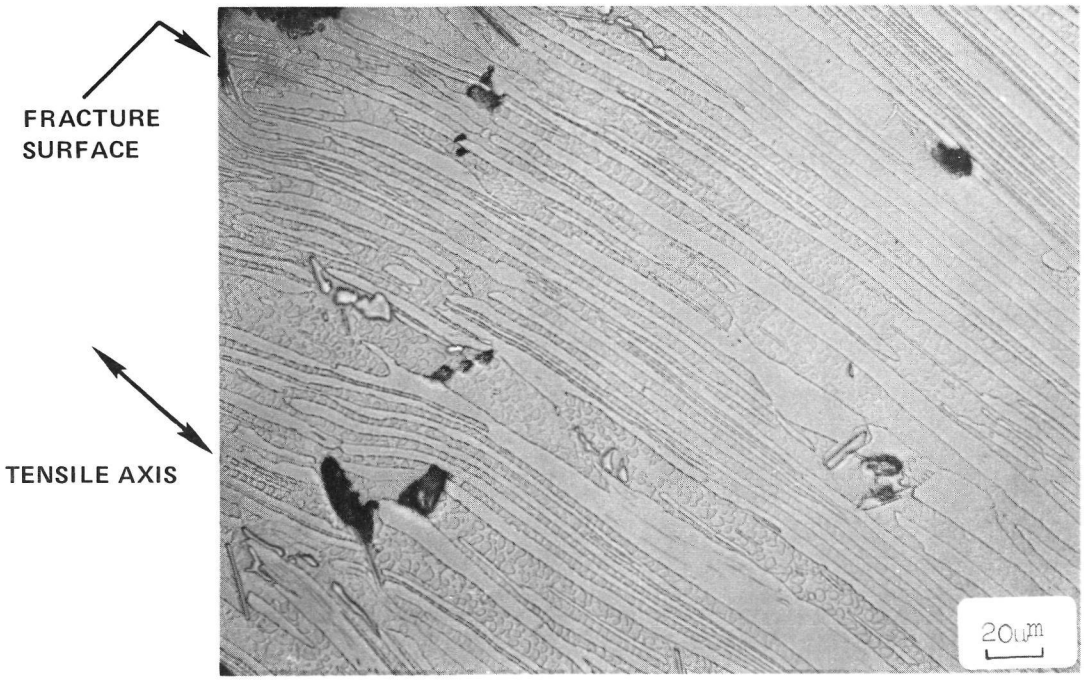
R14-49

Figure 29 Fracture Profiles of Cellular 6 Cr $\gamma/\gamma'$ - $\delta$ Directionally Solidified Eutectic Alloy Broken in Creep-Rupture at Various Stresses and Temperatures




MB 75-23 (B479)

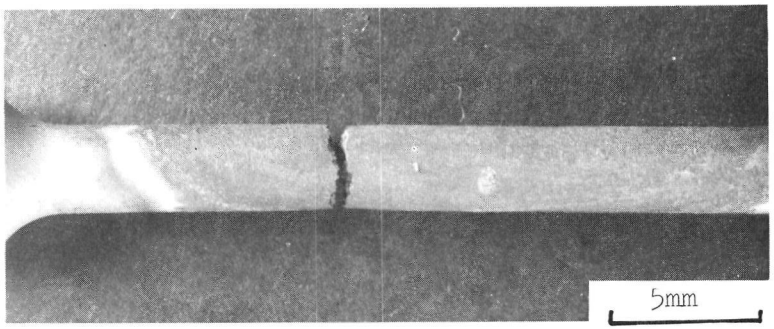
a) Specimen A74-698-02 ruptured in 1073 hours at 871°C/356 MPa (1600°F/51.6 ksi).




MB 75-2 (B481)

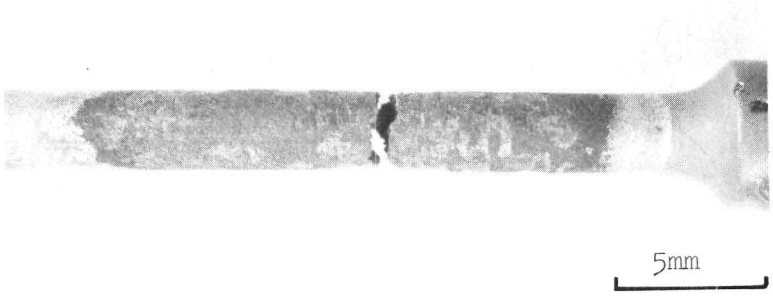
b) Specimen A74-685-02 tested to 1% extension in 1489 hours at 1038°C/92 MPa (1900°F/13.3 ksi) and retested to rupture in 42.2 hours at 1038°C/141 MPa (1900°F/20.4 ksi).

Figure 30 Void Formation in Cellular 6 Cr $\gamma/\gamma'$ - $\delta$ Directionally Solidified Eutectic Specimens Creep Tested at 871°C (1600°F) and 1038°C (1900°F) R14-50



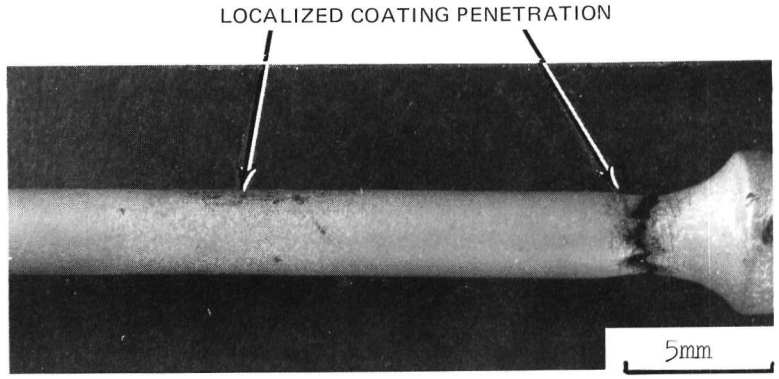

MB 13-3 (B479)

a) Specimen A74-698-02 ruptured in 1073 hours at 871°C/356 MPa (1600°F/51.6 ksi) - coating absent from most of gage section.



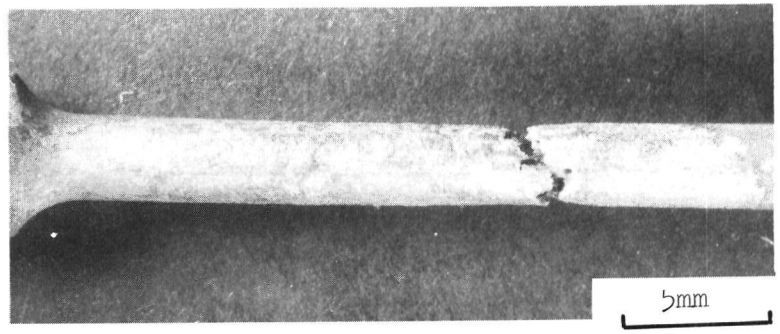

(B527)

b) Specimen A74-676-02 creep tested 2784 hours to 1% extension at 871° C/317 MPa (1600°F/46 ksi) and retested 601 hours to rupture at 871°C/417 (1600°F/60.5 ksi). Coating absent from about 2/3 of gage section.




MB 13-4 (B480)

c) Specimen A74-561-01 ruptured in 846 hours at 1038°C/108 MPa (1900°F/15.7 ksi).

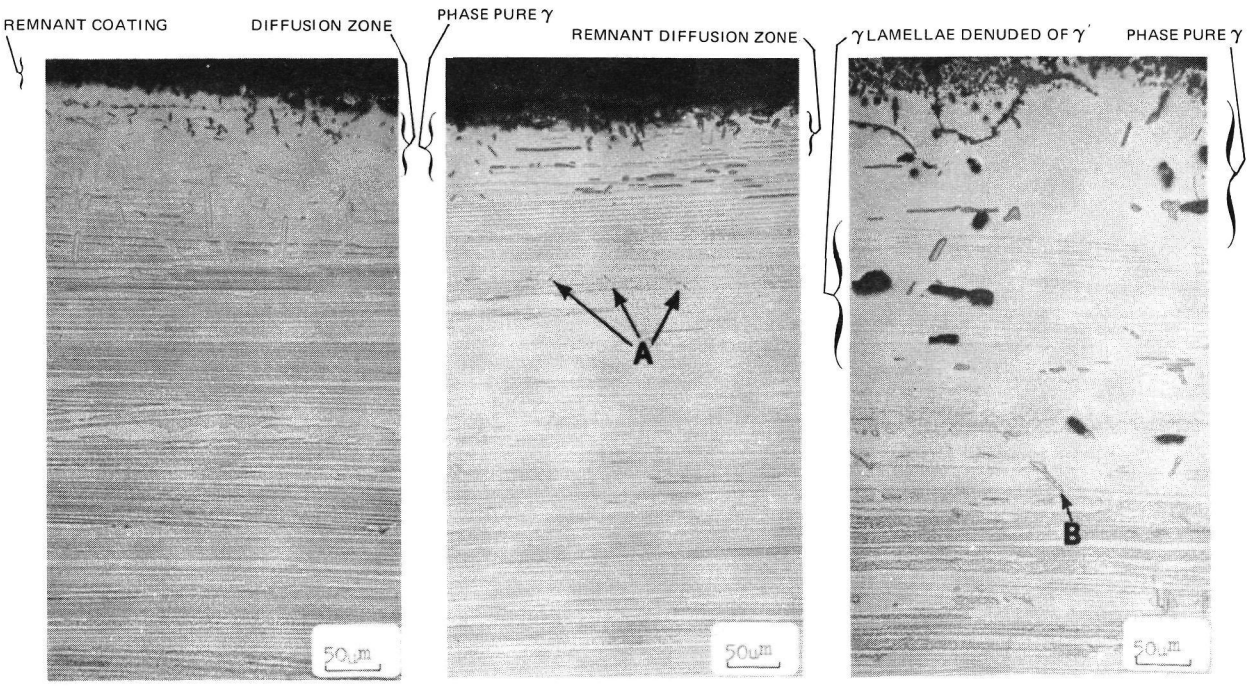



MB 13-2 (B481)

d) Specimen A74-685-02 creep tested 1489 hours to 1% extension at 1038°C/92 MPa (1900°F/13.3 ksi) and retested 42 hours to rupture at 1038°C/141 MPa (1900°F/20.4 ksi) - coating is essentially absent from gage section.

Figure 31 Appearance of Cellular 6 Cr $\gamma/\gamma'$ - $\delta$ Directionally Solidified Eutectic Alloy Creep Test Specimens

R14-51




MB 75-4 (B481)

a) Remnant coating on left, all coating consumed in diffusion zone formation on right.

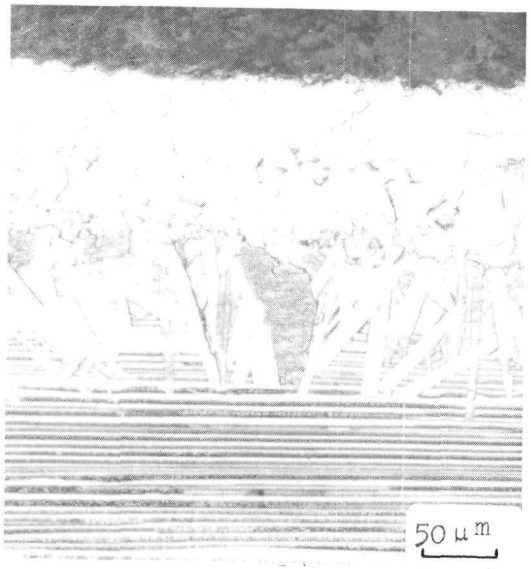
MB 75-3 (B481)

b) Remnant diffusion zone on right, unprotected substrate on left. Note presence of very small unidentified precipitate (A) in substrate under unprotected surface.

BM 75-5 (B481)

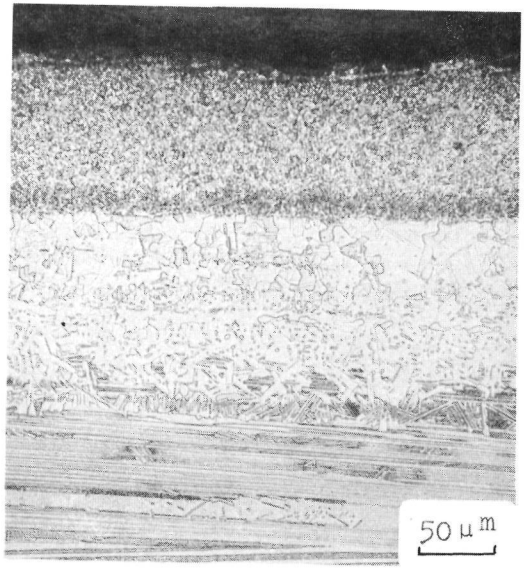
c) Development of a relatively thick layer of phase pure γ. Note that γ lamellae are denuded of γ' phase beneath this layer of γ. Also note development of voids and coarsening of the unidentified precipitate (B).

Figure 32 Illustrating Degrees of Surface Damage Observed in Different Areas of a Long Time Creep Specimen From Which Coating was Partially or Completely Removed During Post-Coat Peening. Specimen A74-685-02 Strained to One Percent Extension at 1038°C/92 MPa (1900°F/13.3 ksi) and Retested to Rupture at 1038°C/141 MPa (1900°F/20.4 ksi). Note That Surface Layer Thicknesses are not Accurately Represented Because of Taper Introduced by Longitudinal Sectioning off the Centerline of Cylindrical Specimens. R14-52



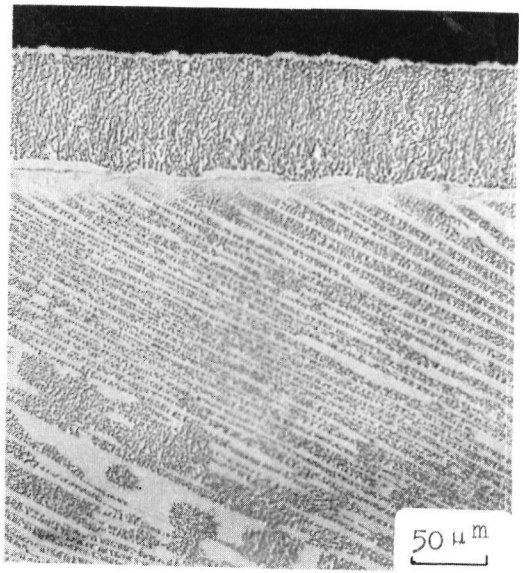

MA 1684-4 (B425)

a) Specimen A74-573-02 creep tested 1232 hours to 1% extension at 1038°C/94 MPa (1900°F/13.6 ksi)




(B478)

b) Specimen A74-216-02 creep tested 2280 hours to 1% extension at 871°C/331 MPa (1600°F/48 ksi)




c) Typical appearance of virgin PWA 270 coating on D. S. 6Cr $\gamma/\gamma' - \delta$ substrate

Figure 33 Influence of Creep Exposure on the Appearance of PWA 270 Coating Applied to Cellular 6 Cr $\gamma/\gamma' - \delta$ Directionally Solidified Eutectic Alloy. Note That Coating Thicknesses on Creep Test Specimens are not Accurately Represented Because of Taper Introduced by Longitudinal Sectioning off the Centerline of Cylindrical Test Specimens

R14-53

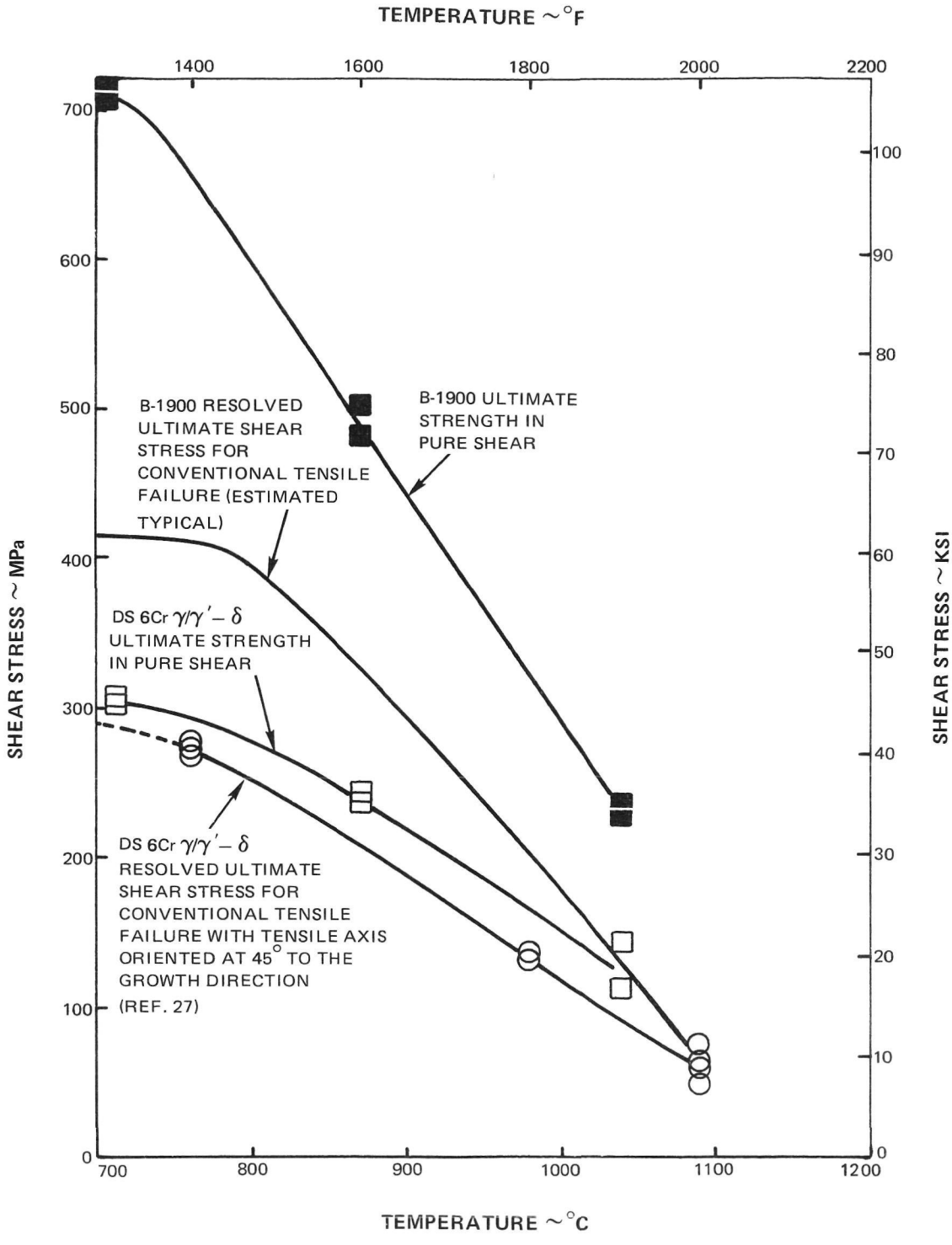
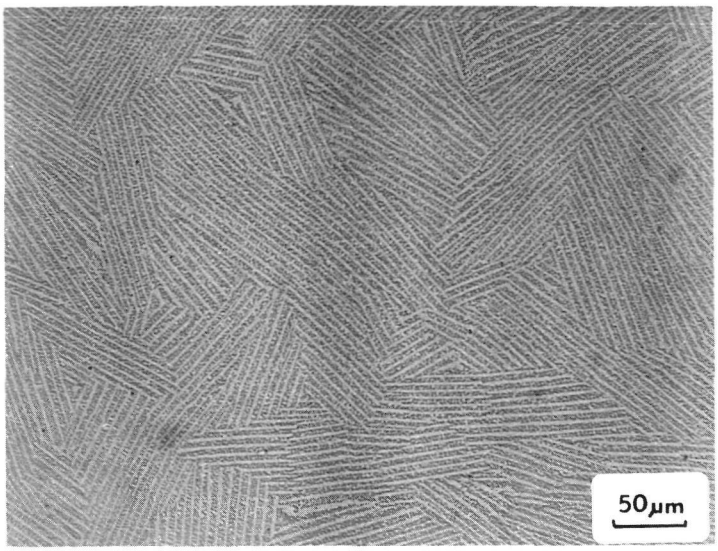
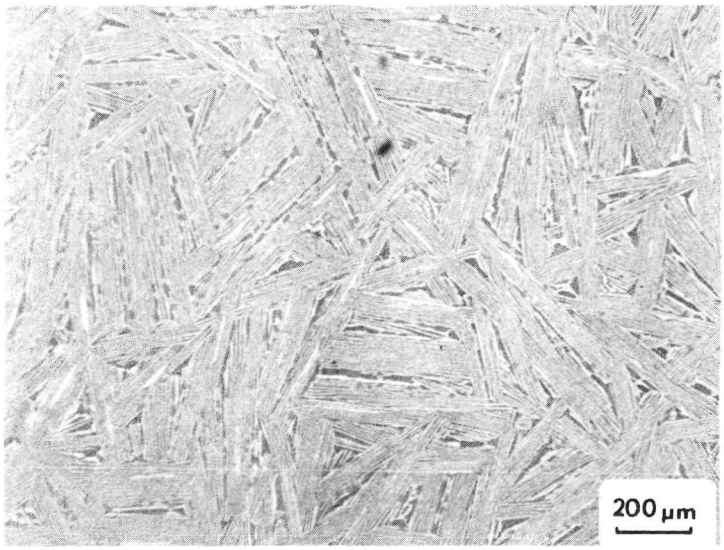



Figure 34 Comparison of Ultimate Shear Strength for Lamellar and Cellular 6 Cr $\gamma/\gamma' - \delta$ Directionally Solidified Eutectic and Conventionally Cast B-1900 Alloy




E-214-2-1

(a) Typical Microstructure Observed In Lamellar Shear Test Specimens.

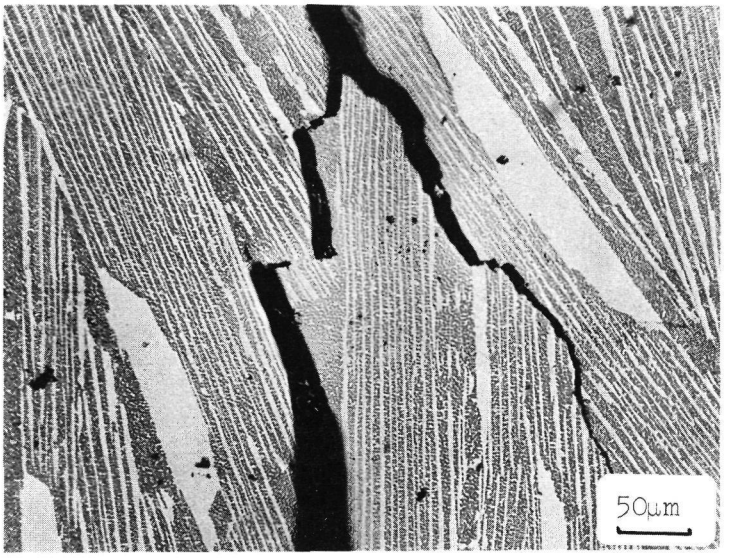



E-214-3-7

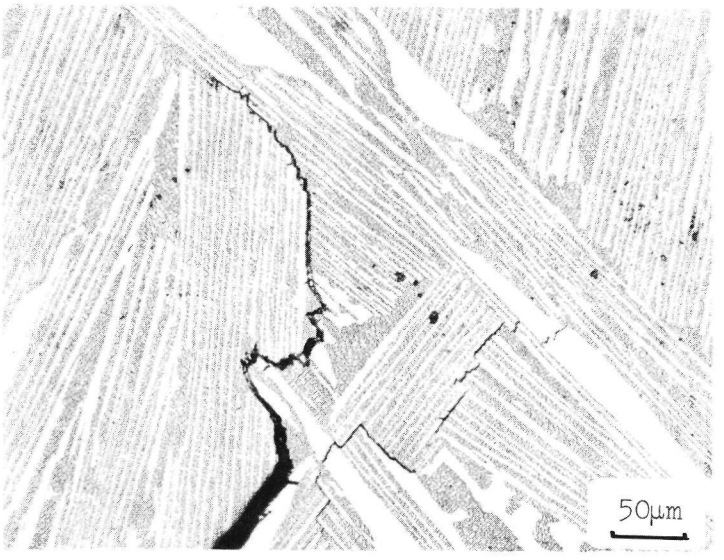
(b) Typical Microstructure Observed In Partially Cellular Shear Test Specimens

R14-55

Figure 35 Comparison of Lamellar and Cellular Microstructures Tested for Measurement of Ultimate Shear Strength in 6 Cr $\gamma/\gamma'$- $\delta$ Directionally Solidified Eutectic Alloy Solidified at 1.3 cm (0.5 inch)/hour




(a) Primary Fracture




(b) Secondary Crack

R14-56

Figure 36 Transverse Sections of Ultimate Shear Strength Specimen E-203-3 Broken at 704°C (1300°F)

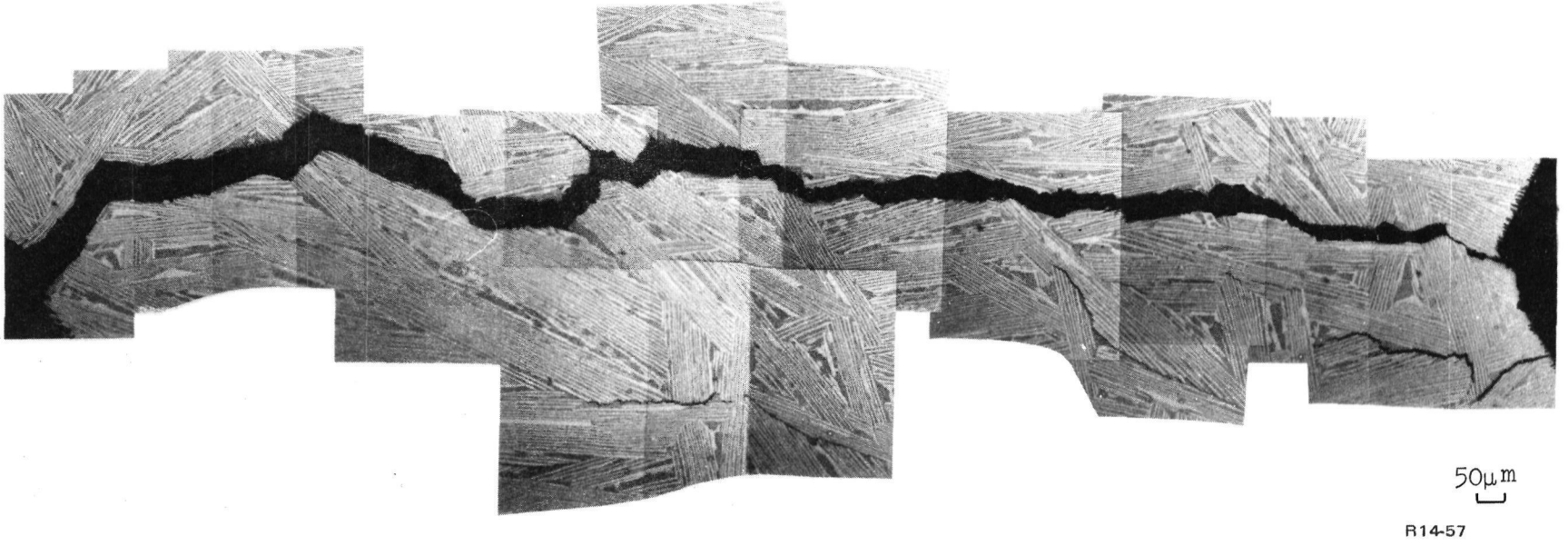



Figure 37 Transverse Section of Ultimate Shear Strength Specimen E-214-37 Broken at 871°C (1600°F)

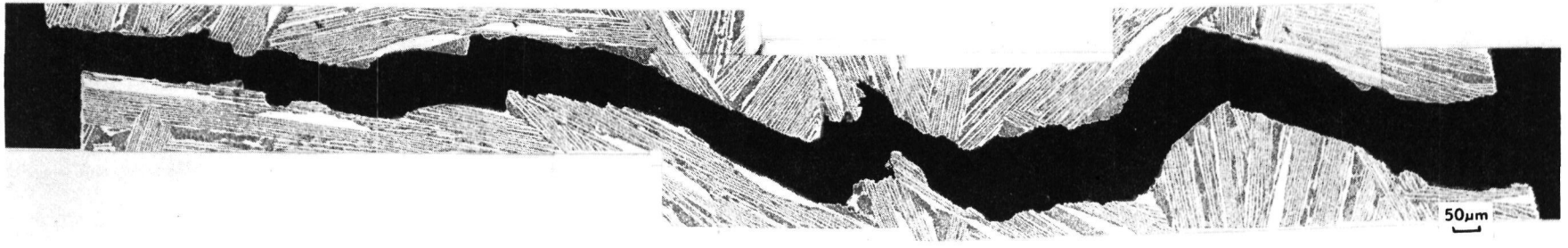



Figure 38 Transverse Section of Ultimate Shear Strength Specimen E-203-2 Broken at 1038°C (1900°F)




R14-59

Figure 39 Transverse Section of Ultimate Shear Strength Specimen E-214-25 Broken at 1038°C (1900°F)

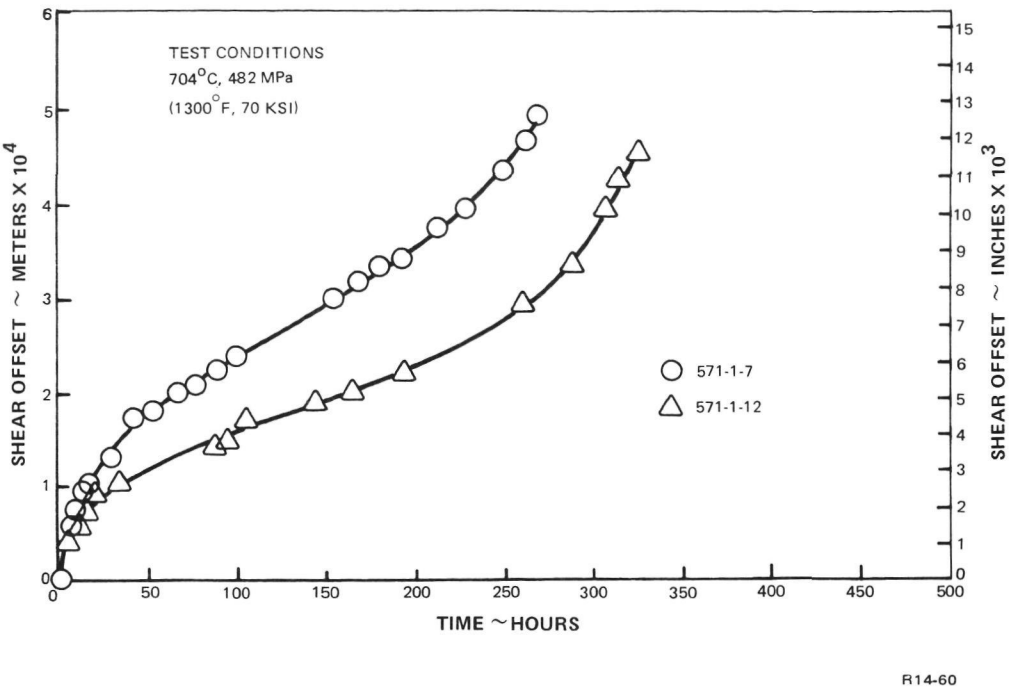



Figure 40 Shear Creep Results for B-1900 Alloy Tested at 704°C (1300°F)

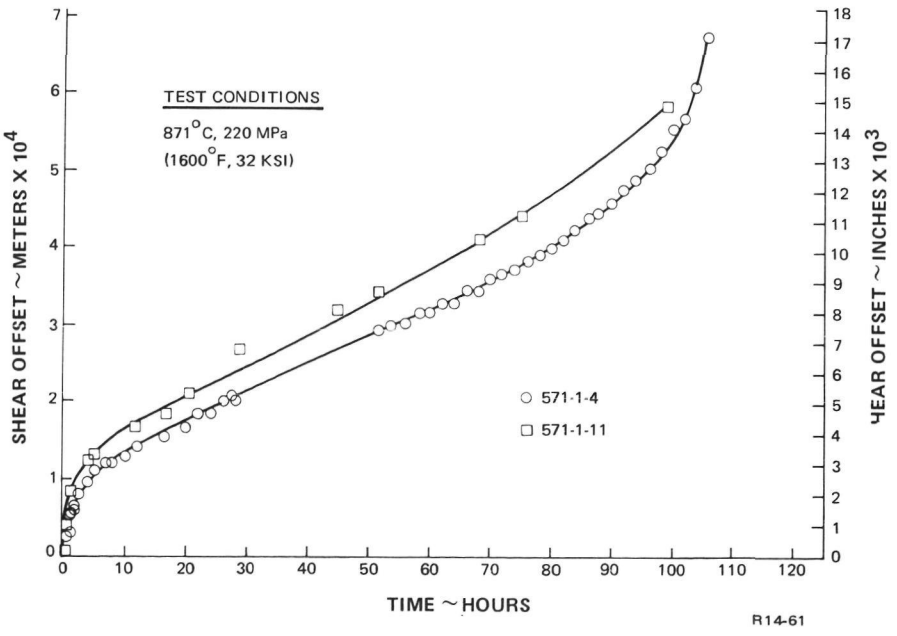



Figure 41 Shear Creep Results for B-1900 Alloy Tested at 871°C (1600°F)

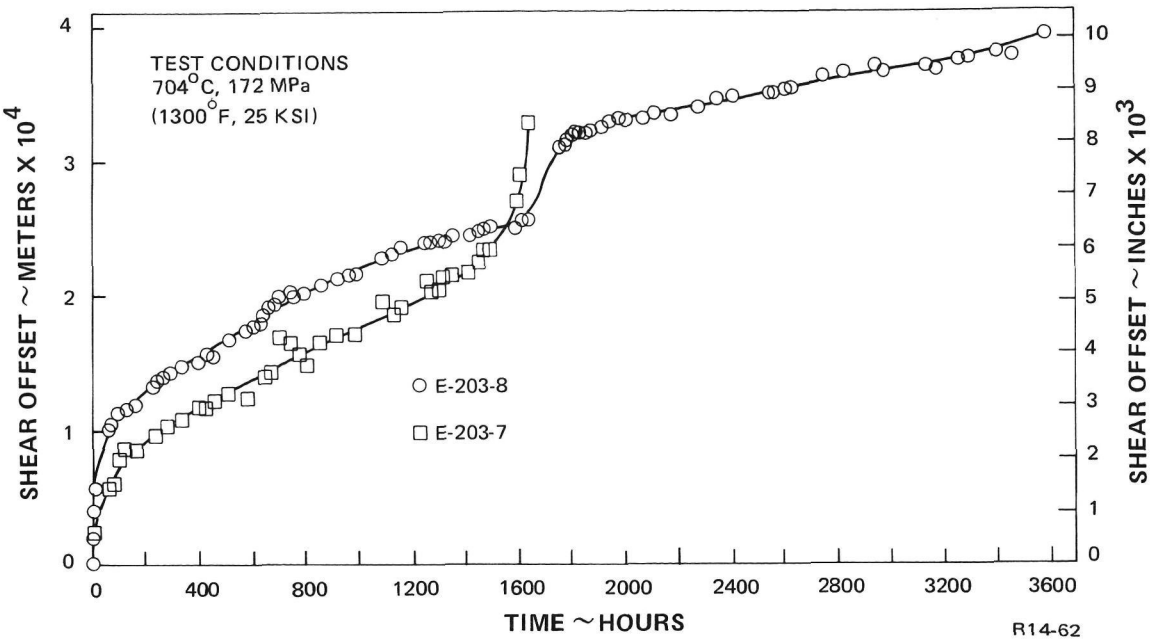



Figure 42 Shear Creep Results for Cellular 6 Cr $\gamma/\gamma'$ - $\delta$ Directionally Solidified Eutectic Alloy Tested at 704°C (1300°F) With the Direction of Shear Loading Parallel to the Growth Direction. Material Grown in Slab Form at a Rate of 1.3 cm (0.5 inch)/hour

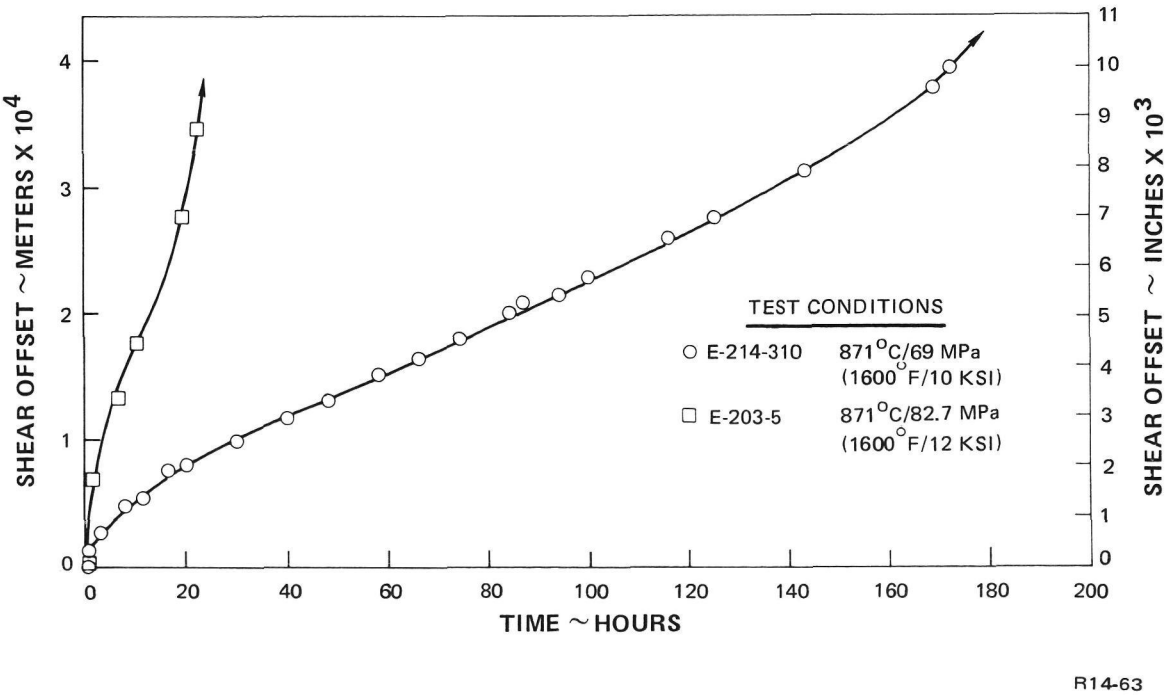



Figure 43 Shear Creep Results on Cellular 6 Cr $\gamma/\gamma'$ - $\delta$ Directionally Solidified Eutectic Alloy Tested at 871°C (1600°F) With the Direction of Shear Loading Parallel to Growth Direction. Material Grown in Slab Form at a Rate of 1.3 cm (0.5 inch)/hour

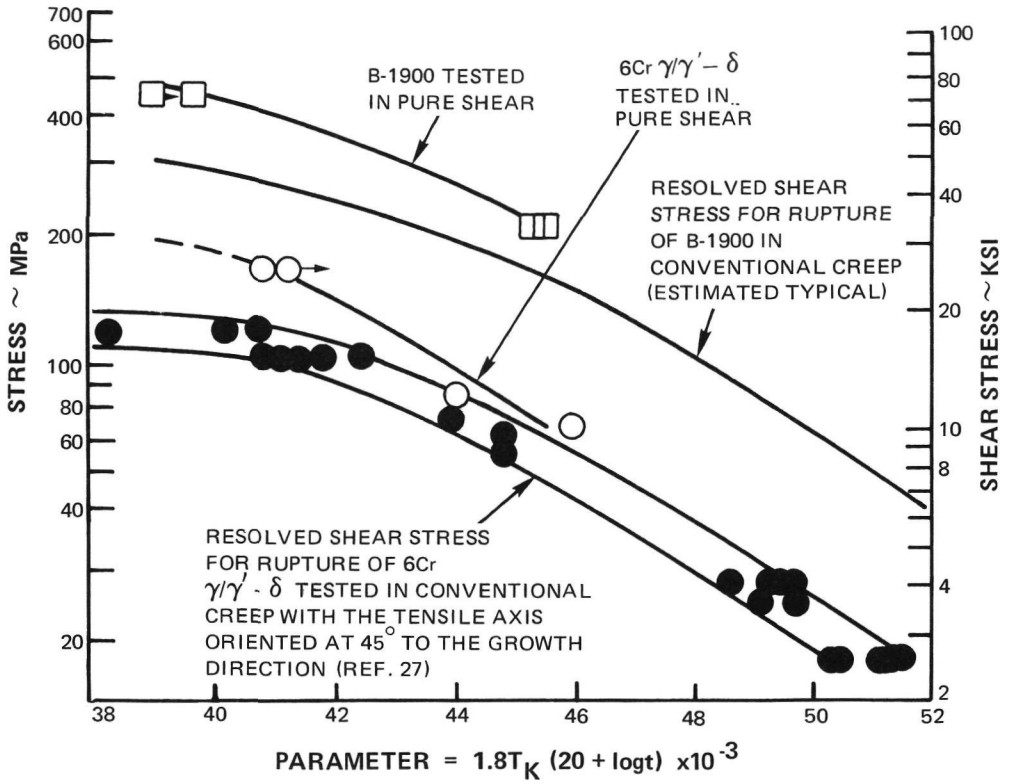



Figure 44 Comparison of Conventionally Cast B-1900 and Cellular 6 Cr $\gamma/\gamma' - \delta$ Directionally Solidified Eutectic Alloy Shear Stress-Rupture Results With Data Obtained From Conventional Tests With the Tensile Axis Oriented at 45 Degrees to the Growth Direction of the Eutectic. Various Processing Conditions Represented

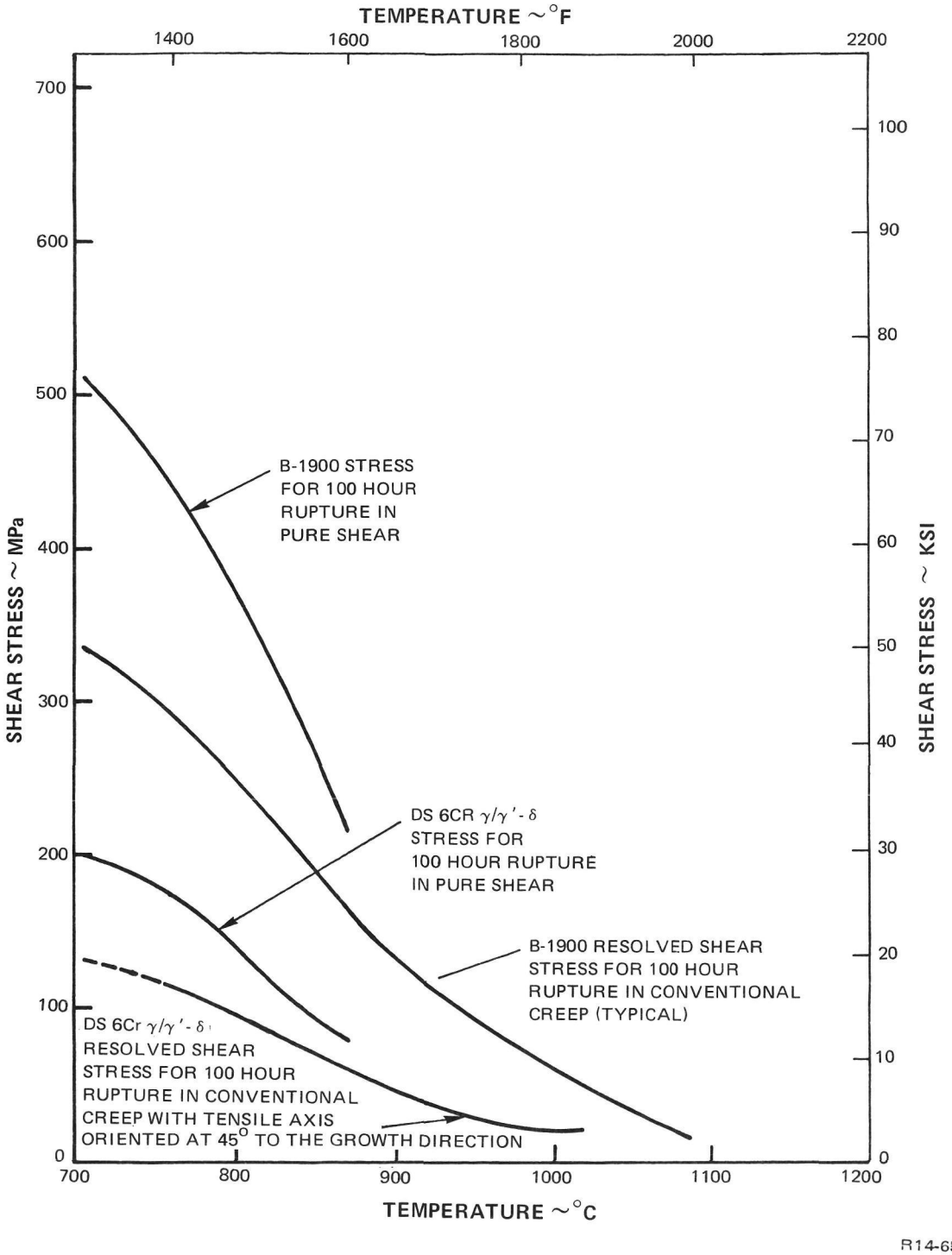



Figure 45 Comparison of Shear-Rupture for Cellular 6 Cr $\gamma/\gamma'$ - $\delta$ Directionally Solidified Eutectic and Conventionally Cast B-1900 Material

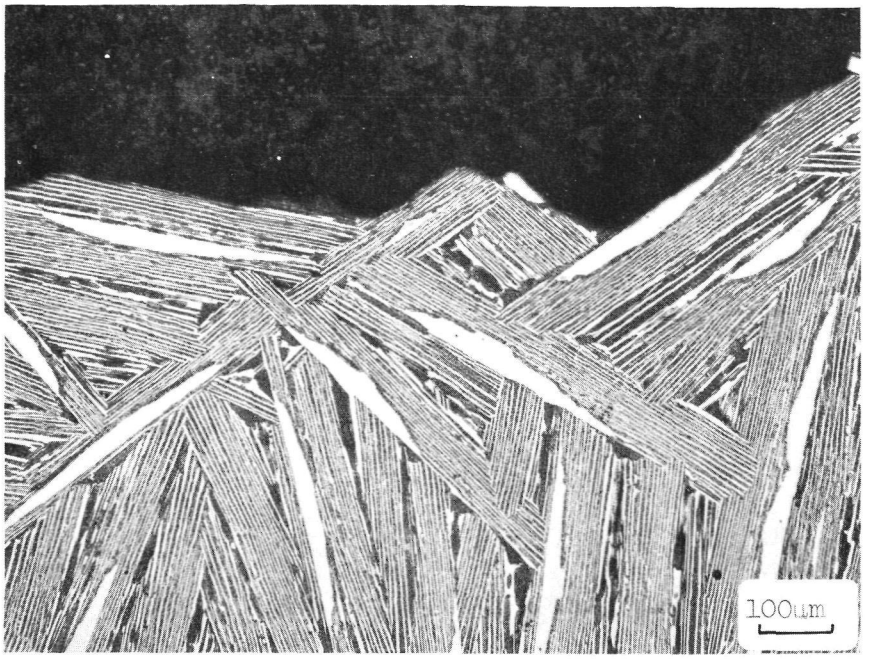



Figure 46 Typical Fracture Appearance Observed in 704 and 871°C (1300 and 1600°F) Shear-Rupture Specimens of Cellular 6 Cr $\gamma/\gamma'$-$\delta$ Directionally Solidified Eutectic Alloy. Specimen Shown is E-203-5 Ruptured in 24 Hours at 871°C/ 83 MPa (1600°F/12 ksi)

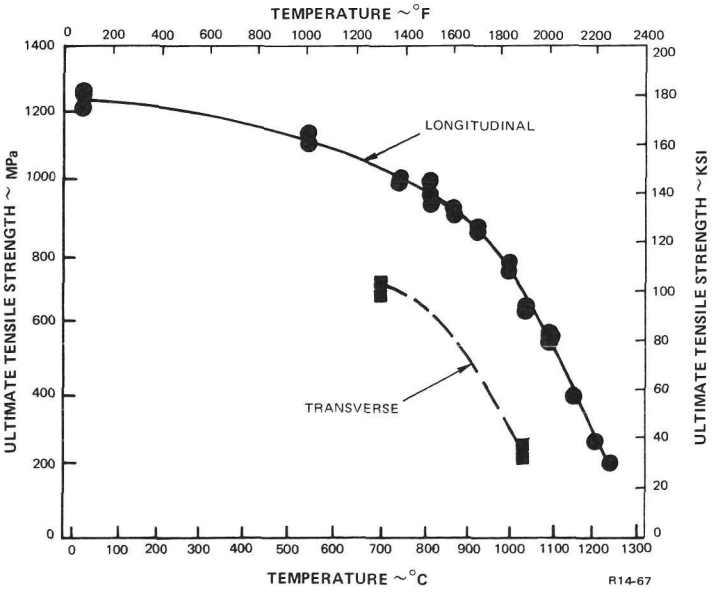



Figure 47 Comparison of Longitudinal and Transverse Tensile Strengths of Cellular 6 Cr $\gamma/\gamma'$ - $\delta$ Directionally Solidified Eutectic Alloy. Various Processing Conditions Represented

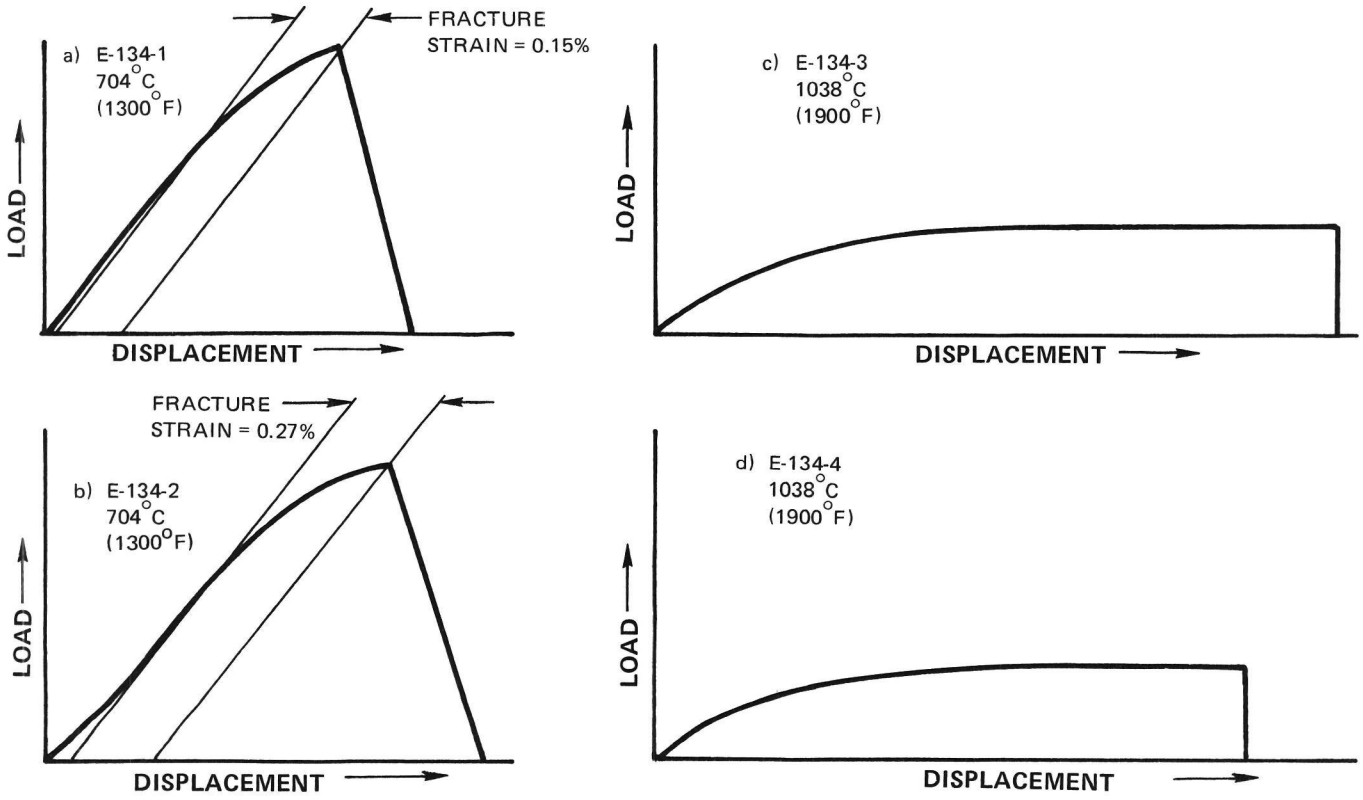
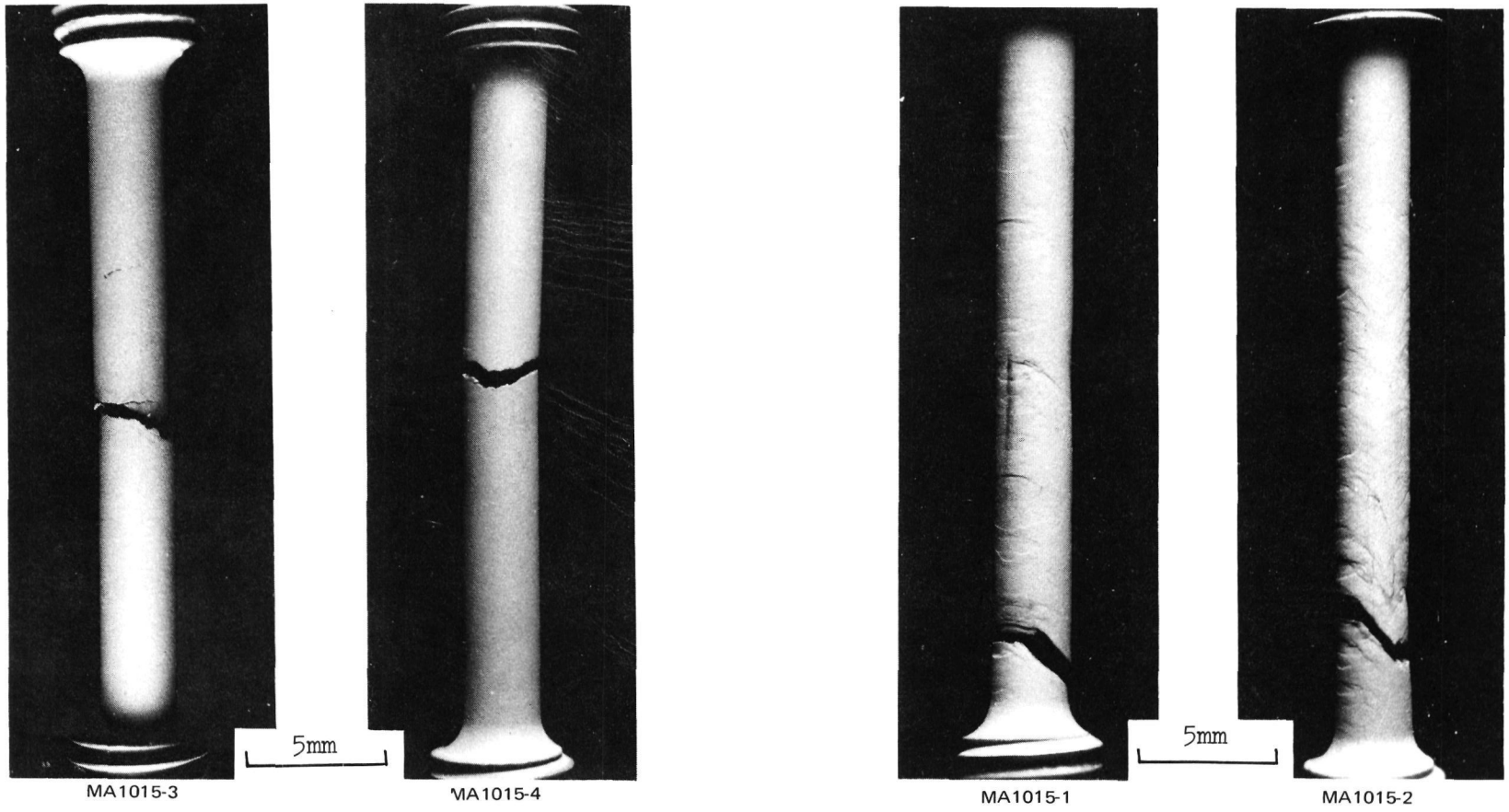



Figure 48 Load Versus Displacement Curves for Cellular 6 Cr $\gamma/\gamma'$ - $\delta$ Directionally Solidified Eutectic Alloy Transverse Tension Tests. (Note: Load and Displacement Scales Arbitrary)




(a) E-134-1 (b) E-134-2

Tested at 704°C (1300°F)

(c) E-134-3 (d) E-134-4

Tested at 1038°C (1900°F)

R14-69

Figure 49 Appearance of Broken Transverse Tension Test Specimens of Cellular 6 Cr $\gamma/\gamma' - \delta$ Directionally Solidified Eutectic Alloy Obtained From Foundry Slab E-134 Grown at 1.3 cm (0.5 inches)/hour

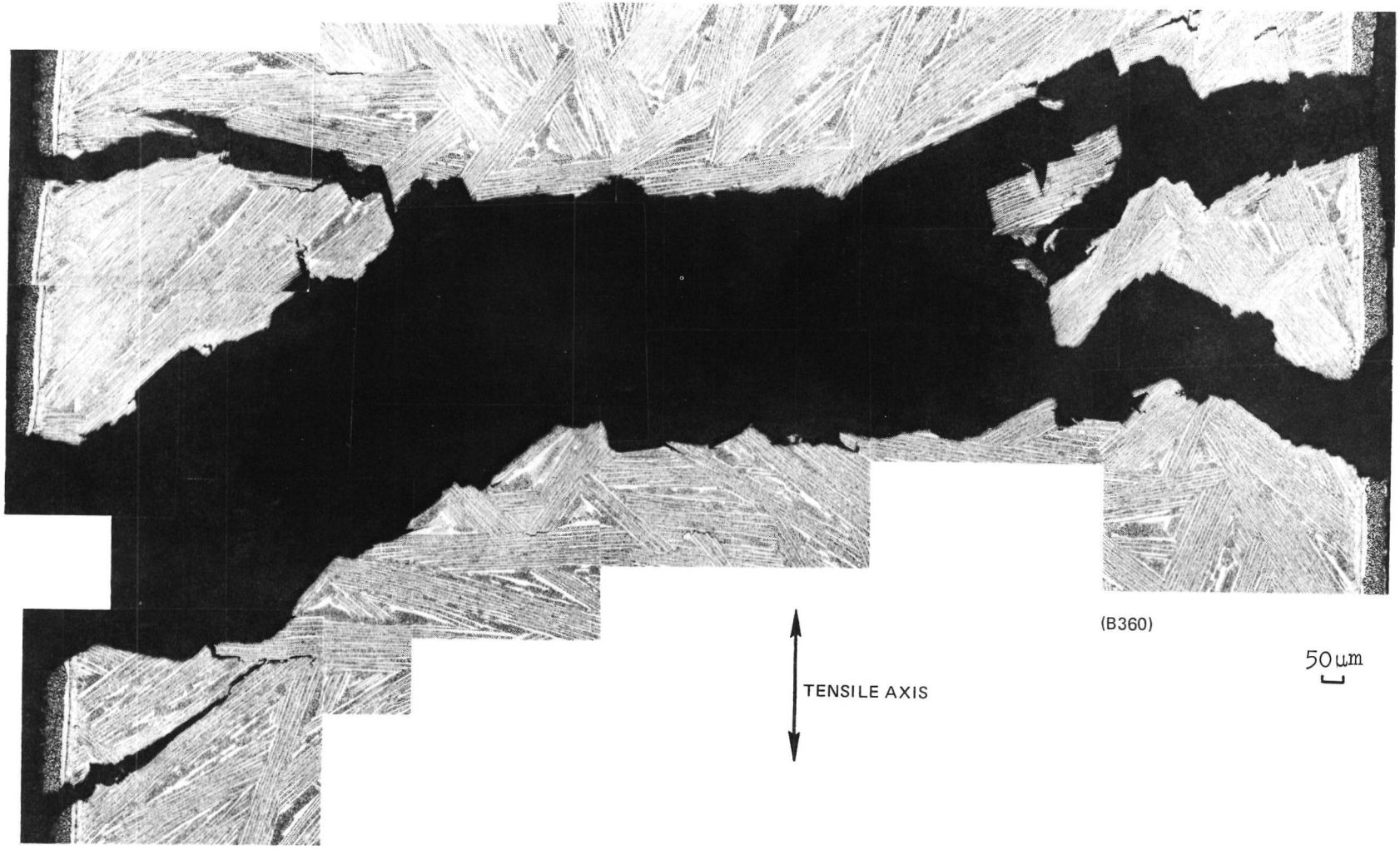
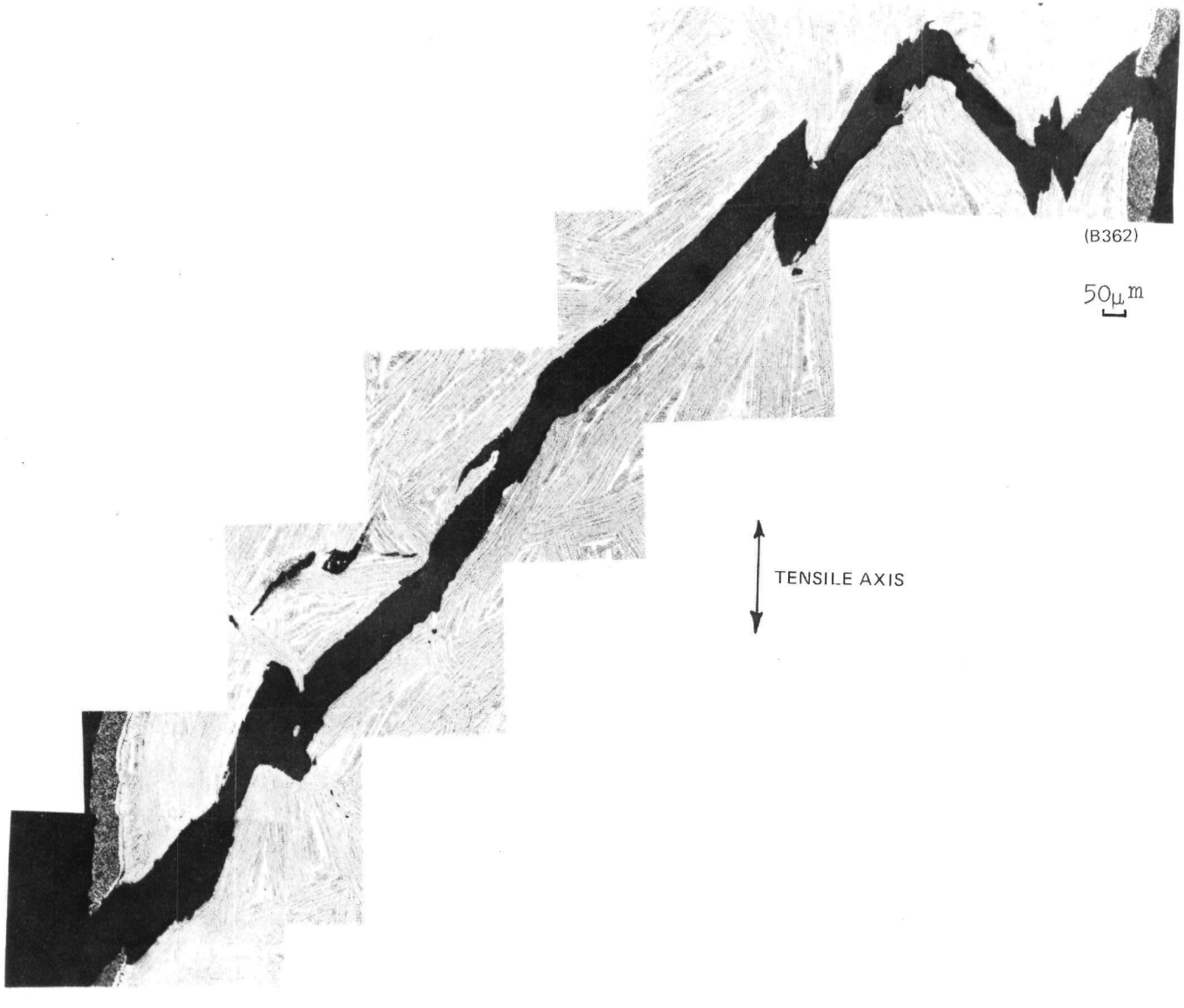


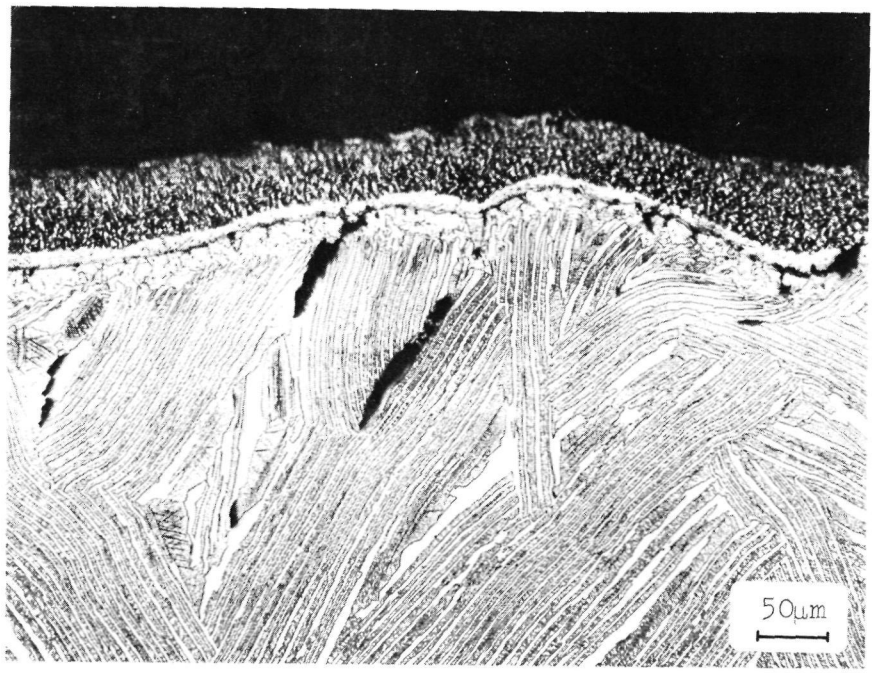

Figure 50 Fracture Profile of Transverse Specimen E-134-2 Broken in Tension at 704°C (1300°F)

R14-70




R14-71

Figure 51 Fracture Profile of Transverse Specimen E-134-4 Broken in Tension at 1038°C (1900°F)




(B362)

R14-72

Figure 52 Subsurface Intergranular Secondary Cracking in Cellular 6 Cr $\gamma/\gamma'$ - $\delta$ Transverse Tension Test Specimen E134-4 Broken in Tension at 1038°C (1900°F)

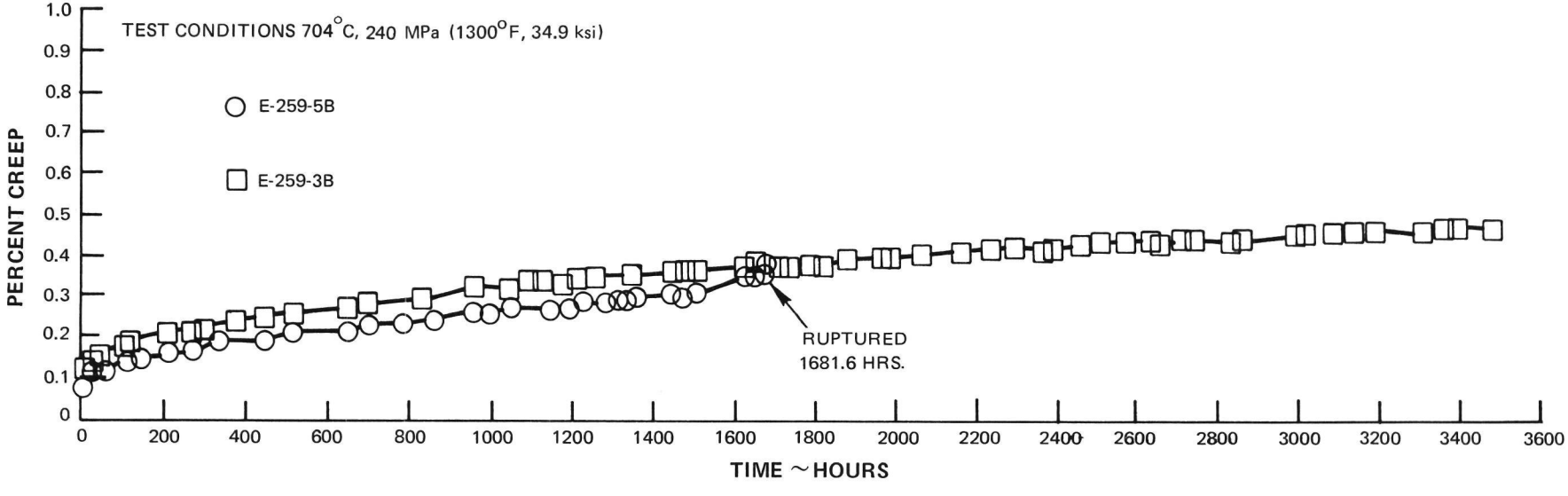
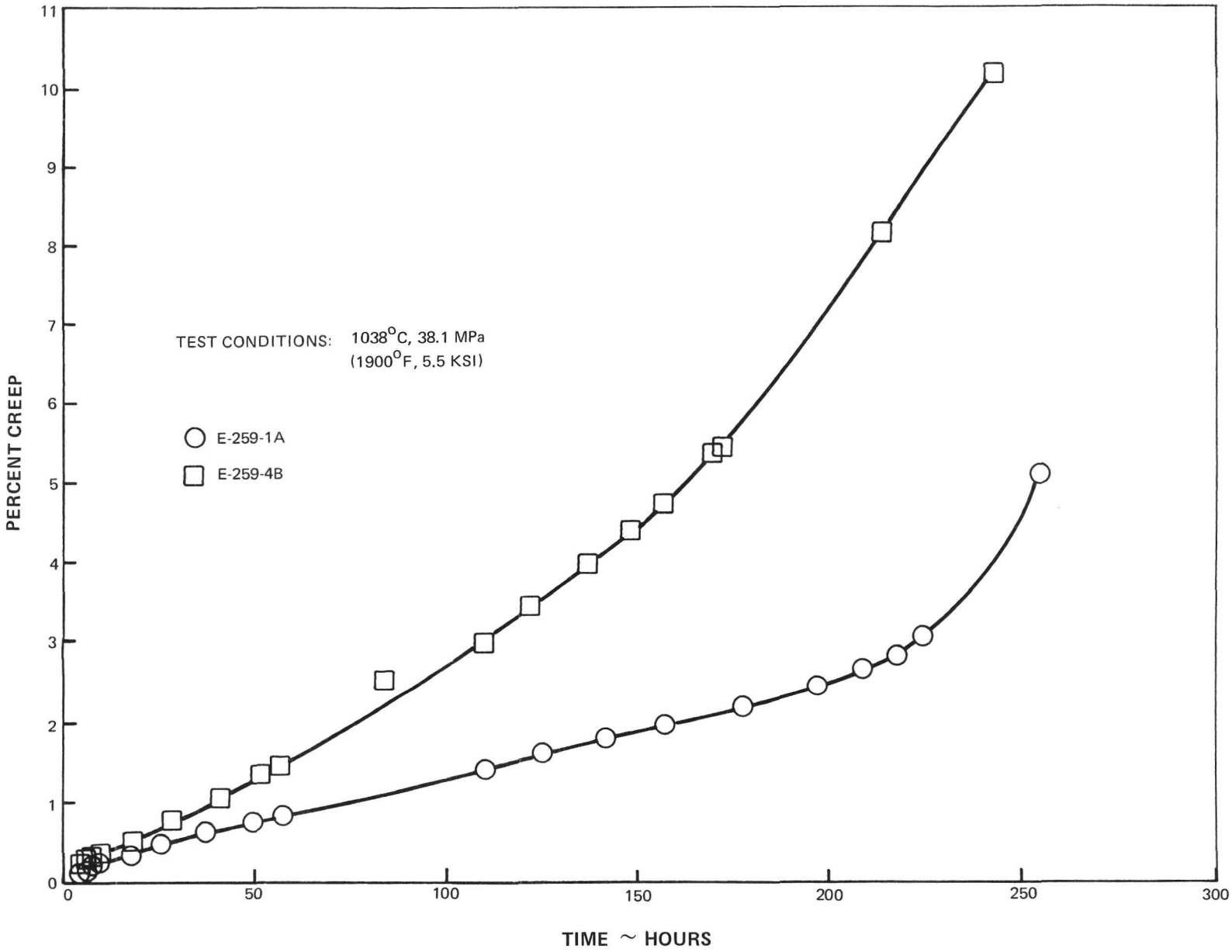



Figure 53 Creep Results for Cellular 6 Cr $\gamma/\gamma'$ - $\delta$ Directionally Solidified Eutectic Alloy Tested at 704°C (1300°F) With the Tensile Axis Oriented at 90 Degrees to the Growth Direction




R14-74

Figure 54 Creep Results for Cellular 6 Cr $\gamma/\gamma'$ - $\delta$ Directionally Solidified Eutectic Alloy Tested at 1038°C (1900°F) With the Tensile Axis Oriented at 90 Degrees to the Growth Direction. Material Grown in Slab Form at a Rate of 1.3 cm (0.5 inches)/hour

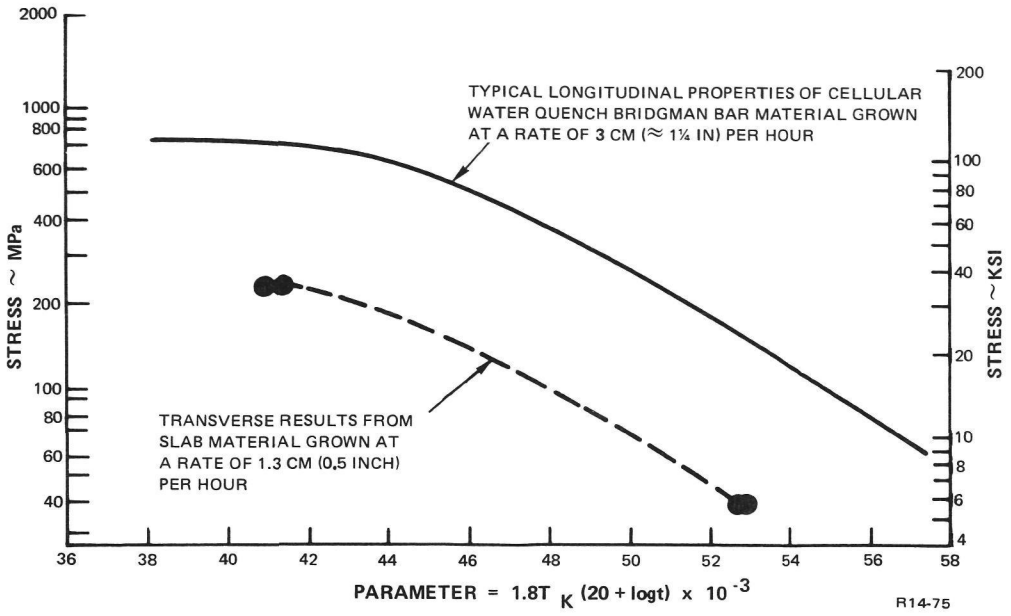
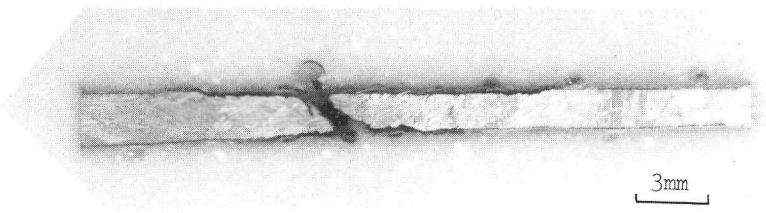
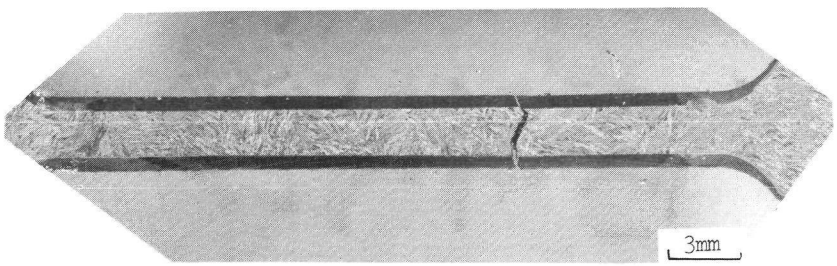



Figure 55 Comparison of Longitudinal and Transverse Rupture Properties of Cellular 6 Cr $\gamma/\gamma'$ - $\delta$ Directionally Solidified Eutectic Alloy



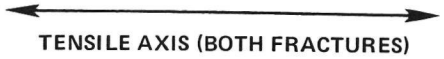

a) Specimen E-259-1A Broken In Creep Rupture at 1038°C/38.1 MPa (1900°F/5.5 KSI). Time to Rupture 74 Hours.

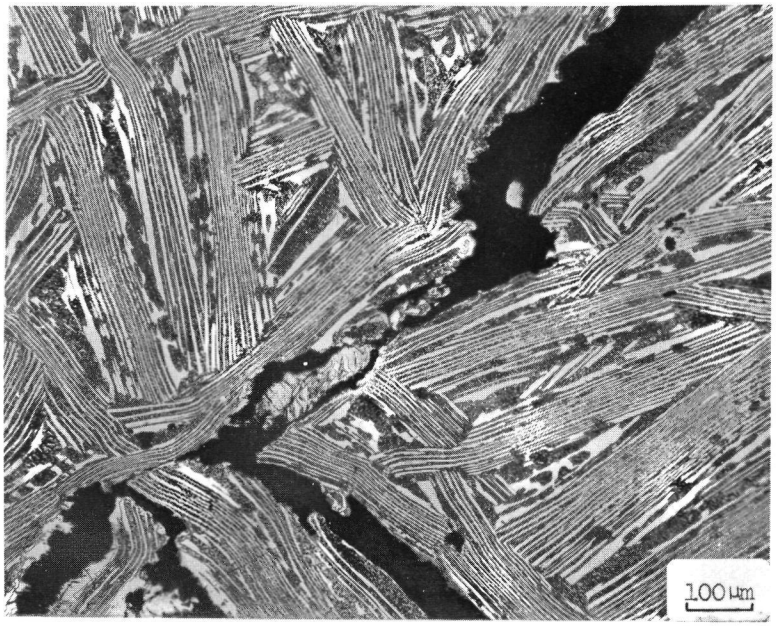



b) Specimen E-259-5B Broken In Creep Rupture at 704°C/241 MPa (1300°F/34.9 KSI). Time to Rupture 1681 Hours.

R14-76

Figure 56 Appearance of Cellular 6 Cr $\gamma/\gamma'$ - $\delta$ Directionally Solidified Eutectic Alloy Creep Specimens Tested With the Tensile Axis Oriented at 90 Degrees to the Growth Direction




MB 124-S (B402)

a) Specimen E-259-4B Broken In Creep Rupture at 1038°C/38.1 MPa (1900°F/5.5 KSI). Time to Rupture 40 Hours.

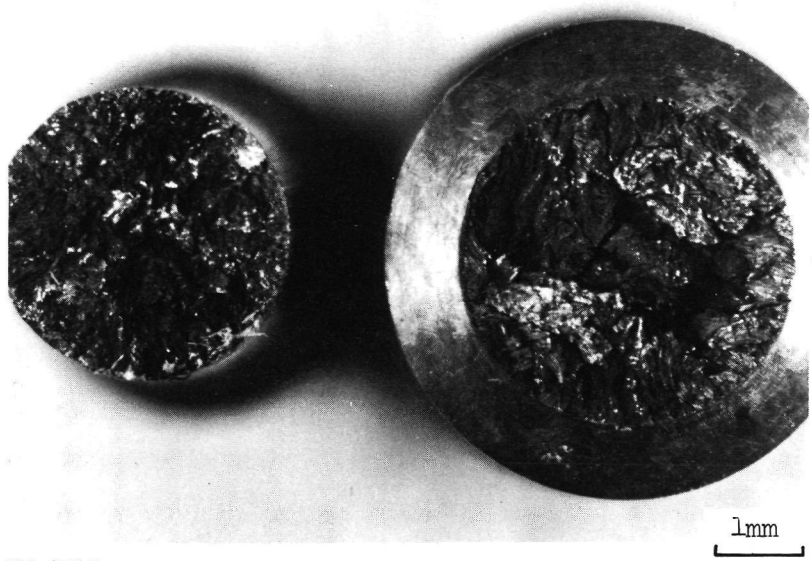



MB 124-6 (B442)

b) Specimen E-259-5B Broken In Creep Rupture at 704°C/241 MPa (1300°F/34.9 KSI). Time to Rupture 1681 Hours.

R14-77

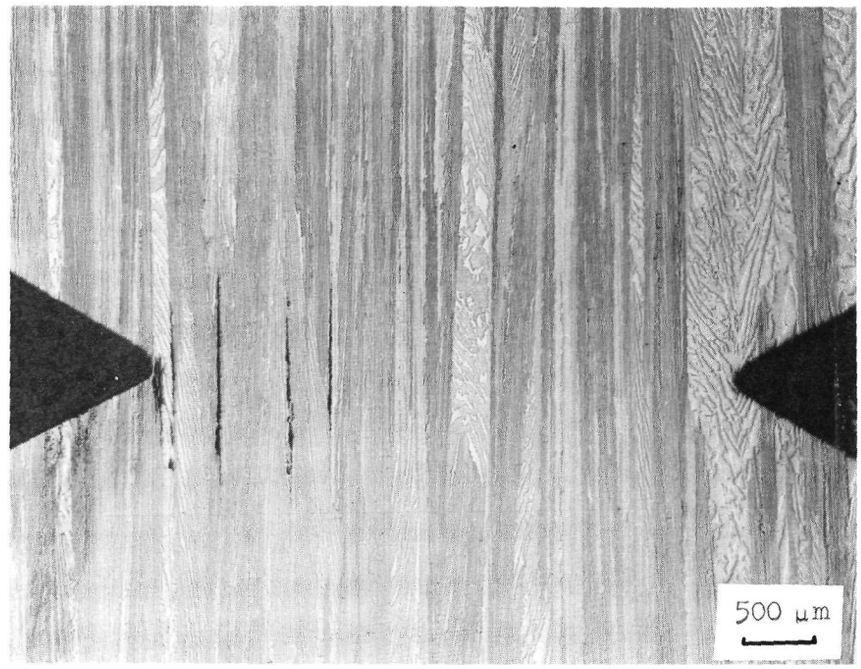
Figure 57 Fracture Appearance Found in Cellular 6 Cr $\gamma/\gamma'$ - $\delta$ Directionally Solidified Eutectic Alloy Creep Specimens Tested With the Tensile Axis Oriented at 90 Degrees to the Growth Direction




MA 479-9

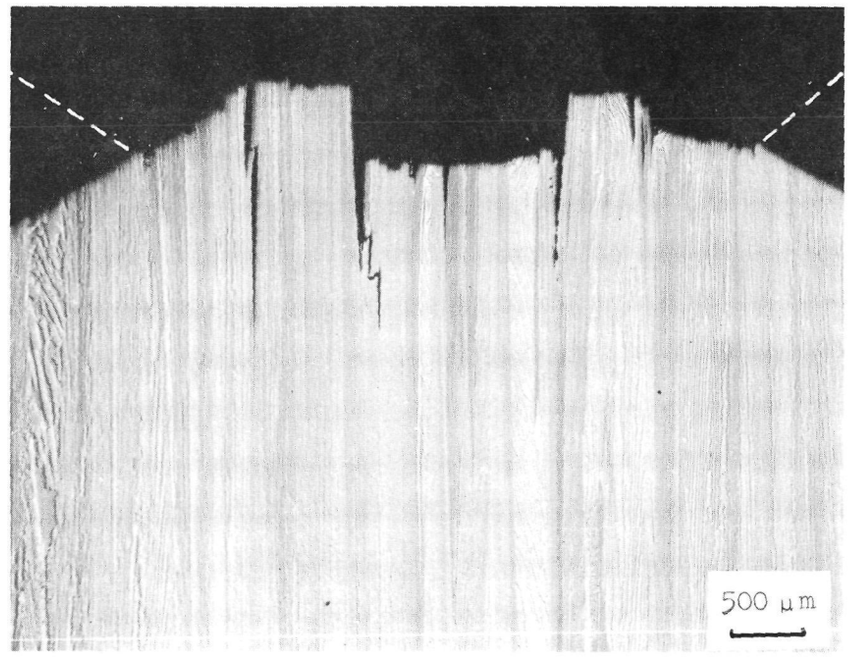
R14-78

Figure 58 Fracture Surfaces of Smooth and Notch Section Failures in Combination Smooth-Notch Specimens A74-055-01 (Smooth Failure) and A74-055-02 (Notch Failure) Broken in Tension at 760°C (1400°F)




MA 479-21 (B330)

a) Transverse Cracking In Notch Zone of Specimen A74-055-01 Which Failed In Smooth Section

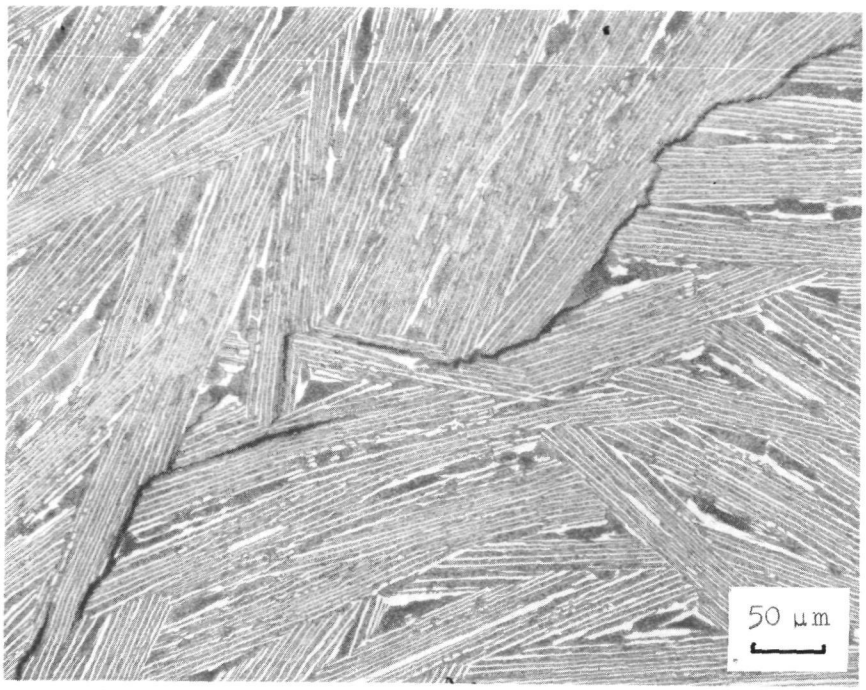



MA 479-17 (B328)

b) Notch Failure In Specimen A74-055-02

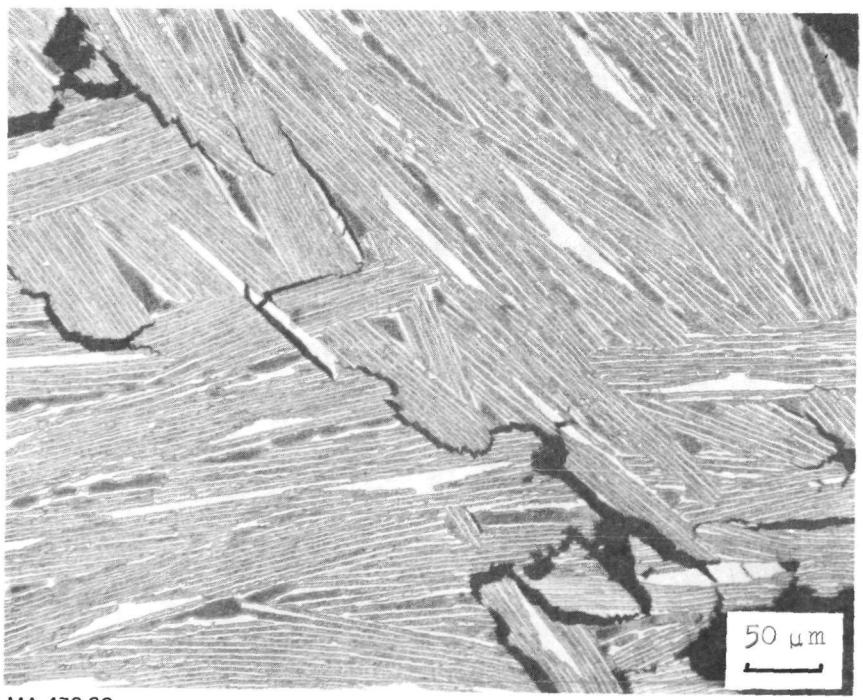
R14-79

Figure 59 Longitudinal Structure in Notch Zone of Combination Smooth-Notch Specimens Broken in Tension at 760°C (1400°F)




MA 479-23

a) Notch Zone of Specimen A74-055-01 Which Failed In Smooth Section

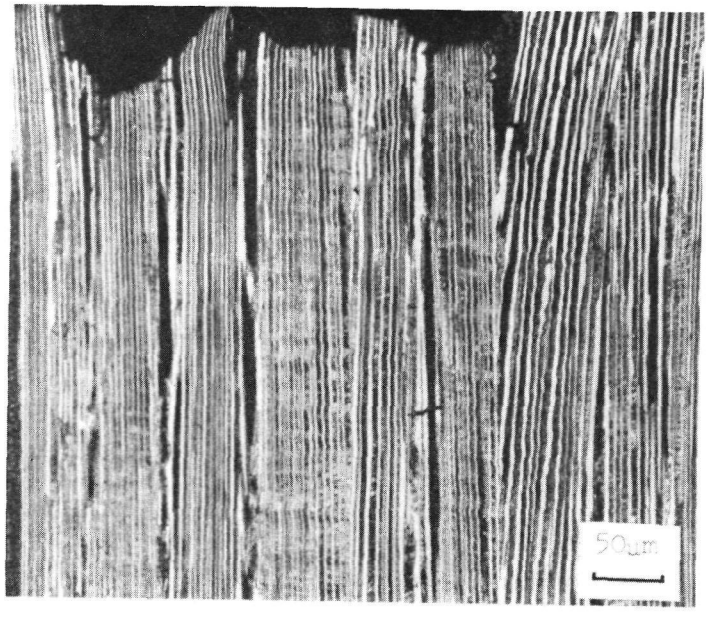



MA 479-22

b) Area Adjacent to Fracture of Specimen A74-055-02 Which Failed In Notch Zone

R14-80

Figure 60 Transverse Sections Through Notch Zone of Combination Smooth-Notch Specimens Broken in Tension at 760°C (1400°F)




R14-81

Figure 61 Fracture Profile of Smooth Section Failure in Combination Smooth-Notch Specimen A74-055-01 Broken in Tension at 760°C (1400°F)

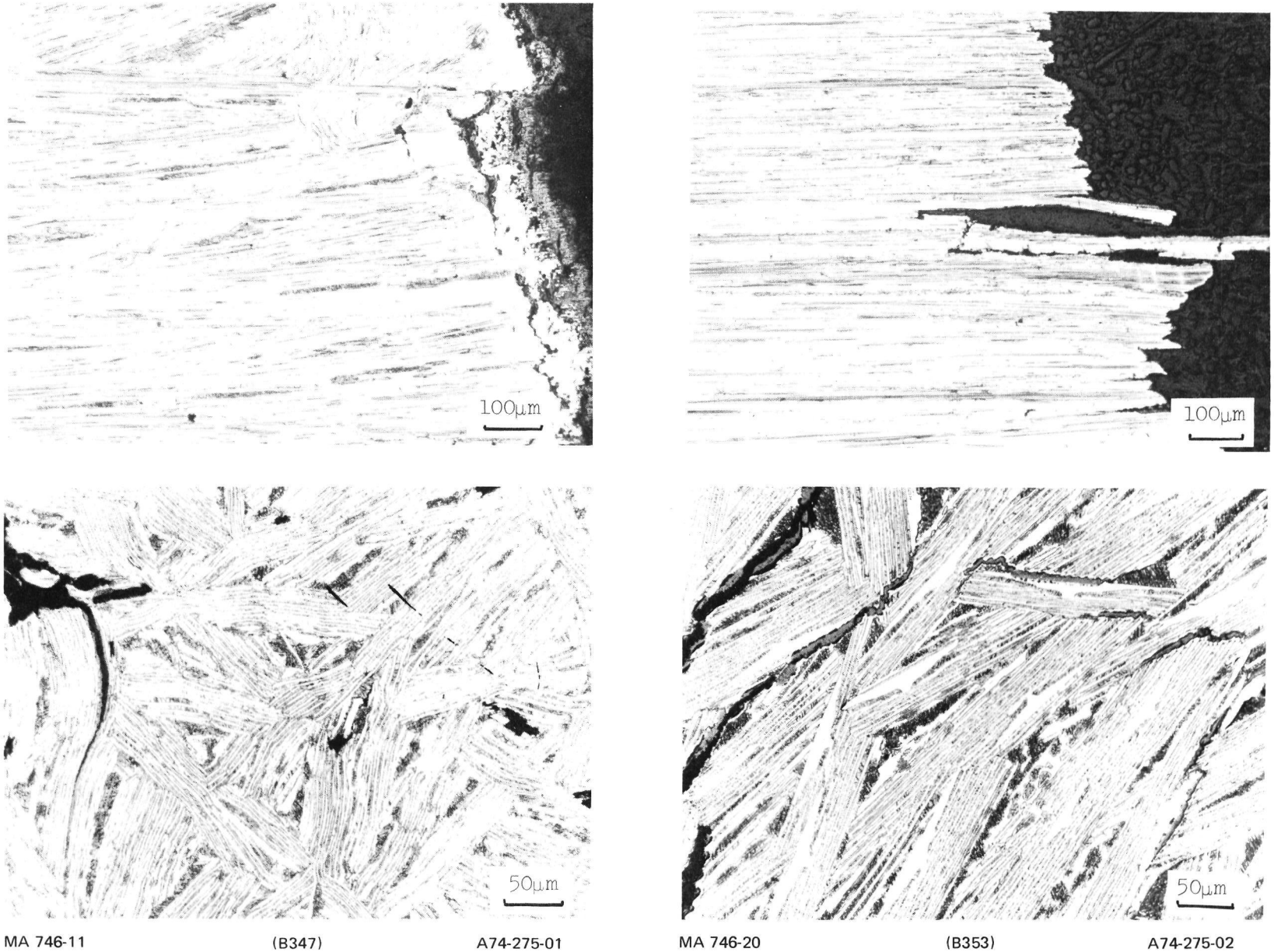
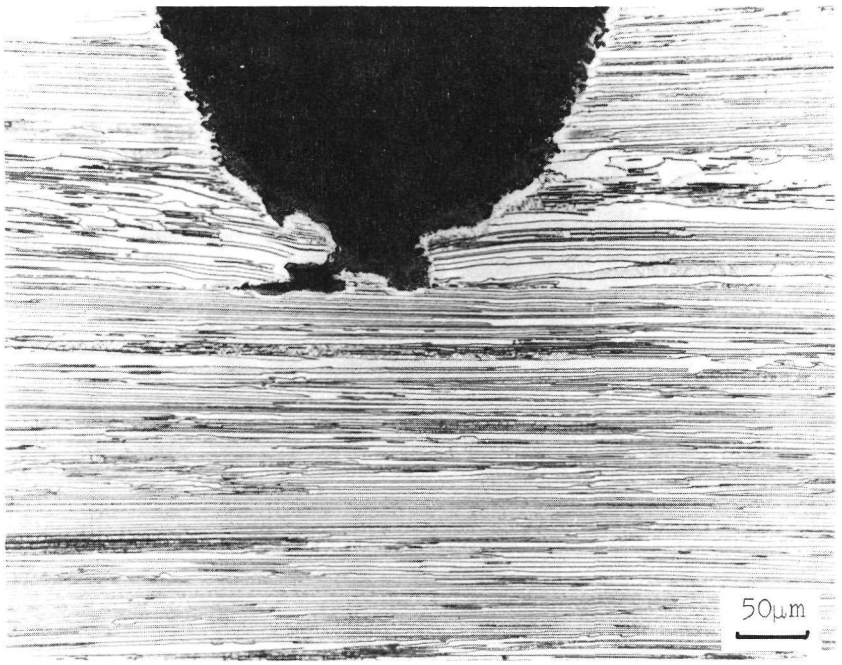
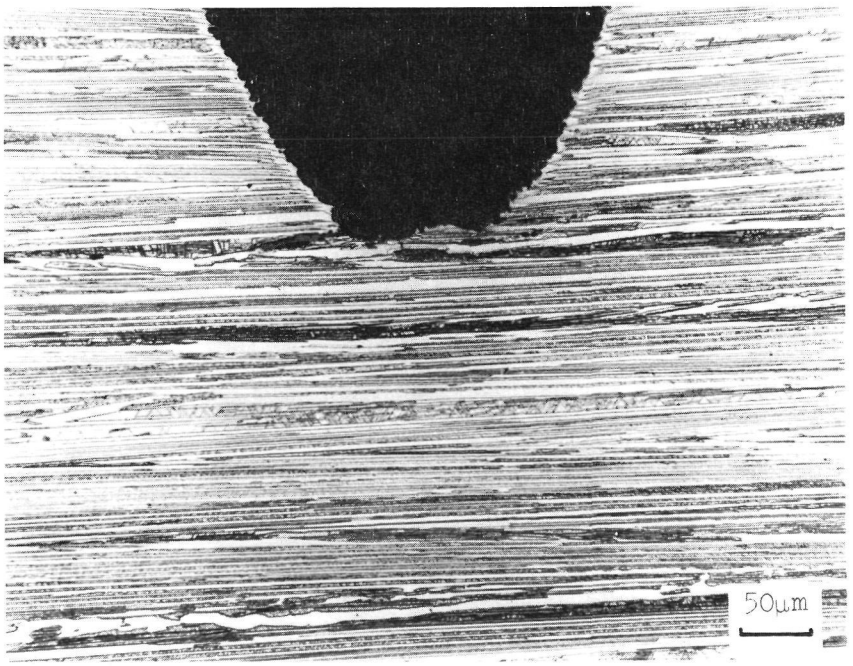



Figure 62 Longitudinal and Transverse Sections Near the Smooth Section Fracture Surface of Combination Smooth-Notch Specimens Broken in Tension at 1038°C (1900°F)

R14-82



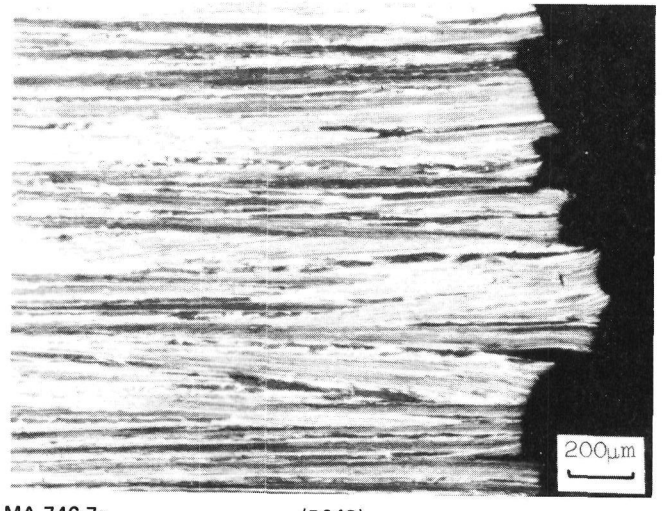

MA 746-14 (B346) A74-275-01



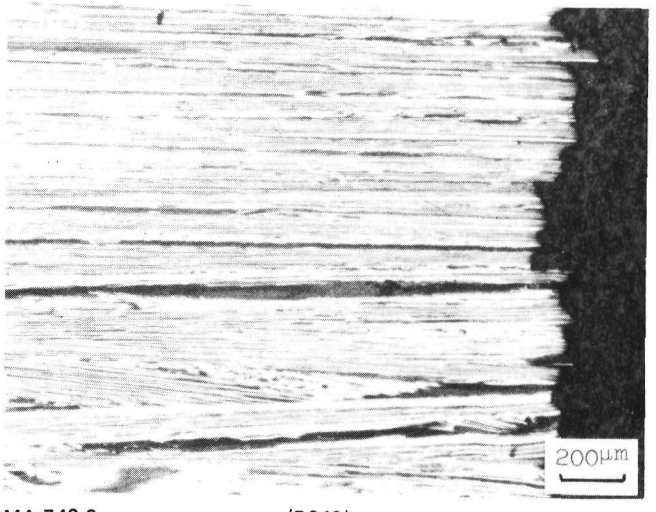

MA 746-15 (B350) A74-381-02

R14-83

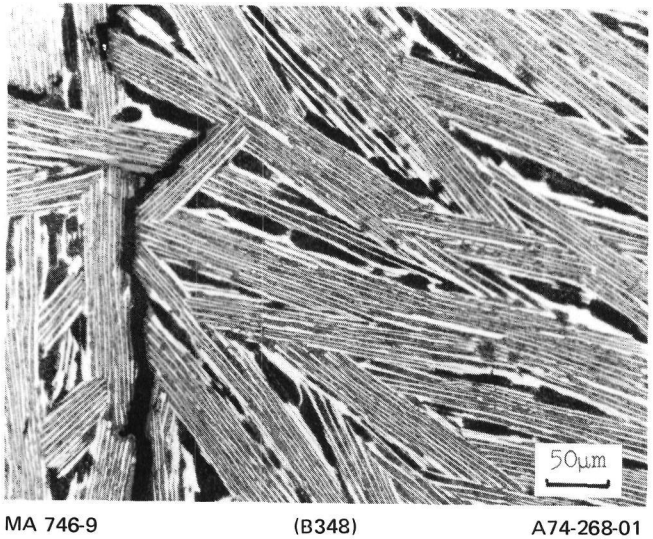
Figure 63 Longitudinal Structure at the Notch Root of Combination Smooth-Notch Specimens Broken in Tension at 1038°C (1900°F)



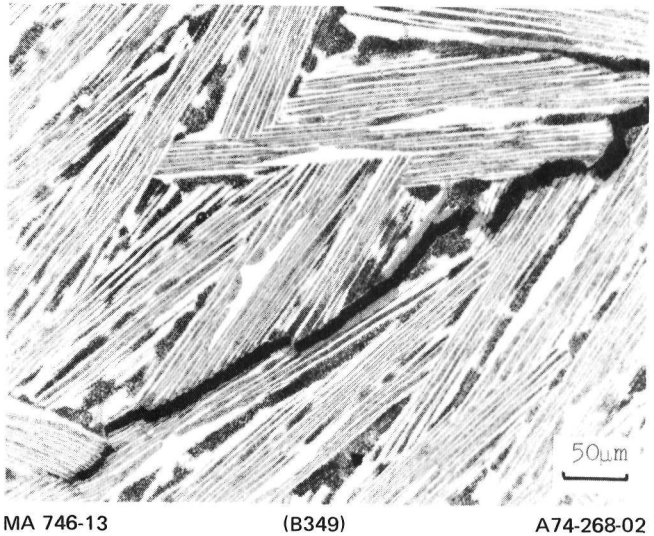

MA 746-7a (B348)




MA 746-6 (B349)




MA 746-9 (B348) A74-268-01

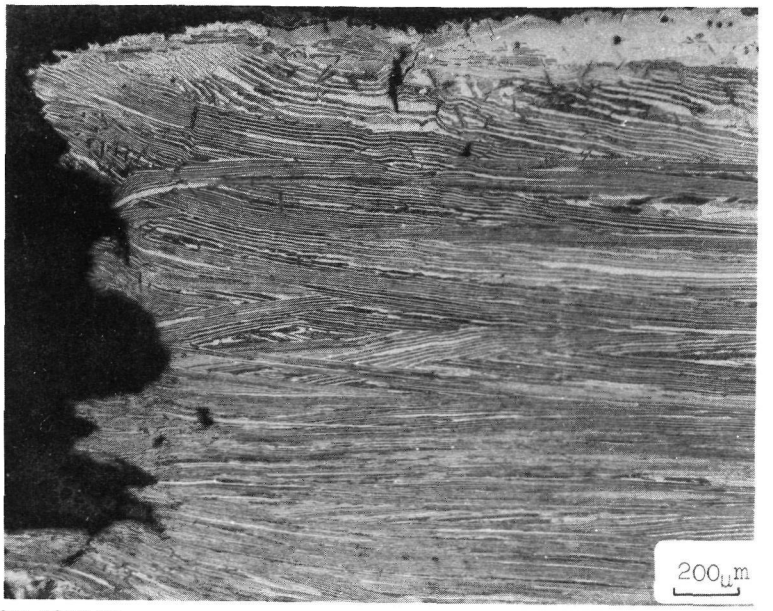



MA 746-13 (B349) A74-268-02

Figure 64 Longitudinal and Transverse Sections in the Fracture Zone of Combination Smooth-Notch Specimens Broken in Stress Rupture at 760°C (1400°F) and 758 MPa (110 ksi)

R14-84

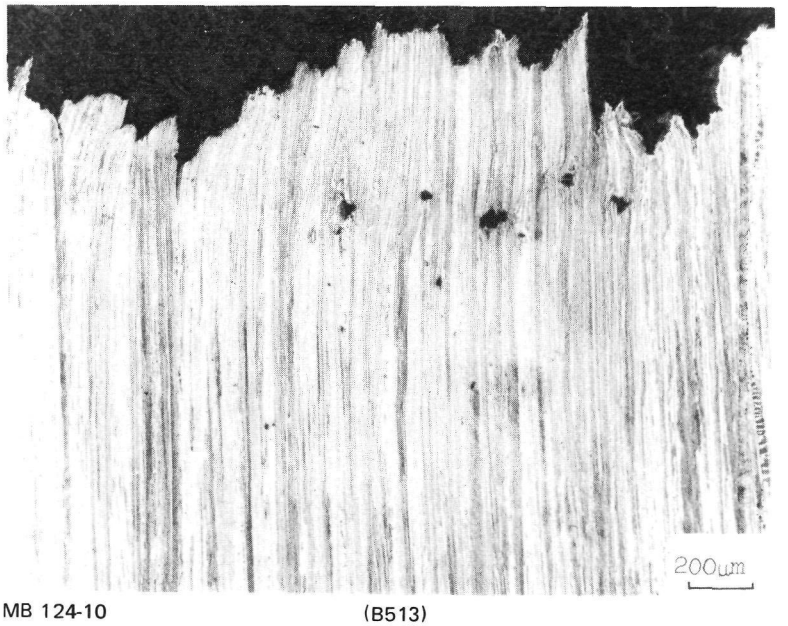
TENSILE AXIS




MA 1372-10

a) Smooth Section Failure, Specimen A74-384-01. Time to Rupture 504 Hours.

TENSILE AXIS

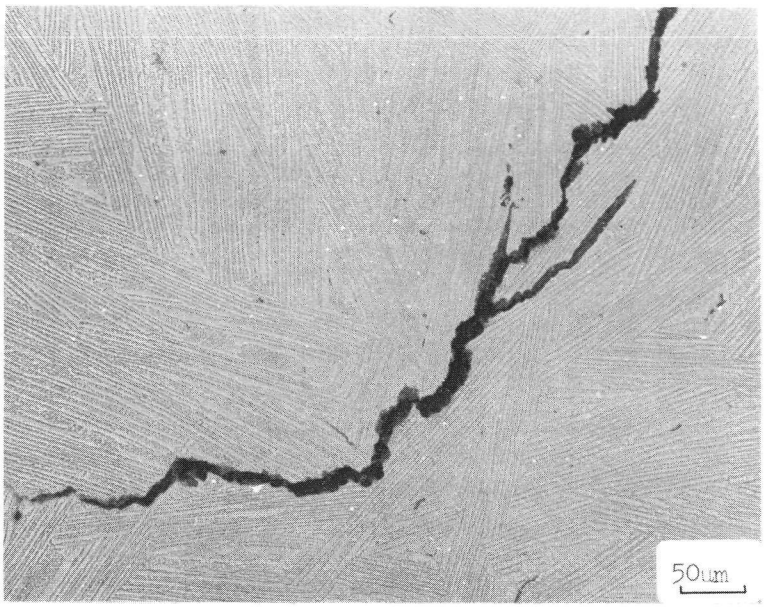



MB 124-10 (B513)

b) Notch Failure, Specimen A74-894-02. Time to Rupture 240 Hours.

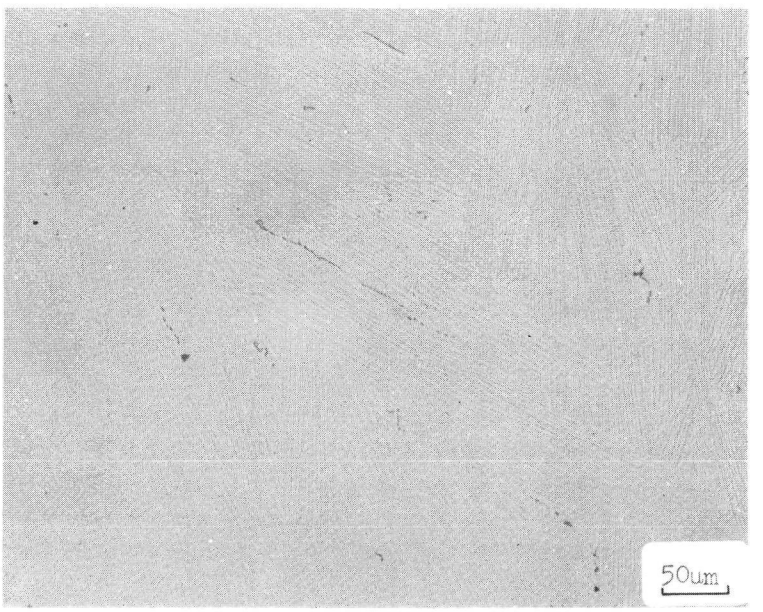
R14-85

Figure 65 Fracture Appearance Found in Cellular 6 Cr $\gamma/\gamma'$ - $\delta$ Directionally Solidified Eutectic Alloy Combination Smooth-Notch Specimen Broken in Stress Rupture at 1038°C/152 MPa (1900°F/22 ksi)




MB 124-9 (B514)

a) Transverse Section Through Notch Fracture In Specimen A74-894-02.




MB 124-7 (B514)

b) Carbide Contamination Found In Specimen A74-894-02. Note Use of a Lighter Than Normal Etch to Highlight Carbides.

R14-86

Figure 66 Metallographic Appearance of Cellular 6 Cr $\gamma/\gamma' - \delta$ Directionally Solidified Eutectic Combination Smooth-Notch Specimen Broken at the Notch in Stress Rupture at 1038°C/152 MPa (1900°F/22 ksi). Time 240 Hours

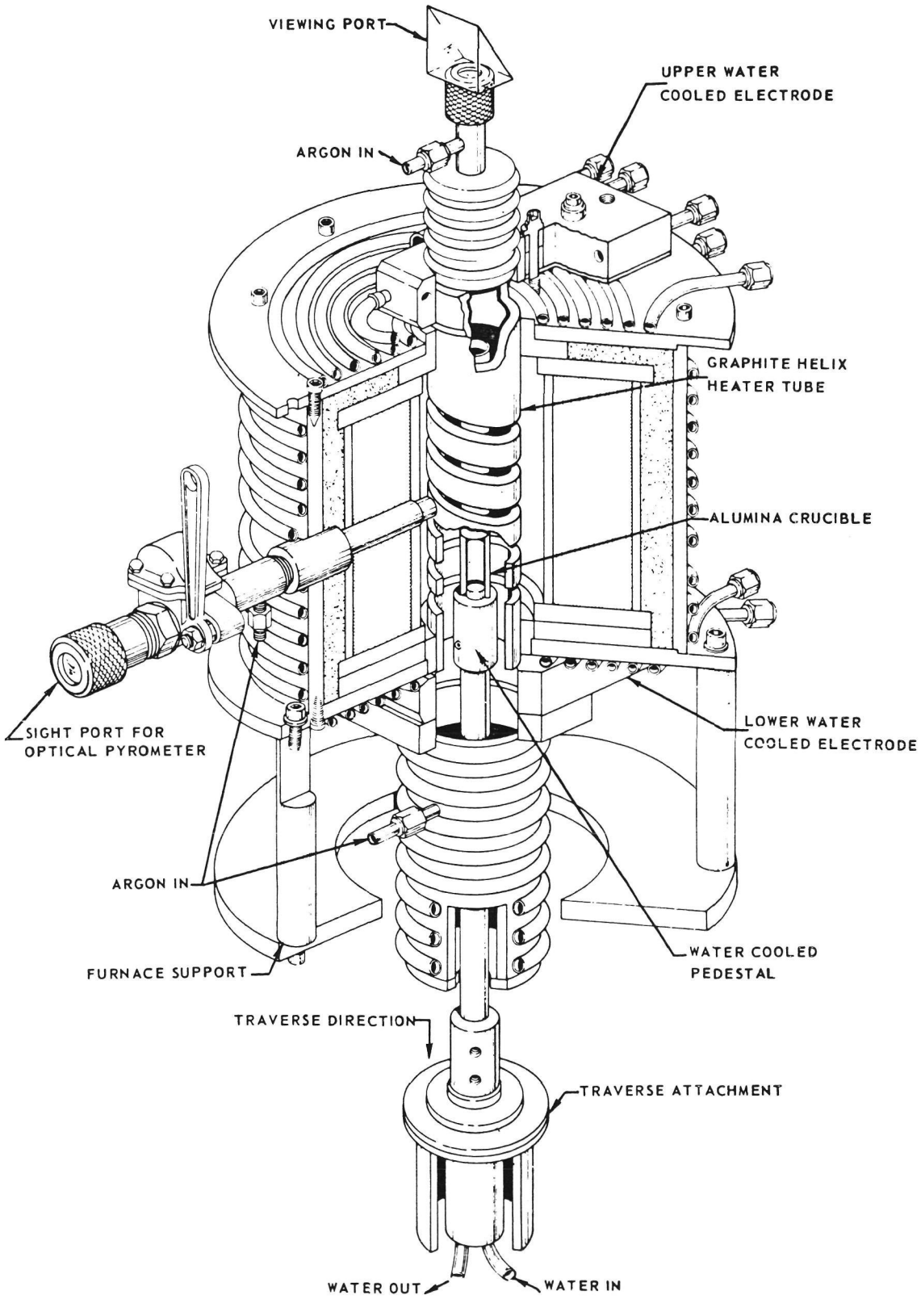



Figure 67 Low Gradient Graphite Heated Directional Solidification Furnace

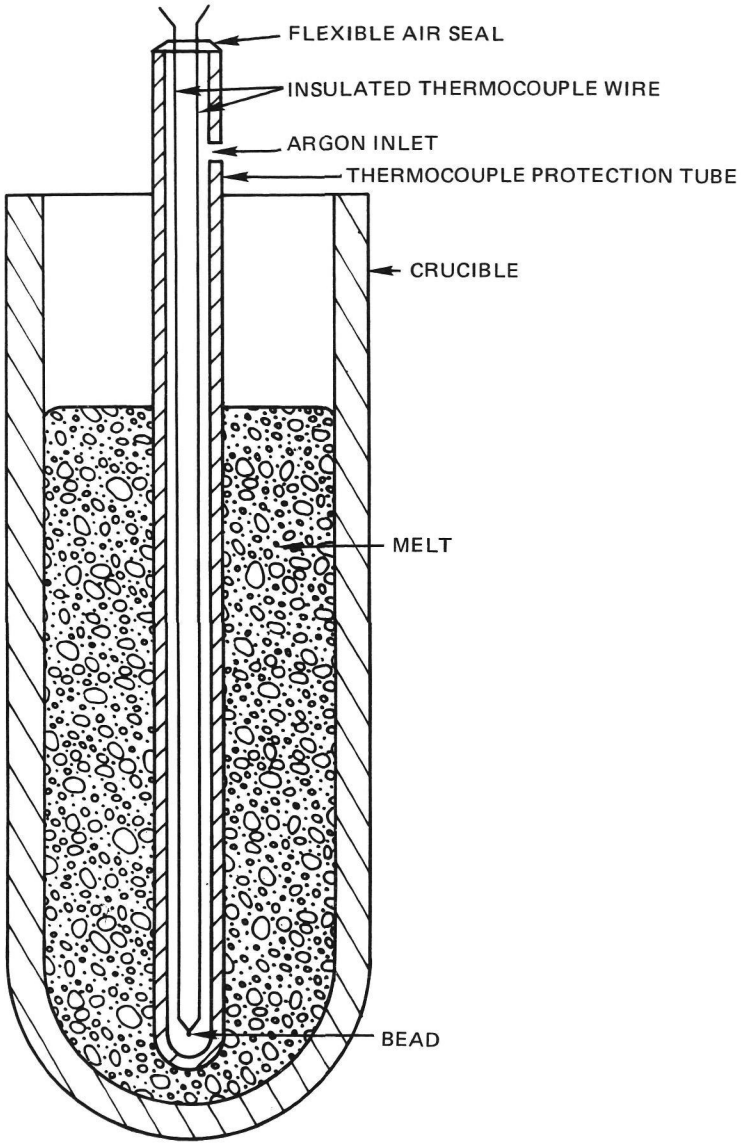



Figure 68 Schematic Illustration of Set-Up for Gradient Measurements (Note: Drawing Not to Scale)

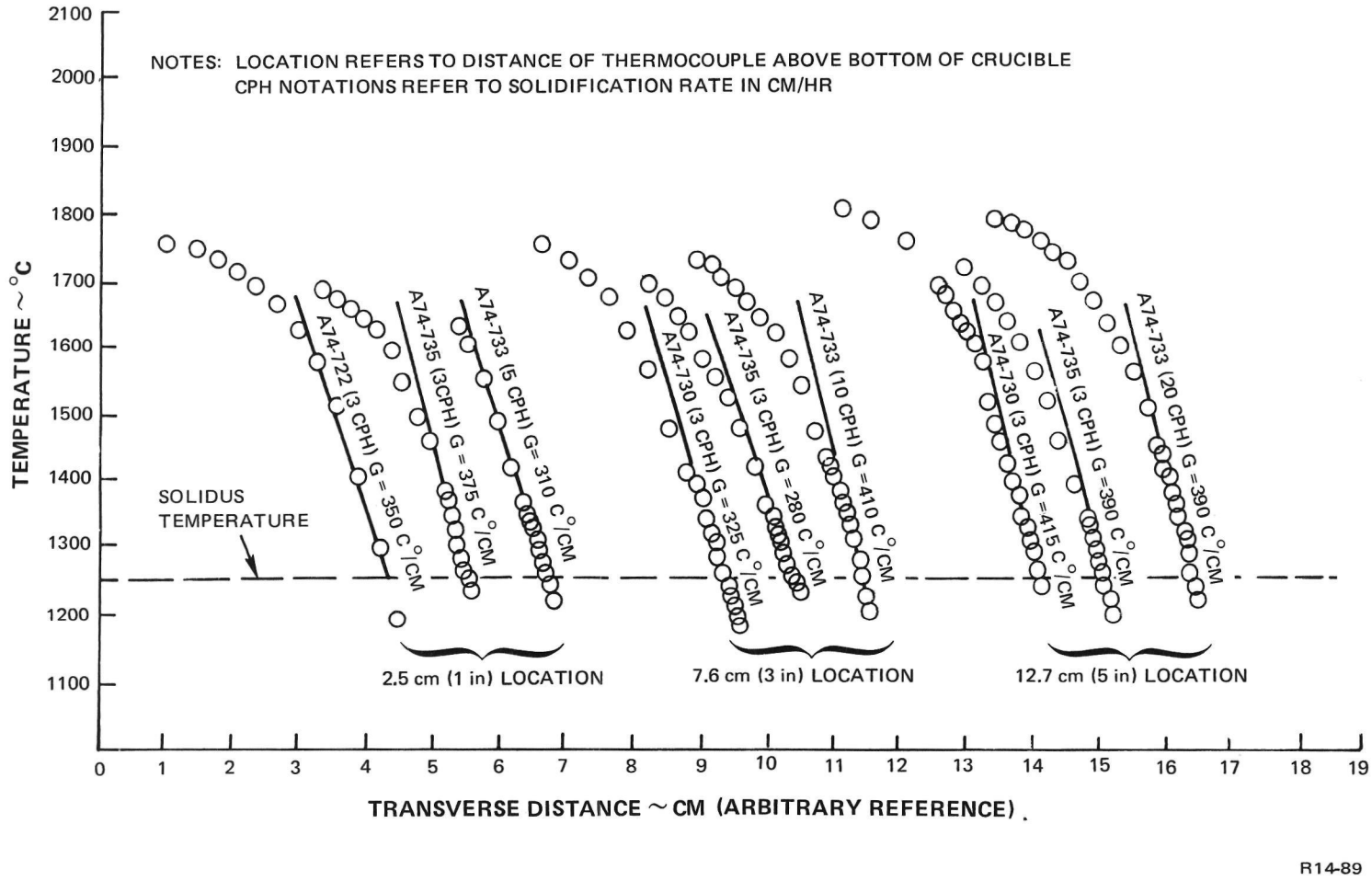



Figure 69 Results of Gradient Measurements In High Gradient Directional Solidification Apparatus

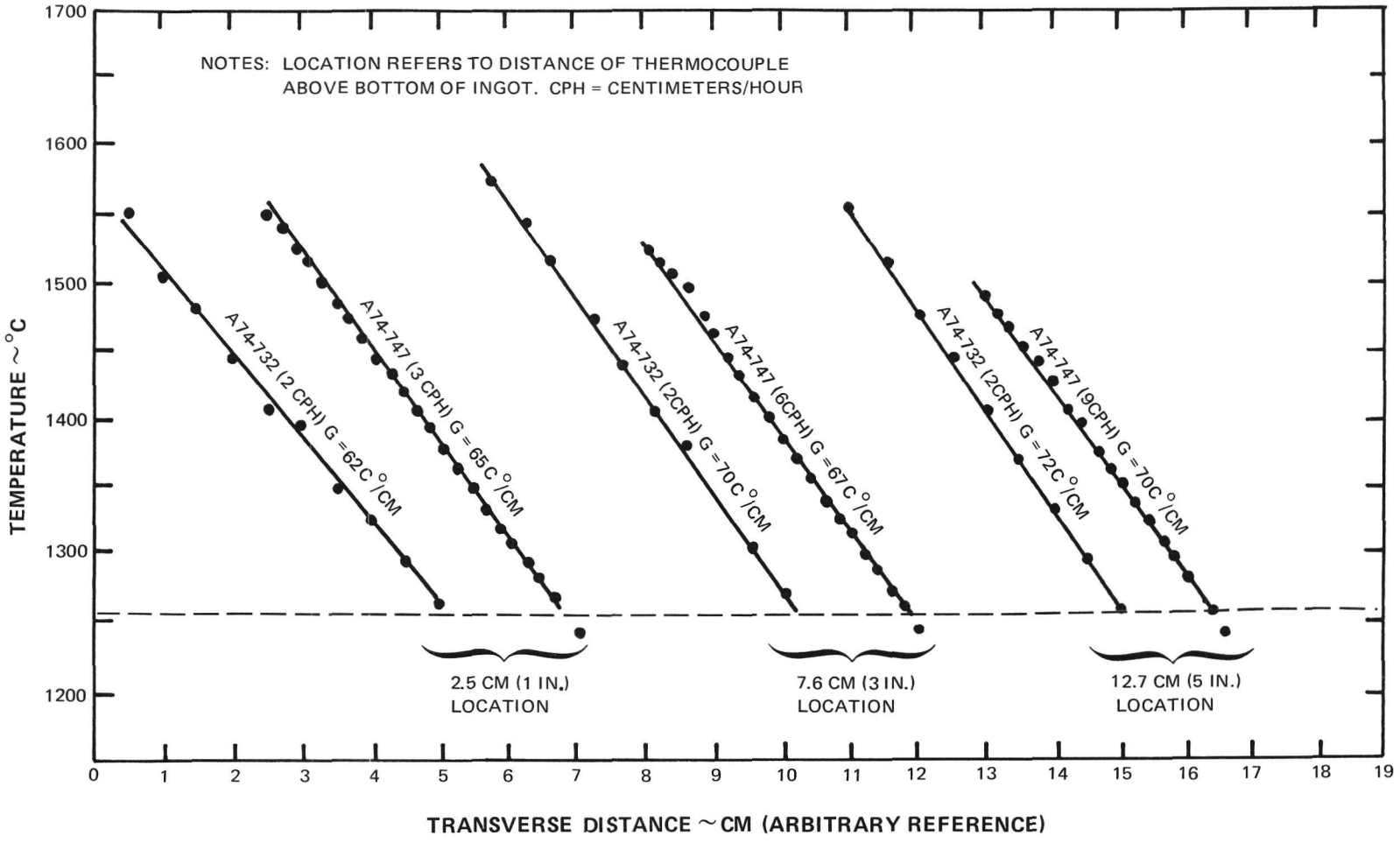



Figure 70 Results of Gradient Measurements In Low Gradient Directional Solidification Apparatus

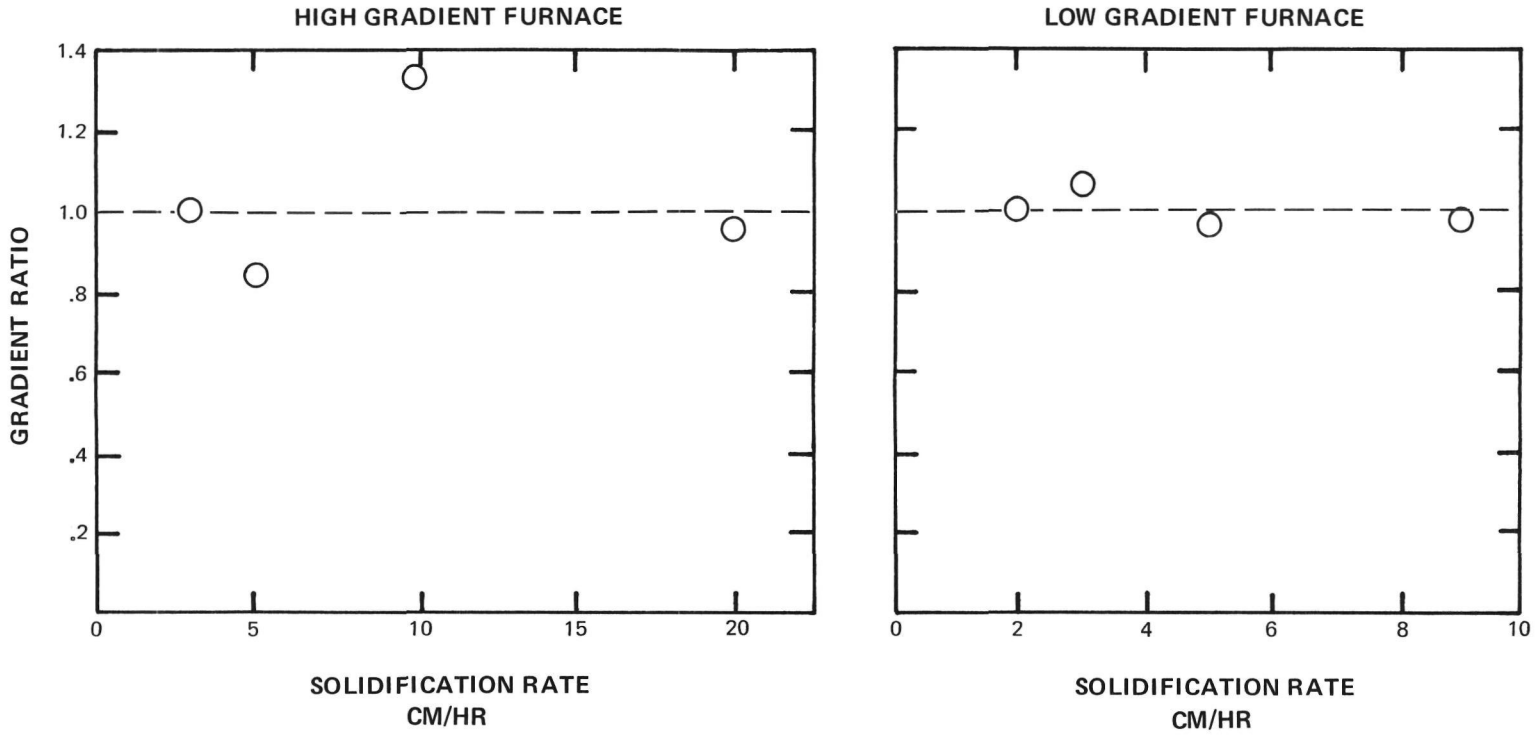
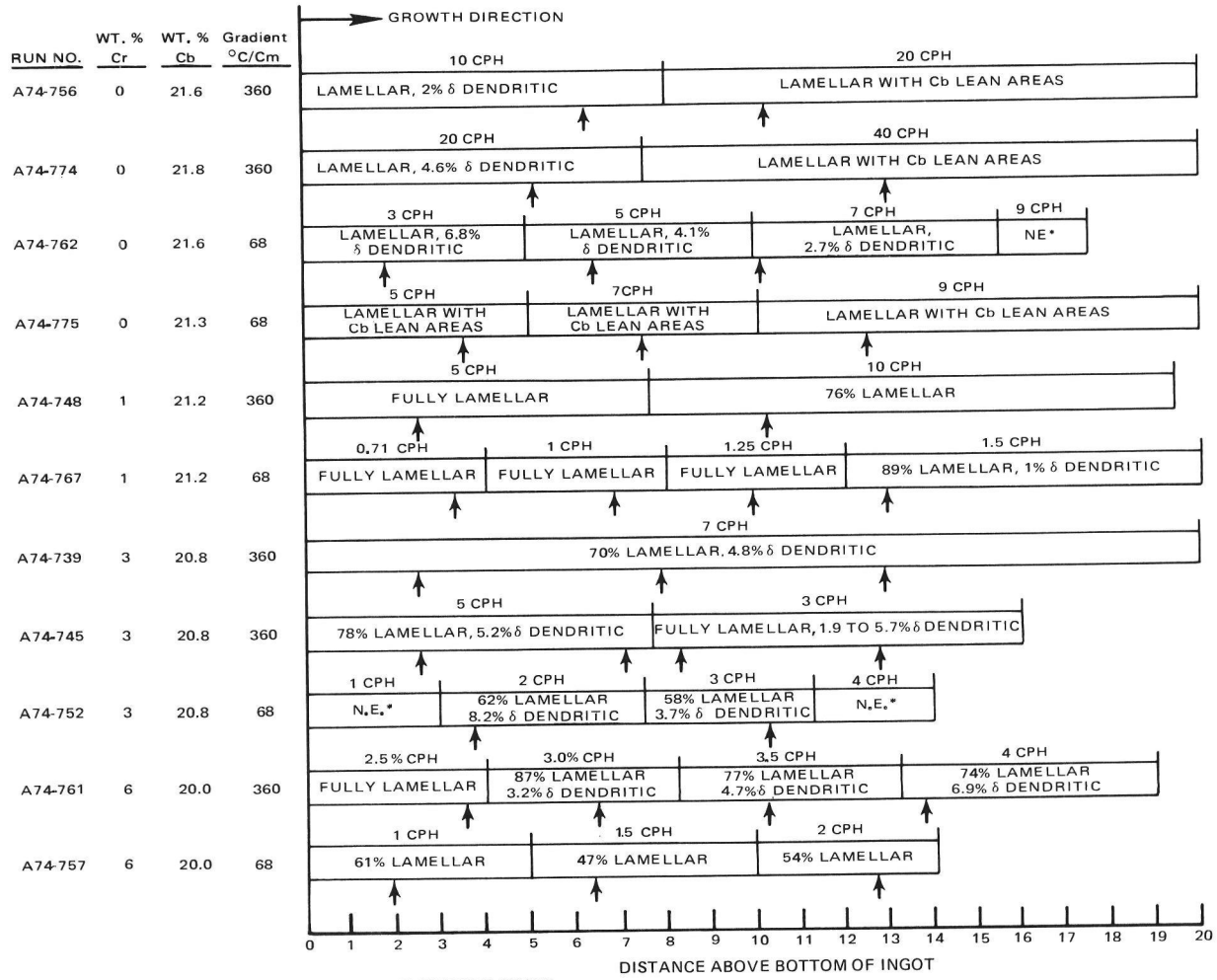


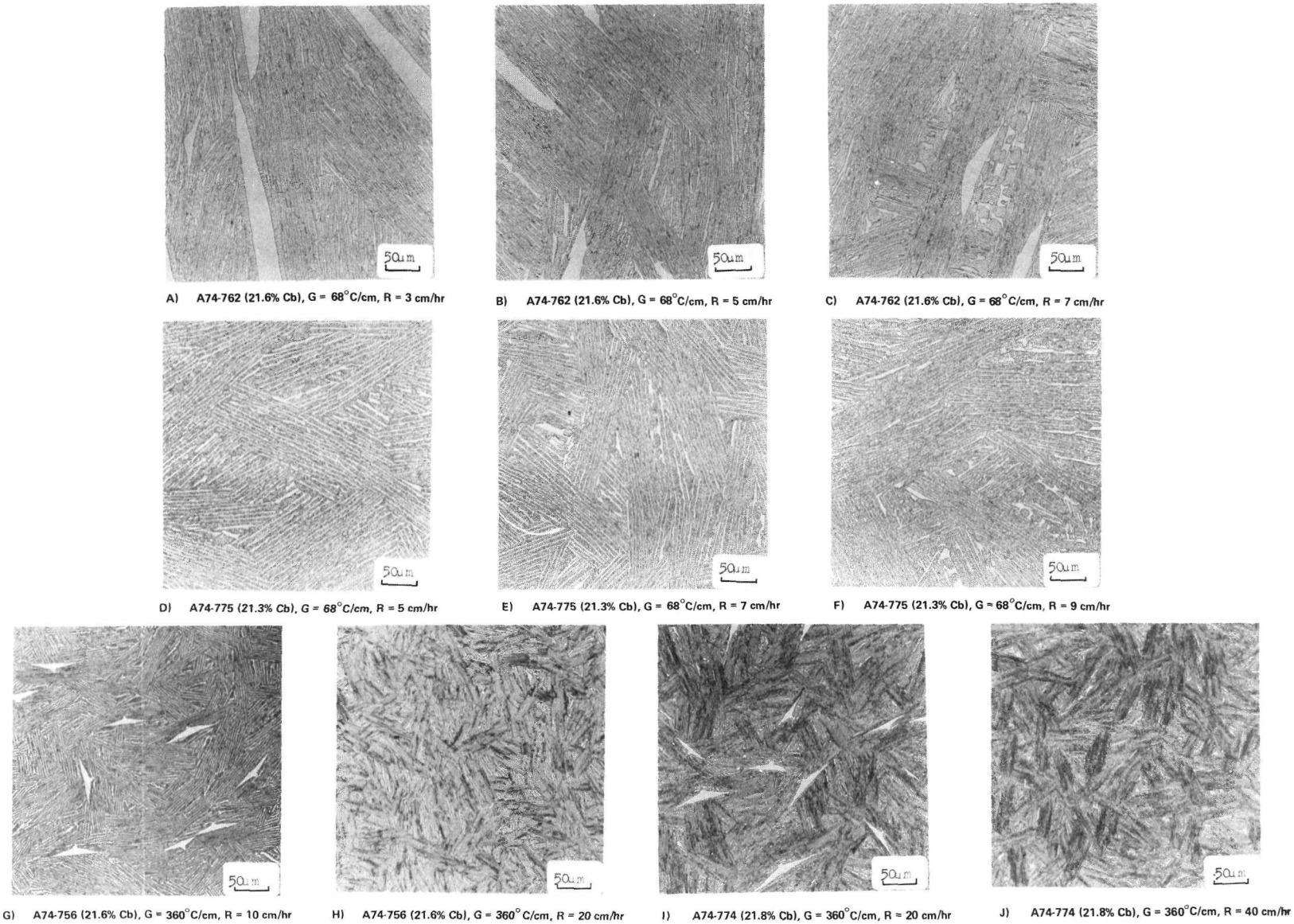

Figure 71 Influence of Solidification Rate On the Ratio of the Thermal Gradient At the Indicated Rate to the Average Gradient In the Same Location At a Rate of 3 cm/hour (High Gradient Furnace) and 2 cm/hour (Low Gradient Apparatus)




CPH INDICATES SOLIDIFICATION RATE CM/HR
* N.E. – NOT EVALUATED

ARROWS (↑) INDICATE LOCATIONS WHERE EACH BAR WAS SECTIONED FOR METALLOGRAPHIC EXAMINATION OF THE TRANSVERSE MICROSTRUCTURE

Figure 72 Summary of Solidification Experiments Performed to Determine Critical G/R As a Function of Chromium Content R14-92




R14-93

Figure 73 Influence of Gradient and Freezing Rate On the Microstructure of a Directionally Solidified Chromium Free $\gamma/\gamma'$-$\delta$ Eutectic Alloy Containing 2.5 Percent Aluminum

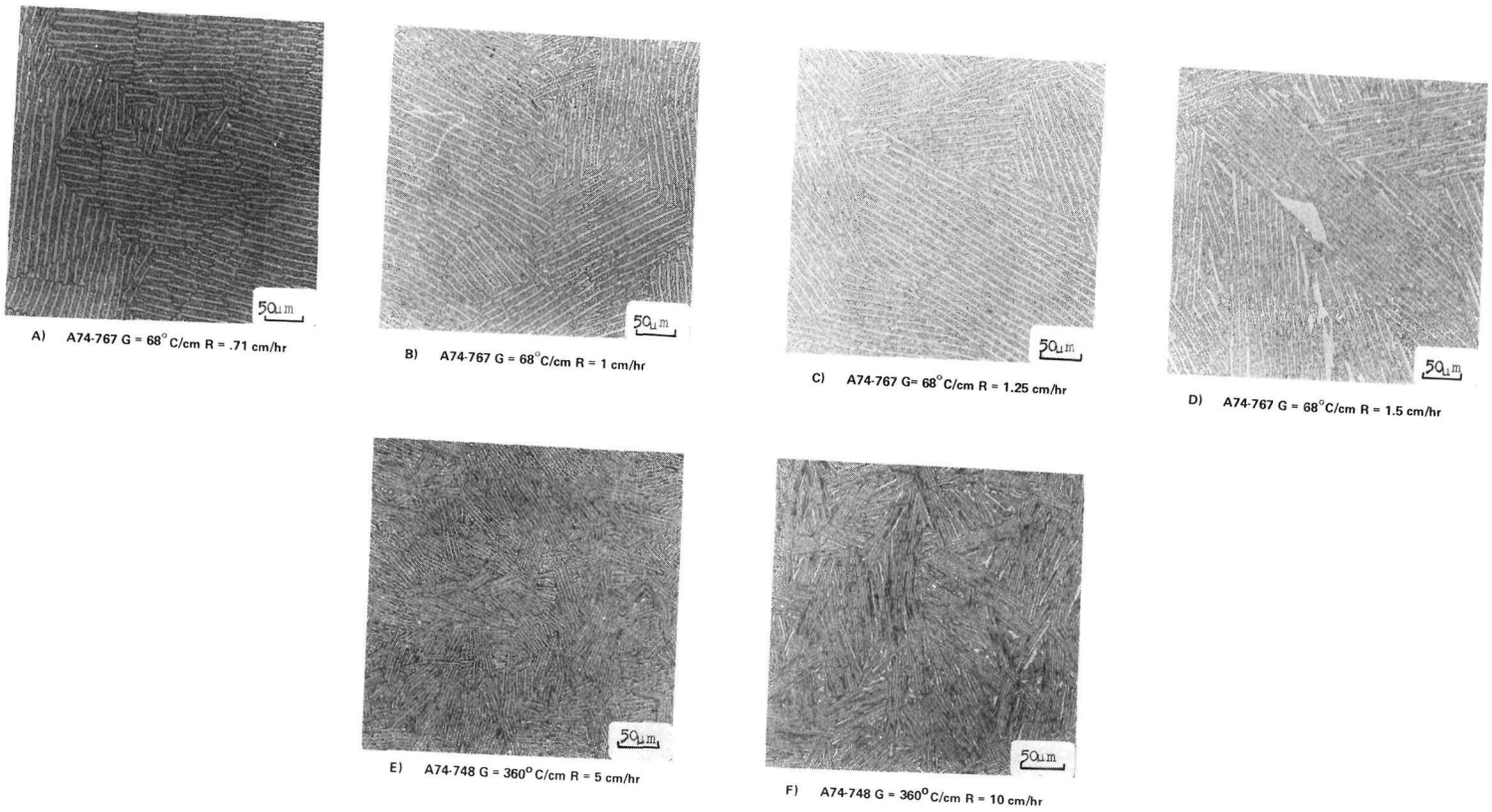



Figure 74 Influence of Gradient and Freezing Rate On the Transverse Microstructure of a Directionally Solidified 1 Percent Chromium $\gamma/\gamma'$-$\delta$ Eutectic Alloy (Composition Ni-21.2% Cb-2.5% Al-1% Cr)

R14-94

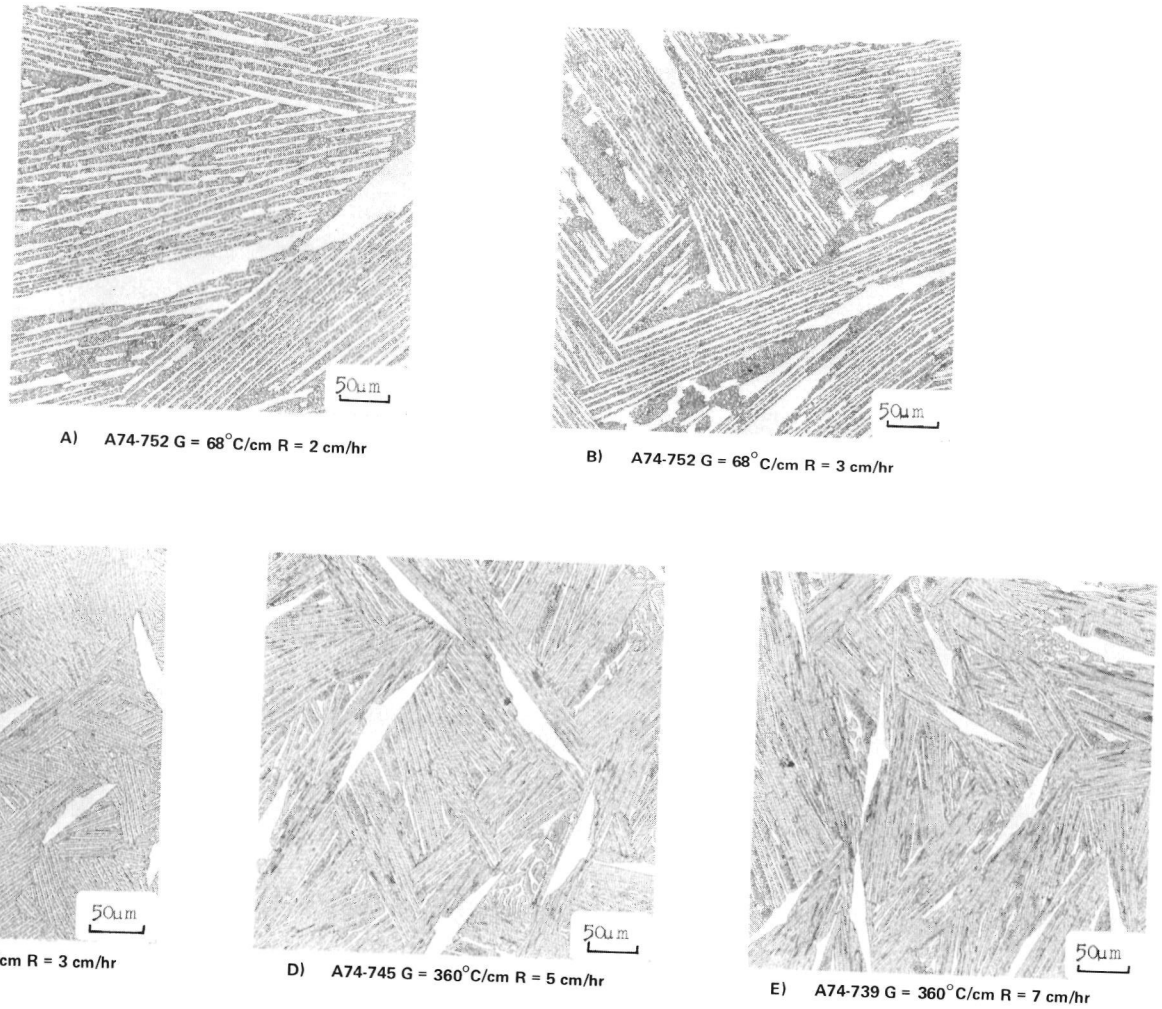



Figure 75 Influence of Gradient and Freezing Rate On the Transverse Microstructure of a Directionally Solidified 3 Percent Chromium $\gamma/\gamma'$-$\delta$ Eutectic Alloy (Composition Ni-20.8% Cb-2.5% Al-3% Cr)

R14-95

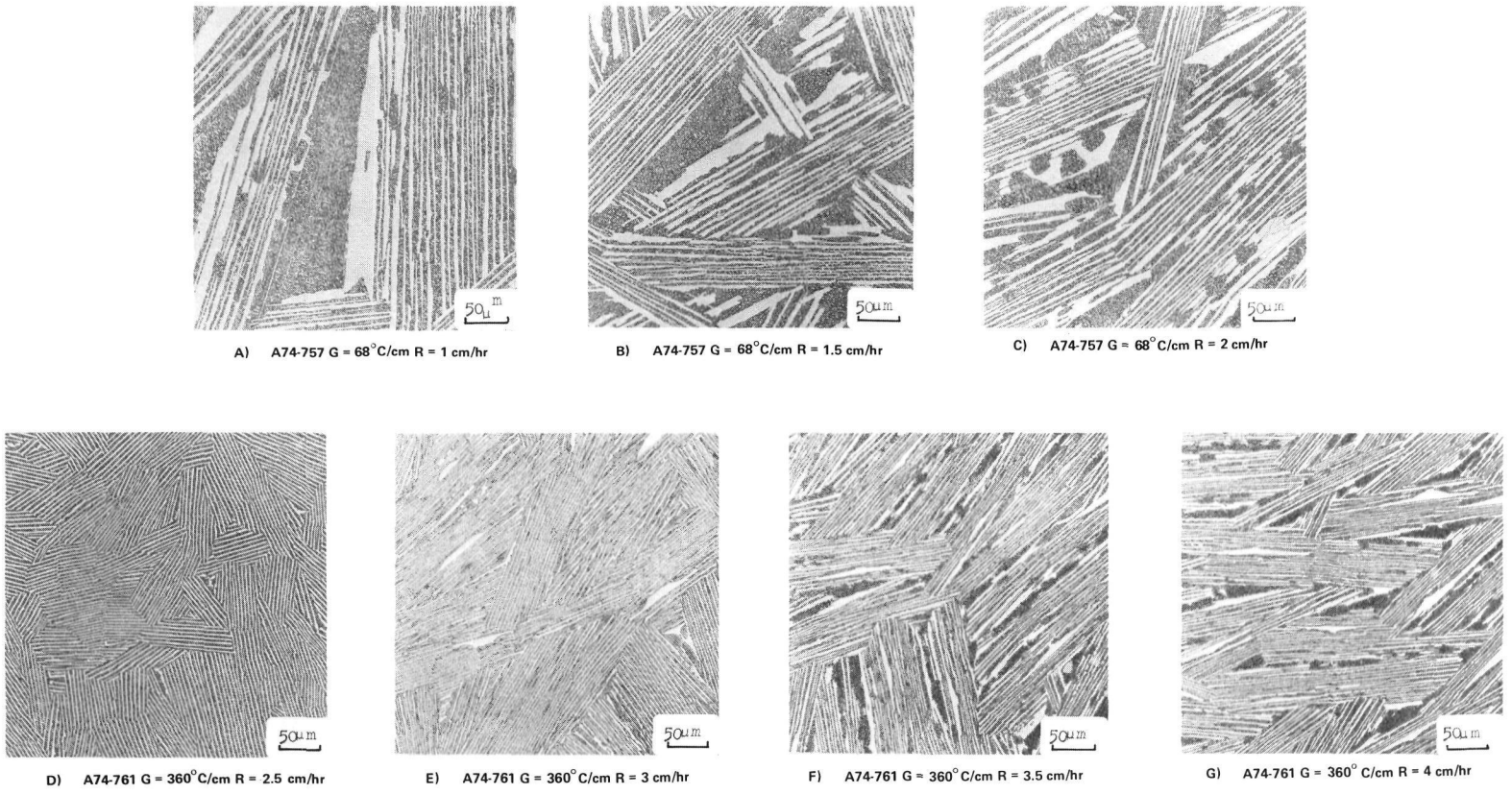



Figure 76 Influence of Gradient and Freezing Rate On the Microstructure of a Directionally Solidified 6 Percent Chromium $\gamma/\gamma'$-$\delta$ Eutectic Alloy (Composition Ni-20% Cb-2.5% Al-6% Cr)

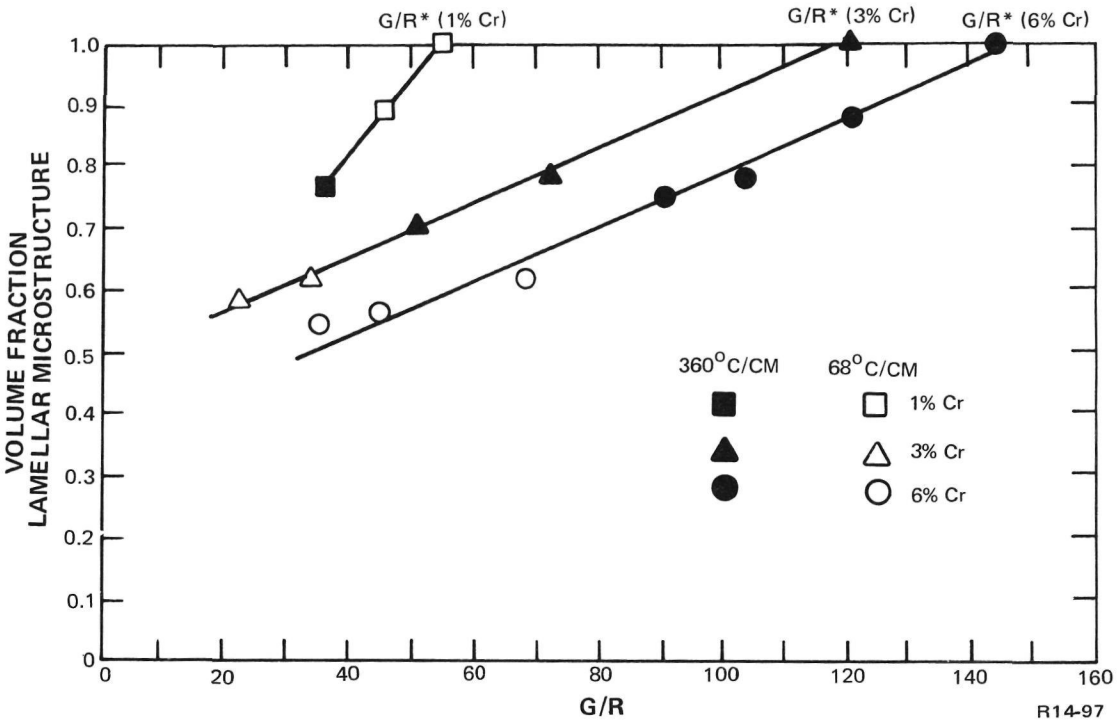



Figure 77 Influence of G/R On the Volume Fraction of Lamellar Microstructure In Directionally Solidified $\gamma/\gamma'$-$\delta$ Eutectic Alloys Containing Various Levels of Chromium

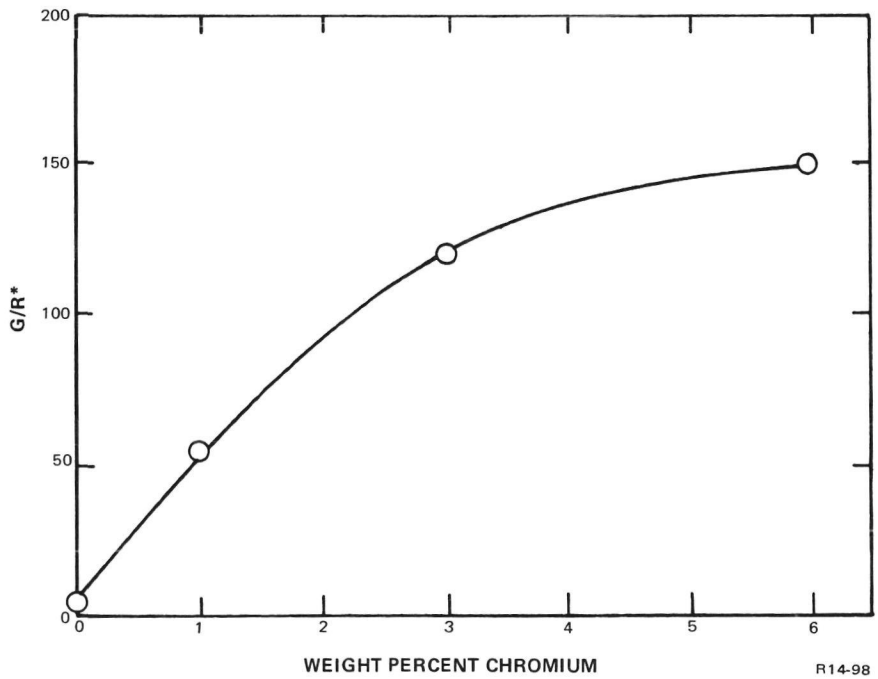
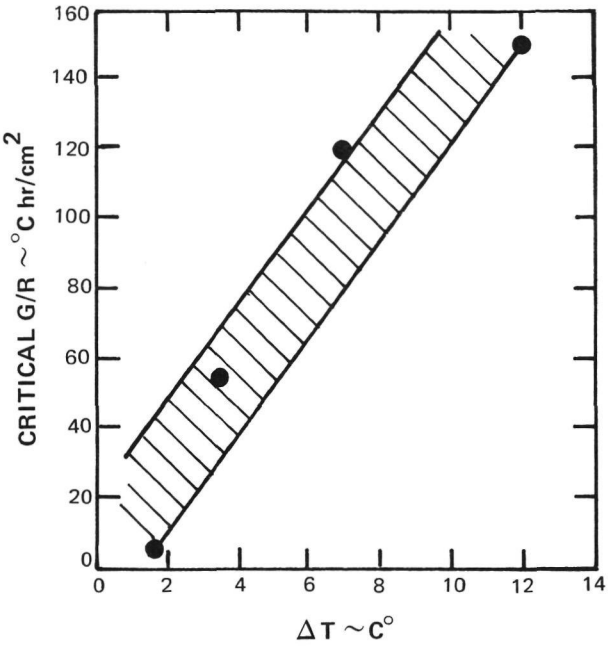
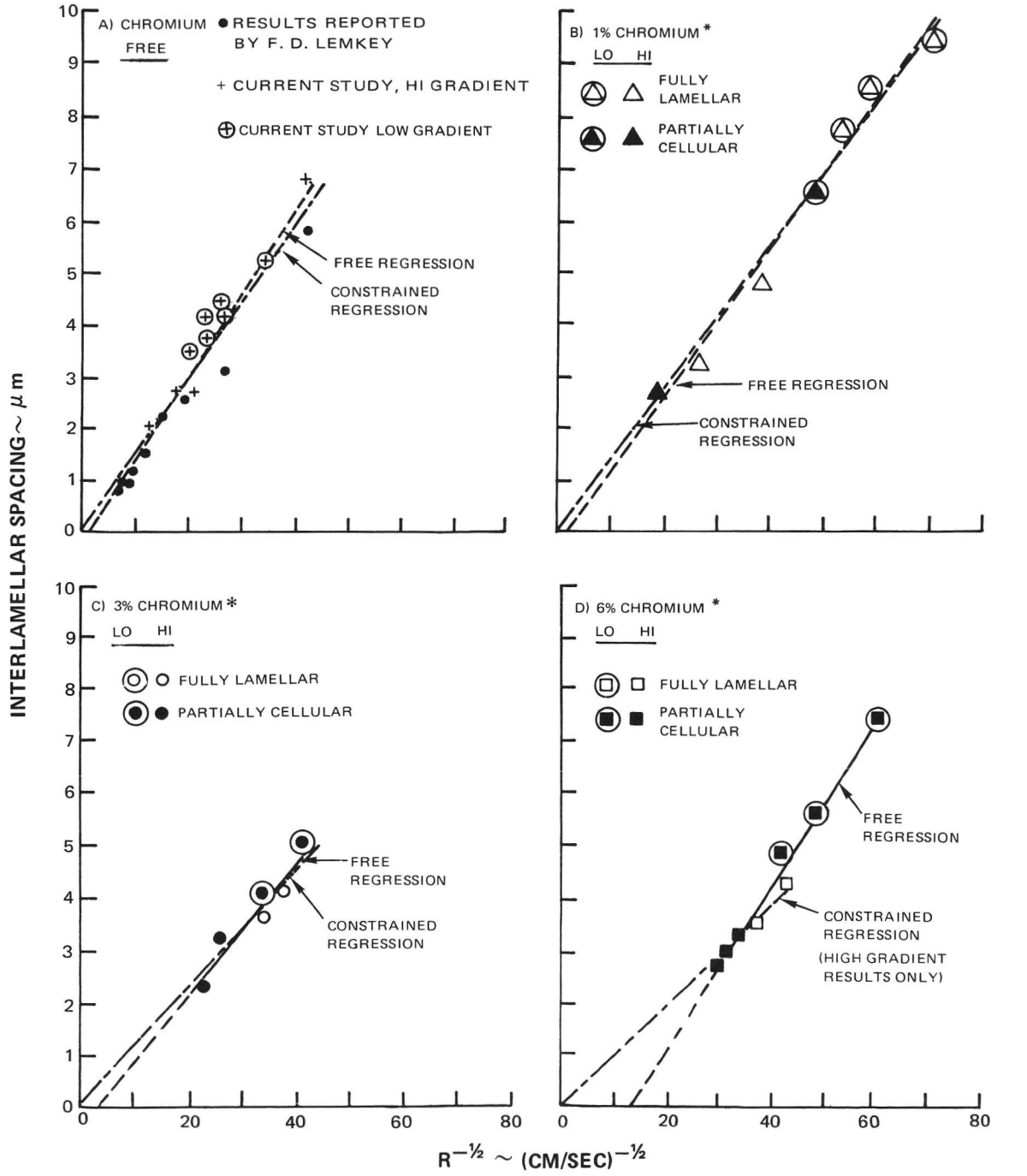



Figure 78 Influence of Chromium On the Critical G/R Ratio for Plane Front Solidification of the $\gamma/\gamma'$-$\delta$ Eutectic Alloy




R14-99

Figure 79 Correlation Between Critical G/R and Liquidus-Solidus Temperature Range ($\Delta T$) for Directionally Solidified $\gamma/\gamma'$-$\delta$ Alloys Containing Various Levels of Chromium




R14-100

Figure 80 Results of Regression Analysis On Interlamellar Spacing As a Function of $R^{-½}$ for Directionally Solidified $\gamma/\gamma'$-$\delta$ Eutectic Alloy Containing Various Levels of Chromium, (* LO – Indicates Low Gradient Furnace, HI – Indicates High Gradient Furnace)

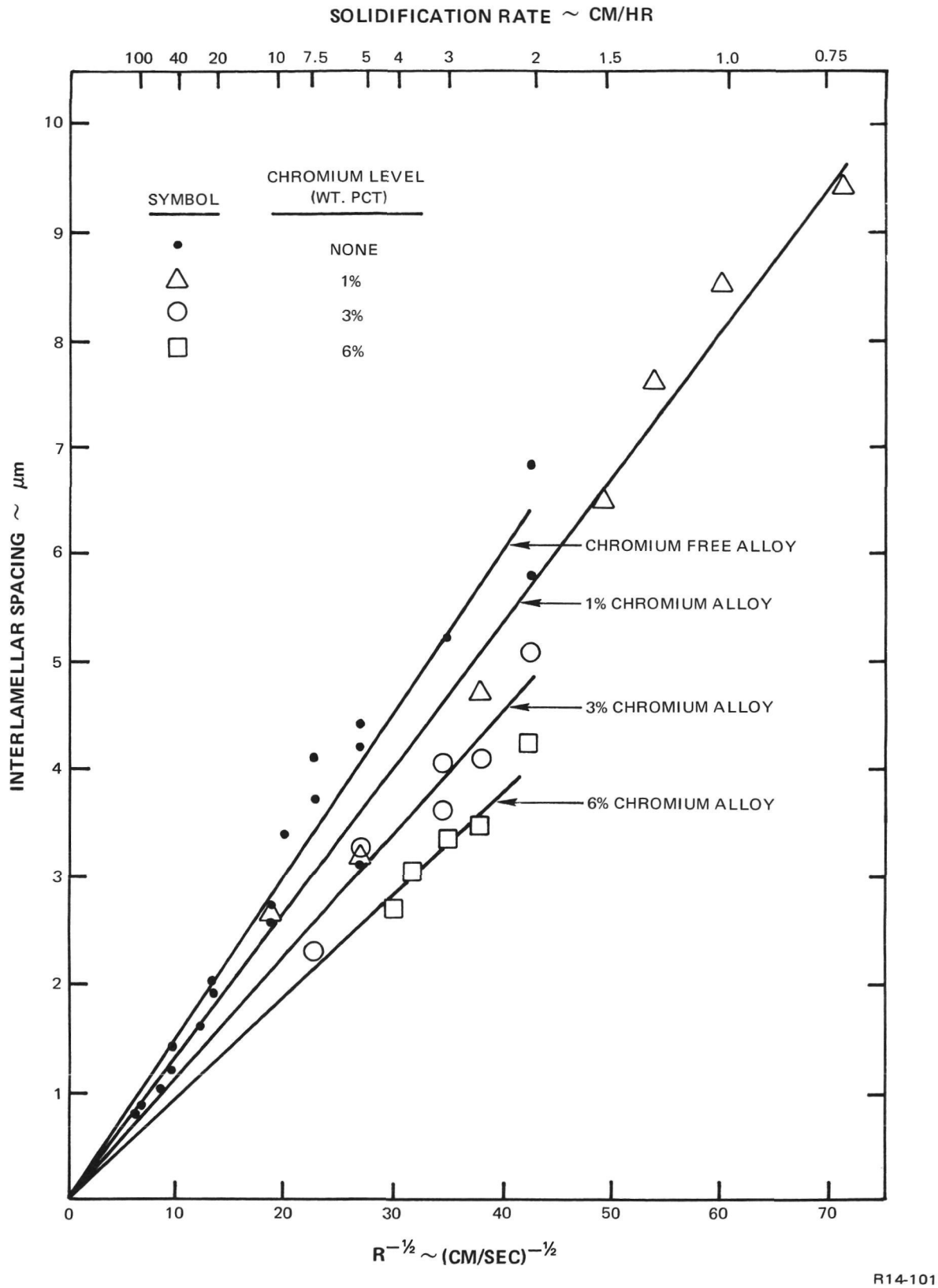



Figure 81 Interlamellar Spacing of Directionally Solidified $\gamma/\gamma'$-$\delta$ Eutectic Alloys Containing Various Levels of Chromium As a Function of Freezing Rate. Straight Lines Were Fit to the Data By a Regression Procedure Which Forced Each Line to Pass Through the Origin

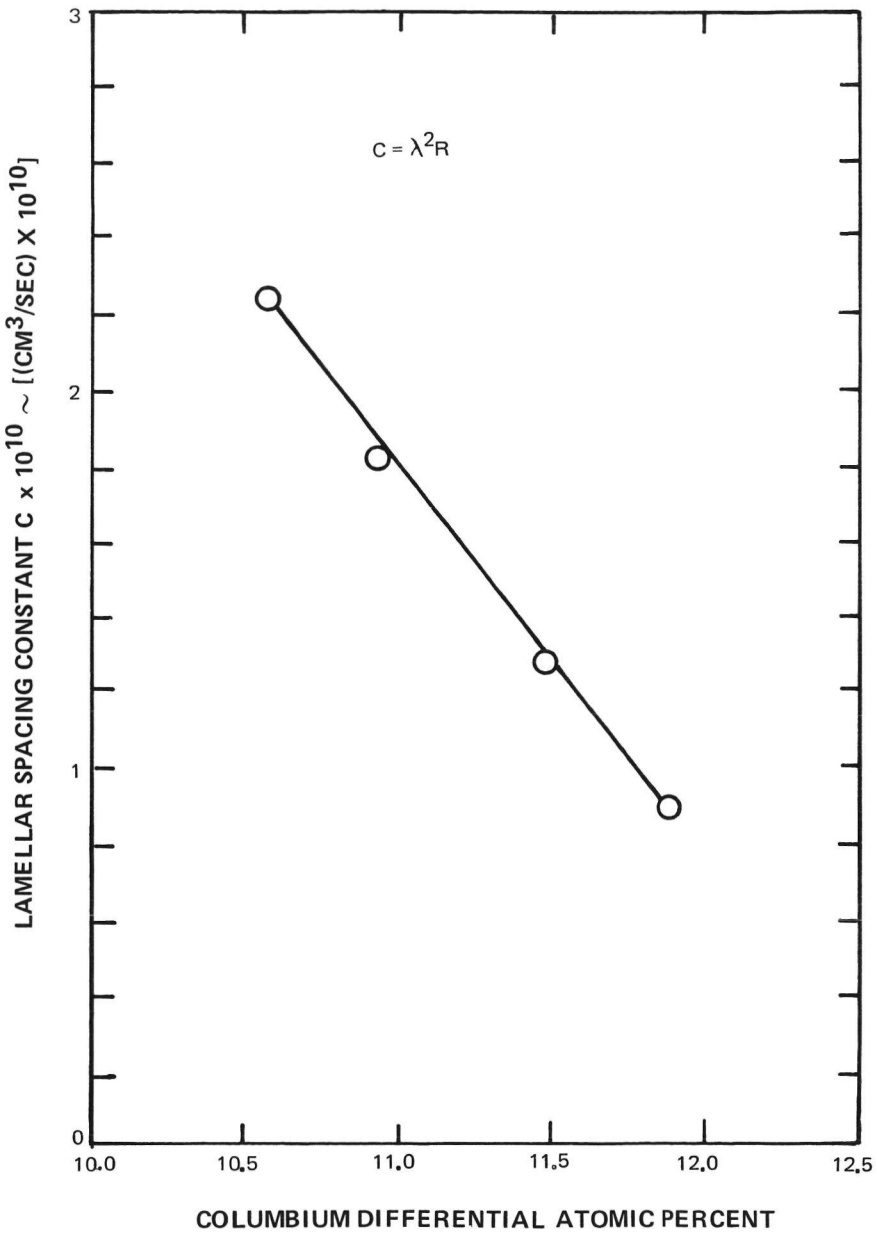



Figure 82 Influence of Columbium Differential (Defined As the Difference Between the Atomic Percentage of Columbium In the Liquid and In the $Ni_3Cb$ Phase) On the Lamellar Spacing Constant for Directionally Solidified $\gamma/\gamma'$-$\delta$ Eutectic Alloys

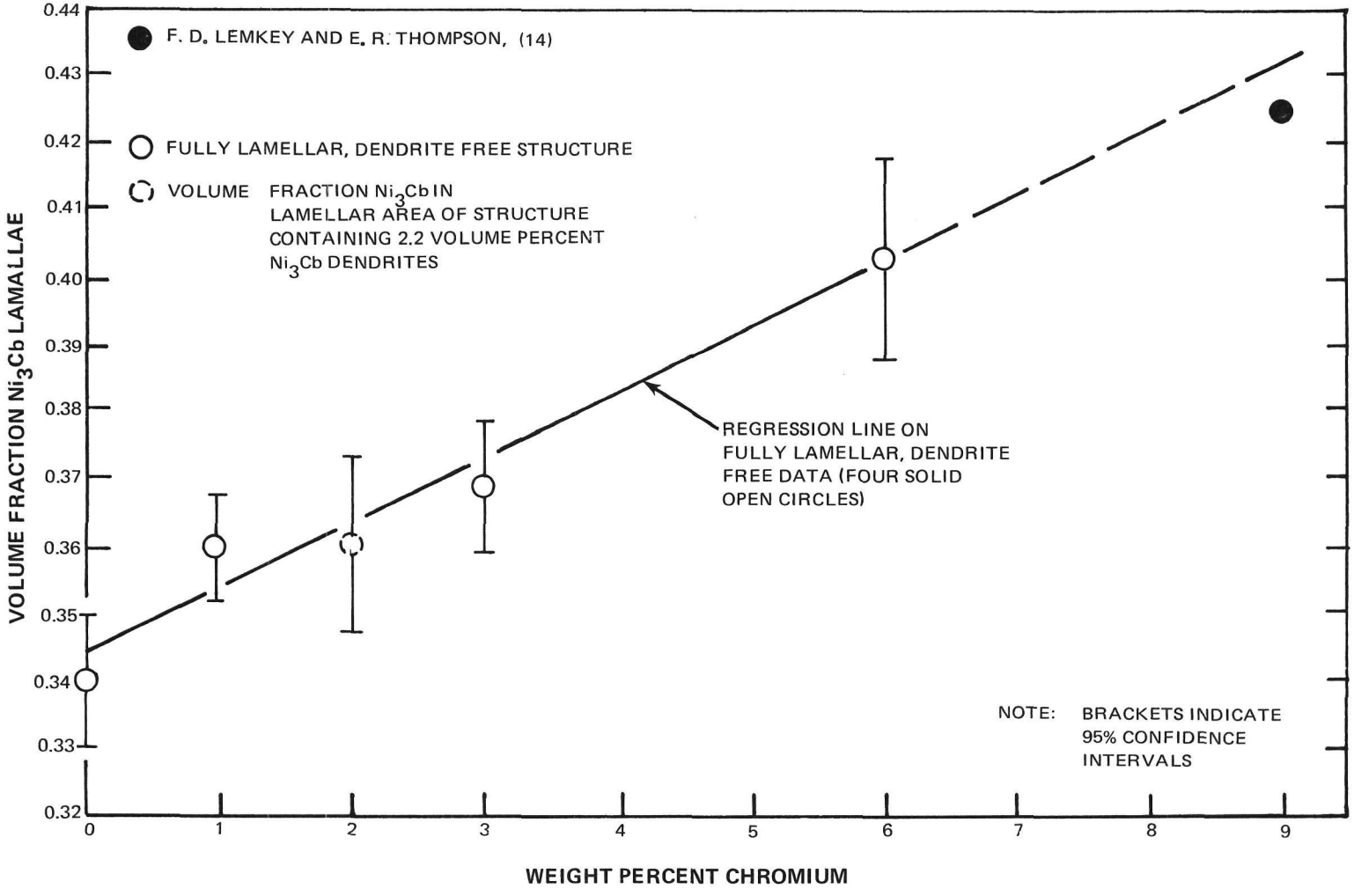



Figure 83 Influence of Chromium Level On Volume Fraction of $Ni_3Cb$ Phase In the Directionally Solidified $\gamma/\gamma'$-$\delta$ Eutectic Alloy System

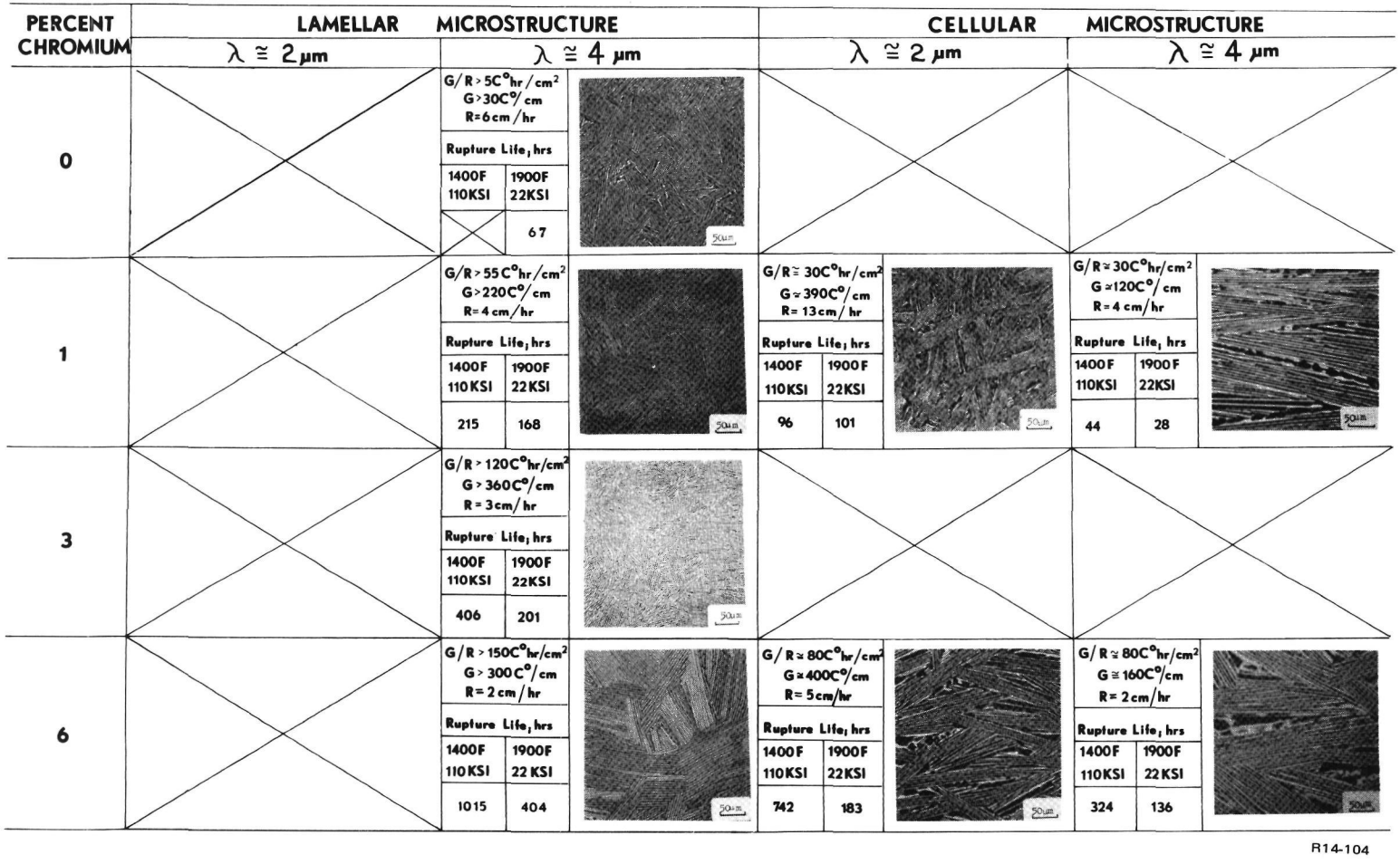



Figure 84 Influence of Composition and Process Conditions On the Microstructure and Rupture Life of $\gamma/\gamma'$-$\delta$ Directionally Solidified Eutectic Alloys

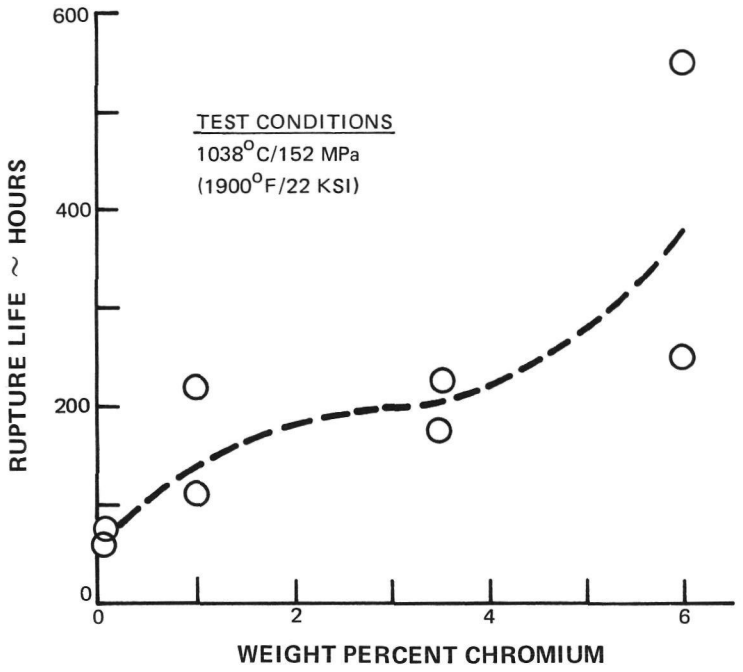



Figure 85 Influence of Chromium On the Rupture Life of Fully Directionally Solidified $\gamma/\gamma'$-$\delta$ Eutectic Alloy Solidified At Various Rates to Provide a Lamellar Spacing of $\approx 4\ \mu m$

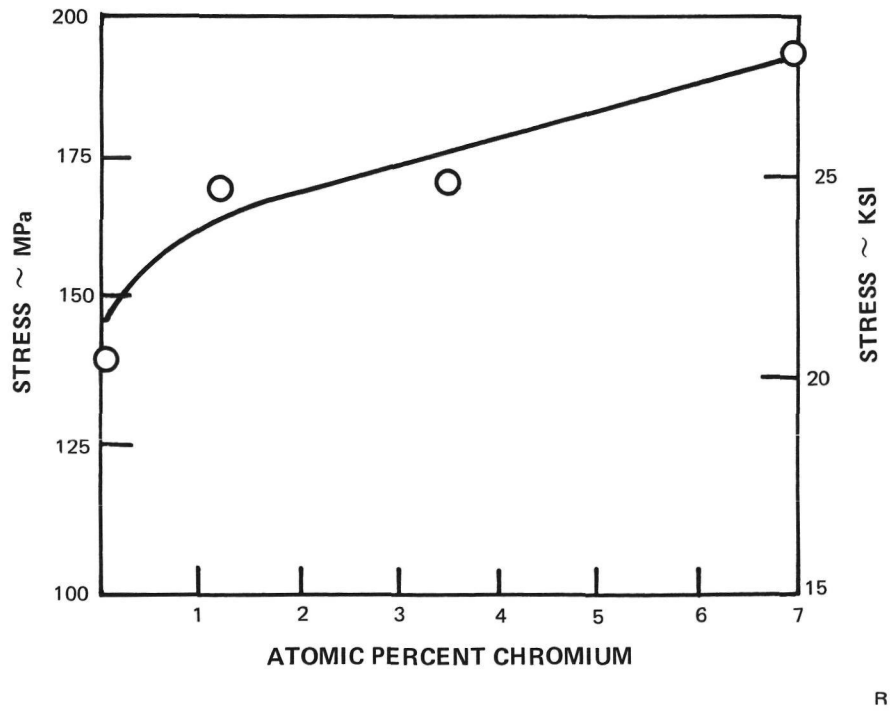
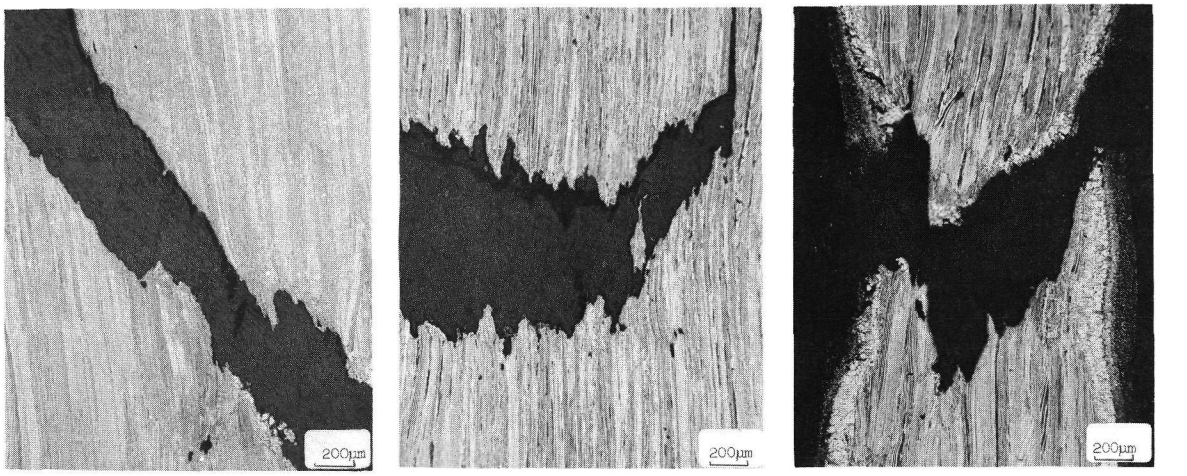


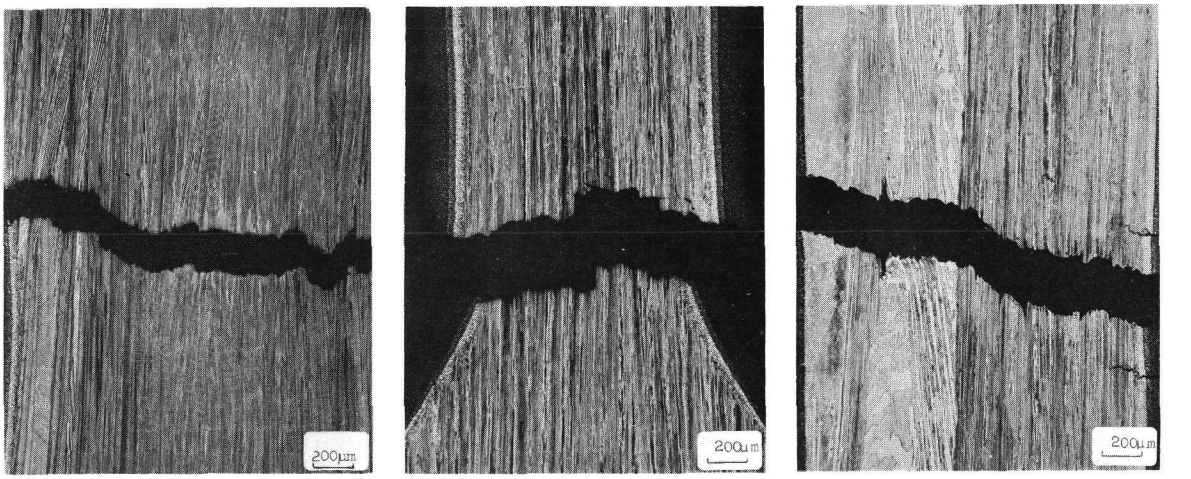

Figure 86 Influence of Chromium On the 1038°C (1900°F) Stress for 100 Hour Rupture of Lamellar Directionally Solidified $\gamma/\gamma'$-$\delta$ Eutectic Alloys Solidified At Various Rates to Provide a Uniform Lamellar Spacing of $\approx 4\ \mu m$




A) A74-1020-01 (B540) 2 cm/hr LAMELLAR, RUPTURE LIFE 556 HRS AT 1038°C/152 MPa (1900°F/22 KSI)

B) A75-003-02 (B543) 5 cm/hr CELLULAR, RUPTURE LIFE 188 HRS AT 1038°C/152 MPa (1900°F/22 KSI)

C) E361-01 (B668) 2 cm/hr CELLULAR, RUPTURE LIFE 142 HRS AT 1038°C/152 MPa (1900°F/22 KSI)



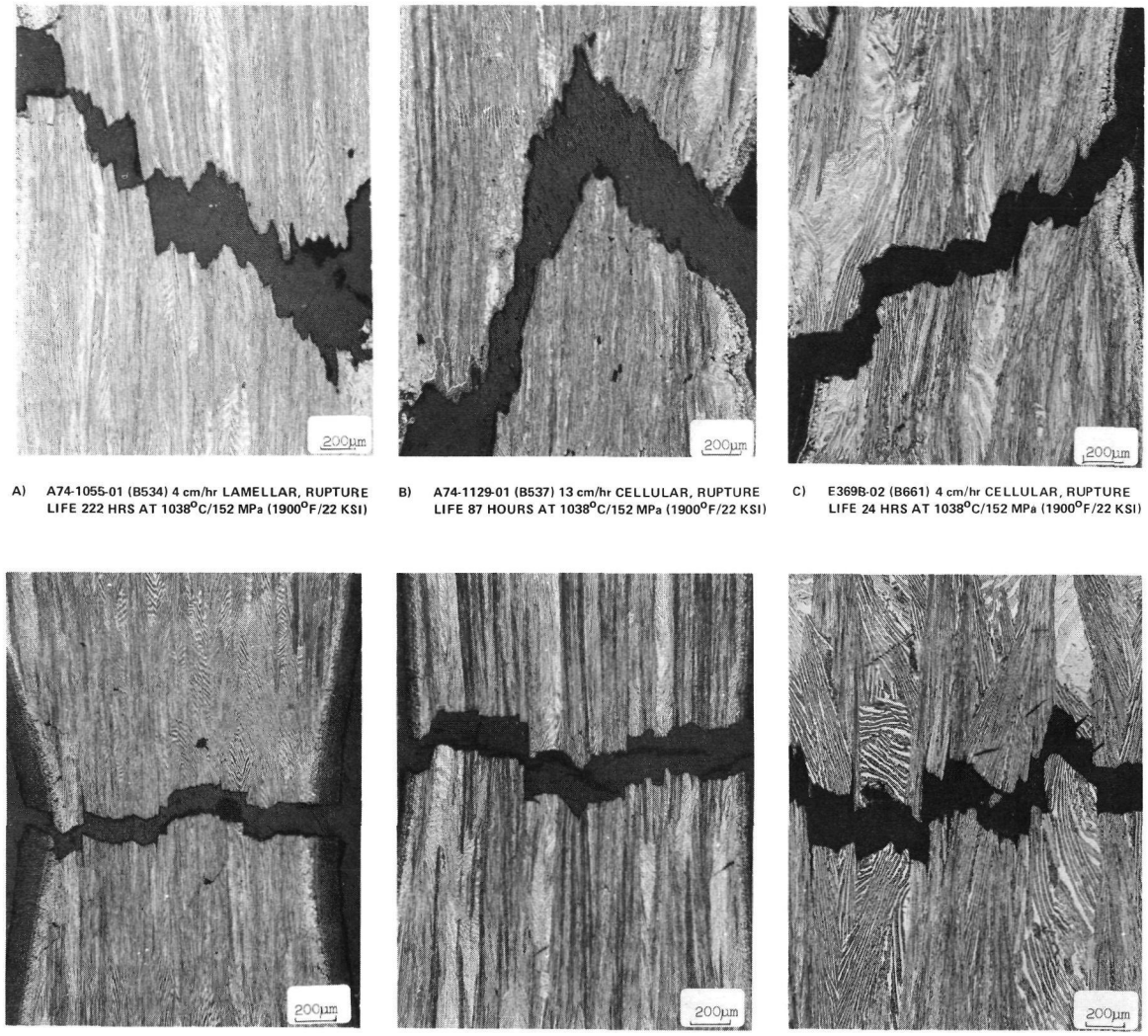

D) A75-451-01 (B781) 2 cm/hr LAMELLAR, RUPTURE LIFE 1015 HRS AT 760°C/758 MPa (1400°F/110 KSI)

E) A75-011-01 (B696) 5 cm/hr CELLULAR, RUPTURE LIFE 272 HRS AT 760°C/758 MPa (1400°F/110 KSI)

F) E370-02 (B730) 2 cm/hr CELLULAR, RUPTURE LIFE 393 HRS AT 760°C/758 MPa (1400°F/110 KSI)

R14-107

Figure 87 Fracture Appearance of 6 Percent Cr $\gamma/\gamma'$-$\delta$ Eutectic Alloy Directionally Solidified Under Various Conditions




A) A74-1055-01 (B534) 4 cm/hr LAMELLAR, RUPTURE LIFE 222 HRS AT 1038°C/152 MPa (1900°F/22 KSI)

B) A74-1129-01 (B537) 13 cm/hr CELLULAR, RUPTURE LIFE 87 HOURS AT 1038°C/152 MPa (1900°F/22 KSI)

C) E369B-02 (B661) 4 cm/hr CELLULAR, RUPTURE LIFE 24 HRS AT 1038°C/152 MPa (1900°F/22 KSI)

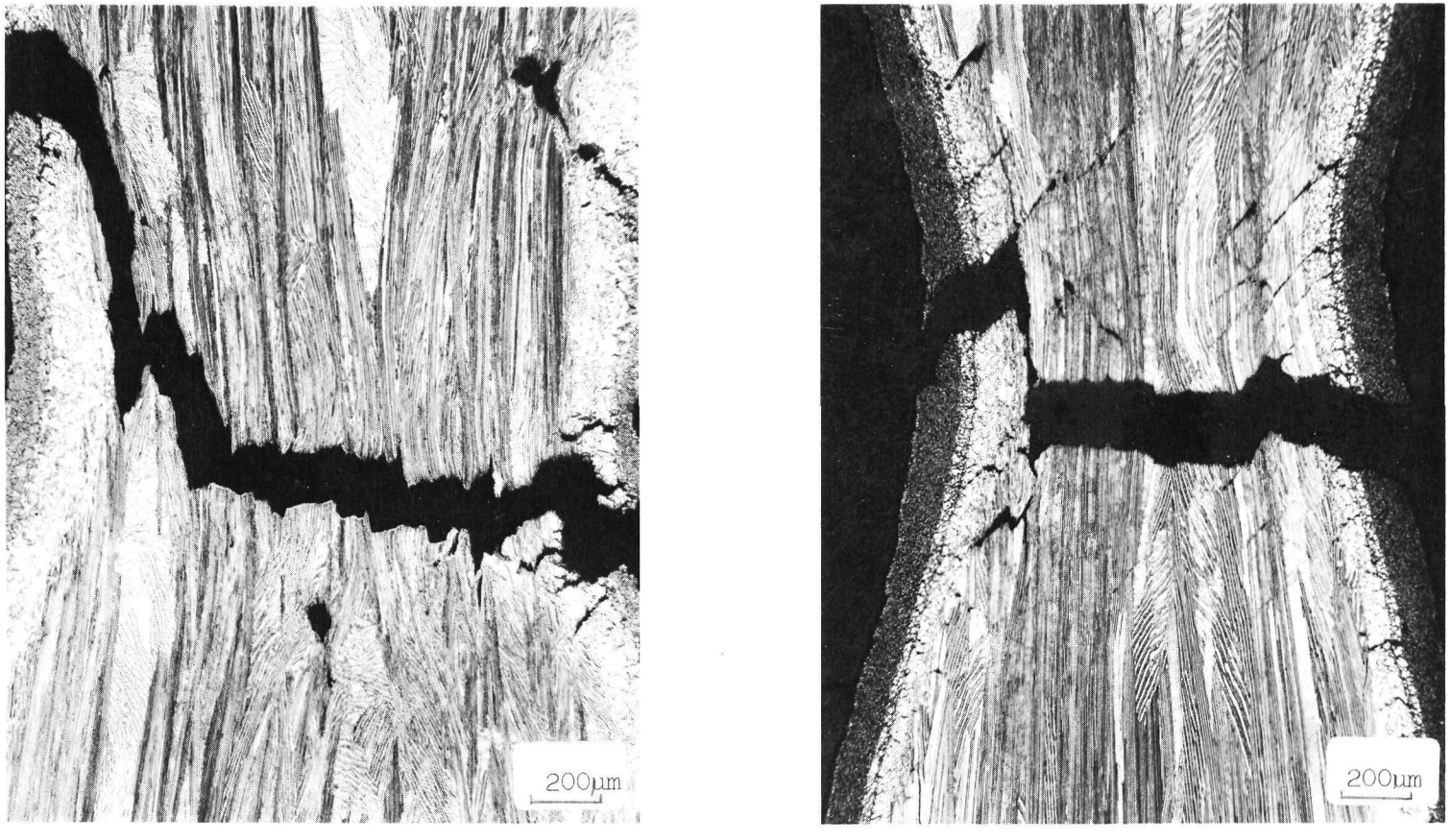
D) A74-1064-02 (B536) 4 cm/hr LAMELLAR, RUPTURE LIFE 202 HRS AT 760°C/758 MPa (1400°F/110 KSI)

E) A74-1132-02 (B539) 13 cm/hr CELLULAR, RUPTURE LIFE 105 HRS AT 760°C/758 MPa (1400°F/110 KSI)

F) E369A-02 (B659) 4 cm/hr CELLULAR, RUPTURE LIFE 28 HRS AT 760°C/758 MPa (1400°F/110 KSI)

R14-108

Figure 88 Fracture Appearance of 1 Percent Cr $\gamma/\gamma'$-$\delta$ Eutectic Alloy Directionally Solidified Under Various Conditions

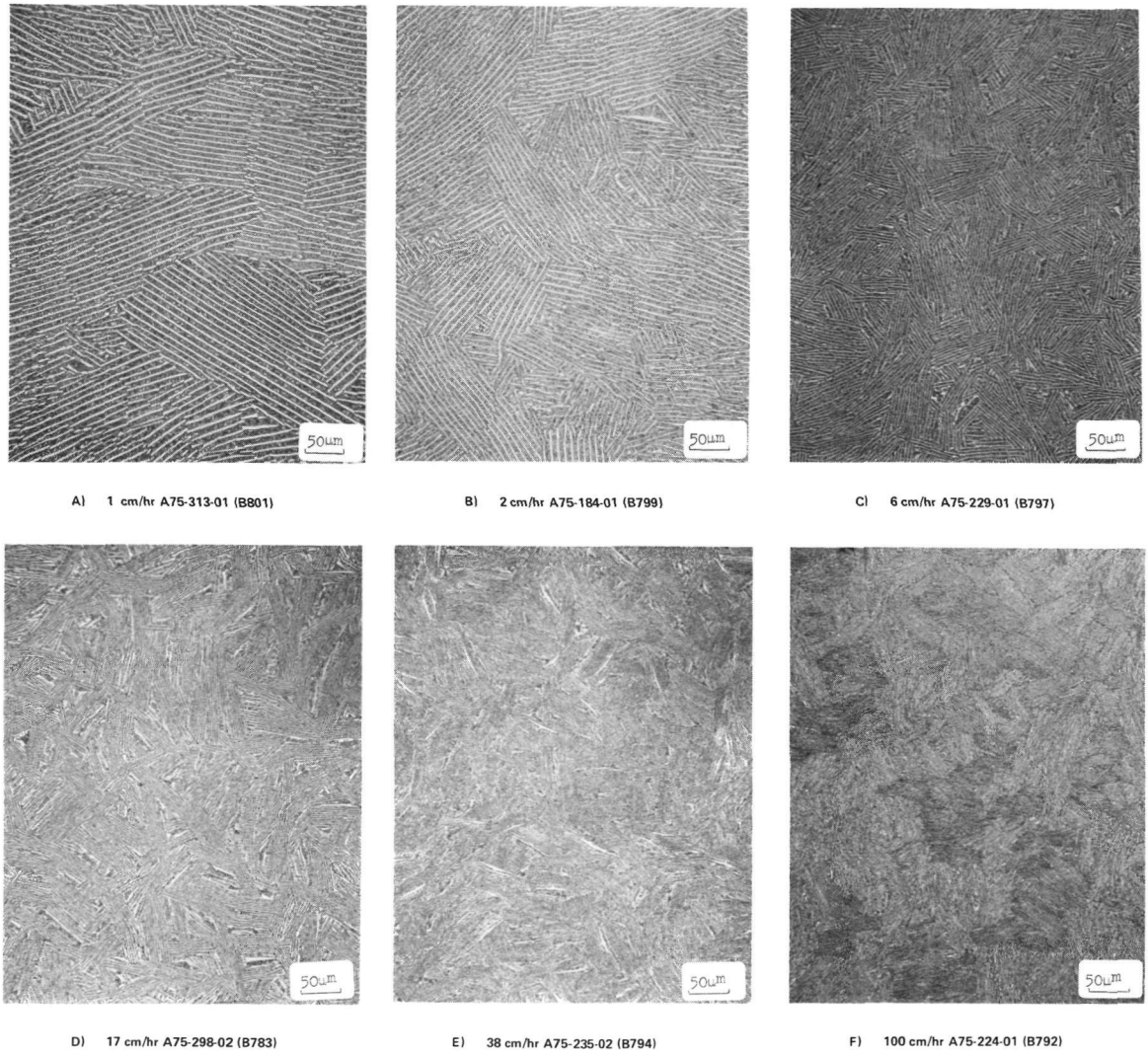



A) A75-259-01 (B725) 3 cm/hr LAMELLAR, RUPTURE LIFE 227 HRS. AT 1038°C/758 MPa (1900°F/22 ksi)

B) A75-301-01 (B744) 3 cm/hr LAMELLAR, RUPTURE LIFE 444 HRS. AT 760°C/758 MPa (1400°F/110 KSI)

R14-109

Figure 89 Fracture Appearance of Directionally Solidified 3 Percent $\gamma/\gamma'$-$\delta$ Eutectic Creep Specimens




A) 1 cm/hr A75-313-01 (B801)

B) 2 cm/hr A75-184-01 (B799)

C) 6 cm/hr A75-229-01 (B797)

D) 17 cm/hr A75-298-02 (B783)

E) 38 cm/hr A75-235-02 (B794)

F) 100 cm/hr A75-224-01 (B792)

R14-110

Figure 90 Influence of Solidification Rate On the Transverse Microstructure of the Chromium Free $\gamma/\gamma'$-$\delta$ Eutectic Alloy

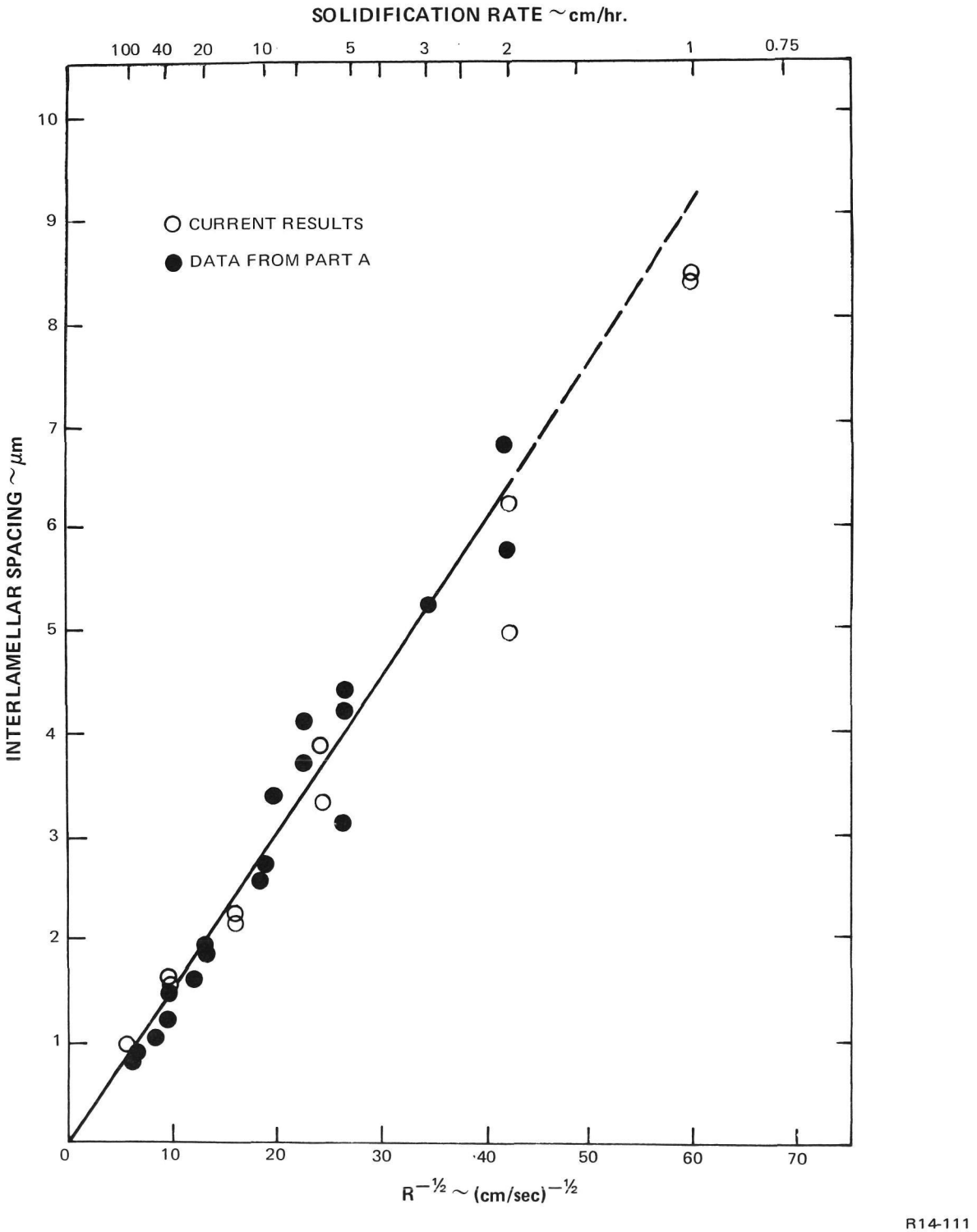



Figure 91 Comparison of Lamellar Spacing Measurements Made On Chromium Free $\gamma/\gamma'$-$\delta$ Mechanical Test Specimens With Results Obtained From the Solidification Part of Phase II

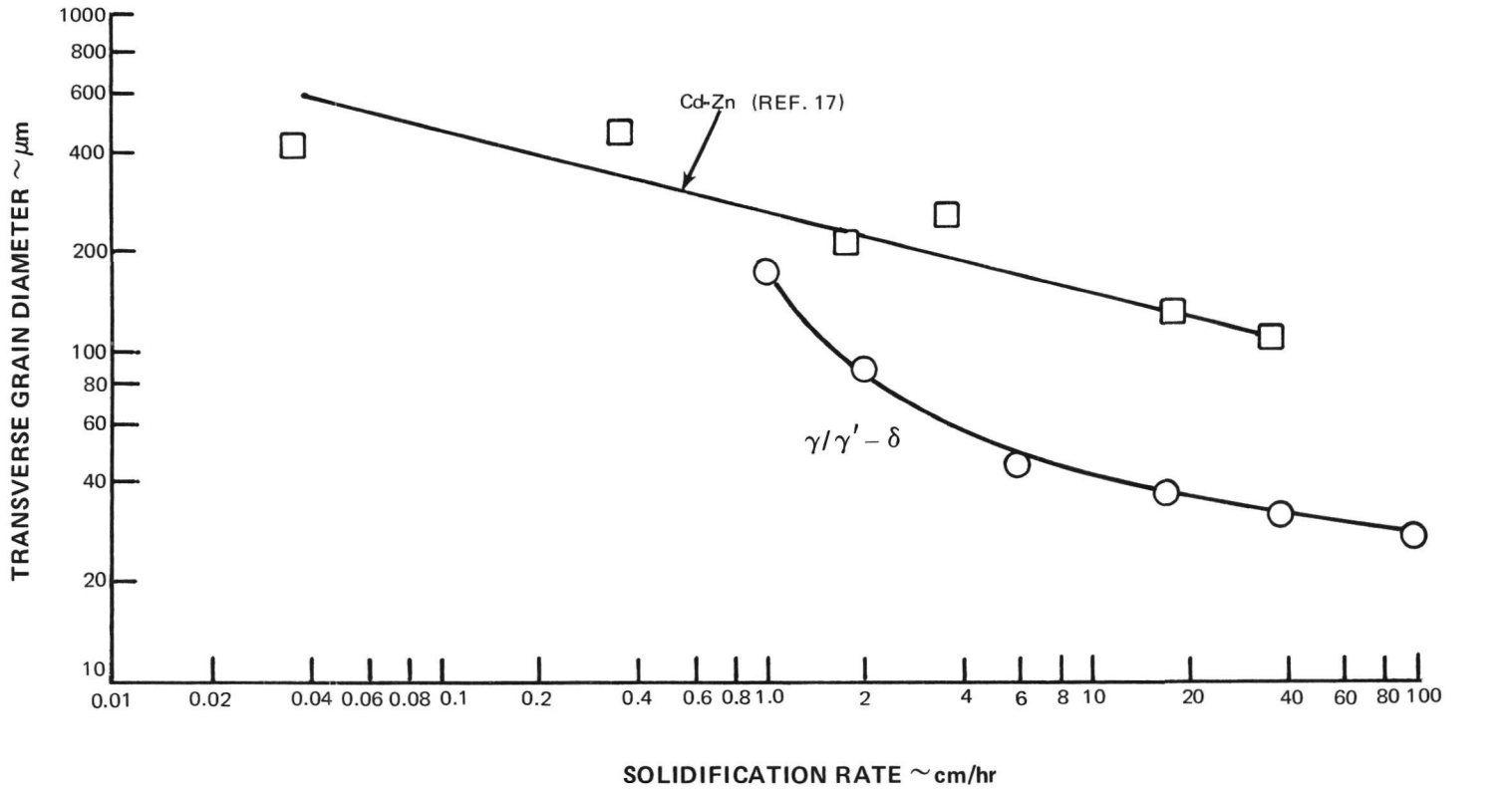



Figure 92 Influence of Solidification Rate On Transverse Grain Diameter

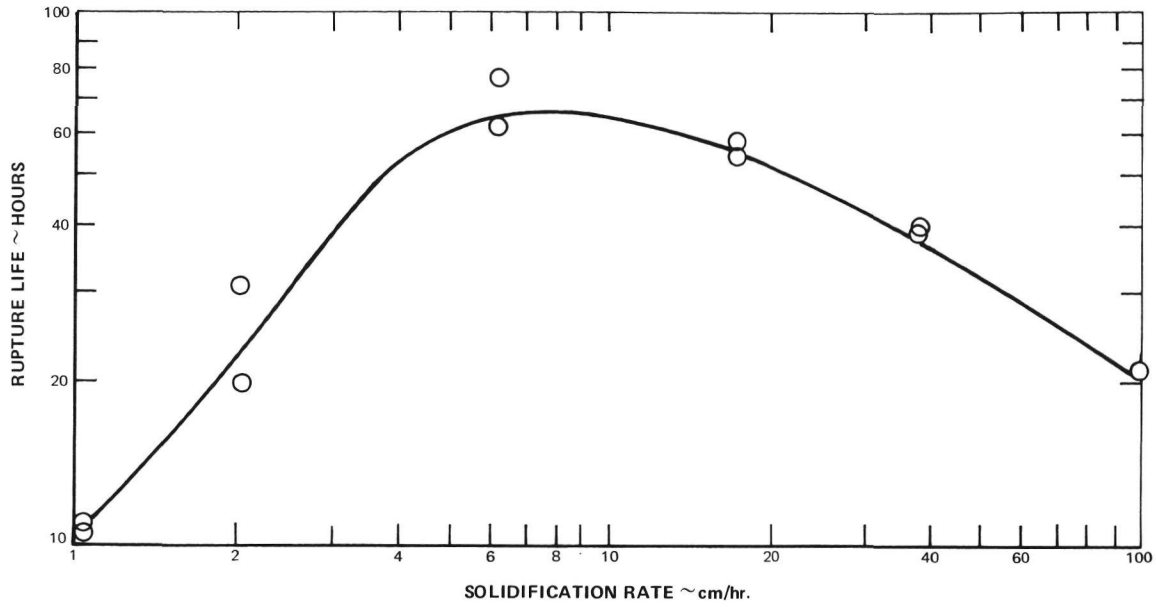



Figure 93 Influence of Solidification Rate On the Rupture Life of Fully Lamellar Chromium Free $\gamma/\gamma'$-$\delta$ Alloy Tested At 1038°C 152 MPa (1900°F/22 ksi)

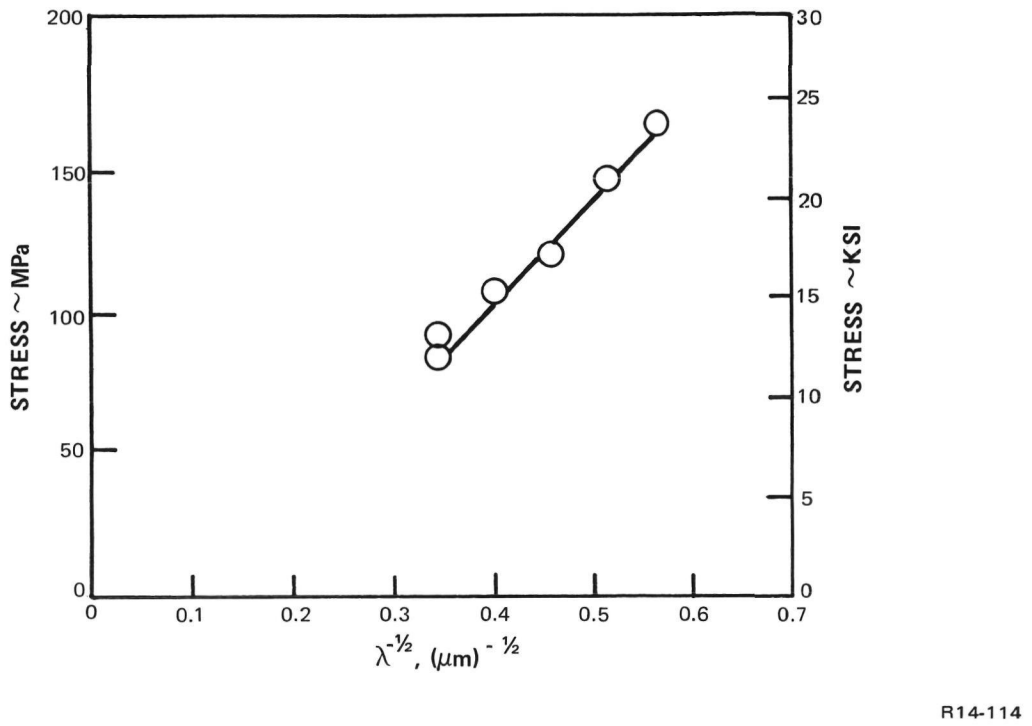
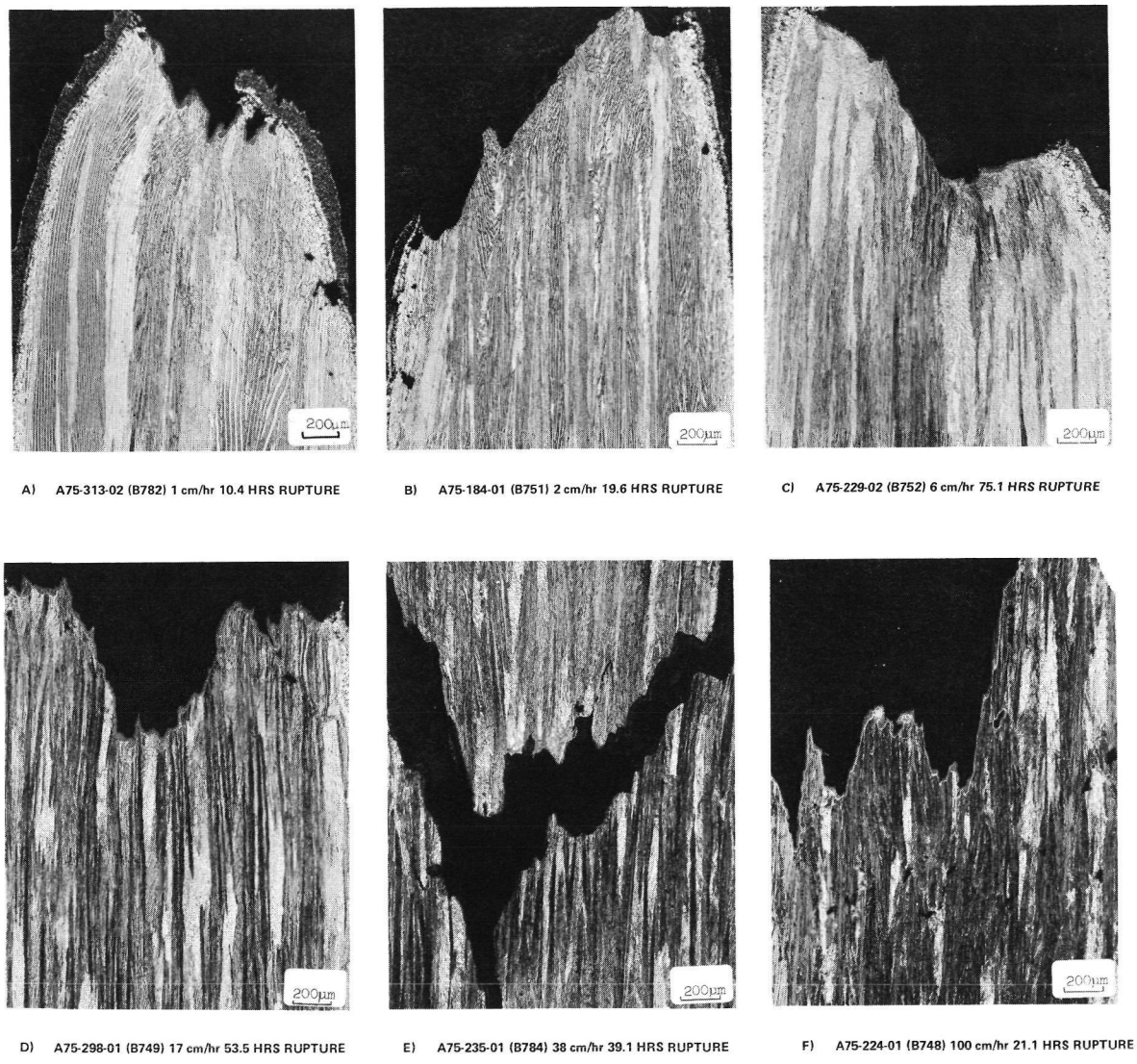



Figure 94 Influence of Lamellar Spacing ($\lambda$) On Stress for a Minimum Creep Rate of $10^{-4}$ $hr^{-1}$ In the Chromium Free $\gamma/\gamma'$-$\delta$ Alloy Solidified At Various Rates In the Range of 1-6 cm/hour




A) A75-313-02 (B782) 1 cm/hr 10.4 HRS RUPTURE

B) A75-184-01 (B751) 2 cm/hr 19.6 HRS RUPTURE

C) A75-229-02 (B752) 6 cm/hr 75.1 HRS RUPTURE

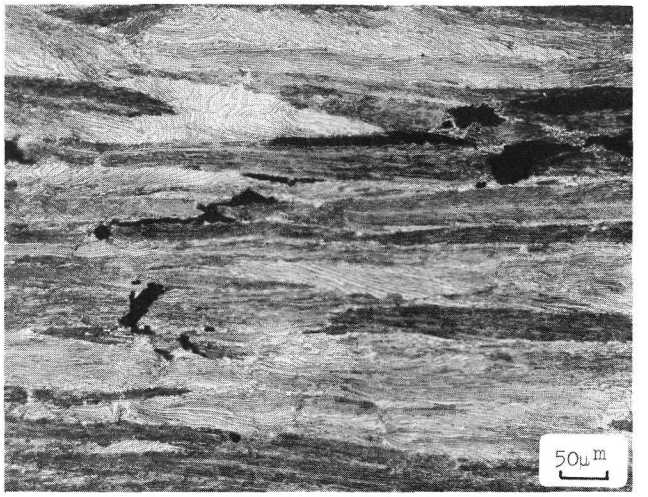
D) A75-298-01 (B749) 17 cm/hr 53.5 HRS RUPTURE

E) A75-235-01 (B784) 38 cm/hr 39.1 HRS RUPTURE

F) A75-224-01 (B748) 100 cm/hr 21.1 HRS RUPTURE

R14-115

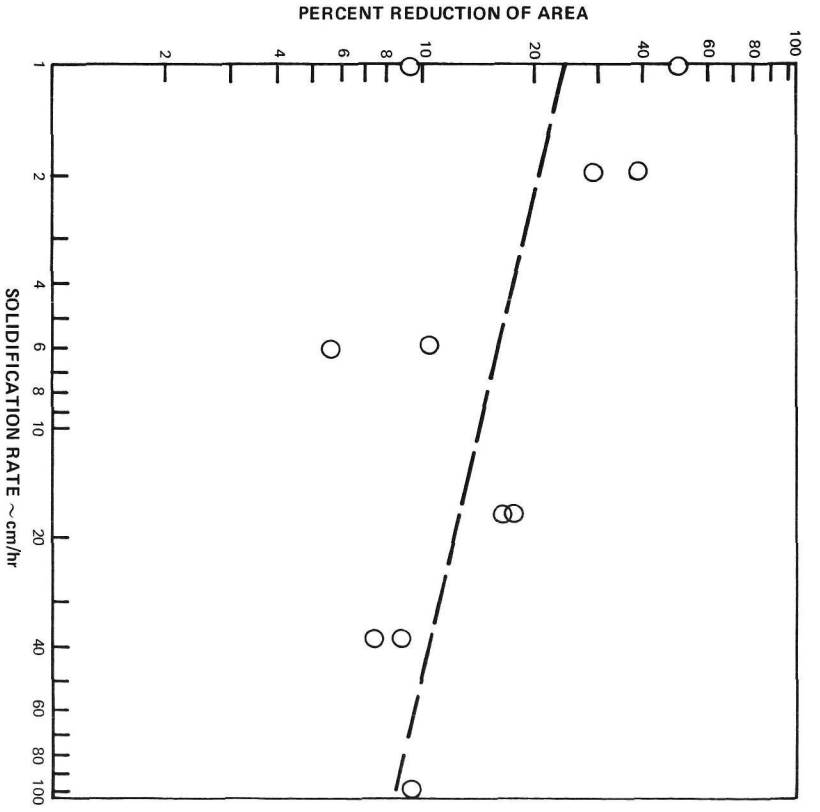
Figure 95 Influence of Solidification Rate On Fracture Appearance of Directionally Solidified Chromium Free $\gamma/\gamma'$-$\delta$ Eutectic Creep Specimens Tested At 1038°C/152 MPa (1900°F/22 ksi). Note Increasing Contribution of Grain Boundary Shear With Increasing Solidification Rate




MB 1169-4 (B748)

R14-116

Figure 96 Example of Intergranular Deformation Formed In Specimen A75-224-01 Produced At 100 cm (40 Inches)/hour




R14-117

Figure 97 Influence of Solidification Rate On Rupture Ductility of the Chromium Free $\gamma/\gamma'$-$\delta$ Directionally Solidified Eutectic Alloy

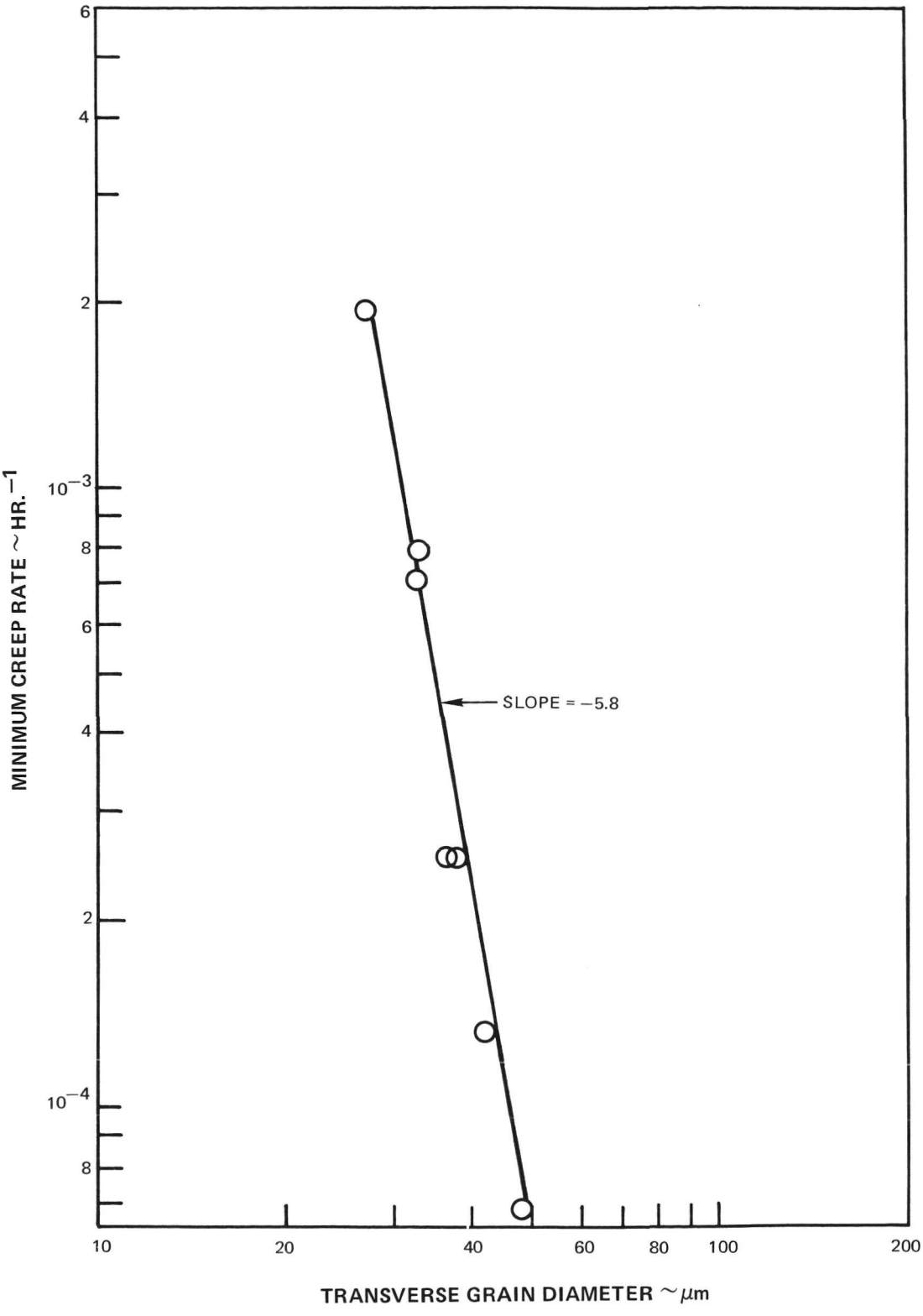



Figure 98 Influence of Transverse Grain Size On Minimum Creep Rate of Chromium Free $\gamma/\gamma'$-$\delta$ Eutectic Creep Specimens Directionally Solidified At Various Rates Between 6 and 100 cm/hour

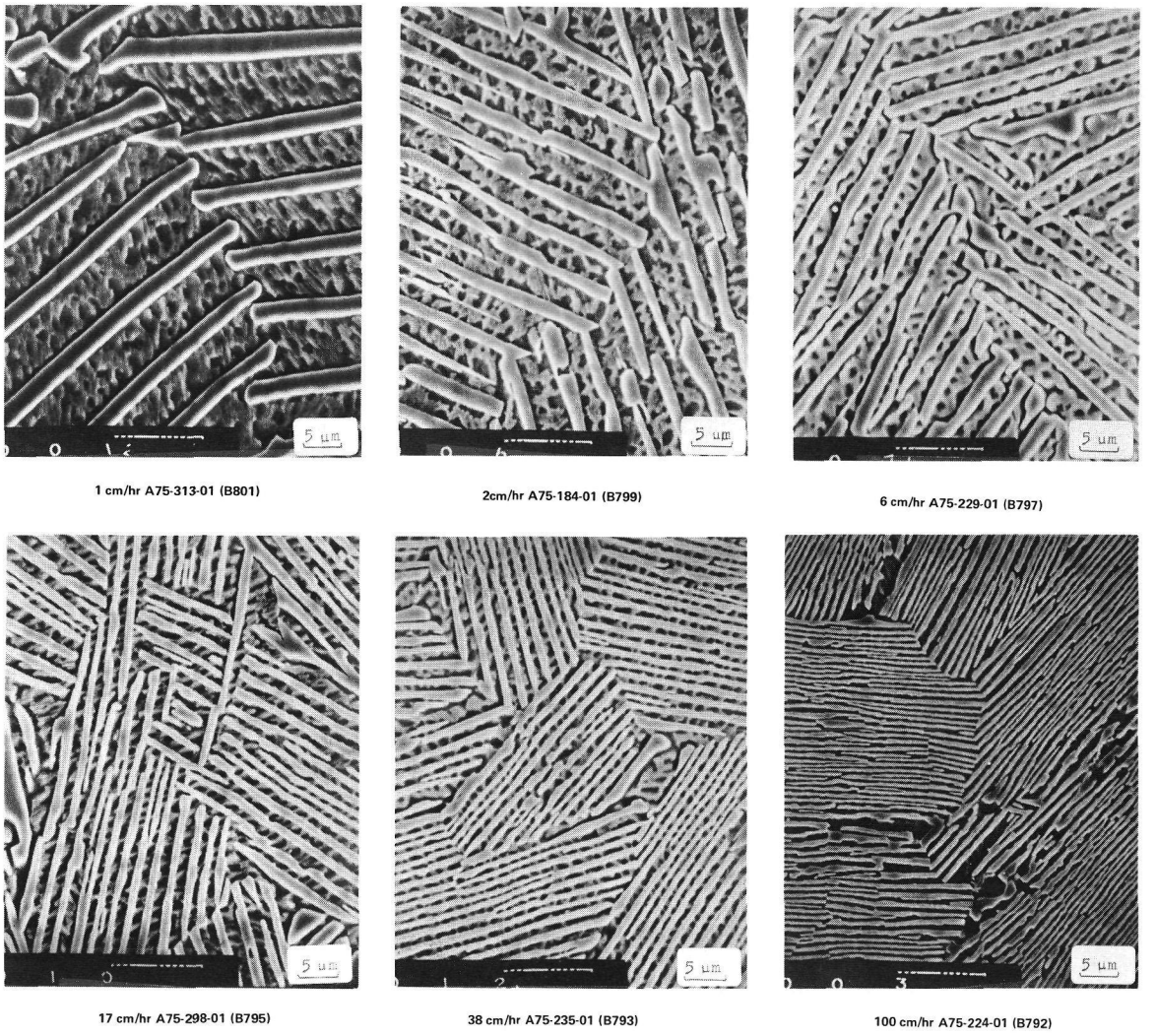
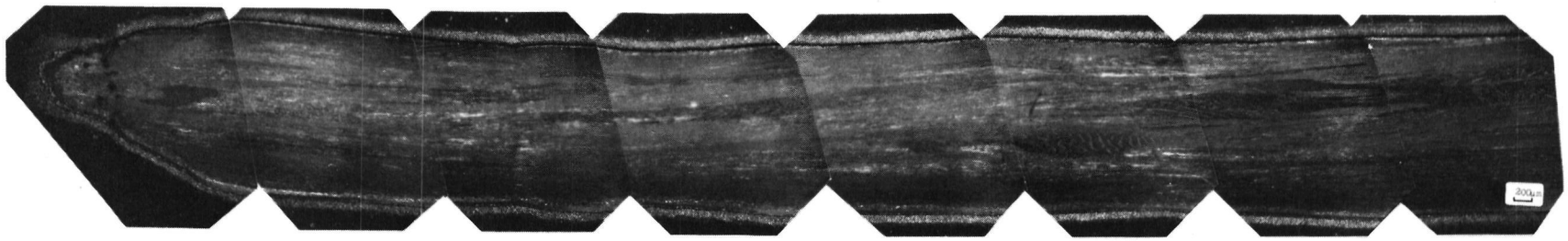
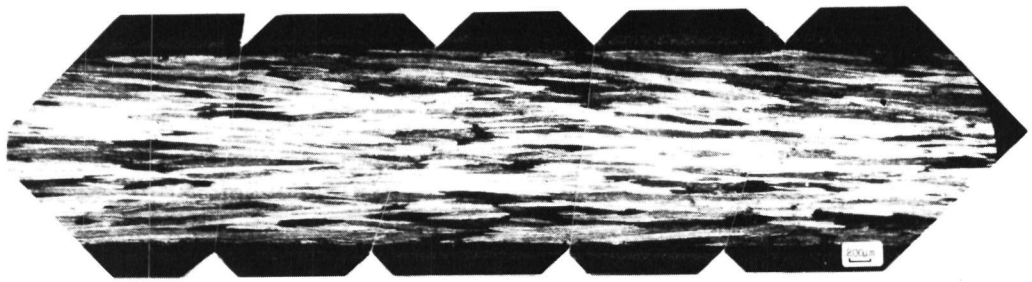



Figure 99 Influence of Solidification Rate On the Grain Boundary Structure of Chromium Free $\gamma/\gamma'$-$\delta$ Eutectic



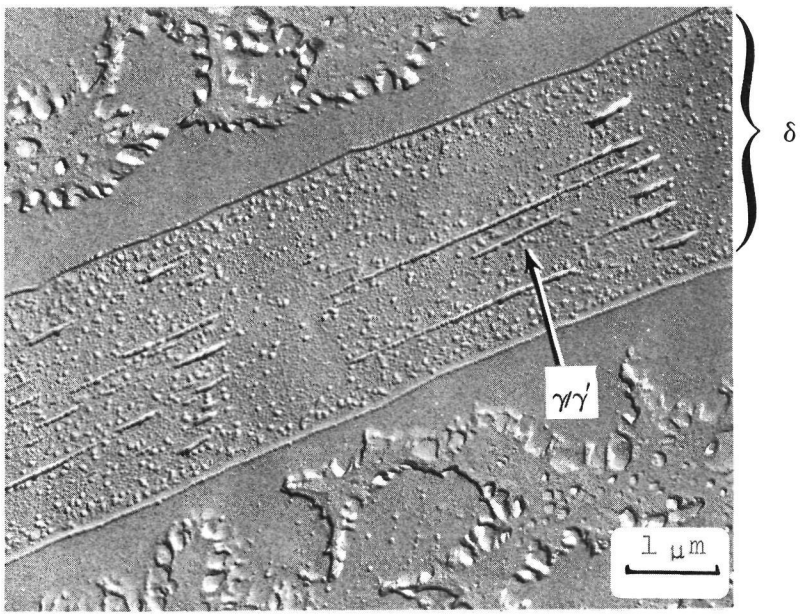
A) FROZEN AT 1 cm/HOUR



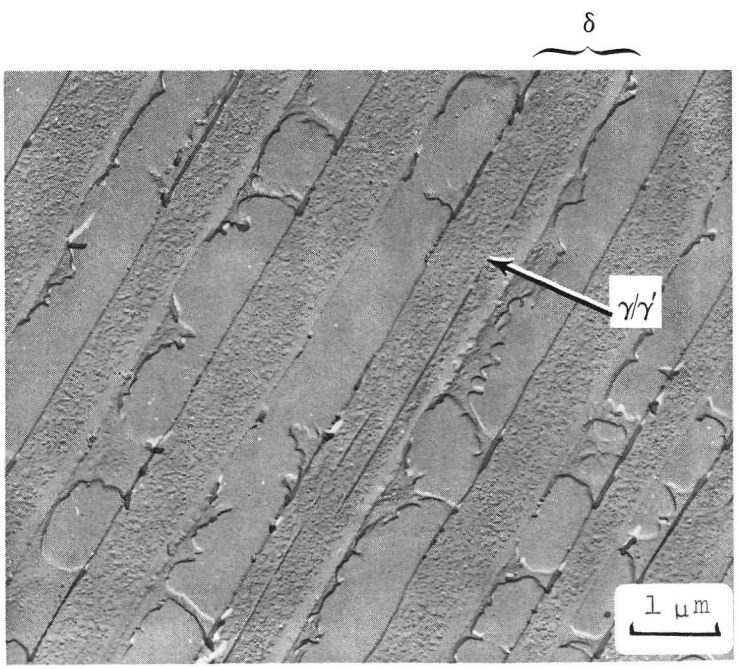
B) FROZEN AT 100 cm/HOUR

R14-120

Figure 100 Longitudinal Grain Structure of Chromium Free $\gamma/\gamma'$-$\delta$ Test Specimens Directionally Solidified At Various Rates. Polarized Illumination




a) SOLIDIFICATION RATE 1 CM/HR.




b) SOLIDIFICATION RATE 38 CM/HR.

R14-121

Figure 101 $\gamma/\gamma'$ Precipitate Found Near the Fracture Surface of Zero Chromium $\gamma/\gamma'$-$\delta$ Alloy Solidified At the Indicated Rates and Tested to Rupture at 1038°C/ 152 MPa (1900°F/22 ksi)

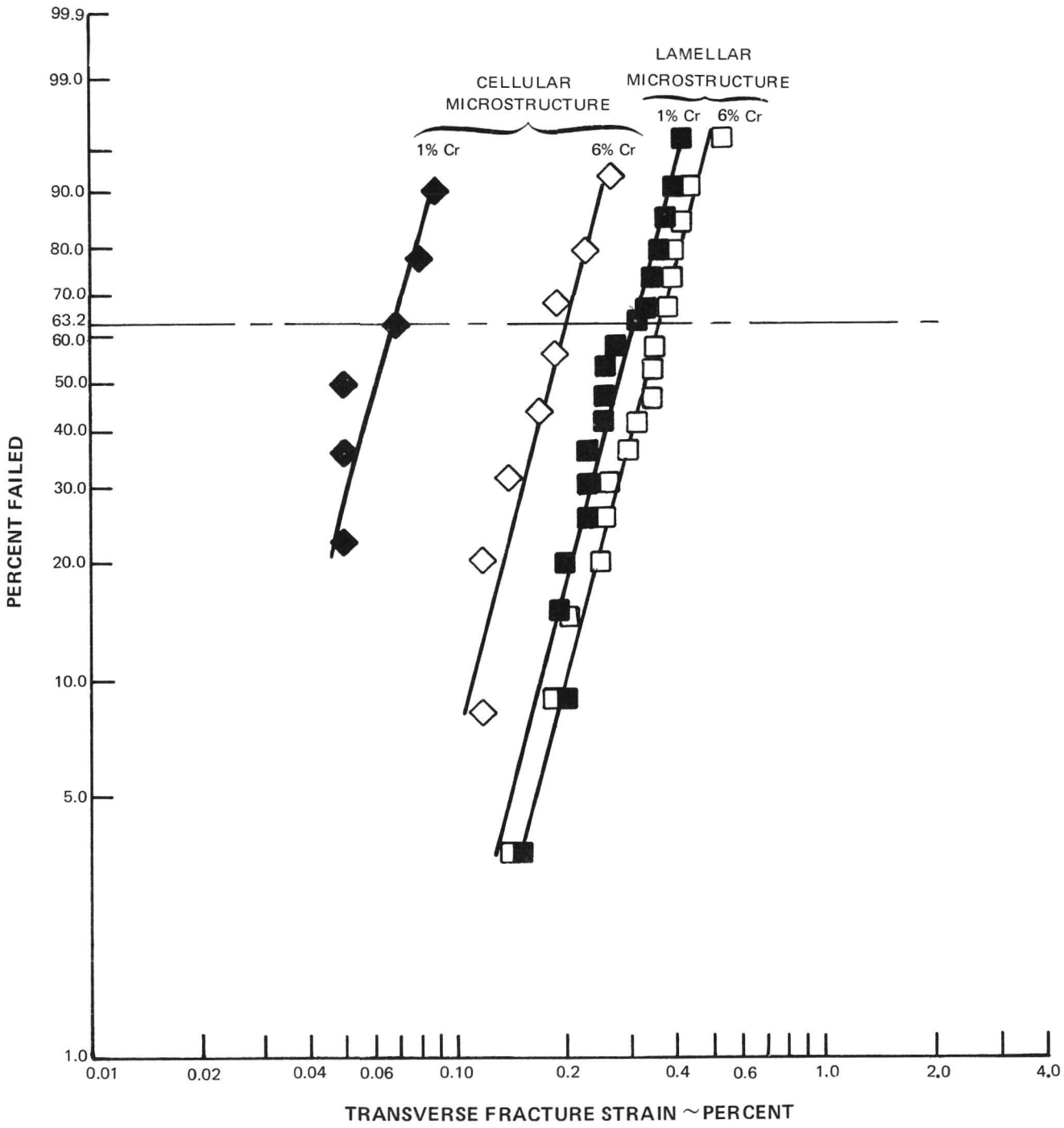
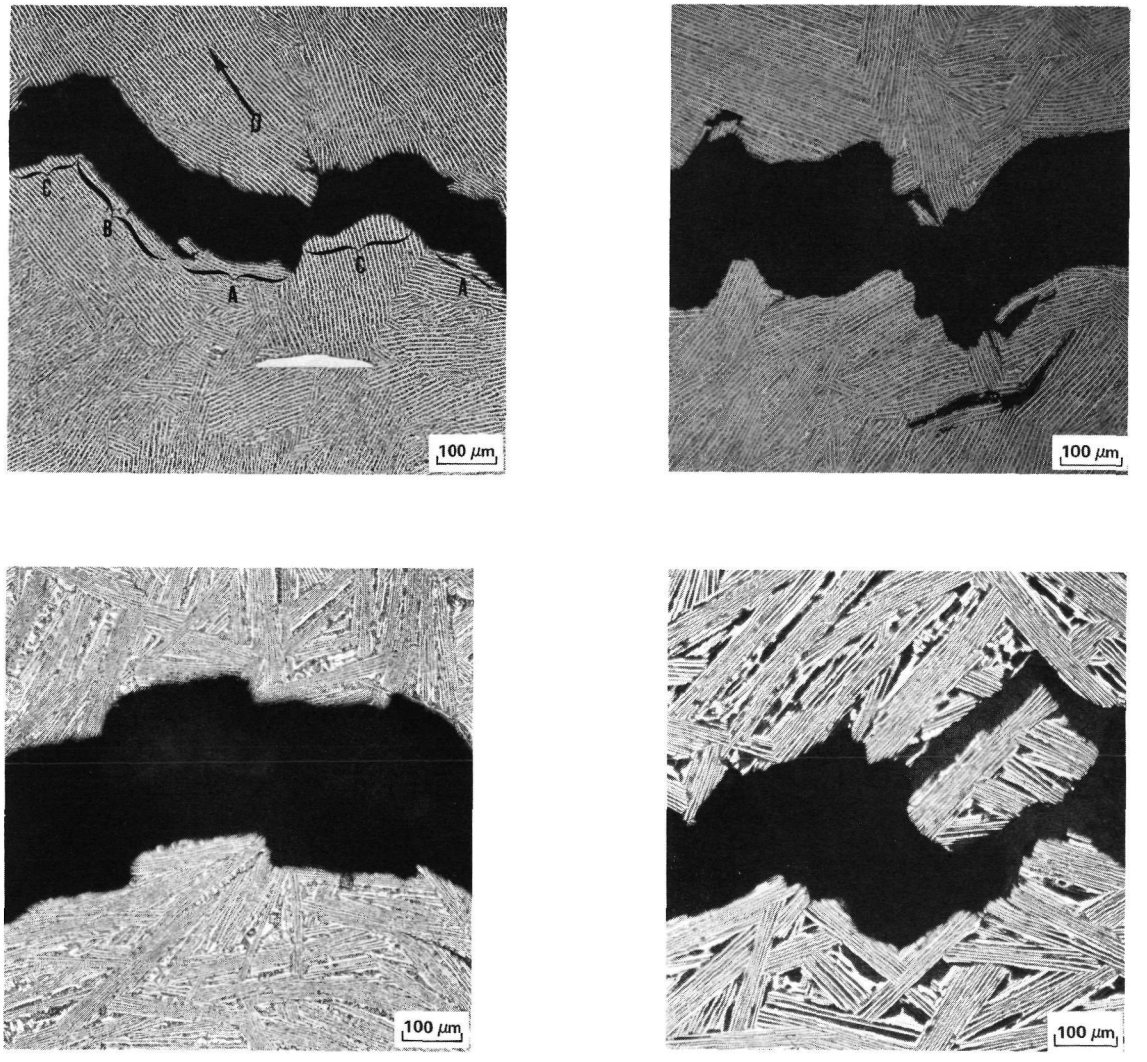



Figure 102 Weibull Analysis of 760°C (1400°F) Transverse Fracture Strains Measured on Various $\gamma/\gamma'$-$\delta$ Directionally Solidified Eutectic Alloys

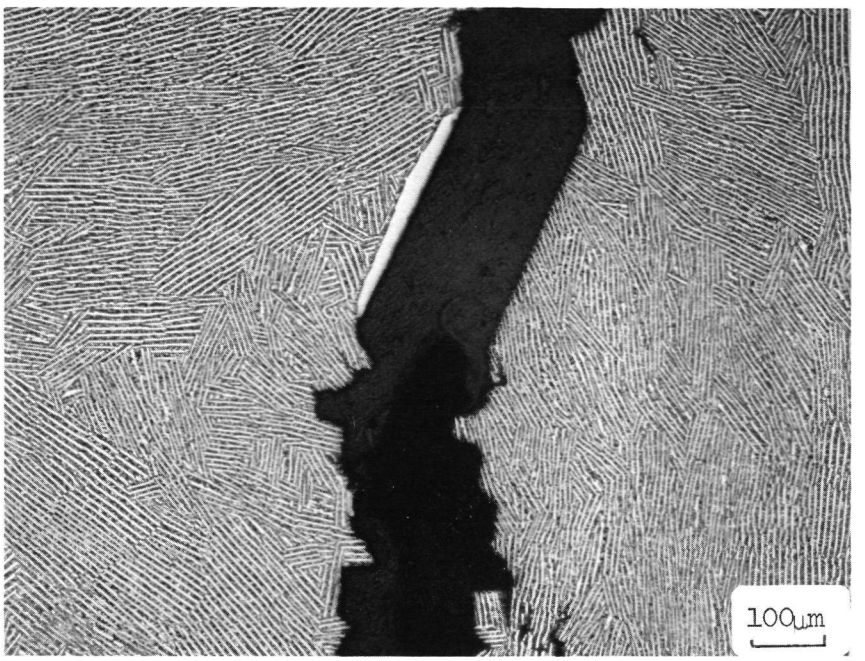



C) 1% Cr, CELLULAR STRUCTURE

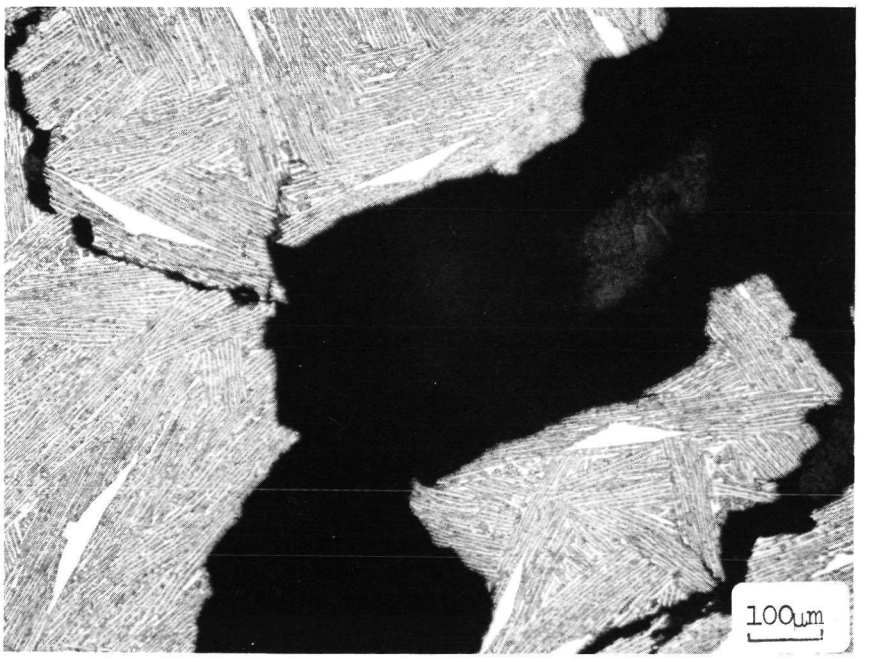
D) 6% Cr, CELLULAR STRUCTURE

R14-123

Figure 103 Fracture Profiles Found In 760°C (1400°F) Transverse Tension Test Specimens. Tensile Axis Vertical




A) LAMELLAR, δ DENDRITIC STRUCTURE




B) CELLULAR, δ DENDRITIC STRUCTURE

R14-124

Figure 104 Comparison of 760°C (1400°F) Transverse Tensile Fracture Profiles Observed In δ Dendritic 1 Percent Directionally Solidified $\gamma/\gamma'$-δ Eutectic Alloy Specimens Having Fully Lamellar and Partially Cellular Microstructures. Tensile Axis Horizontal

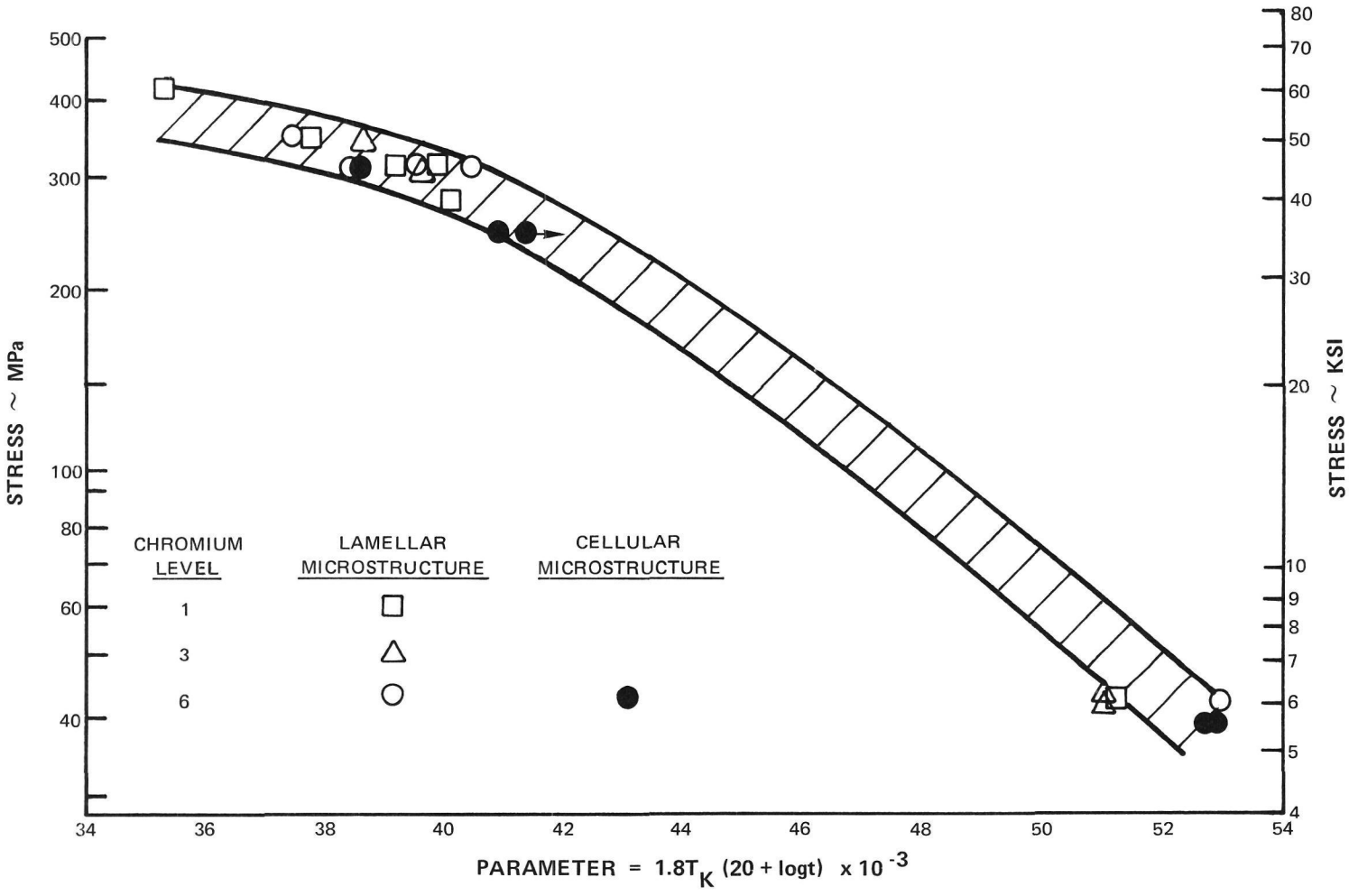
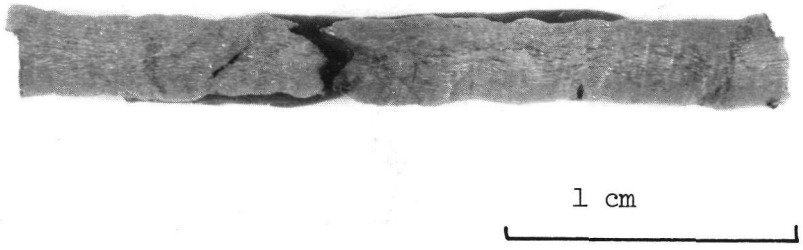
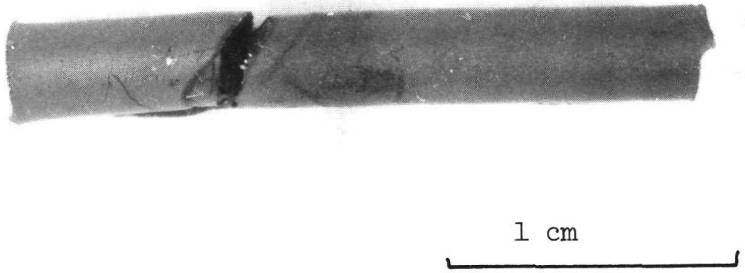



Figure 105 Transverse Creep Results On $\gamma/\gamma'$-$\delta$ Alloy



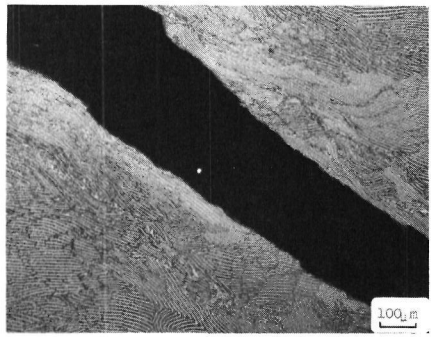

A) SPECIMEN E407E TESTED AT 1038°C/41.3 MPa (1900°F/6 KSI). RUPTURE LIFE 279.3 HOURS. RUPTURE ELONGATION 24% (MB 1342-2).



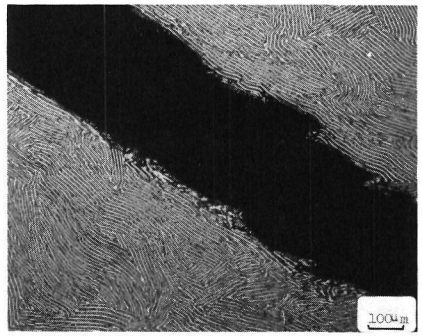

B) SPECIMEN 407D TESTED AT 704°C/310 MPa (1300°F/45 KSI). RUPTURE LIFE 267 HOURS. RUPTURE ELONGATION 1.2% (MB 1342-1).

R14-126

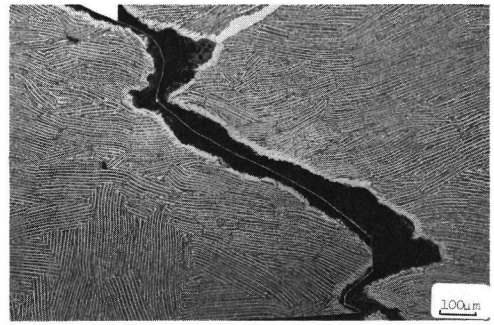
Figure 106 Influence of Test Temperature On Appearance of 6 Percent Cr $\gamma/\gamma'$-$\delta$ Specimens Broken In Transverse Stress Rupture



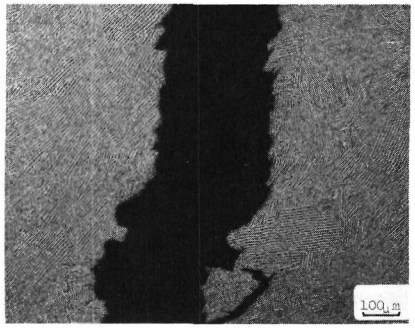

(B848, MB 1342-5)
A) 1% Cr SPECIMEN E406H, TESTED AT 1038°C/41.3 MPa (1900°F/6 KSI).
RUPTURE LIFE 55.2 HOURS.
RUPTURE ELONGATION 27.1%.



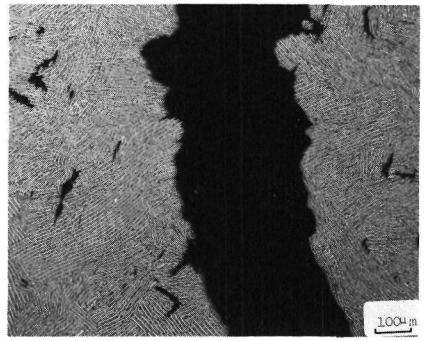

(B850, MB 1342-6)
B) 3% Cr SPECIMEN E384E, TESTED AT 1038°C/41.3 MPa (1900°F/6 KSI).
RUPTURE LIFE 44.7 HOURS.
RUPTURE ELONGATION 12.8%.




(B852, MB 1342-9)
C) 6% Cr SPECIMEN E407E, TESTED AT 1038°C/41.3 MPa (1900°F/6 KSI).
RUPTURE LIFE 279.3 HOURS.
RUPTURE ELONGATION 24%.




(B847, MB 1342-7)
D) 1% Cr SPECIMEN E406G, TESTED AT 704°C/310 MPa (1300°F/45 KSI).
RUPTURE LIFE 458 HOURS.
RUPTURE ELONGATION 2.5%.



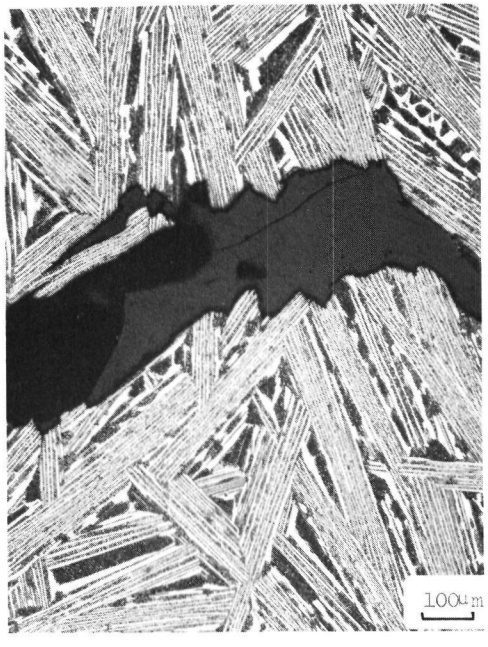

(B849, MB 1342-3)
E) 3% Cr SPECIMEN E384C, TESTED AT 704°C/310 MPa (1300°F/45 KSI).
RUPTURE LIFE 318.4 HOURS.
RUPTURE ELONGATION 5.6%.



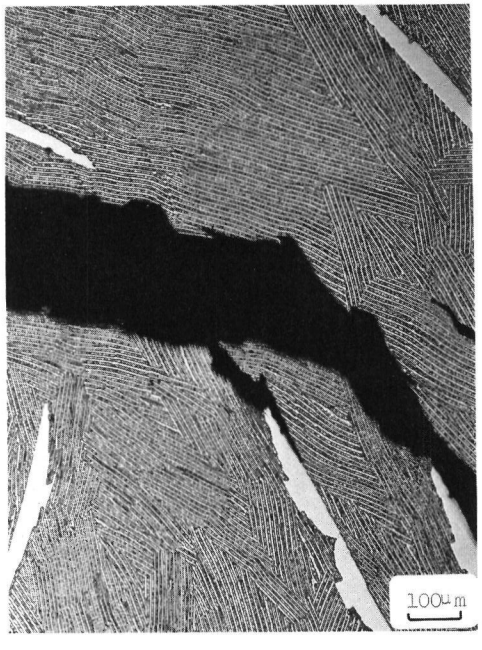

(B851, MB 1342-4)
F) 6% Cr SPECIMEN E407D, TESTED AT 704°C/310 MPa (1300°F/45 KSI).
RUPTURE LIFE 267.0 HOURS.
RUPTURE ELONGATION 2.1%.

R14-127

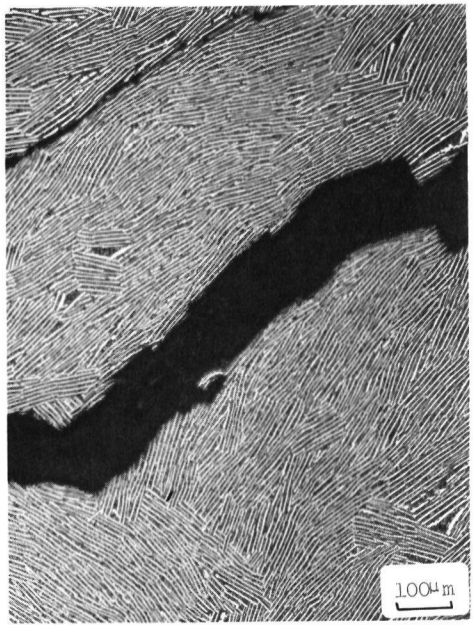
Figure 107 Influence of Chromium Level and Test Temperature On the Fracture Profile Appearance of Fully Lamellar $\gamma/\gamma'$-$\delta$ Specimens Broken In Creep-Rupture At Indicated Conditions. Tensile Axis Horizontal




A) CELLULAR BASELINE COMPOSITION SPECIMEN E259-5B (B442, MB 124-6) TESTED AT 704°C/241 MPa (1300°F/34.9 KSI). RUPTURE LIFE 1681 HOURS. RUPTURE ELONGATION 0.54%.



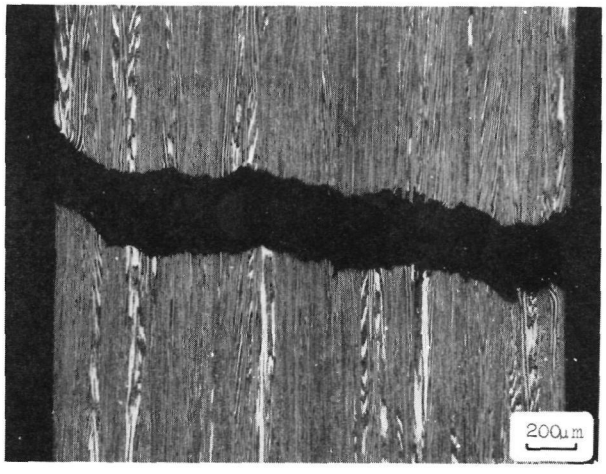

B) LAMELLAR BASELINE COMPOSITION SPECIMEN E407D (B851, MB 1342-4) TESTED AT 704°C/310 MPa (1300°F/45 KSI). RUPTURE LIFE 267 HOURS. RUPTURE ELONGATION 2.1%.



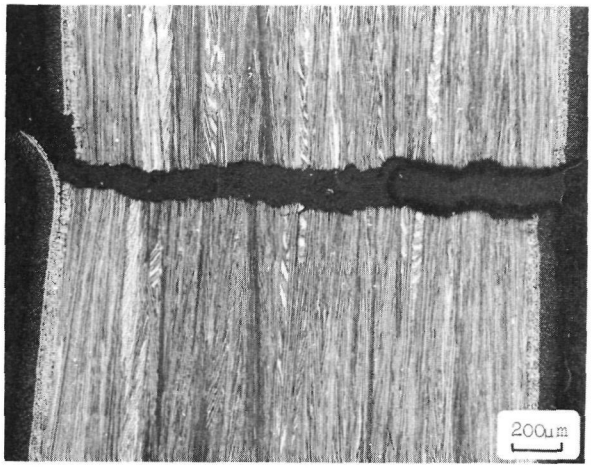

C) CARBON MODIFIED SPECIMEN E438-T1 (B846, MB 1342-8) TESTED AT 760°C/310 MPa (1400°F/45 KSI). RUPTURE LIFE 178.1 HOURS. RUPTURE ELONGATION 1.7%.

R14-128

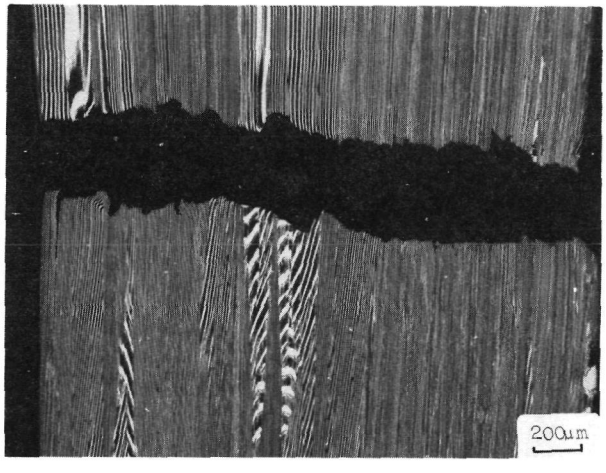
Figure 108 Influence of Microstructure and Composition On the Fracture Profile Appearance of the 6 Percent $\gamma/\gamma'$-$\delta$ Alloy Broken In Transverse Stress Rupture At Indicated Test Conditions. Tensile Axis Vertical



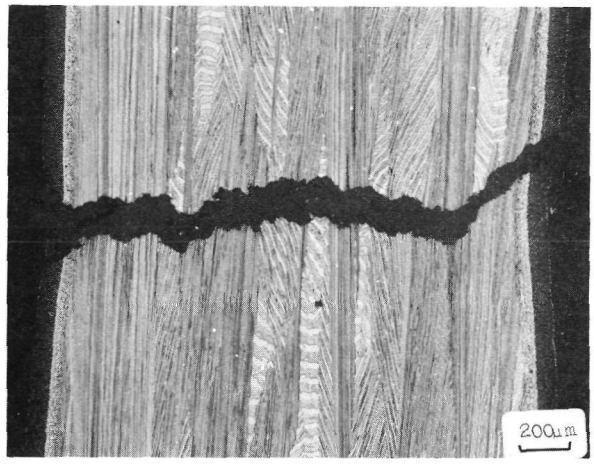

A) UNCOATED 1% Cr SPECIMEN A75-363-01. (B804, MB 1342-17). TOTAL ELONGATION 48.7%.




B) COATED 1% Cr SPECIMEN A75-375-01. (B805, MB 1342-18). TOTAL ELONGATION 7.1%.



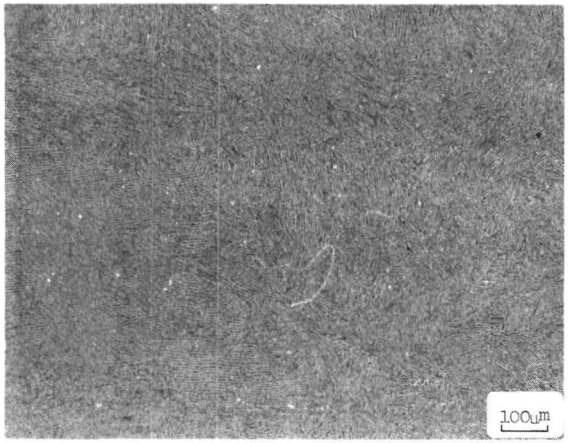

C) UNCOATED 6% Cr SPECIMEN A75-412-01. (B806, MB 1342-19). TOTAL ELONGATION 24%.



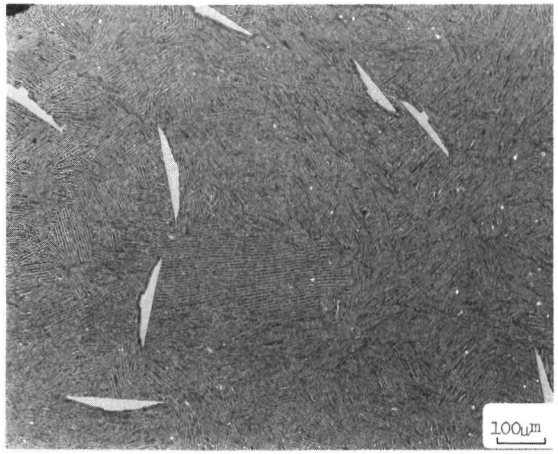

D) COATED 6% Cr SPECIMEN A75-511-01 (B808, MB 1342-20). TOTAL ELONGATION 6.6%.

R14-129

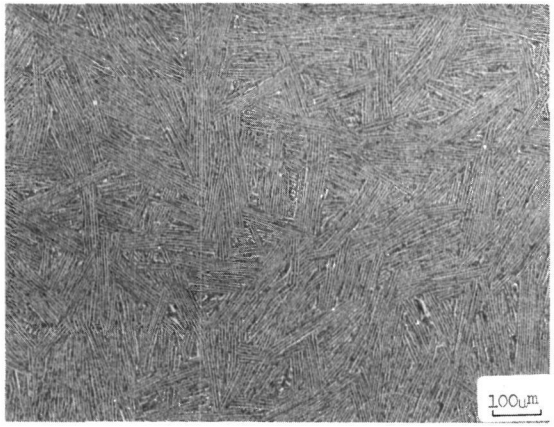
Figure 109 Fracture Profiles Found In Coated and Uncoated Specimens of the 1 and 6 Percent Cr $\gamma/\gamma'$-$\delta$ Eutectic Alloy Broken In Tension At 482°C (900°F). Tensile Axis Vertical



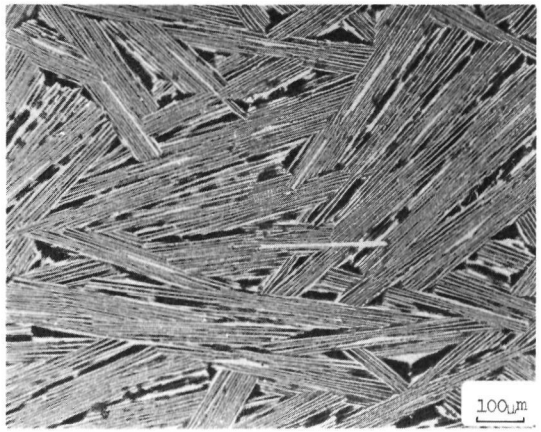

A) CHROMIUM FREE ALLOY – GROWTH RATE 3.2 CM (1.25 INCH)/HOUR.




B) 1% CHROMIUM ALLOY – GROWTH RATE 2.5 CM (1.0 INCH)/HOUR.



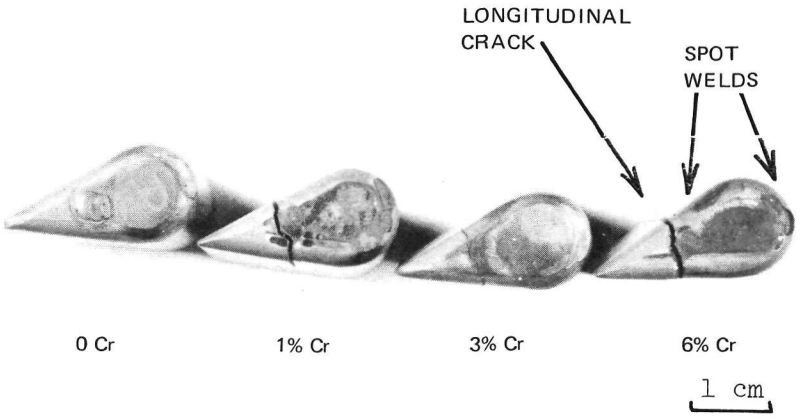

C) 3% CHROMIUM ALLOY – GROWTH RATE 1.9 cm (0.75 INCH)/HOUR.



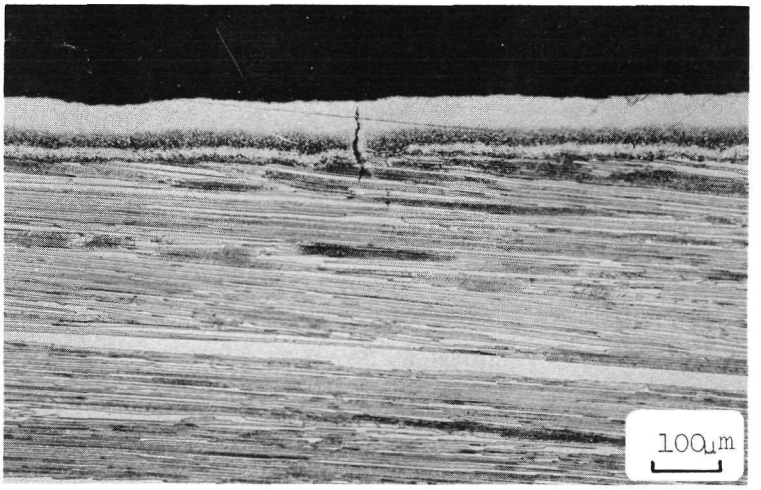

D) 6% CHROMIUM ALLOY – GROWTH RATE 1.3 cm (0.5 INCH)/HOUR.

R14-130

Figure 110 Microstructures Observed In Directionally Solidified $\gamma/\gamma'$-$\delta$ Eutectic Thermal Fatigue Castings With Various Chromium Levels




A) LONGITUDINAL CRACKS (CRACK ON 0 Cr SPECIMEN NOT RESOLVED AT THIS MAGNIFICATION). NOTE THAT CRACKS APPEAR TO BE ASSOCIATED WITH SPOT WELDS USED FOR TEMPORARY ATTACHMENT OF COATING FIXTURES.




B) TYPICAL TRANSVERSE THERMAL FATIGUE CRACK, FOUND IN 6% Cr SPECIMEN E340-A2 (B790).

R14-131

Figure 111 Thermal Fatigue Cracks Found In $\gamma/\gamma'$-$\delta$ Fluidized Bed Thermal Fatigue Wedges Cycled Between Room Temperature and 1038°C (1900°F)

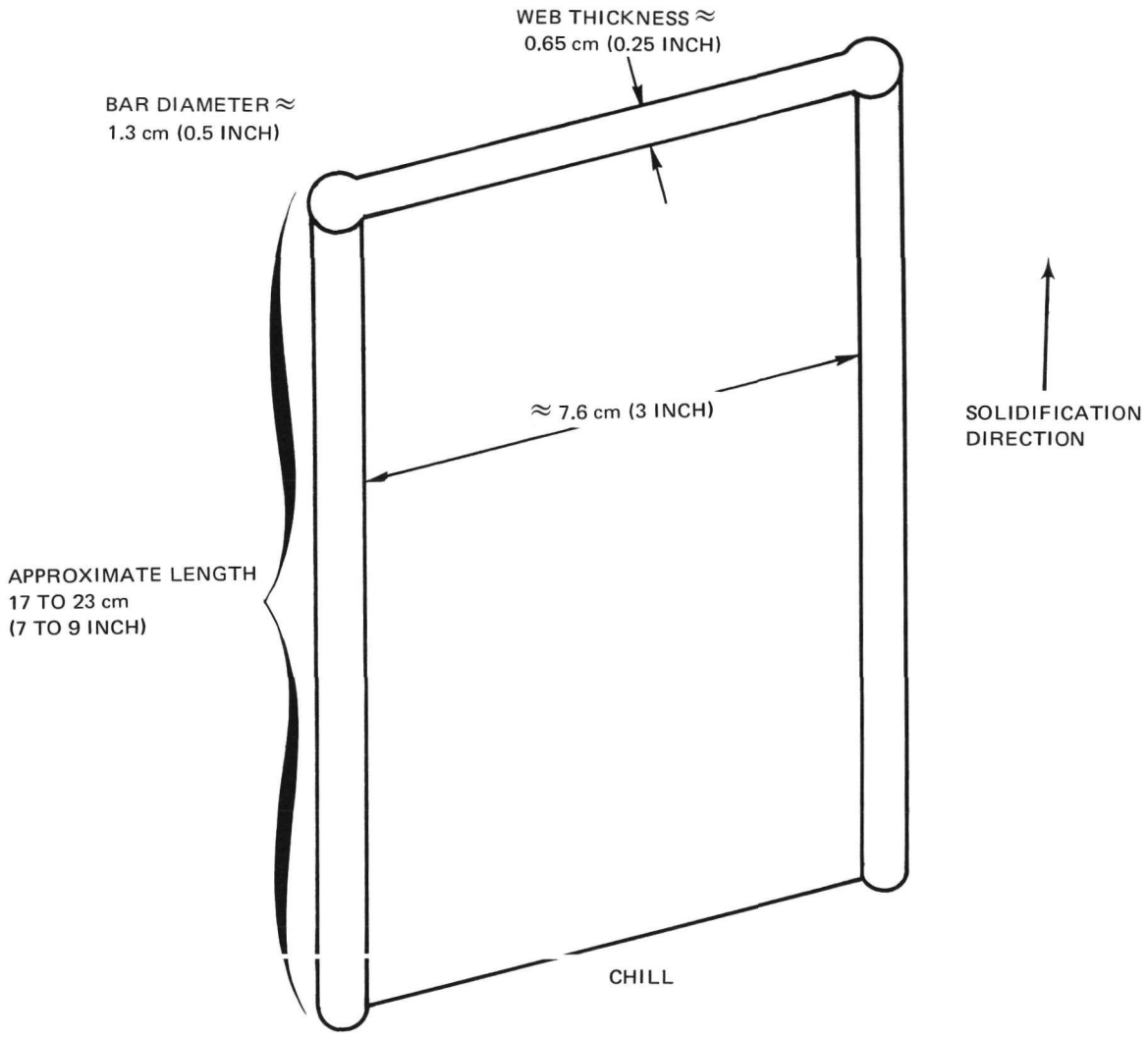
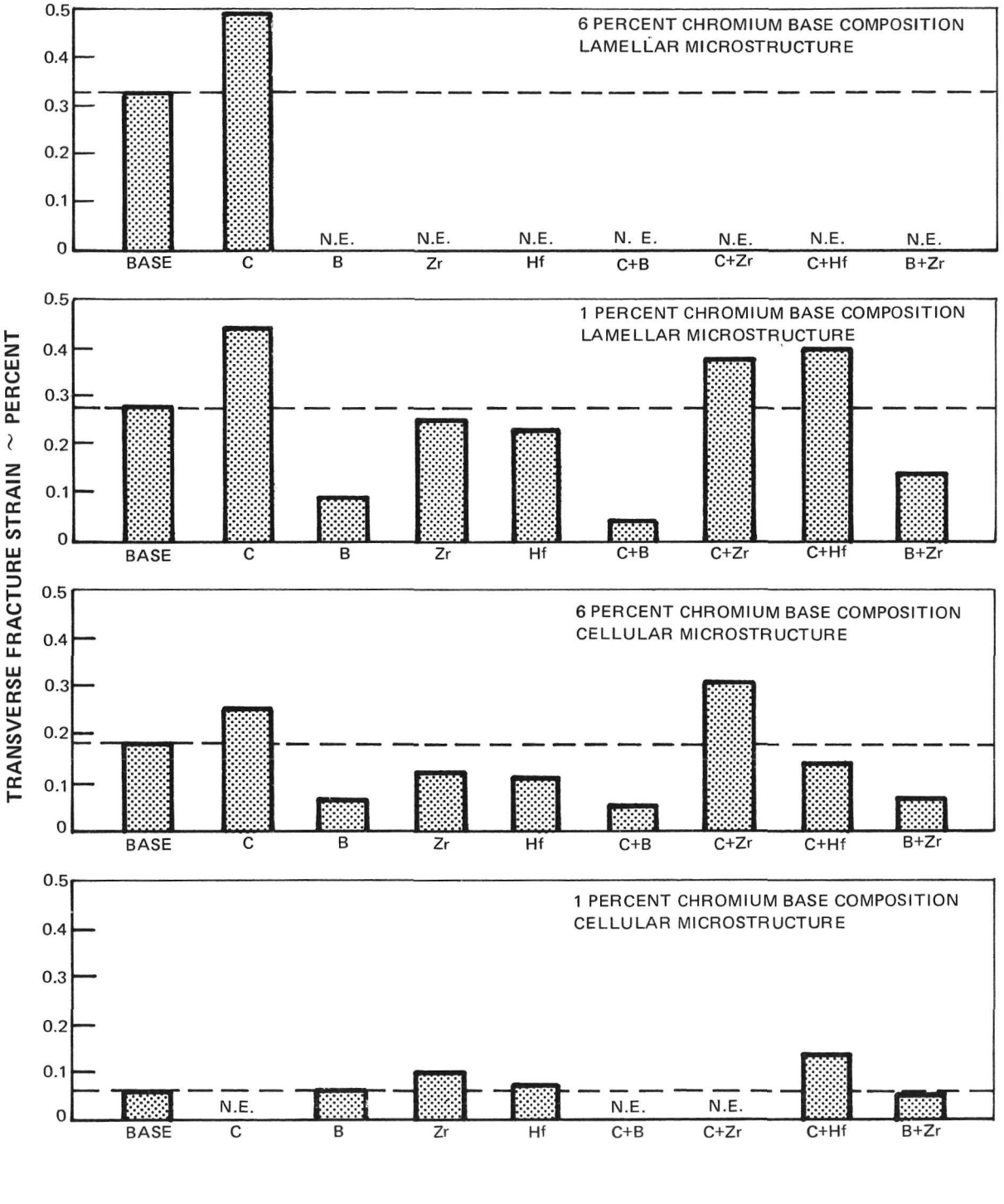



Figure 112 Schematic Illustration of Casting Used for Evaluation of Modified Directionally Solidified Eutectic Alloys




R14-133

Figure 113 Influence of Minor Element Modifications on the 760°C (1400°F) Transverse Tensile Ductility of the $\gamma/\gamma'$-$\delta$ Directionally Solidified Eutectic Alloy (N.E. - Not Evaluated)

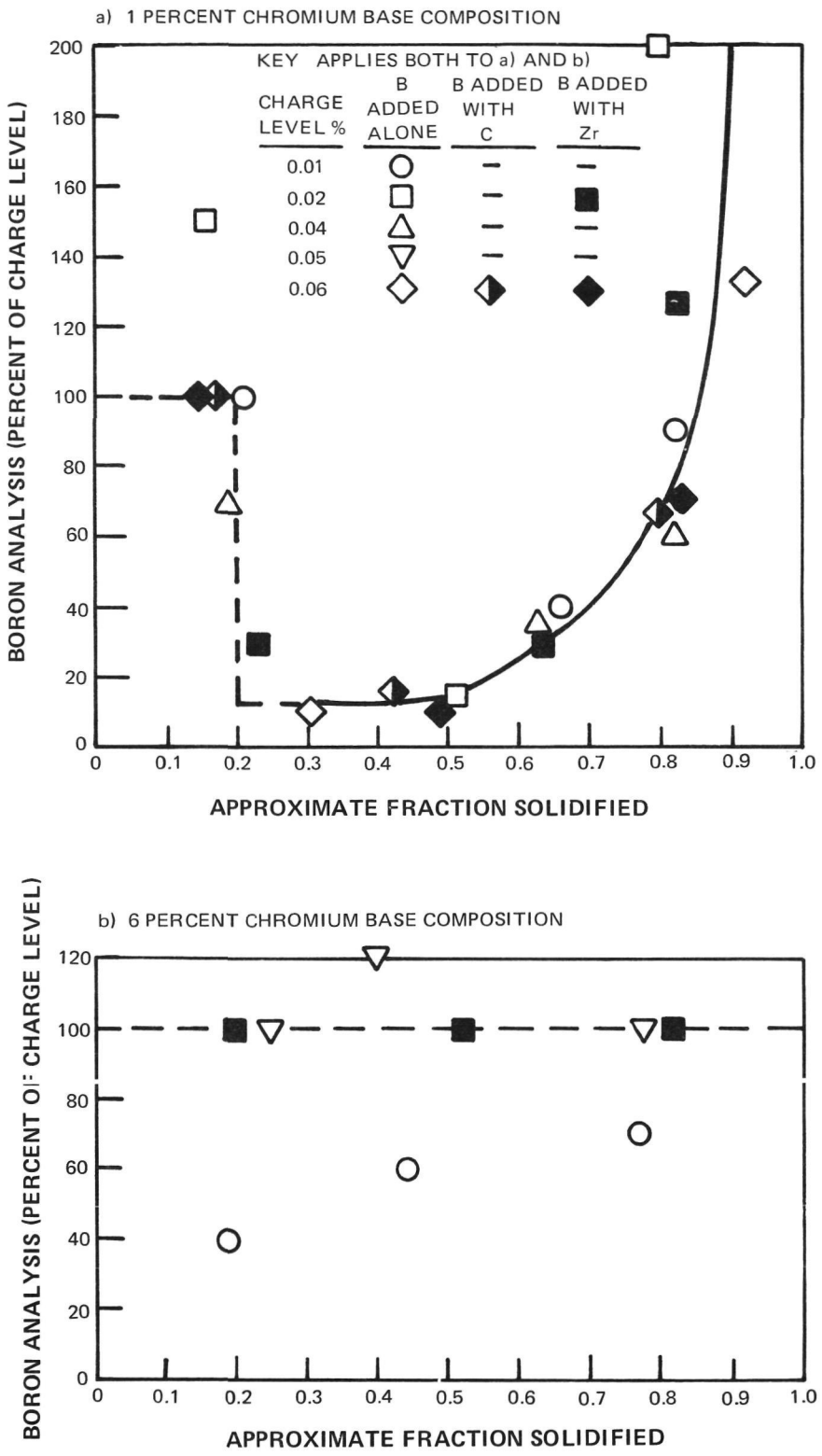
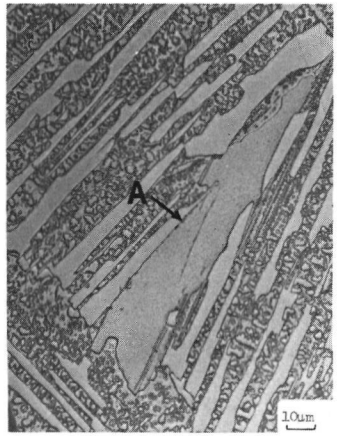
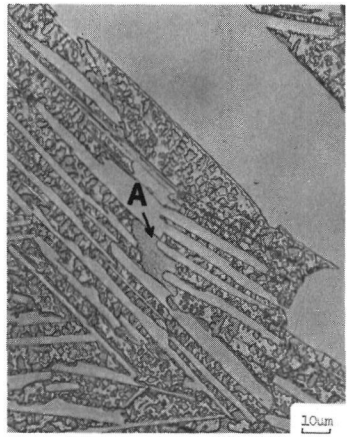


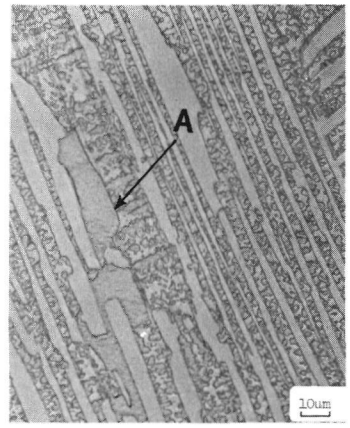

Figure 114 Results of Chemical Analyses Obtained in Boron Modified Slab Castings



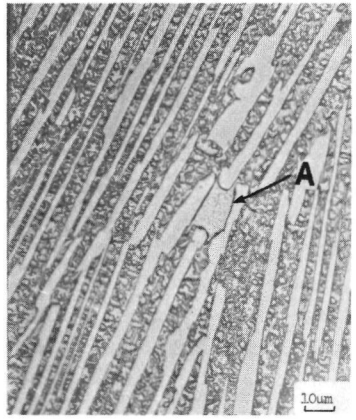

B414, MA 1684-18
A) FOUND THROUGHOUT CASTING E-312 (1.0% Hf ADDITION).



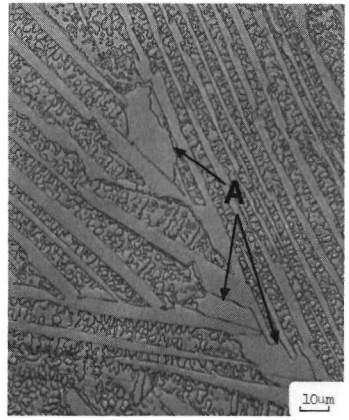

B433 MA 1684-16
B) FOUND NEAR THE BOTTOM AREA OF CASTING E328 (0.6% Hf + 0.05% C ADDITION).




B430, MA 1728-10
C) FOUND IN THE TOP AND CENTER AREAS OF CASTING E323 (0.04% B ADDITION).




B431, MA 1728-13
D) FOUND NEAR THE TOP OF CASTING E324 (0.01% B ADDED).




B432, MA 1728-12
E) FOUND NEAR THE TOP OF CASTING E325 (0.06% Zr + 0.02% B ADDED).

Figure 115 Typical Appearance of Free $\gamma'$ Phase Found in Transverse Sections of Various Modified Ni-21.2% Cb-2.5%Al-1%Cr Castings

R14-135

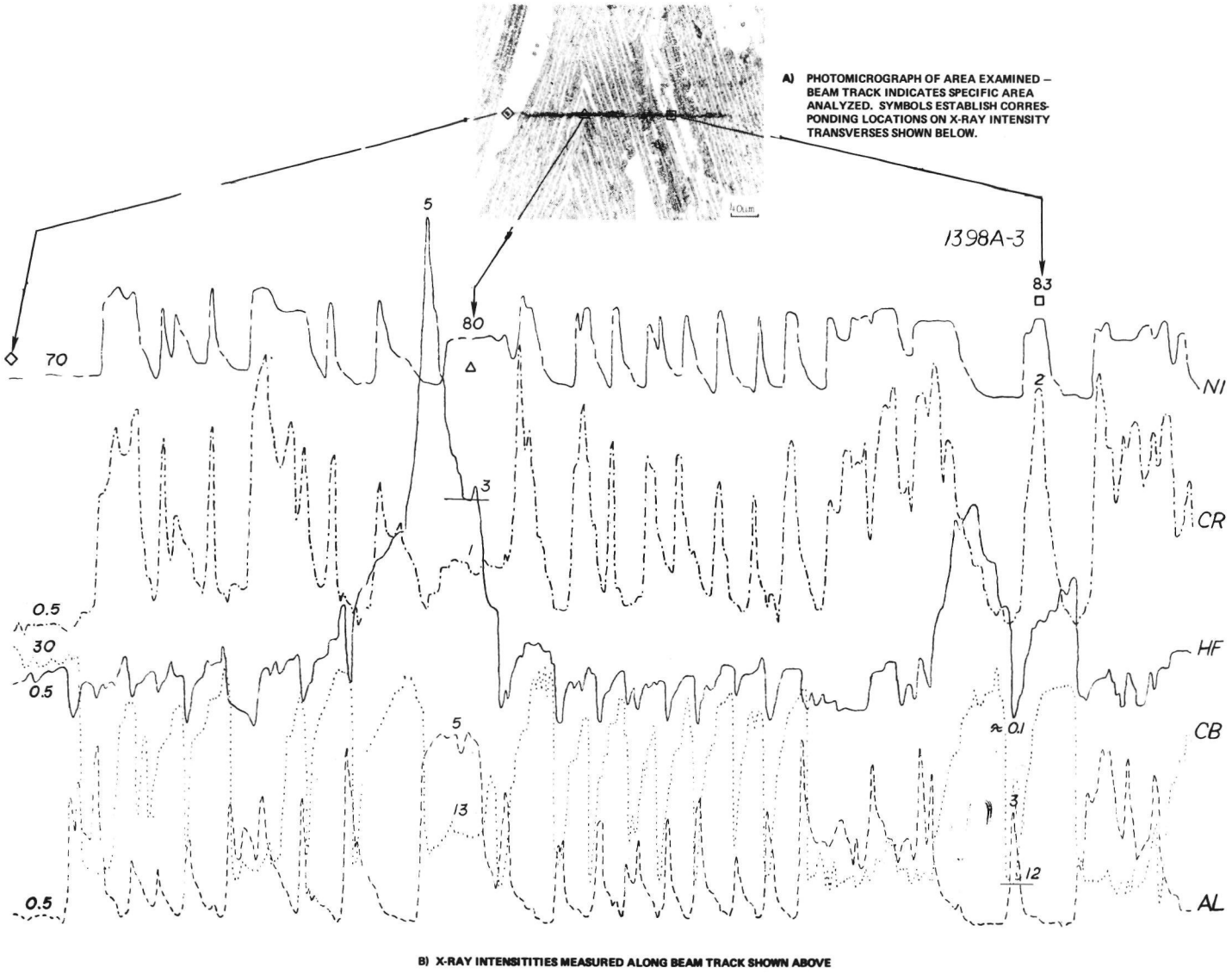
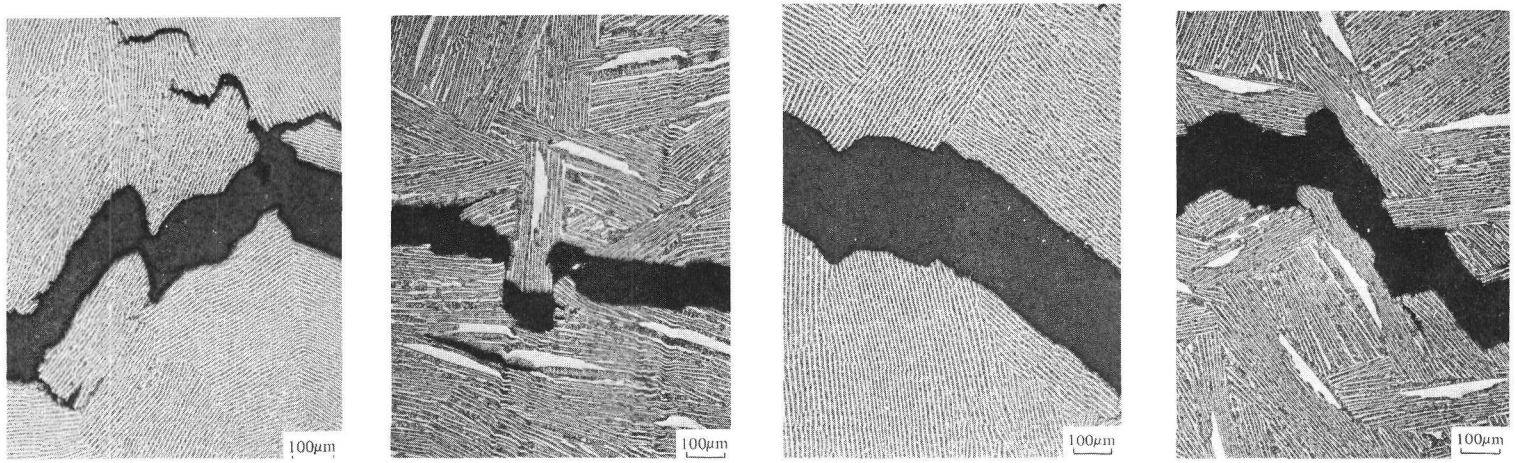



Figure 116 Results of Electron Probe Microanalysis of Casting E312 (Ni-21.2%Cb-2.5%Al-1%Cr-1%Hf Charge Composition)




A) SPECIMEN E382F (0.06% B CHARGED)
ESTIMATED BORON LEVEL 0.006%
FRACTURE STRAIN 0.09%
(B610, MB 483-20)

B) SPECIMEN E323-C4 (0.04% B CHARGED)
ESTIMATED BORON LEVEL 0.014%
FRACTURE STRAIN 0.06%
(B454)

C) SPECIMEN E396F (0.2% Zr + 0.06% B CHARGED)
ESTIMATED BORON LEVEL 0.006%
FRACTURE STRAIN 0.12%
(B621, MB 483-18)

D) SPECIMEN E325J (0.06% Zr + 0.02% B CHARGED)
ESTIMATED BORON LEVEL 0.006%
FRACTURE STRAIN 0.03%
(B459)

R14-137

Figure 117 Fracture Profile Found in Various Boron and Boron Plus Zirconium Modified One Percent Base Composition Transverse Test Specimens Broken in Tension at 760°C (1400°F). Transverse Plane of Polish, Tensile Axis Vertical

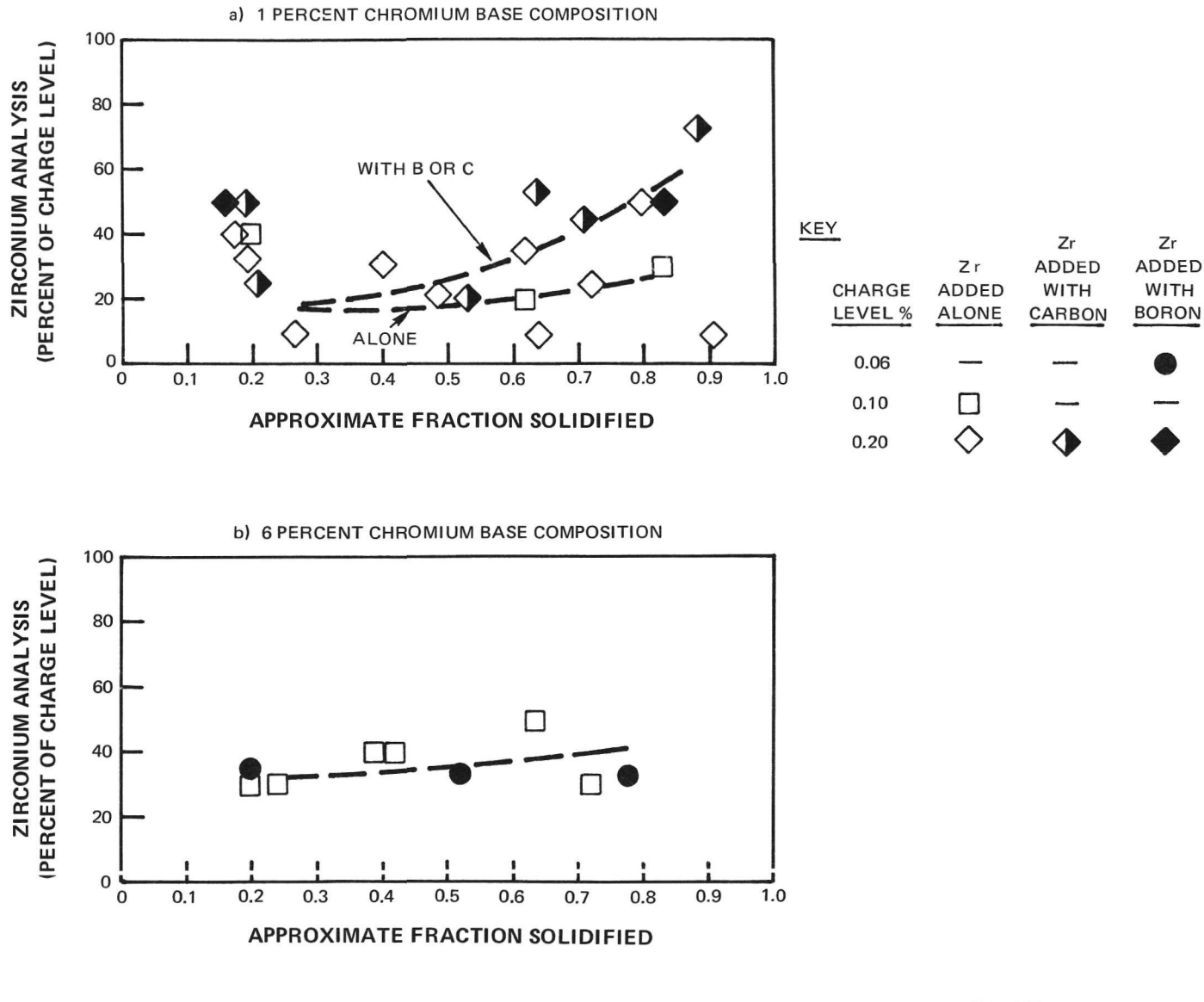



Figure 118 Results of Chemical Analyses Obtained on Zirconium Modified Slab-Castings

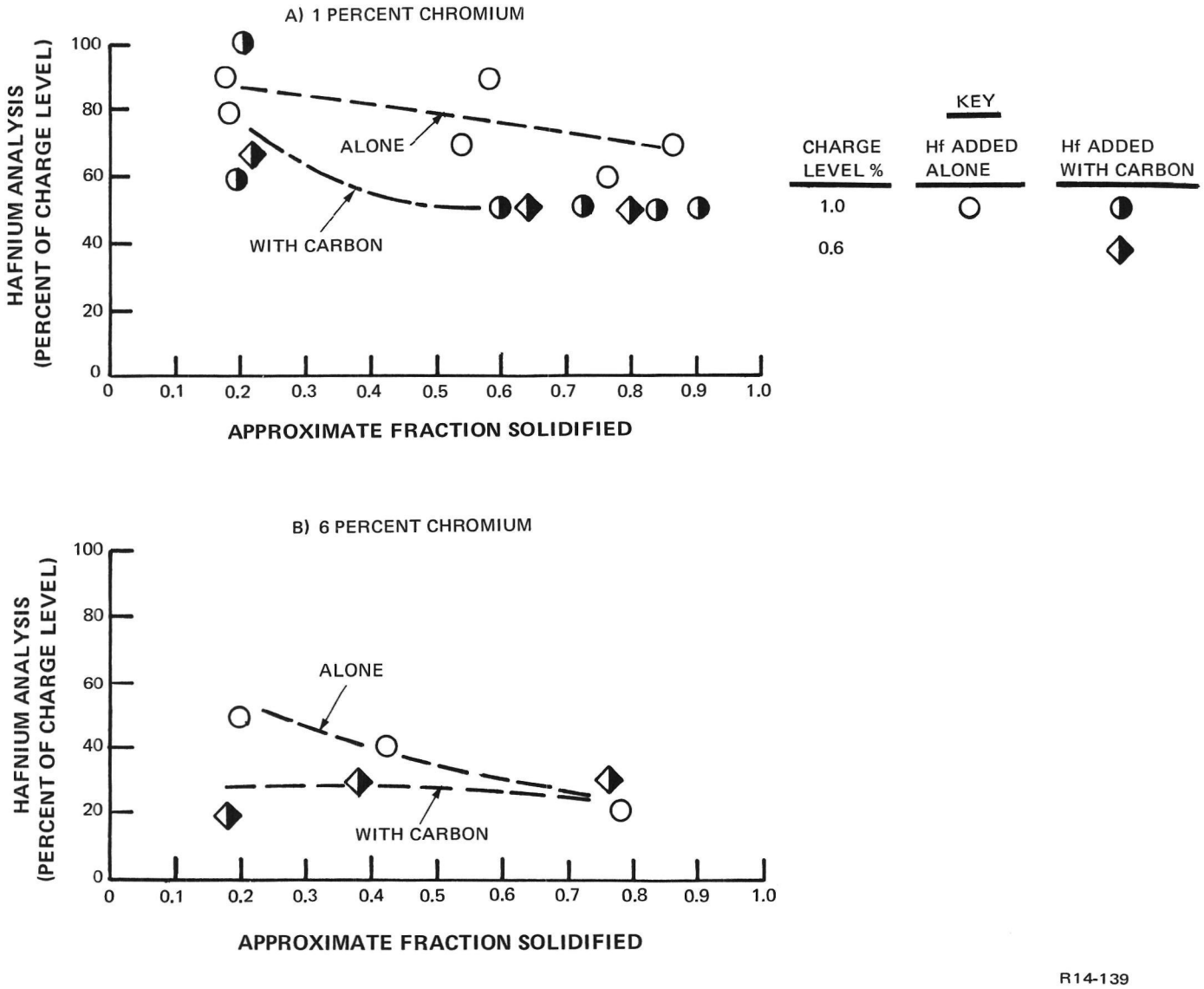
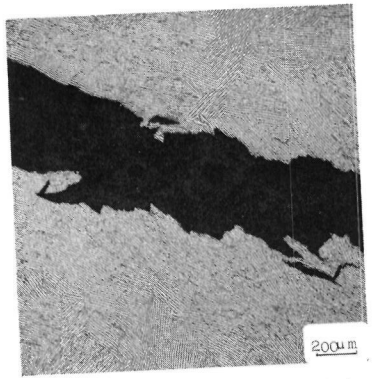
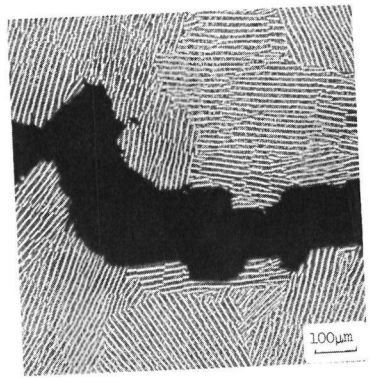


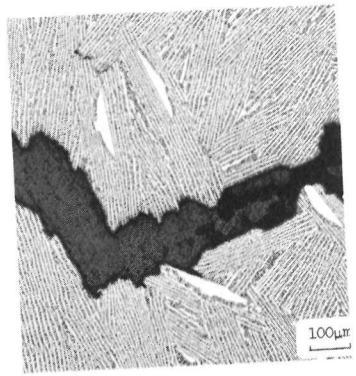

Figure 119 Results of Chemical Analyses Obtained on Hafnium Modified Slab Castings



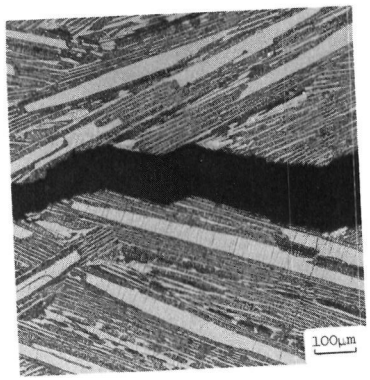

A) SPECIMEN E437-T2 (0.2% Zr CHARGE)
ESTIMATE ZIRCONIUM LEVEL 0.02%
FRACTURE STRAIN 0.21%
(B821)



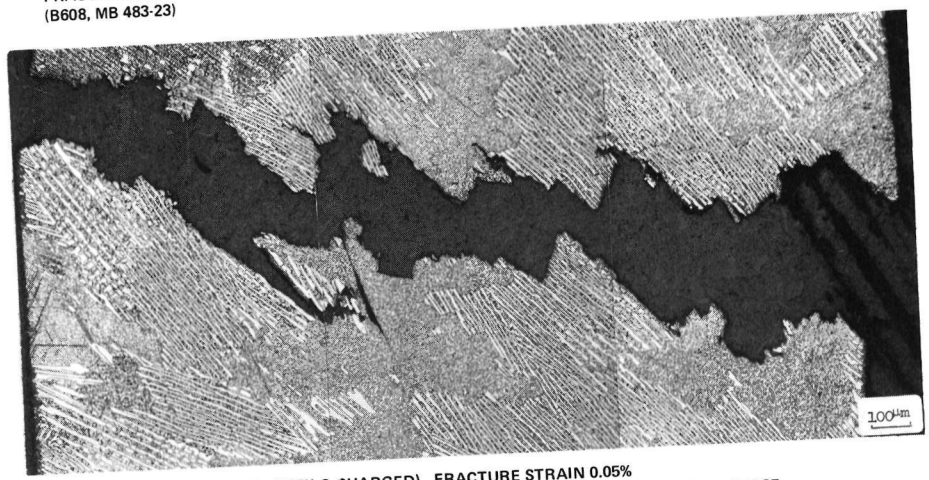

B) SPECIMEN E359-E2 (1% Hf CHARGE)
ESTIMATED HAFNIUM LEVEL 0.8%
FRACTURE STRAIN 0.20%
(B608, MB 483-23)




C) SPECIMEN E383G (0.2% Zr CHARGE)
ESTIMATED Zr LEVEL 0.07%
FRACTURE STRAIN 0.30%
(B612, MB 483-5)




D) SPECIMEN E312-K (1% Hf CHARGE)
ESTIMATED Hf LEVEL 0.7%
FRACTURE STRAIN 0.06%
(B452, MB 26-8)




E) SPECIMEN E392-H (1% Hf + 0.15% C CHARGED) FRACTURE STRAIN 0.05%
NOTE TENDENCY FOR SEPARATION BETWEEN EUTECTIC GRAINS AND DENDRITIC γ PHASE
(B616)

R14-140

Figure 120 Fracture Profiles Found in Various Zirconium and Hafnium Modified One Percent Chromium Base Composition Transverse Test Specimen Broken in Tension at 760°C (1400°F). Transverse Plane of Polish, Tensile Axis Vertical

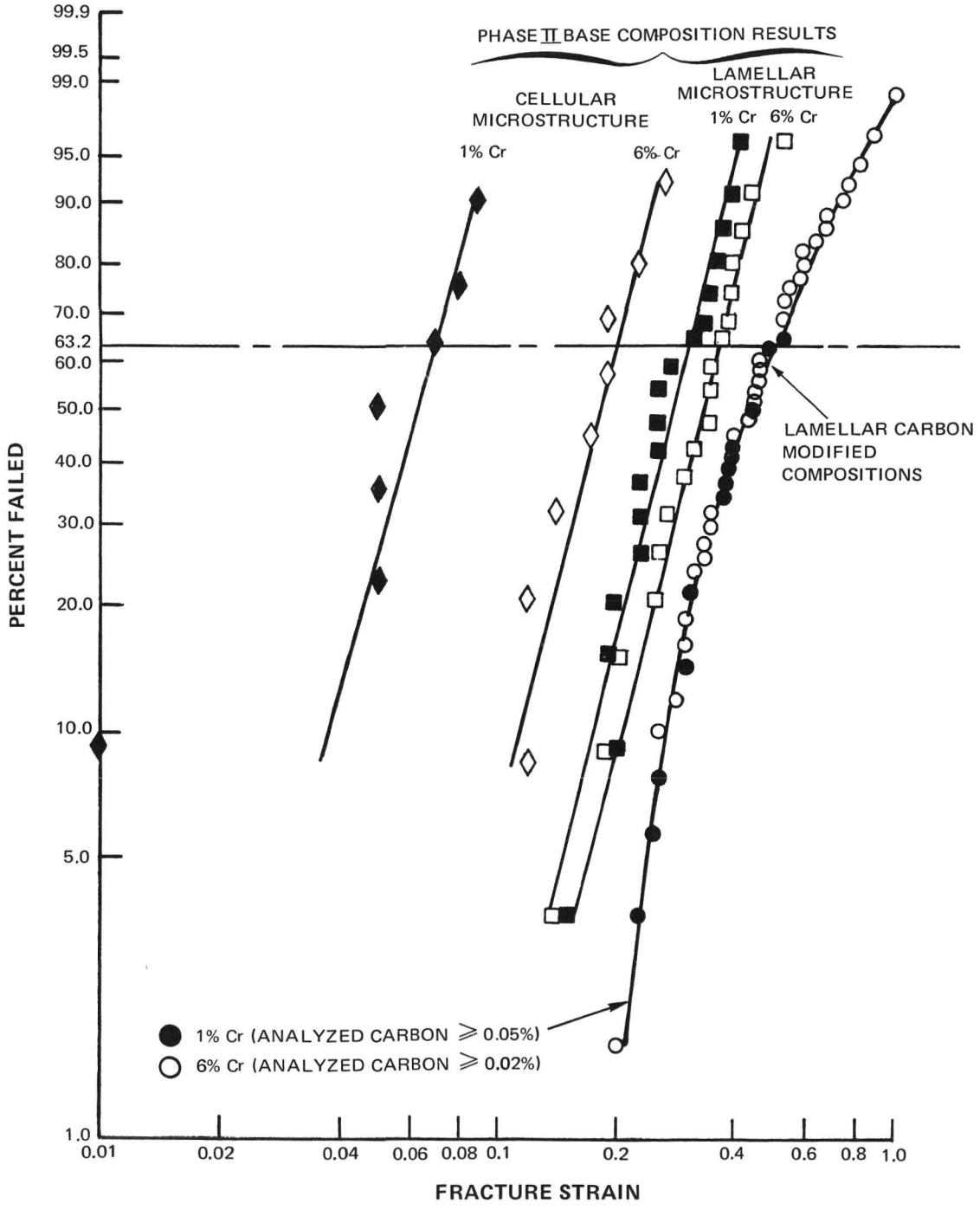



Figure 121 Influence of Carbon on the 760°C (1400°F) Transverse Fracture Strain of $\gamma/\gamma'$-$\delta$ Directionally Solidified Eutectic Alloys Containing One and Six Percent Chromium

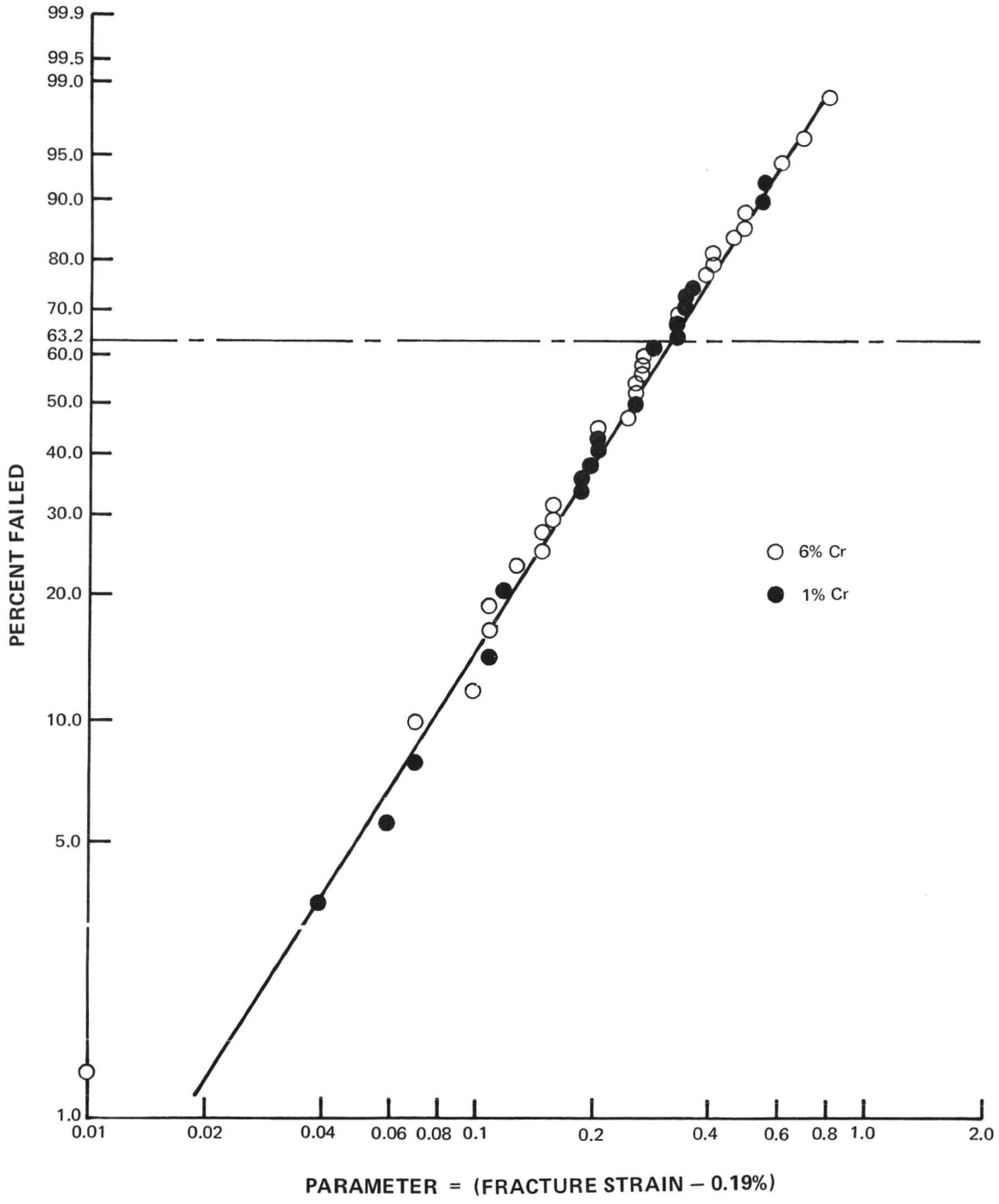



Figure 122 Parametric Adjustment of Carbon Modified Minimum Fracture Strain Results From Figure 121 to Compensate for Finite Minimum Fracture Strain

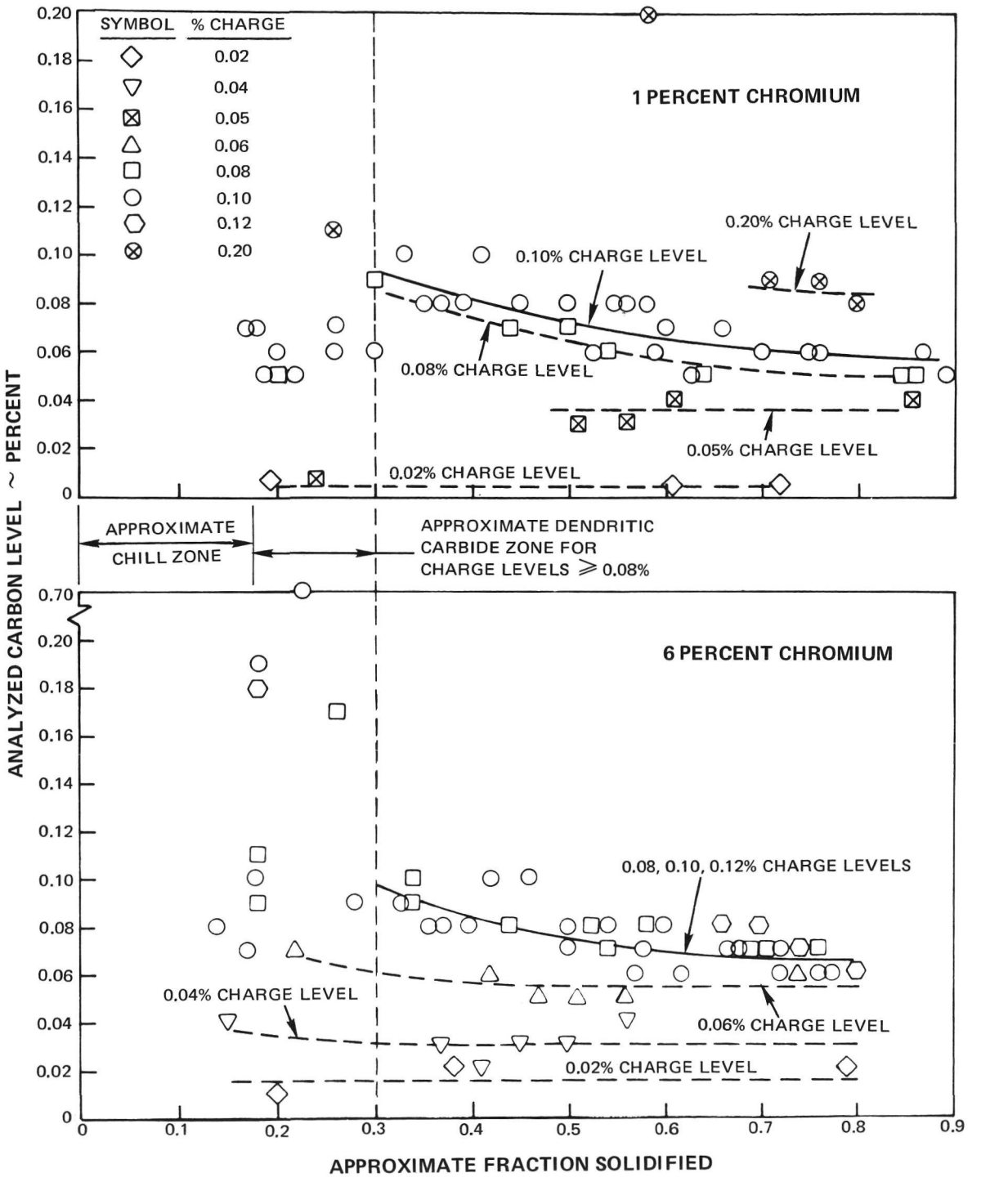
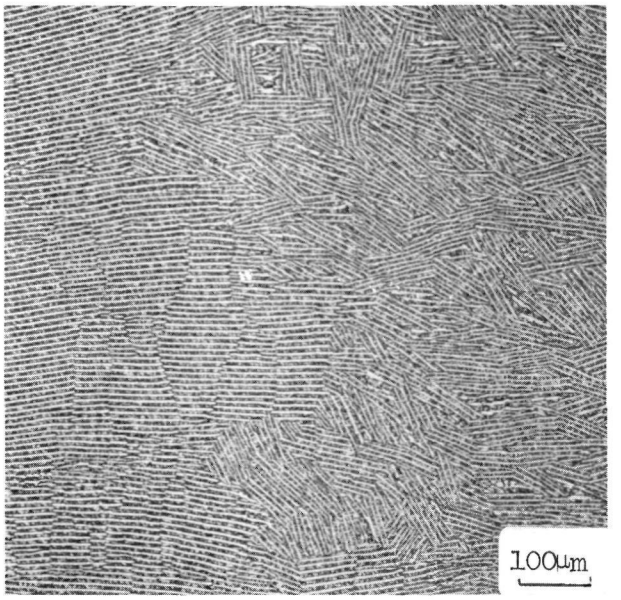
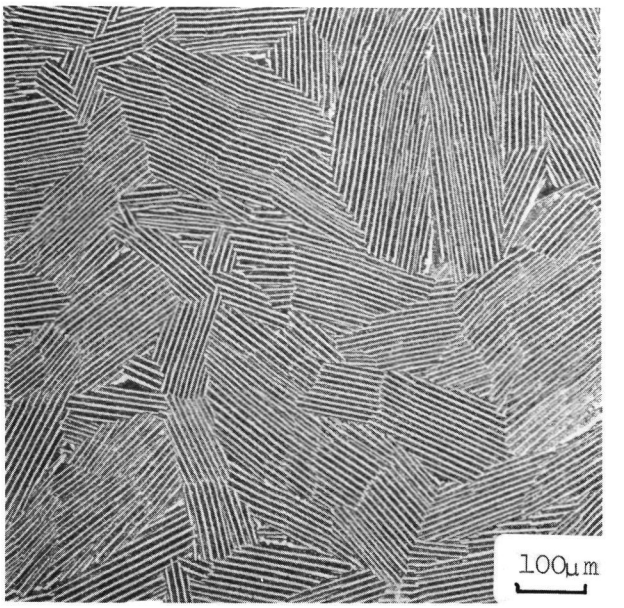


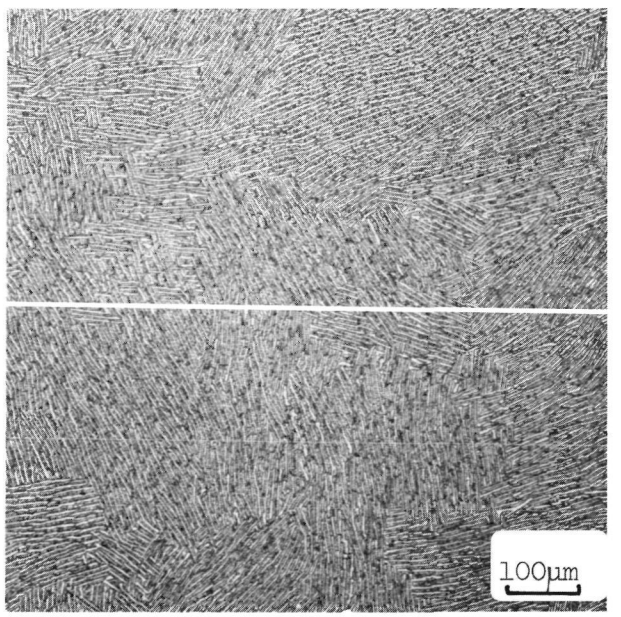

Figure 123 Results of Chemical Analyses Obtained on Carbon Modified Slab Castings



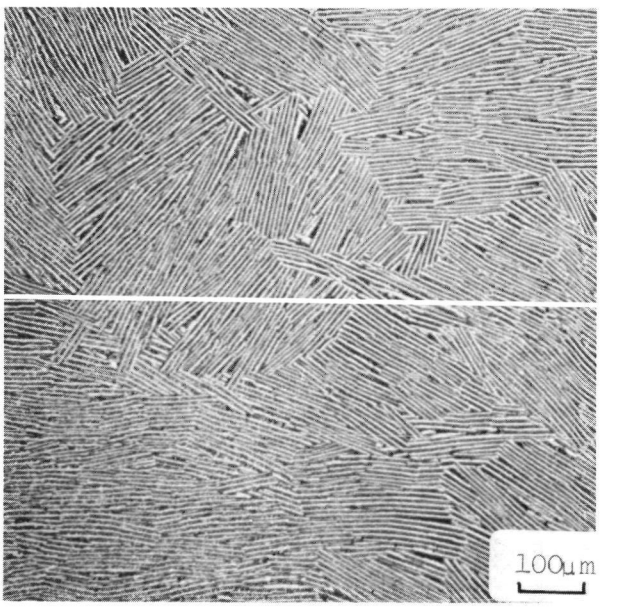

A) 1% Cr BASE COMPOSITION SOLIDIFIED AT 1.3 cm (½ INCH) PER HOUR (B456, MB 660-20)




B) 6% Cr BASE COMPOSITION SOLIDIFIED AT 0.6 Cr (¼ INCH) PER HOUR




C) CARBON MODIFIED 1% Cr COMPOSITION SOLIDIFIED AT 1.3 cm (½ INCH) PER HOUR




D) CARBON MODIFIED 6% Cr COMPOSITION SOLIDIFIED AT 0.6 cm (¼ INCH) PER HOUR

R14-144

Figure 124 Influence of Carbon on the Lamellar Microstructure of the $\gamma/\gamma' - \delta$ Directionally Solidified Eutectic Alloy

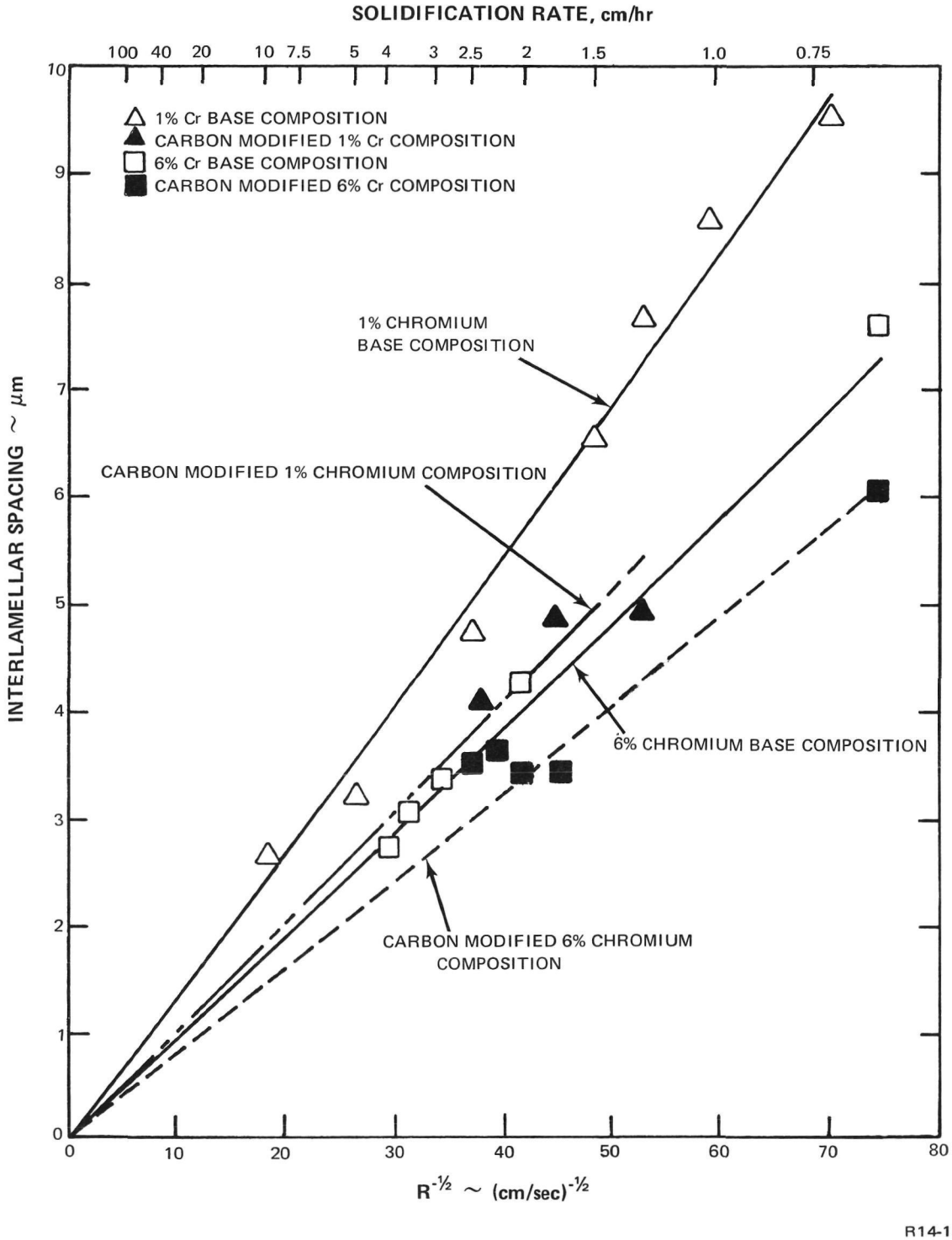
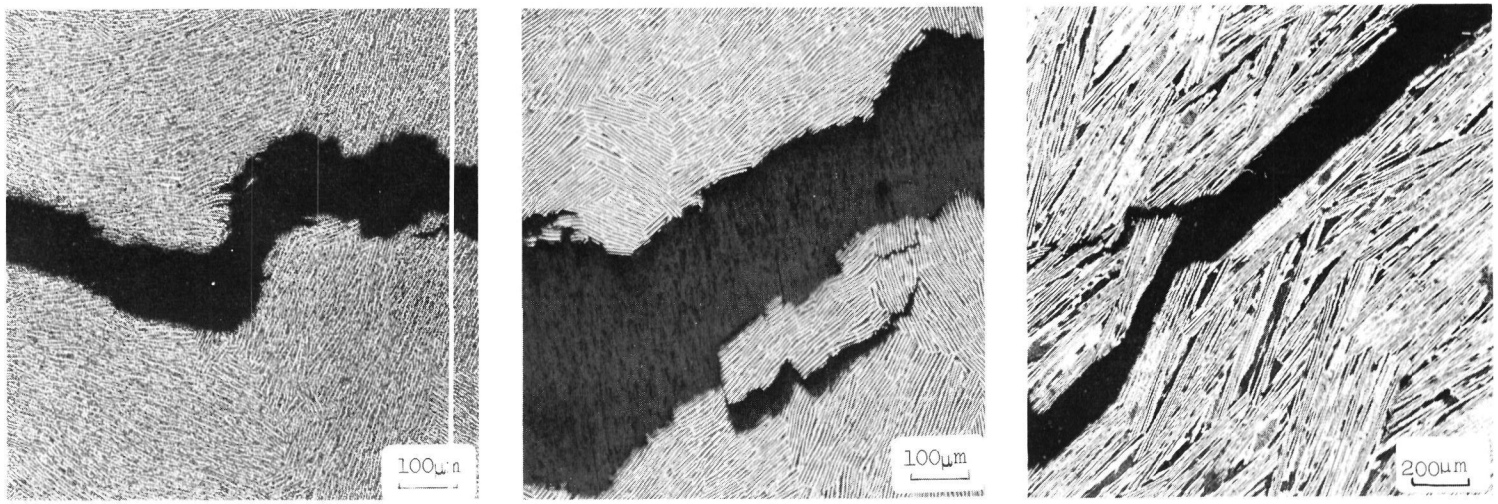



Figure 125 Comparison of Lamellar Spacings Measured on Base Composition and Carbon Modified One and Six Percent Chromium Alloys



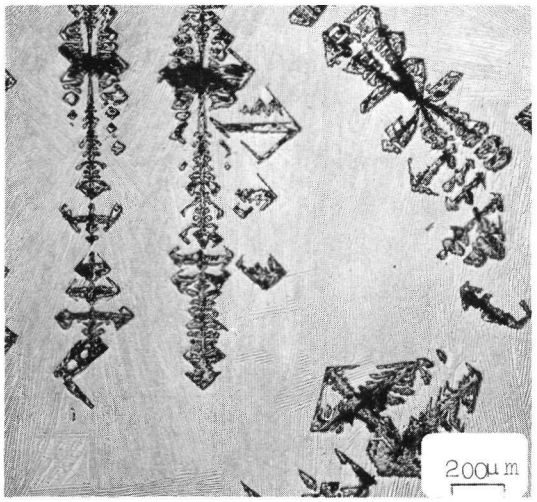

A) SPECIMEN E313J1 (0.1% C CHARGE)
1% Cr BASE COMPOSITION
ESTIMATED CARBON LEVEL (0.07%)
FRACTURE STRAIN 0.48%
(B453, MB 26-6)

B) SPECIMEN E416-I (0.1% C CHARGE)
6% Cr BASE COMPOSITION
ANALYZED CARBON LEVEL 0.07%
FRACTURE STRAIN 0.23%
(B708, MB 1280-12)

C) SPECIMEN E319B (0.1% C CHARGE)
6% Cr BASE COMPOSITION
ESTIMATED CARBON LEVEL 0.08%
FRACTURE STRAIN 0.07%
(B505)

R14-146

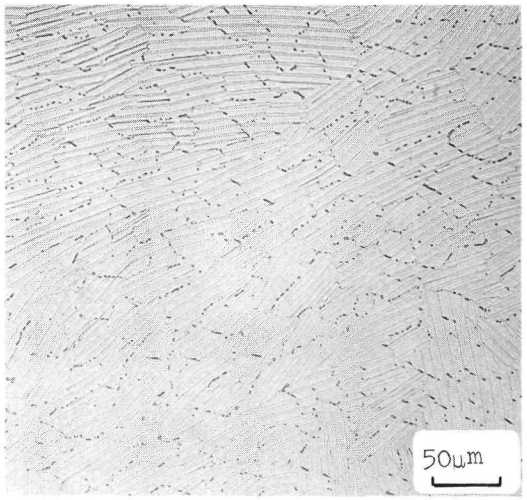
Figure 126 Fracture Profile Found in Carbon Modified $\gamma/\gamma'$-$\delta$ Directionally Solidified Eutectic Transverse Test Specimens Broken in Tension at 760°C (1400°F). Transverse Plane of Polish, Tensile Axis Vertical

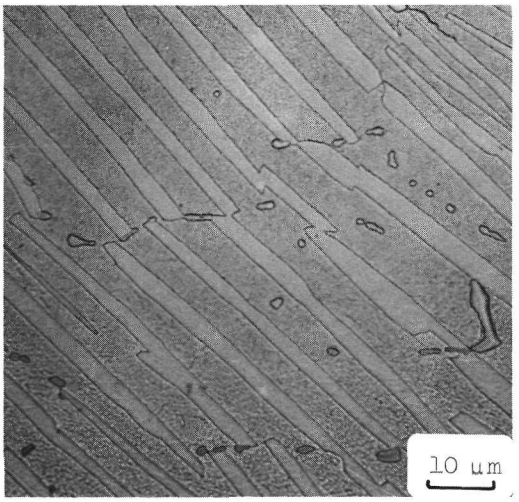



A) DENDRITIC CARBIDES (ASSUMED TO BE MC TYPE) FOUND JUST ABOVE CHILL ZONE AT CHARGE CARBON LEVELS OF 0.08% AND ABOVE (CASTING E416, 6% Cr,0.1% C CHARGE)




B) FINE CARBIDES (ASSUMED TO BE MC TYPE) FOUND CONCENTRATED IN AREAS OF CELLULAR CASTINGS. (CASTING E 426, 1% Cr, 0.15% C CHARGE)

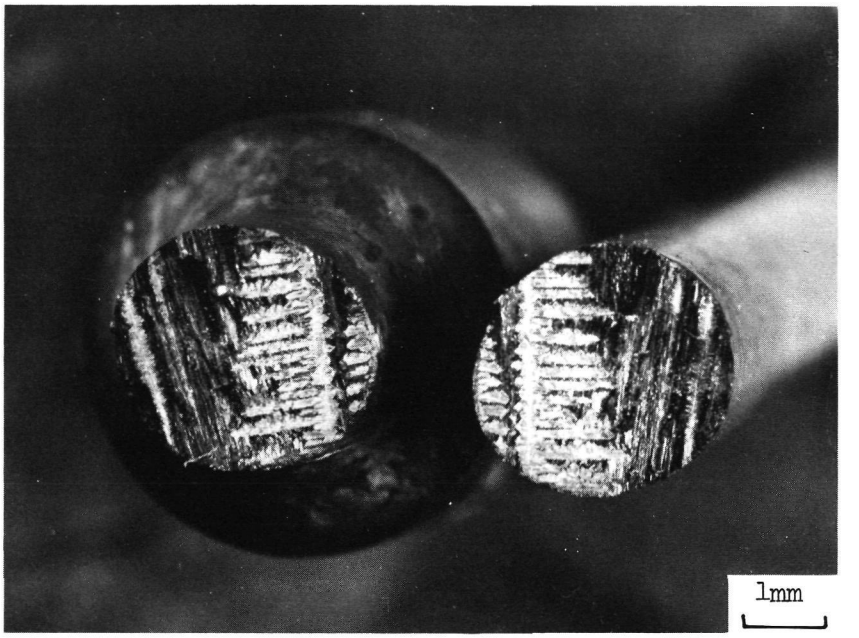



C) CB RICH FINE MC CARBIDES FOUND DISTRIBUTED THROUGHOUT LAMELLAR CARBON MODIFIED CASTINGS (CASTING E 416, 6% Cr, 0.1% C CHARGE) (B705)

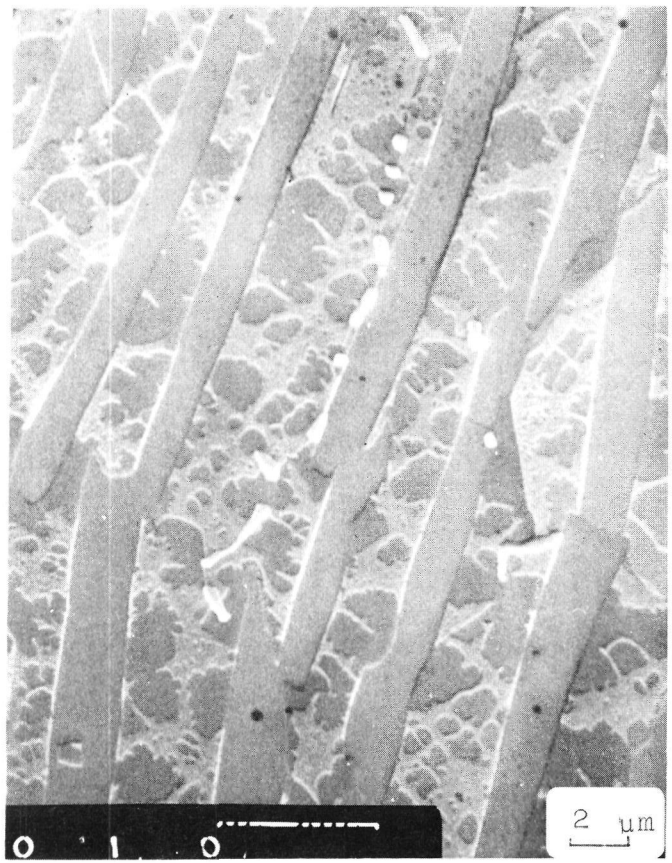
R14-147

Figure 127 Carbide Morphologies Found in Carbon Modified $\gamma/\gamma'$-$\delta$ Directionally Solidified Eutectic Castings

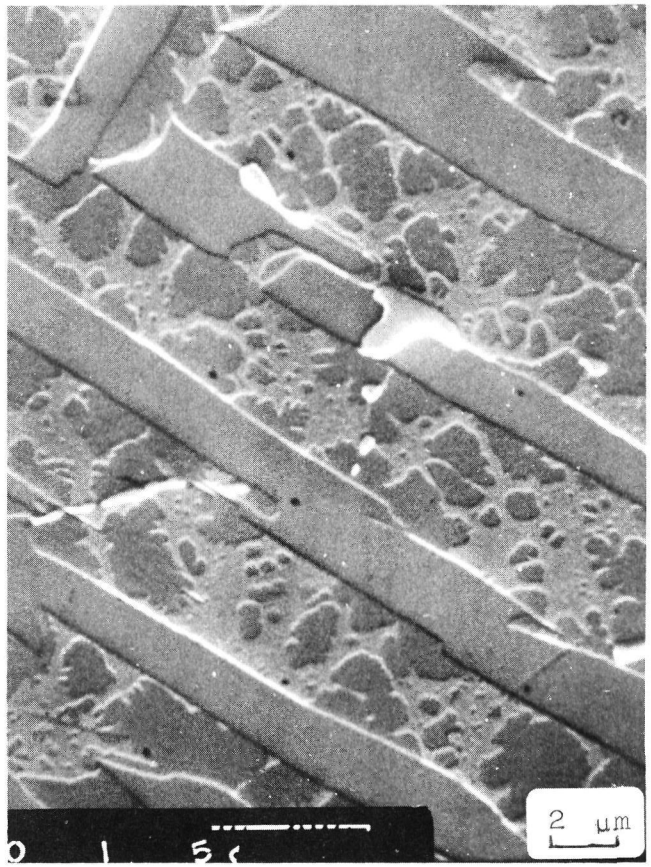



R14-148

Figure 128 Fracture Surface of Cellular Carbon Modified Six Percent Chromium Specimen E319-E Showing Failure at Large Carbide Dendrite




A) PREFERENTIAL DISTRIBUTION OF Cb RICH MC CARBIDES IN $\gamma/\gamma'$ MATRIX AND AT THE LAMELLAR INTERFACE.




B) ILLUSTRATING THE OCCASIONAL OCCURRENCE OF CARBIDE IN THE ($Ni_3Cb$) PHASE

Figure 129 Scanning Electron Micrographs of a Polished and Etched Transverse Section of the One Percent Chromium -0.1% Carbon Modified $\gamma/\gamma'$-$\delta$ Casting E385 Solidified at 1.3cm (0.5 inch)/hour

R14-149

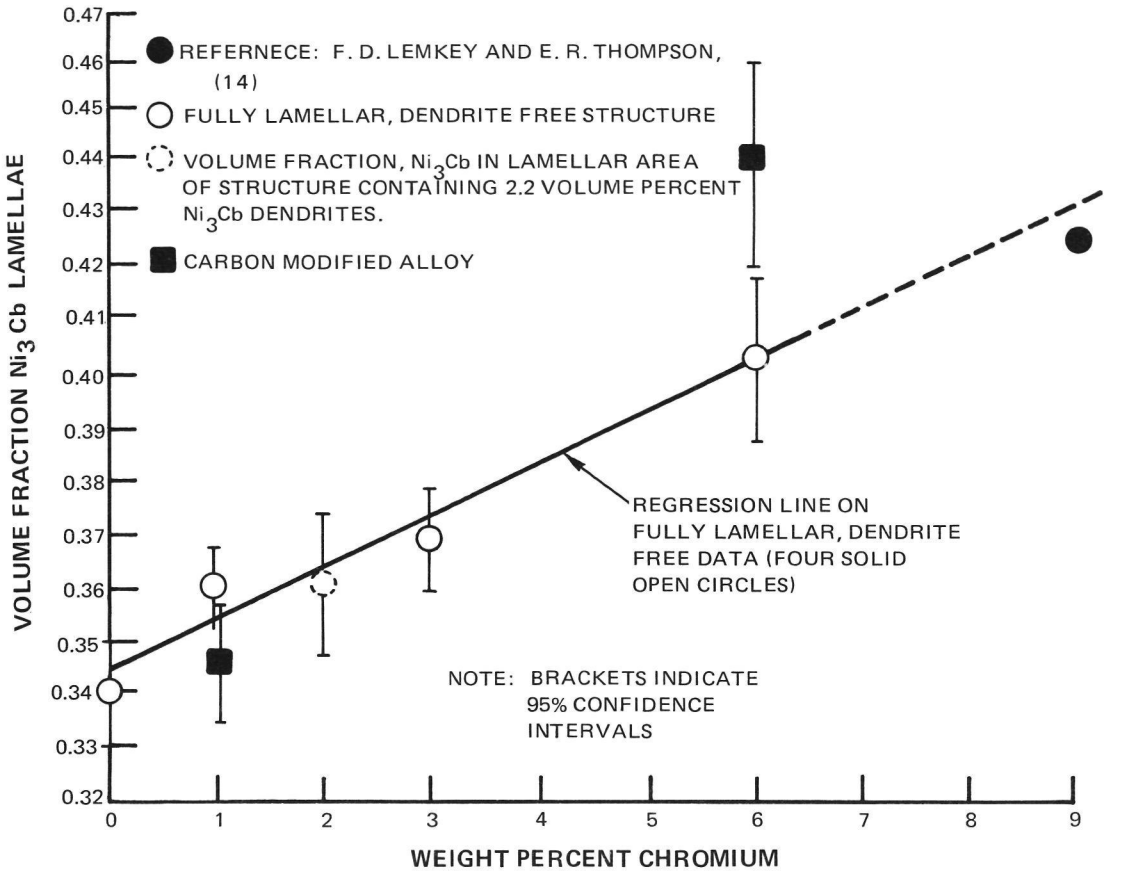



Figure 130 Influence of Carbon Modification on Volume Fraction of $Ni_3Cb$ Phase in Various Directionally Solidified $\gamma/\gamma'$- $\delta$ Eutectic Alloys

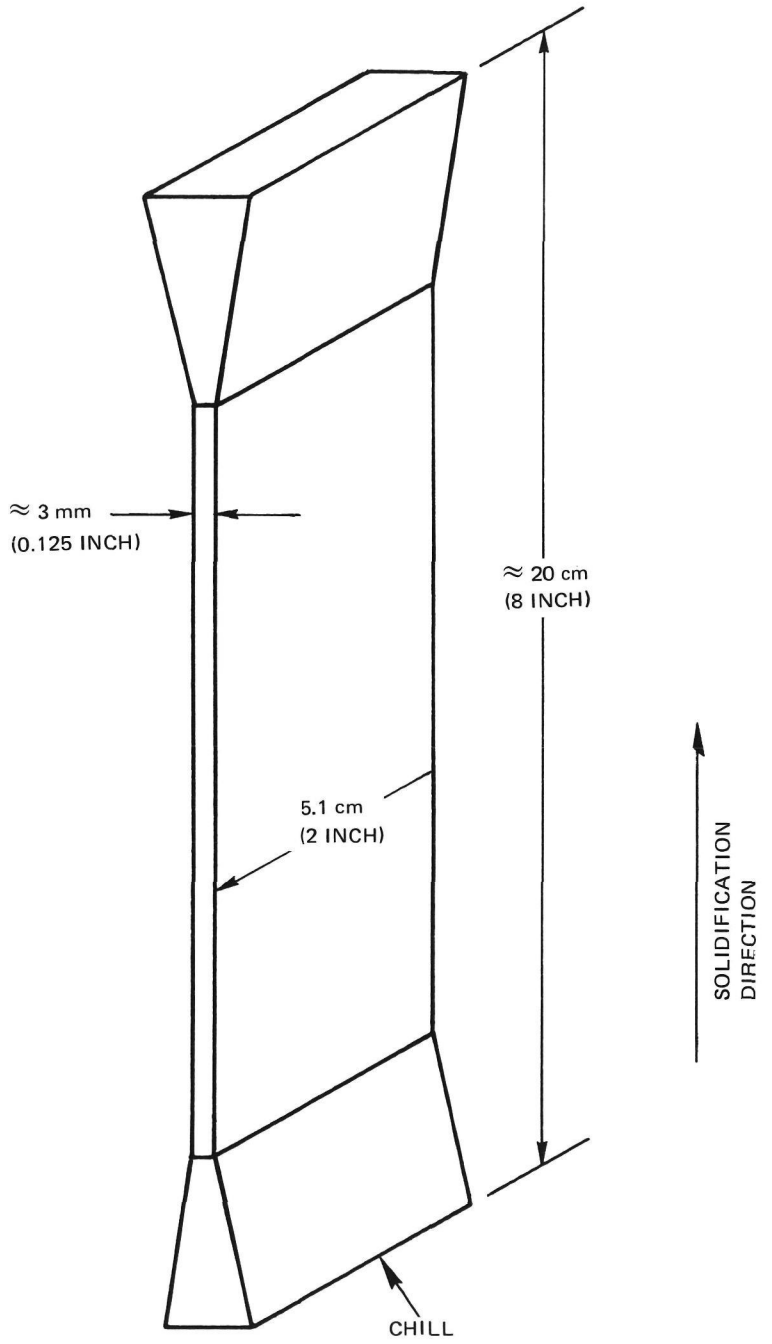



Figure 131 Schematic Diagram of Thin Slab Casting Used to Evaluate Longitudinal Creep Properties

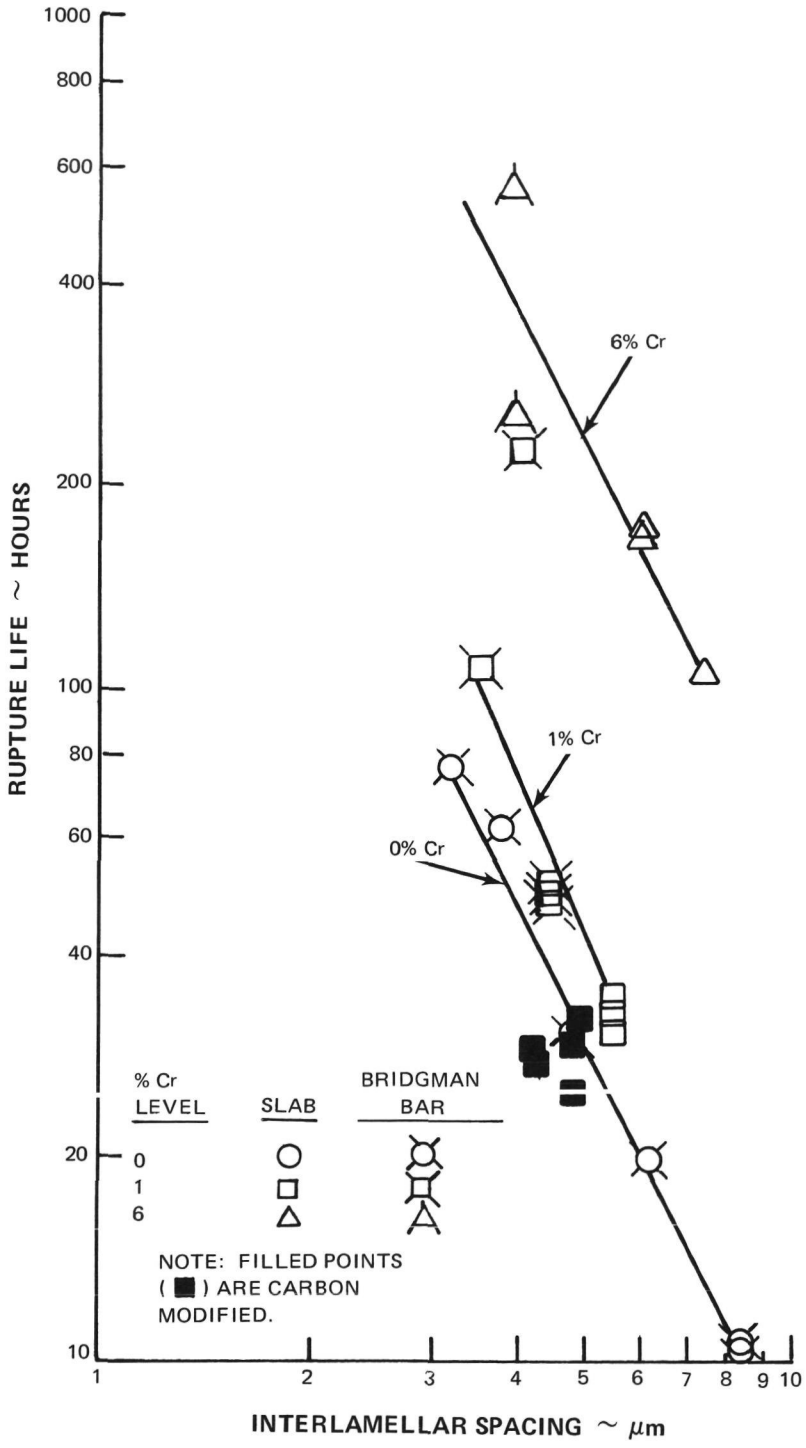
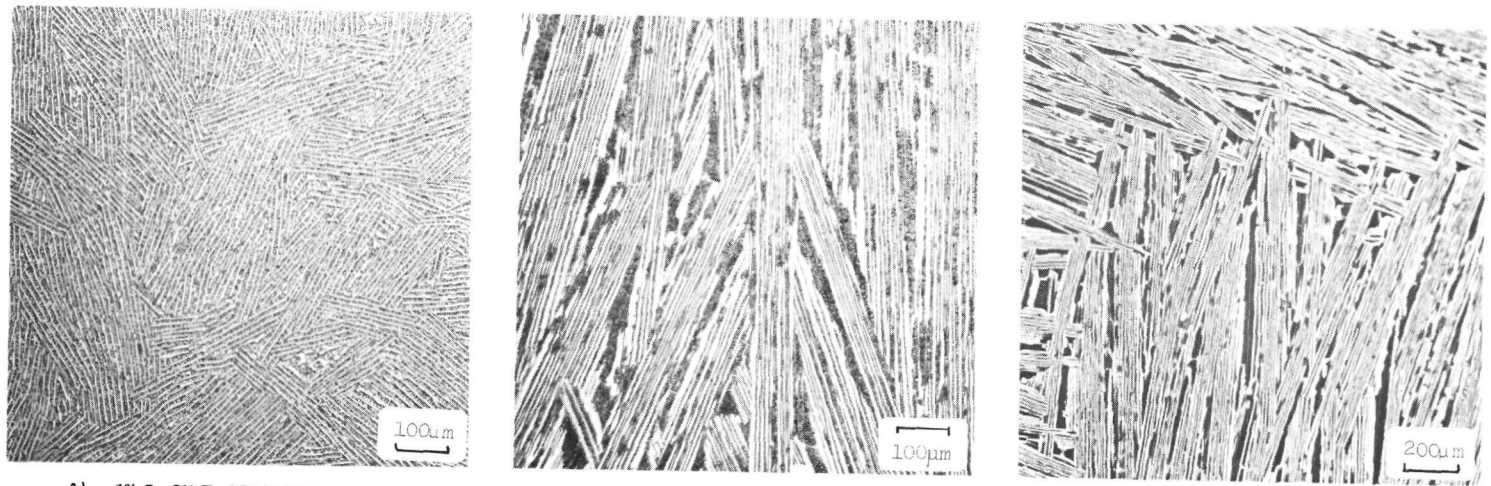



Figure 132 Influence of Interlamellar Spacing on Rupture Life of Various $\gamma/\gamma'$ - $\delta$ Alloys Creep Tested at 1038°C/152 MPa (1900°F/22 ksi)




A) 1% Cr, 3% Ta SOLIDIFIED AT 0.6 cm (¼ INCH) PER HOUR CASTING E 450

B) 1% Cr, 3% Ta SOLIDIFIED AT 0.95 cm (3/8 INCH) PER HOUR CASTING E 417

C) 6% Cr, 3% Ta SOLIDIFIED AT 0.6 cm (¼ INCH) PER HOUR CASTING E-419

Figure 133 Influence of Tantalum on the Microstructure of $\gamma/\gamma'$-$\delta$ Directionally Solidified Eutectic Alloys

R14-153

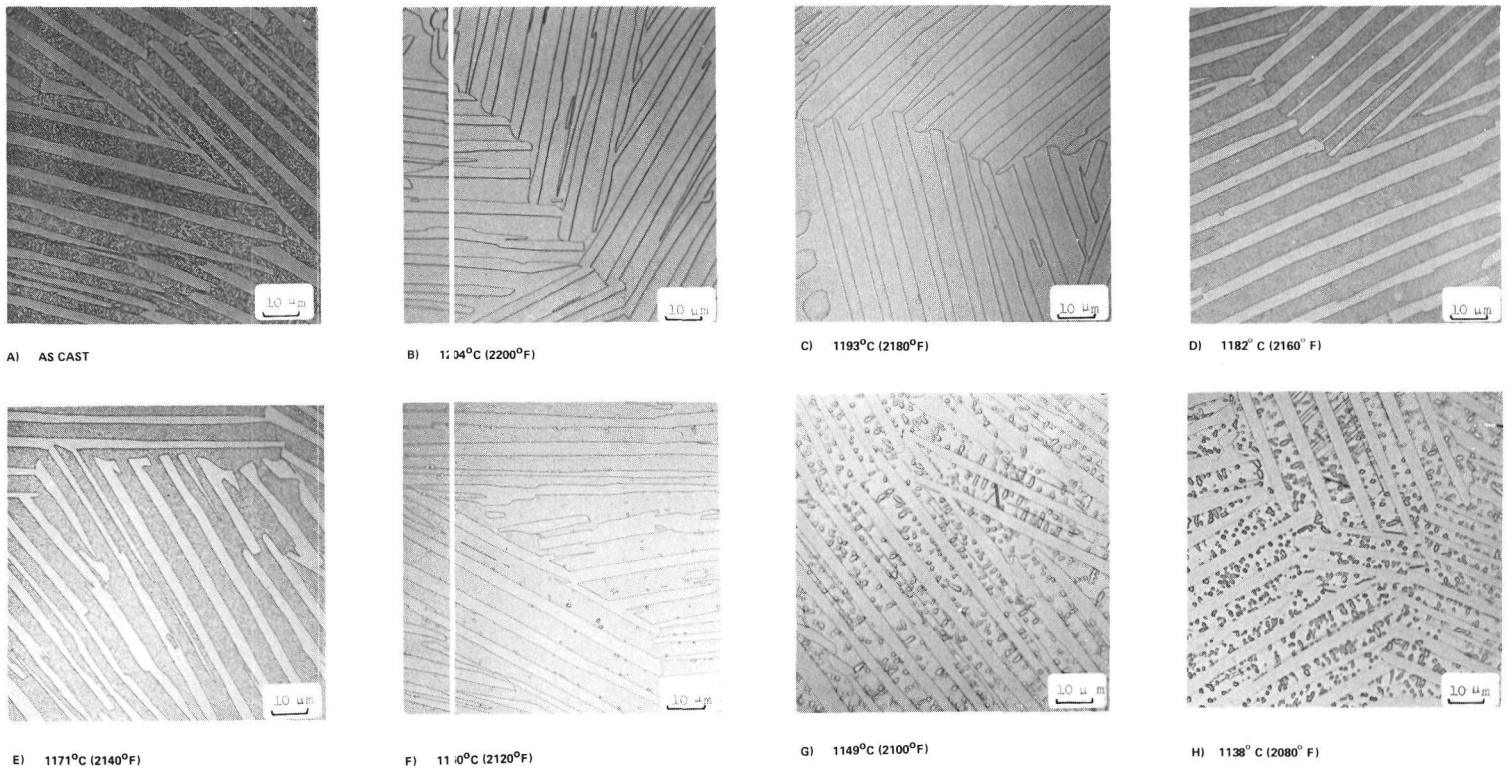
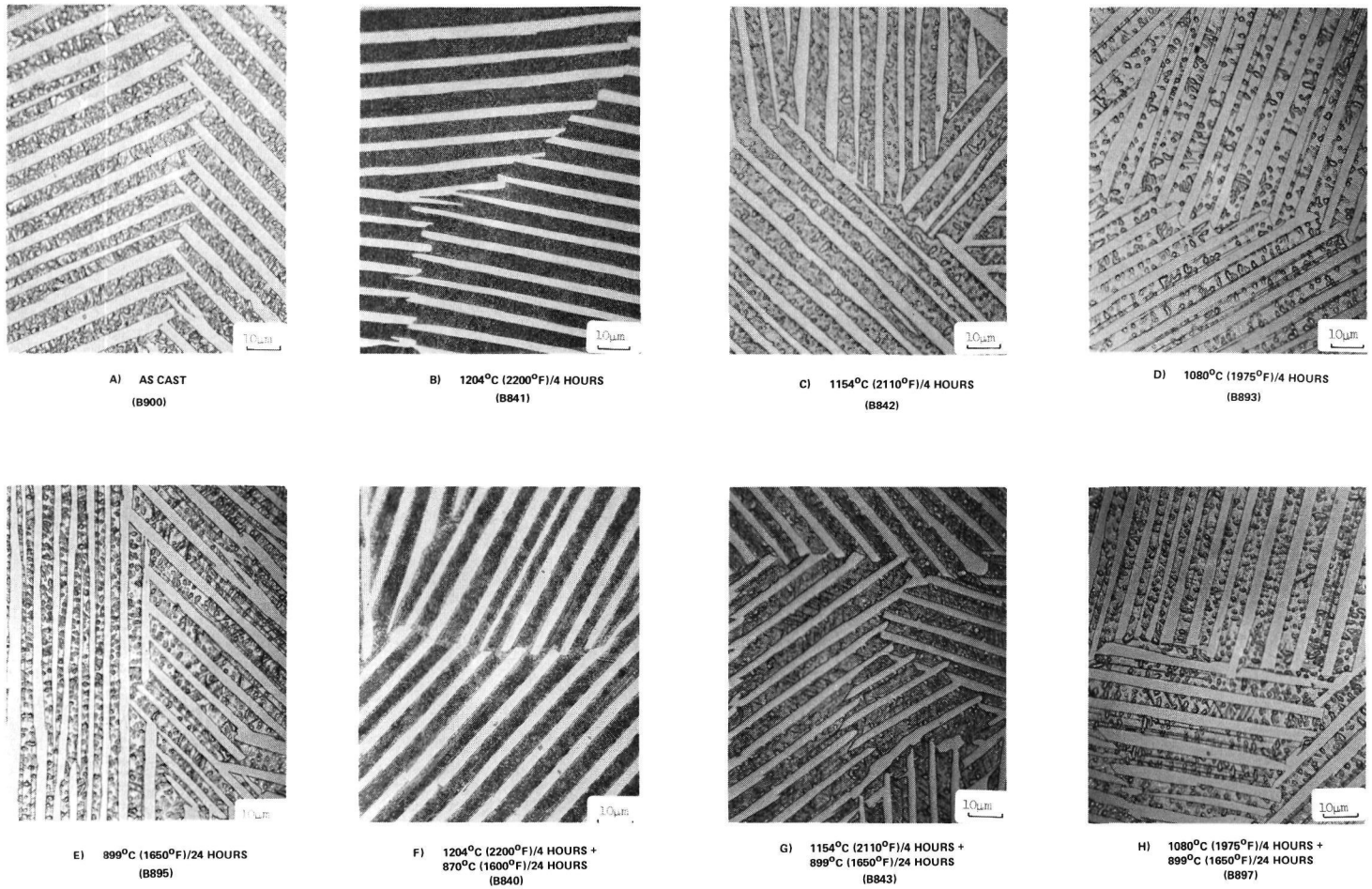


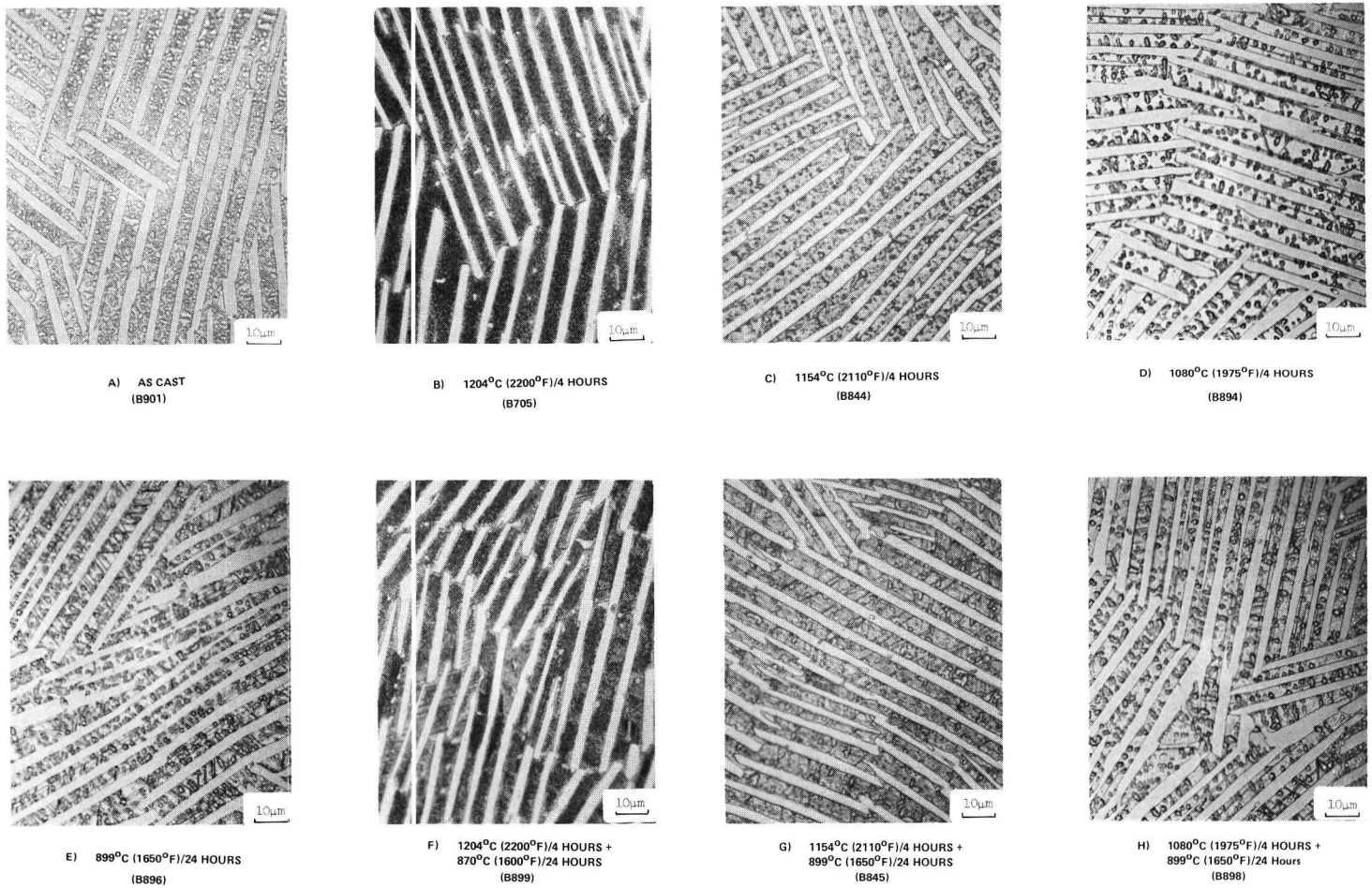

Figure 134 Influence of a Four Hour Thermal Exposure at the Indicated Temperatures on the Microstructures of Fully Lamellar 6%Cr $\gamma/\gamma'$ - $\delta$ Alloy Directionally Solidified at 0.64 cm (0.25 inch)/hour

R14-154




R14-155

Figure 135 Influence of Thermal Treatment on the Microstructure of the Fully Lamellar Base Composition 6%Cr $\gamma/\gamma'$- $\delta$ Eutectic Alloy Directionally Solidified at a Rate of 0.64cm (0.25 inch)/hour




R14-156

Figure 136 Influence of Thermal Treatment on the Microstructure of the Fully Lamellar Carbon Modified 6%Cr $\gamma/\gamma'$-$\delta$ Eutectic Alloy Directionally Solidified at a Rate of 0.64cm (0.25 inch)/hour

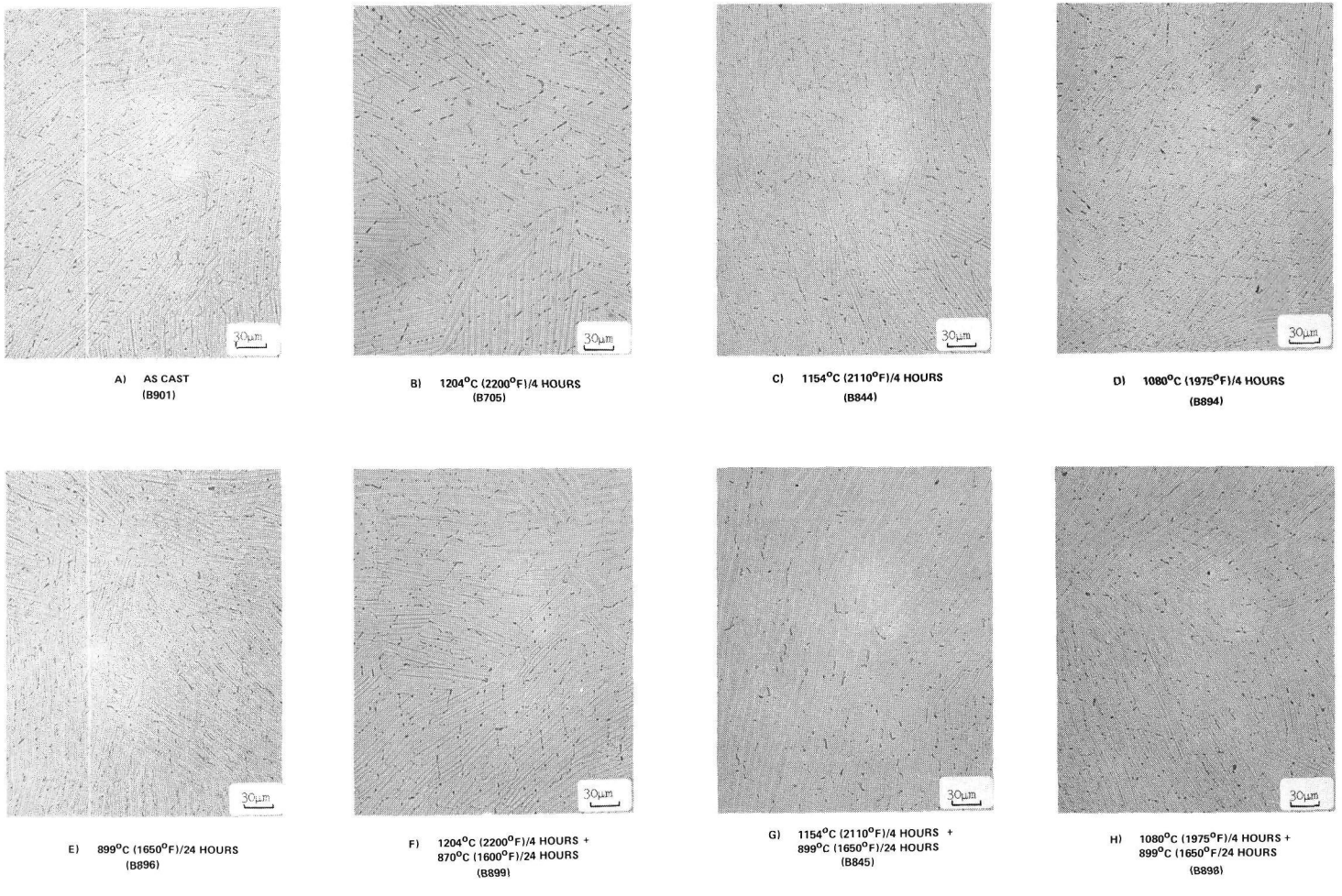



Figure 137 Influence of Thermal Treatment on the Carbide Distribution in a Fully Lamellar Carbon Modified 6%Cr $\gamma/\gamma'$ - $\delta$ Eutectic Alloy Directionally Solidified at a Rate of 0.64cm (0.25 inch) hour

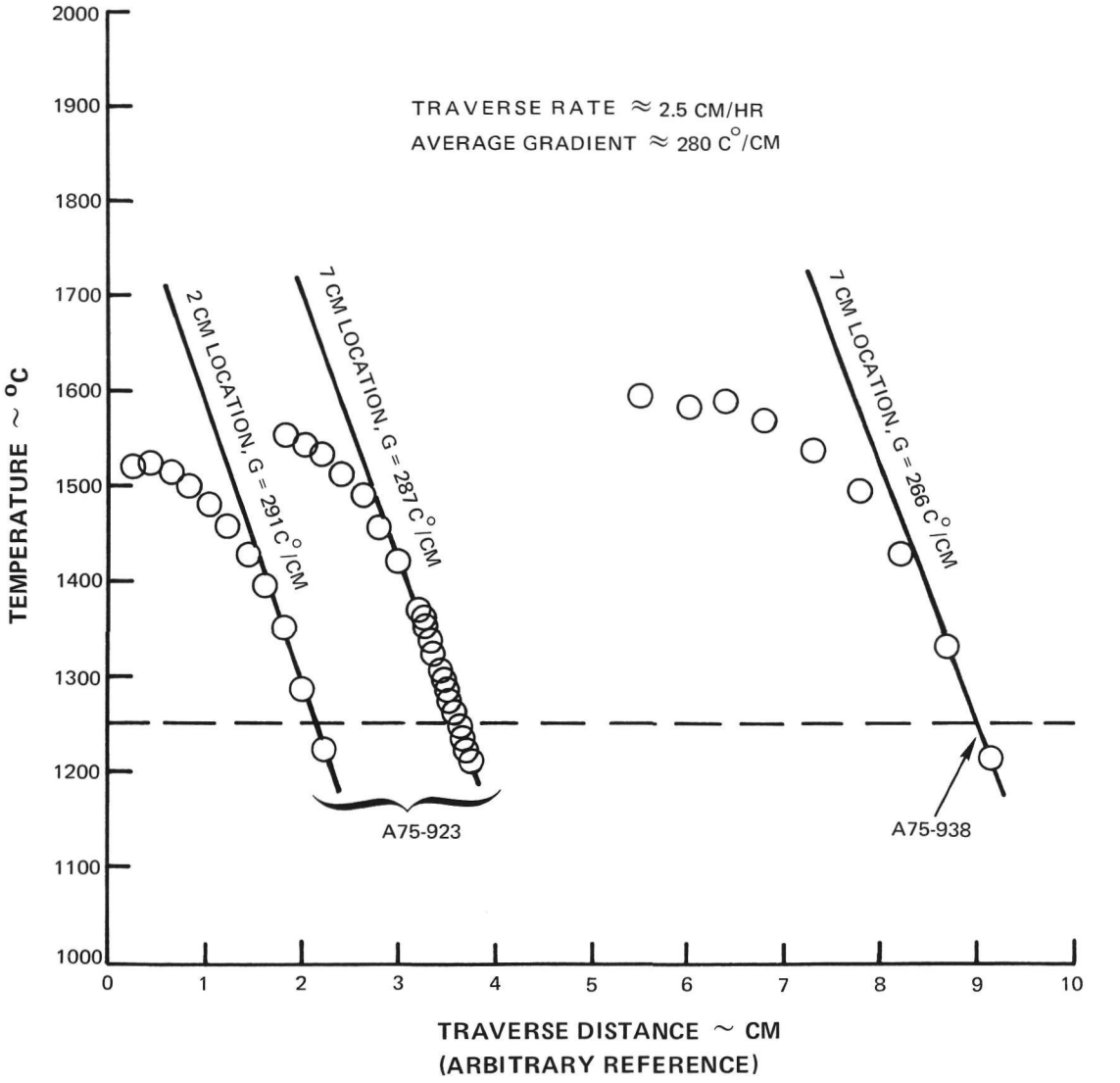
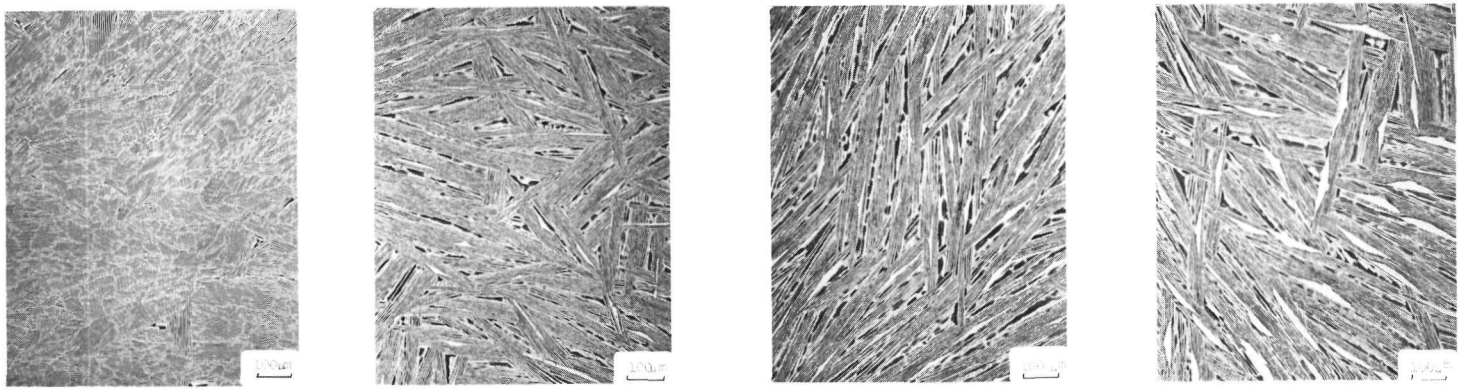



Figure 138 Measurements of Thermal Gradient Made on Water-Quench Bridgman Apparatus Immediately Prior to (Bar A75-923) and Immediately After (Bar A75-928) Phase III Critical G/R Determinations



MB1510-5 B940

A) BASELINE COMPOSITION CASTING A75-931 PROCESSED AT 1.75 cm/hr. G/R ≈ 160C° hr/cm²

MB 1510-6 B940

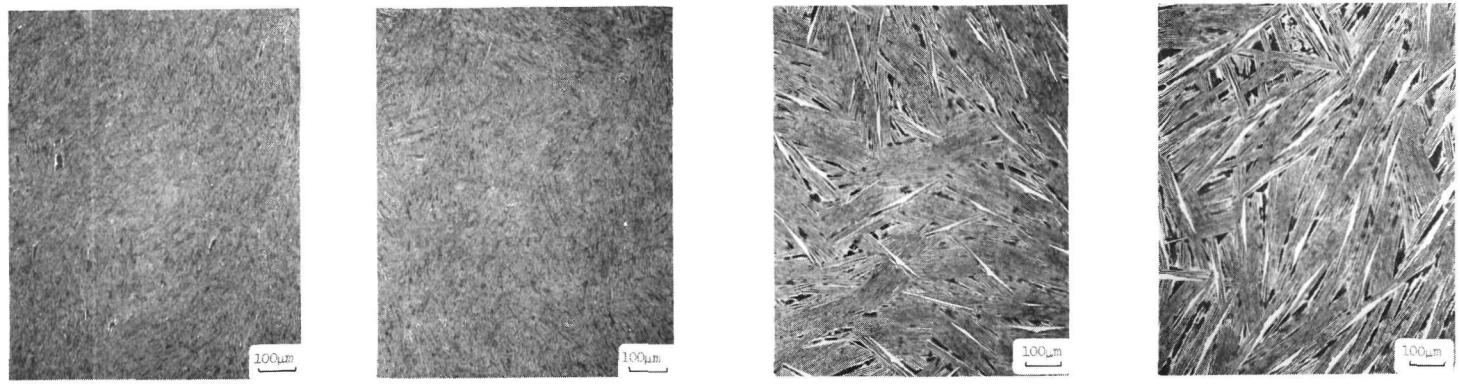
B) BASE COMPOSITION CASTING A75-931 PROCESSED AT 2.0 cm/hr. G/R ≈ 140C° hr/cm²

MB1510-7 B941

C) BASE COMPOSITION CASTING A75-931 PROCESSED AT 2.25 cm/hr. G/R ≈ 125C° hr/cm²

MB1510-8 B941

D) BASE COMPOSITION CASTING A75-931 PROCESSED AT 2.5 cm/hr. G/R ≈ 110C° hr/cm²



MB1510-1 B938

E) CARBON MODIFIED CASTING A75-929 PROCESSED AT 1.75 cm/hr. G/R ≈ 160C° hr/cm²

MB1510-2 B938

F) CARBON MODIFIED CASTING A75-929 PROCESSED AT 2.0 cm/hr. G/R ≈ 140C° hr/cm²

MB1510-3 B939

G) CARBON MODIFIED CASTING A75-929 PROCESSED AT 2.25 cm/hr. G/R ≈ 125C° hr/cm²

MB 1510-4 B939

H) CARBON MODIFIED CASTING A75-929 PROCESSED AT 2.5 cm/hr. G/R ≈ 110C° hr/cm²

R14-159

Figure 139 Influence of Directional Solidification Rate on the Microstructure of Base Composition and 0.06% Carbon Modified 6%Cr $\gamma/\gamma'$-$\delta$ Eutectic Alloys Processed in a Thermal Gradient of $\approx 280C^{\circ}/cm$

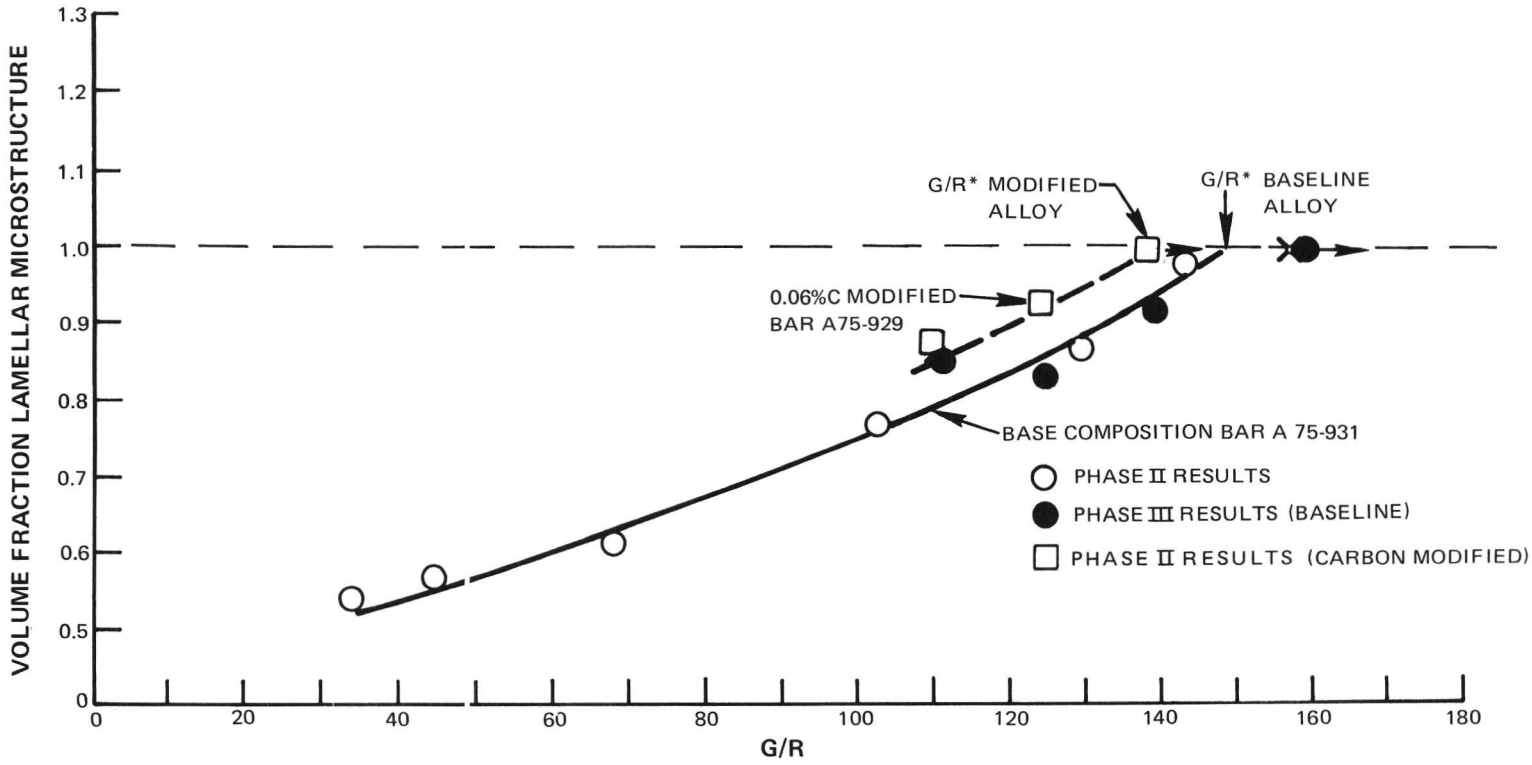



Figure 140 Influence of G/R on the Volume Fraction of Lamellar Microstructure in Base Composition and Carbon Modified 6%Cr $\gamma/\gamma'$-$\delta$ Eutectic Alloys

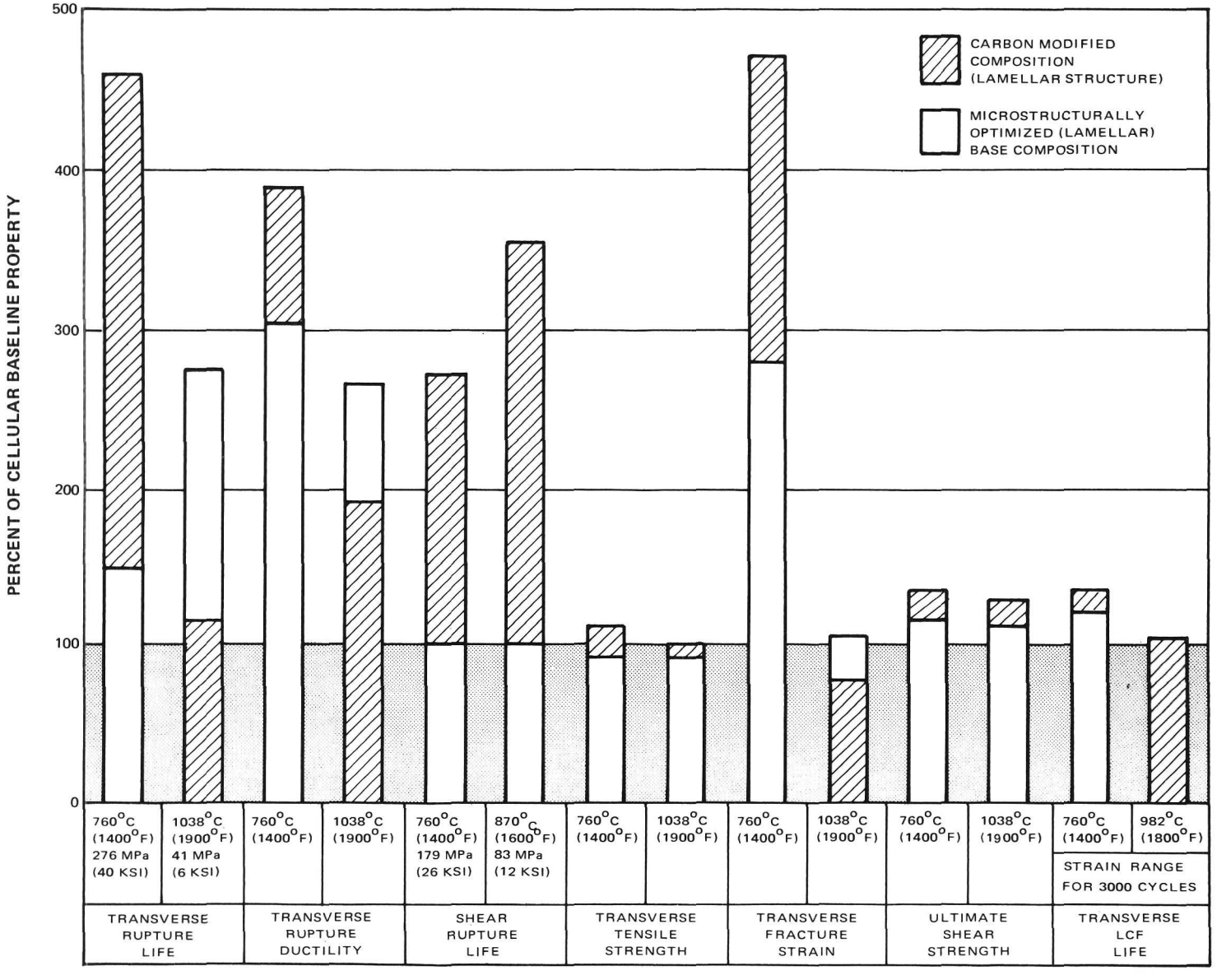



Figure 141 Comparison of Optimized Off-Axis Properties With Cellular Baseline Properties Measured in Phase I and on Other Programs

R14-161

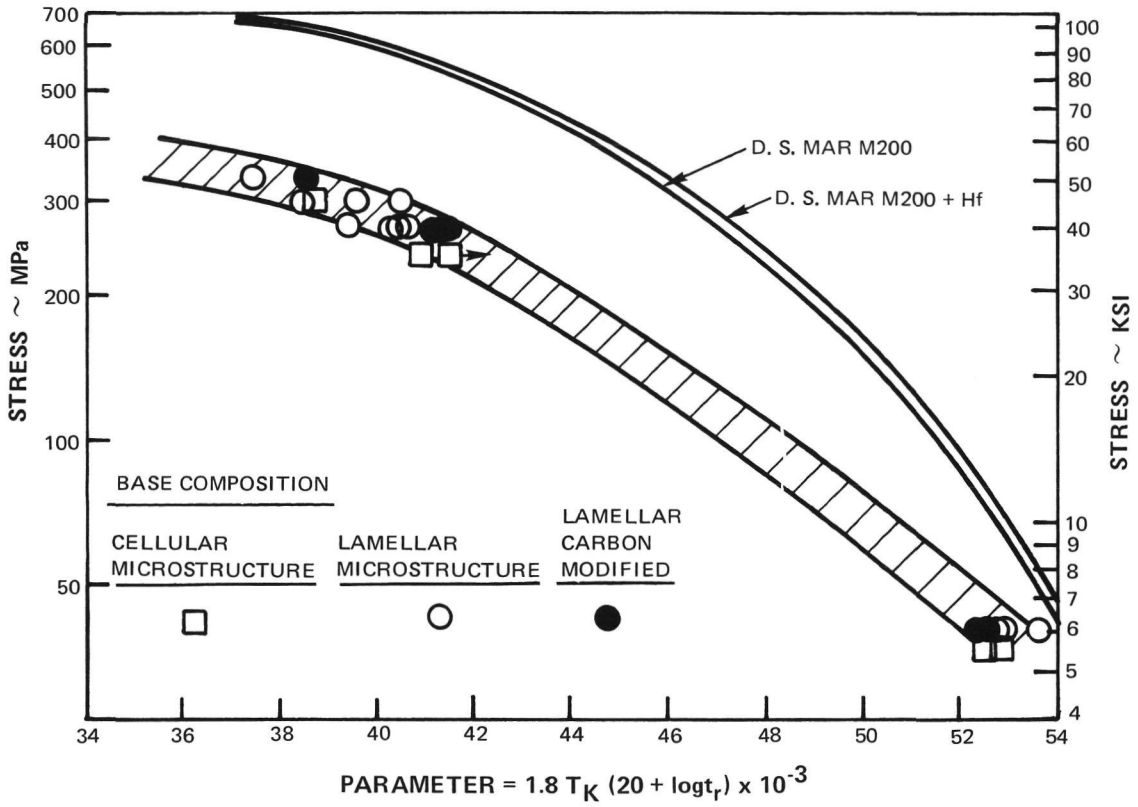
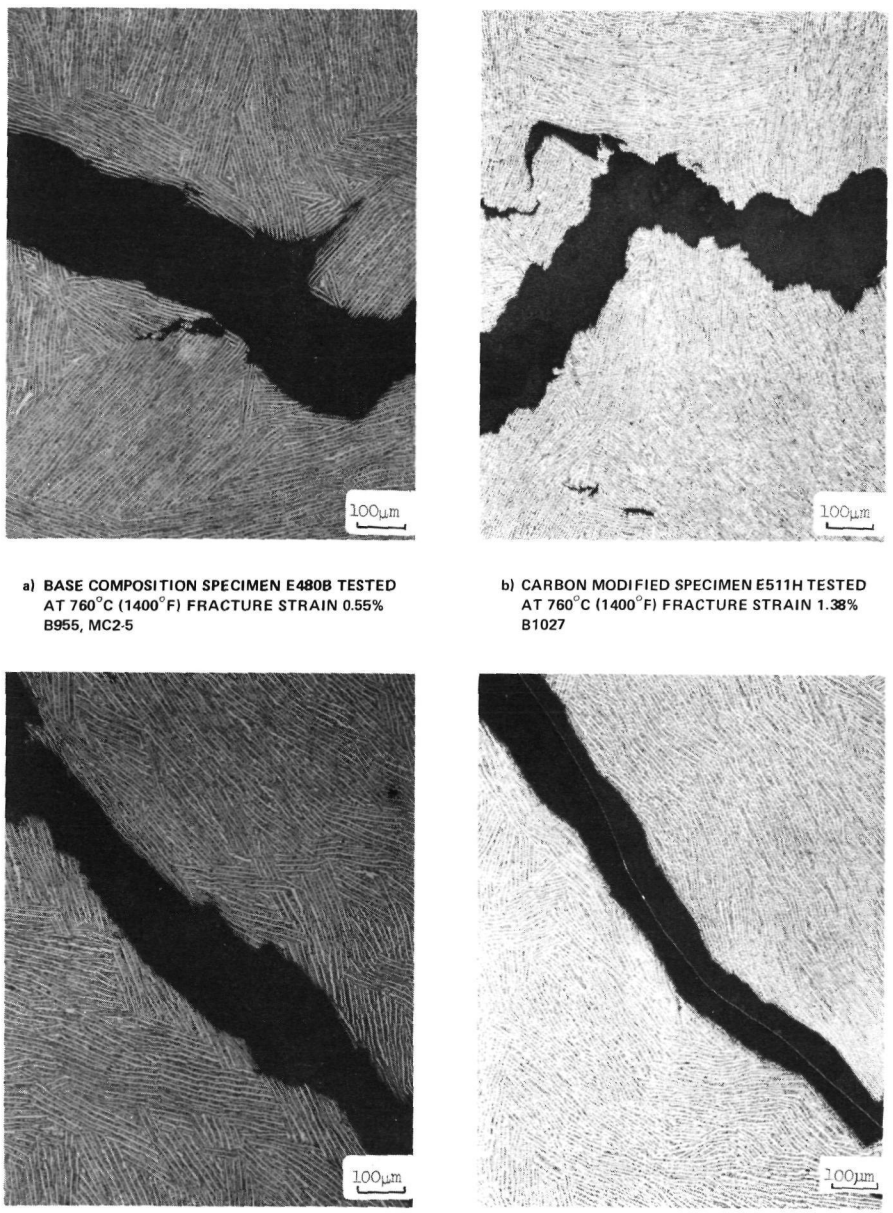



Figure 142 Influence of Microstructure and Composition on the Transverse Creep Properties of 6 Percent Chromium $\gamma/\gamma'$–$\delta$ Directionally Solidified Eutectic Alloy. All Specimens Coated With ≈ 60 $\mu$m (2.5 mils) PWA 270 NiCoCrAlY Coating and Tested in Air




a) BASE COMPOSITION SPECIMEN E480B TESTED AT 760°C (1400°F) FRACTURE STRAIN 0.55% B955, MC2-5

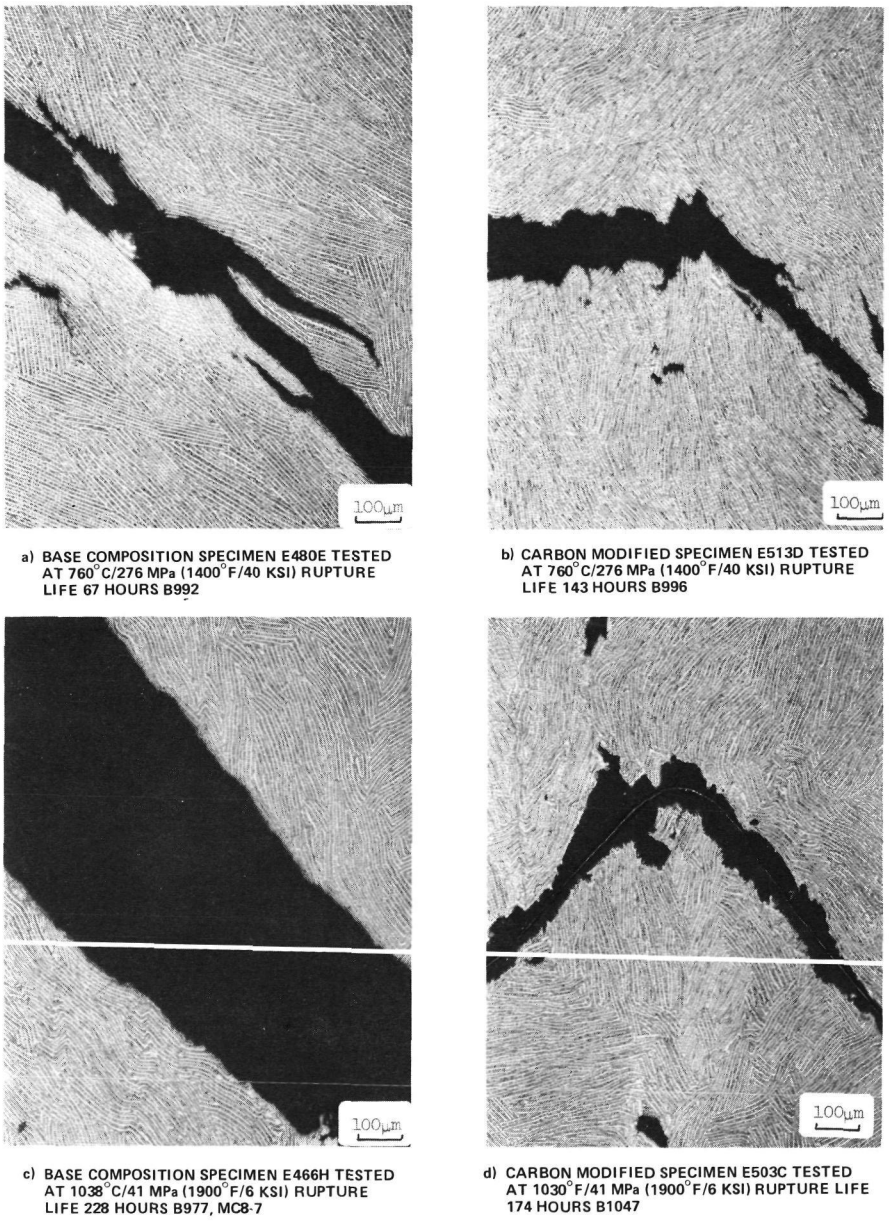
b) CARBON MODIFIED SPECIMEN E511H TESTED AT 760°C (1400°F) FRACTURE STRAIN 1.38% B1027

c) BASE COMPOSITION SPECIMEN E480C TESTED AT 1038°C (1900°F) FRACTURE STRAIN 4.2% B956, MC2-6

d) CARBON MODIFIED SPECIMEN E503B TESTED AT 1038°C (1900°F) FRACTURE STRAIN 4.2% B948, MC2-14A

R14-163

Figure 143 Fracture Profiles Found in Phase IV Transverse Tension Test Specimens Tested at the Indicated Conditions. Test Material Grown in Slab Form at a Rate of 0.64 cm (0.25 inch)/hour. All Specimens Coated with ≈ 60μm (2.5 mils) PWA 270




a) BASE COMPOSITION SPECIMEN E480E TESTED AT 760°C/276 MPa (1400°F/40 KSI) RUPTURE LIFE 67 HOURS B992

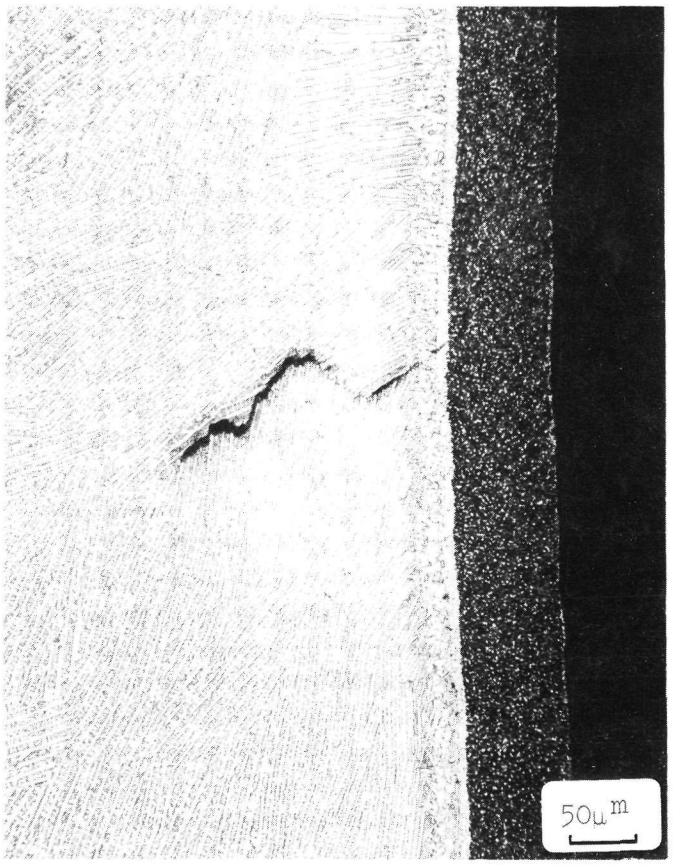
b) CARBON MODIFIED SPECIMEN E513D TESTED AT 760°C/276 MPa (1400°F/40 KSI) RUPTURE LIFE 143 HOURS B996

c) BASE COMPOSITION SPECIMEN E466H TESTED AT 1038°C/41 MPa (1900°F/6 KSI) RUPTURE LIFE 228 HOURS B977, MC8-7

d) CARBON MODIFIED SPECIMEN E503C TESTED AT 1030°F/41 MPa (1900°F/6 KSI) RUPTURE LIFE 174 HOURS B1047

R14-164

Figure 144 Fracture Profiles Found in Phase IV Transverse Creep Specimens Tested at the Indicated Conditions. Test Material Grown in Slab Form at a Rate of 0.64 cm (0.25 inch)/hour. All Specimens Coated With ≈ 60 μm (2.5 mils) PWA 270




B1027

R14-165

Figure 145 Secondary Crack Found at a Location Remote From the Fracture in Specimen E511H Broken in Tension at 760°C (1400°F). Tensile Axis Vertical, Fracture Strain 1.38 Percent

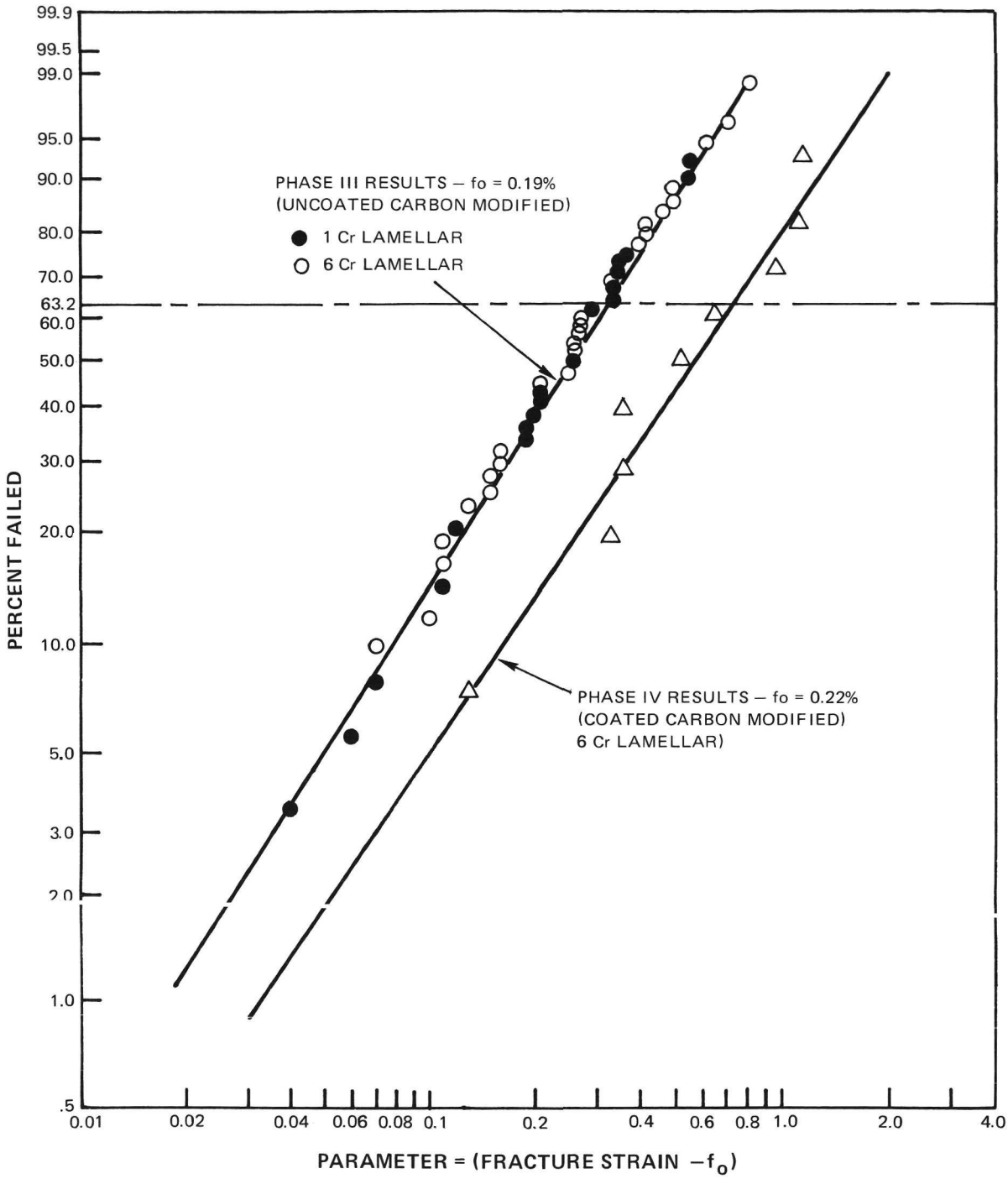



Figure 146 Parametric Weibull Analysis of Phase IV 760°C (1400°F) Coated Carbon Modified Fracture Strains (Phase III Results Included for Comparison)

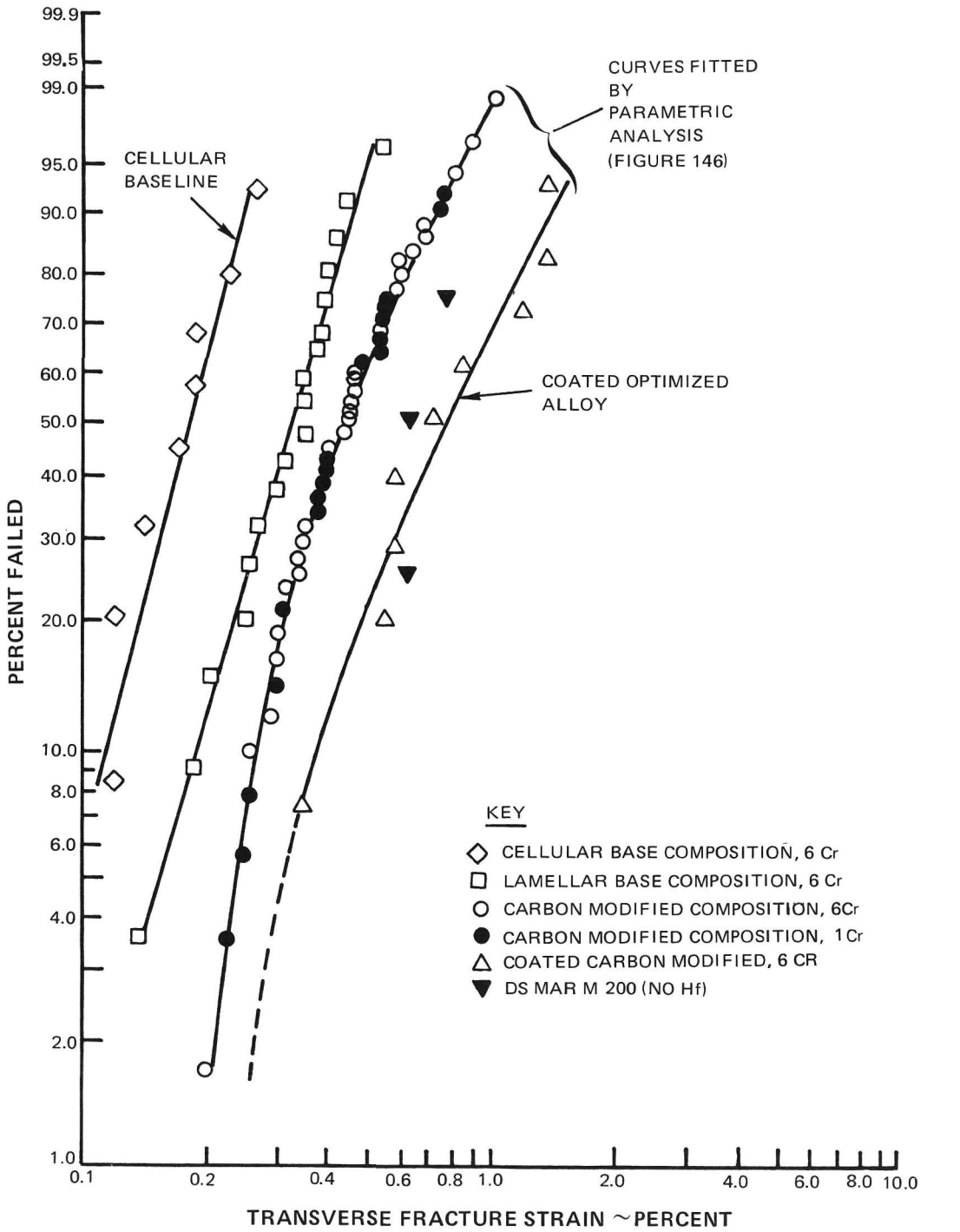



Figure 147 Comparison of 760°C (1400°F) Transverse Fracture Strains for Various Alloy-Structure Combinations

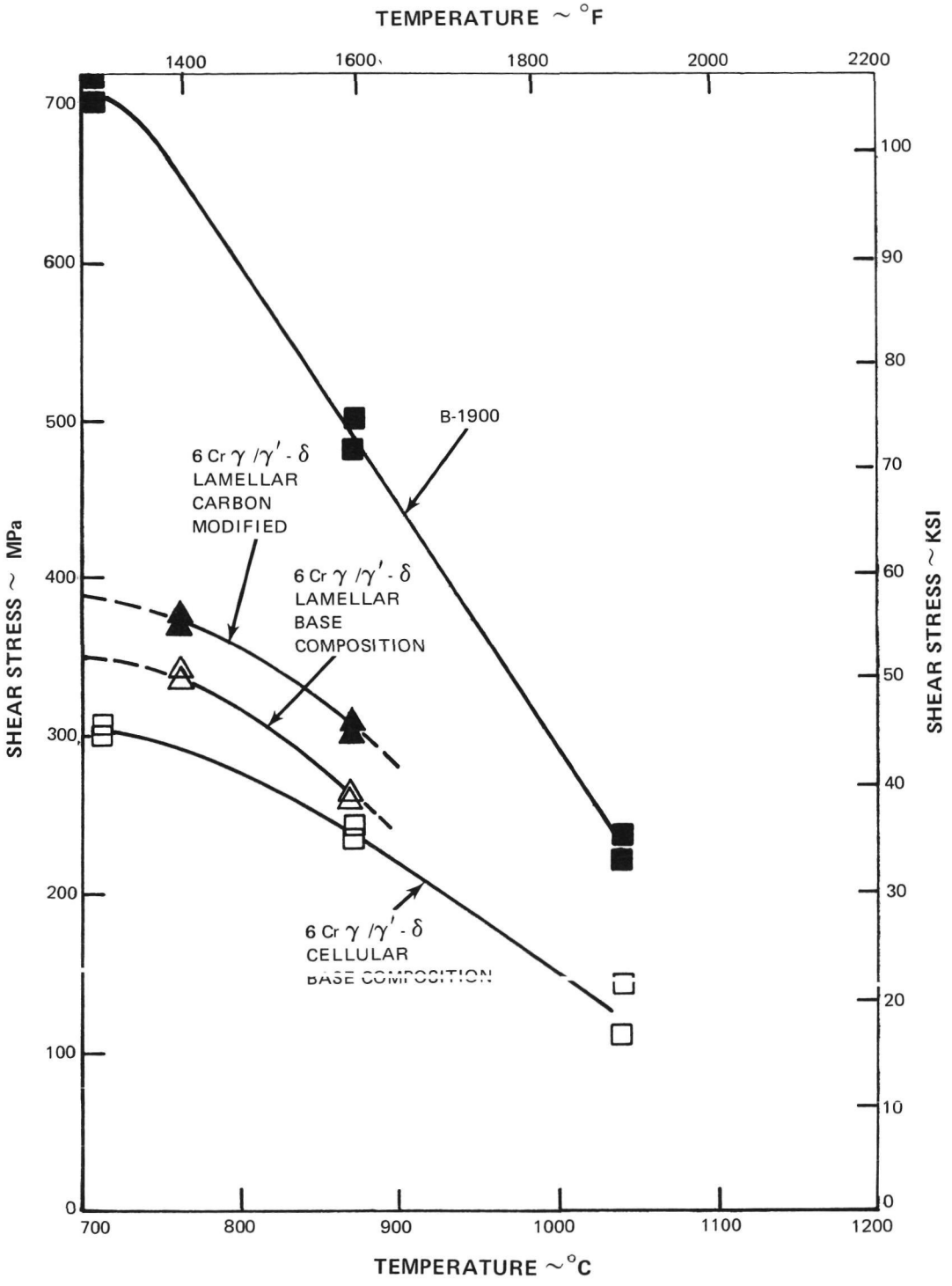



Figure 148 Comparison of $\gamma/\gamma'$ - $\delta$ Baseline and Candidate Optimized Alloy Ultimate Shear Strengths With Conventionally Cast B-1900 Alloy

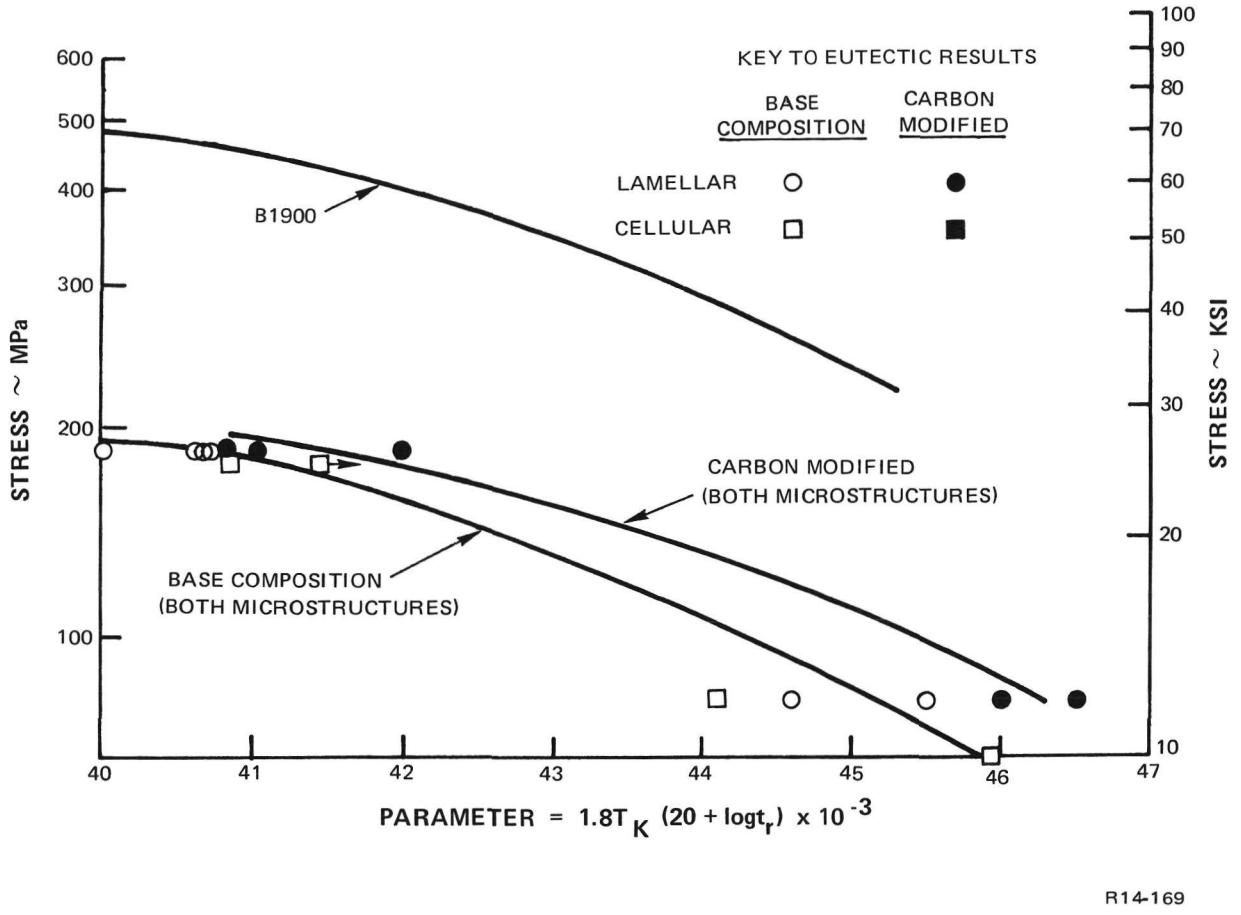
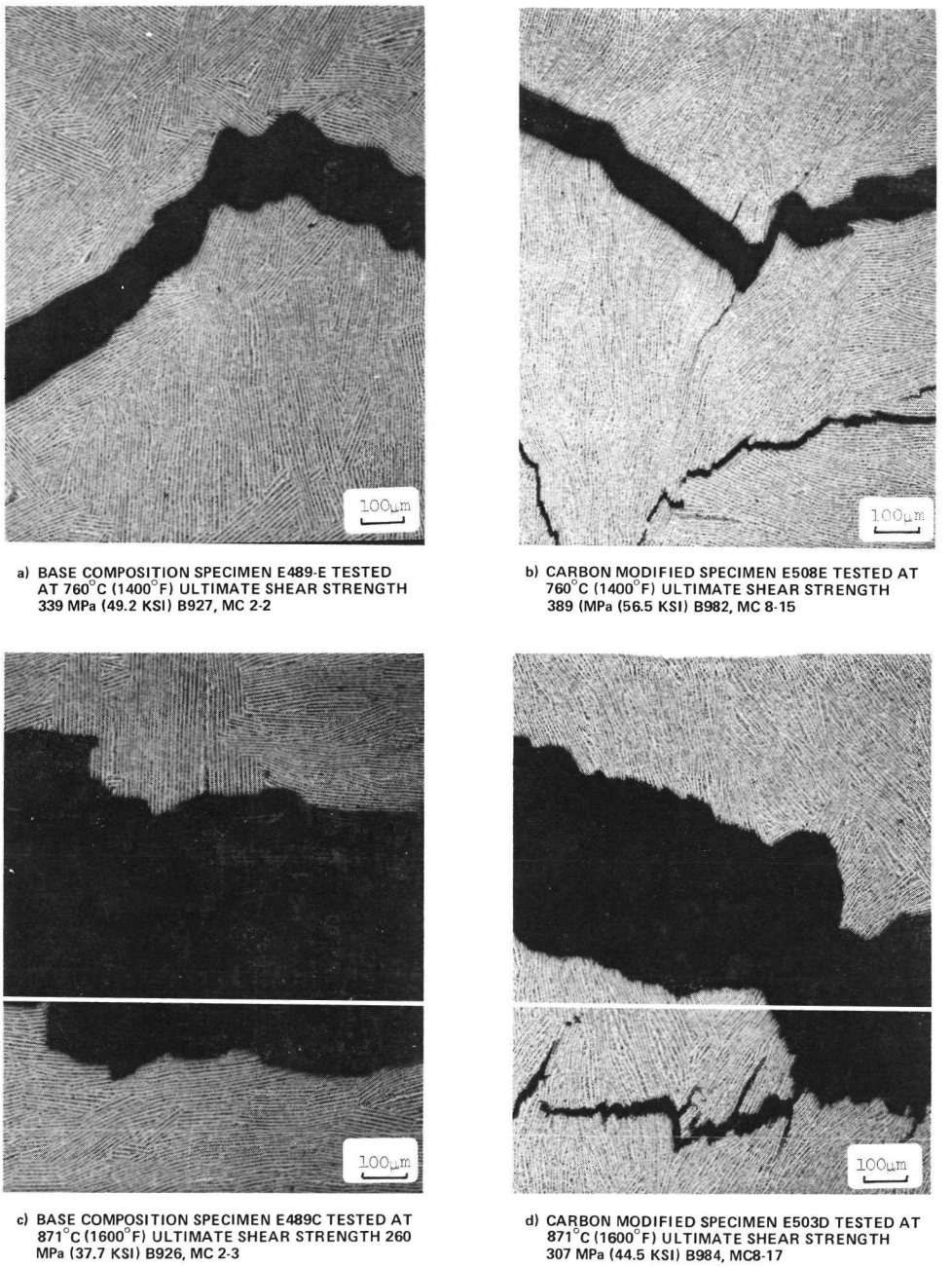



Figure 149 Comparison of Various $\gamma/\gamma'$ - $\delta$ Shear Creep Life Results With Conventionally Cast B-1900 Properties




a) BASE COMPOSITION SPECIMEN E489-E TESTED AT 760°C (1400°F) ULTIMATE SHEAR STRENGTH 339 MPa (49.2 KSI) B927, MC 2-2

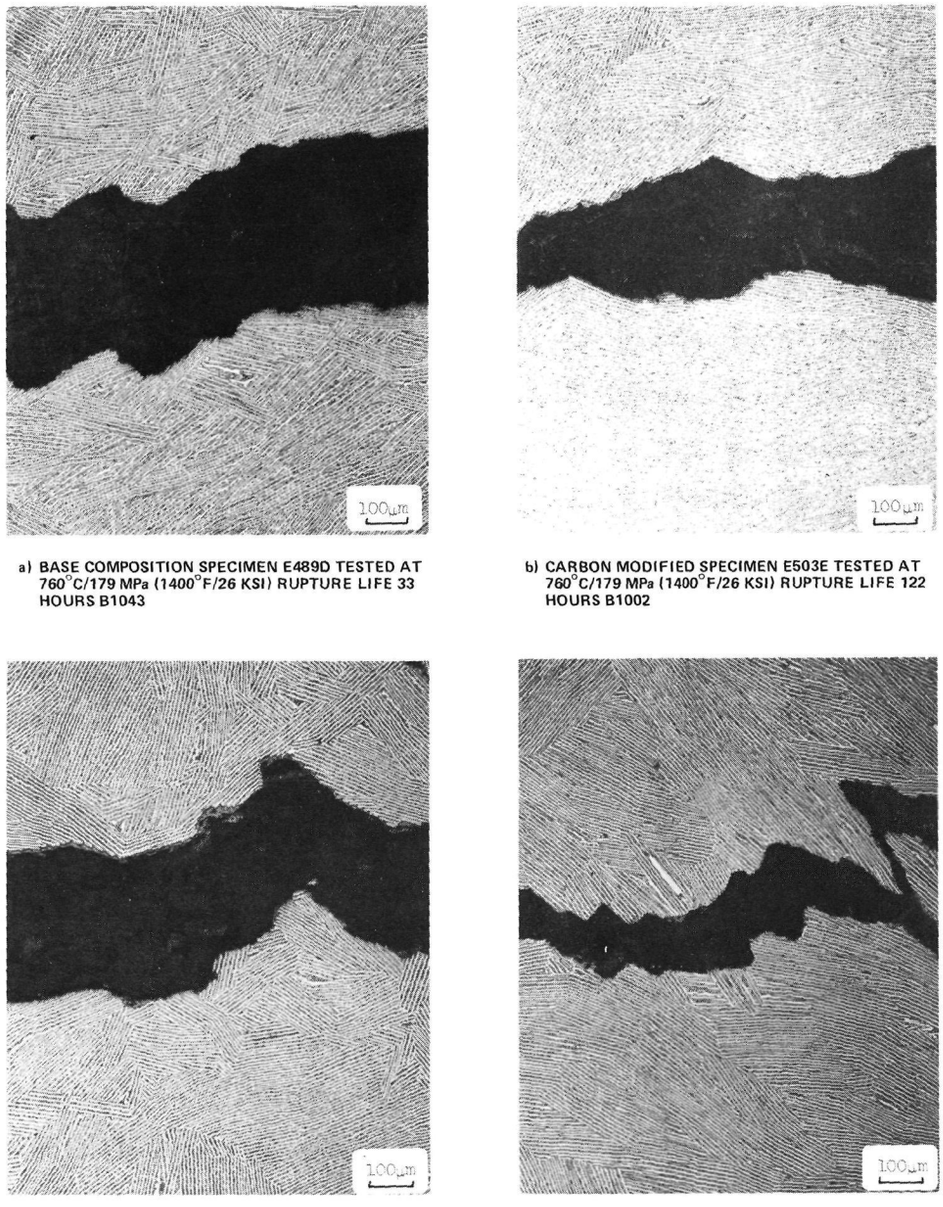
b) CARBON MODIFIED SPECIMEN E508E TESTED AT 760°C (1400°F) ULTIMATE SHEAR STRENGTH 389 (MPa (56.5 KSI) B982, MC 8-15

c) BASE COMPOSITION SPECIMEN E489C TESTED AT 871°C (1600°F) ULTIMATE SHEAR STRENGTH 260 MPa (37.7 KSI) B926, MC 2-3

d) CARBON MODIFIED SPECIMEN E503D TESTED AT 871°C (1600°F) ULTIMATE SHEAR STRENGTH 307 MPa (44.5 KSI) B984, MC8-17

R14-170

Figure 150 Fracture Profiles Found in Phase IV Ultimate Shear Strength Specimens Tested at the Indicated Conditions. Test Material Grown in Slab Form at a Rate of 0.64 cm (0.25 inch)/hour. Shear Stress Applied Normal to the Plane of Polish




a) BASE COMPOSITION SPECIMEN E489D TESTED AT 760°C/179 MPa (1400°F/26 KSI) RUPTURE LIFE 33 HOURS B1043

b) CARBON MODIFIED SPECIMEN E503E TESTED AT 760°C/179 MPa (1400°F/26 KSI) RUPTURE LIFE 122 HOURS B1002

c) BASE COMPOSITION SPECIMEN E482D TESTED AT 871°C/83 MPa (1600°F/12 KSI) RUPTURE LIFE 89 HOURS B983, MC8-16

d) CARBON MODIFIED SPECIMEN E508D TESTED AT 871°C/83 MPa (1600°F/12 KSI) RUPTURE LIFE 216 HOURS B979, MC8-5

R14-171

Figure 151 Fracture Profiles Found in Phase IV Shear Creep Specimens Tested at the Indicated Conditions. Test Material Grown in Slab Form at a Rate of 0.64 cm (0.25 inch)/hour. Shear Stress Applied Normal to the Plane of Polish.

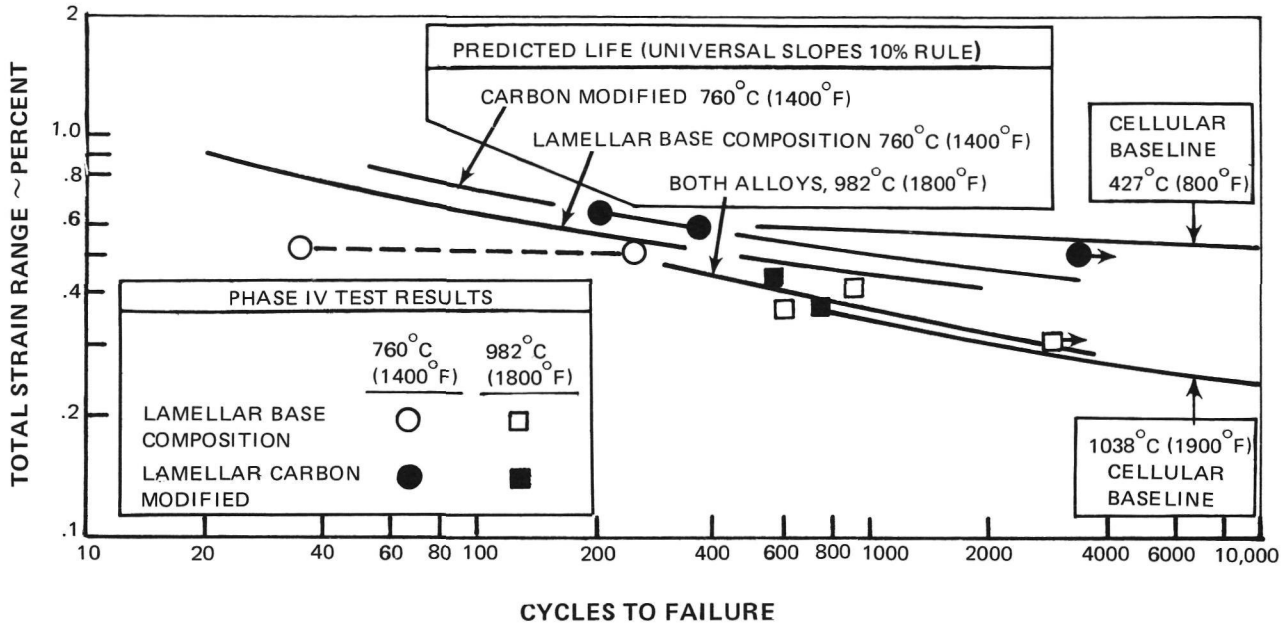
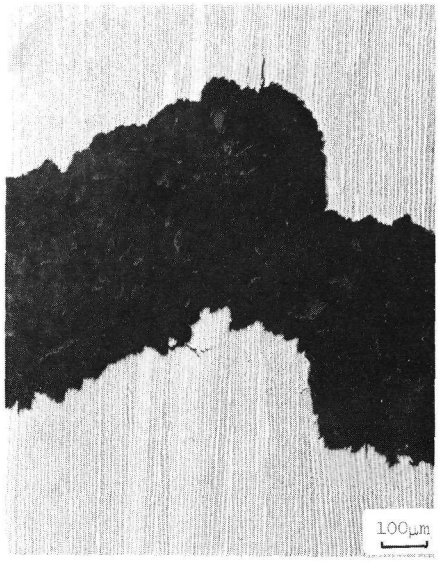
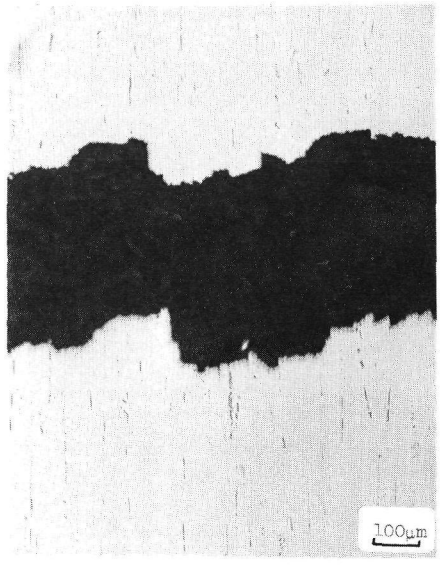


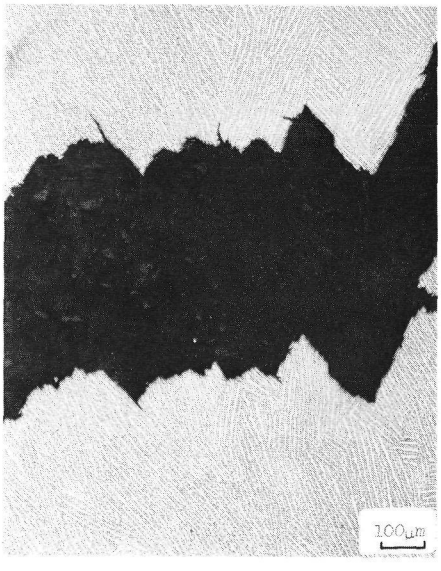

Figure 152 Comparison of Transverse Low Cycle Fatigue Results for Various 6Cr $\gamma/\gamma'$–$\delta$ Directionally Solidified Eutectic Alloy Structure Combinations



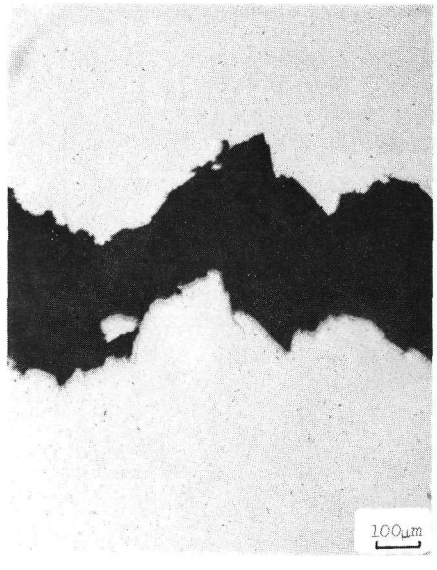

a) BASE COMPOSITION LONGITUDINAL SPECIMEN E492B, IMPACT ENERGY 2.58J (1.90 FT. LB.) B1032




b) CARBON MODIFIED LONGITUDINAL SPECIMEN E513H, IMPACT ENERGY 1.63J (1.20 FT. LB.) B1038



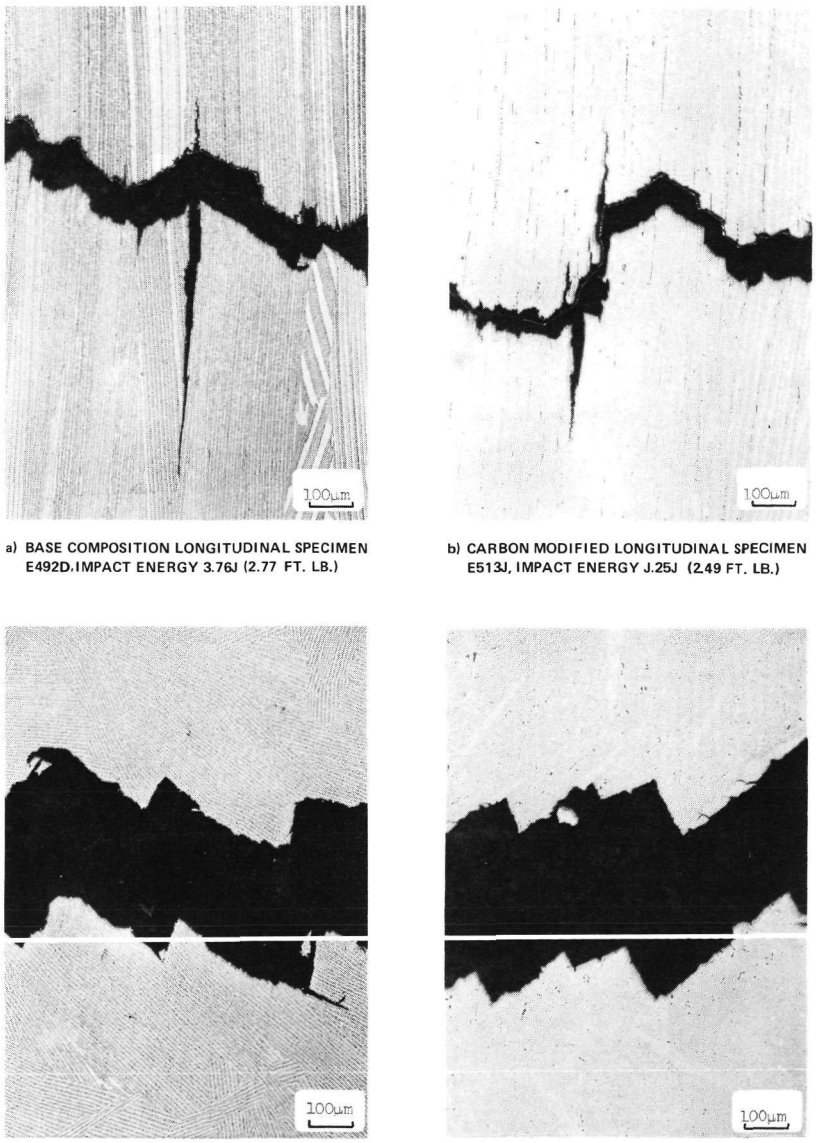

c) BASE COMPOSITION TRANSVERSE SPECIMEN E500C, IMPACT ENERGY 0.66J (0.49 FT. LB.) B1034




d) CARBON MODIFIED TRANSVERSE SPECIMEN E503F, IMPACT ENERGY 0.43J (0.32 FT. LB.) B1036

R14-173

Figure 153 Fracture Profile Found in Room Temperature Eutectic Impact Specimens Impacted Normal to Plane of Polish




a) BASE COMPOSITION LONGITUDINAL SPECIMEN E492D. IMPACT ENERGY 3.76J (2.77 FT. LB.)

b) CARBON MODIFIED LONGITUDINAL SPECIMEN E513J, IMPACT ENERGY J.25J (2.49 FT. LB.)

c) BASE COMPOSITION TRANSVERSE SPECIMEN E500E IMPACT ENERGY 0.71J (0.52 FT. LB.) B1035

d) CARBON MODIFIED TRANSVERSE SPECIMEN E503H IMPACT ENERGY 0.60J (0.44 FT. LB.) B1037

R14-174

Figure 154 Fracture Profiles Found in 760°C (1400°F) Eutectic Impact Specimens Impacted Normal to Plane of Polish

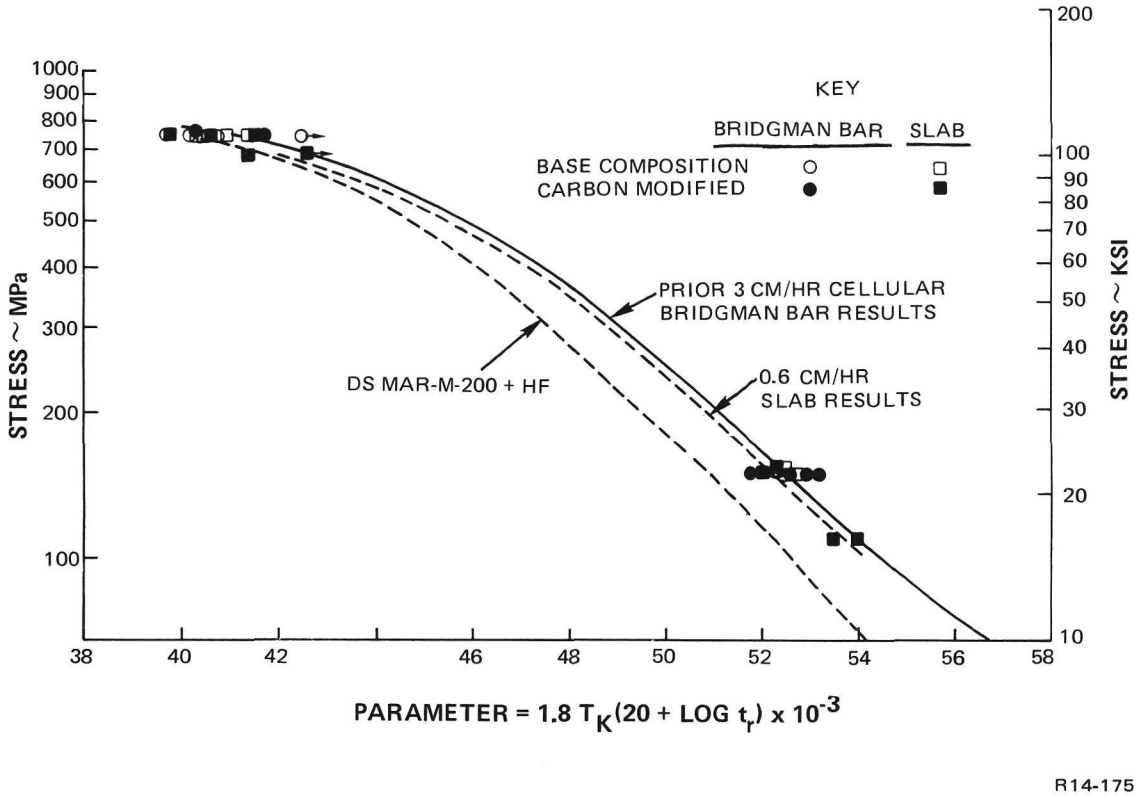
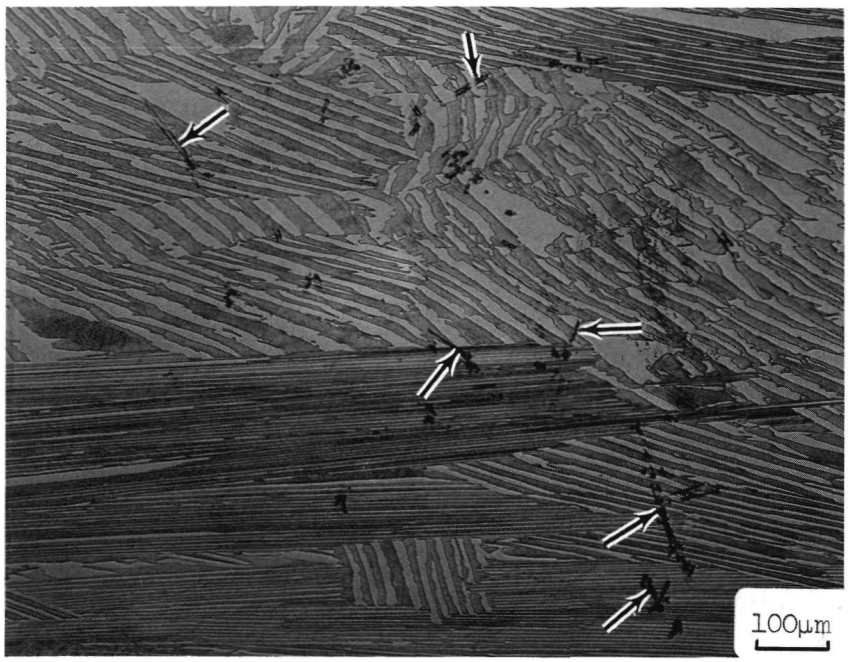
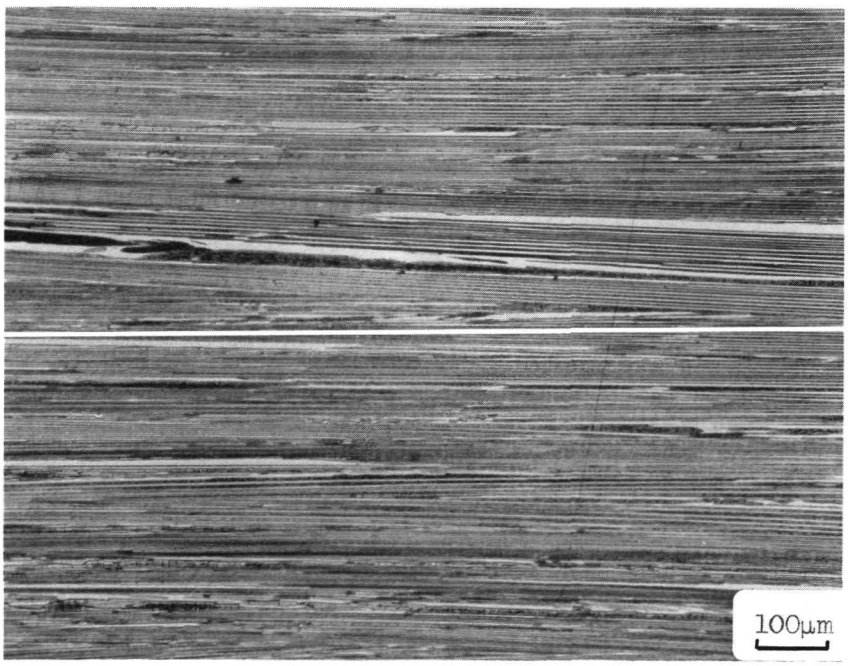



Figure 155 Phase IV Creep Test Results



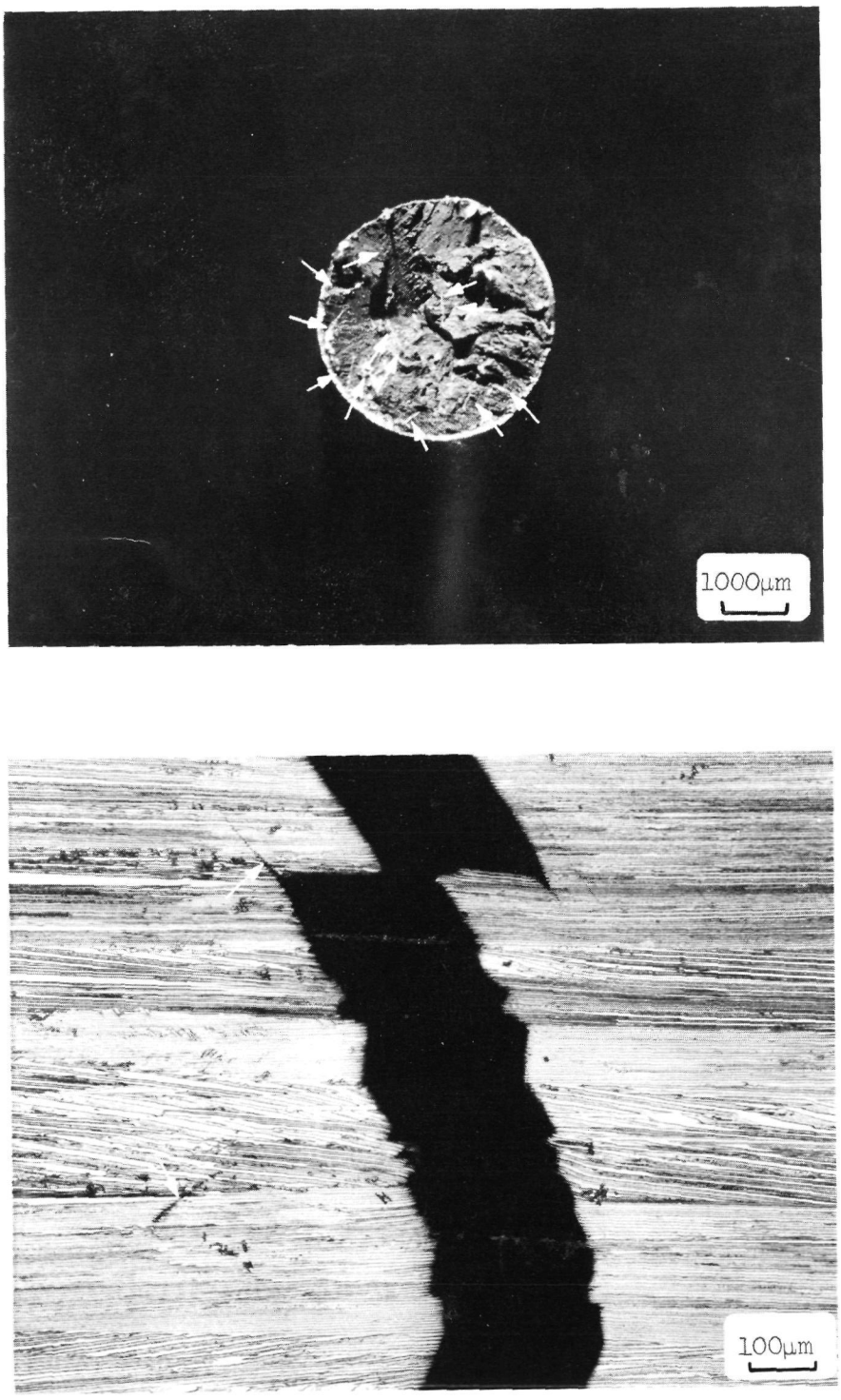

a) OXIDE INCLUSIONS (INDICATED BY ARROWS) FOUND IN CASTING A75-874, B936




b) CELLULAR BAND FOUND IN CASTING A75-806, B1052

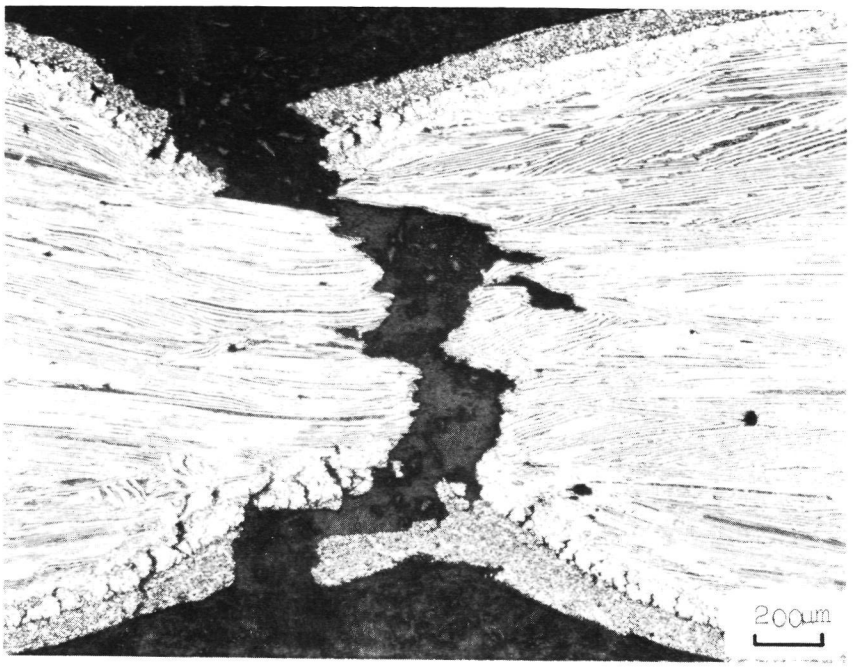
R14-176

Figure 156 Typical Microstructural Defects Found in Phase IV Bridgman Bar Castings




R14-177

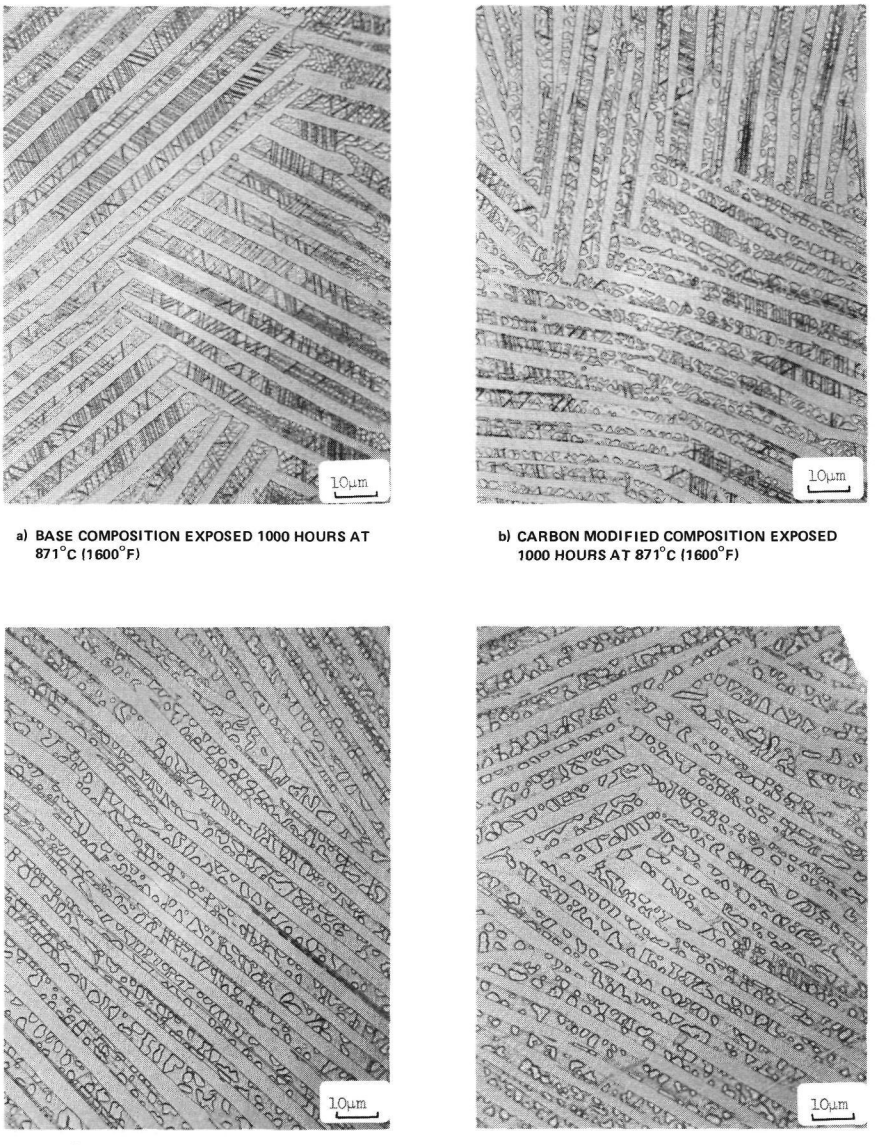
Figure 157 Oxide Inclusions (Indicated By Arrows) Found On Fracture Surface of Specimen No. A75-877-01




B1054

R14-178

Figure 158 Example of Creep Failure Found at a Cellular Band in Phase V Bridgman Bars Creep Specimens (Specimen No. A75-810-01)




a) BASE COMPOSITION EXPOSED 1000 HOURS AT 871°C (1600°F)

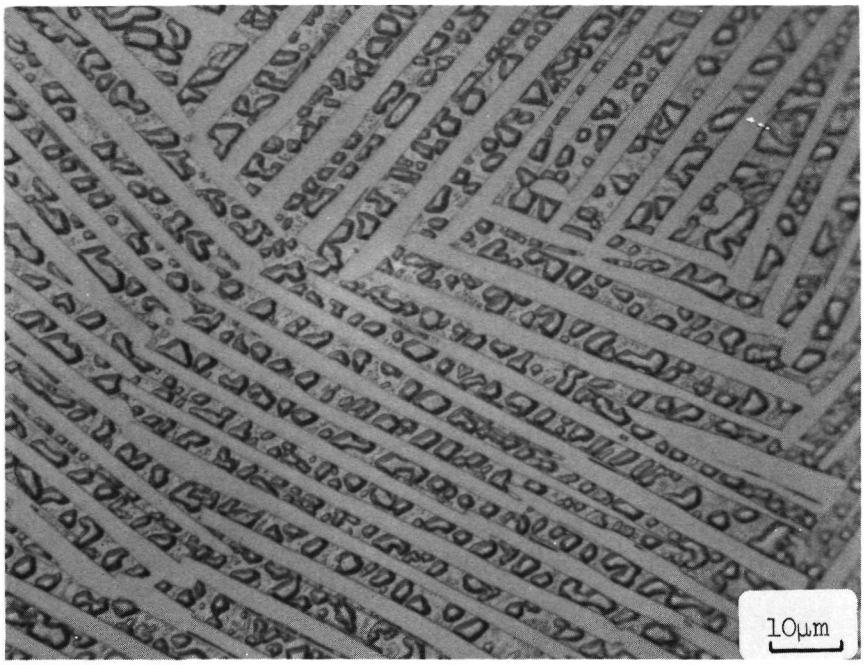
b) CARBON MODIFIED COMPOSITION EXPOSED 1000 HOURS AT 871°C (1600°F)

c) BASE COMPOSITION EXPOSED 1000 HOURS AT 1038°C (1900°F)

d) CARBON MODIFIED COMPOSITION EXPOSED 1000 HOURS AT 1038°C (1900°F)

R14-179

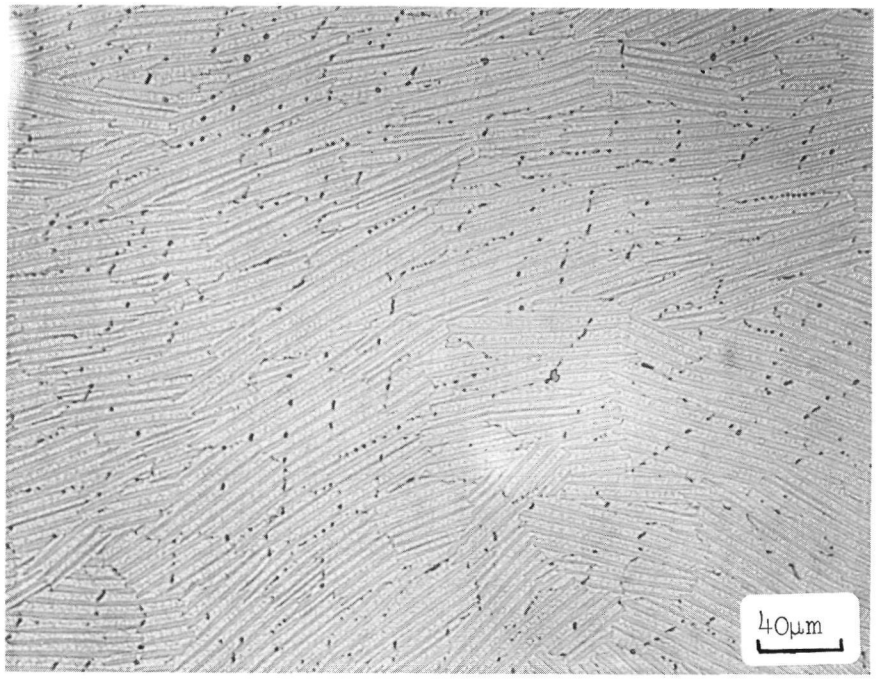
Figure 159 Microstructures Found in $\gamma/\gamma'$–$\delta$ Thermal Exposure Coupons



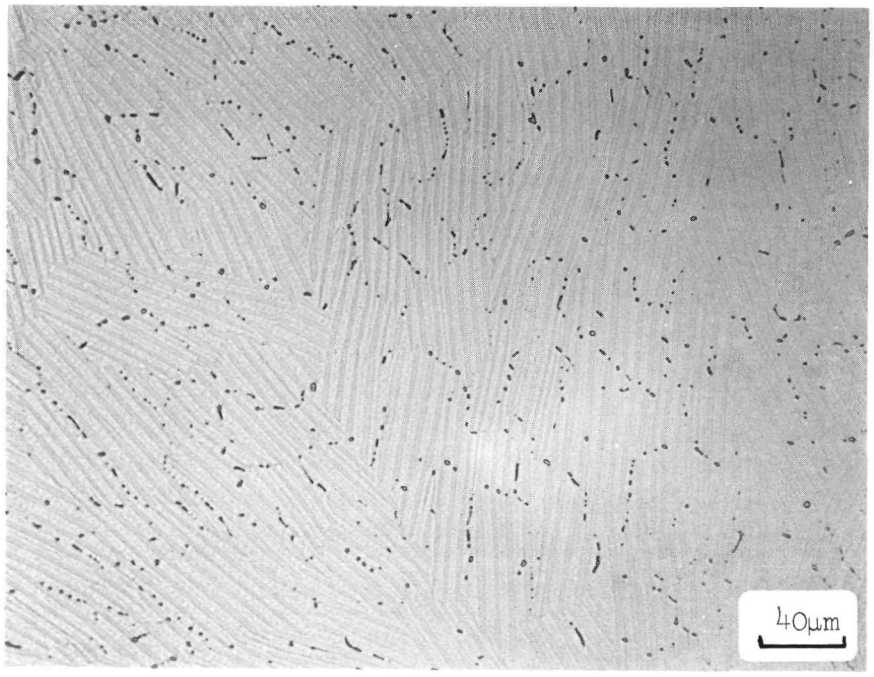

B1079

R14-180

Figure 160 Microstructure Found in Specimen E513M1 Creep Exposed 743 Hours at 1038°C/110MPa (1900°F/16 ksi)



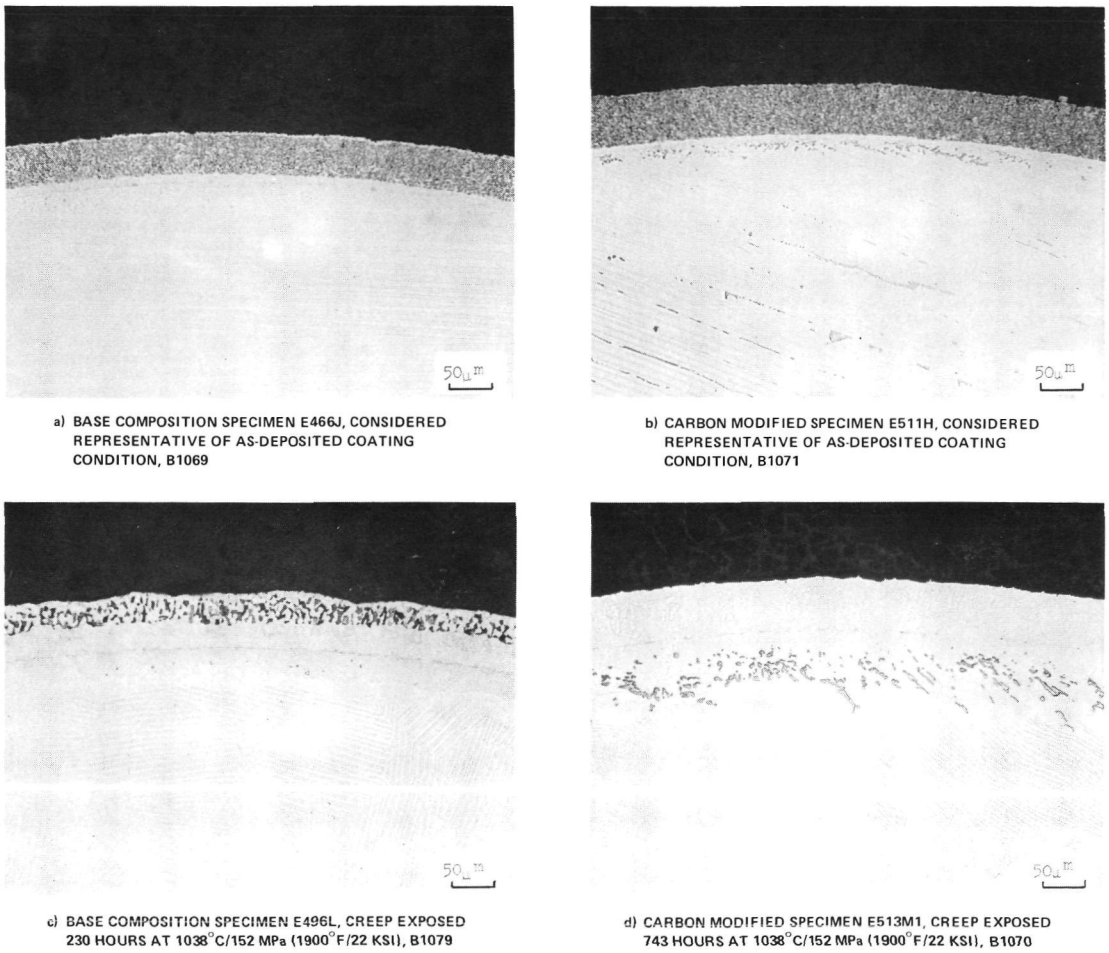

a) EXPOSURE TEMPERATURE 871°C (1600°F) B1055




b) EXPOSURE TEMPERATURE 1038°C (1900°F) B1057

R14-181

Figure 161 Carbide Distributions Found in Fully Lamellar 0.06 Percent Carbon Modified $\gamma/\gamma'$–$\delta$ Coupons Exposed for 1000 Hours in Air at the Indicated Temperatures




a) BASE COMPOSITION SPECIMEN E466J, CONSIDERED REPRESENTATIVE OF AS-DEPOSITED COATING CONDITION, B1069

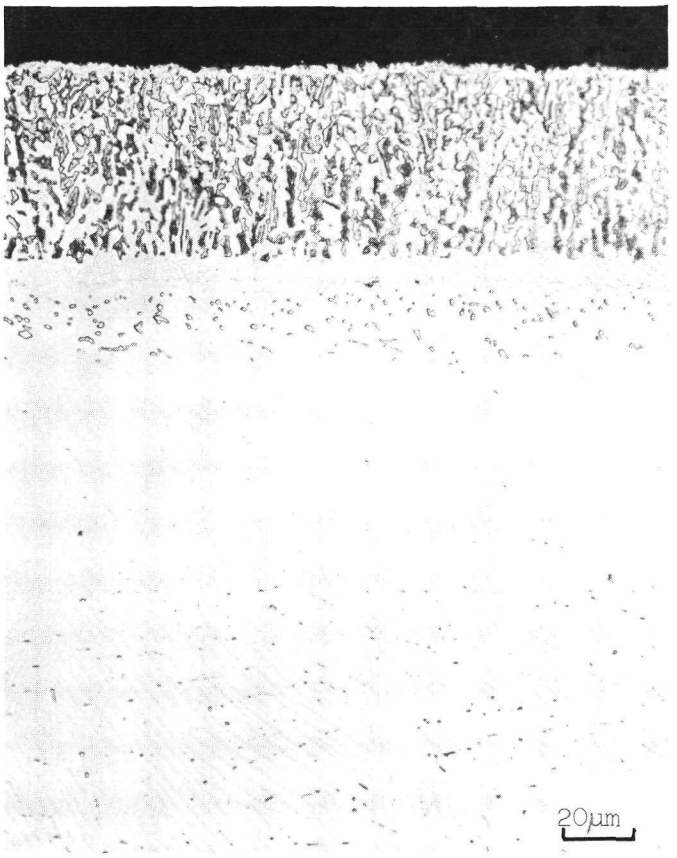
b) CARBON MODIFIED SPECIMEN E511H, CONSIDERED REPRESENTATIVE OF AS-DEPOSITED COATING CONDITION, B1071

c) BASE COMPOSITION SPECIMEN E496L, CREEP EXPOSED 230 HOURS AT 1038°C/152 MPa (1900°F/22 KSI), B1079

d) CARBON MODIFIED SPECIMEN E513M1, CREEP EXPOSED 743 HOURS AT 1038°C/152 MPa (1900°F/22 KSI), B1070

R14-182

Figure 162 Coating Microstructures Found in Various 6Cr $\gamma/\gamma'$–$\delta$ Directionally Solidified Eutectic Specimens Coated With ≈ 60μm (2.5 mils) PWA 270 NiCoCrAlY Overlay Coating




B1081

R14-183

Figure 163 Carbide Distribution Found in Specimen A75-908-01 Tested to Rupture in 225 Hours at 760°C (1400°F)

# APPENDICES

# APPENDIX A
# CASTINGS EVALUATED
## TABLE XLVI
## CASTING DIRECTORY

| Alloy Modification | 0% Cr | | 1% Cr | | 2% Cr | 3% Cr | 6% Cr | | | | B-1900 + Hf |
|---|---|---|---|---|---|---|---|---|---|---|---|
| | Phase II | Phase III | Phase II | Phase III | Phase II | Phase III | Phase I | Phase II | Phase III | Phase IV | Phase I |
| None | A71-651<br>A72-623<br>A74-756<br>A74-762<br>A74-774<br>A74-775<br>A75-184<br>A75-224<br>A75-229<br>A75-235<br>A75-298<br>A75-313<br>E354 | | A73-079 A75-375<br>A74-748 A75-377<br>A74-767 A75-379<br>A74-1036 E288<br>A74-1055 E318<br>A74-1064 E329<br>A74-1129 E345<br>A74-1132 E346<br>A74-1139 E355*<br>A75-351 E369<br>A75-354 E371<br>A75-359 E406<br>A75-363 E435<br>A75-370 E436 | F1665<br>E355* | A73-083 | A73-080<br>A74-739<br>A74-745<br>A74-752<br>A75-204<br>A75-254<br>A75-259<br>A75-301<br>E351<br>E384 | A74-055 E134<br>A74-216 E203<br>A74-268 E214<br>A74-275 E216<br>A74-384 E259<br>A74-561<br>A74-573<br>A74-580<br>A74-650<br>A74-652<br>A74-676<br>A74-685<br>A74-698<br>A74-894 | A74-363 A75-412<br>A74-722 A75-421<br>A74-730 A75-443<br>A74-732 A75-446<br>A74-733 A75-449<br>A74-735 A75-451<br>A74-747 A75-460<br>A74-757 A75-467<br>A74-761 A75-470<br>A74-1020 A75-481<br>A75-003 A75-501<br>A75-011 A75-505<br>A75-017 A75-511<br>A75-026 A75-516 | E340 A75-923 D2-40<br>E341 A75-931 E447*<br>E357 A75-938 E448*<br>E361 E452*<br>E363 E493<br>E370 E517<br>E402 E523<br>E407<br>E433<br>E434<br>E447*<br>E448*<br>E452*<br>E497<br>E525 | A75-382 E465<br>A75-804 E466<br>A75-806 E480<br>A75-810 E482<br>A75-815 E489<br>A75-824 E492<br>A75-857 E496<br>A76-010 E500<br>E510<br>E534 | E571 |
| Carbon | E403 | | | E313 E423<br>E314 E424<br>E385 E425<br>E389 E426<br>E394 E432<br>E418<br>E420<br>E421<br>E422 | | | | | A75-929 E471<br>E319 E472<br>E320 E473<br>E372<br>E388<br>E416<br>E453<br>E459<br>E468<br>E469 | A75-882 E501<br>A75-884 E503<br>A75-887 E508<br>A75-890 E511<br>A75-891 E513<br>A75-904 E524<br>A75-905 E535<br>A75-908 | |
| Boron | | | | E323 E382<br>E324 E398 | | | | | E333<br>E334 | | |
| Zirconium | | | | E315 E427<br>E383 E437 | | | | | E268 E365<br>E332 | | |
| Hafnium | | | | E312 E359 | | | | | E322 | | |
| Tantalum | | | | E414 E450<br>E417 | | | | | E419 | | |
| Carbon and Boron | | | | E397 | | | | | E368 | | |
| Carbon and Zirconium | | | | E395 E428 | | | | | E366 | | |
| Carbon and Hafnium | | | | E328 E392<br>E391 | | | | | E339<br>E367 | | |
| Carbon and Tantalum | | | | E431 | | | | | E430 | | |
| Boron and Zirconium | | | | E325<br>E396 | | | | | E338 | | |

*Material Evaluated in Two Phases

## APPENDIX A (Cont'd)

# TABLE XLVII
# SLAB CASTINGS

| Casting[1] Identification | Solidification Rate cm/hr. | Solidification Rate in./hr. | Cb C | Cr C | Composition Percent[2] C C | C A | B C | B A | Zr C | Zr A | Hf C | Hf A | Ta C | Ta A | Structure and Comments[3] | Method[4] of Carbon Addition | Phase of Program Where Casting Evaluated |
|---|---|---|---|---|---|---|---|---|---|---|---|---|---|---|---|---|---|
| E134 | 1.3 | 0.5 | 20.0 | 6.0 | – | – | – | – | – | – | – | – | – | – | Cellular | – | I |
| E203 | 1.3 | 0.5 | 20.0 | 6.0 | – | – | – | – | – | – | – | – | – | – | Cellular | – | I |
| E214 | 1.3 | 0.5 | 20.0 | 6.0 | – | – | – | – | – | – | – | – | – | – | Cellular, lamellar band (lamellarity not good) | – | I |
| E216 | 1.3 | 0.5 | 20.0 | 6.0 | – | – | – | – | – | – | – | – | – | – | Cellular | – | I |
| E259 | 1.3 | 0.5 | 20.0 | 6.0 | – | – | – | – | – | – | – | – | – | – | Cellular | – | I |
| E268 | 1.3 | 0.5 | 20.0 | 6.0 | – | – | – | – | 0.1 | 0.03 | – | – | – | – | Cellular | – | III |
| E288 | 1.3 | 0.5 | 21.2 | 1.0 | – | – | – | – | – | – | – | – | – | – | Lamellar | – | II |
| E312 | 1.3 | 0.5 | 21.2 | 1.0 | – | – | – | – | – | – | 1.0 | 0.9 to 0.6 | – | – | Cellular, δ dendritic | – | III |
| E313 | 1.3 | 0.5 | 21.2 | 1.0 | 0.1 | 0.07 | – | – | – | – | – | – | – | – | Lamellar | E | III |
| E314 | 1.3 | 0.5 | 21.2 | 1.0 | 0.02 | 0.004 | – | – | – | – | – | – | – | – | Lamellar | E | III |
| E315 | 1.3 | 0.5 | 21.2 | 1.0 | – | – | – | – | 0.1 | 0.03 | – | – | – | – | Lamellar, δ dendritic | – | III |
| E318 | 30, 1.3 | 12,0.5 | 21.2 | 1.0 | – | – | – | – | – | – | – | – | – | – | High rate cellular Transition δ dendritic Low rate lamellar, δ dendritic | – | II |
| E319 | 1.3 | 0.5 | 20.0 | 6.0 | 0.1 | 0.07 | – | – | – | – | – | – | – | – | Cellular δ dendritic | E | III |
| E320 | 1.3 | 0.5 | 20.0 | 6.0 | 0.02 | 0.02 | – | – | – | – | – | – | – | – | Cellular | E | III |
| E322 | 1.3 | 0.5 | 20.0 | 6.0 | – | – | – | – | – | – | 1.0 | 0.5 to 0.2 | – | – | Cellular δ dendritic | – | III |
| E323 | 1.3 | 0.5 | 21.2 | 1.0 | – | – | 0.04 | 0.028 to 0.014 | – | – | – | – | – | – | Lamellar bottom Cellular top δ dendritic | – | III |
| E324 | 1.3 | 0.5 | 21.2 | 1.0 | – | – | 0.01 | 0.010 to 0.004 | – | – | – | – | – | – | Lamellar, δ dendritic | – | III |
| E325 | 1.3 | 0.5 | 21.2 | 1.0 | – | – | 0.02 | 0.006 to 0.025 | 0.06 | <0.02 | – | – | – | – | Lamellar, δ dendritic | – | III |
| E328 | 1.3 | 0.5 | 21.2 | 1.0 | 0.05 | 0.05 | – | – | – | – | 0.6 | 0.3 | – | – | Essentially lamellar, δ dendritic | E | III |
| E329 | 1.3 | 0.5 | 21.2 | 1.0 | – | – | – | – | – | – | – | – | – | – | Lamellar, δ dendritic | – | II |
| E332 | 1.3 | 0.5 | 20.0 | 6.0 | – | – | – | – | 0.1 | 0.03 to 0.05 | – | – | – | – | Cellular | – | III |
| E333 | 1.3 | 0.5 | 20.0 | 6.0 | – | – | 0.05 | 0.05 | – | – | – | – | – | – | Cellular, grossly δ dendritic | – | III |
| E334 | 1.3 | 0.5 | 20.0 | 6.0 | – | – | 0.01 | 0.006 | – | – | – | – | – | – | Cellular, slightly δ dendritic | – | III |

# APPENDIX A (Cont'd)

## TABLE XLVII (Cont'd)

| Casting[1] Identification | Solidification Rate cm/hr. | Solidification Rate in./hr. | Composition Percent[2] Cb C | Cr C | C C | C A | B C | B A | Zr C | Zr A | Hf C | Hf A | Ta C | Ta A | Structure and Comments[3] | Method[4] of Carbon Addition | Phase of Program Where Casting Evaluated |
|---|---|---|---|---|---|---|---|---|---|---|---|---|---|---|---|---|---|
| E338 | 1.3 | 0.5 | 20.0 | 6.0 | – | – | 0.02 | 0.02 | 0.06 | 0.02 | – | – | – | – | Grossly cellular | – | III |
| E339 | 1.3 | 0.5 | 19.7 | 6.0 | 0.05 | 0.05 | – | – | – | – | 0.6 | 0.3 | – | – | Cellular | E | III |
| E340 | 1.3 | 0.5 | 20.0 | 6.0 | – | – | – | – | – | – | – | – | – | – | 3 per thermal fatigue wedges cellular | – | II |
| E341 | 1.3 | 0.5 | 20.0 | 6.0 | – | – | – | – | – | – | – | – | – | – | Cellular | – | II |
| E345 | 4 | 1.6 | 21.2 | 1.0 | – | – | – | – | – | – | – | – | – | – | Single 1 cm (0.375 in.) diameter bar | – | II |
| E346 | 2.5 | 1.0 | 21.2 | 1.0 | – | – | – | – | – | – | – | – | – | – | 3 per thermal fatigue wedges lamellar δ dendritic | | II |
| E351 | 1.9 | 0.75 | 20.5 | 3.0 | – | – | – | – | – | – | – | – | – | – | 3 per thermal fatigue wedges slightly cellular | – | II |
| E353 | 0.6 | 0.25 | 19.4 | 1.0 | – | – | – | – | – | – | 1.0 | – | – | – | γ dendritic | – | III |
| E354 | 3.1 | 1.25 | 21.3 | -0- | – | – | – | – | – | – | – | – | – | – | 3 per thermal fatigue wedges lamellar, | | II |
| E355 | 0.6 | 0.25 | 21.0 | 1.0 | – | – | – | – | – | – | – | – | – | – | Lamellar | – | II, III |
| E357 | 2.0 | 0.78 | 20.0 | 6.0 | – | – | – | – | – | – | – | – | – | – | 1 per 1 cm (3/8 in.) diameter bar - cellular | – | II |
| E359 | 0.6 | 0.25 | 20.3 | 1.0 | – | – | – | – | – | – | 1.0 | 0.8 | – | – | Lamellar - cellular | – | III |
| E361 | 2.0 | 0.78 | 20.0 | 6.0 | – | – | – | – | – | – | – | – | – | – | 1 per 1 cm (0.375 in.) dia. bar-cellular | – | II |
| E363 | 0.6-1.3 | 0.25-0.5 | 19.9 | 6.0 | – | – | – | – | – | – | – | – | – | – | Low rate lamellar high rate cellular | – | II |
| E365 | 1.3 | 0.5 | 20.0 | 6.0 | – | – | – | – | 0.2 | – | – | – | – | – | Cellular, slightly δ dendritic | – | III |
| E366 | 1.3 | 0.5 | 20.0 | 6.0 | 0.02 | 0.009 to 0.018 | – | – | 0.2 | – | – | – | – | – | Cellular | E | III |
| E367 | 1.3 | 0.5 | 20.0 | 6.0 | 0.1 | – | – | – | – | – | 0.6 | – | – | – | Cellular | E | III |
| E368 | 1.3 | 0.5 | 20.0 | 6.0 | 0.05 | – | 0.02 | – | – | – | – | – | – | – | Cellular-lamellar | E | III |
| E369 | 4 | 1.6 | 21.0 | 1.0 | – | – | – | – | – | – | – | – | – | – | 4 per 1.3 cm (0.5 in.) diameter bars-cellular | – | II |
| E370 | 2 | 0.78 | 20.0 | 6.0 | – | – | – | – | – | – | – | – | – | – | 1 per 1 cm (0.375 in.) diameter bar-cellular | – | II |
| E371 | 1.3 | 0.5 | 21.0 | 1.0 | – | – | – | – | – | – | – | – | – | – | 2.5 cm (1 in.) thick slab Alternating lamellar and cellular band | – | II |
| E372 | 1.3 | 0.5 | 20.5 | 6.0 | 0.1 | – | – | – | – | – | – | – | – | – | Grossly δ dendritic | E | III |
| E382 | 1.3 | 0.5 | 20.8 | 1.0 | – | – | 0.06 | 0.006 to 0.08 | – | – | – | – | – | – | Lamellar-cellular (Partial Runout) | – | III |
| E383 | 1.3 | 0.5 | 20.9 | 1.0 | – | – | – | – | 0.2 | 0.08 | – | – | – | – | Lamellar-cellular | – | III |
| E384 | 1.0 | 0.4 | 20.5 | 3.0 | – | – | – | – | – | – | – | – | – | – | Lamellar | – | II |
| E385 | 1.3 | 0.5 | 21.2 | 1.0 | 0.1 | 0.07 | – | – | – | – | – | – | – | – | Lamellar | E | III |
| E388 | 0.6 | 0.25 | 20.2 | 6.0 | 0.1 | 0.07 | – | – | – | – | – | – | – | – | Lamellar | E | III |
| E389 | 1.3 | 0.5 | 21.2 | 1.0 | 0.15 | 0.05 | – | – | – | – | – | – | – | – | Note - Undisolved carbon found in crucible after pour. Lamellar micro-structure | E | III |
| E391 | 0.6 | 0.25 | 20.4 | 1.0 | 0.08 | 0.05 | – | – | – | – | 1.0 | 1.0 to 0.5 | – | – | Cellular-lamellar | C | III |
| E392 | 0.6 | 0.25 | 20.4 | 1.0 | 0.15 | 0.05 | – | – | – | – | 1.0 | 0.5 | – | – | Cellular-lamellar, γ dendritic | E | III |

## APPENDIX A (Cont'd)

### TABLE XLVII (Cont'd)

| Casting[1] Identification | Solidification Rate cm/hr. | Solidification Rate in./hr. | Cb C | Cr C | Composition Percent[2] C C | C A | B C | B A | Zr C | Zr A | Hf C | Hf A | Ta C | Ta A | Structure and Comments[3] | Method[4] of Carbon Addition | Phase of Program Where Casting Evaluated |
|---|---|---|---|---|---|---|---|---|---|---|---|---|---|---|---|---|---|
| E394 | 1.3 | 0.5 | 21.2 | 1.0 | 0.08 | 0.05 | – | – | – | – | – | – | – | – | Lamellar | C | III |
| E395 | 0.6 | 0.25 | 20.9 | 1.0 | 0.08 | 0.05 | – | – | 0.2 | 0.10 to 0.15 | – | – | – | – | Lamellar | C | III |
| E396 | 0.6 | 0.25 | 20.8 | 1.0 | – | – | 0.06 | 0.07 to 0.006 | 0.2 | 0.04 to 0.10 | – | – | – | – | Lamellar | – | III |
| E397 | 1.3 | 0.5 | 20.9 | 1.0 | 0.08 | 0.07 | 0.06 | 0.01 to 0.06 | – | – | – | – | – | – | Lamellar-cellular | C | III |
| E398 | 1.3 | 0.5 | 20.9 | 1.0 | – | – | 0.02 | 0.003 to 0.04 | – | – | – | – | – | – | Lamellar-cellular | – | III |
| E402 | 1.3/0.6/1.3 1.0/25 | 0.5/0.25 0.5/0.38 10 | 20.0 | 6.0 | – | – | – | – | – | – | – | – | – | – | Cellular-lamellar-cellular | – | II |
| E403 | 25 | 10 | 21.6 | -0- | 0.1 | 0.05 | – | – | – | – | – | – | – | – | Lamellar | E | III |
| E406 | 1.3 | 0.5 | 21.0 | 1.0 | – | – | – | – | – | – | – | – | – | – | Lamellar | – | II |
| E407 | 0.6 | 0.25 | 20.0 | 6.0 | – | – | – | – | – | – | – | – | – | – | Lamellar | – | II |
| E414 | 1.3 | 0.5 | 19.1 | 1.0 | – | – | – | – | – | – | – | – | 3.0 | – | Cellular, slightly δ dendritic | – | III |
| E416 | 0.6 | 0.25 | 20.2 | 6.0 | 0.1 | 0.07 | – | – | – | – | – | – | – | – | Lamellar | E | III |
| E417 | 1.0 | 0.38 | 19.0 | 1.0 | – | – | – | – | – | – | – | – | 3.0 | 2.9 | Cellular | – | III |
| E418 | 1.3 | 0.5 | 21.2 | 1.0 | 0.1 | 0.07 | – | – | – | – | – | – | – | – | Lamellar | E | III |
| E419 | 0.6 | 0.25 | 18.0 | 6.0 | – | – | – | – | – | – | – | – | 3.0 | 3.3 | Cellular | – | III |
| E420 | 1.3 | 0.5 | 21.2 | 1.0 | 0.2 | 0.08 | – | – | – | – | – | – | – | – | Lamellar | E | III |
| E421 | 2.5 | 1.0 | 21.2 | 1.0 | 0.1 | 0.08 | – | – | – | – | – | – | – | – | Lamellar | E | III |
| E422 | 1.3 | 0.5 | 21.2 | 1.0 | 0.05 | 0.03 | – | – | – | – | – | – | – | – | Lamellar | E | III |
| E423 | 1.3 | 0.5 | 21.2 | 1.0 | 0.08 | 0.07 | – | – | – | – | – | – | – | – | Lamellar | E | III |
| E424 | 1.9 | 0.75 | 21.2 | 1.0 | 0.1 | 0.06 | – | – | – | – | – | – | – | – | Lamellar | E | III |
| E425 | 30.0 | 12.0 | 21.3 | 1.0 | 0.1 | 0.06 | – | – | – | – | – | – | – | – | Cellular | E | III |
| E426 | 1.3 | 0.5 | 21.2 | 1.0 | 0.15 | 0.03 | – | – | – | – | – | – | – | – | Chamber leak lamellar | E | III |
| E427 | 0.6 | 0.25 | 20.9 | 1.0 | – | – | – | – | 0.2 | 0.06 | – | – | – | – | 2.5 cm (1 inch) DS structure - furnace breakdown | – | III |
| E428 | 0.6 | 0.25 | 20.9 | 1.0 | 0.08 | 0.03 | – | – | 0.2 | 0.04 | – | – | – | – | | E | III |
| E430 | 0.6 | 0.25 | 18.3 | 6.0 | 0.1 | 0.07 | – | – | – | – | – | – | 3.0 | 2.9 | Cellular | E | III |
| E431 | 0.6 | 0.25 | 19.1 | 1.0 | 0.1 | 0.08 | – | – | – | – | – | – | 3.0 | 3.2 | Lamellar | N | III |
| E432 | 1.3 | 0.5 | 21.2 | 1.0 | 0.1 | 0.08 | – | – | – | – | – | – | – | – | Lamellar | N | III |
| E433 | 0.6 | 0.25 | 20.0 | 6.0 | – | – | – | – | – | – | – | – | – | – | Lamellar | – | II |
| E434 | 0.6 | 0.25 | 19.9 | 6.0 | – | – | – | – | – | – | – | – | – | – | Lamellar (short pour) | – | II |
| E435 | 1.3 | 0.5 | 21.0 | 1.0 | – | – | – | – | – | – | – | – | – | – | Lamellar | – | II |
| E436 | 1.3 | 0.5 | 21.1 | 1.0 | – | – | – | – | – | – | – | – | – | – | Lamellar | – | II |
| E437 | 0.6 | 0.25 | 20.9 | 1.0 | – | – | – | – | 0.2 | 0.02 | – | – | – | – | Lamellar | – | II |
| E447 | 0.6 | 0.25 | 20.0 | 6.0 | – | – | – | – | – | – | – | – | – | – | Lamellar | – | II, III |
| E448 | 0.6 | 0.25 | 20.0 | 6.0 | – | – | – | – | – | – | – | – | – | – | Lamellar | – | II, III |
| E450 | 0.6 | 0.25 | 19.0 | 1.0 | – | – | – | – | – | – | – | – | 3.0 | 3.1 | Lamellar | – | III |

# APPENDIX A (Cont'd)

## TABLE XLVII (Cont'd)

| Casting[1] Identification | Solidification Rate cm/hr. | Solidification Rate in./hr. | Composition Percent[2] Cb C | Cr C | C C | C A | B C | B A | Zr C | Zr A | Hf C | Hf A | Ta C | Ta A | Structure and Comments[3] | Method[4] of Carbon Addition | Phase of Program Where Casting Evaluated |
|---|---|---|---|---|---|---|---|---|---|---|---|---|---|---|---|---|---|
| E452 | 0.6 | 0.25 | 20.0 | 6.0 | – | – | – | – | – | – | – | – | – | – | Lamellar, δ dendritic at top | – | II, III |
| E453 | 0.6 | 0.25 | 20.1 | 6.0 | 0.06 | 0.05 | – | – | – | – | – | – | – | – | Lamellar | E | III |
| E459 | 0.6 | 0.25 | 20.1 | 6.0 | 0.08 | 0.08 | – | – | – | – | – | – | – | – | Partial runout lamellar | E | III |
| E465 | 0.6 | 0.25 | 20.1 | 6.0 | – | – | – | – | – | – | – | – | – | – | Lamellar | – | IV |
| E466 | 0.6 | 0.25 | 20.1 | 6.0 | – | – | – | – | – | – | – | – | – | – | Lamellar | – | IV |
| E468 | 0.6 | 0.25 | 20.1 | 6.0 | 0.04 | 0.03 | – | – | – | – | – | – | – | – | Cellular - lamellar | N | III |
| E469 | 0.6 | 0.25 | 20.1 | 6.0 | 0.8 | 0.07 | – | – | – | – | – | – | – | – | Lamellar | N | III |
| E471 | 0.6 | 0.25 | 20.1 | 6.0 | 0.10 | 0.08 | – | – | – | – | – | – | – | – | Lamellar | N | III |
| E472 | 0.6 | 0.25 | 20.1 | 6.0 | 0.12 | 0.08 | – | – | – | – | – | – | – | – | Lamellar | N | III |
| E473 | 0.6 | 0.25 | 20.1 | 6.0 | 0.10 | 0.07 | – | – | – | – | – | – | – | – | Lamellar | N | III |
| E480 | 0.6 | 0.25 | 20.0 | 6.0 | – | – | – | – | – | – | – | – | – | – | Lamellar | – | IV |
| E482 | 0.6 | 0.25 | 20.0 | 6.0 | – | – | – | – | – | – | – | – | – | – | Lamellar | – | IV |
| E489 | 0.6 | 0.25 | 20.0 | 6.0 | – | – | – | – | – | – | – | – | – | – | Lamellar | – | IV |
| E492 | 0.6 | 0.25 | 20.0 | 6.0 | – | – | – | – | – | – | – | – | – | – | Lamellar – short pour | – | IV |
| E493 | 1.0 | 0.38 | 20.0 | 6.0 | – | – | – | – | – | – | – | – | – | – | 0.3 cm (0.125 in.) thick slab - lamellar | – | III |
| E496 | 0.6 | 0.25 | 20.0 | 6.0 | – | – | – | – | – | – | – | – | – | – | Lamellar | – | IV |
| E497 | 0.6 | 0.25 | 20.0 | 6.0 | – | – | – | – | – | – | – | – | – | – | Lamellar | – | II |
| E500 | 0.6 | 0.25 | 20.0 | 6.0 | – | – | – | – | – | – | – | – | – | – | Lamellar | – | IV |
| E501 | 0.6 | 0.25 | 20.1 | 6.0 | 0.06 | – | – | – | – | – | – | – | – | – | Lamellar | N | IV |
| E503 | 0.6 | 0.25 | 20.1 | 6.0 | 0.06 | – | – | – | – | – | – | – | – | – | Lamellar | N | IV |
| E508 | 0.6 | 0.25 | 20.1 | 6.0 | 0.06 | – | – | – | – | – | – | – | – | – | Lamellar | N | IV |
| E510 | 0.6 | 0.25 | 20.0 | 6.0 | – | – | – | – | – | – | – | – | – | – | 1.3 cm (0.5 in.) thick slab | – | IV |
| E511 | 0.6 | 0.25 | 20.1 | 6.0 | 0.06 | – | – | – | – | – | – | – | – | – | Lamellar | N | IV |
| E513 | 0.6 | 0.25 | 20.1 | 6.0 | 0.06 | – | – | – | – | – | – | – | – | – | Lamellar | N | IV |
| E517 | 1.3 | 0.5 | 20.0 | 6.0 | – | – | – | – | – | – | – | – | – | – | 0.3 cm (0.125 in.) thick slab - cellular | – | III |
| E523 | 1.3 | 0.5 | 20.2 | 6.0 | – | – | – | – | – | – | – | – | – | – | 0.3 cm (0.125 in.) thick slab - cellular | – | III |
| E524 | 0.6 | 0.25 | 20.1 | 6.0 | 0.06 | – | – | – | – | – | – | – | – | – | 1.3 cm (0.5 in.) thick slab | N | IV |
| E525 | 1.3 | 0.5 | 20.0 | 6.0 | – | – | | – | – | – | – | – | – | – | Cellular | – | II |
| E534 | 0.6 | 0.25 | 20.0 | 6.0 | – | – | – | – | – | – | – | – | – | – | Lamellar | | IV |
| E535 | 0.6 | 0.25 | 20.1 | 6.0 | 0.06 | – | | – | – | – | – | – | – | – | Lamellar | N | IV |
| D2-40 | 1.0 | 0.38 | 20.0 | 6.0 | – | – | – | – | – | – | – | – | – | – | 0.3 cm (0.125 inch) thick slab made in LMC (Liquid Metal Cooled) Furnace-Cellular | | III |
| F1665 | 1.3 | 0.5 | 21.2 | 1.0 | – | – | – | – | – | – | – | – | – | – | Lamellar | | III |

Notes:

1 0.6 cm (0.25 inch) thick slab unless otherwise indicated

2 C indicates charge level
A indicates approximate analyzed level - See Appendix E for detailed chemical analysis results

3 3 per and 4 per refer to multiple castings made in a single run

4 E indicates carbon added in Elemental Form
C indicates carbon added as a CrC master alloy
N indicates carbon added as a NiC master alloy

APPENDIX A (Cont'd)

TABLE XLVIII
BRIDGMAN BAR CASTINGS

| Casting Identification | Solidification Rate cm/hr. | Solidification Rate in./hr. | Cb | Cr | C | Structure[1] | Phase of Program Where Casting Evaluated |
|---|---|---|---|---|---|---|---|
| A71-651 | 2 | 0.79 | 20.8 | 0 | – | Lamellar | IIA |
| A72-623 | 10 | 3.94 | 21.5 | 0 | – | Lamellar | IIA |
| A73-079 | 2.5 | 0.98 | 21.5 | 1.0 | – | Lamellar | IIA |
| A73-080 | 2.5 | 0.98 | 20.5 | 3.0 | – | Lamellar | IIA |
| A73-082 | 2.5/5/20 | 0.98/1.97 7.87 | 21.0 | 2.0 | – | Lamellar, δ dendritic on area evaluated | IIA |
| A74-055 | 3 | 1.18 | 20 | 6.0 | – | Cellular | I |
| A74-216 | 3 | 1.18 | 20 | 6.0 | – | Cellular | I |
| A74-268 | 3 | 1.18 | 20 | 6.0 | – | Cellular | I |
| A74-275 | 3 | 1.18 | 20 | 6.0 | – | Cellular | I |
| A74-363 | 2 | 0.79 | 20 | 6.0 | – | Lamellar with cellular bands | IIA |
| A74-384 | 3 | 1.18 | 20 | 6.0 | – | Cellular | I |
| A74-561 | 3 | 1.18 | 20 | 6.0 | – | Cellular | I |
| A74-573 | 3 | 1.18 | 20 | 6.0 | – | Cellular | I |
| A74-580 | 3 | 1.18 | 20 | 6.0 | – | Cellular | I |
| A74-650 | 3 | 1.18 | 20 | 6.0 | – | Cellular | I |
| A74-652 | 3 | 1.18 | 20 | 6.0 | – | Cellular | I |
| A74-676 | 3 | 1.18 | 20 | 6.0 | – | Cellular | I |
| A74-685 | 3 | 1.18 | 20 | 6.0 | – | Cellular | I |
| A74-698 | 3 | 1.18 | 20 | 6.0 | – | Cellular | I |
| A74-722 | 3 | 1.18 | 20 | 6.0 | – | Structure not evaluated (gradient measurement) | IIA |
| A74-730 | 3 | 1.18 | 20 | 6.0 | – | Structure not evaluated (gradient measurement) | IIA |
| A74-732 | 2 | 0.8 | 20 | 6.0 | – | Structure not evaluated (gradient measurement) | IIA |
| A74-733 | 5/10/20 | 2.0/3.9/7.9 | 20 | 6.0 | – | Structure not evaluated (gradient measurement) | IIA |
| A74-735 | 3 | 1.18 | 20 | 6.0 | – | Structure not evaluated (gradient measurement) | IIA |
| A74-739 | 7 | 2.76 | 20.8 | 3.0 | – | Cellular, δ dendritic | IIA |
| A74-745 | 5/3 | 1.97/1.18 | 20.8 | 3.0 | – | Various structures – see text, Section VIA | IIA |
| A74-747 | 3/6/9 | 1.18/2.36 3.54 | 20 | 6.0 | – | Structure not evaluated (gradient measurement) | IIA |

APPENDIX A (Cont'd)

TABLE XLVIII (Cont'd)

| Casting Identification | Solidification Rate cm/hr. | Solidification Rate in./hr. | Cb | Cr | C | Structure[1] | Phase of Program Where Casting Evaluated |
|---|---|---|---|---|---|---|---|
| A74-748 | 5/10 | 1.97/3.94 | 21.2 | 1.0 | – | Various structures – see text, Section VIA | IIA |
| A74-752 | 1/2/3/4 | 0.39/0.79/ 1.18/1.57 | 20.8 | 3.0 | – | Various structures – see text, Section VIA | IIA |
| A74-756 | 10/20 | 3.94/7.87 | 21.6 | 0 | – | Various structures – see text, Section VIA | IIA |
| A74-757 | 1/1.5/2 | 0.39/0.59/ 0.79 | 20 | 6.0 | – | Various structures – see text, Section VIA | IIA |
| A74-761 | 2.5/3/3.5/4 | 0.98/1.18/ 1.38/1.57 | 20 | 6.0 | – | Various structures – see text, Section VIA | IIA |
| A74-762 | 3/5/7/9 | 1.18/1.97/ 2.76/3.54 | 21.6 | 0 | – | Various structures – see text, Section VIA | IIA |
| A74-767 | 0.75/1/1.25 1.5 | 0.3/0.39/0.49 0.59 | 21.2 | 1.0 | – | Various structures – See text, Section VIA | IIA |
| A74-774 | 20/40 | 7.87/15.75 | 21.6 | 0 | – | Various structures – see text, Section VIA | IIA |
| A74-775 | 5/7/9 | 1.97/2.76 3.54 | 21.3 | 0 | – | Various structures – see text, Section VIA | IIA |
| A74-894 | 3 | 1.18 | 20 | 6.0 | – | Cellular | I |
| A74-1020 | 2 | 0.79 | 20 | 6.0 | – | Lamellar with cellular bands at low g – heavily oxidized at high g | IIB |
| A74-1036 | 4 | 1.57 | 21.2 | 1.0 | – | Lamellar | IIB |
| A74-1055 | 4 | 1.57 | 21.2 | 1.0 | – | Lamellar | IIB |
| A74-1064 | 4 | 1.57 | 21.2 | 1.0 | – | Lamellar | IIB |
| A74-1129 | 13 | 5.12 | 21.2 | 1.0 | – | Cellular | IIB |
| A74-1132 | 13 | 5.12 | 20 | 1.0 | – | Cellular | IIB |
| A74-1139 | 13 | 5.12 | 20 | 1.0 | – | Cellular | IIB |
| A75-003 | 5 | 1.97 | 20 | 6.0 | – | Cellular | IIB |
| A75-011 | 5 | 1.97 | 20 | 6.0 | – | Cellular | IIB |
| A75-017 | 5 | 1.97 | 20 | 6.0 | – | Cellular | IIB |
| A75-026 | 2 | 0.79 | 19.7 | 6.0 | – | Lamellar with cellular bands at low g – heavily oxidized at high g | IIB |
| A75-184 | 2 | 0.79 | 20.8 | 0 | – | Lamellar | IIB |

APPENDIX A (Cont'd)

TABLE XLVIII (Cont'd)

| Casting Identification | Solidification Rate cm/hr. | Solidification Rate in./hr. | Cb | Cr | C | Structure[1] | Phase of Program Where Casting Evaluated |
|---|---|---|---|---|---|---|---|
| A75-204 | 3 | 1.18 | 20.5 | 3.0 | – | Lamellar at low g, oxidized at high g | IIB |
| A75-224 | 100 | 39.37 | 20.3 | 0 | – | Lamellar | IIB |
| A75-229 | 6 | 2.36 | 21.2 | 0 | – | Lamellar | IIB |
| A75-235 | 38 | 14.96 | 21.9 | 0 | – | Lamellar | IIB |
| A75-254 | 3 | 1.18 | 20.5 | 3.0 | – | Lamellar at low g, oxidized at high g | IIB |
| A75-259 | 3 | 1.18 | 20.5 | 3.0 | – | Lamellar at low g, oxidized at high g | IIB |
| A75-298 | 17 | 6.69 | 21.55 | 0 | – | Lamellar, very slightly Cb lean | IIB |
| A75-301 | 3 | 1.18 | 20.4 | 3.0 | – | Lamellar at low g, oxidized at high g | IIB |
| A75-313 | 1 | 0.39 | 20.6 | 0 | – | Lamellar | IIB |
| A75-351 | 4 | 1.57 | 21.2 | 1.0 | – | Lamellar | IIB |
| A75-354 | 4 | 1.57 | 21.2 | 1.0 | – | Lamellar | IIB |
| A75-359 | 4 | 1.57 | 21.2 | 1.0 | – | Lamellar | IIB |
| A75-363 | 4 | 1.57 | 21.2 | 1.0 | – | Lamellar | IIB |
| A75-370 | 4 | 1.57 | 21.2 | 1.0 | – | Lamellar | IIB |
| A75-375 | 4 | 1.57 | 21.2 | 1.0 | – | Lamellar | IIB |
| A75-377 | 4 | 1.57 | 21.2 | 1.0 | – | Lamellar | IIB |
| A75-379 | 4 | 1.57 | 21.2 | 1.0 | – | Lamellar | IIB |
| A75-382 | 2 | 0.79 | 19.7 | 6.0 | – | Heavily banded, oxidized at high g | IV |
| A75-412 | 2 | 0.79 | 19.7 | 6.0 | – | Lamellar with cellular bands at low g – heavily oxidized at high g | IIB |
| A75-421 | 2 | 0.79 | 19.7 | 6.0 | – | Lamellar with cellular bands at low g – heavily oxidized at high g | IIB |
| A75-443 | 2 | 0.79 | 19.7 | 6.0 | – | Lamellar with cellular bands at low g – heavily oxidized at high g | IIB |
| A75-446 | 2 | 0.79 | 19.7 | 6.0 | – | Lamellar with cellular bands at low g - heavily oxidized at high g | IIB |
| A75-449 | 2 | 0.79 | 19.7 | 6.0 | – | Lamellar with cellular bands at low g – heavily oxidized at high g | IIB |

APPENDIX A (Cont'd)
TABLE XLVIII (Cont'd)

| Casting Identification | Solidification Rate cm/hr. | Solidification Rate in./hr. | Cb | Cr | C | Structure[1] | Phase of Program Where Casting Evaluated |
|---|---|---|---|---|---|---|---|
| A75-451 | 2 | 0.79 | 19.7 | 6.0 | – | Lamellar with cellular bands at low g, heavily oxidized at high g | IIB |
| A75-460 | 2 | 0.79 | 19.7 | 6.0 | – | Lammellar with cellular bands at low g, heavily oxidized at high g | IIB |
| A75-467 | 2 | 0.79 | 19.7 | 6.0 | – | Lamellar with cellular bands at low g, heavily oxidized at high g | IIB |
| A75-470 | 2 | 0.79 | 19.7 | 6.0 | – | Lamellar with cellular bands at low g, heavily oxidized at high g | IIB |
| A75-481 | 2 | 0.79 | 19.7 | 6.0 | – | Lamellar with cellular bands at low g, heavily oxidized at high g | IIB |
| A75-501 | 2 | 0.79 | 19.7 | 6.0 | – | Lamellar with cellular bands at low g, heavily oxidized at high g | IIB |
| A75-505 | 2 | 0.79 | 19.7 | 6.0 | – | Lamellar with cellular bands at low g, heavily oxidized at high g | IIB |
| A75-511 | 2 | 0.79 | 19.7 | 6.0 | – | Lamellar with cellular bands at low g, heavily oxidized at high g | IIB |
| A75-516 | 2 | 0.79 | 19.7 | 6.0 | – | Lamellar with cellular bands at low g, heavily oxidized at high g | IIB |
| A75-804 | 2 | 0.79 | 20 | 6.0 | – | Lamellar with cellular bands – heavily oxidized throughout | IV |
| A75-806 | 2 | 0.79 | 20 | 6.0 | – | Heavily banded – oxidized at high g | IV |
| A75-810 | 2 | 0.79 | 20 | 6.0 | – | Heavily banded, oxidized at high g | IV |
| A75-815 | 2 | 0.79 | 20 | 6.0 | – | Lamellar with cellular bands – oxidized throughout | IV |
| A75-824 | 2 | 0.79 | 20 | 6.0 | – | Lamellar with cellular bands – heavily oxidized throughout | IV |
| A75-857 | 2 | 0.79 | 20 | 6.0 | – | Lamellar with cellular bands – oxidized throughout | IV |
| A75-882 | 2 | 0.79 | 20 | 6.0 | 0.06 | Lamellar with cellular bands – heavily oxidized throughout | IV |
| A75-884 | 2 | 0.79 | 20 | 6.0 | 0.06 | Lamellar with cellular bands – heavily oxidized throughout | IV |

APPENDIX A (Cont'd)

TABLE XLVIII (Cont'd)

| Casting Identification | Solidification Rate cm/hr. | Solidification Rate in./hr. | Cb | Cr | C | Structure[1] | Phase of Program Where Casting Evaluated |
|---|---|---|---|---|---|---|---|
| A75-887 | 2 | 0.79 | 20 | 6.0 | 0.06 | Lamellar with cellular bands – heavily oxidized throughout | IV |
| A75-890 | 2 | 0.79 | 20 | 6.0 | 0.06 | Lamellar with cellular bands – heavily oxidized throughout | IV |
| A75-891 | 2 | 0.79 | 20 | 6.0 | 0.06 | Lamellar, no bands, oxidized at high g | IV |
| A75-904 | 2 | 0.79 | 20 | 6.0 | 0.06 | Lamellar, lightly banded, oxidized at high g | IV |
| A75-905 | 2 | 0.79 | 20 | 6.0 | 0.06 | Lamellar, lightly banded, oxidized throughout | IV |
| A75-908 | 2 | 0.79 | 20 | 6.0 | 0.06 | Lamellar with cellular bands – heavily oxidized throughout | IV |
| A75-923 | 2.5 | 0.98 | 20 | 6.0 | – | Structure not evaluated (gradient measurement) | III |
| A75-929 | 1.75/2/ 2.25/2.5 | 0.69/0.79 0.89/0.98 | 20 | 6.0 | 0.06 | Various structures – see text, Section VII E | III |
| A75-931 | 1.75/2/ 2.25/2.5 | 0.69/0.79 0.89/0.98 | 20 | 6.0 | – | Various structures – see text, Section VII E | III |
| A75-938 | 2.5 | 0.98 | 20 | 6.0 | – | Structure not evaluated (gradient measurement) | III |
| A76-010 | 2 | 0.79 | 20.8 | 6.0 | – | Lamellar with cellular bands at low g, heavily oxidized at high g | IV |

1 Note that while essentially all of the lamellar 6% Cr castings solidified at 2 cm/hour contained cellular bands, it generally was possible to find a band free section at least 2.5 cm (1 nch) in length in which the gage section of the specimen shown in Figure 11 of the text was located. The letter g refers to approximate fraction solidified.

## APPENDIX B

## METHODS USED FOR ANALYSIS OF TENSION TEST RESULTS

The purpose of this Appendix is to describe methods used for accurate measurement of the relatively small (< 1 percent) transverse tensile ductilities of the $\gamma/\gamma' - \delta$ alloy. Methods for modulus measurement will also be discussed. Two specific items require clarification. The first involves measurement of transverse ductility; the following discussion will explain why fracture strain is used instead of total elongation to characterize this property in the directionally solidified eutectic alloy. The second item to be discussed is the method used to calculate elastic modulus from experimental load-extension data.

### A. DUCTILITY MEASUREMENT

For materials of limited ductility, measurement of elongation from specimen length change is subject to relatively large errors associated with fitting the specimen back together after testing. Elongation values reported for low ductility materials thus typically exhibit large amounts of scatter associated with random differences in the exactness with which the broken halves of a specimen are rejoined, and also a systematic error attributable to the fact that the two halves are never rejoined perfectly. Where elongations of less than 1% are involved, fit-up error can equal or exceed the actual amount of plastic strain accumulated at failure and total elongation becomes completely unreliable as a measure of ductility, particularly where comparison of materials with small ductility differences is of primary concern. For this reason, the transverse ductility of the $\gamma/\gamma' - \delta$ eutectic alloy was measured from load-deflection curves obtained from an LVDT type extensometer attached directly to the tension test specimen.

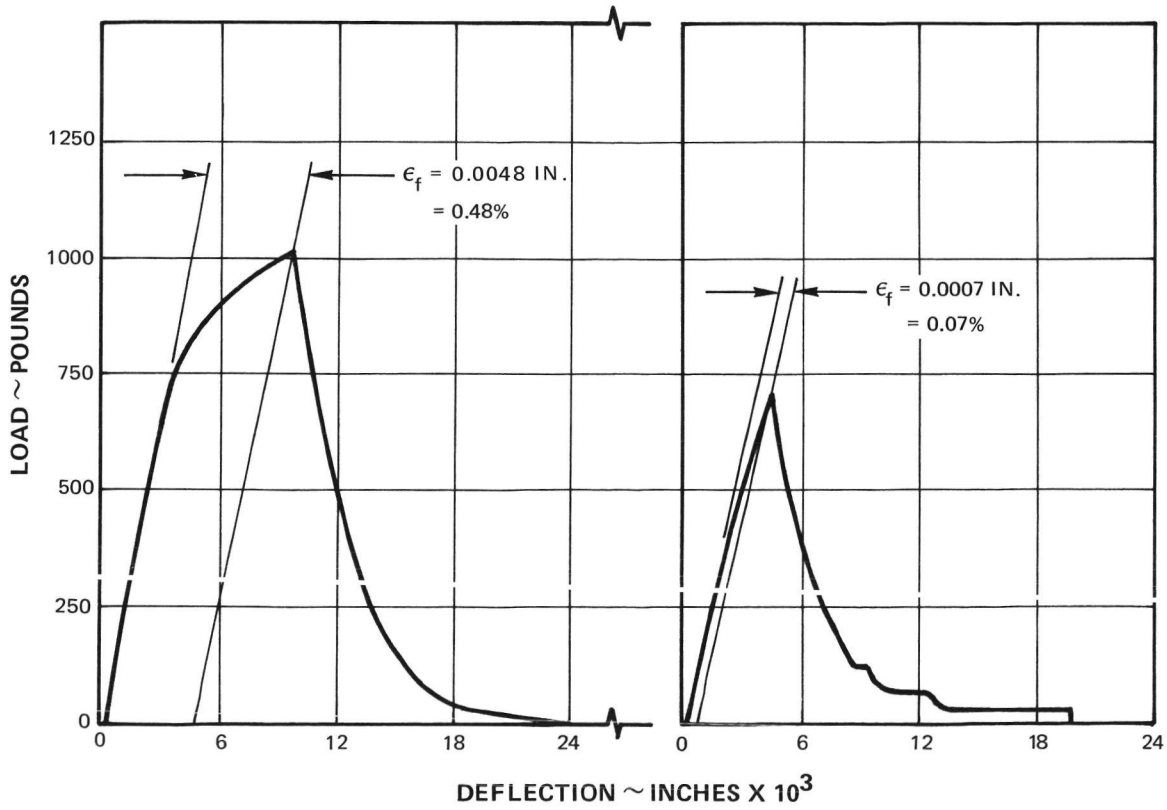
The method used to measure elongation from the load-elongation curve is illustrated in Figure 164. A line is drawn through the point of peak load parallel to the elastic part of the curve, and the offset between this line and the elastic line is taken as the total plastic strain accumulated at fracture. Comparison of the plastic offsets measured in this way with the total elongations measured after test for the two specimens represented in Figure 164 shows how misleading the total elongation figure can be in attempting to evaluate comparative ductilities between two materials with low intrinsic ductility.

### B. CALCULATION OF ELASTIC MODULUS

Where quoted, elastic modulus values were calculated from the slope of the elastic part of the load-deflection curve. Because the extensometer is attached to the shoulder of the specimen used for these tests (see Figure 11 in the main body of the report), it is necessary to correct measured modulus values for elastic deflection which occurs in the shoulder and radius areas of the specimen. Distribution of elastic strain between the extensometer attachment points on this specimen is shown in Figure 165. Areas under various parts of this curve represent displacements in corresponding parts of the specimen. The area under the curve representing the radius section of the specimen was obtained by numerical integration of the equation.

$$\delta = \epsilon^{dx} = \frac{p}{\pi^E} \int \frac{1}{r_o + R - \sqrt{R^2 - x^2}} \qquad \text{(B-1)}$$

where $\delta$ is displacement, p is applied load, and $\epsilon$ is strain (see Figure 166). Areas under the rectangular parts of the curve were obtained by straightforward multiplication of strain times length of section. Percentages of the total area under each part of the curve are noted in Figure 165. These results indicate that the slope of the elastic load-displacement curve must be divided by 0.8628 (the fraction of the total displacement which occurs in the one-inch gage section) to obtain the correct value for modulus. This correction has been applied to all modulus data reported.

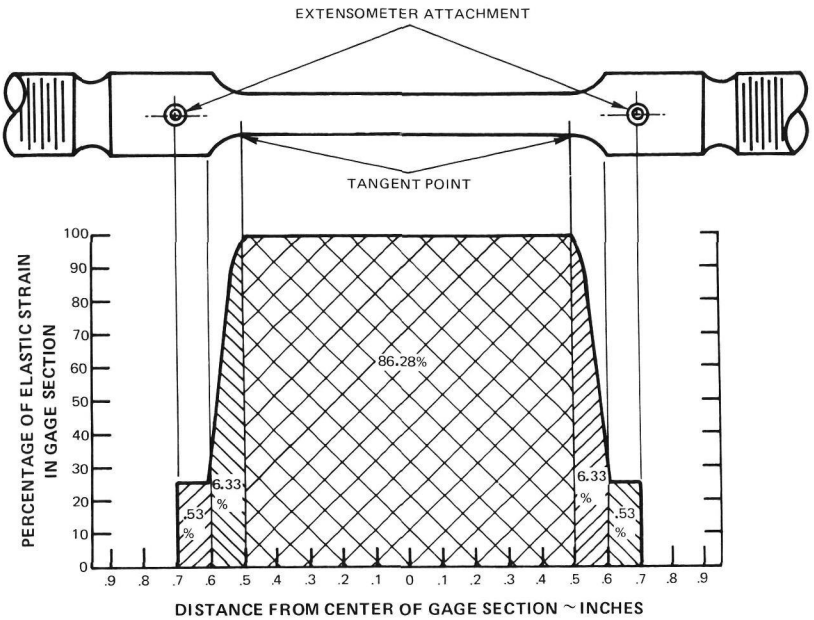



a) SPECIMEN E313-J1
TOTAL ELONGATION - 0.9%

b) SPECIMEN E312K
TOTAL ELONGATION = 2.8%

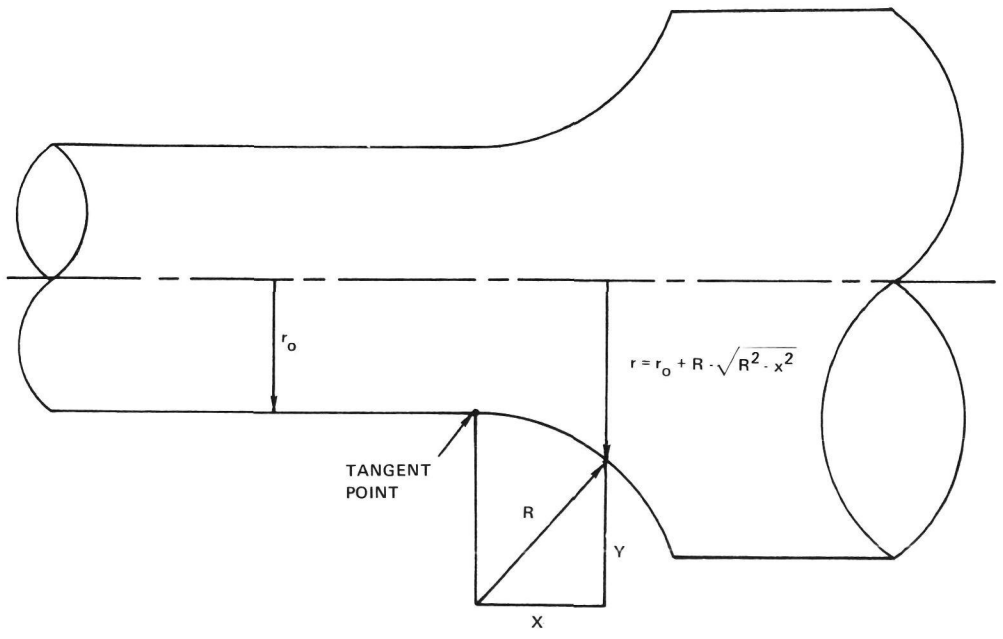
R14-184

Figure 164 Typical Load-Deflection Curves Observed for 760°C (1400°F) Transverse Tensile Tests of Modified 1%Cr $\gamma/\gamma'$ - $\delta$ Eutectic Alloys




R14-185

Figure 165 Distribution of Elastic Strain in Specimen Used for Measurement of Tensile Properties




R14-186

Figure 166 Definition of Symbols Used in Equation 164

## APPENDIX C

## QUANTITATIVE METALLOGRAPHIC MEASUREMENTS

### A. INTERLAMELLAR SPACING MEASUREMENTS

Interlamellar spacing measurements were made on photomicrographs at various magnifications (primarily 200X) using a 10X magnifier and a steel scale ruled at 0.01 inch intervals. For each measurement, an effort was made to span the largest possible number of lamellae having consistent spacings (See, for example, Figure 167a) to obtain statistically significant averages with the smallest possible number of measurements. For the case of partially cellular structures, the reported values represent spacings measured in areas having a lamellar structure, as illustrated in Figure 167b. Results of these measurements are presented in Table XLIX. Composition and processing parameters for each structure examined may be found in Table XIII and Figure 72 in the main body of the report for material produced in this program, and in Table L for previously produced material.

### B. VOLUME FRACTION MEASUREMENTS

Measurements of volume fraction lamellar structure and $Ni_3Cb$ phase were made by the method of point counting on photomicrographs of transverse sections cut from directionally solidified bars. Measurements were made at various magnifications using a 7X7 array of 49 points engraved at 0.25 inch intervals on transparent overlay. Photomicrographs were examined through the overlay with a 2X hand lens to determine where each point was located in the microstructure. The number of points falling within the feature of interest was counted and the total was divided by the number of points applied to determine the volume fraction present. Where the interpretation of point location was not clear (e.g., when the point was located exactly on the edge of a feature), one-half count was accumulated. Except for cases where specific microstructural features (such as dendritic $Ni_3Cb$) were avoided, the array was successively relocated to cover the entire area visible in each of the 8.9 X 11.4 cm (3.5 X 4.5 inch) prints evaluated. Results of these measurements are presented in Table LI. Additonal procedural details relating to the various features evaluated are noted below.

The volume fraction of lamellar $Ni_3Cb$ was measured on 1000X photomicrographs with 10 counts (a total of 490 points applied) being made on each micrograph examined. As illustrated in Figure 168, significant variability of $V_\delta$ was observed from area to area within a given microstructure. While it would have been desirable to make measurements on lower magnification prints so that a statistically significant area could be covered, it was found that sufficient resolution was not available at lower magnifications to clearly distinguish the location of the points in the lamellar microstructure. To cover a larger area and achieve statistical significance, it was therefore necessary to evaluate a large number of 1000X photomicrographs taken in randomly selected locations on each section. As indicated in Table LI, the number of photomicrographs evaluated to measure the volume fraction of lamellar $Ni_3Cb$ in each of the plane front microstructures ranged between 12 and 18.

Volume fraction lamellar structure and dendritic $Ni_3Cb$ measurements were made on photomicrographs with magnifications between 50 and 200X, so that statistical significance was achieved with a substantially smaller number of measurements. Ten counts (490 points applied) were made on each photomicrograph evaluated for volume fraction lamellarity. Because of the lower volume fractions of dendritic $Ni_3Cb$ present in typical structures, it was necessary to make 20 counts (980 points applied) to obtain meaningful measurements.

APPENDIX C (Cont'd)

TABLE XLIX

LAMELLAR SPACING MEASUREMENTS ON DIRECTIONALLY SOLIDIFIED $\gamma/\gamma'$ - $\delta$ EUTECTIC ALLOYS CONTAINING VARIOUS LEVELS OF CHROMIUM

| | 0 Cr A72-623* 10 cph | 0 Cr A71-651* 2 cph | 0 Cr A74-756 10 cph | 0 Cr A74-756* 20 cph | 0 Cr A74-774* 20 cph | 0 Cr A74-774* 40 cph | 0 Cr A74-762 3 cph | 0 Cr A74-762 5 cph | 0 Cr A74-762 7 cph |
|---|---|---|---|---|---|---|---|---|---|
| | 2.6 | 7.6 | 2.6 | 2.1 | 1.9 | 1.4 | 5.7 | 4.3 | 4.7 |
| | 2.4 | 6.3 | 3.0 | 1.6 | 2.1 | 1.7 | 4.0 | 7.0 | 3.8 |
| | 2.2 | 7.3 | 2.9 | 1.5 | 2.0 | 1.1 | 5.9 | 4.0 | 3.6 |
| | 3.3 | 6.7 | 3.0 | 2.5 | 1.5 | 1.4 | 5.3 | 5.6 | 4.9 |
| | 2.2 | 8.4 | 2.6 | 3.2 | 1.6 | 1.2 | 4.7 | 4.0 | 4.9 |
| | 3.4 | 4.9 | 2.6 | 2.1 | 1.8 | 1.5 | 3.1 | 4.7 | 3.7 |
| | 2.3 | 6.2 | 2.6 | 1.4 | 1.6 | 1.7 | 5.4 | 3.6 | 3.7 |
| | 2.7 | – | 2.5 | 2.3 | 1.6 | 1.5 | 7.0 | 3.1 | 3.9 |
| | 3.4 | – | 2.6 | 1.7 | 2.1 | 1.4 | 6.7 | 3.5 | 4.7 |
| | 2.8 | – | 2.5 | 1.8 | 2.3 | 1.3 | 4.9 | 4.3 | 2.8 |
| | – | – | – | – | – | – | 4.8 | – | 4.3 |
| Average | 2.7 | 6.0 | 2.7 | 2.0 | 1.9 | 1.4 | 5.2 | 4.4 | 4.1 |
| Std. Dev. | 0.5 | 1.1 | 0.2 | 0.5 | 0.3 | 0.2 | 1.1 | 1.1 | 0.7 |
| 95% Conf. Int. | ± 0.3 | ± 1.1 | ± 0.1 | ± 0.4 | ± 0.2 | ± 0.1 | ± 0.8 | ± 0.8 | ± 0.4 |

NOTES:

*Measured at 1000X

cph indicates solidification rate in cm/hr

APPENDIX C (Cont'd)

TABLE XLIX (Cont'd)

| | 0 Cr A74-775 5 cph | 0 Cr A74-775 7 cph | 0 Cr A74-775 9 cph | 1 Cr A73-079 2.5 cph | 1 Cr A74-748 5 cph | 1 Cr A74-748 10 cph | 1 Cr A74-767 .71 cph | 1 Cr A74-767 1 cph | 1 Cr A74-767 1.25 cph | 1 Cr A74-767 1.5 cph |
|---|---|---|---|---|---|---|---|---|---|---|
| | 3.7 | 3.7 | 3.4 | 5.0 | 3.5 | 2.3 | 8.7 | 10.0 | 6.7 | 6.4 |
| | 3.8 | 4.4 | 3.6 | 4.0 | 3.3 | 2.8 | 10.3 | 9.8 | 8.6 | 6.4 |
| | 3.4 | 3.5 | 3.4 | 4.8 | 2.8 | 2.2 | 9.3 | 8.9 | 8.5 | 6.0 |
| | 4.7 | 3.8 | 3.3 | 4.0 | 3.3 | 2.7 | 9.3 | 7.4 | 7.7 | 6.6 |
| | 4.3 | 4.0 | 2.5 | 5.0 | 2.9 | 2.8 | 10.6 | 5.9 | 7.2 | 7.1 |
| | 4.1 | 3.8 | 3.1 | 4.5 | 3.2 | 2.8 | 9.4 | 8.5 | 7.0 | 7.1 |
| | 4.3 | 3.2 | 2.5 | 4.7 | 3.2 | 3.1 | 9.3 | 7.4 | 5.7 | 4.2 |
| | 3.3 | 3.2 | 4.1 | 5.5 | 3.5 | 2.9 | 7.7 | 9.1 | 8.0 | 6.5 |
| | 4.6 | 3.8 | 3.6 | – | 3.3 | 2.3 | 8.8 | 8.6 | 7.6 | 7.1 |
| | 5.4 | 3.7 | 4.0 | – | 3.4 | 3.0 | 10.4 | 8.5 | 8.5 | 7.6 |
| | – | 3.7 | – | – | – | – | 10.6 | 9.4 | – | 6.7 |
| | – | – | – | – | – | – | 8.5 | – | – | 5.6 |
| | – | – | – | – | – | – | 9.1 | – | – | 9.9 |
| | – | – | – | – | – | – | 9.6 | – | – | 6.0 |
| | – | – | – | – | – | – | 9.3 | – | – | 4.9 |
| | – | – | – | – | – | – | – | – | – | 7.6 |
| | – | – | – | – | – | – | – | – | – | 4.4 |
| | – | – | – | – | – | – | – | – | – | 7.6 |
| | – | – | – | – | – | – | – | – | – | 7.4 |
| | – | – | – | – | – | – | – | – | – | 4.9 |
| Avg. | 4.2 | 3.7 | 3.4 | 4.7 | 3.2 | 2.7 | 9.4 | 8.5 | 7.6 | 6.5 |
| Std. Dev. | 0.6 | 0.3 | 0.5 | 0.5 | 0.2 | 0.3 | 0.8 | 1.2 | 0.9 | 1.3 |
| 95% Conf. Int. | ± 0.5 | ± 0.2 | ± 0.4 | ± 0.4 | ± 0.2 | ± 0.2 | ± 0.5 | ± 0.8 | ± 0.7 | ± 0.6 |

APPENDIX C (Cont'd)

TABLE XLIX (Cont'd)

| | 3 Cr A73-080 2.5 cph | 3 Cr A74-739* 7 cph | 3 Cr A74-745 3 cph | 3 Cr A74-745 5 cph | 3 Cr A74-752 2 cph | 3 Cr A74-752 3 cph |
|---|---|---|---|---|---|---|
| | 4.0 | 1.9 | 3.4 | 3.8 | 4.5 | 4.8 |
| | 3.8 | 2.1 | 3.3 | 2.6 | 4.7 | 4.1 |
| | 4.0 | 2.5 | 3.8 | 3.0 | 5.9 | 3.4 |
| | 3.8 | 2.1 | 4.1 | 2.7 | 6.4 | 3.6 |
| | 4.3 | 2.6 | 4.2 | 3.0 | 4.7 | 3.8 |
| | 4.6 | 2.3 | 4.0 | 3.1 | 5.0 | 3.8 |
| | – | 2.0 | 3.6 | 3.6 | 5.0 | 3.3 |
| | – | 3.6 | 3.7 | 3.8 | 4.2 | 5.3 |
| | – | 2.6 | 3.9 | 3.7 | 6.1 | 3.9 |
| | – | 2.0 | 4.0 | 2.8 | 4.9 | 4.1 |
| | – | 2.3 | 3.4 | 2.6 | 5.9 | 3.9 |
| | – | 2.1 | 4.2 | 3.1 | 5.0 | 3.7 |
| | – | 1.8 | 4.0 | 3.6 | 4.3 | 4.0 |
| | – | – | 3.6 | 3.8 | 4.2 | 4.8 |
| | – | – | 2.5 | 3.1 | 7.4 | 3.9 |
| | – | – | 3.4 | 2.7 | 5.3 | 4.3 |
| | – | – | 3.1 | 3.3 | 4.7 | 3.4 |
| | – | – | 3.4 | 3.1 | 6.6 | 4.0 |
| | – | – | 3.1 | 3.6 | 2.9 | 3.8 |
| | – | – | 3.7 | 3.9 | 5.1 | 4.0 |
| Avg. | 4.1 | 2.3 | 3.6 | 3.2 | 5.1 | 4.0 |
| Std. Dev. | 0.3 | 0.5 | 0.4 | 0.4 | 1.0 | 0.5 |
| 95% Conf. Int. | ± 0.3 | ± 0.3 | ± 0.2 | ± 0.2 | ± 0.5 | ± 0.2 |

APPENDIX A (Cont'd)

TABLE XLIX (Cont'd)

| | 6 Cr A74-363 2 cph | 6 Cr A74-761 2.5 cph | 6 Cr A74-761 3 cph | 6 Cr A74-761 3.5 cph | 6 Cr A74-761 4 cph | 6 Cr A74-757 1 cph | 6 Cr A74-757 1.5 cph | 6 Cr A74-757 2 cph |
|---|---|---|---|---|---|---|---|---|
| | 4.3 | 4.0 | 3.0 | 3.1 | 2.4 | 5.2 | 4.8 | 3.8 |
| | 4.0 | 2.6 | 3.4 | 2.8 | 2.6 | 9.1 | 8.7 | 4.9 |
| | 3.4 | 3.6 | 3.4 | 2.9 | 2.8 | 7.8 | 4.7 | 9.7 |
| | 3.7 | 3.6 | 3.5 | 3.1 | 2.7 | 7.4 | 6.5 | 4.4 |
| | 4.1 | 3.2 | 2.6 | 3.3 | 2.7 | 6.2 | 5.1 | 5.6 |
| | 4.1 | 3.9 | 3.0 | 2.6 | 2.6 | 5.7 | 5.0 | 4.1 |
| | 4.8 | 3.5 | 3.1 | 2.4 | 2.8 | 5.3 | 4.5 | 4.0 |
| | 4.0 | 3.8 | 4.0 | 3.0 | 2.7 | 5.4 | 7.5 | 6.4 |
| | 5.2 | 3.7 | 2.8 | 3.4 | 2.4 | 8.8 | 4.4 | 4.7 |
| | 4.2 | 3.9 | 4.1 | 3.4 | 2.9 | 12.5 | 5.0 | 3.9 |
| | 4.2 | 3.0 | 3.8 | – | 3.1 | 6.8 | – | 3.7 |
| | – | 3.6 | 3.6 | – | – | 5.8 | – | 4.7 |
| | – | – | 3.2 | – | – | 4.9 | – | 3.4 |
| | – | – | 3.5 | – | – | 6.5 | – | 5.6 |
| | – | – | 3.2 | – | – | 9.5 | – | 3.5 |
| | – | – | – | – | – | 8.3 | – | 3.6 |
| | – | – | – | – | – | 6.9 | – | 6.8 |
| | – | – | – | – | – | 5.9 | – | 4.3 |
| | – | – | – | – | – | 6.5 | – | 5.0 |
| | – | – | – | – | – | 5.4 | – | 4.2 |
| | – | – | – | – | – | 6.1 | – | – |
| | – | – | – | – | – | 8.3 | – | – |
| | – | – | – | – | – | 7.8 | – | – |
| | – | – | – | – | – | 4.5 | – | – |
| | – | – | – | – | – | 7.7 | – | – |
| | – | – | – | – | – | 8.6 | – | – |
| | – | – | – | – | – | 9.2 | – | – |
| | – | – | – | – | – | 4.1 | – | – |
| | – | – | – | – | – | 9.9 | – | – |
| | – | – | – | – | – | 8.7 | – | – |
| Average | 4.2 | 3.5 | 3.3 | 3.0 | 2.7 | 7.2 | 5.6 | 4.8 |
| Std. Dev. | 0.5 | 0.4 | 0.4 | 0.3 | 0.2 | 1.9 | 1.5 | 1.5 |
| 95% Conf. Int. | ± 0.3 | ± 0.3 | ±0.2 | ± 0.2 | ± 0.1 | ± 0.7 | ± 1.0 | ±1.1 |

APPENDIX C (Cont'd)

TABLE L

COMPOSITION AND PROCESSING DETAILS FOR SUPPLEMENTARY MATERIAL SUBJECTED TO MICROSTRUCTURAL EVALUATION

| Run No. | Composition, Wt. Pct. (Bal Ni) Cb | Al | Cr | Solidification Rate, cm/hr |
|---|---|---|---|---|
| A71-651* | 20.8 | 2.8 | 0 | 2 |
| A72-623* | 21.5 | 2.5 | 0 | 10 |
| A73-079 | 21.5 | 2.5 | 1 | Various |
| A73-082 | 21.0 | 2.5 | 2 | Various |
| A73-080 | 20.5 | 2.5 | 3 | Various |
| A74-363 | 20.0 | 2.5 | 6 | 2 |

* These two ingots were produced under contract NAS3-15562; additional documentation may be found in the Final Report by F. D. Lemkey, "Eutectic Superalloys Strengthened by $\delta$, $Ni_3Cb$ Lamellar and $\gamma'$, $Ni_3Al$ Precipitates", NASA-CR-2278, November 1973.

Material grown in the form of 1.3 cm (1/2 inch) diameter bars in a high gradient modified Bridgman furnace. Gradients not measured, but though to be on the order of 300°C/cm.

## APPENDIX C (Cont'd)

## TABLE LI

### RESULTS OF VOLUME FRACTION MEASUREMENTS ON VARIOUS DIRECTIONALLY SOLIDIFIED $\gamma/\gamma'$-$\delta$ EUTECTIC ALLOYS

| Run No. | Wt % Cr | Wt % Cb | Gradient C°/cm | Rate, cm/hr. | G/R C° hr/cm² | (G/R)/ (G/R)* | Measured Volume Fraction Lamellar Structure | Measured Volume Fraction Dendritic $Ni_3Cb$ | Measured Volume Fraction $Ni_3Cb$ in Dendrite Free Areas | Calculated Volume Fraction Lamellar $Ni_3Cb$ in Structure | Total** Volume Fraction $Ni_3Cb$ in Structure |
|---|---|---|---|---|---|---|---|---|---|---|---|
| A74-756 | 0 | 21.6 | 360 | 10 | 36 | – | – | 0.020 | 0.325 | 0.319 | 0.339 (C) |
| | 0 | 21.6 | 360 | 20 | 18 | – | – | 0 | 0.333 | – | 0.333 |
| | 0 | 21.6 | 360 | 20 | 18 | – | – | 0 | 0.331 | – | 0.331 |
| | 0 | 21.6 | 360 | 20 | 18 | – | – | 0 | 0.349 | – | 0.349 |
| | 0 | 21.6 | 360 | 20 | 18 | – | – | 0 | 0.331 | – | 0.331 |
| | 0 | 21.6 | 360 | 20 | 18 | – | – | 0 | 0.376 | – | 0.376 |
| A74-774 | 0 | 21.8 | 360 | 20 | 18 | – | – | 0.046 | 0.301 | 0.287 | 0.333 (C) |
| | 0 | 21.8 | 360 | 40 | 9 | – | – | 0 | 0.350 | – | 0.350 |
| | 0 | 21.8 | 360 | 40 | 9 | – | – | 0 | 0.341 | – | 0.341 |
| | 0 | 21.8 | 360 | 40 | 9 | – | – | 0 | 0.360 | – | 0.360 |
| | 0 | 21.8 | 360 | 40 | 9 | – | – | 0 | 0.331 | – | 0.331 |
| | 0 | 21.8 | 360 | 40 | 9 | – | – | 0 | 0.333 | – | 0.333 |
| A74-775 | 0 | 21.3 | 68 | 5 | 14 | – | – | 0 | 0.326 | – | 0.326 |
| | 0 | 21.3 | 68 | 7 | 10 | – | – | 0 | 0.358 | – | 0.358 |
| | 0 | 21.3 | 68 | 9 | 8 | – | – | 0 | 0.298 | – | 0.298 |
| | 0 | 21.3 | 68 | 9 | 8 | – | – | 0 | 0.350 | – | 0.350 |
| | 0 | 21.3 | 68 | 9 | 8 | – | – | 0 | 0.332 | – | 0.332 |
| A74-762 | 0 | 21.6 | 68 | 3 | 23 | – | – | 0.068 | 0.327 | 0.305 | 0.373 (C) |
| | 0 | 21.6 | 68 | 5 | 14 | – | – | 0.041 | 0.333 | 0.319 | 0.360 (C) |
| | 0 | 21.6 | 68 | 7 | 10 | – | – | 0.027 | 0.343 | 0.334 | 0.361 (C) |

**(C) Calculated from Measured Volume Fraction Dendritic $Ni_3Cb$

# APPENDIX C (Cont'd)

## TABLE LI (Cont'd)

| Run No. | Wt % Cr | Wt % Cb | Gradient C°/cm | Rate, cm/hr. | G/R C° hr/cm² | (G/R)/ (G/R)* | Measured Volume Fraction Lamellar Structure | Measured Volume Fraction Dendritic $Ni_3Cb$ | Measured Volume Fraction $Ni_3Cb$ in Dentrite Free Areas | Calculated Volume Fraction Lamellar $Ni_3Cb$ in Structure | Total** Volume Fraction $Ni_3Cb$ in Structure |
|---|---|---|---|---|---|---|---|---|---|---|---|
| A74-748 | 1 | 20.2 | 360 | 5 | 72 | 1.31 | 1.000 | 0 | 0.363 | – | 0.363 |
| | 1 | 20.2 | 360 | 5 | 72 | 1.31 | 1.000 | 0 | 0.344 | – | 0.344 |
| | 1 | 20.2 | 360 | 5 | 72 | 1.31 | 1.000 | 0 | 0.358 | – | 0.358 |
| | 1 | 20.2 | 360 | 5 | 72 | 1.31 | 1.000 | 0 | 0.351 | – | 0.351 |
| | 1 | 20.2 | 360 | 5 | 72 | 1.31 | 1.000 | 0 | 0.336 | – | 0.336 |
| | 1 | 20.2 | 360 | 10 | 36 | 0.65 | 0.760 | 0 | 0.388 | – | 0.388 |
| A74-767 | 1 | 20.2 | 68 | 0.71 | 96 | 1.78 | 1.000 | 0 | 0.373 | – | 0.373 |
| | 1 | 20.2 | 68 | 1.00 | 68 | 1.24 | 1.000 | 0 | 0.363 | – | 0.363 |
| | 1 | 20.2 | 68 | 1.25 | 54 | 0.98 | 1.000 | 0 | 0.356 | – | 0.356 |
| | 1 | 20.2 | 68 | 1.25 | 54 | 0.98 | 1.000 | 0 | 0.368 | – | 0.368 |
| | 1 | 20.2 | 68 | 1.25 | 54 | 0.98 | 1.000 | 0 | 0.382 | – | 0.382 |
| | 1 | 20.2 | 68 | 1.25 | 54 | 0.98 | 1.000 | 0 | 0.372 | – | 0.372 |
| | 1 | 20.2 | 68 | 1.25 | 54 | 0.98 | 1.000 | 0 | 0.353 | – | 0.353 |
| | 1 | 20.2 | 68 | 1.50 | 45 | 0.82 | 0.885 | 0.010 | 0.389 | 0.385 | 0.395 (C) |
| A73-082 | 2 | 21.0 | N.M.+ | 2.5 | N.M. | N.M. | N.M. | 0.022 | 0.322 | 0.315 | 0.337 (C) |
| | 2 | 21.0 | N.M.+ | 2.5 | N.M. | N.M. | N.M. | 0.022 | 0.328 | 0.321 | 0.343 (C) |
| | 2 | 21.0 | N.M.+ | 2.5 | N.M. | N.M. | N.M. | 0.022 | 0.328 | 0.321 | 0.343 (C) |
| | 2 | 21.0 | N.M.+ | 2.5 | N.M. | N.M. | N.M. | 0.022 | 0.382 | 0.374 | 0.396 (C) |
| | 2 | 21.0 | N.M.+ | 2.5 | N.M. | N.M. | N.M. | 0.022 | 0.370 | 0.362 | 0.384 (C) |
| | 2 | 21.0 | N.M.+ | 2.5 | N.M. | N.M. | N.M. | 0.022 | 0.366 | 0.358 | 0.380 (C) |
| | 2 | 21.0 | N.M.+ | 2.5 | N.M. | N.M. | N.M. | 0.022 | 0.404 | 0.395 | 0.417 (C) |
| | 2 | 21.0 | N.M.+ | 2.5 | N.M. | N.M. | N.M. | 0.022 | 0.345 | 0.337 | 0.359 (C) |
| | 2 | 21.0 | N.M.+ | 2.5 | N.M. | N.M. | N.M. | 0.022 | 0.348 | 0.340 | 0.362 (C) |
| | 2 | 21.0 | N.M.+ | 2.5 | N.M. | N.M. | N.M. | 0.022 | 0.396 | 0.387 | 0.409 (C) |
| | 2 | 21.0 | N.M.+ | 2.5 | N.M. | N.M. | N.M. | 0.022 | 0.373 | 0.365 | 0.387 (C) |
| | 2 | 21.0 | N.M.+ | 2.5 | N.M. | N.M. | N.M. | 0.022 | 0.334 | 0.327 | 0.349 (C) |

## APPENDIX C (Cont'd)

## TABLE LI (Cont'd)

| Run No. | Wt % Cr | Wt % Cb | Gradient C°/cm | Rate, cm/hr | G/R C° hr/cm² | (G/R)* | Measured Volume Fraction Lamellar Structure | Measured Volume Fraction Dendritic $Ni_3Cb$ | Measured Volume Fraction $Ni_3Cb$ in Dentrite Free Areas | Calculated Volume Fraction Lamellar $Ni_3Cb$ in Structure | Total* Volume Fraction $Ni_3Cb$ in Structure |
|---|---|---|---|---|---|---|---|---|---|---|---|
| A73-082 | 2 | 21.0 | N.M.+ | 2.5 | N.M. | N.M. | N.M. | 0.022 | 0.369 | 0.361 | 0.383 (C) |
| | 2 | 21.0 | N.M.+ | 2.5 | N.M. | N.M. | N.M. | 0.022 | 0.391 | 0.382 | 0.404 (C) |
| | 2 | 21.0 | N.M.+ | 2.5 | N.M. | N.M. | N.M. | 0.022 | 0.356 | 0.348 | 0.370 (C) |
| | 2 | 21.0 | N.M.+ | 5.0 | N.M. | N.M. | N.M. | 0.038 | 0.320 | 0.308 | 0.346 (C) |
| | 2 | 21.0 | N.M.+ | 5.0 | N.M. | N.M. | N.M. | 0.038 | 0.351 | 0.338 | 0.376 (C) |
| | 2 | 21.0 | N.M.+ | 10.0 | N.M. | N.M. | N.M. | 0 | 0.323 | – | 0.323 |
| | 2 | 21.0 | N.M.+ | 10.0 | N.M. | N.M. | N.M. | 0 | 0.331 | – | 0.331 |
| A73-080 | 3 | 20.5 | N.M.+ | 2.5 | N.M. | N.M. | 1.000 | 0 | 0.389 | – | 0.389 |
| | 3 | 20.5 | N.M.+ | 2.5 | N.M. | N.M. | 1.000 | 0 | 0.373 | – | 0.373 |
| | 3 | 20.5 | N.M.+ | 2.5 | N.M. | N.M. | 1.000 | 0 | 0.371 | – | 0.371 |
| | 3 | 20.5 | N.M.+ | 2.5 | N.M. | N.M. | 1.000 | 0 | 0.381 | – | 0.381 |
| | 3 | 20.5 | N.M.+ | 2.5 | N.M. | N.M. | 1.000 | 0 | 0.330 | – | 0.330 |
| | 3 | 20.5 | N.M.+ | 2.5 | N.M. | N.M. | 1.000 | 0 | 0.369 | – | 0.369 |
| | 3 | 20.5 | N.M.+ | 2.5 | N.M. | N.M. | 1.000 | 0 | 0.368 | – | 0.368 |
| | 3 | 20.5 | N.M.+ | 2.5 | N.M. | N.M. | 1.000 | 0 | 0.348 | – | 0.348 |
| | 3 | 20.5 | N.M.+ | 2.5 | N.M. | N.M. | 1.000 | 0 | 0.354 | – | 0.354 |
| | 3 | 20.5 | N.M.+ | 2.5 | N.M. | N.M. | 1.000 | 0 | 0.364 | – | 0.364 |
| | 3 | 20.5 | N.M.+ | 2.5 | N.M. | N.M. | 1.000 | 0 | 0.378 | – | 0.378 |
| | 3 | 20.5 | N.M.+ | 2.5 | N.M. | N.M. | 1.000 | 0 | 0.389 | – | 0.389 |
| | 3 | 20.5 | N.M.+ | 2.5 | N.M. | N.M. | 1.000 | 0 | 0.390 | – | 0.390 |
| | 3 | 20.5 | N.M.+ | 2.5 | N.M. | N.M. | 1.000 | 0 | 0.412 | – | 0.412 |
| | 3 | 20.5 | N.M.+ | 2.5 | N.M. | N.M. | 1.000 | 0 | 0.358 | – | 0.358 |
| | 3 | 20.5 | N.M.+ | 2.5 | N.M. | N.M. | 1.000 | 0 | 0.351 | – | 0.354 |
| | 3 | 20.5 | N.M.+ | 2.5 | N.M. | N.M. | 1.000 | 0 | 0.352 | – | 0.352 |

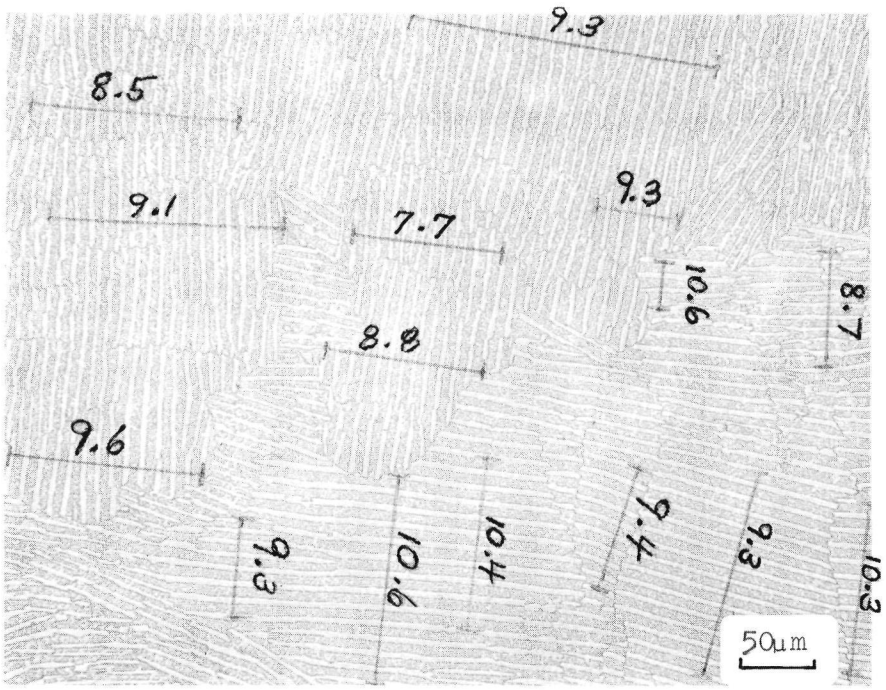
+Not Measured – on the order of 300°C/cm.

# APPENDIX C (Cont'd)
## TABLE LI (Cont'd)

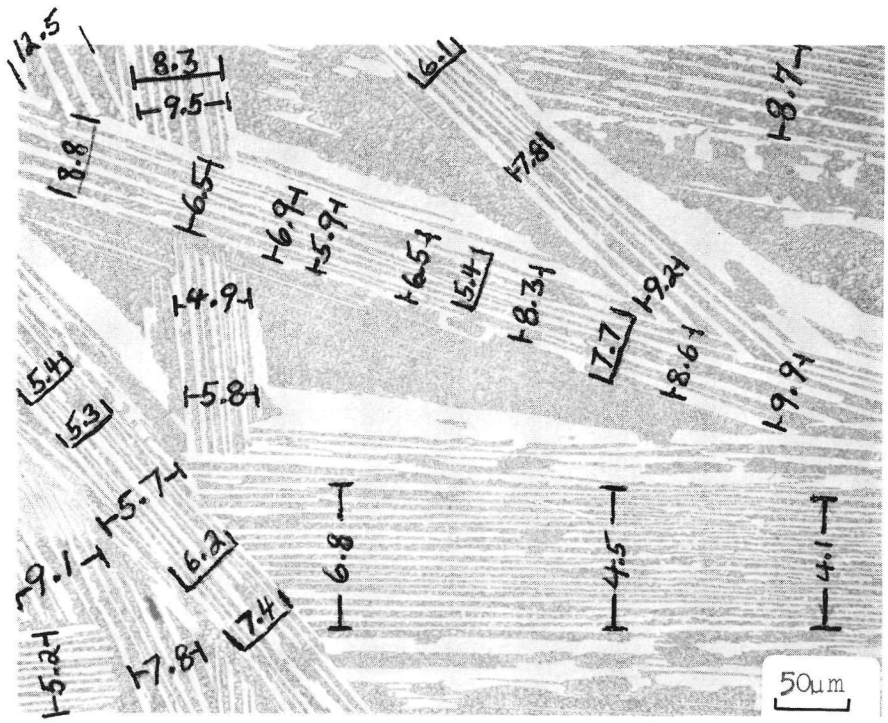
| Run No. | Wt % Cr | Wt % Cb | Gradient C°/cm | Rate, cm/hr | G/R C° hr/cm² | (G/R)* | Measured Volume Fraction Lamellar Structure | Measured Volume Fraction Dendritic $Ni_3Cb$ | Measured Volume Fraction $Ni_3Cb$ in Dentrite Free Areas | Calculated Volume Fraction Lamellar $Ni_3Cb$ in Structure | Total* Volume Fraction $Ni_3Cb$ in Structure |
|---|---|---|---|---|---|---|---|---|---|---|---|
| A74-745 | 3 | 20.8 | 360 | 3.0 | 120 | 1.00 | 1.000 | 0.019 | 0.353 | 0.346 | 0.365 |
| | 3 | 20.8 | 360 | 3.0 | 120 | 1.00 | 1.000 | 0.057 | 0.329 | 0.310 | 0.367 |
| | 3 | 20.8 | 360 | 5.0 | 72 | 0.60 | 0.777 | 0.055 | 0.337 | 0.318 | 0.373 |
| | 3 | 20.8 | 360 | 5.0 | 72 | 0.60 | 0.777 | 0.049 | 0.355 | 0.338 | 0.387 |
| A74-739 | 3 | 20.8 | 360 | 7.0 | 51 | 0.43 | 0.699 | 0.054 | 0.363 | 0.343 | 0.397 (C) |
| | 3 | 20.8 | 360 | 7.0 | 51 | 0.43 | 0.699 | 0.041 | 0.322 | 0.309 | 0.350 (C) |
| | 3 | 20.8 | 360 | 7.0 | 51 | 0.43 | 0.699 | 0.048 | 0.353 | 0.336 | 0.384 (C) |
| A74-752 | 3 | 20.8 | 68 | 2.0 | 34 | 0.28 | 0.615 | 0.086 | N.M. | – | – |
| | 3 | 20.8 | 68 | 3.0 | 23 | 0.19 | 0.581 | 0.037 | N.M. | – | – |
| A74-761 | 6 | 20.0 | 360 | 2.5 | 144 | 0.96 | 0.980 | 0 | 0.467 | 0 | 0.467 |
| | 6 | 20.0 | 360 | 2.5 | 144 | 0.96 | 0.980 | 0 | 0.370 | 0 | 0.370 |
| | 6 | 20.0 | 360 | 2.5 | 144 | 0.96 | 0.980 | 0 | 0.379 | 0 | 0.379 |
| | 6 | 20.0 | 360 | 2.5 | 144 | 0.96 | 0.980 | 0 | 0.394 | 0 | 0.394 |
| | 6 | 20.0 | 360 | 2.5 | 144 | 0.96 | 0.980 | 0 | 0.402 | 0 | 0.402 |
| | 6 | 20.0 | 360 | 2.5 | 144 | 0.96 | 0.980 | 0 | 0.444 | 0 | 0.444 |
| | 6 | 20.0 | 360 | 2.5 | 144 | 0.96 | 0.980 | 0 | 0.372 | 0 | 0.372 |
| | 6 | 20.0 | 360 | 2.5 | 144 | 0.96 | 0.980 | 0 | 0.412 | 0 | 0.412 |
| | 6 | 20.0 | 360 | 2.5 | 144 | 0.96 | 0.980 | 0 | 0.366 | 0 | 0.366 |
| | 6 | 20.0 | 360 | 2.5 | 144 | 0.96 | 0.980 | 0 | 0.396 | 0 | 0.396 |
| | 6 | 20.0 | 360 | 2.5 | 144 | 0.96 | 0.980 | 0 | 0.403 | 0 | 0.403 |
| | 6 | 20.0 | 360 | 2.5 | 144 | 0.96 | 0.980 | 0 | 0.383 | 0 | 0.383 |
| | 6 | 20.0 | 360 | 2.5 | 144 | 0.96 | 0.980 | 0 | 0.386 | 0 | 0.386 |
| | 6 | 20.0 | 360 | 2.5 | 144 | 0.96 | 0.980 | 0 | 0.427 | 0 | 0.427 |
| | 6 | 20.0 | 360 | 2.5 | 144 | 0.96 | 0.980 | 0 | 0.358 | 0 | 0.358 |
| | 6 | 20.0 | 360 | 3.0 | 120 | 0.80 | 0.873 | 0.032 | 0.446 | 0.432 | 0.464 (C) |
| | 6 | 20.0 | 360 | 3.5 | 103 | 0.69 | 0.772 | 0.047 | 0.400 | 0.381 | 0.428 (C) |
| | 6 | 20.0 | 360 | 4.0 | 90 | 0.60 | 0.742 | 0.069 | 0.444 | 0.410 | 0.479 (C) |

APPENDIX C (Cont'd)
TABLE LI (Cont'd)

| Run No. | Wt % Cr | Wt % Cb | Gradient C°/cm | Rate, cm/hr | G/R C° hr/cm² | (G/R) (G/R)* | Measured Volume Fraction Lamellar Structure | Measured Volume Fraction Dendritic $Ni_3Cb$ | Measured Volume Fraction $Ni_3Cb$ in Dendtitic Free Areas | Calculated Volume Fraction Lamellar $Ni_3Cb$ in Structure | Total* Volume Fraction $Ni_3Cb$ in Structure |
|---|---|---|---|---|---|---|---|---|---|---|---|
| A74-363 | 6 | 20.0 | N.M.+ | 2.0 | N.M. | N.M. | 1.000 | 0 | 0.414 | – | 0.414 |
| | 6 | 20.0 | N.M.+ | 2.0 | N.M. | N.M. | 1.000 | 0 | 0.438 | – | 0.438 |
| | 6 | 20.0 | N.M.+ | 2.0 | N.M. | N.M. | 1.000 | 0 | 0.438 | – | 0.438 |
| A74-757 | 6 | 20.0 | 68 | 1.0 | 68 | 0.45 | 0.608 | 0 | N.M. | – | – |
| | 6 | 20.0 | 68 | 1.5 | 45 | 0.30 | 0.568 | 0 | N.M. | – | – |
| | 6 | 20.0 | 68 | 2.0 | 34 | 0.23 | 0.535 | 0 | N.M. | – | – |



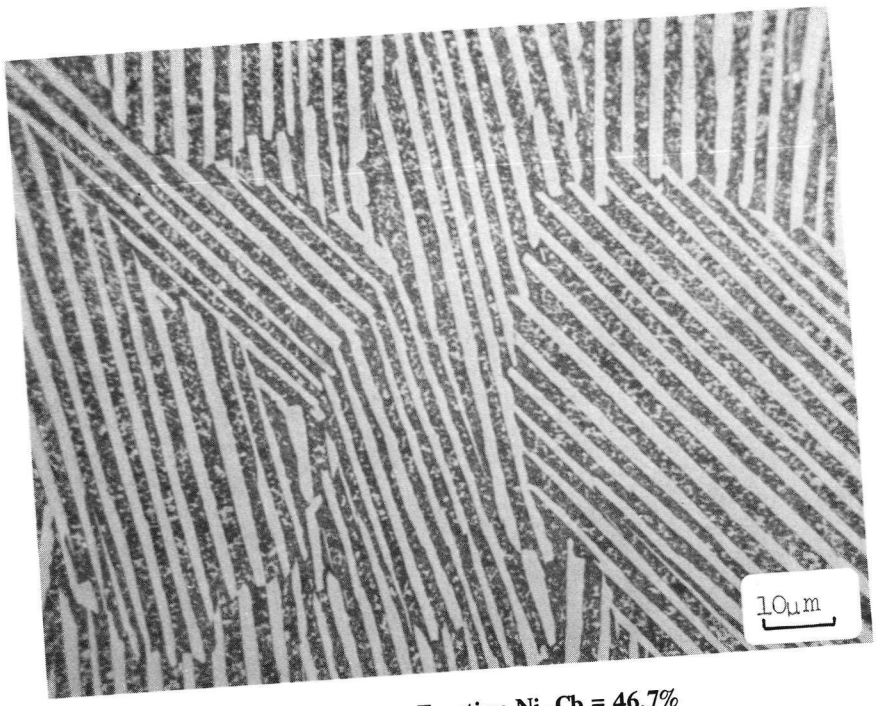

a) **A74-767 1% Chromium Alloy Solidified at 0.71 cm/hr. in a Gradient of 68°C/cm**



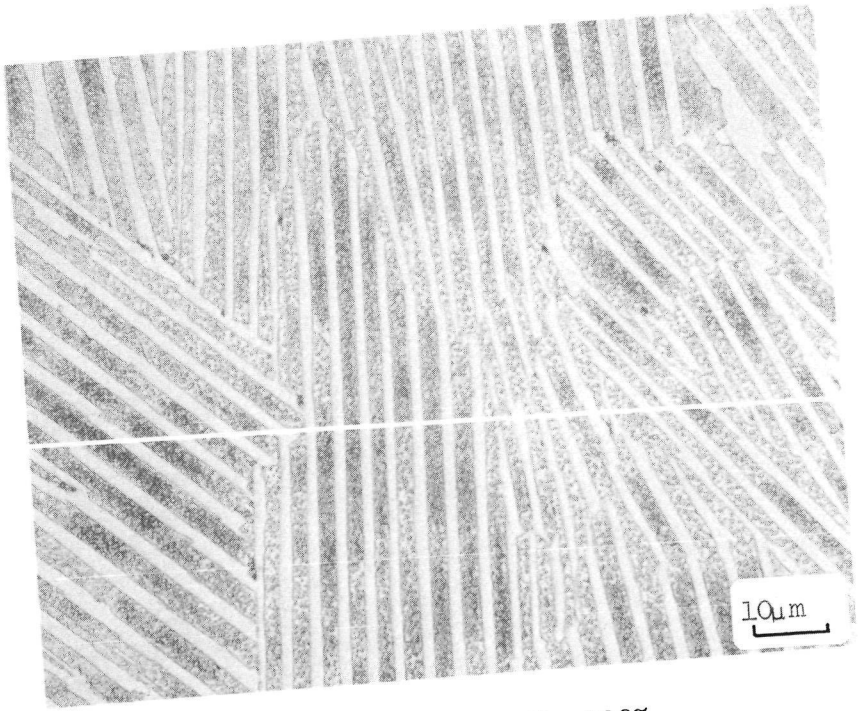

b) **A74-757 6% Chromium Alloy Solidified at 1 cm/hr in a Gradient of 68°C/cm**

R14-187

Figure 167 Illustrating Measurements of Interlamellar Spacing in Fully Lamellar and Partially Cellular Microstructure




a) Volume Fraction $Ni_3Cb$ = 46.7%




b) Volume Fraction $Ni_3Cb$ = 35.8%

R14-188

Figure 168 Illustrating Random Variation of Volume Fraction $Ni_3Cb$ Phase in a Single Section of 6 Percent Chromium Bar Solidified at 2.5 cm/Hour in a Gradient of 360°C/cm (Run No. A74-761)

# APPENDIX D

## MICROSTRUCTURES FOUND IN TYPICAL MODIFIED SLAB CASTINGS EVALUATED IN PHASE III

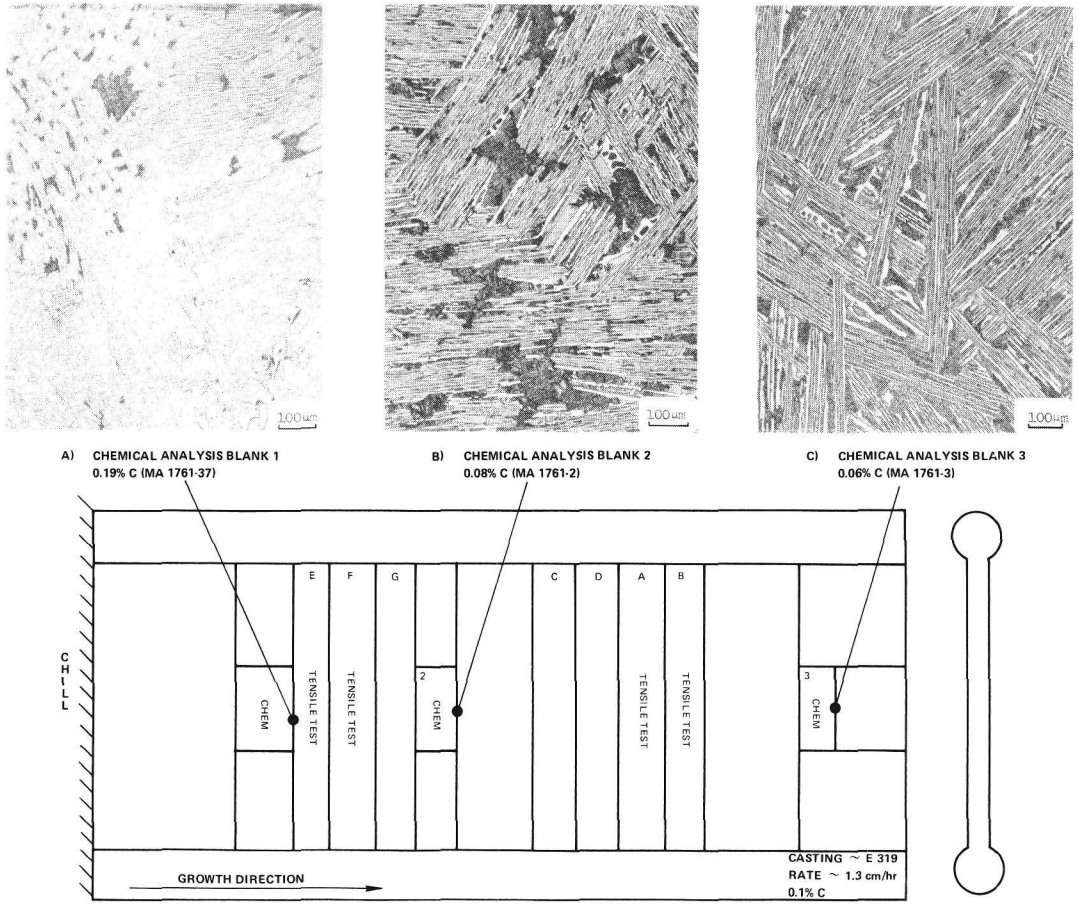



Figure 169 Transverse Microstructures Observed at Various Locations in a Ni-20.0%Cb-2.5%Al-6.0%Cr-0.1%C Charge Composition Slab Directionally Solidified at a Rate of 1.3 cm (0.5 inches)/Hour in a Gradient Estimated to be on the Order of 75 to 100C°/cm. Casting No. E319

R14-189

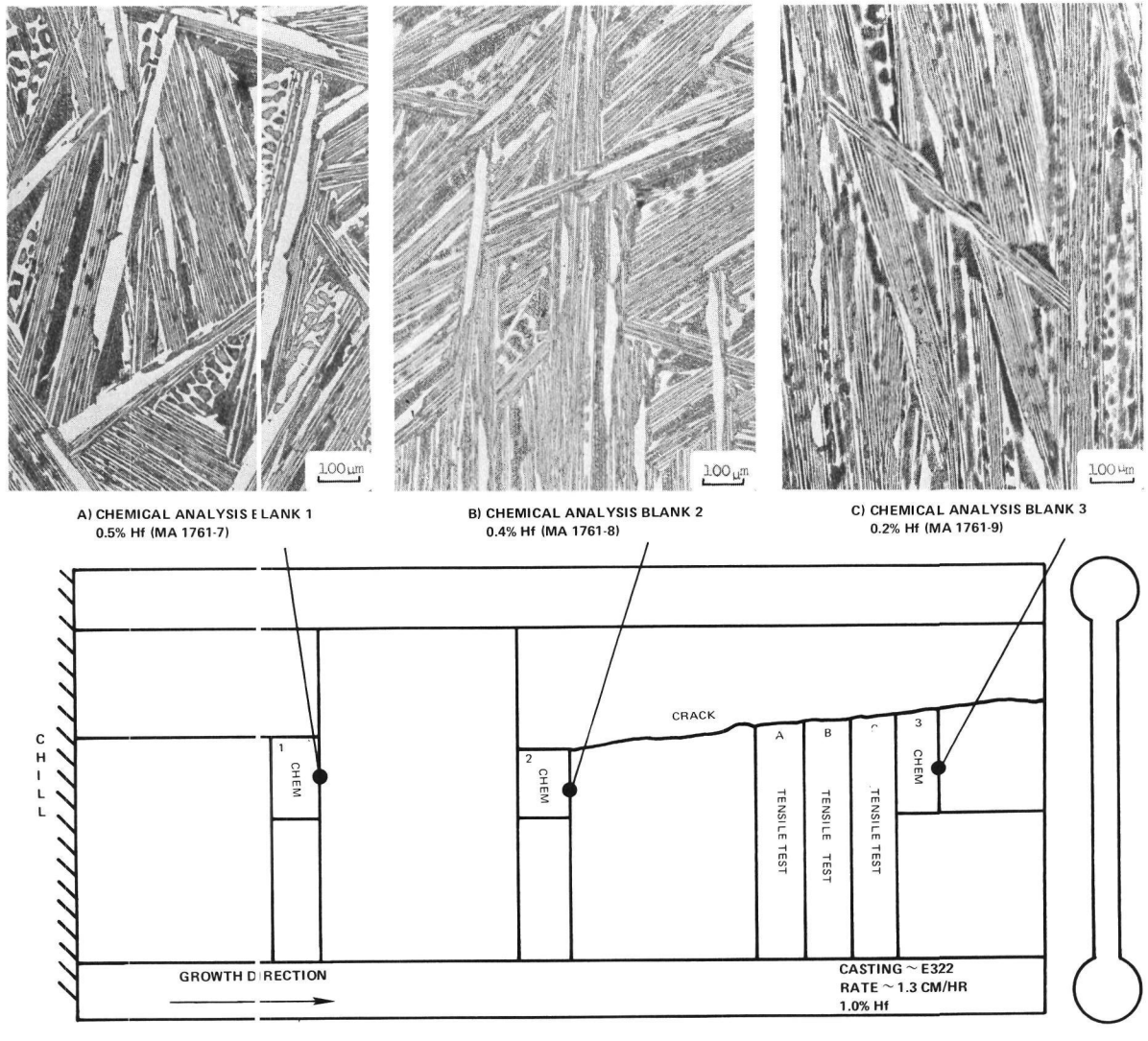



Figure 170 Transverse Microstructures Observed at Various Locations in a Ni-20.0%Cb-2.5%Al-6.0%Cr-1.0%Hf Charge Composition Slab Directionally Solidified at a Rate of 1.3 cm (0.5 inches)/Hour in a Gradient Estimated to be on The Order of 75 to 100C°/cm. Casting No. E322

R14-190

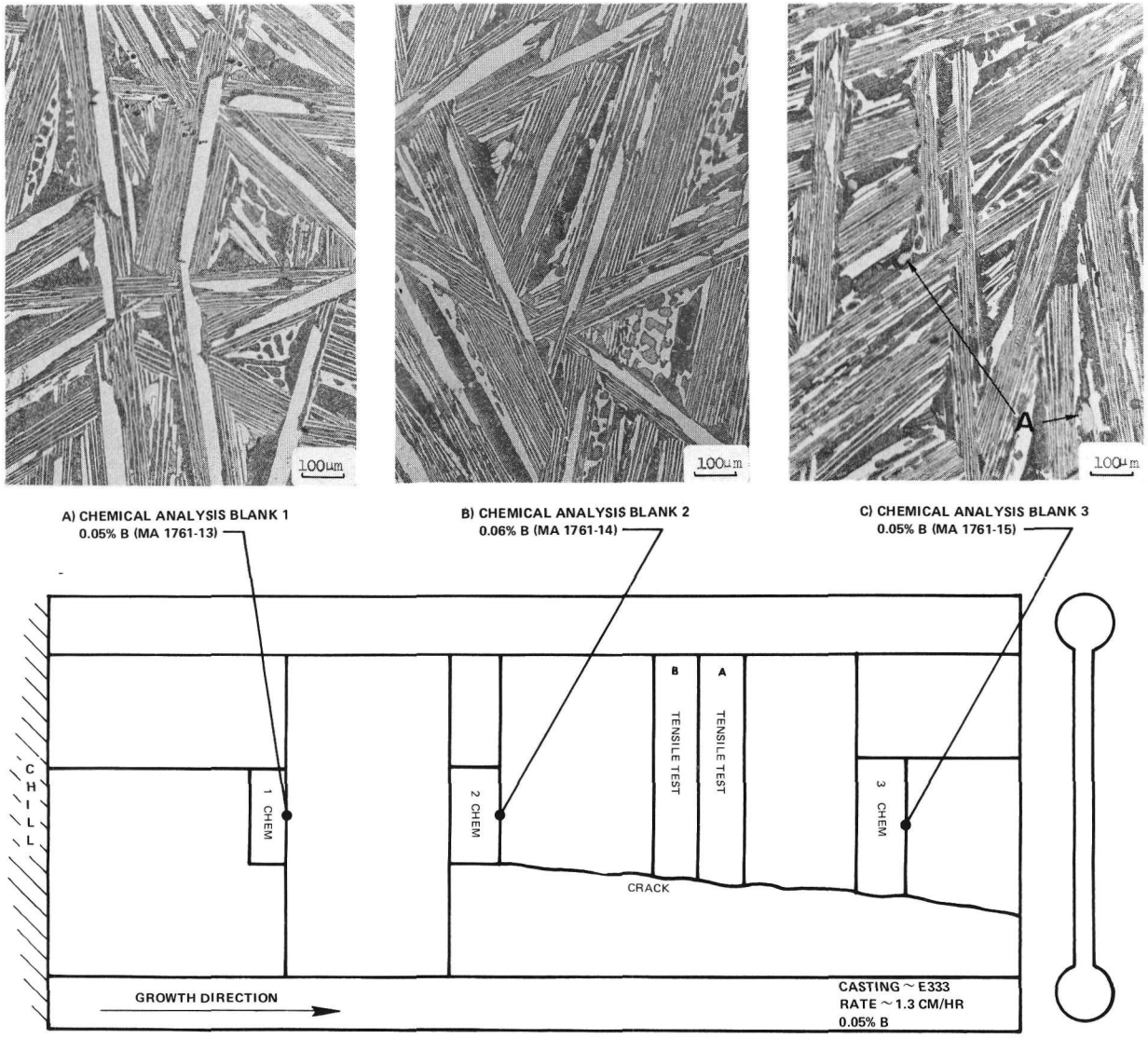



Figure 171 Transverse Microstructure Observed at Various Locations in a Ni-20.0%Cb-2.5%Al-6.0%Cr-0.05%B Charge Composition Slab Directionally Solidified at a Rate of 1.3 cm (0.5 Inches)/Hour in a Gradient Estimated to be on the Order of 75 to 100C°/cm. Casting No. E333

R14-191

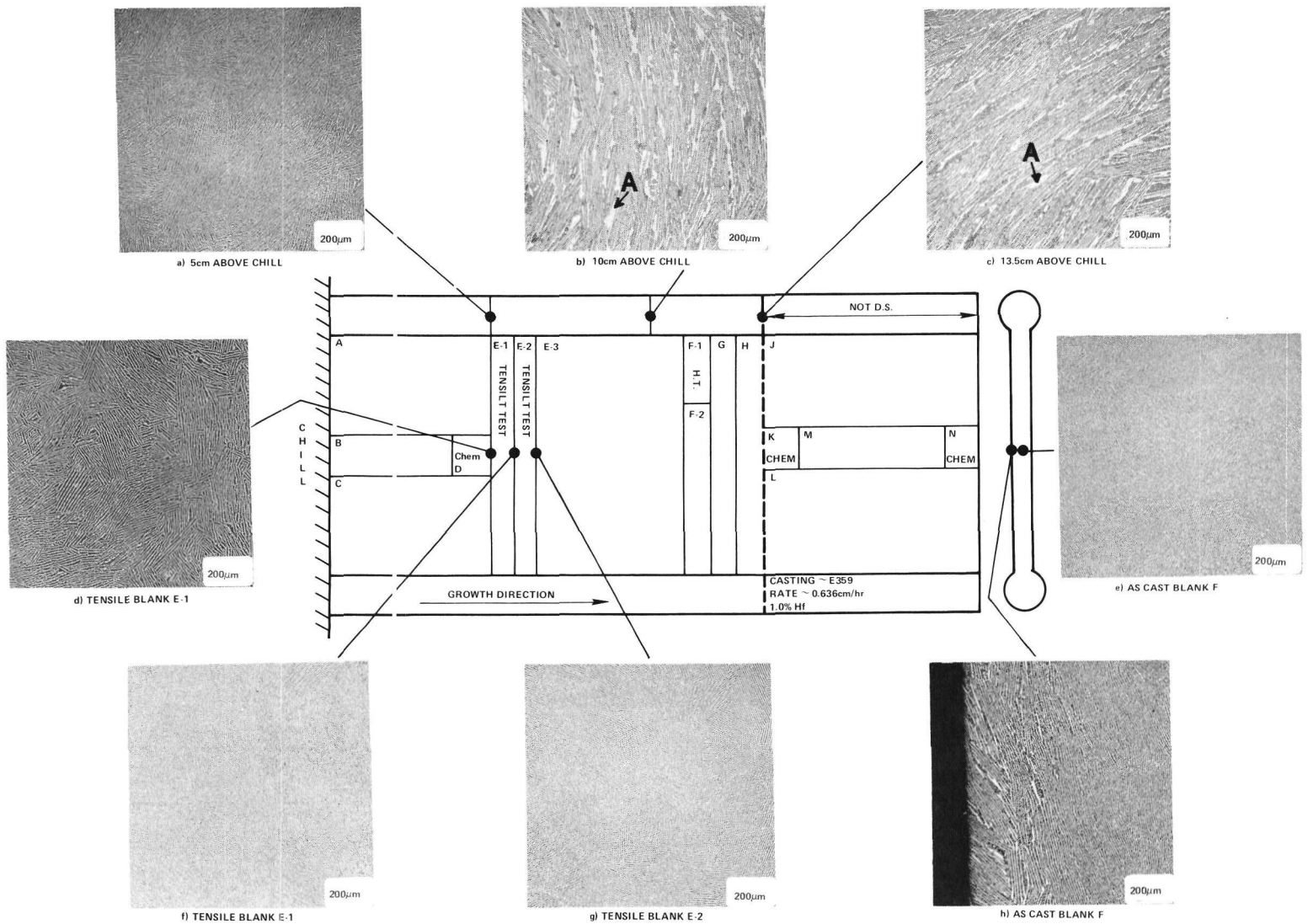



Figure 172 Transverse Microstructure Observed at Various Locations in a Ni-20.3%Cb-2.5%Al-1.0%Cr-1.0%Hf Charge Composition Slab Directionally Solidified at a Rate of 0.6 cm (0.25 Inches)/Hour in a Gradient Estimated to be on the Order of 75 to 100C°/cm. Casting No. E359. Note the Presence of an Extra Phase Previously Identified as $\gamma'$ (Labeled "A") at Various Areas in the Casting R14-192

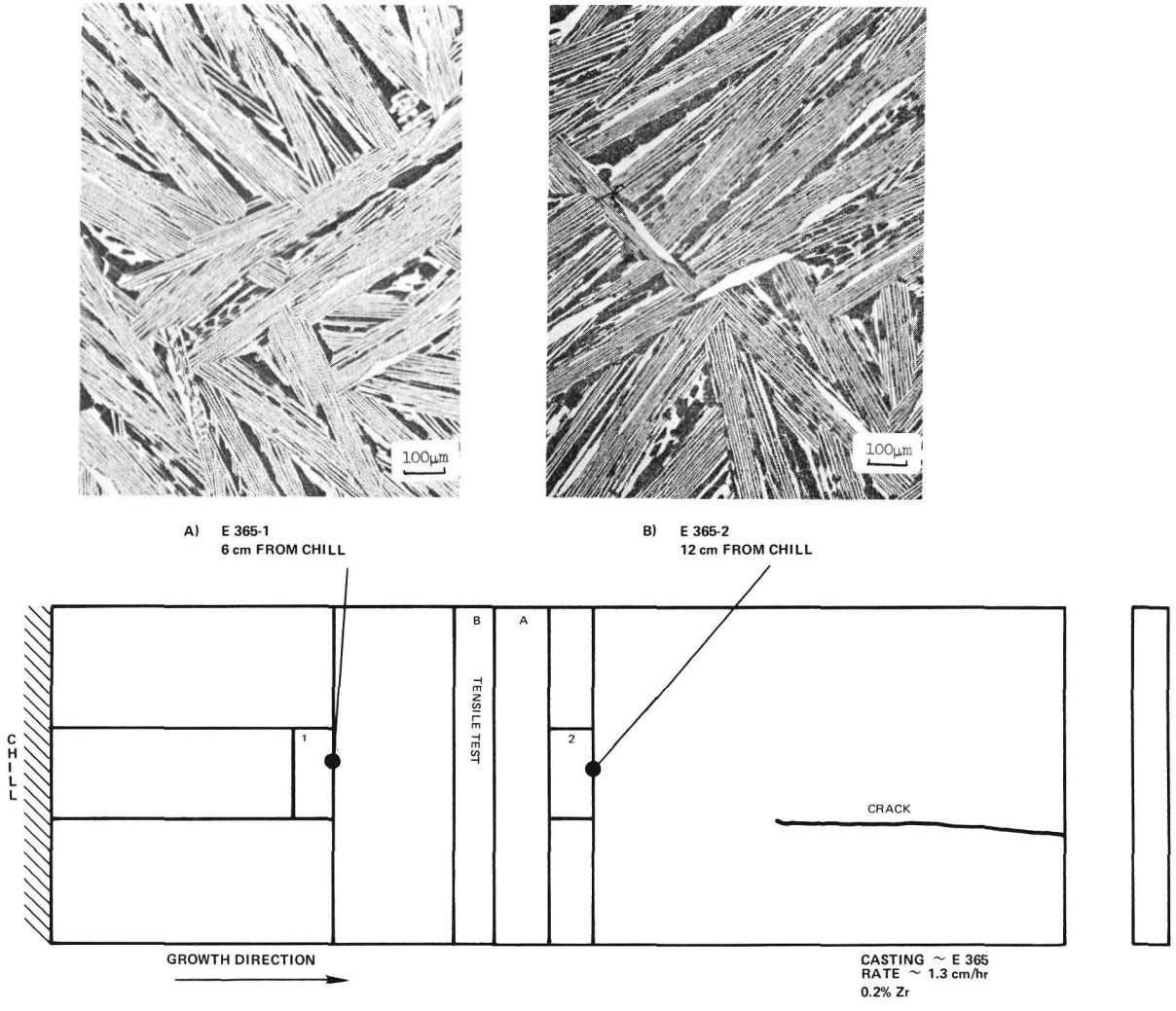



Figure 173 Transverse Microstructures Observed at Various Locations in a Ni-20.0%Cb-2.5%Al-6.0%Cr-0.2%Zr Charge Composition Slab Directionally Solidified at a Rate of 1.3 cm (0.5 Inches)/Hour in a Gradient Estimated to be on the Order of 75 to 100C°/cm. Casting No. E365

R14-193

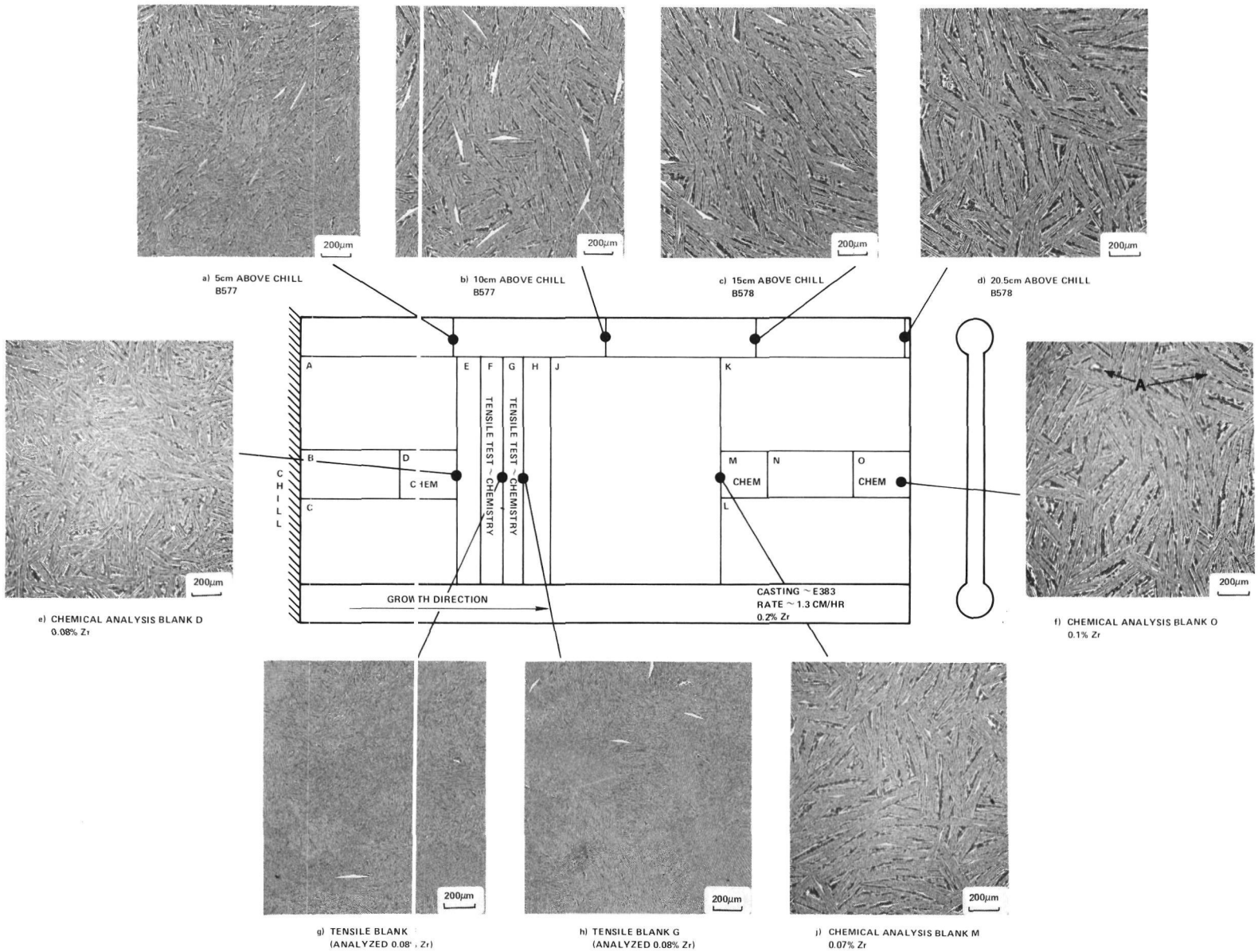



Figure 174 Transverse Microstructures Observed at Various Locations in a Ni-20.9%Cb-2.5%Al-1.0%Cr-0.2%Zr Charge Composition Slab Directionally Solidified at a Rate of 1.3 cm (0.5 Inches)/Hour in a Gradient Estimated to be on the Order of 75 to 100C°/cm. Casting No. E383. Note the Presence of an Extra Phase Previously Identified as $\gamma'$ (Labeled "A") Near the Top of the Casting

R14-194

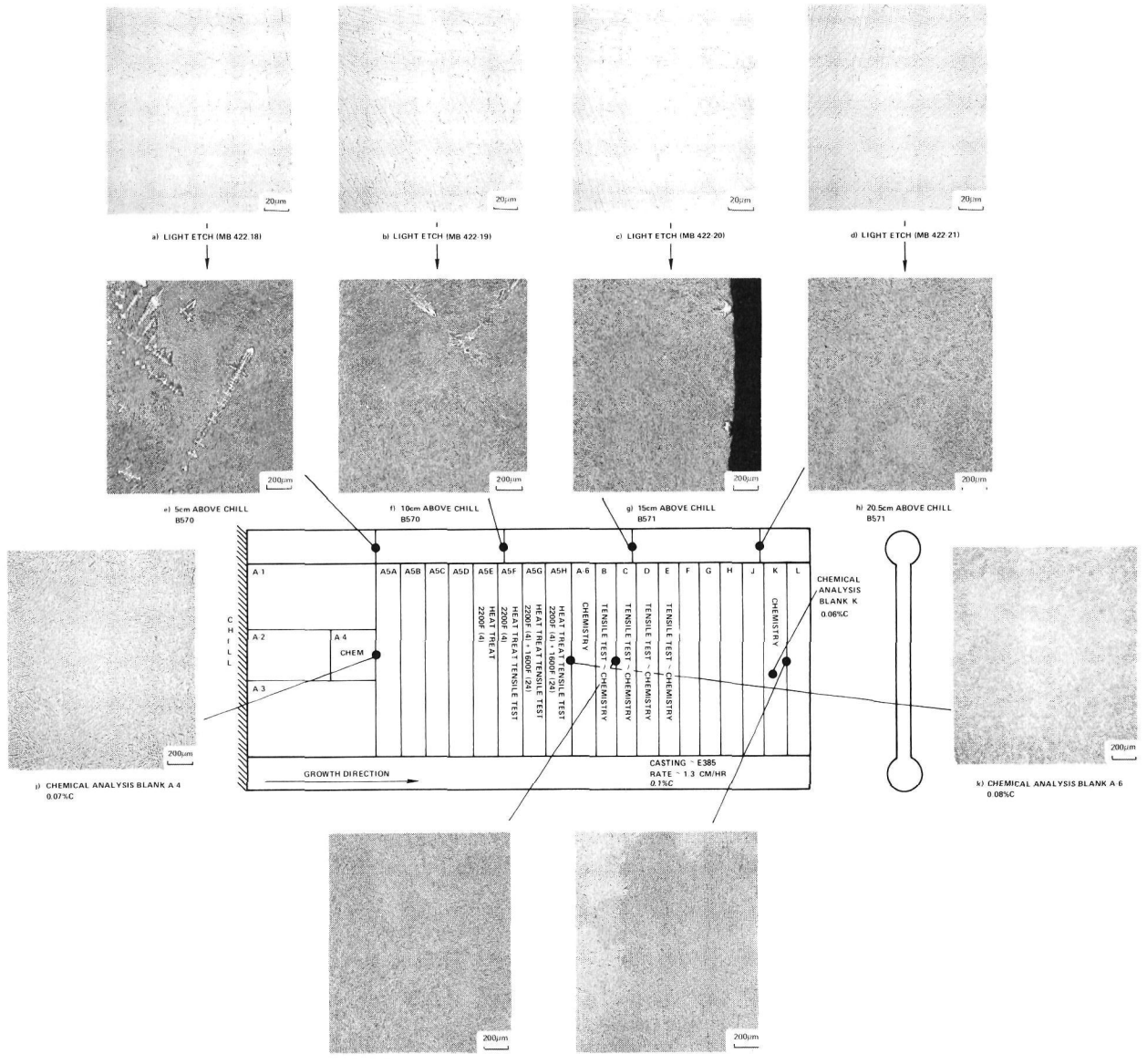



Figure 175 Transverse Microstructures Observed at Various Locations in a Ni-21.2%Cb-2.5%Al-1.0%Cr-0.1%C Charge Composition Slab Directionally Solidified at a Rate of 1.3 cm (0.5 Inches)/Hour in a Gradient Estimated to be on the Order of 75 to 100C°/cm. Casting No. E385 R14-195

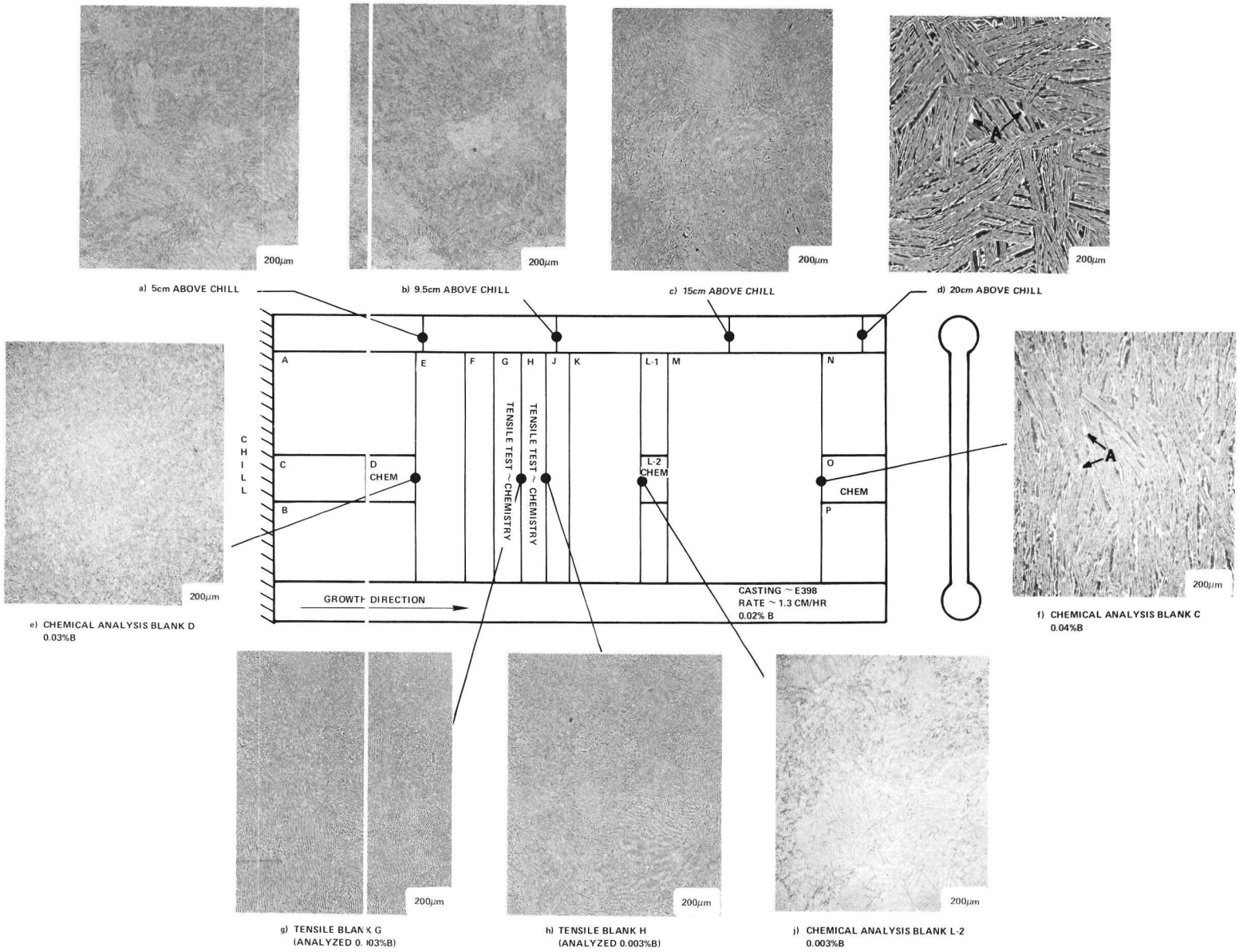



Figure 176 Transverse Microstructures Observed at Various Locations in a Ni-20.9%Cb-2.5%Al-1.0%Cr-0.02%B Charge Composition Slab Directionally Solidified at a Rate of 1.3 cm (0.5 Inches)/Hour in a Gradient Estimated to be on the Order of 75 to 100C°/cm. Casting No. E398. Note the Presence of an Extra Phase Previously Identified as $\gamma'$ (Labelled "A") at the Top of the Casting

R14-196

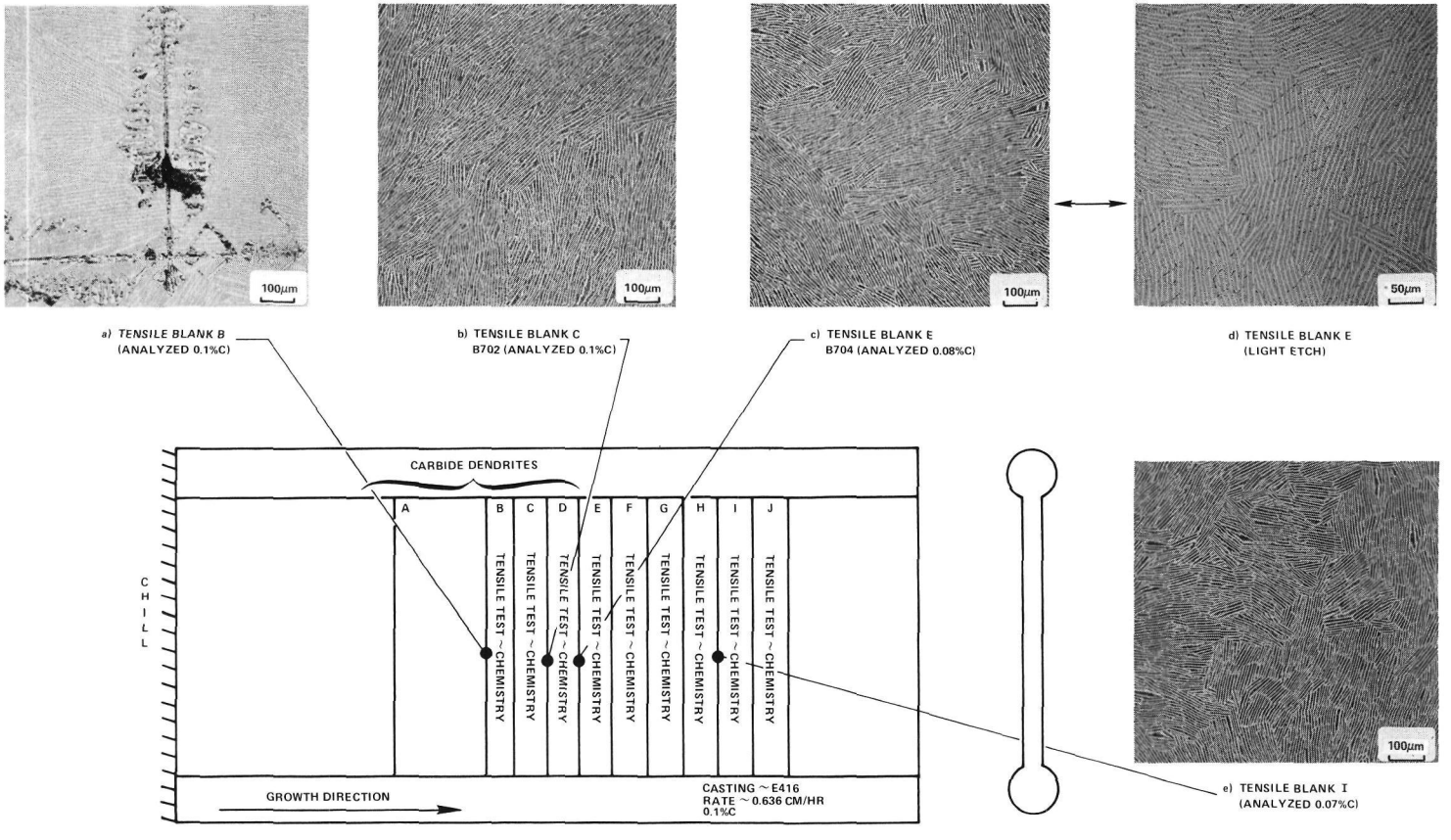



Figure 177 Transverse Microstructures Observed at Various Locations in a Ni-20.2%Cb-2.5%Al-6.0%Cr-0.10%C Charge Composition Slab Directionally Solidified at a Rate of 0.64 cm (0.25 Inches)/Hour in a Gradient Estimated to be on the Order of 75 to 100C°/cm. Casting No. E416 R14-197

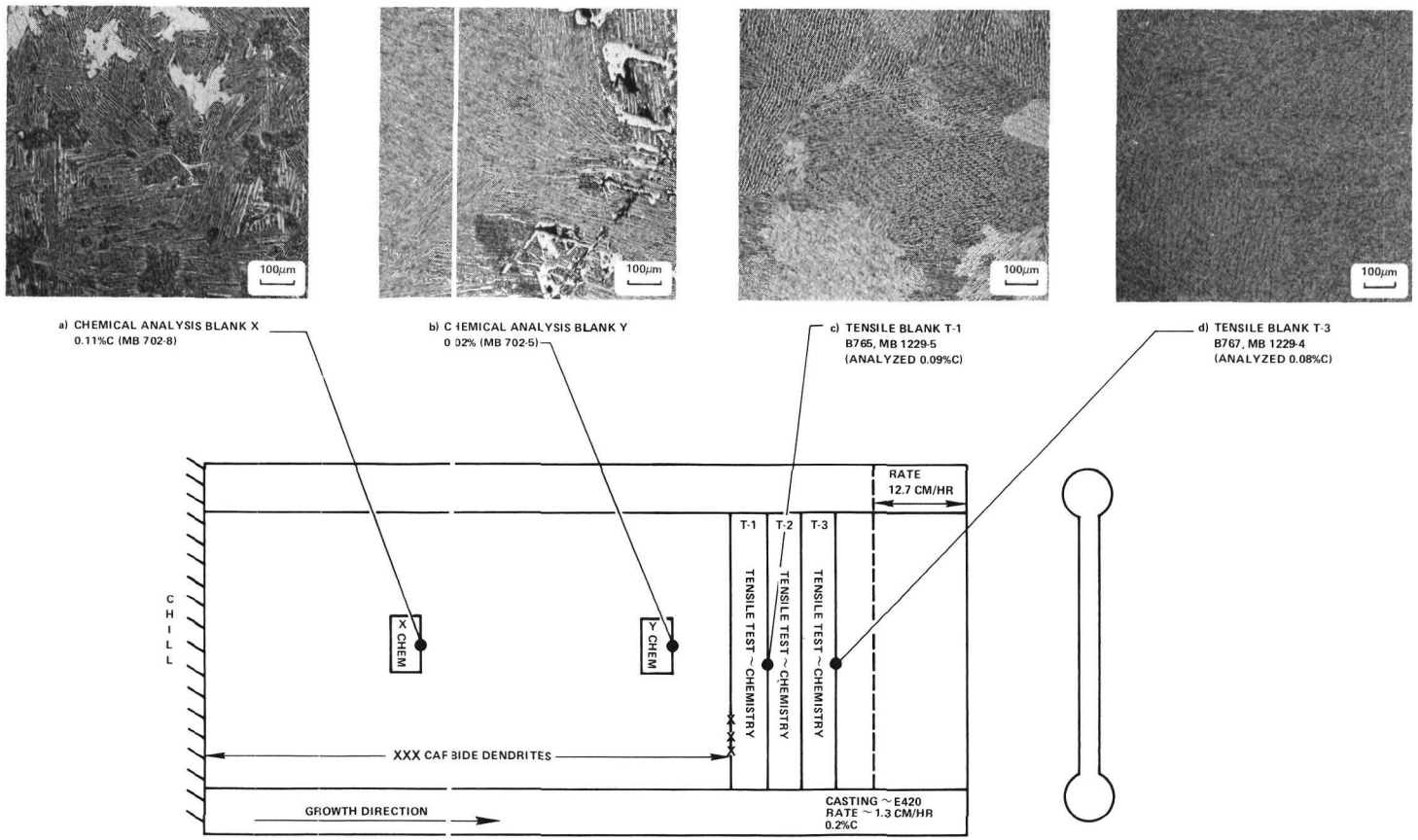



Figure 178 Transverse Microstructures Observed at Various Locations in a Ni-21.2%Cb-2.5%Al-1.0%Cr-0.20%C Charge Composition Slab Directionally Solidified at a Rate of 1.3 cm (0.5 Inches)/Hour in a Gradient Estimated to be on the Order of 75 to 100C°/cm. Casting No. E420 R14-198

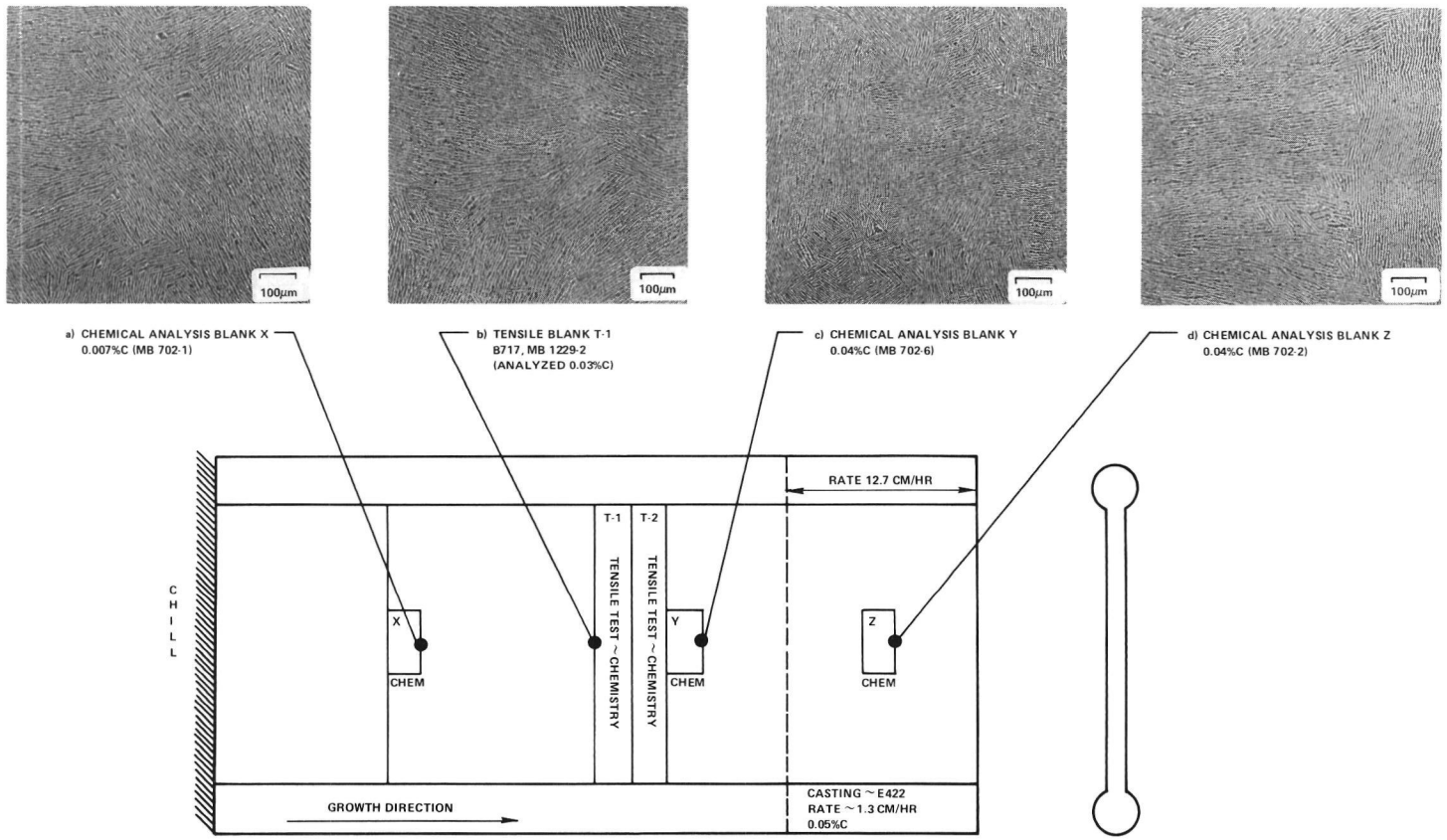



Figure 179 Transverse Microstructures Observed at Various Locations in a Ni-21.2%Cb-2.5%Al-1.0%Cr-0.05%C Charge Composition Slab Directionally Solidified at a Rate of 1.3 cm (0.5 Inches)/Hour in a Gradient Estimated to be on the Order of 75 to 100C°/cm. Casting No. E422 R14-199

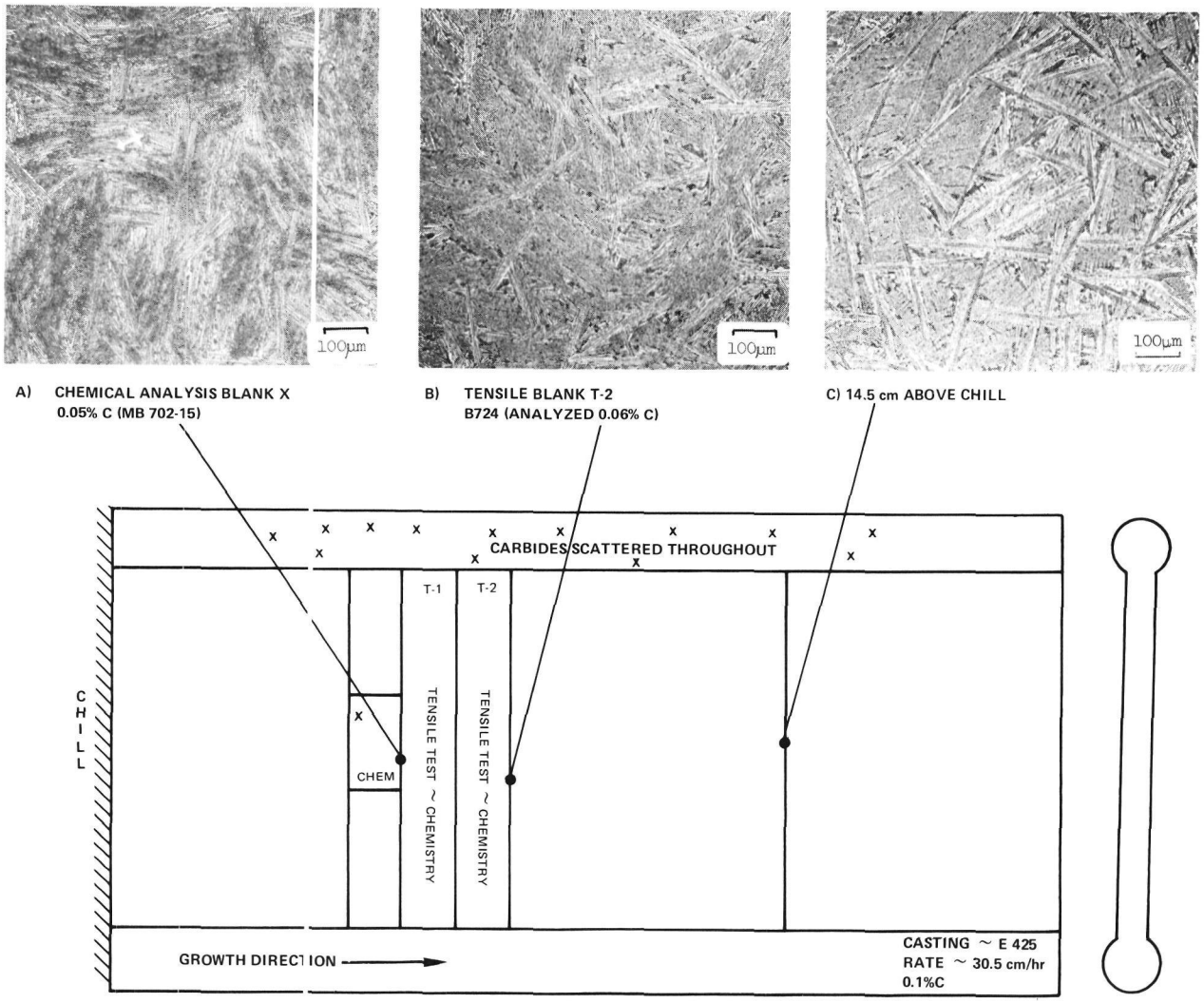



Figure 180 Transverse Microstructures Observed at Various Locations in a Ni-21.3Cb-2.5%Al-1.0%Cr-0.10%C Charge Composition Slab Directionally Solidified at a Rate of 30 cm (12 Inches)/Hour in a Gradient Estimated to be on the Order of 75 to 100C°/cm. Casting No. E425

R14-200

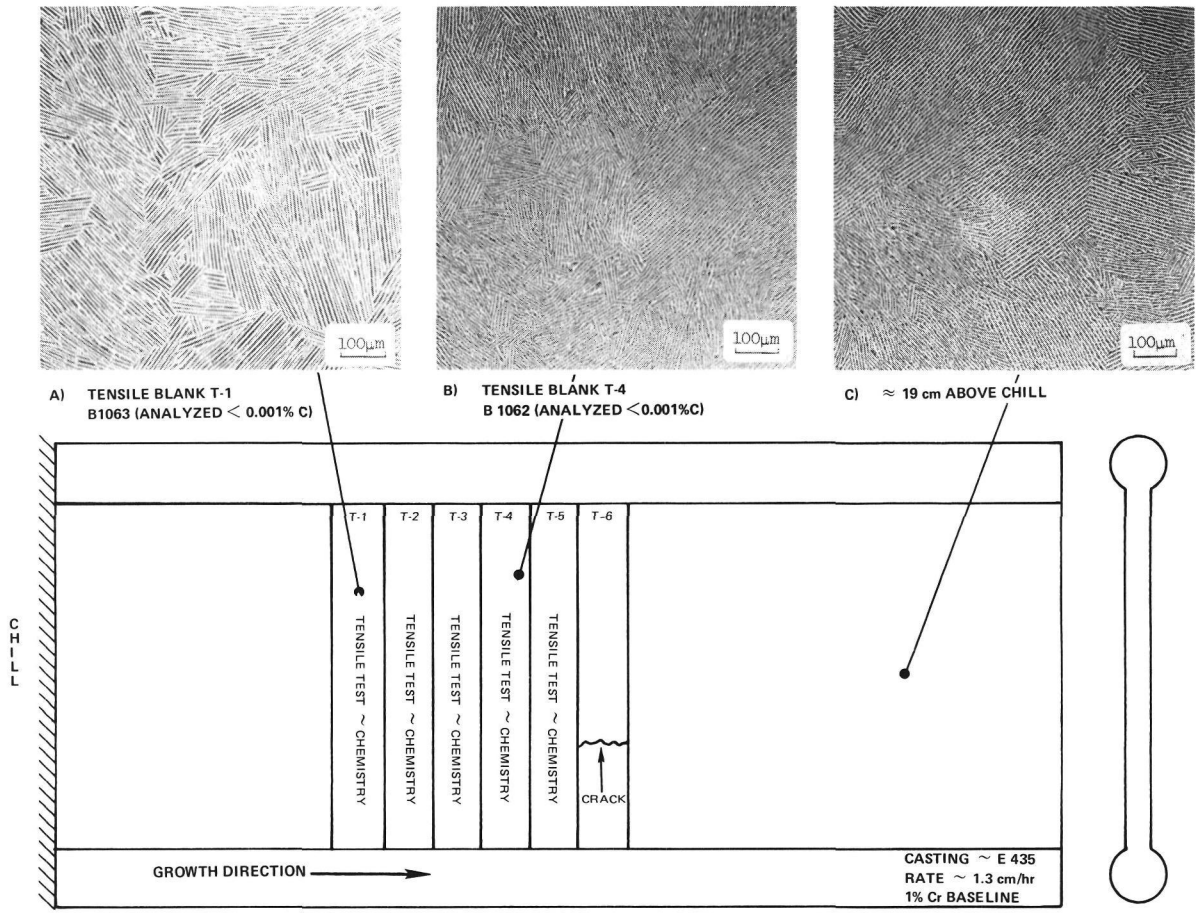



Figure 181 Transverse Microstructures Observed at Various Locations in a Ni-21.0%Cb-2.5%Al-1.0%Cr Charge Composition Slab Directionally Solidified at a Rate of 1.3 cm (0.5 Inches)/Hour in a Gradient Estimated to be on the Order of 75 to 100C°/cm. Casting No. E435 R14-201

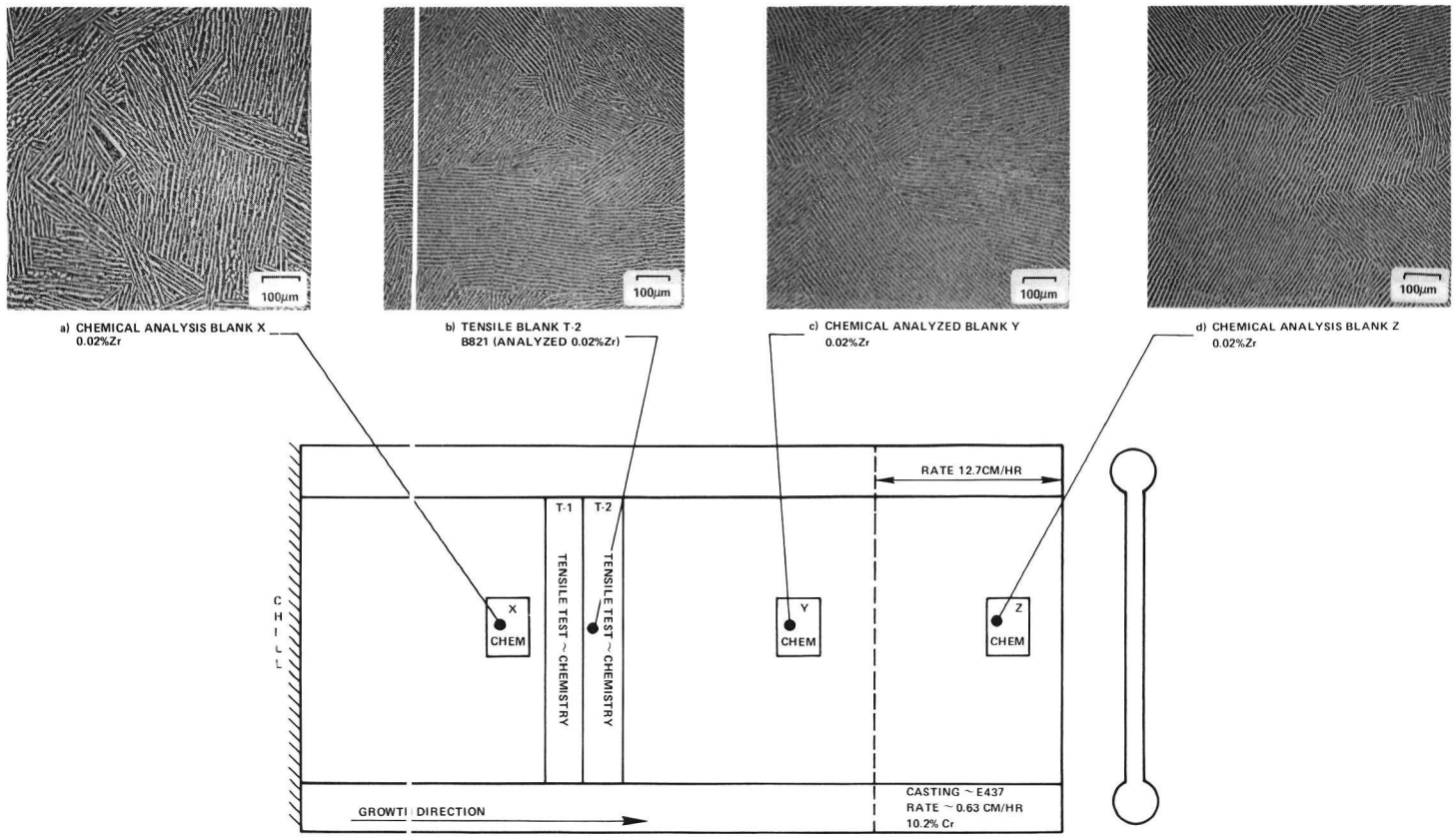



Figure 182 Transverse Microstructures Observed at Various Locations in a Ni-20.9%Cb-2.5%Al-1.0%Cr-0.20%Zr Charge Composition Slab Directionally Solidified at a Rate of 0.64 cm (0.25 Inches)/Hour in a Gradient Estimated to be on the Order of 75 to 100C°/cm. Casting No. E437 R14-202

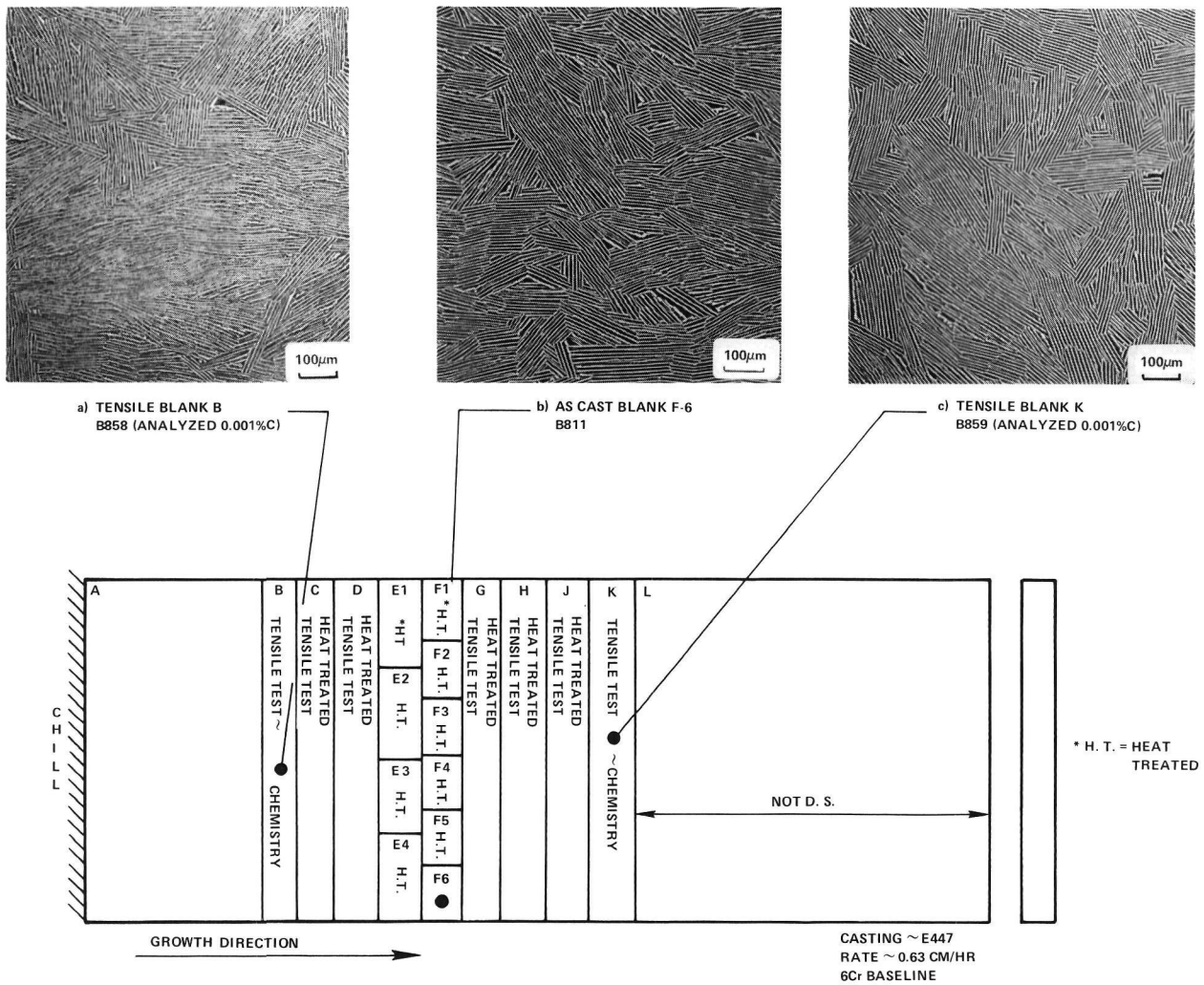



Figure 183 Transverse Microstructures Observed at Various Locations in a Ni-20.0%Cb-2.5%Al-6.0%Cr Charge Composition Slab Directionally Solidified at a Rate of 0.64 cm (0.25 Inches)/Hour in a Gradient Estimated to be on the Order of 75 to 100C°/cm. Casting No. E447 R14-203

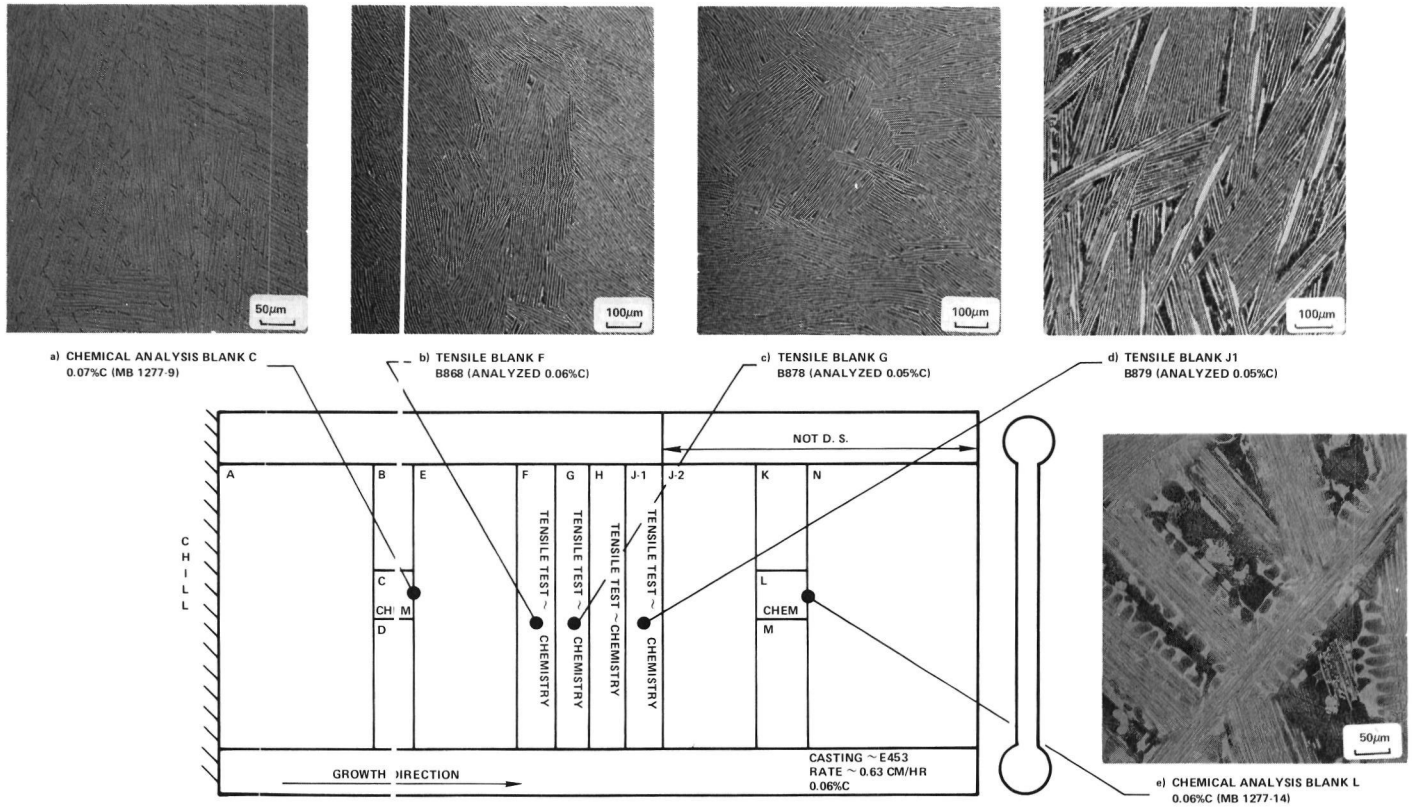



Figure 184 Transverse Microstructures Observed at Various Locations in a Ni-20.1%Cb-2.5%Al-6.0%Cr-0.06%C Charge Composition Slab Directionally Solidified at a Rate of 0.64 cm (0.25 Inches)/Hour in a Gradient Estimated to be on the Order of 75 to 100C°/cm. Casting No. E453

R14-204

# APPENDIX E

## MINOR ELEMENT CHEMICAL ANALYSIS RESULTS

| Casting Identification | SOLIDIFICATION RATE cm/hr | in/hr. | Charge Composition (Percent) Cb | Cr | C | B | Zr | Hf | Ta | Specimen Identification | Approximate Fraction Solidified | Analyzed Composition (Percent) C | B | Zr | Hf | Ta |
|---|---|---|---|---|---|---|---|---|---|---|---|---|---|---|---|---|
| E268 | 1.3 | 0.5 | 20.0 | 6.0 | – | – | 0.1 | – | – | A | 0.24 | – | – | 0.03 | – | – |
| E268 | 1.3 | 0.5 | 20.0 | 6.0 | – | – | 0.1 | – | – | B | 0.42 | – | – | 0.04 | – | – |
| E268 | 1.3 | 0.5 | 20.0 | 6.0 | – | – | 0.1 | – | – | C | 0.72 | – | – | 0.03 | – | – |
| E312 | 1.3 | 0.5 | 21.2 | 1.0 | – | – | – | 1.0 | – | D | 0.18 | – | – | – | 0.9 | – |
| E312 | 1.3 | 0.5 | 21.2 | 1.0 | – | – | – | 1.0 | – | L | 0.54 | – | – | – | 0.7 | – |
| E312 | 1.3 | 0.5 | 21.2 | 1.0 | – | – | – | 1.0 | – | N | 0.76 | – | – | – | 0.6 | – |
| E313 | 1.3 | 0.5 | 21.2 | 1.0 | 0.10(E) | – | – | – | – | D | 0.20 | 0.06 | – | – | – | – |
| E313 | 1.3 | 0.5 | 21.2 | 1.0 | 0.10(E) | – | – | – | – | K | 0.56 | 0.08 | – | – | – | – |
| E313 | 1.3 | 0.5 | 21.2 | 1.0 | 0.10(E) | – | – | – | – | M | 0.76 | 0.06 | – | – | – | – |
| E314 | 1.3 | 0.5 | 21.2 | 1.0 | 0.02(E) | – | – | – | – | D | 0.20 | 0.006 | – | – | – | – |
| E314 | 1.3 | 0.5 | 21.2 | 1.0 | 0.02(E) | – | – | – | – | K | 0.61 | 0.003 | – | – | – | – |
| E314 | 1.3 | 0.5 | 21.2 | 1.0 | 0.02(E) | – | – | – | – | M | 0.72 | 0.004 | – | – | – | – |
| E315 | 1.3 | 0.5 | 21.2 | 1.0 | – | – | 0.10 | – | – | A4 | 0.20 | – | – | 0.04 | – | – |
| E315 | 1.3 | 0.5 | 21.2 | 1.0 | – | – | 0.10 | – | – | G | 0.62 | – | – | 0.02 | – | – |
| E315 | 1.3 | 0.5 | 21.2 | 1.0 | – | – | 0.10 | – | – | J | 0.83 | – | – | 0.03 | – | – |
| E318 | 1.3 | 0.5 | 21.2 | 1.0 | – | – | – | – | – | 1 | 0.61 | 0.004 | – | – | – | – |
| E318 | 1.3 | 0.5 | 21.2 | 1.0 | – | – | – | – | – | 2 | 0.66 | <0.002 | – | – | – | – |
| E318 | 1.3 | 0.5 | 21.2 | 1.0 | – | – | – | – | – | 3 | 0.71 | 0.006 | – | – | – | – |
| E318 | 1.3 | 0.5 | 21.2 | 1.0 | – | – | – | – | – | 4 | 0.77 | 0.005 | – | – | – | – |
| E318 | 1.3 | 0.5 | 21.2 | 1.0 | – | – | – | – | – | 5 | 0.82 | <0.002 | – | – | – | – |
| E318 | 1.3 | 0.5 | 21.2 | 1.0 | – | – | – | – | – | 6 | 0.87 | <0.002 | – | – | – | – |
| E319 | 1.3 | 0.5 | 20.0 | 6.0 | 0.10(E) | – | – | – | – | 1 | 0.18 | 0.19 | – | – | – | – |
| E319 | 1.3 | 0.5 | 20.0 | 6.0 | 0.10(E) | – | – | – | – | 2 | 0.37 | 0.08 | – | – | – | – |
| E319 | 1.3 | 0.5 | 20.0 | 6.0 | 0.10(E) | – | – | – | – | 3 | 0.76 | 0.06 | – | – | – | – |

## APPENDIX E (Cont'd)

| Casting Identification | Solidification Rate cm/hr | Solidification Rate in/hr. | Charge Composition (Percent) Cb | Cr | C | B | Zr | Hf | Ta | Specimen Identification | Approximate Fraction Solidified | Analyzed Composition (Percent) C | B | Zr | Hf | Ta |
|---|---|---|---|---|---|---|---|---|---|---|---|---|---|---|---|---|
| E320 | 1.3 | 0.5 | 20.0 | 6.0 | 0.02(E) | – | – | – | – | 1 | 0.20 | .01 | – | – | – | – |
| E320 | 1.3 | 0.5 | 20.0 | 6.0 | 0.02(E) | – | – | – | – | 2 | 0.38 | .02 | – | – | – | – |
| E320 | 1.3 | 0.5 | 20.0 | 6.0 | 0.02(E) | – | – | – | – | 3 | 0.79 | .02 | – | – | – | – |
| E322 | 1.3 | 0.5 | 20.0 | 6.0 | – | – | – | 1.0 | – | 1 | 0.20 | – | – | – | 0.5 | – |
| E322 | 1.3 | 0.5 | 20.0 | 6.0 | – | – | – | 1.0 | – | 2 | 0.43 | – | – | – | 0.4 | – |
| E322 | 1.3 | 0.5 | 20.0 | 6.0 | – | – | – | 1.0 | – | 3 | 0.78 | – | – | – | 0.2 | – |
| E323 | 1.3 | 0.5 | 21.2 | 1.0 | – | 0.04 | – | – | – | A4 | 0.19 | – | 0.028 | – | – | – |
| E323 | 1.3 | 0.5 | 21.2 | 1.0 | – | 0.04 | – | – | – | J | 0.62 | – | 0.014 | – | – | – |
| E323 | 1.3 | 0.5 | 21.2 | 1.0 | – | 0.04 | – | – | – | L | 0.84 | – | 0.024 | – | – | – |
| E324 | 1.3 | 0.5 | 21.2 | 1.0 | – | 0.01 | – | – | – | D | 0.22 | – | 0.010 | – | – | – |
| E324 | 1.3 | 0.5 | 21.2 | 1.0 | – | 0.01 | – | – | – | K | 0.66 | – | 0.004 | – | – | – |
| E324 | 1.3 | 0.5 | 21.2 | 1.0 | – | 0.01 | – | – | – | M | 0.84 | – | 0.009 | – | – | – |
| E325 | 1.3 | 0.5 | 21.2 | 1.0 | – | 0.02 | 0.06 | – | – | D | 0.26 | – | .006 | <.02 | – | – |
| E325 | 1.3 | 0.5 | 21.2 | 1.0 | – | 0.02 | 0.06 | – | – | K | 0.66 | – | .006 | <.02 | – | – |
| E325 | 1.3 | 0.5 | 21.2 | 1.0 | – | 0.02 | 0.06 | – | – | M | 0.84 | – | .025 | <.02 | – | – |
| E328 | 1.3 | 0.5 | 21.2 | 1.0 | 0.05(E) | – | – | 0.6 | – | A4 | 0.22 | 0.06 | – | – | 0.4 | – |
| E328 | 1.3 | 0.5 | 21.2 | 1.0 | 0.05(E) | – | – | 0.6 | – | H | 0.64 | 0.04 | – | – | 0.3 | – |
| E328 | 1.3 | 0.5 | 21.2 | 1.0 | 0.05(E) | – | – | 0.6 | – | K | 0.80 | 0.04 | – | – | 0.3 | – |
| E332 | 1.3 | 0.5 | 20.0 | 6.0 | – | – | 0.1 | – | – | 1 | 0.20 | – | – | 0.03 | – | – |
| E332 | 1.3 | 0.5 | 20.0 | 6.0 | – | – | 0.1 | – | – | 2 | 0.40 | – | – | 0.04 | – | – |
| E332 | 1.3 | 0.5 | 20.0 | 6.0 | – | – | 0.1 | – | – | 3 | 0.64 | – | – | 0.05 | – | – |
| E333 | 1.3 | 0.5 | 20.0 | 6.0 | – | 0.05 | – | – | – | 1 | 0.25 | – | 0.05 | – | – | – |
| E333 | 1.3 | 0.5 | 20.0 | 6.0 | – | 0.05 | – | – | – | 2 | 0.40 | – | 0.06 | – | – | – |
| E333 | 1.3 | 0.5 | 20.0 | 6.0 | – | 0.05 | – | – | – | 3 | 0.78 | – | 0.05 | – | – | – |

## APPENDIX E (Cont'd)

| Casting Identification | Solidification Rate cm/hr | Solidification Rate in/hr | Charge Composition (Percent) Cb | Cr | C | B | Zr | Hf | Ta | Specimen Identification | Approximate Fraction Solidified | Analyzed Composition (Percent) C | B | Zr | Hf | Ta |
|---|---|---|---|---|---|---|---|---|---|---|---|---|---|---|---|---|
| E334 | 1.3 | 0.5 | 20.0 | 6.0 | – | 0.01 | – | – | – | 1 | 0.19 | – | .004 | – | – | – |
| E334 | 1.3 | 0.5 | 20.0 | 6.0 | – | 0.01 | – | – | – | 2 | 0.44 | – | .006 | – | – | – |
| E334 | 1.3 | 0.5 | 20.0 | 6.0 | – | 0.01 | – | – | – | 3 | 0.77 | – | .007 | – | – | – |
| E338 | 1.3 | 0.5 | 20.0 | 6.0 | – | 0.02 | 0.06 | – | – | 1 | 0.20 | – | 0.02 | 0.02 | – | – |
| E338 | 1.3 | 0.5 | 20.0 | 6.0 | – | 0.02 | 0.06 | – | – | 2 | 0.52 | – | 0.02 | 0.02 | – | – |
| E338 | 1.3 | 0.5 | 20.0 | 6.0 | – | 0.02 | 0.06 | – | – | 3 | 0.78 | – | 0.02 | 0.02 | – | – |
| E339 | 1.3 | 0.5 | 20.0 | 6.0 | 0.05(E) | – | – | 0.6 | – | 1 | 0.18 | 0.02 | – | – | 0.2 | – |
| E339 | 1.3 | 0.5 | 20.0 | 6.0 | 0.05(E) | – | – | 0.6 | – | 2 | 0.39 | 0.05 | – | – | 0.3 | – |
| E339 | 1.3 | 0.5 | 20.0 | 6.0 | 0.05(E) | – | – | 0.6 | – | 3 | 0.77 | 0.05 | – | – | 0.3 | – |
| E359 | 0.6 | 0.25 | 20.3 | 1.0 | – | – | – | 1.0 | – | D | 0.18 | – | – | – | 0.8 | – |
| E359 | 0.6 | 0.25 | 20.3 | 1.0 | – | – | – | 1.0 | – | K | 0.58 | – | – | – | 0.9 | – |
| E359 | 0.6 | 0.25 | 20.3 | 1.0 | – | – | – | 1.0 | – | N | 0.86 | – | – | – | 0.7 | – |
| E363 | 0.6/1.3 | 0.25/0.5 | 19.9 | 6.0 | – | – | – | – | – | T4 | 0.41 | <0.002 | – | – | – | – |
| E366 | 1.3 | 0.5 | 20.0 | 6.0 | 0.02(E) | – | 0.2 | – | – | 1 | 0.23 | 0.009 | – | – | – | – |
| E366 | 1.3 | 0.5 | 20.0 | 6.0 | 0.02(E) | – | 0.2 | – | – | 2 | 0.47 | 0.018 | – | – | – | – |
| E382 | 1.3 | 0.5 | 20.8 | 1.0 | – | 0.06 | – | – | – | D | 0.31 | – | 0.006 | – | – | – |
| E382 | 1.3 | 0.5 | 20.8 | 1.0 | – | 0.06 | – | – | – | L | 0.94 | – | 0.08 | – | – | – |
| E383 | 1.3 | 0.5 | 20.9 | 1.0 | – | – | 0.2 | – | – | D | 0.18 | – | – | 0.08 | – | – |
| E383 | 1.3 | 0.5 | 20.9 | 1.0 | – | – | 0.2 | – | – | M | 0.62 | – | – | 0.07 | – | – |
| E383 | 1.3 | 0.5 | 20.9 | 1.0 | – | – | 0.2 | – | – | O | 0.80 | – | – | 0.10 | – | – |
| E385 | 1.3 | 0.5 | 21.2 | 1.0 | 0.10(E) | – | – | – | – | A4 | 0.18 | 0.07 | – | – | – | – |
| E385 | 1.3 | 0.5 | 21.2 | 1.0 | 0.10(E) | – | – | – | – | A6 | 0.58 | 0.08 | – | – | – | – |
| E385 | 1.3 | 0.5 | 21.2 | 1.0 | 0.10(E) | – | – | – | – | K | 0.87 | 0.06 | – | – | – | – |
| E388 | 0.6 | 0.25 | 20.2 | 6.0 | 0.10(E) | – | – | – | – | X | 0.17 | 0.07 | – | – | – | – |
| E388 | 0.6 | 0.25 | 20.2 | 6.0 | 0.10(E) | – | – | – | – | Y | 0.22 | > 0.70 | – | – | – | – |
| E388 | 0.6 | 0.25 | 20.2 | 6.0 | 0.10(E) | – | – | – | – | Z | 0.57 | 0.06 | – | – | – | – |

## APPENDIX E (Cont'd)

| Casting Identification | Solidification Rate cm/hr | Solidification Rate in/hr | Charge Composition (Percent) Cb | Cr | C | B | Zr | Hf | Ta | Specimen Identification | Approximate Fraction Solidified | Analyzed Composition (Percent) C | B | Zr | Hf | Ta |
|---|---|---|---|---|---|---|---|---|---|---|---|---|---|---|---|---|
| E389 | 1.3 | 0.5 | 21.2 | 1.0 | 0.15(E) | – | – | – | – | C | 0.16 | 0.05 | – | – | – | – |
| E389 | 1.3 | 0.5 | 21.2 | 1.0 | 0.15(E) | – | – | – | – | M | 0.61 | 0.05 | – | – | – | – |
| E389 | 1.3 | 0.5 | 21.2 | 1.0 | 0.15(E) | – | – | – | – | O | 0.74 | 0.05 | – | – | – | – |
| E391 | 0.6 | 0.25 | 20.4 | 1.0 | 0.08(C) | – | – | 1.0 | – | D | 0.20 | 0.06 | – | – | 1.0 | – |
| E391 | 0.6 | 0.25 | 20.4 | 1.0 | 0.08(C) | – | – | 1.0 | – | M | 0.72 | 0.05 | – | – | 0.5 | – |
| E391 | 0.6 | 0.25 | 20.4 | 1.0 | 0.08(C) | – | – | 1.0 | – | O | 0.90 | 0.04 | – | – | 0.5 | – |
| E392 | 0.6 | 0.25 | 20.4 | 1.0 | 0.15(E) | – | – | 1.0 | – | D | 0.20 | 0.10 | – | – | 0.6 | – |
| E392 | 0.6 | 0.25 | 20.4 | 1.0 | 0.15(E) | – | – | 1.0 | – | M | 0.60 | 0.05 | – | – | 0.5 | – |
| E392 | 0.6 | 0.25 | 20.4 | 1.0 | 0.15(E) | – | – | 1.0 | – | O | 0.84 | 0.05 | – | – | 0.5 | – |
| E394 | 1.3 | 0.5 | 21.2 | 1.0 | 0.08(C) | – | – | – | – | D | 0.20 | 0.05 | – | – | – | – |
| E394 | 1.3 | 0.5 | 21.2 | 1.0 | 0.08(C) | – | – | – | – | L | 0.64 | 0.05 | – | – | – | – |
| E394 | 1.3 | 0.5 | 21.2 | 1.0 | 0.08(C) | – | – | – | – | O | 0.86 | 0.05 | – | – | – | – |
| E395 | 0.6 | 0.25 | 20.9 | 1.0 | 0.08(C) | – | 0.2 | – | – | D | 0.20 | 0.06 | – | 0.10 | – | – |
| E395 | 0.6 | 0.25 | 20.9 | 1.0 | 0.08(C) | – | 0.2 | – | – | M | 0.64 | 0.05 | – | 0.11 | – | – |
| E395 | 0.6 | 0.25 | 20.9 | 1.0 | 0.08(C) | – | 0.2 | – | – | O | 0.88 | 0.04 | – | 0.15 | – | – |
| E396 | 0.6 | 0.25 | 20.8 | 1.0 | – | 0.06 | 0.2 | – | – | D | 0.18 | – | 0.06 | 0.10 | – | – |
| E396 | 0.6 | 0.25 | 20.8 | 1.0 | – | 0.06 | 0.2 | – | – | L | 0.49 | – | 0.006 | 0.04 | – | – |
| E396 | 0.6 | 0.25 | 20.8 | 1.0 | – | 0.06 | 0.2 | – | – | P | 0.83 | – | 0.07 | 0.10 | – | – |
| E397 | 1.3 | 0.5 | 20.9 | 1.0 | 0.08(C) | 0.06 | – | – | – | D | 0.17 | 0.07 | 0.06 | – | – | – |
| E397 | 1.3 | 0.5 | 20.9 | 1.0 | 0.08(C) | 0.06 | – | – | – | K2 | 0.44 | 0.09 | 0.01 | – | – | – |
| E397 | 1.3 | 0.5 | 20.9 | 1.0 | 0.08(C) | 0.06 | – | – | – | N | 0.80 | 0.06 | 0.04 | – | – | – |
| E398 | 1.3 | 0.5 | 20.9 | 1.0 | – | 0.02 | – | – | – | D | 0.16 | – | 0.03 | – | – | – |
| E398 | 1.3 | 0.5 | 20.9 | 1.0 | – | 0.02 | – | – | – | L2 | 0.52 | – | 0.003 | – | – | – |
| E398 | 1.3 | 0.5 | 20.9 | 1.0 | – | 0.02 | – | – | – | O | 0.80 | – | 0.04 | – | – | – |
| E403 | 25 | 10 | 21.6 | – | 0.10(E) | – | – | – | – | X | 0.17 | 0.06 | – | – | – | – |
| E403 | 25 | 10 | 21.6 | – | 0.10(E) | – | – | – | – | Y | 0.20 | 0.05 | – | – | – | – |

## APPENDIX E (Cont'd)

| Casting Identification | Solidification Rate cm/hr | Solidification Rate in/hr | Charge Composition (Percent) Cb | Cr | C | B | Zr | Hf | Ta | Specimen Identification | Approximate Fraction Solidified | Analyzed Composition (Percent) C | B | Zr | Hf | Ta |
|---|---|---|---|---|---|---|---|---|---|---|---|---|---|---|---|---|
| E416 | 0.6 | 0.25 | 20.2 | 6.0 | 0.10(E) | – | – | – | – | B | 0.42 | 0.10 | – | – | – | – |
| E416 | 0.6 | 0.25 | 20.2 | 6.0 | 0.10(E) | – | – | – | – | C | 0.46 | 0.10 | – | – | – | – |
| E416 | 0.6 | 0.25 | 20.2 | 6.0 | 0.10(E) | – | – | – | – | D | 0.50 | 0.08 | – | – | – | – |
| E416 | 0.6 | 0.25 | 20.2 | 6.0 | 0.10(E) | – | – | – | – | E | 0.54 | 0.08 | – | – | – | – |
| E416 | 0.6 | 0.25 | 20.2 | 6.0 | 0.10(E) | – | – | – | – | F | 0.58 | 0.07 | – | – | – | – |
| E416 | 0.6 | 0.25 | 20.2 | 6.0 | 0.10(E) | – | – | – | – | H | 0.68 | 0.07 | – | – | – | – |
| E416 | 0.6 | 0.25 | 20.2 | 6.0 | 0.10(E) | – | – | – | – | I | 0.72 | 0.07 | – | – | – | – |
| E416 | 0.6 | 0.25 | 20.2 | 6.0 | 0.10(E) | – | – | – | – | J | 0.76 | 0.06 | – | – | – | – |
| E417 | 1.0 | 0.38 | 19.0 | 1.0 | – | – | – | – | 3.0 | X | 0.21 | 0.003 | – | – | – | 2.9 |
| E417 | 1.0 | 0.38 | 19.0 | 1.0 | – | – | – | – | 3.0 | Y | 0.62 | 0.005 | – | – | – | 2.9 |
| E418 | 1.3 | 0.5 | 21.2 | 1.0 | 0.10(E) | – | – | – | – | X | 0.26 | 0.07 | – | – | – | – |
| E418 | 1.3 | 0.5 | 21.2 | 1.0 | 0.10(E) | – | – | – | – | T1 | 0.45 | 0.08 | – | – | – | – |
| E418 | 1.3 | 0.5 | 21.2 | 1.0 | 0.10(E) | – | – | – | – | T2 | 0.50 | 0.08 | – | – | – | – |
| E418 | 1.3 | 0.5 | 21.2 | 1.0 | 0.10(E) | – | – | – | – | T3 | 0.55 | 0.08 | – | – | – | – |
| E418 | 1.3 | 0.5 | 21.2 | 1.0 | 0.10(E) | – | – | – | – | T4 | 0.60 | 0.07 | – | – | – | – |
| E418 | 1.3 | 0.5 | 21.2 | 1.0 | 0.10(E) | – | – | – | – | T5 | 0.66 | 0.07 | – | – | – | – |
| E418 | 1.3 | 0.5 | 21.2 | 1.0 | 0.10(E) | – | – | – | – | T6 | 0.70 | 0.06 | – | – | – | – |
| E418 | 1.3 | 0.5 | 21.2 | 1.0 | 0.10(E) | – | – | – | – | T | 0.90 | 0.05 | – | – | – | – |
| E419 | 0.6 | 0.25 | 18.0 | 6.0 | – | – | – | – | 3.0 | X | 0.24 | 0.003 | – | – | – | 3.7 |
| E419 | 0.6 | 0.25 | 18.0 | 6.0 | – | – | – | – | 3.0 | Y | 0.70 | 0.004 | – | – | – | 3.0 |
| E420 | 1.3 | 0.5 | 21.2 | 1.0 | 0.20(E) | – | – | – | – | X | 0.26 | 0.11 | – | – | – | – |
| E420 | 1.3 | 0.5 | 21.2 | 1.0 | 0.20(E) | – | – | – | – | Y | 0.59 | 0.20 | – | – | – | – |
| E420 | 1.3 | 0.5 | 21.2 | 1.0 | 0.20(E) | – | – | – | – | T1 | 0.71 | 0.09 | – | – | – | – |
| E420 | 1.3 | 0.5 | 21.2 | 1.0 | 0.20(E) | – | – | – | – | T2 | 0.76 | 0.09 | – | – | – | – |
| E420 | 1.3 | 0.5 | 21.2 | 1.0 | 0.20(E) | – | – | – | – | T3 | 0.80 | 0.08 | – | – | – | – |
| E421 | 2.5 | 1.0 | 21.2 | 1.0 | 0.10(E) | – | – | – | – | X | 0.18 | 0.07 | – | – | – | – |
| E421 | 2.5 | 1.0 | 21.2 | 1.0 | 0.10(E) | – | – | – | – | T1 | 0.33 | 0.10 | – | – | – | – |
| E421 | 2.5 | 1.0 | 21.2 | 1.0 | 0.10(E) | – | – | – | – | T2 | 0.37 | 0.08 | – | – | – | – |
| E421 | 2.5 | 1.0 | 21.2 | 1.0 | 0.10(E) | – | – | – | – | Y | 0.41 | 0.10 | – | – | – | – |
| E421 | 2.5 | 1.0 | 21.2 | 1.0 | 0.10(E) | – | – | – | – | Z | 0.75 | 0.06 | – | – | – | – |

## APPENDIX E (Cont'd)

| Casting Identification | Solidification Rate cm/hr | Solidification Rate in/hr | Charge Composition (Percent) Cb | Cr | C | B | Zr | Hf | Ta | Specimen Identification | Approximate Fraction Solidified | Analyzed Composition (Percent) C | B | Zr | Hf | Ta |
|---|---|---|---|---|---|---|---|---|---|---|---|---|---|---|---|---|
| E422 | 1.3 | 0.5 | 21.2 | 1.0 | 0.05(E) | – | – | – | – | X | 0.24 | 0.007 | – | – | – | – |
| E422 | 1.3 | 0.5 | 21.2 | 1.0 | 0.05(E) | – | – | – | – | T1 | 0.51 | 0.03 | – | – | – | – |
| E422 | 1.3 | 0.5 | 21.2 | 1.0 | 0.05(E) | – | – | – | – | T2 | 0.56 | 0.03 | – | – | – | – |
| E422 | 1.3 | 0.5 | 21.2 | 1.0 | 0.05(E) | – | – | – | – | Y | 0.61 | 0.04 | – | – | – | – |
| E422 | 1.3 | 0.5 | 21.2 | 1.0 | 0.05(E) | – | – | – | – | Z | 0.86 | 0.04 | – | – | – | – |
| E423 | 1.3 | 0.5 | 21.2 | 1.0 | 0.08(E) | – | – | – | – | X | 0.30 | 0.09 | – | – | – | – |
| E423 | 1.3 | 0.5 | 21.2 | 1.0 | 0.08(E) | – | – | – | – | T1 | 0.44 | 0.07 | – | – | – | – |
| E423 | 1.3 | 0.5 | 21.2 | 1.0 | 0.08(E) | – | – | – | – | T2 | 0.50 | 0.07 | – | – | – | – |
| E423 | 1.3 | 0.5 | 21.2 | 1.0 | 0.08(E) | – | – | – | – | Y | 0.54 | 0.06 | – | – | – | – |
| E423 | 1.3 | 0.5 | 21.2 | 1.0 | 0.08(E) | – | – | – | – | Z | 0.85 | 0.05 | – | – | – | – |
| E424 | 1.9 | 0.75 | 21.2 | 1.0 | 0.10(E) | – | – | – | – | X | 0.19 | 0.05 | – | – | – | – |
| E424 | 1.9 | 0.75 | 21.2 | 1.0 | 0.10(E) | – | – | – | – | T1 | 0.54 | 0.06 | – | – | – | – |
| E424 | 1.9 | 0.75 | 21.2 | 1.0 | 0.10(E) | – | – | – | – | T2 | 0.59 | 0.06 | – | – | – | – |
| E424 | 1.9 | 0.75 | 21.2 | 1.0 | 0.10(E) | – | – | – | – | Y | 0.63 | 0.05 | – | – | – | – |
| E425 | 30.0 | 12.0 | 21.3 | 1.0 | 0.10(E) | – | – | – | – | X | 0.22 | 0.05 | – | – | – | – |
| E425 | 30.0 | 12.0 | 21.3 | 1.0 | 0.10(E) | – | – | – | – | T1 | 0.26 | 0.06 | – | – | – | – |
| E425 | 30.0 | 12.0 | 21.3 | 1.0 | 0.10(E) | – | – | – | – | T2 | 0.30 | 0.06 | – | – | – | – |
| E426 | 1.3 | 0.5 | 21.2 | 1.0 | 0.15(E) | – | – | – | – | X | 0.22 | 0.06 | – | – | – | – |
| E426 | 1.3 | 0.5 | 21.2 | 1.0 | 0.15(E) | – | – | – | – | T1 | 0.45 | 0.02 | – | – | – | – |
| E426 | 1.3 | 0.5 | 21.2 | 1.0 | 0.15(E) | – | – | – | – | T2 | 0.50 | 0.03 | – | – | – | – |
| E426 | 1.3 | 0.5 | 21.2 | 1.0 | 0.15(E) | – | – | – | – | Y | 0.56 | 0.03 | – | – | – | – |
| E426 | 1.3 | 0.5 | 21.2 | 1.0 | 0.15(E) | – | – | – | – | Z | 0.82 | 0.03 | – | – | – | – |
| E427 | 0.6 | 0.25 | 20.9 | 1.0 | – | – | 0.2 | – | – | XO | 0.19 | 0.006 | – | 0.07 | – | – |
| E427 | 0.6 | 0.25 | 20.9 | 1.0 | – | – | 0.2 | – | – | X1 | 0.19 | 0.010 | – | 0.06 | – | – |
| E427 | 0.6 | 0.25 | 20.9 | 1.0 | – | – | 0.2 | – | – | Y | 0.40 | 0.007 | – | 0.06 | – | – |
| E427 | 0.6 | 0.25 | 20.9 | 1.0 | – | – | 0.2 | – | – | Z | 0.72 | 0.020 | – | 0.05 | – | – |

## APPENDIX E (Cont'd)

| Casting Identification | Solidification Rate cm/hr | Solidification Rate in/hr | Charge Composition (Percent) Cb | Cr | C | B | Zr | Hf | Ta | Specimen Identification | Approximate Fraction Solidified | Analyzed Composition (Percent) C | B | Zr | Hf | Ta |
|---|---|---|---|---|---|---|---|---|---|---|---|---|---|---|---|---|
| E428 | 0.6 | 0.25 | 20.9 | 1.0 | 0.08(E) | – | 0.2 | – | – | X | 0.21 | 0.03 | – | 0.05 | – | – |
| E428 | 0.6 | 0.25 | 20.9 | 1.0 | 0.08(E) | – | 0.2 | – | – | T3 | 0.28 | 0.004 | – | – | – | – |
| E428 | 0.6 | 0.25 | 20.9 | 1.0 | 0.08(E) | – | 0.2 | – | – | T1 | 0.47 | 0.03 | – | – | – | – |
| E428 | 0.6 | 0.25 | 20.9 | 1.0 | 0.08(E) | – | 0.2 | – | – | T2 | 0.51 | 0.04 | – | – | – | – |
| E428 | 0.6 | 0.25 | 20.9 | 1.0 | 0.08(E) | – | 0.2 | – | – | Y | 0.55 | 0.03 | – | 0.04 | – | – |
| E428 | 0.6 | 0.25 | 20.9 | 1.0 | 0.08(E) | – | 0.2 | – | – | Z | 0.72 | 0.04 | – | 0.09 | – | – |
| E430 | 0.6 | 0.25 | 18.3 | 6.0 | 0.10(E) | – | – | – | 3.0 | T1 | 0.48 | 0.08 | – | – | – | – |
| E430 | 0.6 | 0.25 | 18.3 | 6.0 | 0.10(E) | – | – | – | 3.0 | T2 | 0.52 | 0.07 | – | – | – | – |
| E430 | 0.6 | 0.25 | 18.3 | 6.0 | 0.10(E) | – | – | – | 3.0 | L1 | 0.72 | – | – | – | – | 3.2 |
| E430 | 0.6 | 0.25 | 18.3 | 6.0 | 0.10(E) | – | – | – | 3.0 | L2 | 0.72 | – | – | – | – | 2.7 |
| E430 | 0.6 | 0.25 | 18.3 | 6.0 | 0.10(E) | – | – | – | 3.0 | L3 | 0.72 | – | – | – | – | 2.9 |
| E431 | 0.6 | 0.25 | 19.1 | 1.0 | 0.10(N) | – | – | – | 3.0 | T1 | 0.28 | 0.08 | – | – | – | – |
| E431 | 0.6 | 0.25 | 19.1 | 1.0 | 0.10(N) | – | – | – | 3.0 | T2 | 0.33 | 0.08 | – | – | – | – |
| E431 | 0.6 | 0.25 | 19.1 | 1.0 | 0.10(N) | – | – | – | 3.0 | L1 | 0.48 | – | – | – | – | 3.2 |
| E431 | 0.6 | 0.25 | 19.1 | 1.0 | 0.10(N) | – | – | – | 3.0 | L6 | 0.48 | – | – | – | – | 3.2 |
| E432 | 1.3 | 0.5 | 21.2 | 1.0 | 0.10(N) | – | – | – | – | T1 | 0.35 | 0.08 | – | – | – | – |
| E432 | 1.3 | 0.5 | 21.2 | 1.0 | 0.10(N) | – | – | – | – | T2 | 0.39 | 0.08 | – | – | – | – |
| E433 | 0.6 | 0.25 | 20.0 | 6.0 | – | – | – | – | – | T1 | 0.26 | 0.009 | – | – | – | – |
| E433 | 0.6 | 0.25 | 20.0 | 6.0 | – | – | – | – | – | T2 | 0.30 | <0.001 | – | – | – | – |
| E433 | 0.6 | 0.25 | 20.0 | 6.0 | – | – | – | – | – | T3 | 0.35 | <0.001 | – | – | – | – |
| E433 | 0.6 | 0.25 | 20.0 | 6.0 | – | – | – | – | – | T4 | 0.39 | <0.001 | – | – | – | – |
| E433 | 0.6 | 0.25 | 20.0 | 6.0 | – | – | – | – | – | T5 | 0.43 | <0.001 | – | – | – | – |
| E435 | 1.3 | 0.5 | 21.0 | 1.0 | – | – | – | – | – | T1 | 0.26 | <0.001 | – | – | – | – |
| E435 | 1.3 | 0.5 | 21.0 | 1.0 | – | – | – | – | – | T2 | 0.31 | <0.001 | – | – | – | – |
| E435 | 1.3 | 0.5 | 21.0 | 1.0 | – | – | – | – | – | T3 | 0.36 | <0.001 | – | – | – | – |
| E435 | 1.3 | 0.5 | 21.0 | 1.0 | – | – | – | – | – | T4 | 0.40 | <0.001 | – | – | – | – |
| E435 | 1.3 | 0.5 | 21.0 | 1.0 | – | – | – | – | – | T5 | 0.45 | <0.001 | – | – | – | – |

## APPENDIX E (Cont'd)

| Casting Identification | Solidification Rate cm/hr | Solidification Rate in/hr | Charge Composition (Percent) Cb | Cr | C | B | Zr | Hf | Ta | Specimen Identification | Approximate Fraction Solidified | Analyzed Composition (Percent) C | B | Zr | Hf | Ta |
|---|---|---|---|---|---|---|---|---|---|---|---|---|---|---|---|---|
| E437 | 0.6 | 0.25 | 20.9 | 1.0 | – | – | 0.2 | – | – | X | 0.27 | – | – | 0.02 | – | – |
| E437 | 0.6 | 0.25 | 20.9 | 1.0 | – | – | 0.2 | – | – | Y | 0.64 | – | – | 0.02 | – | – |
| E437 | 0.6 | 0.25 | 20.9 | 1.0 | – | – | 0.2 | – | – | Z | 0.91 | – | – | 0.02 | – | – |
| E447 | 0.6 | 0.25 | 20.0 | 6.0 | – | – | – | – | – | B | 0.20 | 0.001 | – | – | – | – |
| E447 | 0.6 | 0.25 | 20.0 | 6.0 | – | – | – | – | – | K | 0.47 | 0.001 | – | – | – | – |
| E448 | 0.6 | 0.25 | 20.0 | 6.0 | – | – | – | – | – | B | 0.18 | 0.002 | – | – | – | – |
| E448 | 0.6 | 0.25 | 20.0 | 6.0 | – | – | – | – | – | H | 0.40 | 0.002 | – | – | – | – |
| E450 | 0.6 | 0.25 | 19.0 | 1.0 | – | – | – | – | 3.0 | C | 0.20 | – | – | – | – | 4.0 |
| E450 | 0.6 | 0.25 | 19.0 | 1.0 | – | – | – | – | 3.0 | N | 0.54 | – | – | – | – | 3.1 |
| E450 | 0.6 | 0.25 | 19.0 | 1.0 | – | – | – | – | 3.0 | O | 0.58 | – | – | – | – | 3.2 |
| E450 | 0.6 | 0.25 | 19.0 | 1.0 | – | – | – | – | 3.0 | Q | 0.72 | – | – | – | – | 3.0 |
| E452 | 0.6 | 0.25 | 20.0 | 6.0 | – | – | – | – | – | B | 0.26 | 0.002 | – | – | – | – |
| E452 | 0.6 | 0.25 | 20.0 | 6.0 | – | – | – | – | – | E | 0.42 | 0.004 | – | – | – | – |
| E452 | 0.6 | 0.25 | 20.0 | 6.0 | – | – | – | – | – | G | 0.52 | 0.001 | – | – | – | – |
| E452 | 0.6 | 0.25 | 20.0 | 6.0 | – | – | – | – | – | L | 0.72 | 0.005 | – | – | – | – |
| E453 | 0.6 | 0.25 | 20.1 | 6.0 | 0.06(E) | – | – | – | – | C | 0.22 | 0.07 | – | – | – | – |
| E453 | 0.6 | 0.25 | 20.1 | 6.0 | 0.06(E) | – | – | – | – | F | 0.42 | 0.06 | – | – | – | – |
| E453 | 0.6 | 0.25 | 20.1 | 6.0 | 0.06(E) | – | – | – | – | G | 0.47 | 0.05 | – | – | – | – |
| E453 | 0.6 | 0.25 | 20.1 | 6.0 | 0.06(E) | – | – | – | – | H | 0.51 | 0.05 | – | – | – | – |
| E453 | 0.6 | 0.25 | 20.1 | 6.0 | 0.06(E) | – | – | – | – | J1 | 0.56 | 0.05 | – | – | – | – |
| E453 | 0.6 | 0.25 | 20.1 | 6.0 | 0.06(E) | – | – | – | – | L | 0.74 | 0.06 | – | – | – | – |
| E459 | 0.6 | 0.25 | 20.1 | 6.0 | 0.08(E) | – | – | – | – | C | 0.18 | 0.11 | – | – | – | – |
| E459 | 0.6 | 0.25 | 20.1 | 6.0 | 0.08(E) | – | – | – | – | D | 0.26 | 0.17 | – | – | – | – |
| E459 | 0.6 | 0.25 | 20.1 | 6.0 | 0.08(E) | – | – | – | – | F | 0.34 | 0.10 | – | – | – | – |
| E459 | 0.6 | 0.25 | 20.1 | 6.0 | 0.08(E) | – | – | – | – | H | 0.44 | 0.08 | – | – | – | – |
| E459 | 0.6 | 0.25 | 20.1 | 6.0 | 0.08(E) | – | – | – | – | K | 0.54 | 0.07 | – | – | – | – |
| E459 | 0.6 | 0.25 | 20.1 | 6.0 | 0.08(E) | – | – | – | – | M | 0.58 | 0.08 | – | – | – | – |

## APPENDIX E (Cont'd)

| Casting Identification | Solidification Rate cm/hr | Solidification Rate in/hr | Charge Composition (Percent) Cb | Cr | C | B | Zr | Hf | Ta | Specimen Identification | Approximate Fraction Solidified | Analyzed Composition (Percent) C | B | Zr | Hf | Ta |
|---|---|---|---|---|---|---|---|---|---|---|---|---|---|---|---|---|
| E468 | 0.6 | 0.25 | 20.1 | 6.0 | 0.04(N) | – | – | – | – | B | 0.15 | 0.04 | – | – | – | – |
| E468 | 0.6 | 0.25 | 20.1 | 6.0 | 0.04(N) | – | – | – | – | F | 0.37 | 0.03 | – | – | – | – |
| E468 | 0.6 | 0.25 | 20.1 | 6.0 | 0.04(N) | – | – | – | – | G | 0.41 | 0.02 | – | – | – | – |
| E468 | 0.6 | 0.25 | 20.1 | 6.0 | 0.04(N) | – | – | – | – | H | 0.45 | 0.03 | – | – | – | – |
| E468 | 0.6 | 0.25 | 20.1 | 6.0 | 0.04(N) | – | – | – | – | J | 0.50 | 0.03 | – | – | – | – |
| E468 | 0.6 | 0.25 | 20.1 | 6.0 | 0.04(N) | – | – | – | – | L | 0.56 | 0.04 | – | – | – | – |
| E469 | 0.6 | 0.25 | 20.1 | 6.0 | 0.08(N) | – | – | – | – | C | 0.18 | 0.09 | – | – | – | – |
| E469 | 0.6 | 0.25 | 20.1 | 6.0 | 0.08(N) | – | – | – | – | G | 0.34 | 0.09 | – | – | – | – |
| E469 | 0.6 | 0.25 | 20.1 | 6.0 | 0.08(N) | – | – | – | – | K2 | 0.54 | 0.07 | – | – | – | – |
| E469 | 0.6 | 0.25 | 20.1 | 6.0 | 0.08(N) | – | – | – | – | K5 | 0.67 | 0.07 | – | – | – | – |
| E469 | 0.6 | 0.25 | 20.1 | 6.0 | 0.08(N) | – | – | – | – | K6 | 0.71 | 0.07 | – | – | – | – |
| E469 | 0.6 | 0.25 | 20.1 | 6.0 | 0.08(N) | – | – | – | – | M | 0.76 | 0.07 | – | – | – | – |
| E471 | 0.6 | 0.25 | 20.1 | 6.0 | 0.10(N) | – | – | – | – | C | 0.18 | 0.10 | – | – | – | – |
| E471 | 0.6 | 0.25 | 20.1 | 6.0 | 0.10(N) | – | – | – | – | F | 0.28 | 0.09 | – | – | – | – |
| E471 | 0.6 | 0.25 | 20.1 | 6.0 | 0.10(N) | – | – | – | – | H | 0.36 | 0.08 | – | – | – | – |
| E471 | 0.6 | 0.25 | 20.1 | 6.0 | 0.10(N) | – | – | – | – | J | 0.40 | 0.08 | – | – | – | – |
| E471 | 0.6 | 0.25 | 20.1 | 6.0 | 0.10(N) | – | – | – | – | M | 0.68 | 0.07 | – | – | – | – |
| E472 | 0.6 | 0.25 | 20.1 | 6.0 | 0.12(N) | – | – | – | – | C | 0.18 | 0.18 | – | – | – | – |
| E472 | 0.6 | 0.25 | 20.1 | 6.0 | 0.12(N) | – | – | – | – | F | 0.60 | 0.08 | – | – | – | – |
| E472 | 0.6 | 0.25 | 20.1 | 6.0 | 0.12(N) | – | – | – | – | G | 0.66 | 0.08 | – | – | – | – |
| E472 | 0.6 | 0.25 | 20.1 | 6.0 | 0.12(N) | – | – | – | – | H | 0.70 | 0.08 | – | – | – | – |
| E472 | 0.6 | 0.25 | 20.1 | 6.0 | 0.12(N) | – | – | – | – | J | 0.74 | 0.07 | – | – | – | – |
| E472 | 0.6 | 0.25 | 20.1 | 6.0 | 0.12(N) | – | – | – | – | L | 0.80 | 0.06 | – | – | – | – |
| E473 | 0.6 | 0.25 | 20.1 | 6.0 | 0.10(N) | – | – | – | – | C | 0.14 | 0.08 | – | – | – | – |
| E473 | 0.6 | 0.25 | 20.1 | 6.0 | 0.10(N) | – | – | – | – | F | 0.34 | 0.09 | – | – | – | – |
| E473 | 0.6 | 0.25 | 20.1 | 6.0 | 0.10(N) | – | – | – | – | K | 0.50 | 0.07 | – | – | – | – |
| E473 | 0.6 | 0.25 | 20.1 | 6.0 | 0.10(N) | – | – | – | – | N | 0.62 | 0.06 | – | – | – | – |
| E473 | 0.6 | 0.25 | 20.1 | 6.0 | 0.10(N) | – | – | – | – | Q | 0.72 | 0.06 | – | – | – | – |

# APPENDIX F
# RESULTS OF PHASE II AND III 760°C (1400°F) TRANSVERSE TENSION TESTS

| Casting Identification | Solidification Rate cm/hr | Solidification Rate in/hr | Chromium Level, Pct. | Alloy Modification (Charge Composition Percent) | Specimen Identification | Thermal Treatment Code (1) | Analyzed(2) Composition, Pct. | Microstructure In Test Specimen | 0.2% Yield Strength MPa | 0.2% Yield Strength KSI | Ultimate Strength MPa | Ultimate Strength KSI | Fracture Strain Percent |
|---|---|---|---|---|---|---|---|---|---|---|---|---|---|
| E268 | 1.3 | 0.5 | 6.0 | 0.1 Zr | 5 | – | 0.03 Zr* | Cellular | – | – | 624 | 90.5 | 0.12 |
| E268 | 1.3 | 0.5 | 6.0 | 0.1 Zr | 6 | – | 0.03 Zr* | Cellular | – | – | 628 | 91.1 | 0.10 |
| E312 | 1.3 | 0.5 | 1.0 | 1.0 Hf | G | – | 0.7 Hf* | Cellular, grossly δ dendritic | – | – | 515 | 74.8 | 0.08 |
| E312 | 1.3 | 0.5 | 1.0 | 1.0 Hf | K | – | 0.7 Hf* | Cellular, grossly δ dendritic | – | – | 493 | 71.5 | 0.06 |
| E313 | 1.3 | 0.5 | 1.0 | 0.1 C | H | – | 0.07 C* | Lamellar | 630 | 91.5 | 679 | 98.6 | 0.76 |
| E313 | 1.3 | 0.5 | 1.0 | 0.1 C | J | – | 0.07 C* | Lamellar | 650 | 94.3 | 685 | 99.4 | 0.48 |
| E314 | 1.3 | 0.5 | 1.0 | 0.02 C | H | – | 0.003 C* | Lamellar | 598 | 86.8 | 616 | 89.4 | 0.34 |
| E314 | 1.3 | 0.5 | 1.0 | 0.02 C | J1 | – | 0.003 C* | Lamellar | 609 | 88.4 | 632 | 91.7 | 0.26 |
| E315 | 1.3 | 0.5 | 1.0 | 0.1 Zr | E | – | 0.02 Zr* | Lamellar, δ dendritic | 610 | 88.6 | 612 | 88.8 | 0.24 |
| E315 | 1.3 | 0.5 | 1.0 | 0.1 Zr | F | – | 0.02 Zr* | Lamellar, δ dendritic | – | – | 525 | 76.2 | 0.06 |
| E318 Bot. | 30 | 12 | 1.0 | None | B | – | – | Cellular, fine grain | – | – | 498 | 72.3 | 0.01 |
| E318 Bot. | 30 | 12 | 1.0 | None | C | – | – | Cellular, fine grain | – | – | 491 | 71.3 | 0.02 |
| E318 Bot. | 30 | 12 | 1.0 | None | D | – | – | Cellular, fine grain | – | – | 451 | 65.4 | 0.03 |
| E318 Top | 1.3 | 0.5 | 1.0 | None | F | – | – | Cellular, δ dendritic | – | – | 517 | 75.0 | 0.05 |
| E318 Top | 1.3 | 0.5 | 1.0 | None | G | – | – | Cellular, δ dendritic | – | – | 474 | 83.3 | 0.08 |
| E318 Top | 1.3 | 0.5 | 1.0 | None | 1 | – | 0.004 C | Lamellar | 628 | 91.1 | 629 | 91.3 | 0.20 |
| E318 Top | 1.3 | 0.5 | 1.0 | None | 2 | – | <0.002 C | Lamellar | 636 | 92.3 | 640 | 92.9 | 0.26 |
| E318 Top | 1.3 | 0.5 | 1.0 | None | 3 | – | 0.006 C | Lamellar | 616 | 89.4 | 640 | 92.9 | 0.36 |
| E318 Top | 1.3 | 0.5 | 1.0 | None | 4 | – | 0.005 C | Lamellar | 678 | 98.4 | 688 | 99.8 | 0.26 |
| E318 Top | 1.3 | 0.5 | 1.0 | None | 5 | – | <0.002 C | Lamellar | 672 | 97.5 | 679 | 98.5 | 0.24 |
| E318 Top | 1.3 | 0.5 | 1.0 | None | 6 | – | <0.002 C | Lamellar | 566 | 82.1 | 595 | 86.4 | 0.28 |
| E319 | 1.3 | 0.5 | 6.0 | 0.1 C | A | – | 0.06* | Cellular, slightly γ dendritic | – | – | 520 | 75.4 | 0.11 |
| E319 | 1.3 | 0.5 | 6.0 | 0.1 C | B | – | 0.06* | Cellular, slightly γ dendritic | – | – | 497 | 72.2 | 0.07 |
| E319 | 1.3 | 0.5 | 6.0 | 0.1 C | E | – | 0.19* | Carbide dendrite on fracture surface | – | – | 310 | 45.0 | <0.01 |
| E319 | 1.3 | 0.5 | 6.0 | 0.1 C | F | – | 0.19* | Lamellar, slightly γ dendritic | 635 | 92.2 | 658 | 95.5 | 0.35 |
| E320 | 1.3 | 0.5 | 6.0 | 0.02 C | A | – | 0.02 C* | Cellular | 610 | 88.5 | 633 | 91.8 | 0.27 |
| E320 | 1.3 | 0.5 | 6.0 | 0.02 C | B | – | 0.02 C* | Cellular | 639 | 92.7 | 643 | 93.3 | 0.27 |
| E322 | 1.3 | 0.5 | 6.0 | 1.0 Hf | A | – | 0.2 Hf* | Cellular, slightly δ dendritic | – | – | 739 | 107.2 | 0.14 |
| E322 | 1.3 | 0.5 | 6.0 | 1.0 Hf | B | – | 0.2 Hf* | Cellular, slightly δ dendritic | – | – | 756 | 109.7 | 0.12 |
| E322 | 1.3 | 0.5 | 6.0 | 1.0 Hf | C | – | 0.2 Hf* | Cellular, slightly δ dendritic | – | – | 683 | 99.1 | 0.07 |
| E323 | 1.3 | 0.5 | 1.0 | 0.04 B | C4 | – | 0.14 B* | Slightly cellular δ dendritic | – | – | 609 | 88.4 | 0.06 |
| E324 | 1.3 | 0.5 | 1.0 | 0.01 B | H | – | 0.004 B* | Lamellar, δ dendritic | – | – | 657 | 95.3 | 0.12 |
| E324 | 1.3 | 0.5 | 1.0 | 0.01 B | J | – | 0.004 B* | Lamellar, δ dendritic | – | – | 637 | 92.5 | 0.06 |

# APPENDIX F (Cont'd)

| Casting Identification | Solidification Rate cm/hr | Solidification Rate in/hr | Chromium Level, Pct. | Alloy Modification (Charge Composition Percent) | Specimen Identification | Thermal Treatment Code (1) | Analyzed(2) Composition, Pct. | Microstructure In Test Specimen | 0.2% Yield Strength MPa | 0.2% Yield Strength KSI | Ultimate Strength MPa | Ultimate Strength KSI | Fracture Strain Percent |
|---|---|---|---|---|---|---|---|---|---|---|---|---|---|
| E325 | 1.3 | 0.5 | 1.0 | 0.06 Zr + 0.02 B | H | – | <0.02 Zr*, 0.006 B* | Lamellar, δ dendritic | – | – | 648 | 94.1 | 0.06 |
| E325 | 1.3 | 0.5 | 1.0 | 0.06 Zr + 0.02 B | J | – | <0.02 Zr*, 0.006 B* | Lamellar, δ dendritic | – | – | 593 | 86.0 | 0.03 |
| E328 | 1.3 | 0.5 | 1.0 | 0.6 Hf + 0.05 C | F | – | 0.3 Hf*, 0.04C* | Slightly cellular, grossly δ dendritic | – | – | 280 | 40.7 | 0.01 |
| E328 | 1.3 | 0.5 | 1.0 | 0.6 Hf + 0.05 C | G | – | 0.3 Hf*, 0.04C* | Slightly cellular, grossly δ dendritic | – | – | 590 | 85.6 | 0.14 |
| E329 | 1.3 | 0.5 | 1.0 | None | B | – | – | Lamellar, δ dendritic | 595 | 86.3 | 595 | 86.3 | 0.20 |
| E332 | 1.3 | 0.5 | 6.0 | 0.1 Zr | B | – | 0.04 Zr* | Cellular | – | – | 576 | 83.6 | 0.15 |
| E332 | 1.3 | 0.5 | 6.0 | 0.1 Zr | C | – | 0.04 Zr* | Cellular | – | – | 566 | 82.1 | 0.12 |
| E333 | 1.3 | 0.5 | 6.0 | 0.05 B | A | – | 0.05 B* | Cellular, δ dendritic | – | – | 468 | 67.9 | 0.01 |
| E333 | 1.3 | 0.5 | 6.0 | 0.05 B | B | – | 0.05 B* | Cellular, δ dendritic | – | – | 433 | 62.8 | 0.01 |
| E334 | 1.3 | 0.5 | 6.0 | 0.01 B | A | – | 0.004 B* | Cellular | – | – | 672 | 97.5 | 0.15 |
| E334 | 1.3 | 0.5 | 6.0 | 0.01 B | B | – | 0.004 B* | Cellular | – | – | 672 | 97.5 | 0.07 |
| E338 | 1.3 | 0.5 | 6.0 | 0.06 Zr + 0.02 B | A | – | 0.02 B*, 0.02 Zr* | Cellular | – | – | 548 | 79.5 | 0.07 |
| E338 | 1.3 | 0.5 | 6.0 | 0.06 Zr + 0.02 B | B | – | 0.02 B*, 0.02 Zr* | Cellular | – | – | 603 | 87.5 | 0.06 |
| E339 | 1.3 | 0.5 | 6.0 | 0.6 Hf + 0.05 C | A | – | 0.3 Hf*, 0.05 C* | Cellular | – | – | 493 | 71.5 | 0.06 |
| E341 | 1.3 | 0.5 | 6.0 | None | A | – | – | Cellular, heavily δ dendritic | – | – | 522 | 75.8 | 0.03 |
| E341 | 1.3 | 0.5 | 6.0 | None | B | – | – | Cellular, heavily δ dendritic | – | – | 528 | 76.6 | 0.02 |
| E341 | 1.3 | 0.5 | 6.0 | None | C | – | – | Cellular, heavily δ dendritic | – | – | 545 | 79.1 | 0.06 |
| E355 | 0.6 | 0.25 | 1.0 | None | E | – | – | Lamellar | – | – | 616 | 89.4 | 0.18 |
| E355 | 0.6 | 0.25 | 1.0 | None | G | – | – | Lamellar | 640 | 92.9 | 640 | 92.9 | 0,21 |
| E359 | 0.6 | 0.25 | 1.0 | 1.0 Hf | E1 | – | 0.08 Hf* | Lamellar | 629 | 91.3 | 630 | 91.5 | 0.25 |
| E359 | 0.6 | 0.25 | 1.0 | 1.0 Hf | E2 | – | 0.08 Hf* | Lamellar | 599 | 86.9 | 599 | 86.9 | 0.20 |
| E363 Bot. | 0.6 | 0.25 | 6.0 | None | T1 | – | – | Lamellar | 629 | 91.2 | 652 | 94.6 | 0.39 |
| E363 Bot. | 0.6 | 0.25 | 6.0 | None | T2 | – | – | Lamellar | 656 | 95.2 | 684 | 99.2 | 0.42 |
| E363 Top | 1.3 | 0.5 | 6.0 | None | T6 | – | – | Cellular | 610 | 88.5 | 652 | 94.7 | 0.27 |
| E365 | 1.3 | 0.5 | 6.0 | 0.2 Zr | B | – | – | Cellular, slightly δ dendritic | – | – | 532 | 77.2 | 0.10 |
| E366 | 1.3 | 0.5 | 6.0 | 0.2 Zr + 0.02 C | A | – | 0.018 C* | Cellular | 617 | 89.5 | 628 | 91.1 | 0.30 |
| E366 | 1.3 | 0.5 | 6.0 | 0.2 Zr + 0.02 C | B | – | 0.018 C* | Cellular | 590 | 85.7 | 613 | 88.9 | 0.31 |
| E367 | 1.3 | 0.5 | 6.0 | 0.6 Hf + 0.1 C | A | – | – | Cellular, slightly δ dendritic | – | – | 371 | 53.8 | 0.01 |
| E367 | 1.3 | 0.5 | 6.0 | 0.6 Hf + 0.1 C | B | – | – | Cellular, slightly δ dendritic | 522 | 75.8 | 531 | 77.0 | 0.22 |
| E368 | 1.3 | 0.5 | 6.0 | 0.02 B + 0.05 C | A | – | – | Lamellar, very slightly Cb lean | – | – | 617 | 89.6 | 0.10 |
| E368 | 1.3 | 0.5 | 6.0 | 0.02 B + 0.05 C | B | – | – | Lamellar | – | – | 310 | 45.0 | 0.01 |
| E368 | 1.3 | 0.5 | 6.0 | 0.02 B + 0.05 C | C | – | – | Cellular | – | – | 418 | 60.7 | 0.01 |

# APPENDIX F (Cont'd)

| Casting Identification | Solidification Rate cm/hr | Solidification Rate in/hr | Chromium Level, Pct. | Alloy Modification (Charge Composition Percent) | Specimen Identification | Thermal Treatment Code (1) | Analyzed(2) Composition, Pct. | Microstructure In Test Specimen | 0.2% Yield Strength MPa | 0.2% Yield Strength KSI | Ultimate Strength MPa | Ultimate Strength KSI | Fracture Strain Percent |
|---|---|---|---|---|---|---|---|---|---|---|---|---|---|
| E371 | 1.3 | 0.5 | 1.0 | None | B1 | – | – | Cellular | – | – | 536 | 77.8 | 0.05 |
| E371 | 1.3 | 0.5 | 1.0 | None | B2 | – | – | Cellular | – | – | 426 | 61.9 | 0.01 |
| E371 | 1.3 | 0.5 | 1.0 | None | B3 | – | – | Cellular | – | – | 605 | 87.8 | 0.09 |
| E371 | 1.3 | 0.5 | 1.0 | None | B4 | – | – | Cellular | – | – | 491 | 71.3 | 0.05 |
| E371 | 1.3 | 0.5 | 1.0 | None | B5 | – | – | Cellular | – | – | 556 | 80.7 | 0.07 |
| E372 | 1.3 | 0.5 | 6.0 | 0.1 C | B | – | – | Cellular, grossly δ dendritic | – | – | 385 | 55.9 | 0.02 |
| E382 | 1.3 | 0.5 | 1.0 | 0.06 B | E | – | 0.006 B* | Lamellar | – | – | 661 | 96.0 | 0.12 |
| E382 | 1.3 | 0.5 | 1.0 | 0.06 B | F | – | 0.006 B* | Lamellar | – | – | 632 | 91.8 | 0.09 |
| E383 | 1.3 | 0.5 | 1.0 | 0.2 Zr | F | – | 0.08 Zr* | Very slightly cellular | – | – | 565 | 82.0 | 0.08 |
| E383 | 1.3 | 0.5 | 1.0 | 0.2 Zr | G | – | 0.08 Zr* | Very slightly cellular | 444 | 64.4 | 455 | 66.0 | 0.30 |
| E385 | 1.3 | 0.5 | 1.0 | 0.1 C | A5F | 2200 (4) | 0.07 C* | Lamellar | – | – | 664 | 96.3 | 0.13 |
| E385 | 1.3 | 0.5 | 1.0 | 0.1 C | A5G | 2200 (4)+1600 (24) | 0.07 C* | Lamellar | – | – | 684 | 99.2 | 0.11 |
| E385 | 1.3 | 0.5 | 1.0 | 0.1 C | A5H | 2200 (4)+1600 (24) | 0.07 C* | Lamellar | – | – | 609 | 88.3 | 0.17 |
| E385 | 1.3 | 0.5 | 1.0 | 0.1 C | B | – | 0.07 C* | Lamellar | 656 | 95.2 | 660 | 95.8 | 0.30 |
| E385 | 1.3 | 0.5 | 1.0 | 0.1 C | C | – | 0.07 C* | Lamellar | 672 | 97.6 | 678 | 98.4 | 0.31 |
| E385 | 1.3 | 0.5 | 1.0 | 0.1 C | D | – | 0.07 C* | Lamellar | 688 | 99.8 | 688 | 99.8 | 0.23 |
| E385 | 1.3 | 0.5 | 1.0 | 0.1 C | E | – | 0.07 C* | Lamellar | 678 | 98.4 | 689 | 100.0 | 0.38 |
| E388 | 0.6 | 0.25 | 6.0 | 0.1 C | C | – | 0.06 C* | Lamellar | 496 | 71.9 | 517 | 75.0 | 1.02 |
| E388 | 0.6 | 0.25 | 6.0 | 0.1 C | E | – | 0.06 C* | Lamellar | 676 | 98.0 | 676 | 98.0 | 0.20 |
| E389 | 1.3 | 0.5 | 1.0 | 0.15 C | F | – | 0.05 C* | Lamellar | 504 | 73.1 | 535 | 77.6 | 0.75 |
| E389 | 1.3 | 0.5 | 1.0 | 0.15 C | G | – | 0.05 C* | Lamellar | 567 | 82.3 | 608 | 88.3 | 0.54 |
| E391 | 0.6 | 0.25 | 1.0 | 1.0 Hf + 0.08 C | G | – | 0.5 Hf*, 0.05 C* | Lamellar | 552 | 80.1 | 575 | 83.4 | 0.40 |
| E392 | 0.6 | 0.25 | 1.0 | 1.0 Hf + 0.15 C | H | – | 0.5 Hf*, 0.05 C* | Lamellar, γ dendritic | – | – | 434 | 63.0 | 0.05 |
| E394 | 1.3 | 0.5 | 1.0 | 0.08 C | F | – | 0.05 C* | Lamellar | 523 | 75.9 | 554 | 80.4 | 0.53 |
| E394 | 1.3 | 0.5 | 1.0 | 0.08 C | G | – | 0.05 C* | Lamellar | 591 | 85.8 | 615 | 89.3 | 0.34 |
| E395 | 0.6 | 0.25 | 1.0 | 0.2 Zr + 0.08 C | G | – | 0.11 Zr*, 0.05 C* | Lamellar | 528 | 76.7 | 551 | 80.0 | 0.53 |
| E395 | 0.6 | 0.25 | 1.0 | 0.2 Zr + 0.08 C | H | – | 0.11 Zr*, 0.05 C* | Lamellar | 541 | 78.5 | 558 | 81.0 | 0.49 |
| E396 | 0.6 | 0.25 | 1.0 | 0.2 Zr + 0.06 B | F | – | 0.04 Zr*, 0.006 B* | Lamellar | – | – | 650 | 94.3 | 0.12 |
| E396 | 0.6 | 0.25 | 1.0 | 0.2 Zr + 0.06 B | G | – | 0.04 Zr*, 0.006 B* | Lamellar | – | – | 668 | 97.0 | 0.18 |
| E397 | 0.6 | 0.25 | 1.0 | 0.08 C + 0.06 B | H | – | 0.08 C*, 0.01 B* | Very slightly cellular or Cb lean | – | | 608 | 88.2 | 0.03 |
| E397 | 0.6 | 0.25 | 1.0 | 0.08 C + 0.06 B | J | – | 0.08 C*, 0.01 B* | Very slightly cellular or Cb lean | – | – | 604 | 87.7 | 0.04 |
| E398 | 1.3 | 0.5 | 1.0 | 0.02 B | G | – | 0.003 B* | Lamellar | – | – | 604 | 87.6 | 0.12 |
| E398 | 1.3 | 0.5 | 1.0 | 0.02 B | H | – | 0.003 B* | Lamellar | – | – | 648 | 94.0 | 0.03 |

# APPENDIX F (Cont'd)

| Casting Identification | Solidification Rate cm/hr | Solidification Rate in/hr | Chromium Level, Pct. | Alloy Modification (Charge Composition Percent) | Specimen Identification | Thermal Treatment Code (1) | Analyzed(2) Composition, Pct. | Microstructure In Test Specimen | 0.2% Yield Strength MPa | 0.2% Yield Strength KSI | Ultimate Strength MPa | Ultimate Strength KSI | Fracture Strain Percent |
|---|---|---|---|---|---|---|---|---|---|---|---|---|---|
| E402 | 25 | 10 | 6.0 | None | K | – | – | Cellular, fine grained | – | – | 396 | 57.5 | 0.01 |
| E402 | 25 | 10 | 6.0 | None | L | – | – | Cellular, fine grained | – | – | 476 | 69.1 | 0.02 |
| E403 | 25 | 10 | -0- | 0.1 C | A | – | 0.05 C* | Lamellar | – | – | 647 | 93.9 | 0.07 |
| E403 | 25 | 10 | -0- | 0.1 C | B | – | 0.05 C* | Lamellar | – | – | 594 | 86.2 | 0.08 |
| E403 | 25 | 10 | -0- | 0.1 C | C | – | 0.05 C* | Lamellar, slightly Cb lean | – | – | 577 | 83.8 | 0.05 |
| E414 | 1.3 | 0.5 | 1.0 | 3.0 Ta | T1 | – | 0.008 | Cellular | – | – | 389 | 56.5 | 0.01 |
| E414 | 1.3 | 0.5 | 1.0 | 3.0 Ta | T2 | – | 0.008 | Cellular | – | – | 439 | 63.7 | 0.01 |
| E416 | 0.6 | 0.25 | 6.0 | 0.1 C | B | – | 0.1 | Lamellar | 663 | 96.2 | 696 | 101.0 | 0.46 |
| E416 | 0.6 | 0.25 | 6.0 | 0.1 C | C | – | 0.1 | Lamellar | 647 | 93.9 | 689 | 100.0 | 0.60 |
| E416 | 0.6 | 0.25 | 6.0 | 0.1 C | D | 2200(4)+1600(24) | 0.08 | Lamellar | 689 | 100.0 | 711 | 103.1 | 0.25 |
| E416 | 0.6 | 0.25 | 6.0 | 0.1 C | E | – | 0.08 | Lamellar | 655 | 95.0 | 698 | 101.3 | 0.69 |
| E416 | 0.6 | 0.25 | 6.0 | 0.1 C | F | 2200(4) | 0.07 | Lamellar | 698 | 101.2 | 710 | 103.0 | 0.23 |
| E416 | 0.6 | 0.25 | 6.0 | 0.1 C | G | – | 0.07* | Lamellar | 643 | 93.2 | 676 | 98.0 | 0.30 |
| E416 | 0.6 | 0.25 | 6.0 | 0.1 C | H | 2200(4)+(1600(24) | 0.07 | Lamellar | 712 | 103.2 | 751 | 108.9 | 0.40 |
| E416 | 0.6 | 0.25 | 6.0 | 0.1 C | I | 2200(4) | 0.07 | Lamellar | 725 | 105.1 | 748 | 108.5 | 0.23 |
| E416 | 0.6 | 0.25 | 6.0 | 0.1 C | J | – | 0.06 | Lamellar | 641 | 92.9 | 677 | 98.2 | 0.40 |
| E417 | 1.0 | 0.38 | 1.0 | 3.0 Ta | T2 | – | 2.9 Ta* | Cellular | – | – | 432 | 62.7 | 0.01 |
| E418 | 1.3 | 0.5 | 1.0 | 0.1 C | T1 | – | .08 C | Lamellar | 667 | 96.7 | 692 | 100.4 | 0.40 |
| E418 | 1.3 | 0.5 | 1.0 | 0.1 C | T2 | – | .08C | Lamellar | 621 | 90.0 | 635 | 92.1 | 0.26 |
| E418 | 1.3 | 0.5 | 1.0 | 0.1 C | T3 | – | .08C | Lamellar | 651 | 94.4 | 677 | 98.2 | 0.40 |
| E418 | 1.3 | 0.5 | 1.0 | 0.1 C | T4 | – | .07C | Lamellar | 631 | 91.5 | 654 | 94.9 | 0.39 |
| E418 | 1.3 | 0.5 | 1.0 | 0.1 C | T5 | – | .07C | Lamellar | 617 | 89.5 | 636 | 92.3 | 0.53 |
| E418 | 1.3 | 0.5 | 1.0 | 0.1 C | T6 | – | .06C | Lamellar | 600 | 87.0 | 623 | 90.3 | 0.45 |
| E419 | 0.6 | 0.25 | 6.0 | 3.0 Ta | T1 | – | 3.3 Ta*, 0.003C* | Cellular | – | – | 486 | 70.5 | 0.10 |
| E419 | 0.6 | 0.25 | 6.0 | 3.0 Ta | T2 | – | 3.3 Ta*, 0.003C* | Cellular | – | – | 508 | 73.7 | 0.03 |
| E420 | 1.3 | 0.5 | 1.0 | 0.2 C | T1 | – | 0.09 C | Carbide dendrite on fracture | – | – | 345 | 50.0 | Nil |
| E420 | 1.3 | 0.5 | 1.0 | 0.2 C | T2 | – | 0.09 C | Lamellar | 638 | 92.5 | 654 | 94.8 | 0.30 |
| E420 | 1.3 | 0.5 | 1.0 | 0.2 C | T3 | – | 0.08 C | Lamellar | 638 | 92.5 | 646 | 93.7 | 0.35 |
| E421 | 2.5 | 1.0 | 1.0 | 0.1 C | T1 | – | 0.10 C | Carbide dendrite on fracture | – | – | 504 | 73.1 | 0.02 |
| E421 | 2.5 | 1.0 | 1.0 | 0.1 C | T2 | – | 0.08 C | Lamellar | 585 | 84.8 | 614 | 89.1 | 0.42 |
| E422 | 1.3 | 0.5 | 1.0 | 0.05 C | T1 | – | 0.03 C | Lamellar | 699 | 101.4 | 709 | 102.8 | 0.30 |
| E422 | 1.3 | 0.5 | 1.0 | 0.05 C | T2 | – | 0.03 C | Lamellar | 631 | 91.5 | 657 | 95.3 | 0.34 |
| E423 | 1.3 | 0.5 | 1.0 | 0.08 C | T1 | – | 0.07 C | Lamellar | 678 | 98.3 | 680 | 98.7 | 0.25 |
| E423 | 1.3 | 0.5 | 1.0 | 0.08 C | T2 | – | 0.07 C | Lamellar | 641 | 92.9 | 671 | 97.3 | 0.56 |
| E424 | 1.9 | 0.75 | 1.0 | 0.1 C | T1 | – | 0.06 C | Lamellar | 570 | 82.7 | 594 | 86.2 | 0.44 |
| E424 | 1.9 | 0.75 | 1.0 | 0.1 C | T2 | – | 0.06 C | Lamellar | 647 | 93.9 | 650 | 94.3 | 0.23 |

# APPENDIX F (Cont'd)

| Casting Identification | Solidification Rate cm/hr | Solidification Rate in/hr | Chromium Level, Pct. | Alloy Modification Charge Composition Percent | Specimen Identification | Thermal Treatment Code (1) | Analyzed(2) Composition, Pct. | Microstructure In Test Specimen | 0.2% Yield Strength MPa | 0.2% Yield Strength KSI | Ultimate Strength MPa | Ultimate Strength KSI | Fracture Strain Percent |
|---|---|---|---|---|---|---|---|---|---|---|---|---|---|
| E425 | 30 | 12 | 1.0 | 0.1 C | T1 | – | 0.06 C | Cellular | – | – | 538 | 78.0 | 0.04 |
| E425 | 30 | 12 | 1.0 | 0.1 C | T2 | – | 0.06 C | Cellular | – | – | 538 | 78.0 | 0.06 |
| E426 | 1.3 | 0.5 | 1.0 | 0.15 C | T1 | – | 0.02 C | Lamellar | 674 | 97.8 | 678 | 98.3 | 0.22 |
| E426 | 1.3 | 0.5 | 1.0 | 0.15 C | T2 | – | 0.03 C | Lamellar | 689 | 100.0 | 691 | 100.2 | 0.21 |
| E427 | 0.6 | 0.25 | 1.0 | 0.2 Zr | T1 | – | 0.06 Zr*, 0.007 C* | Not Directionally Solidified | – | – | 449 | 65.1 | 0.01 |
| E427 | 0.6 | 0.25 | 1.0 | 0.2 Zr | T2 | – | 0.06 Zr*, 0.007 C* | Not Directionally Solidified | – | – | 415 | 60.3 | 0.01 |
| E428 | 0.6 | 0.25 | 1.0 | 0.2 Zr + 0.08 C | T1 | – | 0.03 C, 0.04 Zr* | Lamellar | – | – | 590 | 85.7 | 0.18 |
| E428 | 0.6 | 0.25 | 1.0 | 0.2 Zr + 0.08 C | T2 | – | 0.04 C, 0.04 Zr* | Lamellar | 582 | 84.4 | 603 | 87.5 | 0.50 |
| E428 | 0.6 | 0.25 | 1.0 | 0.2 Zr + 0.08 C | T3 | – | 0.04 C, 0.05 Zr* | Lamellar | – | – | 624 | 90.5 | 0.18 |
| E430 | 0.6 | 0.25 | 6.0 | 3.0 Ta + 0.1 C | T1 | – | 3.1 Ta*, 0.08 C | Cellular | – | – | 500 | 72.5 | 0.05 |
| E430 | 0.6 | 0.25 | 6.0 | 3.0 Ta + 0.1 C | T2 | – | 3.1 Ta*, 0.07 C | Cellular | – | – | 520 | 75.4 | 0.08 |
| E431 | 0.6 | 0.25 | 1.0 | 3.0 Ta + 0.1 C | T1 | – | 3.2 Ta*, 0.08 C | Lamellar | – | – | 615 | 89.2 | 0.16 |
| E431 | 0.6 | 0.25 | 1.0 | 3.0 Ta + 0.1 C | T2 | – | 3.2 Ta*, 0.08 C | Lamellar | 598 | 86.7 | 598 | 86.7 | 0.20 |
| E432 | 1.3 | 0.5 | 1.0 | 0.1 C | T1 | – | 0.08 C | Carbide dendrite on fracture | – | – | 565 | 82.0 | 0.08 |
| E432 | 1.3 | 0.5 | 1.0 | 0.1 C | T2 | – | 0.08 C | Lamellar | 614 | 89.1 | 638 | 92.6 | 0.38 |
| E433 | 0.6 | 0.25 | 6.0 | None | T1 | – | 0.009 | Lamellar | 629 | 91.2 | 643 | 93.2 | 0.27 |
| E433 | 0.6 | 0.25 | 6.0 | None | T2 | – | <0.001 | Lamellar | 596 | 86.4 | 621 | 90.0 | 0.40 |
| E433 | 0.6 | 0.25 | 6.0 | None | T3 | – | <0.001 | Lamellar | 635 | 92.1 | 653 | 94.7 | 0.30 |
| E433 | 0.6 | 0.25 | 6.0 | None | T4 | – | <0.001 | Lamellar | 617 | 89.5 | 654 | 94.9 | 0.40 |
| E433 | 0.6 | 0.25 | 6.0 | None | T5 | – | <0.001 | Lamellar | 631 | 91.5 | 665 | 96.5 | 0.38 |
| E434 | 0.6 | 0.25 | 6.0 | None | T1 | – | – | Lamellar | 627 | 91.0 | 652 | 94.7 | 0.35 |
| E434 | 0.6 | 0.25 | 6.0 | None | T2 | – | – | Lamellar | 627 | 91.0 | 652 | 94.7 | 0.32 |
| E435 | 1.3 | 0.5 | 1.0 | None | T1 | – | <0.001 | Lamellar | 610 | 88.5 | 610 | 88.5 | 0.20 |
| E435 | 1.3 | 0.5 | 1.0 | None | T2 | – | <0.001 | Lamellar | – | – | 591 | 85.7 | 0.15 |
| E435 | 1.3 | 0.5 | 1.0 | None | T3 | – | <0.001 | Lamellar | 561 | 81.4 | 585 | 84.9 | 0.32 |
| E435 | 1.3 | 0.5 | 1.0 | None | T4 | – | <0.001 | Lamellar | 636 | 92.3 | 636 | 92.3 | 0.24 |
| E435 | 1.3 | 0.5 | 1.0 | None | T5 | – | <0.001 | Lamellar | 617 | 89.5 | 625 | 90.7 | 0.24 |
| E436 | 1.3 | 0.5 | 1.0 | None | T1 | – | – | Lamellar | 607 | 88.1 | 621 | 90.1 | 0.42 |
| E436 | 1.3 | 0.5 | 1.0 | None | T2 | – | – | Lamellar | 593 | 86.1 | 610 | 88.5 | 0.40 |
| E436 | 1.3 | 0.5 | 1.0 | None | T3 | – | – | Lamellar | 609 | 88.4 | 615 | 89.3 | 0.35 |
| E436 | 1.3 | 0.5 | 1.0 | None | T4 | – | – | Lamellar | 569 | 82.6 | 584 | 84.7 | 0.38 |
| E437 | 0.6 | 0.25 | 1.0 | 0.2 Zr | T1 | – | 0.02* | Lamellar | 588 | 85.3 | 603 | 87.5 | 0.30 |
| E437 | 0.6 | 0.25 | 1.0 | 0.2 Zr | T2 | – | 0.02* | Lamellar | 615 | 89.2 | 618 | 89.7 | 0.21 |

# APPENDIX F (Cont'd)

| Casting Identification | Solidification Rate cm/hr | Solidification Rate in/hr | Chromium Level, Pct. | Alloy Modification (Charge Composition Percent) | Specimen Identification | Thermal Treatment Code (1) | Analyzed(2) Composition, Pct. | Microstructure In Test Specimen | 0.2% Yield Strength MPa | 0.2% Yield Strength KSI | Ultimate Strength MPa | Ultimate Strength KSI | Fracture Strain Percent |
|---|---|---|---|---|---|---|---|---|---|---|---|---|---|
| E447 | 0.6 | 0.25 | 6.0 | None | B | – | 0.001 C | Lamellar | 566 | 82.1 | 624 | 90.5 | 0.44 |
| E447 | 0.6 | 0.25 | 6.0 | None | C | 2110(4) | – | Lamellar | 650 | 94.4 | 678 | 98.8 | 0.28 |
| E447 | 0.6 | 0.25 | 6.0 | None | D | 2110(4)+1650(24) | – | Lamellar | 613 | 89.0 | 637 | 92.4 | 0.66 |
| E447 | 0.6 | 0.25 | 6.0 | None | G | 1975(4) | – | Lamellar | 650 | 94.3 | 671 | 97.4 | 0.27 |
| E447 | 0.6 | 0.25 | 6.0 | None | H | 1975(4)+1650(24) | – | Lamellar | 630 | 91.5 | 688 | 99.8 | 0.45 |
| E447 | 0.6 | 0.25 | 6.0 | None | J | 1650(24) | – | Lamellar | 650 | 94.3 | 684 | 99.3 | 0.75 |
| E447 | 0.6 | 0.25 | 6.0 | None | K | – | 0.001 C | Lamellar | 654 | 94.9 | 755 | 109.6 | 0.55 |
| E448 | 0.6 | 0.25 | 6.0 | None | B | – | 0.002 C | Lamellar | 647 | 93.9 | 658 | 95.5 | 0.26 |
| E448 | 0.6 | 0.25 | 6.0 | None | C | 1650(24) | – | Lamellar | 657 | 95.3 | 676 | 98.1 | 0.33 |
| E448 | 0.6 | 0.25 | 6.0 | None | D | 1975(4)+1650(24) | – | Lamellar | 619 | 89.8 | 647 | 93.2 | 0.50 |
| E448 | 0.6 | 0.25 | 6.0 | None | E | 1975(4) | – | Lamellar | 573 | 83.2 | 610 | 88.6 | 0.37 |
| E448 | 0.6 | 0.25 | 6.0 | None | F | 2110(4)+1650(24) | – | Lamellar | 619 | 89.8 | 648 | 94.0 | 0.50 |
| E448 | 0.6 | 0.25 | 6.0 | None | G | 2110(4) | – | Lamellar | 666 | 96.7 | 722 | 104.8 | 0.33 |
| E448 | 0.6 | 0.25 | 6.0 | None | H | – | 0.002 C | Lamellar | 728 | 105.7 | 754 | 109.4 | 0.35 |
| E450 | 0.6 | 0.25 | 1.0 | 3.0 Ta | M | – | – | Lamellar | – | – | 471 | 68.4 | 0.04 |
| E450 | 0.6 | 0.25 | 1.0 | 3.0 Ta | N | – | 3.1 Ta | Lamellar | – | – | 633 | 91.9 | 0.16 |
| E450 | 0.6 | 0.25 | 1.0 | 3.0 Ta | O | – | 3.2 Ta | Lamellar | 633 | 91.9 | 633 | 91.9 | 0.20 |
| E452 | 0.6 | 0.25 | 6.0 | None | B | – | 0.002 C | Lamellar | 448 | 65.0 | 465 | 67.5 | 0.25 |
| E452 | 0.6 | 0.25 | 6.0 | None | C | 2200(4) | – | Lamellar | 666 | 96.6 | 689 | 100.0 | 0.26 |
| E452 | 0.6 | 0.25 | 6.0 | None | D | 2200(4)+1600(24) | – | Lamellar | – | – | 624 | 90.5 | 0.13 |
| E452 | 0.6 | 0.25 | 6.0 | None | E | – | 0.004 C | Lamellar | – | – | 607 | 88.1 | 0.14 |
| E452 | 0.6 | 0.25 | 6.0 | None | G | – | 0.001 C | Lamellar δ dendritic | – | – | 618 | 89.7 | 0.19 |
| E452 | 0.6 | 0.25 | 6.0 | None | H | 2200(4)+1600(24) | – | Lamellar | 683 | 99.1 | 702 | 101.9 | 0.26 |
| E452 | 0.6 | 0.25 | 6.0 | None | L | – | 0.005 C | Cellular, δ dendritic | – | – | 597 | 86.7 | 0.10 |
| E453 | 0.6 | 0.25 | 6.0 | 0.06 C | F | – | 0.06 C | Lamellar | 662 | 96.1 | 692 | 100.4 | 0.45 |
| E453 | 0.6 | 0.25 | 6.0 | 0.06 C | G | – | 0.05 C | Lamellar | 634 | 92.0 | 648 | 94.0 | 0.59 |
| E453 | 0.6 | 0.25 | 6.0 | 0.06 C | H | – | 0.05 C | Lamellar | 683 | 99.2 | 695 | 100.8 | 0.30 |
| E453 | 0.6 | 0.25 | 6.0 | 0.06 C | J1 | – | 0.05 C | Cellular, δ dendritic | – | – | 634 | 92.0 | 0.10 |
| E459 | 0.6 | 0.25 | 6.0 | 0.06 C | F | – | 0.10 C | Lamellar | 640 | 92.9 | 672 | 97.6 | 0.46 |
| E459 | 0.6 | 0.25 | 6.0 | 0.06 C | H | – | 0.08 C | Lamellar | 683 | 99.2 | 703 | 102.1 | 0.35 |
| E459 | 0.6 | 0.25 | 6.0 | 0.06 C | K | – | 0.07 C | Lamellar | 608 | 88.3 | 635 | 92.1 | 0.46 |
| E466 | 0.6 | 0.25 | 6.0 | None | J(3) | 1975(4)+1650(24) | – | Lamellar | 689 | 100.0 | 715 | 103.8 | 0.54 |

# APPENDIX F (Cont'd)

| Casting Identification | Solidification Rate cm/hr | Solidification Rate in/hr | Chromium Level, Pct. | Alloy Modification (Charge Composition Percent) | Specimen Identification | Thermal Treatment Code (1) | Analyzed(2) Composition, Pct. | Microstructure In Test Specimen | 0.2% Yield Strength MPa | 0.2% Yield Strength KSI | Ultimate Strength MPa | Ultimate Strength KSI | Fracture Strain Percent |
|---|---|---|---|---|---|---|---|---|---|---|---|---|---|
| E468 | 0.6 | 0.25 | 6.0 | 0.04C | F | – | 0.03C | Cellular | 635 | 92.2 | 635 | 92.2 | 0.20 |
| E468 | 0.6 | 0.25 | 6.0 | 0.04C | G | – | 0.02C | Lamellar | 610 | 88.5 | 633 | 91.8 | 0.44 |
| E468 | 0.6 | 0.25 | 6.0 | 0.04C | H | – | 0.03C | Lamellar | 656 | 95.2 | 697 | 101.2 | 0.53 |
| E468 | 0.6 | 0.25 | 6.0 | 0.04C | J | – | 0.03C | Lamellar | 630 | 91.5 | 661 | 96.0 | 0.66 |
| E469 | 0.6 | 0.25 | 6.0 | 0.08C | G | – | 0.09C | Carbide dendrite on fracture | 583 | 84.6 | 597 | 86.7 | 0.30 |
| E469 | 0.6 | 0.25 | 6.0 | 0.08C | H | 1650(24) | – | Lamellar | 574 | 83.3 | 601 | 87.3 | 0.52 |
| E469 | 0.6 | 0.25 | 6.0 | 0.08C | J | 1975(4) + 1650(24) | – | Lamellar | 639 | 92.8 | 703 | 102.1 | 0.55 |
| E469 | 0.6 | 0.25 | 6.0 | 0.08C | K1 | 1975(4) | – | Lamellar | 635 | 92.1 | 689 | 100.0 | 0.58 |
| E469 | 0.6 | 0.25 | 6.0 | 0.08C | K2 | – | 0.07C | Lamellar | 621 | 90.2 | 672 | 99.6 | 0.32 |
| E469 | 0.6 | 0.25 | 6.0 | 0.08C | K3 | 2110(4) + 1650(24) | – | Lamellar | 666 | 96.6 | 712 | 103.4 | 0.47 |
| E469 | 0.6 | 0.25 | 6.0 | 0.08C | K4 | 2110(4) | – | Lamellar | 719 | 104.3 | 742 | 107.7 | 0.28 |
| E469 | 0.6 | 0.25 | 6.0 | 0.08C | K5 | – | 0.07C | Lamellar δ dentritic | 652 | 94.6 | 694 | 100.7 | 0.35 |
| E469 | 0.6 | 0.25 | 6.0 | 0.08C | K6 | – | 0.07C | Lamellar | 661 | 95.9 | 700 | 101.6 | 0.45 |
| E471 | 0.6 | 0.25 | 6.0 | 0.10C | F | – | 0.09C | δ dendritic, broke in radius | – | – | 164 | 23.8 | 0.03 |
| E471 | 0.6 | 0.25 | 6.0 | 0.10C | H | – | 0.08C | Lamellar | 644 | 93.5 | 675 | 98.0 | 0.82 |
| E471 | 0.6 | 0.25 | 6.0 | 0.10C | J | – | 0.08C | Lamellar | 482 | 70.0 | 534 | 77.5 | 0.69 |
| E472 | 0.6 | 0.25 | 6.0 | 0.12C | F | – | 0.08C | Lamellar | 573 | 83.1 | 607 | 88.1 | 0.60 |
| E472 | 0.6 | 0.25 | 6.0 | 0.12C | G | – | 0.08C | Lamellar | 674 | 97.8 | 693 | 100.6 | 0.29 |
| E472 | 0.6 | 0.25 | 6.0 | 0.12C | H | – | 0.08C | Lamellar | 706 | 102.4 | 720 | 104.5 | 0.26 |
| E472 | 0.6 | 0.25 | 6.0 | 0.12C | J | – | 0.07C | Lamellar | 695 | 100.9 | 719 | 104.4 | 0.34 |
| E473 | 0.6 | 0.25 | 6.0 | 0.10C | F | – | 0.09C | Lamellar | 681 | 98.8 | 715 | 103.8 | 0.34 |
| E473 | 0.6 | 0.25 | 6.0 | 0.10C | G | 2110(4) | – | Lamellar | 683 | 99.2 | 723 | 104.9 | 0.30 |
| E473 | 0.6 | 0.25 | 6.0 | 0.10C | H | 2110(4) + 1650(24) | – | Lamellar | 628 | 91.2 | 651 | 94.5 | 0.37 |
| E473 | 0.6 | 0.25 | 6.0 | 0.10C | J | 1975(4) | – | Lamellar | 632 | 91.7 | 672 | 97.5 | 0.36 |
| E473 | 0.6 | 0.25 | 6.0 | 0.10C | K | – | 0.07C | Lamellar | 580 | 84.2 | 601 | 87.3 | 0.90 |
| E473 | 0.6 | 0.25 | 6.0 | 0.10C | L | 1975(4) + 1650(24) | – | Lamellar | 665 | 96.5 | 692 | 100.4 | 0.34 |
| E473 | 0.6 | 0.25 | 6.0 | 0.10C | M | 1650(24) | – | Lamellar | 646 | 93.8 | 670 | 97.3 | 0.35 |
| E473 | 0.6 | 0.25 | 6.0 | 0.10C | N | – | 0.06C | δ needle on fracture surface | 642 | 93.2 | 658 | 95.5 | 0.34 |
| E480 | 0.6 | 0.25 | 6.0 | None | B(3) | 1975(4) + 1650(24) | – | Lamellar | 602 | 87.4 | 635 | 92.1 | 0.54 |
| E497 | 0.6 | 0.25 | 6.0 | None | T1 | – | – | Cellular | – | – | 557 | 80.9 | 0.08 |
| E497 | 0.6 | 0.25 | 6.0 | None | T2 | – | – | Lamellar | 651 | 94.5 | 681 | 98.8 | 0.35 |
| E497 | 0.6 | 0.25 | 6.0 | None | T3 | – | – | Lamellar | 670 | 97.2 | 670 | 97.2 | 0.20 |

# APPENDIX F (Cont'd)

| Casting Identification | Solidification Rate cm/hr | Solidification Rate in/hr | Chromium Level, Pct. | Alloy Modification (Charge Composition Percent) | Specimen Identification | Thermal Treatment Code (1) | Analyzed(2) Composition, Pct. | Microstructure In Test Specimen | 0.2% Yield Strength MPa | 0.2% Yield Strength KSI | Ultimate Strength MPa | Ultimate Strength KSI | Fracture Strain Percent |
|---|---|---|---|---|---|---|---|---|---|---|---|---|---|
| E501 | 0.6 | 0.25 | 6.0 | 0.06C | F(3) | 1975(4) | – | Lamellar | 695 | 100.9 | 749 | 108.7 | 0.87 |
| E501 | 0.6 | 0.25 | 6.0 | 0.06C | G(3) | 1975(4) | – | Lamellar | 640 | 92.9 | 686 | 99.6 | 0.58 |
| E511 | 0.6 | 0.25 | 6.0 | 0.06C | F(3) | 1975(4) | – | Lamellar | 716 | 103.9 | 752 | 109.1 | 0.55 |
| E511 | 0.6 | 0.25 | 6.0 | 0.06C | G(3) | 1975(4) | – | Lamellar | 719 | 104.3 | 783 | 113.7 | 1.35 |
| E511 | 0.6 | 0.25 | 6.0 | 0.06C | H(3) | 1975(4) | – | Lamellar | 739 | 107.3 | 762 | 110.6 | 1.38 |
| E511 | 0.6 | 0.25 | 6.0 | 0.06C | J(3) | 1975(4) | – | Lamellar | 749 | 108.7 | 797 | 115.7 | 0.75 |
| E511 | 0.6 | 0.25 | 6.0 | 0.06C | L(3) | 1975(4) | – | Lamellar | 678 | 98.4 | 722 | 104.8 | 0.58 |
| E525 | 1.3 | 0.5 | 6.0 | None | B | – | – | Lamellar | 628 | 91.1 | 669 | 97.1 | 0.39 |
| E525 | 1.3 | 0.5 | 6.0 | None | C | – | – | Cellular | – | – | 600 | 87.1 | 0.17 |
| E525 | 1.3 | 0.5 | 6.0 | None | E | – | – | Cellular | – | – | 639 | 92.7 | 0.12 |
| E525 | 1.3 | 0.5 | 6.0 | None | F | – | – | Cellular | – | – | 641 | 93.0 | 0.19 |
| E525 | 1.3 | 0.5 | 6.0 | None | G | – | – | Cellular | – | – | 645 | 93.6 | 0.19 |
| E525 | 1.3 | 0.5 | 6.0 | None | H | – | – | Cellular | 628 | 91.1 | 637 | 92.4 | 0.23 |
| E525 | 1.3 | 0.5 | 6.0 | None | K | – | – | Cellular | – | – | 656 | 95.2 | 0.14 |
| E525 | 1.3 | 0.5 | 6.0 | None | L | – | – | Cellular | – | – | 626 | 90.9 | 0.12 |
| E535 | 0.6 | 0.25 | 6.0 | 0.06C | E(3) | 1975(4) | – | Lamellar | 724 | 105.1 | 787 | 114.2 | 1.20 |
| E535 | 0.6 | 0.25 | 6.0 | 0.06C | G(3) | 1975(4) | – | Lamellar | 734 | 106.5 | 753 | 109.3 | 0.33 |

Notes:

(1) See Table below for explanation of thermal treatment code.
(2) Analyzed on specimen threads except as indicated (*), where analysis was estimated from analyses obtained at other locations in casting.
(3) Coated.

Explanation of Thermal Treatment Code

| Code | Exposure Time (hours) | Treatment Temperature (°C) | Treatment Temperature (°F) |
|---|---|---|---|
| 2200 (4) | 4 | 1204 | 2200 |
| 2110 (4) | 4 | 1154 | 2110 |
| 1975 (4) | 4 | 1079 | 1975 |
| 1650 (24) | 24 | 899 | 1650 |
| 1600 (24) | 24 | 871 | 1600 |

## APPENDIX G
## PHASE III LONGITUDINAL CREEP TEST RESULTS

| Casting Number | Charge Composition, % Cr | C | Ta | Analyzed Comp, %* C | Ta | Solidification Rate cm/hr | in/hr | Specimen Identification | Microstructure in Test Specimen | Stress MPa | ksi | Temperature °C | °F | Rupture Life Hours | Prior Creep % | % El | Larson-Miller Parameter (C = 20) |
|---|---|---|---|---|---|---|---|---|---|---|---|---|---|---|---|---|---|
| E355 | 1 | – | – | – | – | 1.3 | 1/2 | H3 | Lamellar | 172 | 25 | 982 | 1800 | 103.2 | 8.6 | 17.0 | 49.8 |
| E355 | 1 | – | – | – | – | 1.3 | 1/2 | H4 | Lamellar | 152 | 22 | 1038 | 1900 | 29.7 | 9.7 | 19.0 | 50.7 |
| F1665 | 1 | – | – | – | – | 0.64 | 1/4 | C | Lamellar | 276 | 40 | 982 | 1800 | 10.3 | 4.5 | 13.5 | 47.5 |
| F1665 | 1 | – | – | – | – | 0.64 | 1/4 | D | Lamellar | 176 | 25 | 982 | 1800 | 114.7 | 10.1 | 16.7 | 49.9 |
| F1665 | 1 | – | – | – | – | 0.64 | 1/4 | B | Lamellar | 152 | 22 | 1038 | 1900 | 30.0 | 6.7 | N.M. | 50.7 |
| E288 | 1 | – | – | – | – | 1.3 | 1/2 | 2 | Lamellar | 724 | 105 | 760 | 1400 | 40.0 | 1.7 | 2.5 | 40.2 |
| E313 | 1 | 0.10 | – | 0.07 | – | 1.3 | 1/2 | O2 | Lamellar | 724 | 105 | 760 | 1400 | 81.6 | 2.1 | 3.5 | 40.8 |
| E313 | 1 | 0.10 | – | 0.07 | – | 1.3 | 1/2 | O1 | Lamellar | 758 | 110 | 760 | 1400 | 11.1 | 0.8 | 1.2 | 39.1 |
| E313 | 1 | 0.10 | – | 0.07 | – | 1.3 | 1/2 | O3 | Lamellar | 176 | 25 | 982 | 1800 | 111.9 | 11.2 | 17.9 | 49.8 |
| E313 | 1 | 0.10 | – | 0.07 | – | 1.3 | 1/2 | P3 | Lamellar | 276 | 40 | 982 | 1800 | 9.5 | 3.2 | 10.1 | 47.4 |
| E313 | 1 | 0.10 | – | 0.07 | – | 1.3 | 1/2 | P1 | Lamellar | 103 | 15 | 1038 | 1900 | 248.0 | 9.2 | 14.4 | 52.9 |
| E313 | 1 | 0.10 | – | 0.07 | – | 1.3 | 1/2 | P2 | Lamellar | 152 | 22 | 1038 | 1900 | 31.2 | 10.0 | 18.9 | 50.7 |
| E424 | 1 | 0.10 | – | .06 | – | 1.9 | 3/4 | A | Lamellar | 758 | 110 | 760 | 1400 | 4.8 | 0.9 | 1.2 | 38.5 |
| E424 | 1 | 0.10 | – | .06 | – | 1.9 | 3/4 | D | Lamellar | 758 | 110 | 760 | 1400 | 66.6 | 2.4 | 3.3 | 40.6 |
| E424 | 1 | 0.10 | – | .06 | – | 1.9 | 3/4 | B | Lamellar | 276 | 40 | 982 | 1800 | 7.9 | 1.3 | 8.2 | 47.2 |
| E424 | 1 | 0.10 | – | .06 | – | 1.9 | 3/4 | E | Lamellar | 276 | 40 | 982 | 1800 | 10.0 | 7.8 | 19.1 | 47.5 |
| E424 | 1 | 0.10 | – | .06 | – | 1.9 | 3/4 | C | Lamellar | 152 | 22 | 1038 | 1900 | 29.2 | 5.7 | 11.5 | 50.7 |
| E424 | 1 | 0.10 | – | .06 | – | 1.9 | 3/4 | F | Lamellar | 152 | 22 | 1028 | 1900 | 24.4 | 4.0 | 8.6 | 50.5 |
| E421 | 1 | 0.10 | – | .08 | – | 2.5 | 1 | A | Lamellar | 758 | 110 | 760 | 1400 | 2.2 | 0.7 | 1.4 | 37.8 |
| E421 | 1 | 0.10 | – | .08 | – | 2.5 | 1 | D | Lamellar | 758 | 110 | 760 | 1400 | 7.7 | 0.7 | 1.2 | 38.8 |
| E421 | 1 | 0.10 | – | .08 | – | 2.5 | 1 | B | Lamellar | 276 | 40 | 982 | 1800 | 8.4 | 8.7 | 16.2 | 47.3 |
| E421 | 1 | 0.10 | – | .08 | – | 2.5 | 1 | E | Lamellar | 276 | 40 | 982 | 1800 | 9.5 | 3.8 | 11.6 | 47.4 |
| E421 | 1 | 0.10 | – | .08 | – | 2.5 | 1 | C | Lamellar | 152 | 22 | 1038 | 1900 | 27.2 | 5.9 | 10.6 | 50.6 |

## APPENDIX G (Cont'd)

| Casting Number | Charge Composition, % Cr | C | Ta | Analyzed Comp, %* C | Ta | Solidification Rate cm/hr | in/hr | Specimen Identification | Microstructure in Test Specimen | Stress MPa | ksi | Temperature °C | °F | Rupture Life Hours | Prior Creep % | % El | Larson-Miller Parameter (C=20) |
|---|---|---|---|---|---|---|---|---|---|---|---|---|---|---|---|---|---|
| E421 | 1 | 0.10 | – | .08 | – | 2.5 | 1 | F | Lamellar | 152 | 22 | 1038 | 1900 | 27.4 | 4.7 | 10.5 | 50.6 |
| E450 | 1 | – | 3.0 | – | 3.2 | 0.64 | 1/4 | L | Lamellar | 758 | 110 | 760 | 1400 | 1.1 | .2 | 17.3 | 37.3 |
| E450 | 1 | – | 3.0 | – | 3.2 | 0.64 | 1/4 | H | Lamellar | 758 | 110 | 760 | 1400 | 35.0 | 2.9 | 6.9 | 49.1 |
| E450 | 1 | – | 3.0 | – | 3.2 | 0.64 | 1/4 | J | Lamellar | 276 | 40 | 982 | 1800 | 15.0 | 3.7 | 12.2 | 47.9 |
| E450 | 1 | – | 3.0 | – | 3.2 | 0.64 | 1/4 | F | Lamellar | 276 | 40 | 982 | 1800 | 6.2 | .8 | 6.7 | 47.0 |
| E450 | 1 | – | 3.0 | – | 3.2 | 0.64 | 1/4 | K | Lamellar | 152 | 22 | 1038 | 1900 | 48.3 | 9.0 | 14.5 | 51.2 |
| E450 | 1 | – | 3.0 | – | 3.2 | 0.64 | 1/4 | G | Lamellar | 152 | 22 | 1038 | 1900 | 38.3 | 10.4 | 16.9 | 50.9 |
| E417 | 1 | – | 3.0 | – | 2.9 | 0.95 | 3/8 | A | Cellular | 758 | 110 | 760 | 1400 | 0.7 | 6.9 | 11.4 | 36.9 |
| E417 | 1 | – | 3.0 | – | 2.9 | 0.95 | 3/8 | B | Cellular | 758 | 110 | 760 | 1400 | 0.4 | 6.5 | 14.0 | 36.5 |
| E417 | 1 | – | 3.0 | – | 2.9 | 0.95 | 3/8 | C | Cellular | 276 | 40 | 982 | 1800 | 33.9 | 4.5 | 8.0 | 48.7 |
| E417 | 1 | – | 3.0 | – | 2.9 | 0.95 | 3/8 | D | Cellular | 276 | 40 | 982 | 1800 | 10.8 | 18.9 | 16.8 | 47.5 |
| E417 | 1 | – | 3.0 | – | 2.9 | 0.95 | 3/8 | E | Cellular | 152 | 22 | 1038 | 1900 | 34.1 | 8.0 | 18.0 | 50.8 |
| E417 | 1 | – | 3.0 | – | 2.9 | 0.95 | 3/8 | F | Cellular | 152 | 22 | 1038 | 1900 | 31.5 | | 16.5 | 50.7 |
| E414 | 1 | – | 3.0 | – | Not | 1.3 | 1/2 | E | Cellular | 758 | 110 | 760 | 1400 | 0.6 | 7.7 | 14.3 | 39.3 |
| E414 | 1 | – | 3.0 | – | Analyz- | 1.3 | 1/2 | F | Cellular | 758 | 110 | 760 | 1400 | 0.7 | 9.6 | 14.3 | 39.3 |
| E414 | 1 | – | 3.0 | – | ed | 1.3 | 1/2 | A | Cellular | 276 | 40 | 982 | 1800 | 11.7 | 8.6 | 15.4 | 47.9 |
| E414 | 1 | – | 3.0 | – | " | 1.3 | 1/2 | B | Cellular | 276 | 40 | 982 | 1800 | 12.7 | 6.3 | 13.3 | 47.7 |
| E414 | 1 | – | 3.0 | – | " | 1.3 | 1/2 | C | Cellular | 152 | 22 | 1038 | 1900 | 36.7 | 9.2 | 15.0 | 50.0 |
| E414 | 1 | – | 3.0 | – | " | 1.3 | 1/2 | D | Cellular | 152 | 22 | 1038 | 1900 | 36.5 | 8.4 | 13.8 | 49.9 |
| E431 | 1 | 0.10 | 3.0 | .08 | 3.2 | 0.64 | 1/4 | L1 | Lamellar | 758 | 110 | 760 | 1400 | 1.1 | –– | 9.3 | 37.3 |
| E431 | 1 | 0.10 | 3.0 | .08 | 3.2 | 0.64 | 1/4 | L2 | Lamellar | 758 | 110 | 760 | 1400 | 0.4 | 1.4 | 5.7 | 36.5 |
| E431 | 1 | 0.10 | 3.0 | .08 | 3.2 | 0.64 | 1/4 | L3 | Lamellar | 276 | 40 | 982 | 1800 | 10.1 | 2.2 | 9.3 | 47.5 |
| E431 | 1 | 0.10 | 3.0 | .08 | 3.2 | 0.64 | 1/4 | L4 | Lamellar | 276 | 40 | 982 | 1800 | 9.2 | 2.8 | 13.1 | 47.4 |
| E431 | 1 | 0.10 | 3.0 | .08 | 3.2 | 0.64 | 1/4 | L5 | Lamellar | 152 | 22 | 1038 | 1900 | 29.5 | 6.6 | 12.6 | 50.7 |
| E431 | 1 | 0.10 | 3.0 | .08 | 3.2 | 0.64 | 1/4 | L6 | Lamellar | 152 | 22 | 1038 | 1900 | 22.1 | | 9.8 | 50.4 |

## APPENDIX G (Cont'd)

| Casting Number | Charge Composition, % Cr | C | Ta | Analyzed Comp, %* C | Ta | Solidification Rate cm/hr | in/hr | Specimen Identification | Microstructure in Test Specimen | Stress MPa | ksi | Temperature °C | °F | Rupture Life Hours | Prior Creep % | % El | Larson-Miller Parameter (C=20) |
|---|---|---|---|---|---|---|---|---|---|---|---|---|---|---|---|---|---|
| E216 | 6 | – | – | – | – | 1.3 | 1/2 | 1 | Cellular | 758 | 110 | 760 | 1400 | 0.3 | – | 6.8 | 36.2 |
| E216 | 6 | – | – | – | – | 1.3 | 1/2 | 2 | Cellular | 758 | 110 | 760 | 1400 | 0.4 | – | 5.7 | 36.5 |
| E216 | 6 | – | – | – | – | 1.3 | 1/2 | 3 | Cellular | 276 | 40 | 982 | 1800 | 53.9 | – | 6.8 | 49.1 |
| E216 | 6 | – | – | – | – | 1.3 | 1/2 | 4 | Cellular | 276 | 40 | 982 | 1800 | 59.5 | – | 9.8 | 49.2 |
| E216 | 6 | – | – | – | – | 1.3 | 1/2 | 5 | Cellular | 689 | 100 | 760 | 1400 | 231.9 | 0.4 | – | 41.6 |
| E216 | 6 | – | – | – | – | 1.3 | 1/2 | 6 | Cellular | 152 | 22 | 1038 | 1900 | 96.1 | – | 12.8 | 51.9 |
| E216 | 6 | – | – | – | – | 1.3 | 1/2 | 7 | Cellular | 310 | 45 | 982 | 1800 | 21.2 | 5.0 | 8.7 | 49.1 |
| E216 | 6 | – | – | – | – | 1.3 | 1/2 | 8 | Cellular | 517 | 75 | 871 | 1600 | 74.1 | 2.3 | 4.0 | 45.1 |
| E363 | 6 | – | – | – | – | 1.3 | 1/2 | L5 | Cellular | 724 | 105 | 760 | 1400 | 22.1 | 0.96 | 1.6 | 39.7 |
| E363 | 6 | – | – | – | – | 0.64 | 1/4 | L1 | Lamellar | 758 | 110 | 760 | 1400 | 35.6 | 0.98 | 1.9 | 40.1 |
| E363 | 6 | – | – | – | – | 0.64 | 1/4 | L2 | Lamellar | 276 | 40 | 982 | 1800 | 53.1 | 3.4 | 10.4 | 49.1 |
| E388 | 6 | 0.10 | – | .06 | – | 0.64 | 1/4 | G1 | Lamellar | 276 | 40 | 982 | 1800 | 40.0 | 3.0 | 9.0 | 48.8 |
| E388 | 6 | 0.10 | – | .06 | – | 0.64 | 1/4 | G2 | Lamellar | 152 | 22 | 1038 | 1900 | 105.5 | 4.4 | 8.4 | 52.0 |
| E419 | 6 | – | 3.0 | – | 3.3 | 0.64 | 1/4 | A | Cellular | 758 | 110 | 760 | 1400 | 0.8 | 7.3 | 6.1 | 37.0 |
| E419 | 6 | – | 3.0 | – | 3.3 | 0.64 | 1/4 | D | Cellular | 758 | 110 | 760 | 1400 | 0.2 | 4.6 | 9.0 | 35.9 |
| E419 | 6 | – | 3.0 | – | 3.3 | 0.64 | 1/4 | B | Cellular | 276 | 40 | 982 | 1800 | 10.7 | 3.9 | 11.7 | 47.5 |
| E419 | 6 | – | 3.0 | – | 3.3 | 0.64 | 1/4 | E | Cellular | 276 | 40 | 982 | 1800 | 31.0 | 1.9 | 7.8 | 48.6 |
| E419 | 6 | – | 3.0 | – | 3.3 | 0.64 | 1/4 | C | Cellular | 152 | 22 | 1038 | 1900 | 84.6 | 6.5 | 10.7 | 51.7 |
| E419 | 6 | – | 3.0 | – | 3.3 | 0.64 | 1/4 | G | Cellular | 152 | 22 | 1038 | 1900 | 91.3 | 3.6 | 21.6 | 51.8 |
| E430 | 6 | 0.10 | 3.0 | .07 | 3.1 | 0.64 | 1/4 | L1 | Cellular | 758 | 110 | 760 | 1400 | 0.1 | — | 1.7 | 35.3 |
| E430 | 6 | 0.10 | 3.0 | .07 | 3.1 | 0.64 | 1/4 | L2 | Cellular | 276 | 40 | 982 | 1800 | 27.2 | 2.8 | 4.2 | 48.4 |
| E430 | 6 | 0.10 | 3.0 | .07 | 3.1 | 0.64 | 1/4 | L3 | Cellular | 152 | 22 | 1038 | 1900 | 48.7 | 3.5 | 16.2 | 51.2 |
| E430 | 6 | 0.10 | 3.0 | .07 | 3.1 | 0.64 | 1/4 | L4 | Cellular | 152 | 22 | 1038 | 1900 | 65.6 | 3.5 | 5.5 | 51.5 |

## APPENDIX G (Cont'd)

| Casting Number | Charge Composition, % Cr | C | Ta | Analyzed Comp, %* C | Ta | Solidification Rate cm/hr | in/hr | Specimen Identification | Microstructure in Test Specimen | Stress MPa | ksi | Temperature °C | °F | Rupture Life Hours | Prior Creep % | % El | Larson-Miller Parameter (C=20) |
|---|---|---|---|---|---|---|---|---|---|---|---|---|---|---|---|---|---|
| D2-40 | 6 | – | – | – | – | 0.95 | 3/8 | A | Cellular | 152 | 22 | 1038 | 1900 | 95.3 | N.M. | N.M. | 51.9 |
| D2-40 | 6 | – | – | – | – | 0.95 | 3/8 | B | Cellular | 152 | 22 | 1038 | 1900 | 89.8 | N.M. | N.M. | 51.8 |
| E493 | 6 | – | – | – | – | 0.95 | 3/8 | C | Lamellar | 152 | 22 | 1038 | 1900 | 165 | N.M. | N.M. | 52.4 |
| E493 | 6 | – | – | – | – | 0.95 | 3/8 | D | Lamellar | 152 | 22 | 1038 | 1900 | 169 | N.M. | N.M. | 52.5 |
| E-517 | 6 | – | – | – | – | 1.3 | 1/2 | B | Cellular | 152 | 22 | 1038 | 1900 | 63.1 | N.M. | N.M. | 51.4 |
| E-517 | 6 | – | – | – | – | 1.3 | 1/2 | C | Cellular | 152 | 22 | 1038 | 1900 | 68.9 | N.M. | N.M. | 51.5 |
| E-523 | 6 | – | – | – | – | 1.3 | 1/2 | B | Cellular | 152 | 22 | 1038 | 1900 | 18.5 | N.M. | N.M. | 50.2 |
| E-523 | 6 | – | – | – | – | 1.3 | 1/2 | C | Cellular | 152 | 22 | 1038 | 1900 | 27.9 | N.M. | N.M. | 50.6 |

*Estimated from slab analysis.
N. M. – Not measured

## DISTRIBUTION LIST

| | Copies |
|---|---|
| Mr. J. Acurio - MS 77-5<br>NASA Lewis Research Center<br>21000 Brookpark Road<br>Cleveland, Ohio 44135 | 1 |
| Dr. R. L. Ashbrook - MS 49-3<br>NASA Lewis Research Center<br>21000 Brookpark Road<br>Cleveland, Ohio 44135 | 1 |
| Mr. C. P. Blankenship - MS 105-1<br>NASA Lewis Research Center<br>21000 Brookpark Road<br>Cleveland, Ohio 44135 | 1 |
| Dr. H. R. Gray - MS 49-1<br>NASA Lewis Research Center<br>21000 Brookpark Road<br>Cleveland, Ohio 44135 | 10 |
| Mr. F. H. Harf - MS 49-3<br>NASA Lewis Research Center<br>21000 Brookpark Road<br>Cleveland, Ohio 44135 | 10 |
| Dr. H. B. Probst - MS 49-3<br>NASA Lewis Research Center<br>21000 Brookpark Road<br>Cleveland, Ohio 44135 | 1 |
| Mr. C. M. Schuermann - MS 49-1<br>NASA Lewis Research Center<br>21000 Brookpark Road<br>Cleveland, Ohio 44135 | 1 |
| Mr. J. W. Weeton - MS 49-3<br>NASA Lewis Research Center<br>21000 Brookpark Road<br>Cleveland, Ohio 44135 | 1 |
| Mr. G. C. Deutsch/RW<br>NASA Headquarters<br>Washington, DC 20546 | 1 |
| Dr. C. W. Andrews - MS 49-3<br>NASA Lewis Research Center<br>21000 Brookpark Road<br>Cleveland, Ohio 44135 | 1 |
| Mr. G. M. Ault - MS 3-5<br>NASA Lewis Research Center<br>21000 Brookpark Road<br>Cleveland, Ohio 44135 | 1 |
| Mr. J. C. Freche - MS 49-1<br>NASA Lewis Research Center<br>21000 Brookpark Road<br>Cleveland, Ohio 44135 | 1 |
| Mr. R. W. Hall - MS 49-1<br>NASA Lewis Research Center<br>21000 Brookpark Road<br>Cleveland, Ohio 44135 | 1 |
| Mr. M. H. Hirschberg - MS 49-1<br>NASA Lewis Research Center<br>21000 Brookpark Road<br>Cleveland, Ohio 44135 | 1 |
| Mr. N. T. Saunders - MS 105-1<br>NASA Lewis Research Center<br>21000 Brookpark Road<br>Cleveland, Ohio 44135 | 1 |
| Mr. R. A. Signorelli - MS 106-1<br>NASA Lewis Research Center<br>21000 Brookpark Road<br>Cleveland, Ohio 44135 | 1 |
| Maj. F. J. Gasperich<br>AFSC Liaison MS 501-3<br>NASA Lewis Research Center<br>21000 Brookpark Road<br>Cleveland, Ohio 44135 | 1 |
| Mr. J. Gangler/RWM<br>NASA Headquarters<br>Washington, DC 20546 | 1 |

## DISTRIBUTION LIST (Cont'd)

| | Copies |
|---|---|
| Mr. J. Maltz/RWM<br>NASA Headquarters<br>Washington, DC 20546 | 1 |
| Mr. W. J. Schulz<br>AFML/<br>Headquarters<br>Wright Patterson AFB<br>Ohio 45433 | 1 |
| Dr. P. J. Ahearn AMXMR-RM<br>Army Materials and<br>Mechanics Research Center<br>Watertown, MA 02172 | 1 |
| Mr. I. Machlin AIR-52031B<br>Naval Air Systems Command<br>Navy Department<br>Washington, DC 20361 | 1 |
| Mr. J. W. Glatz<br>Navy Department<br>Naval Air Prop. Tr. Center<br>Trenton, NJ 08628 | 1 |
| Mr. J. P. Gudas<br>Navy Department<br>Naval Ship R&D Center<br>Annapolis, Maryland 21402 | 1 |
| Mr. R. D. Fitzsimmons<br>National Aeronautics and<br>Space Council<br>Exec. Off. of the President<br>Washington, DC 20502 | 1 |
| Dr. C. W. Spencer<br>Materials Adv. Bd.<br>Nat. Acad. of Sciences<br>2101 Constitution Ave.<br>Washington, DC 20418 | 1 |
| Mr. N. Griesenauer<br>Battelle Memorial Inst.<br>505 King Avenue<br>Columbus, Ohio 43201 | 1 |
| Capt. R. Dunco<br>AFML/LLC<br>Wright Patterson AFB, OH 45433 | 1 |
| Capt. D. W. Zabierek<br>AFAPL/TBP<br>Headquarters<br>Wright Patterson AFB<br>Ohio 45433 | 1 |
| Dr. J. C. Hurt<br>Army Research Office<br>Box CM<br>Durham, NC 27706 | 1 |
| Mr. R. Schmidt AIR-52031A<br>Naval Air Systems Command<br>Navy Department<br>Washington, DC 20361 | 1 |
| Mr. M. K. Thomas (MAMM-5)<br>Vehicle Tech. Department<br>Nav. Air Dev. Center<br>Warminster, PA 18974 | 1 |
| Dr. B. McDonald<br>Code 471, ONR<br>Department of the Navy<br>Arlington, VA 22217 | 1 |
| Mr. J. R. Lane<br>Materials Adv. Bd.<br>Nat. Acad. of Sciences<br>2101 Constitution Ave.<br>Washington, DC 20418 | 1 |
| Mr. H. E. Boyer<br>Am. Society for Metals<br>Metals Park<br>Novelty, OH 44073 | 1 |
| Mr. D. J. Maykuth<br>Battelle Memorial Inst.<br>Cobalt Information Center<br>505 King Avenue<br>Columbus, Ohio 43201 | 1 |

## DISTRIBUTION LIST (Cont'd)

| | Copies |
|---|---|
| MCIC<br>Battelle Memorial Inst.<br>505 King Avenue<br>Columbus, Ohio 43201 | 1 |
| Dr. J. K. Tien<br>Henry Krumb Sch. of Mines<br>Columbia University<br>New York, NY 10027 | 1 |
| Prof. A. Lawley<br>Dept. of Metall. Engrg.<br>Drexel University<br>Philadelphia, PA 19104 | 1 |
| Dr. D. L. Albright<br>Dept. Met. & Matl. Engrg.<br>Ill. Inst. of Techn.<br>Chicago, IL 60616 | 1 |
| Prof. J. D. Verhoeven<br>Department of Metallurgy<br>Iowa State University<br>Ames, Iowa 50010 | 1 |
| Dr. W. R. Kraft<br>Dept. Met. & Matl. Sci.<br>Lehigh University<br>Bethlehem, PA 18015 | 1 |
| Prof. T. H. Courtney<br>Michigan Technological<br>University<br>Houghton, MI 48602 | 1 |
| Prof. N. S. Stoloff<br>Rensselaer Polytechnical Institute<br>Troy, NY 12100 | 1 |
| Mr. L. J. Fiedler<br>Avco Lycoming Div.<br>550 S. Main Street<br>Stratford, CT 06497 | 1 |

| | Copies |
|---|---|
| Dr. M. S. Seltzer<br>Battelle Memorial Inst.<br>505 King Avenue<br>Columbus, Ohio 43201 | 1 |
| Mr. T. Z. Kattamis<br>School of Engineering<br>University of Connecticut<br>Storrs, CT 06268 | 1 |
| Mr. A. T. Chapman<br>Georgia Inst. of Techn.<br>Atlanta, GA 30080 | 1 |
| Dr. R. A. Gottschall<br>University of Illinois<br>Urbana, IL 61801 | 1 |
| Dr. W. Hertzberg<br>Dept. Met. & Matl. Sci.<br>Lehigh University<br>Bethlehem, PA 18015 | 1 |
| Prof. M. C. Flemmings<br>Dept. of Metallurgy<br>Mass. Inst. of Technology<br>Cambridge, MA 02139 | 1 |
| Dr. S. A. David<br>Dept. of Metallurgy<br>University of Pittsburgh<br>Pittsburgh, PA 15213 | 1 |
| Dr. T. T. Courtney<br>University of Texas<br>Matls. Sci. Lab.<br>Austin, TX 78712 | 1 |
| Mr. B. Goldblatt<br>Avco Lycoming Div.<br>550 S. Main Street<br>Stratford, CT 06497 | 1 |

## DISTRIBUTION LIST (Cont'd)

| | Copies |
|---|---|
| Dr. S. T. Wlodek<br>Stellite Division<br>Cabot Corporation<br>1020 W. Park Ave.<br>Kokomo, IN 46901 | 1 |
| Mr. H. Morrow<br>Climax Molybdenum Corp.<br>1 Greenwich Place<br>Greenwich, CT 06830 | 1 |
| Dr. M. G. Benz<br>CRD<br>General Electric Company<br>Schenectady, N. Y. 12301 | 1 |
| Dr. M. F. Henry<br>CRD<br>General Electric Company<br>P. O. Box 8<br>Schenectady, NY 12301 | 1 |
| Library<br>Advanced Technology Lab.<br>General Electric Company<br>Schenectady, NY 12345 | 1 |
| Dr. P. Aldred<br>AEG/GED<br>General Electric Company<br>Cincinnati, OH 45215 | 1 |
| Mr. R. W. Smashey<br>AEG/GED<br>General Electric Company<br>Cincinnati, OH 45215 | 1 |
| Library<br>Materials Science Lab. W5<br>Detroit Diesel Allison<br>General Motors<br>Indianapolis, IN 46206 | 1 |
| Dr. D. R. Muzyka<br>Carpenter Technology Corp.<br>Res. & Dev. Center<br>P. O. Box 662<br>Reading, PA 19603 | 1 |
| Dr. R. F. Kirby<br>Chief, Materials Eng.<br>Garrett Airesearch<br>402 S. 36th Street<br>Phoenix, AR 85034 | 1 |
| Dr. M. F. X. Gigliotti<br>R. & D. Center<br>General Electric Company<br>Schenectady, N. Y. 12301 | 1 |
| Mr. J. L. Walter<br>CRD<br>General Electric Company<br>P. O. Box 8<br>Schenectady, NY 12301 | 1 |
| Tech. Information Center<br>AEG<br>General Electric Company<br>Cincinnati, OH 45215 | 1 |
| Dr. J. W. Semmel<br>AEG/GED<br>General Electric Company<br>Cincinnati, OH 45215 | 1 |
| Dr. M. Herman<br>Detroit Deisel Allison Div.<br>P. O. Box 894<br>Indianapolis, IN 46206 | 1 |
| Mr. F. Jaeger<br>Howmet Corporation<br>Austenal Division<br>Dover, NJ 07801 | 1 |

## DISTRIBUTION LIST (Cont'd)

| | Copies |
|---|---|
| Dr. A. Chalder<br>Howmet Corporation<br>Misco Division<br>One Misco Drive<br>Whitehall, Michigan 49461 | 1 |
| Dr. J. Benjamin<br>International Nickel Co.<br>Merica Research Lab<br>Sterling Forest<br>Suffern, NY 10901 | 1 |
| Dr. G. Garmong<br>Rockwell International<br>Science Center<br>Thousand Oaks, CA 91360 | 1 |
| Dr. T. Piwonka<br>Materials Technology<br>TRW Equipment Group<br>23555 Euclid Avenue<br>Cleveland, OH 44117 | 1 |
| Dr. E. A. Steigerwald<br>TRW Metals Division<br>Minerva, OH 44657 | 1 |
| M&S Division Files<br>MS 49-1<br>NASA Lewis Research Center<br>21000 Brookpark Road<br>Cleveland, OH 44135 | 1 |
| Contracts Section B - MS 500-313<br>NASA Lewis Research Center<br>21000 Brookpark Road<br>Cleveland, OH 44135 | 1 |
| Report Control Office - MS 5-5<br>NASA Lewis Research Center<br>21000 Brookpark Road<br>Cleveland, OH 44135 | 1 |

| | Copies |
|---|---|
| Dr. R. F. Decker<br>International Nickel Co.<br>One New York Plaza<br>NY, NY 10004 | 1 |
| Dr. L. Kaufman<br>Manlabs, Inc.<br>21 Erie Street<br>Cambridge, MA 02139 | 1 |
| Dr. W. Sutton<br>Special Metals<br>Corporation<br>New Hartford, NY 13413 | 1 |
| Library<br>Materials Technology<br>TRW Equipment Group<br>23555 Euclid Avenue<br>Cleveland, OH 44117 | 1 |
| Mr. R. W. Fawley<br>Williams Research Corp.<br>2280 W. Maple Road<br>Walled Lake, MI 48088 | 1 |
| Mr. J. P. Merutka<br>MS 49-3<br>NASA Lewis Research Center<br>21000 Brookpark Road<br>Cleveland, OH 44135 | 1 |
| Library - MS 60-3<br>NASA Lewis Research Center<br>21000 Brookpark Road<br>Cleveland, OH 44135 | 2 |
| Technology Utilization - MS 3-19<br>NASA Lewis Research Center<br>21000 Brookpark Road<br>Cleveland, OH 44135 | 1 |

## DISTRIBUTION LIST (Cont'd)

| | Copies |
|---|---|
| Library<br>NASA<br>Goddard Space Flight Center<br>Greenbelt, Maryland 20771 | 1 |
| Library<br>NASA<br>Marshall Space Flight Center<br>Huntsville, AL 35812 | 1 |
| Library – Acquisitions<br>Jet Propulsion Lab.<br>4800 Oak Grove Drive<br>Pasadena, CA 91102 | 1 |
| Library – Reports-MS 202-3<br>NASA Ames Research Center<br>Moffett Field, CA 94035 | 1 |
| Defense Documentation Center<br>Cameron Station<br>5010 Duke Street<br>Alexandria, Virginia 22314 | 1 |
| Technical Reports Library<br>ERDA<br>Washington, DC 20545 | 1 |
| Mr. W. F. Brown–MS 105-1<br>NASA Lewis Research Center<br>21000 Brookpark Road<br>Cleveland, Ohio 44135 | 1 |
| Mr. S. J. Grisaffe–MS 49-3<br>NASA-Lewis Research Center<br>21000 Brookpark Road<br>Cleveland, Ohio 44135 | 1 |
| Mr. J. L. Smialek–MS 49-3<br>NASA Lewis Research Center<br>21000 Brookpark Road<br>Cleveland, Ohio 44135 | 1 |
| Library – MS 185<br>NASA<br>Langley Research Center<br>Langley Field, VA 23365 | 1 |
| Technical Library/JM6<br>NASA<br>Johnson Space Center<br>Houston, TX 77058 | 1 |
| Library<br>NASA<br>Dryden Flight Res. Center<br>P. O. Box 273<br>Edwards, CA 93523 | 1 |
| Acquisitions Branch<br>NASA Scientific & Tech.<br>Information Facility<br>Box 33<br>College Park, MD 20740 | 10 |
| Technical Library<br>AFML/LAM<br>Headquarters<br>Wright Patterson AFB, OH 45433 | 1 |
| Mr. P. T. Bizon–MS 49-1<br>NASA Lewis Research Center<br>21000 Brookpark Road<br>Cleveland, Ohio 44135 | 1 |
| Dr. R. L. Dreshfield–MS 105-1<br>NASA Lewis Research Center<br>21000 Brookpark Road<br>Cleveland, Ohio 44135 | 1 |
| Mr. R. H. Kemp–MS 49-3<br>NASA Lewis Research Center<br>21000 Brookpark Road<br>Cleveland, Ohio 44135 | 1 |
| Dr. Y. G. Kim–MS 49-1<br>NASA Lewis Research Center<br>21000 Brookpark Road<br>Cleveland, Ohio 44135 | 1 |

## DISTRIBUTION LIST (Cont'd)

| | Copies |
|---|---|
| Dr. S. N. Tewari–MS 49-3<br>NASA Lewis Research Center<br>21000 Brookpark Road<br>Cleveland, Ohio 44135 | 1 |
| Dr. B. A. Wilcox<br>National Science<br>Foundation<br>Washington, DC 20550 | 1 |
| Mr. R. Bragg<br>Dept. of Matls. & Engrg.<br>University of California<br>Berkeley, CA 94720 | 1 |
| Dr. F. H. Cocks<br>School of Engineering<br>Duke University<br>Durham, NC 27706 | 1 |
| Prof. B. Avitzur<br>Dept. Met. & Matl. Sci.<br>Lehigh University<br>Bethlehem, PA 18015 | 1 |
| Dr. B. F. Oliver<br>Dept. Chem. & Met. Engrg.<br>University of Tennessee<br>Knoxville, TE 37916 | 1 |
| Library<br>Chrysler Corporation<br>Defense-Space Group<br>P. O. Box 757<br>Detroit, MI 48231 | 1 |
| Technical Library<br>Space Division<br>General Electric Company<br>P. O. Box 8555<br>Philadelphia, PA 19101 | 1 |
| Mr. M. Slawsky<br>USAF Off Scientific Res.<br>Propulsion Research Div.<br>Washington, DC 20525 | 1 |
| Dr. G. F. Hurley<br>University of California<br>Los Alamos Sci. Lab.<br>P. O. Box 1663<br>Los Alamos, NM 87544 | 1 |
| Prof. J. E. Davison<br>University of Dayton<br>Research Institute<br>300 College Park Ave.<br>Dayton, Ohio 45409 | 1 |
| Mr. W. B. Johnston<br>George Mason University<br>4400 University Drive<br>Faifax, VA 22030 | 1 |
| Prof. P. Winchell<br>Matl. Sci. & Met. Eng.<br>Purdue University<br>West Lafayette, IN 47906 | 1 |
| Dr. K. A. Jackson<br>Bell Telephone Labs.<br>600 Mountain Avenue<br>Murray Hill, NJ 07974 | 1 |
| Dr. D. L. Sponseller<br>Climax Molybdenum Company<br>1600 Huron Parkway<br>Ann Arbor, Michigan 48106 | 1 |
| Dr. E. E. Reynolds<br>Technical Center<br>General Motors Corp.<br>Warren, MI 48090 | 1 |

## DISTRIBUTION LIST (Cont'd)

| | Copies |
|---|---|
| Dr. F. M. Dunlevey<br>Gould Laboratories<br>Gould Inc.<br>540 East 105th Street<br>Cleveland, OH 44108 | 1 |
| Technical Information Center<br>Matls. & Science Lab.<br>Lockheed Research Labs.<br>3251 Hanover Street<br>Palo Alto, CAL. 94304 | 1 |
| Dr. A. I. Mlavsky<br>Tyco Laboratories, Inc.<br>16 Hickory Drive<br>Waltham, MA 02154 | 1 |
| Mr. W. A. Compton<br>Solar Division<br>International Harvester<br>2200 Pacific Highway<br>San Diego, CAL. 92112 | 1 |
| Dr. J. F. Radavich<br>Micromet Laboratories<br>202 South Street<br>West Lafayette, Indiana 47906 | 1 |